9-4-2019

Effect of Surfactant, Oil:Water Ratio and Temperature on the Rheology of Emulsion-Suspension Complex Fluids: Implications for Oil-Based Drilling Fluids

Gilles Landry Numkam
Louisiana State University and Agricultural and Mechanical College

EFFECT OF SURFACTANT, OIL:WATER RATIO AND TEMPERATURE ON THE RHEOLOGY OF EMULSION-SUSPENSION COMPLEX FLUIDS: IMPLICATIONS FOR OIL-BASED DRILLING FLUIDS

A Dissertation

Submitted to the Graduate Faculty of the
Louisiana State University and
Agricultural & Mechanical College
in partial fulfillment of the
requirements for the degree of
Doctor of Philosophy

in

The Craft & Hawkins Department of Petroleum Engineering

by
Gilles Landry Numkam
BS Chemistry, University of Buea, 2011
MS Chemical Engineering, Katholieke Universiteit Leuven, 2015
December 2019

I wish to dedicate this work to my family; my sisters and brothers, Patricia, Celia, and Stephane; and to my parents Josephine Kouomo and Pierre Numkam. With a special thank you to my mother who was my main source of motivation.

Acknowledgments

I am deeply thankful to my research advisor, Dr. Babak Akbari, whose guidance and support was key in the evolution and successful completion of the project. I equally wish to thank my committee members; Dr. Dandina Rao, Dr. Andrew Wojtanowicz, and Dr. James Dorman for their invaluable feedback and recommendations. I also wish to acknowledge my friends and colleagues for their encouragements.

Finally, I wish to express my gratitude to Dr. Seung Kam (Louisiana State University), Mr. Dan Ortiz (Chevron Refinery), Mr. Mike Redburn and Mr. Ryan Shurshen (Newpark Drilling Fluids), Mr. Mike Gilless (Vermeer Texas), Mr. Jorge Fernandez (Sasol USA), Mr. Matthew Offenbacher (AES Drilling Fluids) and Mr. Stephen Bohnet (ConocoPhillips) for fruitful discussions, feedback and chemical supplies. Deep appreciations also go to Dr. Bhuvnesh Bharti and JinGyun Lee (Louisiana State University) for making accessible some important lab instruments.

Table of Contents

List of Abbreviations

CMC: Critical Micelle Concentration

CPI: Catastrophic Phase Inversion

ECD: Equivalent Circulation Density

ESD: Equivalent Static Density

FRIDF: Flat Rheology Invert Drilling Fluid

GoM: Gulf of Mexico

HLB: Hydrophilic Lipophilic Balance

HPHT: High Pressure High Temperature

LPLT: Low Pressure Low Temperature

LPM: Litres per Minute

NPT: Non-Productive Time

MWD: Measurement While Drilling

PIT: Phase Inversion Temperature

PV: Plastic Viscosity

OBM: Oil-Based Mud

OCF: Oil-base Complex Fluid

O:W : Oil-to-Water ratio

O/W: Oil-in-Water Base Emulsion

ROP: Rate of Penetration

TIPI: Temperature-Induced Phase Inversion

TPI: Transitional Phase Inversion

vol.%: Volume Percent

WBM: Water-Based Mud

WCF: Water-base Complex Fluid

YP: Yield Point

wt.%: Weight Percent

W/O: Water-in-Oil Emulsion

List of Symbols

a_o: Hydrophilic head group area

P: Surfactant packing parameter

$\oslash_{disp}$: Dispersed phase volume fraction

$\oslash_{RCP}$: Random close packing fraction

q: Flow rate per unit area

μ_a: Apparent viscosity

μ_r: Emulsion relative viscosity

μ_i: Dispersed phase viscosity

μ_o: Continuous phase viscosity

a_g: Rate of penetration constant

$\Delta \mathrm{P}_{La}$: Laplace pressure

σ_{IFT}: Interfacial tension

R_1, R_2: Radii of curvature

k_1: Einstein's coefficient

k_2: Droplet interaction coefficient

τ: Shear stress

τ_w: Wall shear stress

τ_y: Yield stress

n: Flow behavior index

v: Hydrophobic chain volume

K: Flow Consistency index

$\dot{\gamma}$: Shear rate

γ: Shear strain

a: Droplet radius of dispersed phase

dD/dt: Rate of penetration

dP_f/dL: Frictional pressure loss gradient

U_s: Slip velocity

τ_R: Shear stress at edge of disk

δ: Slip layer thickness

a: Diffusivity coefficient

θ: Contact angle

U_{sb}: Binder slip velocity

σ_s: Surface tension

ϵ: Absolute roughness

d_p: Drill pipe diameter

ϵ/d_p: Relative roughness

$\Delta\rho$: Density difference

μ_p: Plastic viscosity

r_H: Hydraulic radius

r_p: Drill pipe radius

v: Hydrophobic chain length

k_B: Bolztmann's constant

$\bar{v_n}$: Nozzle velocity

d_n: Nozzle diameter

f: Friction coefficient

μ_f: Filtrate volume viscosity

h_{mc}: Mudcake thickness

Ca: Capillary number

Re: Reynold's number

Pe: Peclet number

C_{surf}: Surfactant concentration

T: Temperature

Abstract

Drilling fluids are non-Newtonian mixtures that play a critical role in the timely and successful completion of oil and gas wells. In the particular case of offshore operations, proper design of drilling fluids is of paramount importance in the constant quest to lower break-even prices. Most downhole problems are directly or in-directly related to the rheological and physical properties of drilling fluids, thereby calling for a better understanding of the underlying changes of these properties with respect to drilling fluid composition and external conditions.

The current stance in the design of drilling fluids involves the selection of components and their concentration based on their known attributes. Surfactants and Oil:Water ratio are examples of typical parameters used in the design of drilling fluids. However, the laid emphasis on these attributes tends to overlook other effects of these components that equally affect their end rheology and physical properties, possibly greater extents.

This project sought to assess the underlying effects of typical components used in the preparation of oil-based drilling fluids (OBM), through the investigation of oil-base complex fluids (OCF). Where OCFs refer to emulsion-suspension mixtures having oil as continuous phase. Surfactants and Oil:Water ratio were the composition variables investigated, with temperature as the external variable. The variables in the project were thus both qualitative and quantitative.

Results of the experimental analysis found the underlying effects of both composition and external variables to significantly affect the flow curve, yield stress and stability of OCFs. Comparison between OCFs and OBMs showed similarities on the effect of composition and temperature on their flow and yield properties. Phenomena such as phase inversion, depletion flocculation and wall slip were equally found to affect the mechanical properties of both fluids, albeit to different extents.

Chapter 1
Introduction

1.1 Motivation

In the oil and gas industry, the drilling of wellbores is the first and most expensive step of all operations [1]. The type, depth and location of the well determines the drilling cost, which can represent 25 % of the total oilfield exploration budget. For both on- and offshore operations it is essential for drilling fluids to display desired rheological properties. Via the aforementioned, these viscoelastic mixtures are able to meet their defined functions allowing timely and successful completion of the well; maintain the safety of rig personnel and equipment; and preserve the environment by avoiding spillage and other well-control related issues. In the current economic stance of oil prices, lowering break-even prices is continuously sought by operators via different means amongst which is the performance of drilling fluids through a sound understanding of their mechanical properties.

Drilling environments in deepwaters pose additional challenges in comparison to their onshore counterparts. This is due to the extreme environmetal conditions, Figure 1.1, drilling fluids are subjected to when flowing through the different geometric conduits that make the circulation loop of the rotary system. With these highly varying conditions come undesirable changes in the intrinsic physical and flow properties of drilling fluids that are detrimental to their established functions. Examples of such operations are the drilling of wells in water depths greater than 10,000 ft and 40,000 ft total measured depth in the Gulf of Mexico (GoM) [2][3], where water temperatures can be as low as < 40 °F . On the other hand, temperatures at the opposite end of the scale exceeding 450 and 500 °F have been experienced in the Gulf of Thailand and Red Sea respectively [2][4].

Figure 1.1. Offshore rig [5].

The main challenges encountered in deepwater drilling have been classified under 10 points, namely: (1) lost circulation, (2) mud properties, (3) solids transport, (4) stuck pipe, (5) wellbore stability, (6) shallow gas hazards, (7) gas hydrates, (8) reservoir productivity, (9) environmental issues and (10) fluid-related logistics [6][7]. Research and development (R & D) efforts have been focused on minimizing the costs resulting from the aforementioned challenges and unscheduled events which collectively cost operators in the GoM more than $1 billion in non-productive time (NPT) on an annual basis [7]. About 10 - 40 % of total drilling time is non-productive, with up to 15 % accounted for by downhole problems [8]. With the latter reported to account for more than 40 % of total NPT costs [7]. Figures 1.2 and 1.3 respectively show a breakdown of the source of NPT and the trend in offshore daily rig rates over the past years.

Recognizing the need to address the operational challenges that pose risks to personnel

and equipment safety, induce significant costs and may result in environmental issues, the deepwater drilling industry amongst other measures developed what is today known as flat rheology invert drilling fluids (FRIDF). These drilling fluid systems were developed to overcome the issues observed with the use of conventional oil-based drilling fluids (OBM) as a result of the drastic changes in their apparent viscosity and gel strength with temperature and pressure (Figure 1.4) [7][9][10]. The benefits associated to the use of FRIDFs have allowed them to be used in the drilling of hundreds of deepwater wells, where improvements in rate of penetration (ROP), hole cleaning efficiency, equivalent circulation density (ECD) reduction and lost circulation minimization has been observed [9].

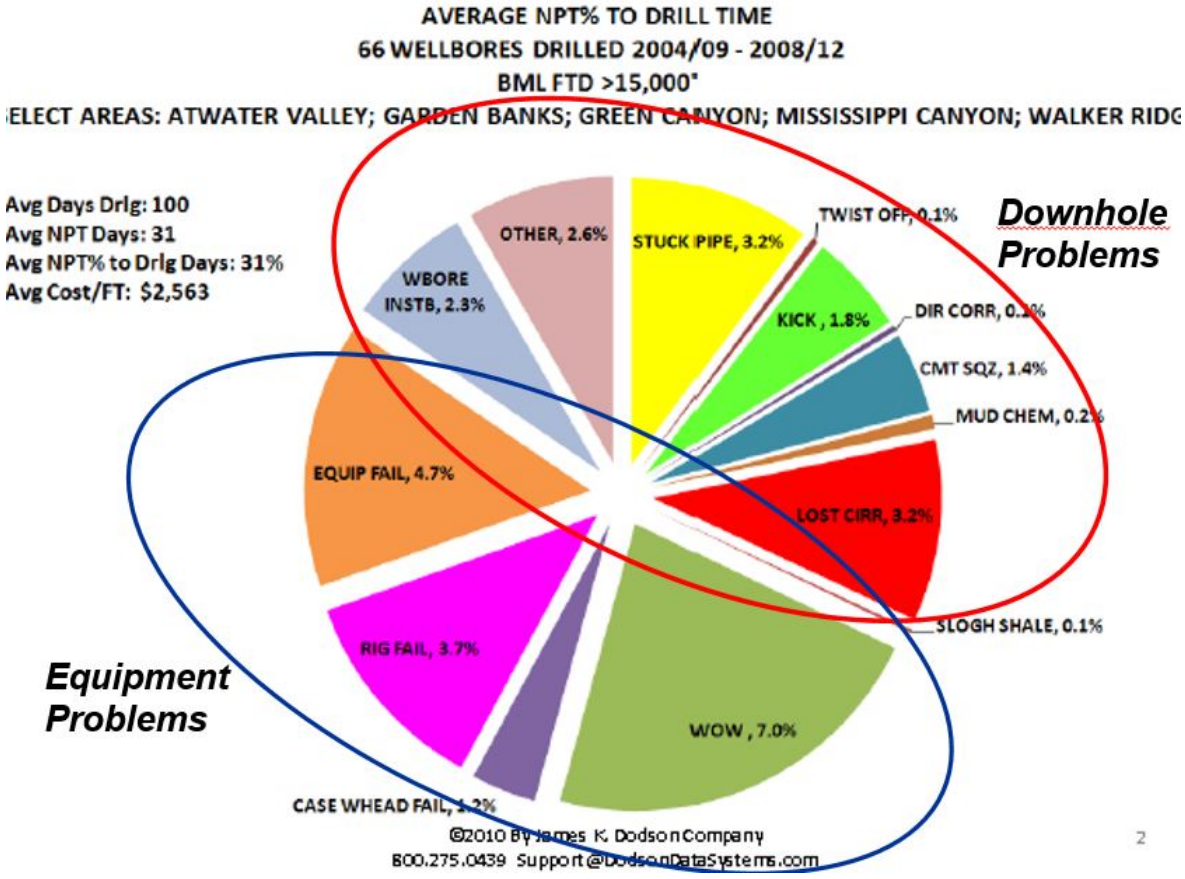

Figure 1.2. Sources of NPT - Deepwater industry [8].

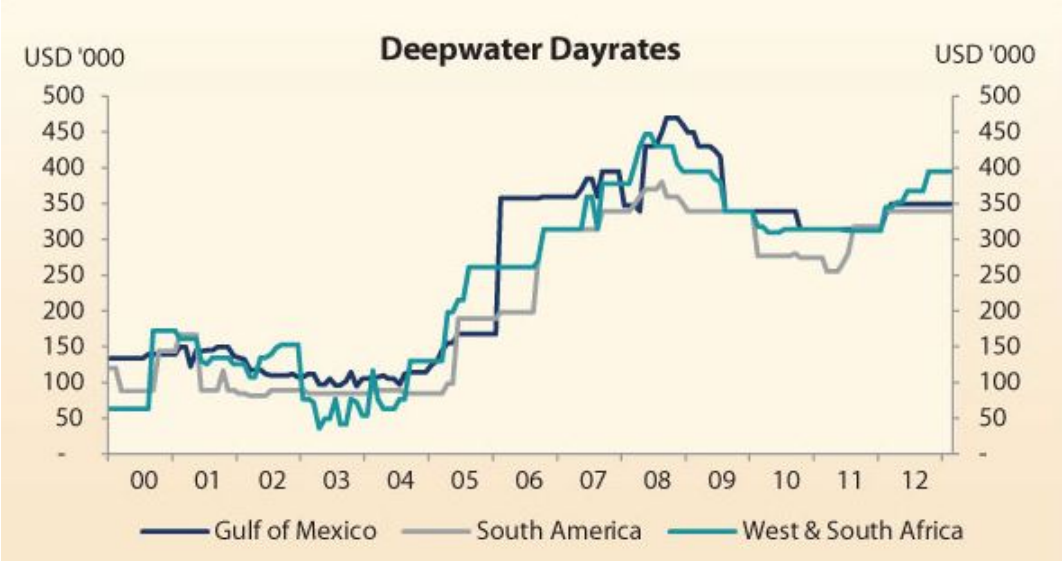

Figure 1.3. Deepwater rig rates [11].

However, despite the multiple benefits related to the application of FRIDFs in the field its been recognized that drawbacks that were overlooked need to be addressed [9]. These drawbacks include the difficult field maintenance and engineering of the fluid system because of its complex and multicomposition, the very high gel strength observed when contaminated with low specific gravity solids. Furthermore, the ineffectiveness of certain rheology modifiers beyond 250 °F has been reported requiring the introduction of another to maintain the flat rheology. To continue, although FRIDFs provide uniform ECD under extreme temperatures and pressures, 'uniform' has been found not to always translate to 'uniformly low' [10]. Finally, drawbacks associated to the use of conventional OBMs such as compressibility, lower formation breakdown gradient (FBG), and gas compressibility remain due to the inherent features of the oil (hydrocarbon) continuous phase [10].

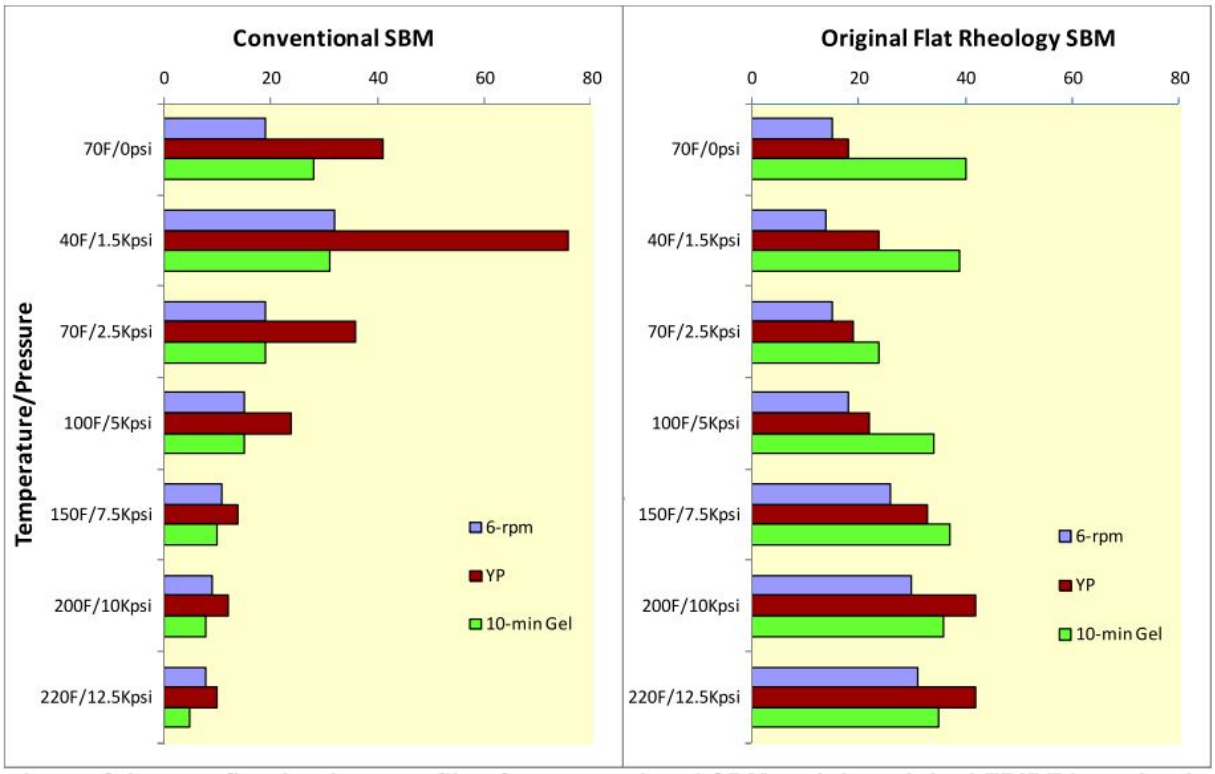

Figure 1.4. A comparison of the non-flat rheology profile of a conventional OBM (SBM) and the original FRIDF in a simulated deepwater well profile, where temperature and pressure changes are aligned with depth increase along the y-axis [9].

The change in mechanical properties of drilling fluids in general, and FRIDFs in particular, to changing environmental conditions is determined by their viscoelastic properties which in turn are defined by their composition. For FRIDFs the number of components typically used in their preparation usually exceeds 13 [10]. The use of rheology modifiers, oil wetters, stabilizers, and complex emulsifier packages amongst other components used in the preparation of FRIDFs underscores the need for a sound understanding of the possible interactions that can induce unaccounted phenomena. Assessing the conditions under which these phenomena occur would enable the mitigation of downhole problems (Figure 1.2) which are all directly or indirectly related to drilling fluid rheology, and will at the same time provide a route for the optimal design of novel drilling fluids.

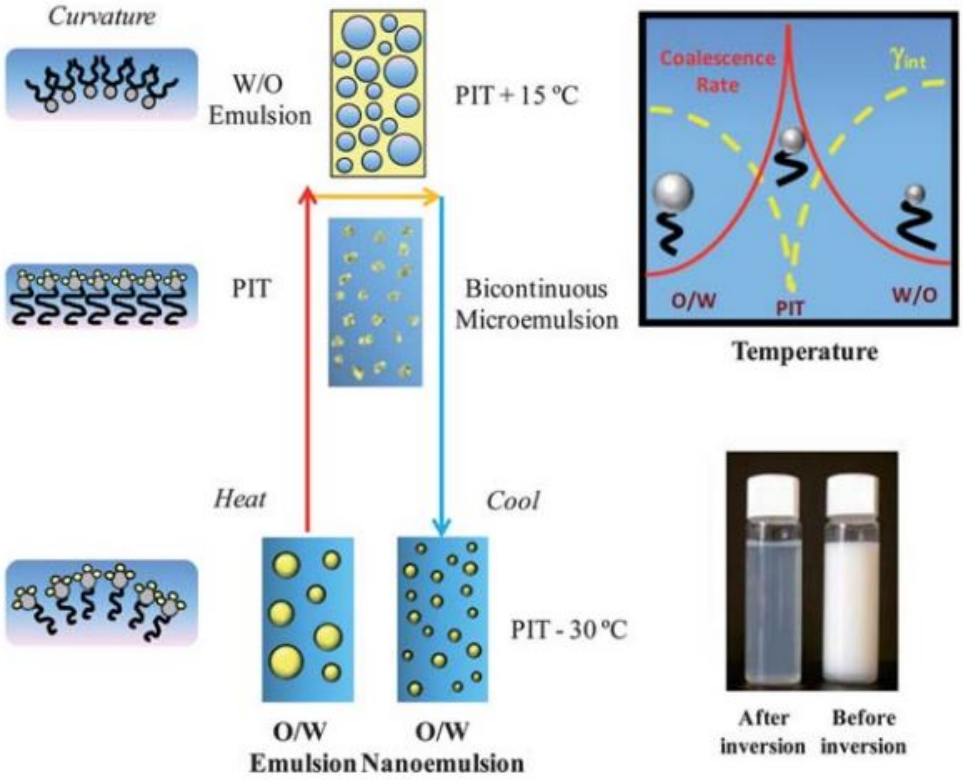

Figure 1.5. Schematic diagram of the formation of nanoemulsions by the PIT method [12].

Temperature-induced phase inversion (TIPI) and wall slip are examples of phenomena unaccounted for in drilling fluids. TIPI is a phenomenon whereby a drilling fluid would transition from one type (WBM or OBM) to another (OBM or WBM) at a temperature known as the phase inversion temperature (PIT). This phenomenon is well established in the chemical and food industries, and is peculiar to emulsion systems stabilized by nonionic surfactants. Figure 2.37 shows a schematic representative of the TIPI process. At temperatures well below the PIT ($\sim$T < PIT - 30 °C), the formation of oil-in-water (O/W) emulsions is favored while at those greater ($\sim$T > PIT + 20 °C) water-in-oil (W/O) emulsions are favored [12]. The low and high temperatures to which drilling fluids are subjected to when flowing through the different geometric conduits of the circulation loop in deepwater operations, make them highly prone to undergo phase inversion leading to changes in their rheological properties.

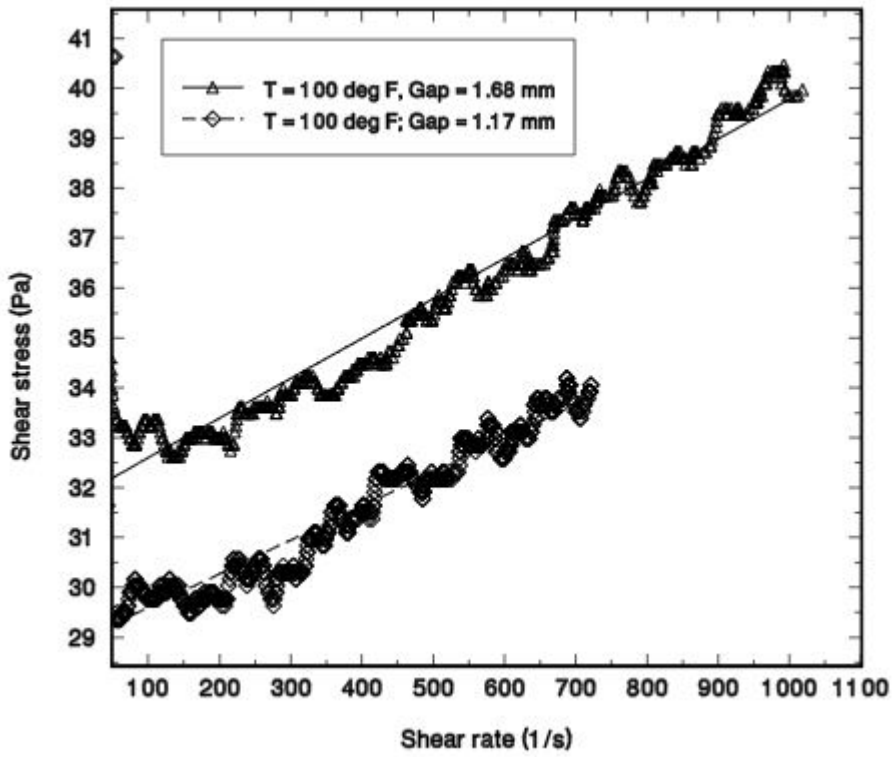

Figure 1.6. The effect of gap width on the flow curves of a 10 wt.% bentonite mud at temperature of 100 °F at 100 psi. Lines represent regressions to experimental data [13].

Wall slip phenomenon, just like TIPI, depends on both composition and temperatures to which non-Newtonian fluids are subjected to. The major consequences for cases of wall slip occurrence in drilling fluids reside in: (1) excessive pump power requirements and (2) greater risks of kicks/blowouts. During drilling fluid circulation, the ECD of the fluid is set to remain within the drilling window, which tend more often than not to be narrow in the ever increasingly challenging environments in which more operations are been conducted [2][7][9]. Frictional pressure loss used in determining ECD are a function of the drilling fluid's rheology characterized on the field with viscometers. Figure 1.6 shows the increasing and decreasing shear stresses of a drilling mud as a result of wall slip. As shown by Tables 1.1 and 1.2, a case can be made on wall slip being a contributing (if not major) factor in the high kick frequencies observed during operations. This is well illustrated by the 55 % kick frequency observed in shallow exploration wells in the GoM.

Table 1.1: GoM - Development Wells Kick Frequencies: 2011 - 2015 [14].

Water Depth Grouped	< 600 m	> 600 m	Total
number of wells spudded	699	122	821
number of kicks	95	27	122
number of wells with kicks	71	23	94
kick frequency per well	0.14	0.22	0.15
percentage number of wells with kicks	10.2 %	18.9 %	11.4 %

Table 1.2: GoM - Exploration Wells Kick Frequencies: 2011 - 2015 [14].

Water Depth Grouped	< 600 m	> 600 m	Total
number of wells spudded	110	190	300
number of kicks	61	82	143
number of wells with kicks	33	56	89
kick frequency per well	0.55	0.43	0.48
percentage number of wells with kicks	30.0 %	29.5 %	29.7 %

1.2 Problem Statements

1. Components used in the preparation of conventional drilling fluids for both on- and offshore operations consist of: (i) immiscible liquid phases (water, oil), differing surfactant: (ii) polarity and (iii) concentrations.

   Emphasis on certain benefits related to these components tend to overlook embedded effects:

   (a) Volume Fraction of Oil phase - Emphasis: high volume fraction of oil phase for better lubrication of drilling string, inhibition of water-sensitive formations. Overlooked: effect of emulsion viscoelastic properties on flow behavior.

   (b) Surfactant polarity (hydrophilic lipophilic balance) - Emphasis: stabilizing O/W or W/O base emulsion. Overlooked: temperature-induced phase inversion, degree of emulsification, interaction with viscosifier (bentonite).

   (c) Surfactant Concentration - Emphasis: interfacial tension reduction for emulsification, wettability alteration of cuttings to facilitate transport. Overlooked: effect of micelle concentration on rheology e.g. depletion flocculation.

2. Drilling fluids (FRIDF) used in offshore operations in general, and deepwater drilling in particular, contain multiple components to generate 'flat rheology'. The plausible use of nonionic surfactants as part of the large and complex components, make the likelihood of phase inversion occurrence high given the large temperature variations (low to high) drilling fluids are subjected to in offshore operations.

3. Wall slip is a phenomenon overwhelmingly observed in multiple non-Newtonian fluids such as polymers, suspensions and emulsions. Despite drilling fluids being emulsion-suspension mixtures, insufficient attention has been put on the in-depth assessment of the occurrence and conditions favoring slip.

1.3 Research Objectives

1. Experimentally determine the effect of composition (internal) and temperature (external) variables on rheology (flow curve, yield stress) of oil-base complex fluids (OCF). Where OCFs are emulsion-suspension mixtures having oil as continuous phase. Internal and external variables include:

   (a) surfactant polarity

   (b) surfactant concentration

   (c) Oil:Water ratio

   (d) temperature

2. Experimentally determine the electrical stability of OCFs.

3. Experimentally determine catastrophic and transitional phase inversion of OCFs.

4. Experimentally determine transitional phase inversion of water-base complex fluids (WCF). Where WCFs are emulsion-suspension mixtures having water as continuous phase.

5. Experimentally determine the effect of composition and temperature on the different forms of wall slip in OCFs.

6. Experimentally determine the effect of composition on fluid loss of OCF:

Chapter 2
Literature Review

2.1 Drilling Fluids

2.1.1 Functions & Composition

Drilling fluids (muds) refer to any fluid that is circulated during operations through geometric conduits going from the surface, down the drill string, through the bit and back to the surface via the annulus [15]. These fluids perform the following functions: (1) cleaning rock fragments from beneath the bit and carrying them to the surface, (2) generate sufficient hydrostatic pressure against formations to prevent formation fluid influx, (3) maintain wellbore stability, (4) cool and lubricate the drill string and bit, (4) minimize formation damage, (5) enable adequate formation evaluation and (6) minimize environmental impact [15][16]. Amongst the functions performed by drilling fluids the one most critical to drilling operation efficiency is the removal of cuttings beneath the bit and their proper transportation to the surface via the annulus (Figure 2.1) [17]. All downhole drilling problems are directly or indirectly related to the physical and rheological properties of drilling fluids, that can result in well abandonment when it is unable to adequately perform its functions.

To meet the established functions mentioned earlier, drilling fluids must posses a number of properties. Among these properties are: (*i*) rheological, (*ii*) fluid loss control, (*iii*) specific fluid weight, (*iv*) inhibition and (*v*) lubrication properties [19]. Rheological properties of drilling fluids determine their ability to achieve good hydraulic requirements and good cuttings carrying capacity. Formation fluid influx of drilling fluids is determined by the fluid loss control properties, this can be measured through static, dynamic and high pressure high temperature (HPHT) tests [19]. The specific fluid weight property of drilling fluids allow them to preserve the well column integrity during operations. Avoiding cuttings from sticking to the drill bit to achieve greater ROP and maintaining wellbore stability is defined by the fluid's inhibition properties. Finally, lubrication properties of the drilling fluid assist in the prevention of problems such as stuck pipe. Generally, oil-based drilling

fluids provide better lubrication properties over their water counterparts [19]. Drilling fluids are classified based on the type of the continuous (base) fluid and other primary components as follows [16][17]:

- Gaseous: air, nitrogen, natural gas
- Gas-Liquid mixtures: foam, aerated water
- Aqueous: water-based muds (WBM)
- Nonaqueous: oil-based muds (OBM)

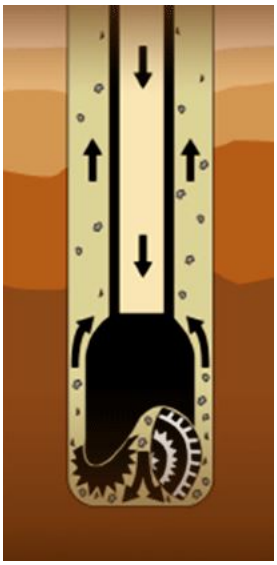

Figure 2.1. Cuttings in circulating drilling fluid [18]

The selection of one drilling fluid over another for a given operation (or depth interval) is governed by the following criteria: (1) formation type(s) to be drilled, (2) temperature range, strength, permeability and pore fluid pressure of the formation, (3) water quality available, (4) formation evaluation procedure and (5) ecological and environmental considerations [16]. A significant fraction of total drilling costs is often associated with drilling fluids, underscoring the importance of its selection and design [17]. The emulsification of oil in a water continuous medium yields an O/W base emulsion in WBMs, while that of water

in a continuous oil medium yields a W/O base emulsion in an OBM. A major difference between conventional OBMs and WBMs is that all solid additives in OBMs are considered inactive because they do not react with the oil phase, while these solids can be inactive (e.g. barite) and active (e.g. hydratable clay) in WBMs [16].

Table 2.1: Composition of Typical Onshore Water- and Oil-Based Muds [19].

WBM	OBM
water continuous phase	oil continuous phase
clay, biopolymers, polymers	modified organophilic clay
weight additives	weight additives
bridging agents	wetting agents
surfactants	surfactants
	calcium chloride

The liquid phase of oil (synthetic base fluid) used in OBMs is either 100 % base fluid or W/O emulsions [19]. The selection of the oil type depends on several factors. The selection of oil used is important as it affects emulsion stability, ease of emulsification, the drilling fluid's odor and its effect on rubber it contacts [22]. The other components used in OBM are: modified organophilic clay, calcium chloride brine, surfactants for emulsification and wetting solid-additives (barium sulfate) as well as drill cuttings.

Elevated costs of paraffins and olefins is one of the reasons that drives the tendency to emulsify water into an oil continuous phase. By doing so, reductions in the cost per barrel of the drilling fluid are achieved [19]. The emulsification is done with surfactants with hydrophilic lipophilic balance (HLB) values ranging between 4 and 6 [23][24][25]. HLB is an empirical quantitative scale which determines the type of emulsion stabilized by a single or mixture of surfactants. Alkanolamides and imidazolines are commonly used as surfactants in OBMs [19]. Although it is possible for a single surfactant to deliver the emulsification and solid wetting properties needed for the OBM (Figure 2.2), two are

commonly applied to meet each purpose. The Oil:Water (O:W) ratio commonly applied in OBMs ranges from 60:40 - 90:10 [19].

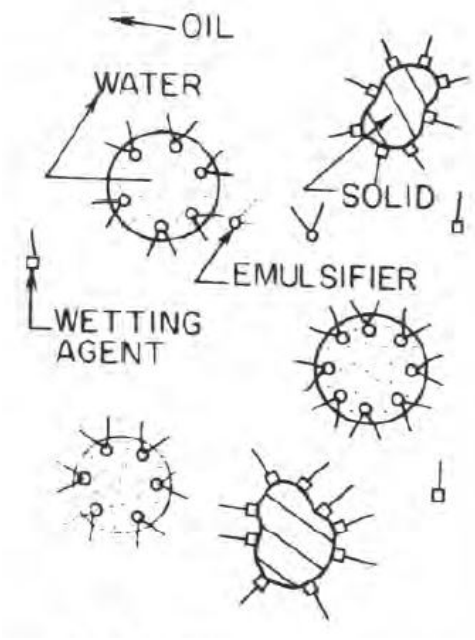

Figure 2.2. Schematic of an oil mud [16].

For conventional WBMs, components typically used in their preparation include: water, clay (or polymers), weighting additives and bridging agents [19]. The use of clays provide the rheological properties needed for cuttings suspension and transportation to the surface. Weighting additives and bridging agents on the other hand are respectively used for density control and formation damage prevention [19]. Stabilization of the base O/W emulsion is done using anionic, nonionic and different possible blends of surfactants [26][27]. Figure 2.3 shows the beneficial effect of surfactant on bit balling reduction.

Composition and physicochemical variables involved in O/W formulations include among others: concentration and nature of surfactant, oil type and mixing temperature [28]. In the past Oil:Water ratios used in WBMs ranged from 40:60 - 75:25 [19], current field applications however have Oil:Water ratios rarely exceeding 10:90. One of the many benefits of emulsion presence in drilling fluids, is the reduced concentration of additives

required to achieve desired rheological properties and added lubricity. To continue, lower amounts of bridging agents are required in comparison to non-emulsified WBMs [19].

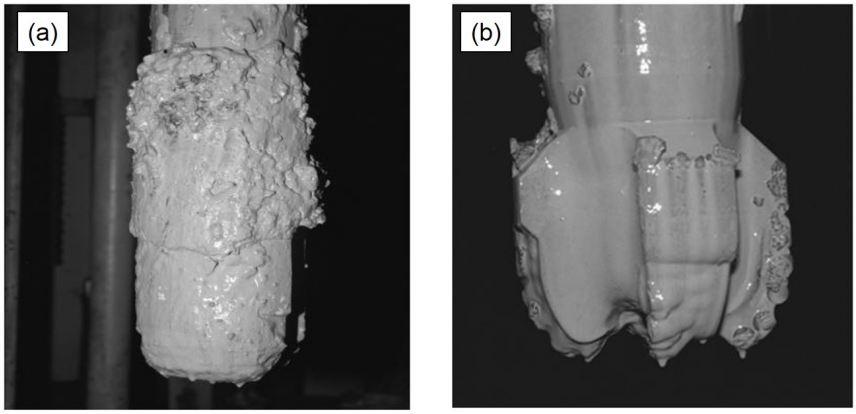

Figure 2.3. Balled drilled bit used with water-based fluid that: (a) does not contain surfactant and (b) contains a surfactant that prevents bit balling [19].

Holistically, OBMs find greater application in conventional drilling operations over WBMs [10]. Their technical superiority over their water counterparts has consistently been proven in the areas of cuttings conditioning, borehole stability, ionic inhibition, ROP, and drill string sticking avoidance (Figure 2.4). The technical benefits associated to the use of OBMs stem from their continuous organic phase [10].

They are considered to be more tolerant to contaminants (e.g. drill cuttings) and easier to maintain, thereby accounting for their widespread selection for most challenging wells [10]. However, some inherent features that make them attractive for onshore drilling operations prove to be counter-productive for offshore deepwater drilling [10]. The setbacks observed with their use for deepwater drilling include excessive increase in fluid viscosity and gel strength with low temperatures, gas solubility, compressibility, and the prospect of downhole pressure losses due to high ECD [9][10].

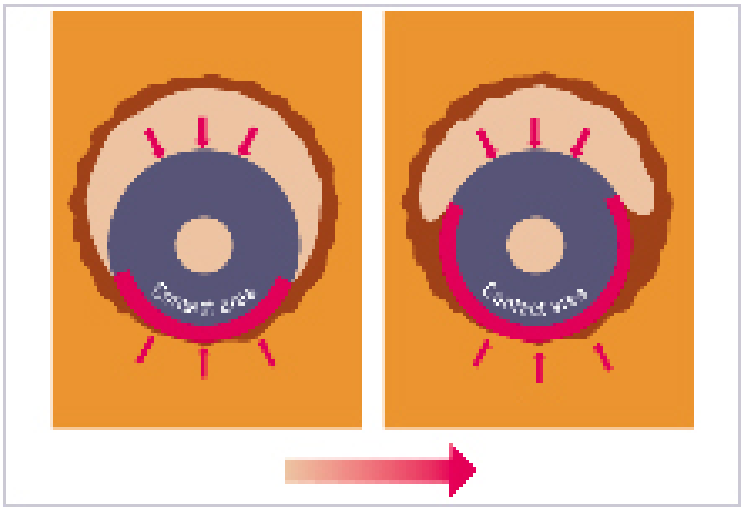

Figure 2.4. Differential sticking due to pressure differential between the drilling fluid and formation. As time passes, if the drillstring remains stationary the area of contact can increase as shown from left to right making it more difficult to free the drillstring [20].

The use of emulsified drilling fluids in operations has been reported to present numerous technical benefits. These include lower filtrate volume losses through the formation of a thin filter cake by the emulsion droplets, Figure 2.5. Additionally, higher return permeabilities due to the minimization of the infiltration of damaging solids and polymers were found through the use of emulsified drilling fluids [1][21]. To continue, emulsified drilling fluids allow higher ROPs to be achieved [22].

They have also been found to reduce bit balling in comparison to non-emulsified WBMs [1]. An increase in bit life from 5 - 50 % has been observed amongst users of emulsified drilling fluids. This has made them highly suitable in directional well drilling because of the improved borehole conditions and low torques associated to their use [29] [30]. They have equally been associated to thin filter cakes, thereby minimizing friction between the drill pipe and wellbore and reducing the risk of differential sticking which is an important trait when drilling in shallow horizontal wells [1][31][32].

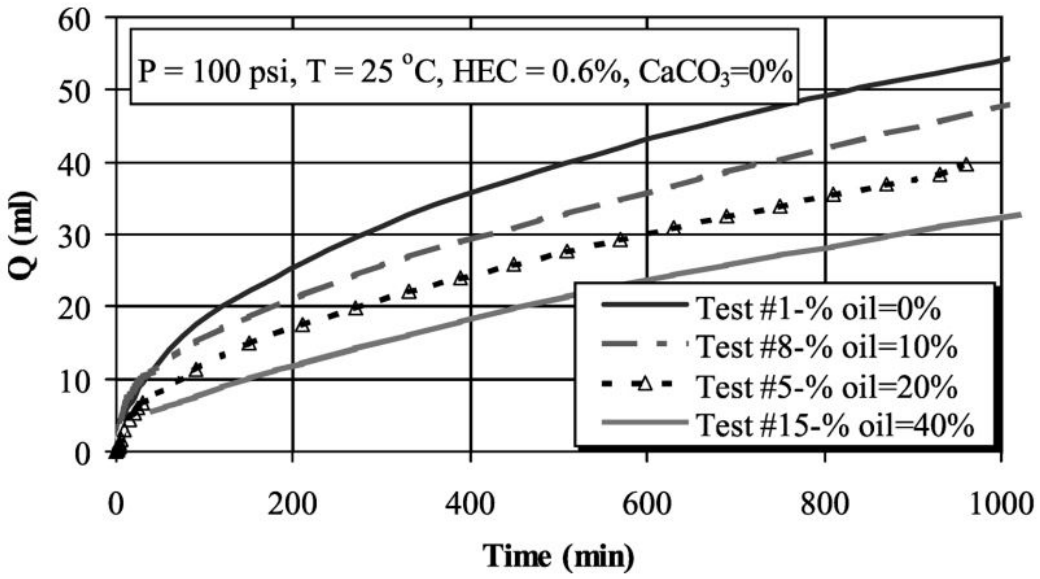

Figure 2.5. Effect of percent oil on the cumulative filtrate volume for Texas limestone [21].

When drilling through low pore pressure formations, emulsified drilling fluids present an advantage due to the presence of an oil phase thereby conferring them lower densities. Through the increase of the O:W ratio both reaction with water-sensitive formations (e.g. shale) and lower mud weight are achieved. Technical challenges however, do exist. These arise from the ability of surfactants to alter the wettability of mineral surfaces. When drilling through producing formations, it has been postulated that reduction of the production potential of reservoirs through different formation damage mechanisms could be caused by surfactants used in emulsified drilling fluids [19][33]. These formation damage mechanisms include (*i*) surfactant invasion and alteration of reservoir rock wettability and (*ii*) promotion of an emulsion barrier formation in the reservoir area surrounding the wellbore by the surfactants [19].

2.1.2 Deepwater Drilling

Majority of deepwater operations occur in the Gulf of Mexico (GoM), Brazil and West Africa. However major initiatives have been recently launched in areas like India, East

Africa, New Zealand, Eastern Mediterranean, Eastern Canada and parts of the North Sea [7][34]. Over the last two decades wells have been drilled in water depths going up to 10,000 ft (3,048 m) of water. The significant prospects for deepwater and ultra-deepwater exploration in conjunction with the elevated rates for floating rigs, have driven continuous R & D efforts to improve safety, economics and efficiency in these environments [7].

Figure 2.6. Deepwater drilling [35].

The deepwater temperature and pressure operating conditions to which conventional drilling fluids are subjected to when flowing through the different geometric conduits of the flow loop often lead to drastic changes in their physical and rheological properties. These include high viscosity buildup with low temperatures that prevail when flowing through the riser leading to high gel strengths and surge/swab pressures after making a trip or connection [9]. These same fluids were found to show excessive shear thinning at high downhole temperatures leading to poor hole cleaning and barite sagging, which would often result in lost circulation due to the formation of barite plugs and cutting beds [9].

The technical challenges resulting from the use of conventional drilling fluids can be classified under 10 main points namely: (1) lost circulation, (2) mud properties, (3) solids transport, (4) stuck pipe, (5) wellbore stability, (6) shallow gas hazards, (7) gas hydrates,

(8) reservoir productivity, (9) environmental issues and (10) fluid-related logistics [7]. Majority of these problems were addressed through the design and application of flat rheology invert drilling fluids (FRIDFs), Figure 2.7.

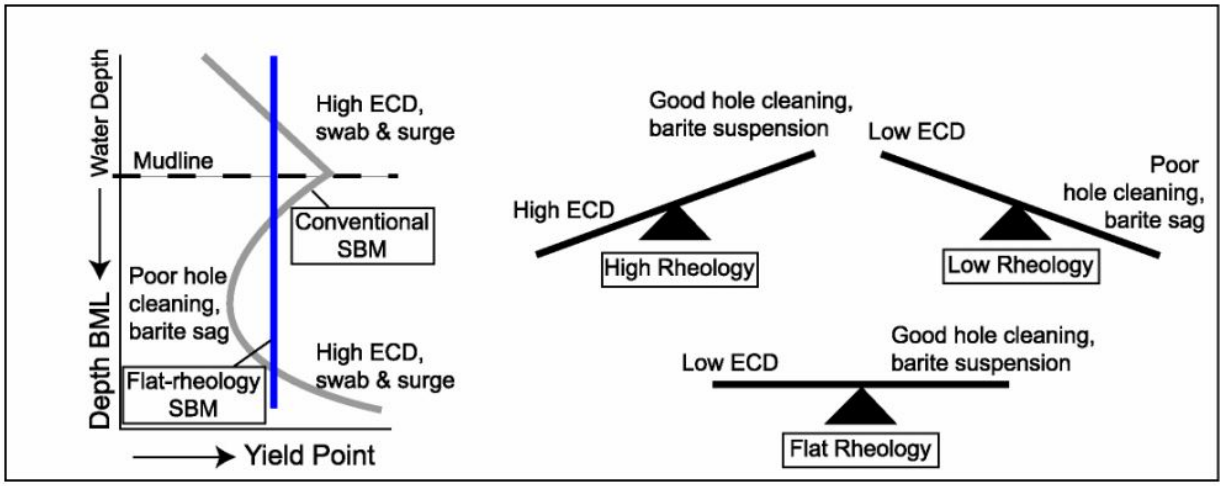

Figure 2.7. Flat rheology concept [36].

These fluids were developed for deepwater application and have been observed to be less sensitive to the wide temperature and pressure variations encountered [7][9][10]. They are defined as drilling fluids that show relatively consistent readings of 6 rpm, yield point and 10 min gel strength over wide ranges of temperature [9]. The 'flat rheology' profile achieved in these fluids is the result of a complex composition of emulsifier packages, rheology modifiers and viscosifiers. The interaction of all these components helps in reducing viscosity at low temperatures while raising them at elevated values [7].

Both FRIDFs and conventional OBMs because of the intrinsic properties of their continuous oil phase pose challenges in reliable hydrostatic pressure estimations. This is due to the degree of compressibility of the the oil phase that will lead to variations in mud density at different points along the annulus, leading to variations in the actual hydrostatic pressure exerted on the formation [10]. This problem tends to be exacerbated in deepwater conditions where large variations in temperature and pressures prevail. Kick detection is another challenge faced by non-aqueous drilling fluids that are OBMs and FRIDFs. Due to the very high solubility of formation gas in oil, 10 to 100 times greater than water, kick

detection is difficult with oil-based systems [10].

Table 2.2: Non-aqueous Drilling Fluid Composition with 70:30 Oil:Water Ratio [37].

Additive	Function	Concentration
base oil	oil continuous phase	67 vol.%
primary emulsifier	emulsifier	2.5 wt.%
Calcium Oxide	alkalinity	1.5 wt.%
NaCl-saturated brine	internal phase	34 vol.%
secondary emulsifier	fluid-loss reducer	0.4 - 1.7 wt.%
organophilic clay	viscosifier	0.5 - 0.6 wt.%
rheology modifier	viscosifier	0.5 - 0.6 wt.%
wetting agent	wettability	as needed
barite	weighting agent	as needed

The technical challenges associated to the use of FRIDFs that highlight the importance of a better understanding of the chemical and physical interactions between its components include the following:

- Uniform hydraulics, ECD, observed does not always translate to uniformly 'low' [10].
- Multiple field reports have indicated its difficult maintenance and engineering [9]. Typical formulations of FRIDFs contain more than thirteen components [10].
- Excessive 10 min gel strength following contamination by low specific gravity solids and ineffectiveness of certain rheology modifiers beyond elevated temperatures have equally been reported [9].

2.1.3 Drilling Hydraulics

The large fluid pressures created by the presence of drilling fluids in the long slender wellbore and tubular pipe strings, make the science of fluid mechanics important to the drilling engineer [16]. These subsurface pressures must be factored into every well problem encountered. The three commonly encountered well conditions during drilling operations include: (1) static conditions, (2) circulating and (3) tripping operations. Static condition refers to situations where both the fluid and central pipe are at rest, while circulating operations refer to periods during which the drilling fluid is being circulated down the drill string and up the annulus, Figure 2.8. Finally, tripping operations refer to those instances in which the central pipe is displaced up or down through the drilling fluid. The second and third conditions are complicated by the non-Newtonian behavior of the drilling fluid [16].

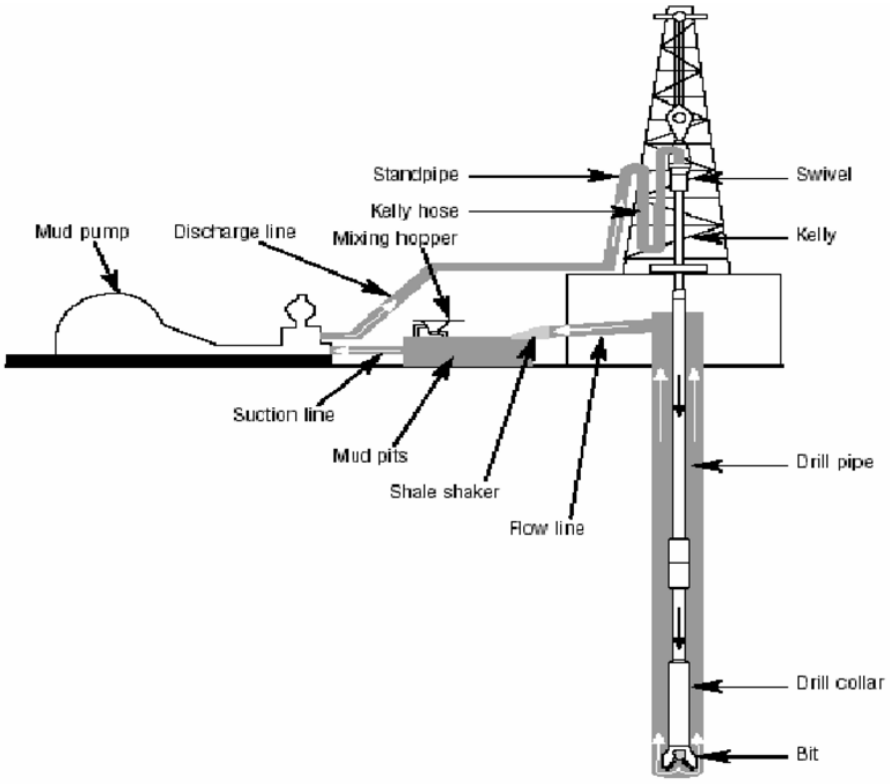

Figure 2.8. Drilling fluid circulation loop [40].

Pressure determination at various points along the well can be quite challenging when

the drill string or fluid is in motion [16]. Furthermore, mathematical description of frictional forces present in the well can be difficult. Nevertheless, these forces must be determined for the calculation of: (1) flowing bottomhole pressure (ECD) during drilling, (2) bottomhole pressure or ECD during tripping operations, (3) optimum pump pressure, (4) cuttings-carrying capacity of the mud and (5) the surface and downhole pressure present in the drill string at different mud flow rates [16].

Controlling frictional pressure losses is important, they define pump pressure requirements, Equation 2.1, and allow the well to be drilled safely with overpressure without fracturing the formation [16][38]. Where ΔP_s, ΔP_{dp}, ΔP_{dc}, ΔP_{dca}, ΔP_{dpa} and ΔP_{bit} represent the frictional pressure loss in the surface equipment, drill pipe, drill collar, drill collar annulus, drill pipe annulus and bit nozzles respectively. P_p represents the pump pressure [16].

$$P_p = \Delta P_s + \Delta P_{dp} + \Delta P_{dc} + \Delta P_{dca} + \Delta P_{dpa} + \Delta P_{bit} \tag{2.1}$$

Continuous adjustment of parameters such as pump rate, drillstring rotation rate and ROP are conducted in order to maintain annular pressure within the drilling window [38]. Frictional pressure losses generated can become critical especially when extermely large viscous forces must be overcome to move the drilling fluid through the different geometric conduits of the flow loop. Development of frictional pressure loss equations require mathematical representation of these forces. This has been done through the use of popular rheological models such as Bingham Plastic, Power Law and Herschel-Bulkley (Yield Pseudoplastic) models, Figure 2.9 [16][39].

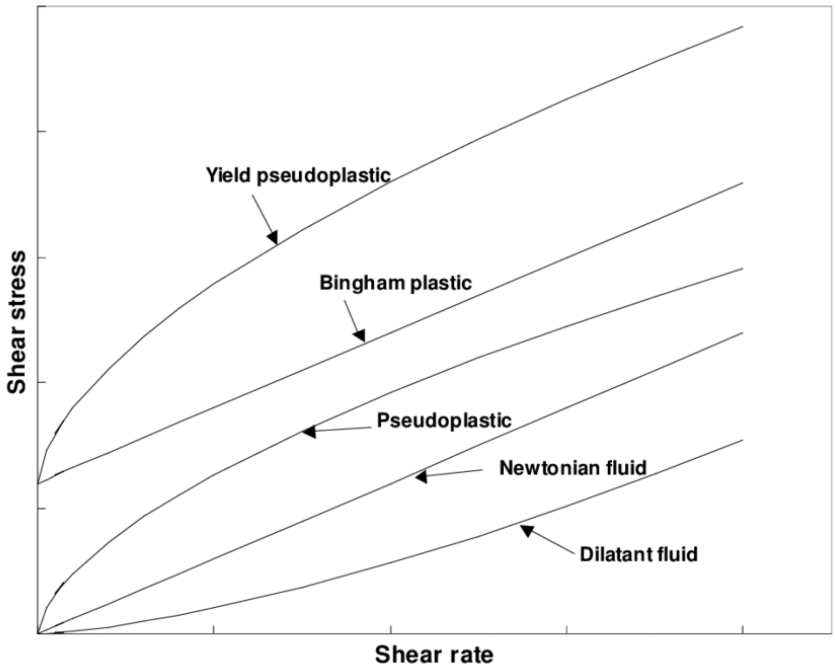

Figure 2.9. Rheological models [41].

These models are respectively represented by Equations 2.3 - 2.5, where τ is the drilling fluid shear stress, τ_y its yield stress, μ stands for its apparent viscosity, μ_p plastic viscosity, $\dot{\gamma}$ represents the applied shear rate, k is the fluid's consistency index and n flow behavior index. Equation 2.2 is the Newtonian rheological model which rarely describes the flow properties of drilling fluids. The relationship between these models and frictional pressure loss is defined by Equations 2.6 and 2.7 for the laminar and turbulent flow regimes respectively [16]. Where r and d represent the radius and diameter of the geometric conduit, dP_f/dL represent the fluid's frictional pressure loss gradient, ρ its density and f the friction factor. c_1 is a constant of integration which for the case of pipe flow equals zero.

$$\tau = \mu\dot{\gamma} \tag{2.2}$$

$$\tau = \tau_y + \mu_p\dot{\gamma} \tag{2.3}$$

$$\tau = k\dot{\gamma^n} \tag{2.4}$$

$$\tau = \tau_y + k\dot{\gamma}^n \tag{2.5}$$

$$\tau = \frac{r}{2}\frac{dP_f}{dL} + \frac{c_1}{r} \tag{2.6}$$

$$\frac{dP_f}{dL} \propto \frac{f\rho\bar{v}}{r} \tag{2.7}$$

Major assumptions are made in the derivation of the analytical expressions of frictional pressure loss. These include: (1) that the drill string is concentrically centered in the casing or open hole, (2) the drill string is not rotated, (3) circular sections of known diameters of the open hole are present, (4) the drilling fluid is incompressible and (5) the flow is isothermal . The computational complexity required to remove these assumptions, is seldom justified [16]. No-flow conditions is the next condition commonly encountered during drilling. This may arise when circulation is interrupted to make a trip or connection. Under such conditions it is important for the drilling fluid to prevent settling of drill cuttings as described by Equation 2.8 [16]. The rheological property of drilling fluids which defines their ability to meet the aforementioned is their yield stress, τ_y.

$$\tau_y = \frac{1}{6}\Delta\rho g \tag{2.8}$$

$$\frac{dP_f}{dL} = \frac{\tau_g}{2}r_w \tag{2.9}$$

The gel strength, τ_g, of the drilling fluid determines the frictional pressure loss that must be overcome by the pump to (re)initiate flow as defined by Equation 2.9. Where r_w represents the radius of the geometric conduit. In some cases the required pressure gradient can be extremely high, especially in the riser where low temperatures prevail. Figure 2.10 summarizes the importance of drilling fluid rheology on drilling hydraulics.

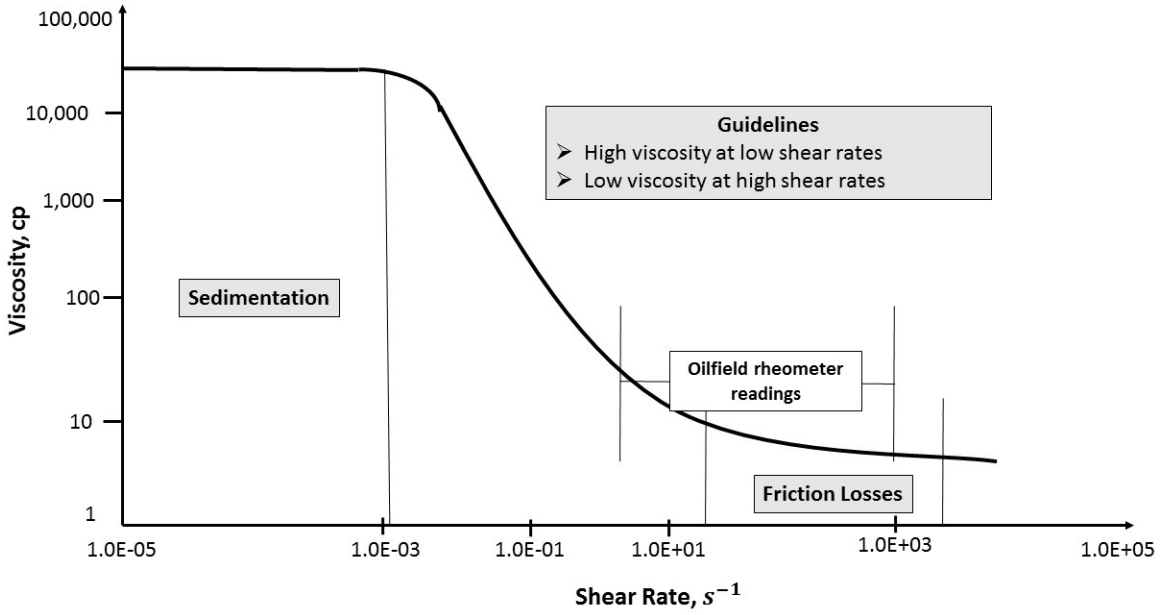

Figure 2.10. The role of fluid rheology [37].

The transportation of cuttings from the hole back to the surface is one of the primary functions of drilling fluids. The adequate transportation of cuttings mitigates multiple technical challenges such as stuck pipe, low ROP, high torque, formation fracturing, premature bit wear and drag on the drill string [42]. Many factors influence the transportation of cuttings to the surface, these include hole diameter, well deviation angle, drill pipe diameter, drill pipe rotation, drill pipe eccentricity, ROP and cuttings characteristics (size, shape, bed porosity), drilling fluid velocity, type and rheology [42].

Cuttings transport ratio (F_T), Equation 2.10, is an excellent measure of the cuttings carrying capacity of drilling fluids [16]. Cuttings in drilling fluids advance at a rate equal to the difference between the fluid velocity ($\bar{v}_a$) and the cuttings' slip velocity ($\bar{v}_{sl}$). The particle's velocity relative to the fluid's velocity is referred to as the transport velocity ($\bar{v}_T$).

$$F_T = \frac{\bar{v}_T}{\bar{v}_a} = \frac{\bar{v}_a - \bar{v}_{sl}}{\bar{v}_a} = 1 - \frac{\bar{v}_{sl}}{\bar{v}_a} \tag{2.10}$$

Computational fluid dynamics (CFD) simulations provides a means to analyze phenomena that are otherwise quite difficult to observe through experimental studies [42]. It

is defined as the analysis of systems involving fluid flow, heat transfer, and mass transport and associated chemical reactions using computer-based simulations [43]. CFD analysis provides an interesting alternative to the experimental studies, particularly for the simulation of real flows and theoretical advances under conditions otherwise unavailable experimentally [44].

Multiple investigations into the effect of rheological properties of drilling fluids on cuttings transport have conducted. Numerical and experimental analysis conducted have found rheological parameters of popular non-Newtonian models used to describe the flow behavior of drilling fluids, (n), consistency index (k), yield stress (τ_y) and plastic viscosity (μ_p), to affect hole cleaning efficiency in different ways [45] [46] [47] [48].

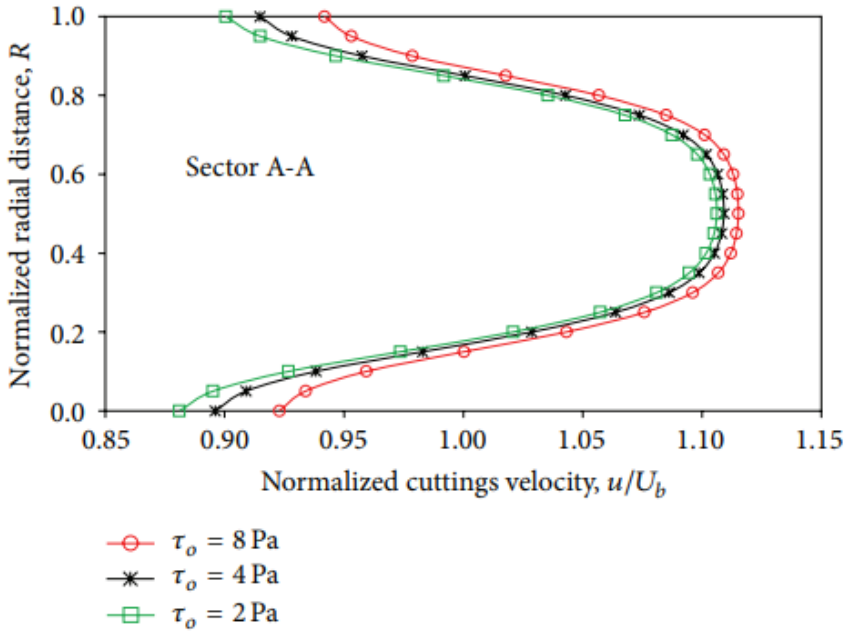

Figure 2.11. Effect of yield stress on cuttings transport velocity in wide annulus [49].

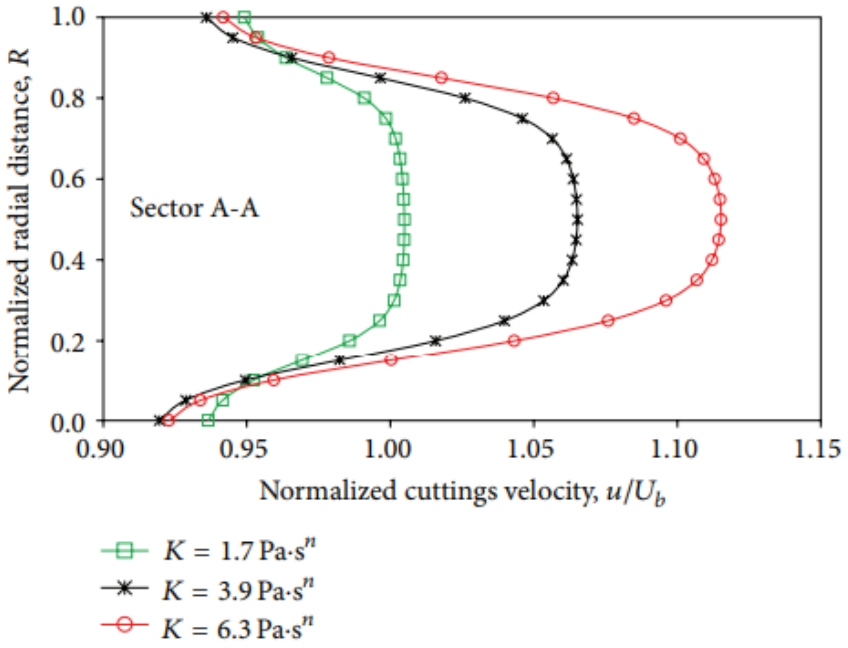

Figure 2.12. Effect of consistency index on cuttings transport velocity in wide annulus [49].

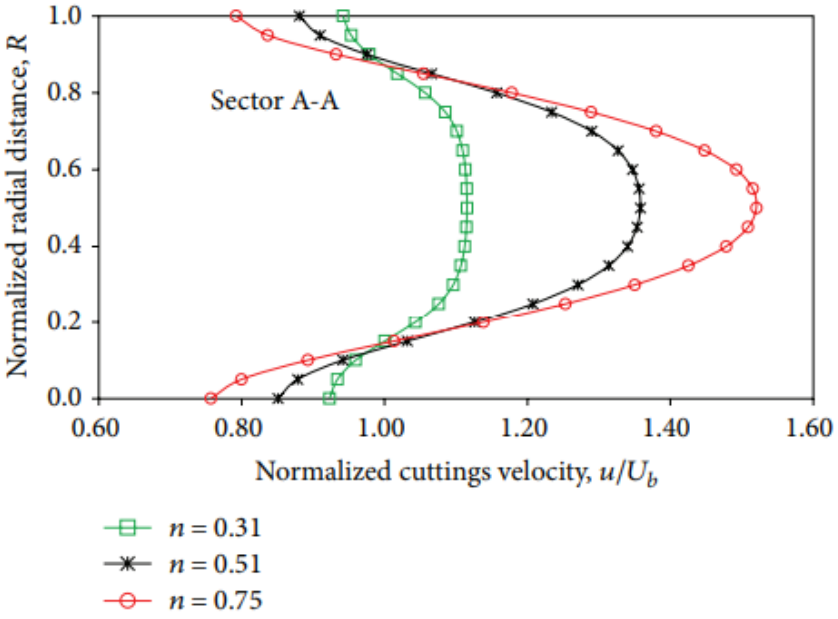

Figure 2.13. Effect of flow behavior index on cuttings transport velocity in wide annulus [49].

Decrease in the values of the flow behavior index has been found to yield a decrease in stationary bed formation, while increasing moving bed layers [45]. To continue, increase in

the ratio of the flow behavior to consistency index (n/k) was found to lead to a reduction in cuttings bed height [46]. The yield stress and plastic viscosity of drilling fluids were found to increase hole cleaning efficiency with decrease in their values at reduced flow rates [48]. Figures 2.11 - 2.13 show the effect of different rheological parameters on cuttings transport velocity for a CFD analysis conducted for a horizontal well geometry [49].

Results shown in Figure 2.11, indicate that high yield stress translate to better cutting transport capacity by drilling fluids, however this effect is less significant in the core. The same trend is observed for the flow consistency index, which is a rheological parameter that relates the cohesion of individual particles, their ability to deform and resist flow [49]. Figure 2.12 shows that high k values translate to better cuttings transport. This rheological property is directly proportional to the drilling fluid's effective viscosity, implying cuttings will be suspended longer and hence travel faster and further in fluids having high k values. As shown in Figure 2.13, increase in the n leads to improved cuttings transport as well. A difference in cuttings transport performance can however be observed when comparing the core and the vicinity of the wall boundaries, where the drilling fluid with the lowest n displays better cuttings transport in the latter region.

2.2 Surfactant: Polarity, HLB, & Concentration

Surfactants refer to amphiphilic molecules that find application in many industrial processes. 'Amphiphile' is indicative of the fact that one part of the molecule likes a given solvent while the other part likes another, with both solvents being immiscible [50]. The term surfactant is a contraction of the phrase "surface active agent". Their properties are important as they dominant interfacial phenomena, examples of which are liquid-liquid, liquid-solid and liquid-gas interfaces [51]. Typically, one of the solvents is water and the water-loving part of the surfactant is referred to as hydrophilic, with the other part usually preferring to be in an oily environment or air and is referred to as hydrophobic (Figure **??**) [50].

Hydrophobic parts of surfactants tend to consist of long, straight alkyl chains ($CH_3(CH_2)_{n_C-1} \sim$, n_C = 8 - 20) [50]. Surfactants can be divided into four groups based on the nature of the electrostatic charge on the hydrophilic head group. These are: anionic, negative charge; cationic, positive charge; nonionic, neutral (no charge); and zwitterionic, whose head group possess both positive and negative charges so that the resultant charge is zero [50]. Commonly used surfactants are nonionic and anionic in nature, cationic surfactants pose environmental problems due to their non-biodegradability while zwitterionic surfactants are expensive and therefore used only for special applications [50].

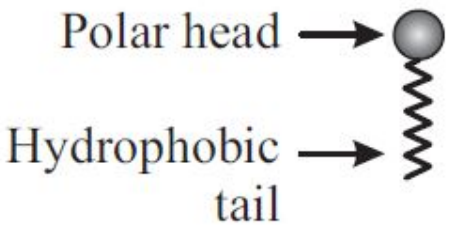

Figure 2.14. Conventional surfactant [50].

A characteristic property of surfactants is their spontaneous aggregation in water to form structures such as spherical micelles, cylinders or bilayers (Figure 2.15) [52]. Micelles play a critical role in the ability of aqueous solutions to solubilize hydrophobic substances (e.g. oil) at concentrations above their critical micelle concentration (CMC) [50]. When dissolved in two (immiscible) phases, surfactants adsorb at the interface with the hydrophobic chain oriented towards the oil phase and hydrophilic head towards the water phase.

Decrease in interfacial tension occurs with continuous increase of surfactant concentration till the critical micelle concentration (CMC) is reached [50]. Above the CMC the interfacial tension remains constant. A number of physical properties of liquids are dependent on surfactant concentration, these include osmotic pressure, electrical conductance and optical turbidity. A key property of high practical relevance equally changes, which is the capacity of solubilizing another hydrophobic substance (oil) in an immiscible liquid

(water) [50].

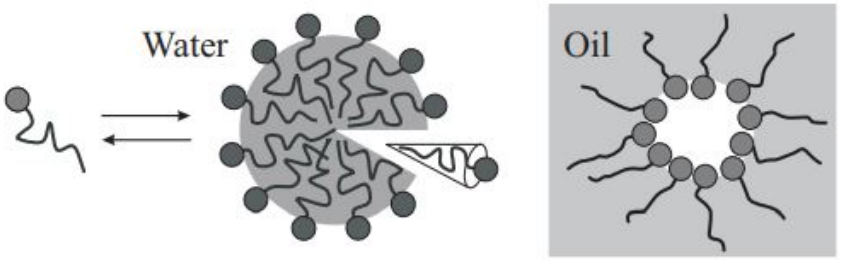

Figure 2.15. Schematic cross-section through a spherical micelle in water. A shell of polar head groups surrounds the hydrophobic core formed by the hydrocarbons chains. The micellar structure is in equilibrium with monomers in solution. Right: inverted micelle in oil [50].

As surfactant concentration increases above values of those of the CMC, the capacity to solubilize a hydrophobic (oil) substance in an aqueous phase increases due to the aggregation of surfactant molecules to form micelles [50]. On average, spherical micelles contain 30 - 100 surfactant molecules with outer diameters of 3 - 6 nm [50]. The tally of surfactant molecules in micelles tend to differ. Some micelles may contain more or less surfactants than others, such that there is a significant polydispersity. The distribution of aggregation number of surfactants is schematically shown in Figure 2.16. The structure and nature of head group polarity are the two competing factors driving micelle formation of surfactants. Surfactants with long alkyl chains (hydrophobic tail) have smaller CMCs in comparison to those with short ones, this is driven by an entropic effect called hydrophobic effect [53].

On the other hand, micelle formation tends to be opposed by the lateral repulsion of the polar head groups. In addition as the surfactants are brought closer to each other, the thermal fluctuations of the head groups are reduced leading to steric repulsion [50]. Nonionic surfactants tend to have lower CMCs than those of ionic surfactants due to the additional electrostatic repulsion that is present in the latter [50]. Figure 2.17 shows the effect of surfactant (micelle) concentration on the stabilization of emulsions. Where stability here is referred to the time taken for 50 % of the aqueous to phase separate [56].

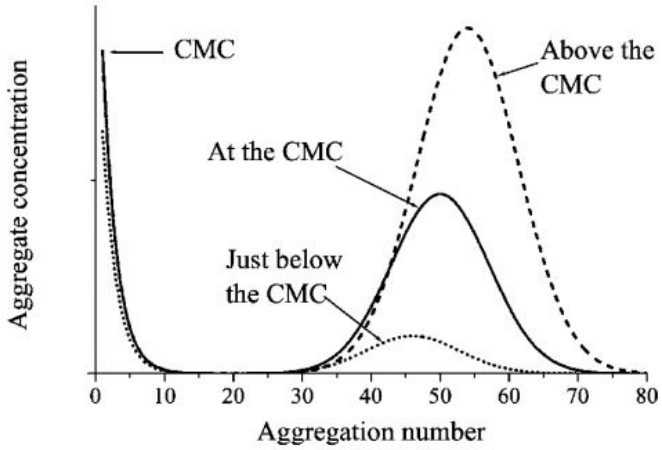

Figure 2.16. Schematic distribution of surfactant aggregates as a function of the aggregation number for three different concentrations. When the total surfactant concentration is equal to the CMC we assumed a mean aggregation number of $N_{agg} = 50$ [50].

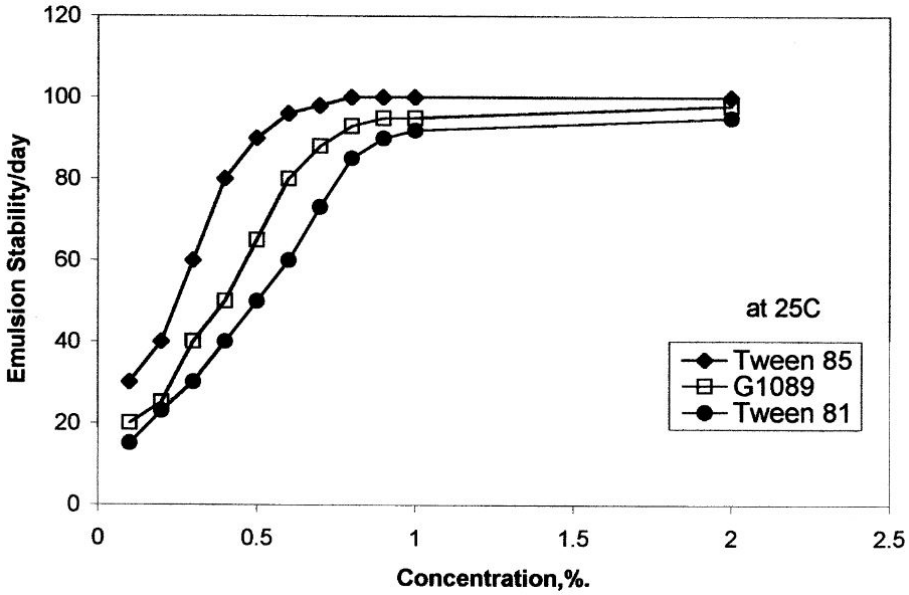

Figure 2.17. Effect of concentration on the stability of asphalt emulsions for Tween 85, G1089 and Tween 81 after 60 days at 50 % asphaltene content [56].

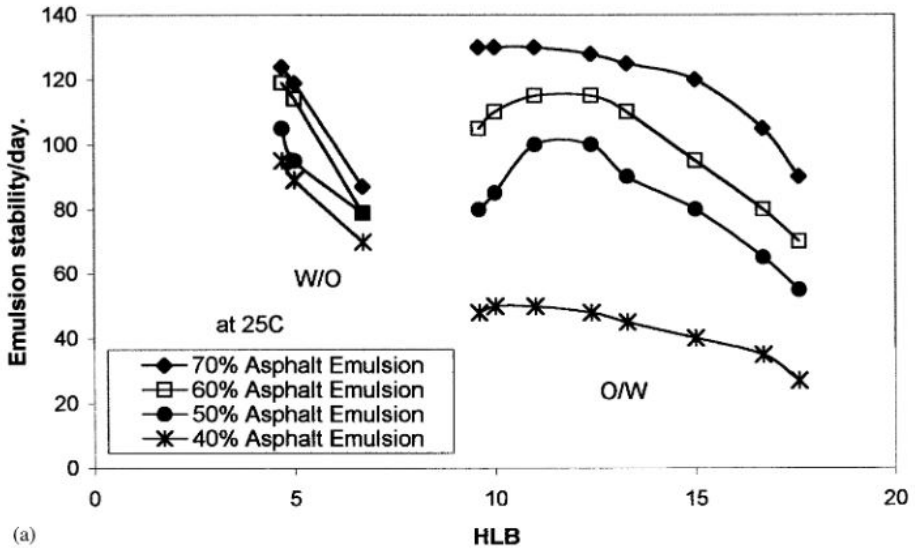

Figure 2.18. HLB versus the stability for individual surfactants (1 -11) at 8 % concentration [56].

Hydrophilic lipophilic balance (HLB) is the other key property of surfactants. Whether an O/W or W/O emulsion was obtained upon mixing oil, water and surfactant was a central problem in emulsion technology. It was determined that the volume fractions of oil and water are not important and that the type of emulsion is primarily determined by the surfactant nature [50]. Figure 2.18 shows the effect of HLB on emulsions stability for asphalt emulsions.

The type of emulsion formed by surfactants is defined by their packing parameter (N_s), Equation 2.11. Where V_c is the volume of the hydrophobic part, L_c the length of the hydrophobic tail and σ_A the effective area of the head group [50]. There are two additional guidelines which are used for the practical formulation of emulsions, these are Bancroft's rule of thumb and the more quantitative HLB scale concept. Bancroft's rule of thumb states that continuous phase of an emulsion will be that in which the surfactant is preferentially soluble [54][55]. Griffin on the other hand suggested an empirical quantitative HLB scale which determines the tendency of surfactants to form W/O or O/W emulsions. The scale runs from 0 - 20 for most surfactants and establishes that those with HLB values between 3 - 6 stabilize W/O emulsions while those with values between 8 - 18 stabilize O/W emulsions

[23].

$$N_s = \frac{V_c}{L_c \sigma_A} \tag{2.11}$$

Surfactants play critical roles in the custom design of drilling fluid formulations as emulsifiers, wetting agents, shale-swelling inhibitors, differential sticking prevention, mitigation of cuttings adhering to the drill bit etc. [19]. Their selection not only depends on the desired formulation but equally varies with respect to the drilling fluid type, aqueous- versus oil-based drilling fluids. Among the properties sought to be modified in drilling fluid formulations are [19]:

- rheological properties - that allow the achievement of hydraulic requirements and good transportation capacity of drill cuttings.
- fluid loss control - that prevents formation damage through fluid invasion.
- specific fluid weight - that ensures the drilling fluid provides required hydrostatic control of the well at all times.
- inhibition properties - that prevent cuttings from sticking to the bit and maintain wellbore stability.
- lubricant properties - that prevents issues such as stuck pipe.

2.3 Oil:Water Ratio: Emulsion Rheology

Fluid systems composed of at least two immiscible phases are known as emulsions [57]. The finely distributed phase is referred to as the dispersed phase while the other phase acting as a dispersing agent is called the continuous or outer phase [50]. Emulsions find great applications in industries such as that of oil & gas, where they are commonly known to assist upstream processes (drilling fluids, oil recovery).

Two types of emulsions can be distinguished from a thermodynamic perspective. Emulsions that are thermodynamically stable are referred to as microemulsions, while those that show metastability (or unstability) are called macroemulsions. Dispersed droplets in microemulsions have diameters between 5 - 100 nm while those in macroemulsions have droplets of the order of wavelength of visible light, 0.5 - 10 μm [50]. O/W and W/O emulsions constitute the two most important emulsion systems, oil here referring to any liquid not soluble in water (Figure 2.19).

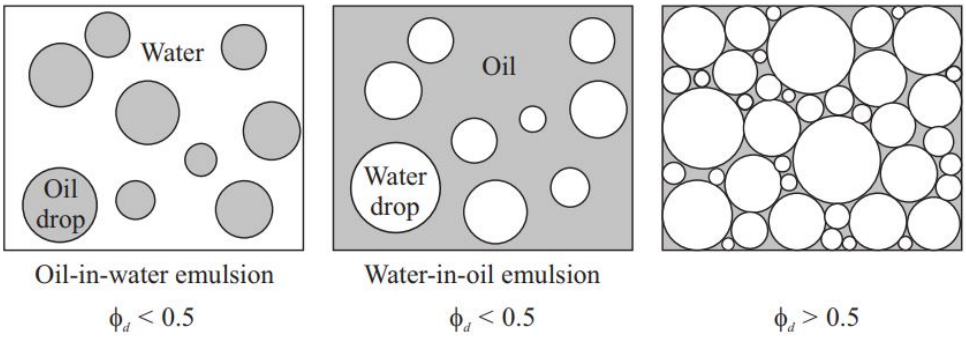

Figure 2.19. An O/W and W/O emulsion with low volume fractions of the dispersed phase $\oslash_{disp}$. In addition, a W/O emulsion with high volume fraction is shown. $\oslash_{disp}$ above 0.74 can occur due to polydispersity of the drops. Small drops can fill the spaces between large ones [50].

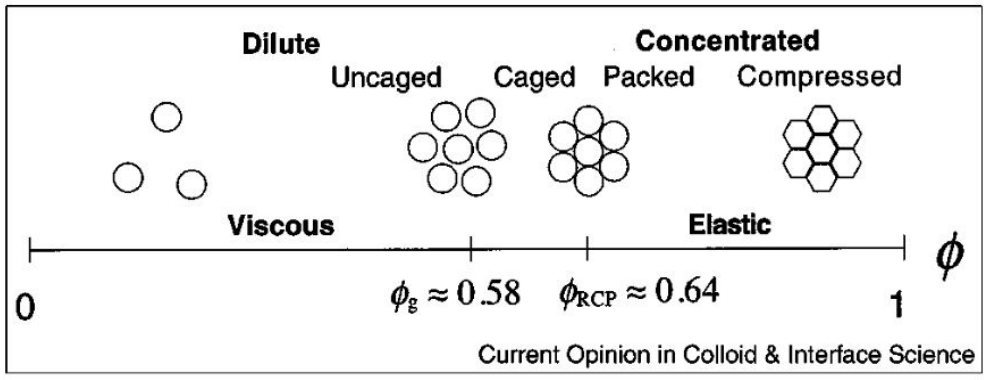

Figure 2.20. Schematic diagram of droplet positional structure and interfacial morphology for disordered monodisperse emulsions of repulsive droplets as a function of the volume fraction of the dispersed phase, $\oslash_{disp}$. In the dilute regime at low $\oslash_{disp}$, the droplets are spherical in the absence of shear. As $\oslash_{disp} \rightarrow 1$, the droplets become nearly polyhedral in shape and form a biliquid foam. Dilute emulsions behave as visous liquids, whereas concentrated emulsions exhibit solid-like elasticity [58].

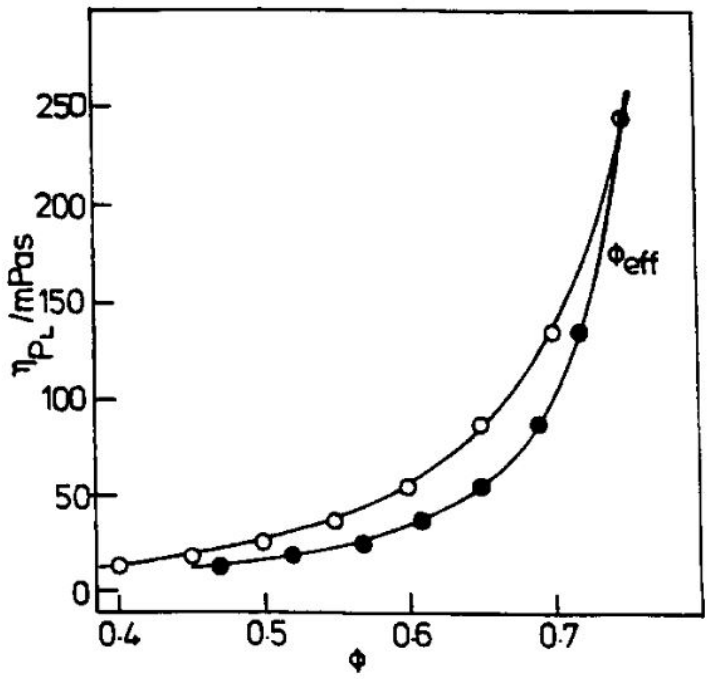

Figure 2.21. Viscosity-volume fraction curve for O/W emulsions [59].

Volume fraction of dispersed phase ($\oslash_{disp}$) is an important property which characterizes macroemulsions. Although one would intuitively assume that $\oslash_{disp}$ should be significantly lower than 50 %, much higher $\oslash_{disp}$ can actually be attained [50][58]. For monodispersed spherical droplets, the maximum volume fraction is that of closed packed spheres ($\oslash_{disp} = 0.74$), Figure 2.20 [50][58]. Preparation of emulsions with much higher $\oslash_{disp}$ have however been achieved with values going as high as 99 % [50] [58].

By controlling the $\oslash_{disp}$, the mechanical properties of an emulsion can be changed from that of a viscous liquid at low $\oslash_{disp}$ to that of an elastic solid at elevated $\oslash_{disp}$ [58]. The display of elasticity at high $\oslash_{disp}$ is the result of the work that needs to be done against interfacial tension, σ_{IFT}, to increase the surface area of droplets when the shear further deforms the already compressed droplets (Figure 2.20) [58]. The aforementioned is best described by the Young-Laplace equation, Equation 2.12 [50]. Figure 2.21 shows the effect of $\oslash_{disp}$ on viscosity of emulsions.

$$\Delta P_{La} = \sigma_{IFT}(\frac{1}{R_1} + \frac{1}{R_2}) \tag{2.12}$$

- ΔP_{La}: pressure difference across the oil-water interface
- R_1 and R_2: are the principal radii of curvature and
- σ_{IFT}: is the interfacial tension

Rheology of emulsions can be considered a direct manifestation of the various interaction forces occurring within the system [59]. Phenomena such as flocculation, creaming and sedimentation, coalescence and Ostwald ripening occurring within emulsion systems are reflected in their rheological behavior [59]. Figure 2.22 depicts the aforementioned. For the case of highly immiscible liquids, molecules of the dispersed phase cannot be exchanged between droplets. Thus coarsening of the droplet size distribution as a result of Ostwald ripening can be considered negligible for most oil-water emulsion systems [58]. Surfactants play a key role in the stabilization of emulsions (coalescence) and their altered morphology (flow fracture) during flow [61].

The driving force for the coalescence of dispersed droplets is the lower Gibbs free energy that results from the reduced total interfacial area [50]. The coalescence, and thus demulsification, of emulsions is first initiated by the molecular contact between surfactant films as a result of the attractive Van der Waals forces, Figure 2.23 [50]. If the repulsive forces between the two surfactant films is not significant enough the surfactant films will fuse, forming a neck. The aforementioned being favored if the surfactant film is not fully saturated. Ultimately the neck grows so that the two drops completely merge, with the surfactant film remaining intact although its area and curvature changes [50].

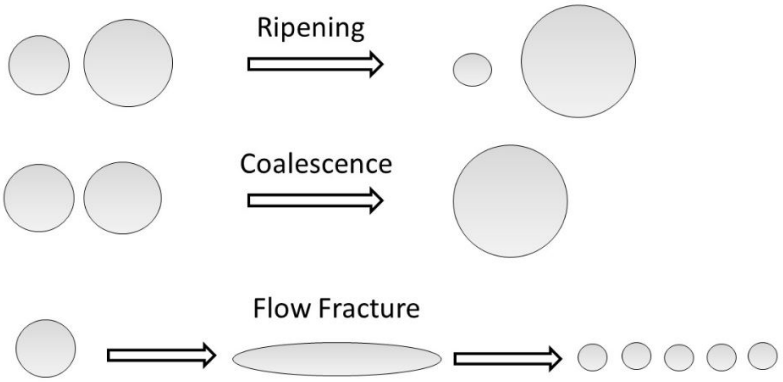

Figure 2.22. Evolution of the topology of an emulsion. Ripening induces the growth of the largest droplets by interdiffusion of the fluids. Coalescence decreases the number of droplets. Both ripening and coalescence decrease the amount of interface. Conversely, flow-induced fracture allows emulsions to be prepared by increasing the amount of interface [62].

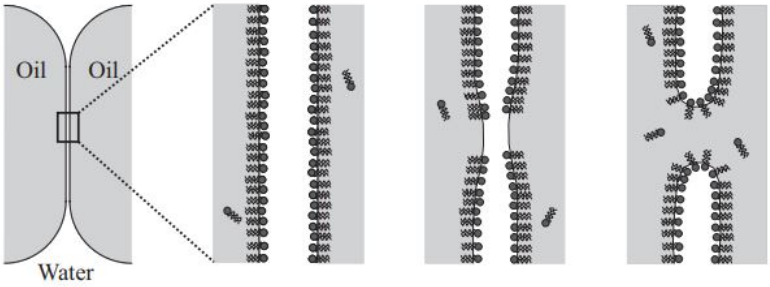

Figure 2.23. Three steps of droplet coalescence after flocculation or creaming for an O/W emulsion [50].

Stabilization of (macro)emulsions is achieved through the mitigation of molecular contact between the dispersed phase. Although surfactants are ubiquitously used in the stabilization of emulsions by adhering at the liquid-liquid interface, they are not the only form of emulsifiers that can be used. Macromolecules such as proteins, polysaccharides or synthetic polymers find great industrial applications in the stabilization of emulsions. In the drilling industry, active solids such as bentonite, starch, Xanthan gum and carboxymethyl celldoes do not limit their-self to the alteration of the flow behavior (shear thinning or thickening) of drilling and/or mitigation of fluid loss through thin filter cake formation.

These particles stabilize emulsion through steric and electrostatic repulsion [1][63][64]. Identical trends have been observed for inactive solids such as barite, whose primary purpose is a density-additive, that also stabilize emulsions through steric hindrance and modification of the rheology of the oil-water interface [31]. The reason for the stabilizing effect stems from the size of the particles that allow them to adsorb practically irreversibly at the interface [50]. Particles assume stable position at the oil-water interface for contact angles different from zero, Figure 2.24, but ultimately do desorb upon coalescence.

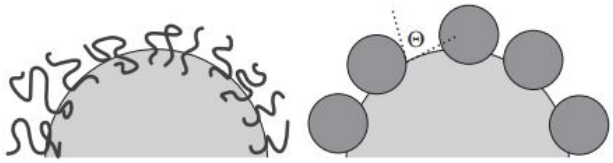

Figure 2.24. Droplet stabilized by polymer (left) and by adsorbed solid particle (right). The contact angles (θ) of the solid particles with the continuous phase should be smaller than 90 ° [50].

Surfactants however remain the main agent used in the preparation of emulsions [50]. Stabilization of emulsions as a result of the presence of surfactants can be summarized into the following key points. In the case of W/O emulsions, the steric repulsion between the hydrophobic tails of surfactants prevents aggregation of surfactant molecules. In the case of O/W emulsions, the hydrophilic head groups prevent droplets from coalescing by hydration repulsion [50]. When ions are present within the emulsion system, additional forces come into play.

The high dielectric permittivity of water, allows ions to readily dissolve within it [50]. This leads to the formation of charged surfaces and thus the presence of an electric double layer, Figure 2.25. With anions showing a greater solubility in oil media than cations, dispersed oil droplets tend to be negatively charged leading to electrostatic repulsion. However, the increase in associated concentration of cations tends to reduce the Debye length weakening the electrostatic force. Hence, emulsion stability for system containing ions

tends to be exhibit a maximum based on the concentration of ions [50].

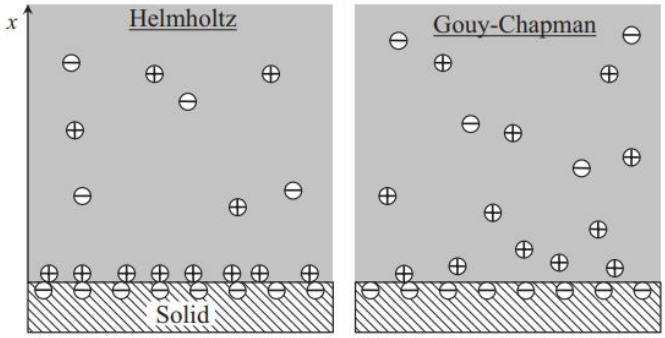

Figure 2.25. Helmholtz and Gouy-Chapman model of the electric double layer [50].

Different additives are used in the preparation of emulsified drilling fluids (surfactants, viscosifiers, O:W ratio etc.) with each affecting the fluid's rheology in different ways. The O:W ratio or the ratio of dispersed to continuous medium volume fraction is one of the most important parameters to affect emulsion rheology [59]. For dilute emulsion systems having $\oslash_{disp} < 0.01$ the relative viscosity (μ_r) of the system can be related to $\oslash_{disp}$ using Einstein's equation, Equation 2.13 [65]. For greater $\oslash_{disp}$, μ_r becomes a more complex function of $\oslash_{disp}$ and is described by Equation 2.14. Where k_1 represents Einstein's coefficient and $k \neq k_1$ are the droplet hydrodynamic interaction coefficients. The number of interaction terms increases with increasing volume fraction of the dispersed phase [59].

$$\mu_r = 1 + 2.5\oslash_{disp} \tag{2.13}$$

$$\mu_r = 1 + k_1 \oslash_{disp} + k_2 \oslash_{disp}^{2} + k_3 \oslash_{disp}^{3} ... \tag{2.14}$$

The next variable affecting the rheology of emulsions, is the viscosity of the dispersed phase with respect to that of the continuous medium. This was considered by Taylor who extended Einstein's hydrodynamic treatment for suspensions to emulsions, Equation 2.15 [66]. Equation 2.15 assumes that tangential and normal stresses from the continuous medium are not mitigated by the emulsifier film around the droplet, which for very low surfactant concentrations is a fair approximation.

As shown by Equation 2.15, for instances where the viscosity of the dispersed phase (μ_i) is far greater than that of the continuous phase (μ_o), $\mu_i \gg \mu_o$, as is the case for O/W emulsions. The term between the brackets reduces to unity giving a coefficient of 2.5, as opposed to a coefficient of 1 for cases where $\mu_i \ll \mu_o$ as is the case for W/O emulsions or foams [59].

$$\mu_r = 1 + 2.5(\frac{\mu_i + 0.4\mu_o}{\mu_i + \mu_o})\oslash_{disp} \tag{2.15}$$

$$h_m = d_m((\frac{\oslash_{max}}{\oslash_{disp}})^{1/3} - 1) \tag{2.16}$$

To continue, the third factor that affects emulsion rheology is the droplet size distribution of the dispersed phase. This tends to be the case, particularly at elevated $\oslash_{disp}$ (> 0.60). Under such conditions, μ_r is inversely proportional to the reciprocal of the the droplet diameter [67]. The structure of emulsions are completely destroyed (deflocculated) at high shear rates as shown in Figure 2.26 and tend to be equidistant under such conditions [59]. At low shear rates, where $\tau < \Delta P_{La}$ the rearrangement of droplets occurs but the coalescence, stretching or rupturing of droplets only begins as $\tau \approx \Delta P_{La}$ [58].

Dimensionless numbers such as the Capillary (Ca) (Equation 2.17) and Peclet (Pe) numbers (Equation 2.18) allow the determination of dominant forces prevailing in emulsions under given conditions. At a critical distance of separation between droplets, the viscosity of emulsions tends to increase rapidly. The average distance of separation between droplets (h_m) is related to droplet diameter (d_m) and dispersed phase volume fraction ($\oslash_{disp}$) by the expression shown in Equation 2.16. Where $\oslash_{max}$ is the maximum packing fraction for hexagonally packed monodispersed spheres [59].

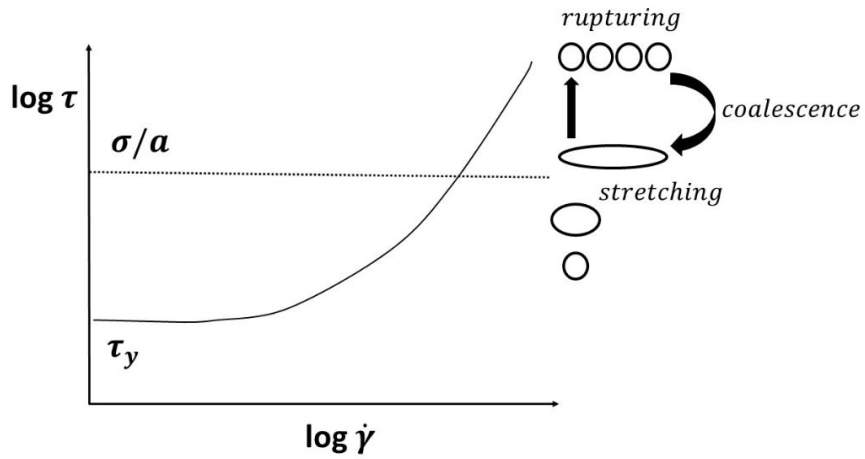

Figure 2.26. Schematic log-log diagram of the steady shear stress, τ, as a function of shear rate, $\dot{\gamma}$, (solid) line for a concentrated emulsion. As $\dot{\gamma}$ increases, τ rises above the elastic yield stress, τ_y, as viscous contributions become important. As τ approaches the Laplace pressure scale, σ_{IFT}/a (dashed line) the droplets deform, stretch, and rupture as shown at right. Depending upon the interfacial properties, the droplets may also recombine through coalescence [58].

$$Ca = \frac{\mu\dot{\gamma}}{\sigma_{IFT}/a} \tag{2.17}$$

$$Pe = \frac{\mu\dot{\gamma}a^3}{k_B T} \tag{2.18}$$

where:

- $\dot{\gamma}$: flow shear rate
- σ_{IFT}: interfacial tension between the two fluids
- μ: fluid viscosity
- k_B: Boltzmann's constant
- T: temperature
- a: particle radius

In addition to the properties affecting emulsion rheology that pertain to the dispersed phase, several other factors affect the rheology of emulsions that are related to the properties of the continuous phase and interfacial film [59]. Three main properties of the continuous

phase may be considered. First is the viscosity of the medium, which is affected by the presence of additives such as excess emulsifiers and thickeners. The aforementioned being added for various reasons amongst which the prevention of sedimentation and creaming [59]. The next property of the continuous medium is its chemical composition (pH, polarity etc.) which affects the charges on the droplets and thus the presence of electrostatic repulsive forces. These electrostatic repulsive forces are affected by the concentration of electrolyte, which represents the third important property of the continuous medium [59].

Electroviscous effect(s) is the term commonly used to describe the effect of charges and repulsion on the interaction between droplets in an emulsion. The distortion of the electric double layer of droplets during shear represents the first form of this effect. This effect leads to a small increase in relative viscosity in comparison to the second form which arises from the overlapping of the double layers of the droplets in concentrated emulsions. With the magnitude of the aforementioned being $\propto \oslash_{disp}^{2}$ [59].

Rheology of emulsions can equally be influenced by the interfacial rheology of the emulsifier surrounding the droplet. When the interfacial film is subjected to an applied shear, its constituent molecules as well as those of water and oil are displaced from their equilibrium position [60]. The stress which develops will have an effect on the interfacial viscosity of the film, which will in turn affect the bulk rheology of the emulsion [59]. This tends to be predominantly the case for large deformable droplets, that have low amount of surfactant molecules at their interface [59].

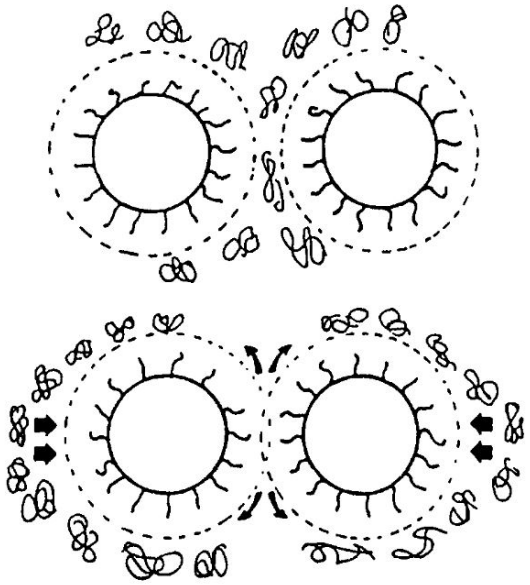

Figure 2.27. Schematic representation of depletion flocculation [59].

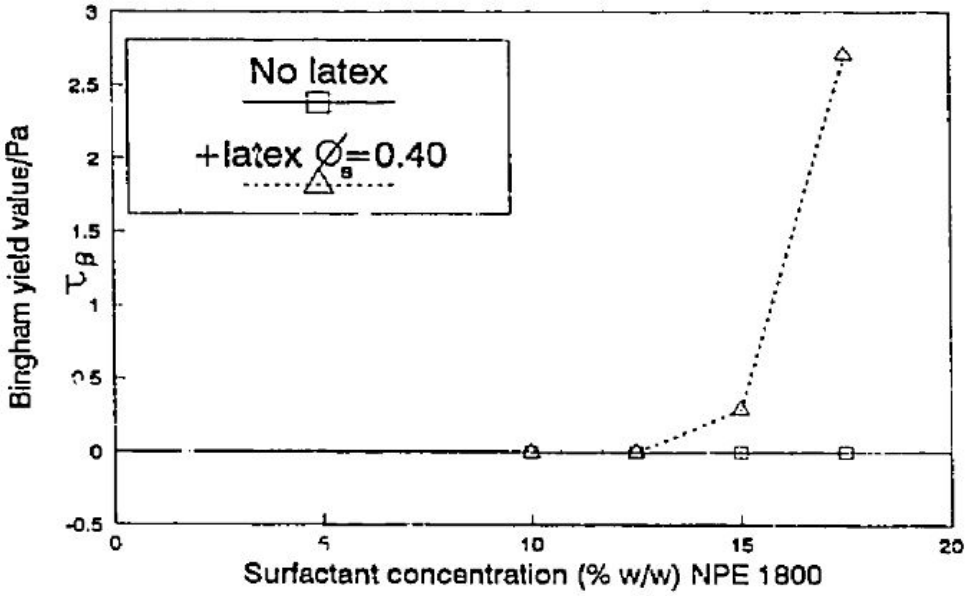

Figure 2.28. Effect of surfactant concentration (wt.%) for NPE 1800 surfactant [68].

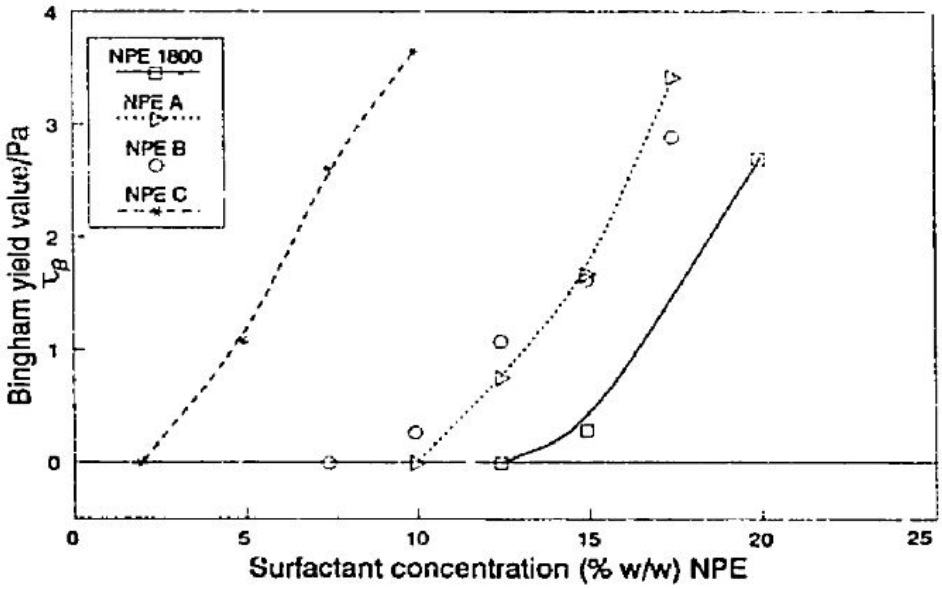

Figure 2.29. Variation of yield stress with surfactant concentration (wt.%) for different surfactant systems [68].

At elevated surfactant concentrations, emulsion systems are prone to a phenomenon known as depletion flocculation. This phenomenon leads to a change in the viscoelastic properties of emulsions, basically changing their mechanical properties from viscous to elastic-like [59]. Depletion flocculation causes dispersed droplets within the emulsion system to be brought together as depicted in Figure 2.27, as a result of elevated micelle concentrations [59].

The onset of the phenomenon occurs at surfactant concentrations exceeding a critical value, which varies based on the surfactant's physical properties as shown in Figures 2.28 and 2.29. Figure 2.28 shows that in the absence of dispersed particles the dispersion systems shows no yield stress at all surfactant concentrations. However, in the presence of latex particles a yield stress is displayed by the system at a critical concentration. This highlights the effect of elevated micelle concentration on the flocculation of dispersed particles (hard or soft) within non-Newtonian mixtures.

2.4 Temperature

When drilling through shallow wells, temperature changes are not large and it is thus a fair approximation to assume the rheological properties of drilling fluids not to change significantly with respect to the aforementioned [69]. However, the drive in global demand for hydrocarbon brings operators to drill in deeper reservoirs where extreme temperatures and pressures prevail [70]. For such wells, the drilling window tends to be narrow and thus careful evaluation and analysis of temperature and pressure on wellbore hydraulics is required [69].

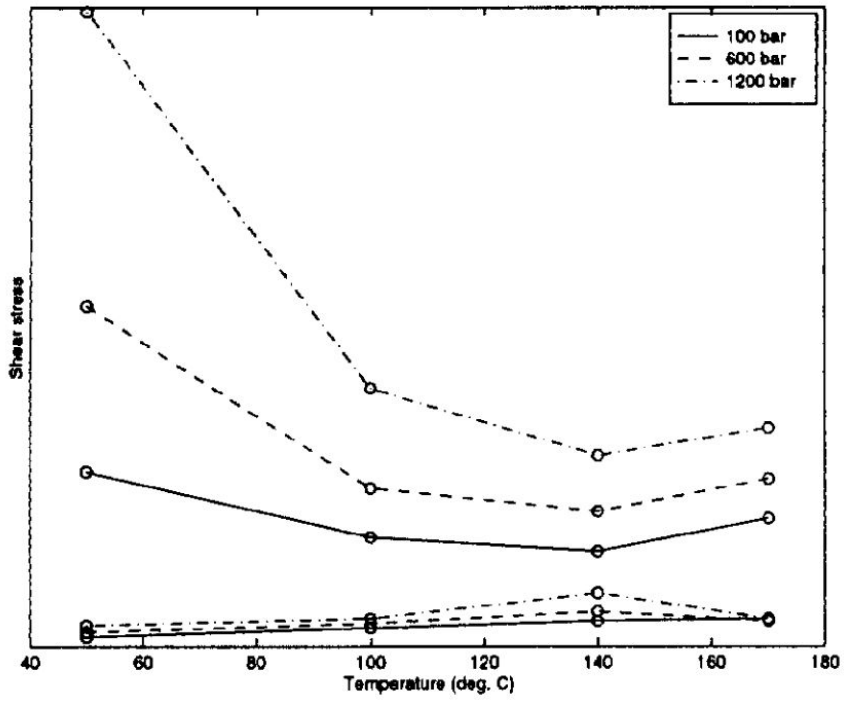

Figure 2.30. Shear stress at 3 (lower four lines) and 600 rpm (upper four lines) as a function of temperature for HPHT OBM [69].

Figures 2.30 and 2.31 show the effect of temperature on drilling fluid rheology. It can be observed that the shear stress of the fluids decrease significantly with increasing temperatures [69]. The temperature and pressure effects for OBMs have generally been found to cancel out when pressure increases from 1 - 1,000 bar and temperature from 50 - 150 °C. For aqueous drilling fluids, the effect of pressure on apparent viscosity is typically

smaller than that of temperature [69].

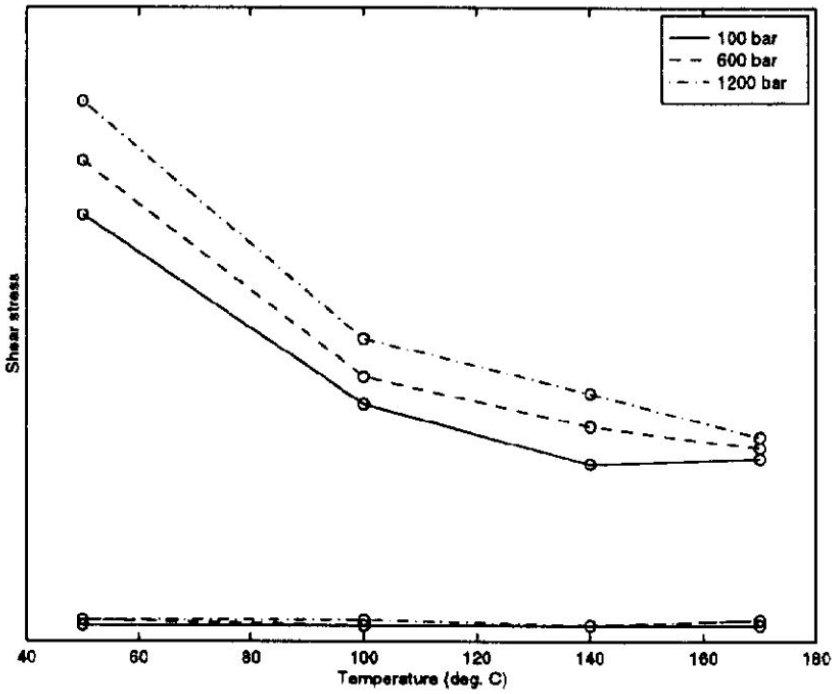

Figure 2.31. Shear stress at 3 (lower four lines) and 600 rpm (upper four lines) as a function of temperature for HPHT WBM [69].

In the case of OBMs, a noticeable deviation in the decreasing trend of shear stress with temperature can be seen at values greater than 150 °C. A plausible reason for this deviation is the thermal degradation of the mud sample[70] resulting in its instability and as a consequence compromising the physical and mechanical properties that enable the fluid to prevent the settling and effective transportation of cuttings to the surface.

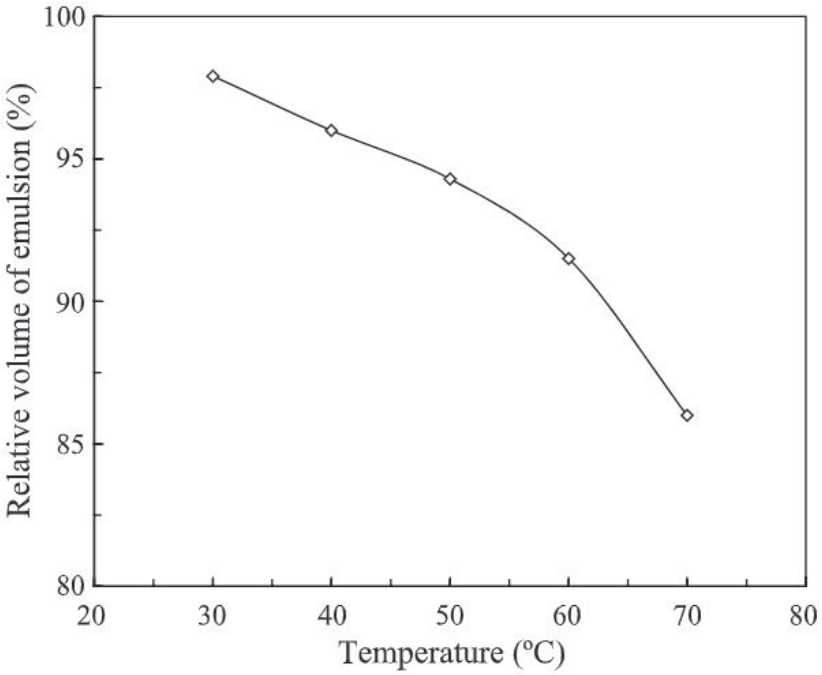

Figure 2.32. Relationship between mixing temperature and emulsification after 24 hrs [71].

Figure 2.32 shows the effect of temperature on the stability of emulsions. The reduced stability comes as a result of the greater number of collisions between dispersed droplets and the desorption of surfactant molecules from the oil-water interface [31][71][72]. For the most part the effect of temperature on the apparent viscosity of drilling fluids can be modeled using Arrheniu's equation, Equation 2.19 [73]. Where μ represents the viscosity of the liquid, μ_0 its viscosity at some reference temperature (T), R the universal gas constant and E the viscosity temperature coefficient. As shown in Figure 2.33, the apparent viscosity of drilling fluids tends to decrease with increasing temperature [73].

$$\mu = \mu_0 e^{E/RT} \tag{2.19}$$

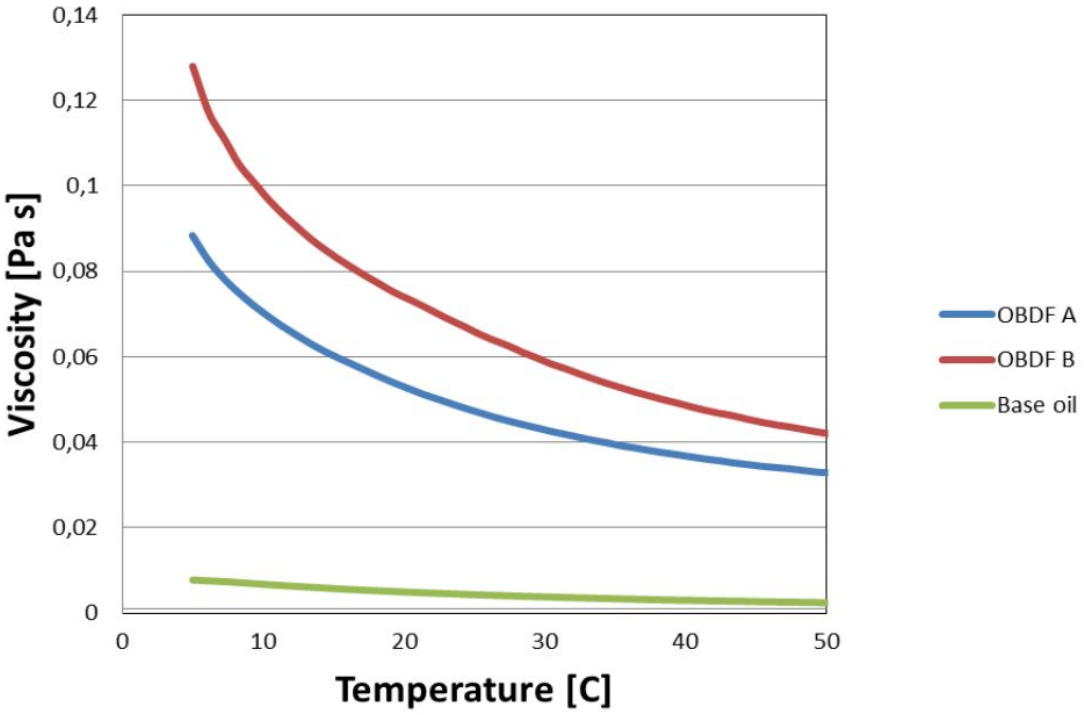

Figure 2.33. Temperature sweeps of OBMs and Base Oils at a temperature ramp of 1 °C/min and shear rate of 100 s^{-1} [73].

2.5 Phase Inversion

Despite the large temperature variations that prevail in offshore operations, temperature-induced phase inversion (TIPI) has seen little to no study in the drilling fluid industry. This phenomenon involves the transition of emulsions, stabilized by nonionic surfactants, from one type to another when a critical temperature known as the phase inversion temperature (PIT) is reached. Above the PIT, emulsions transition from O/W to W/O or vice-versa depending on the direction of temperature change [12][50][78]. This form of phase inversion is referred to as transitional phase inverison (TPI).

It is brought about by the alteration of the affinity of nonionic surfactant(s) molecules for a phase by etiher: changing the temperature the emulsion is subjected to or changing the composition of the surfactant mixture (at constant temperature) [50][77]. Affinity of surfactants towards a given phase is defined by their hydrophilic lipophilic balance (HLB),

thus an alteration of the HLB is required for TPI to occur.

Mixtures instead of individual surfactants are used, because the desired HLBs required for emulsion stability is normally not achieved through the use of single surfactants [77]. In other words, reduction of interfacial tension and enhanced emulsion stability is best obtained through the use of surfactants with different HLBs [87]. Figure 2.34 shows the phase inversion process for an O/W emulsion (2.34a) and a schematic for the preparation of nano-emulsions via phase inversion (2.34b).

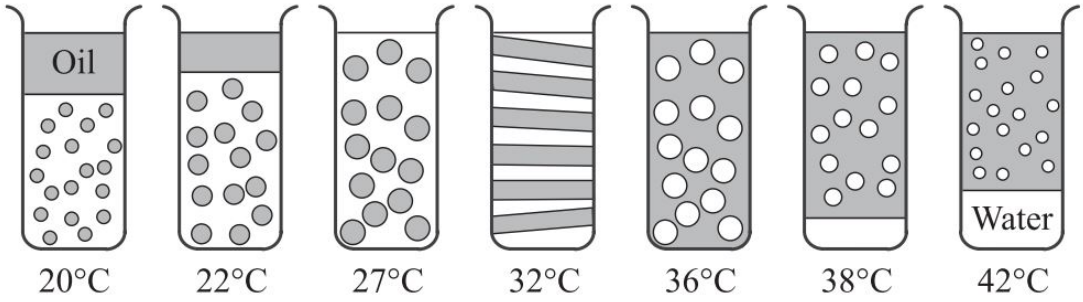

(a) Phase diagram of a water-in-octane-$C_{12}E_5$ emulsion [50].

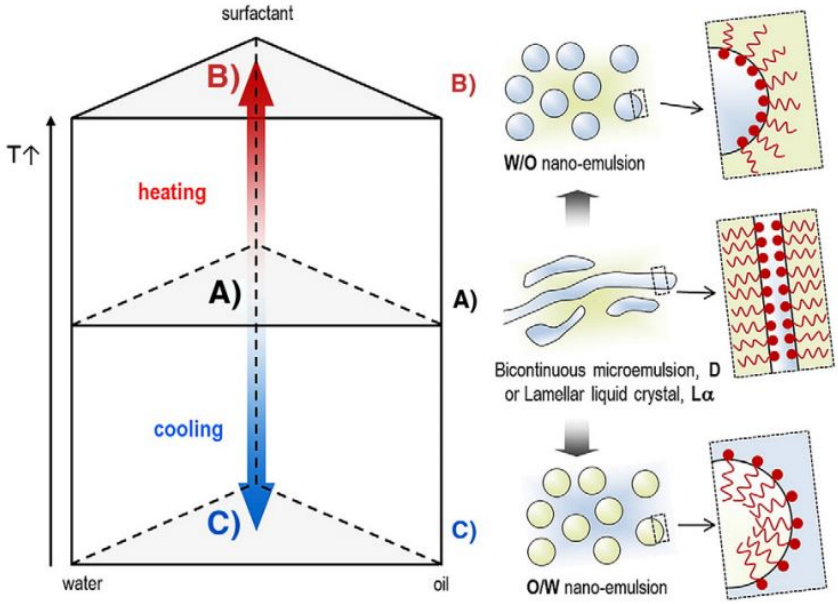

(b) Schematic representation of nano-emulsion formation by PIT method [78].

Figure 2.34. Temperature-Induced Phase Inversion (TIPI).

Phase inversion of emulsions driven by temperature variation, comes as a result of

the change in the optimum curvature (molecular geometry) and solubility of nonionic surfactants with the aforementioned [79][80][81]. The molecular geometry of surfactants is defined by their packing parameter (N_s) (Equation 2.11) [12][50][82]. At low temperatures, the surfactant tends to be more soluble in the aqueous phase and its packing parameter is N_s <1, thus favoring the stabilization of a O/W emulsion [12].

With increasing temperatures, the hydrophilic head group of the nonionic surfactants become dehydrated thereby decreasing their solubility in water and bringing their packing parameter towards unity (N_s =1). The temperature at which the N_s of the surfactants equals unity, is referred to as the phase inversion temperature (PIT) [50][12][78]. At temperatures greater than the PIT, the surfactants show greater solubility in the oil phase and their packing parameter becomes greater than unity ($N_s > 1$) and favors the stabilization of W/O emulsion [12].

The dimension of the dispersed droplets obtained and consequently the stability of the emulsion system, Table 2.3, depends on the rate at which it is cooled (heated). Rapid cooling of emulsion systems to temperatures well below their PIT has been found to lead to the formation of nanoemulsions [12].

Table 2.3: Comparison of the Properties of Different Emulsion Types that can be Prepared from Oil, Water and Surfactant [12].

Emulsion Type	Radius Range	Stability	Appearance
macroemulsion	100 nm - 100 μm	metastable	turbid/opaque
nanoemulsion	10 - 100 nm	metastable	clear/turbid
microemulsion	2 - 50 nm	stable	clear

An 'intermediate 'bicontinuous' phase is usually involved in the transformation of one emulsion type to another via phase inversion. Micro- and nano-emulsion systems, Figure 2.35, have a number of advantages over macro-systems. These include their better stability to particle aggregation and gravitational separation [83][84], the novel rheological properties

(e.g. high viscosity and gel strength) that can result from their design [84][85][86]. The latter being of practical relevance to the drilling industry, where frictional pressure losses and hole cleaning efficiency all depend on the apparent viscosity of drilling fluids.

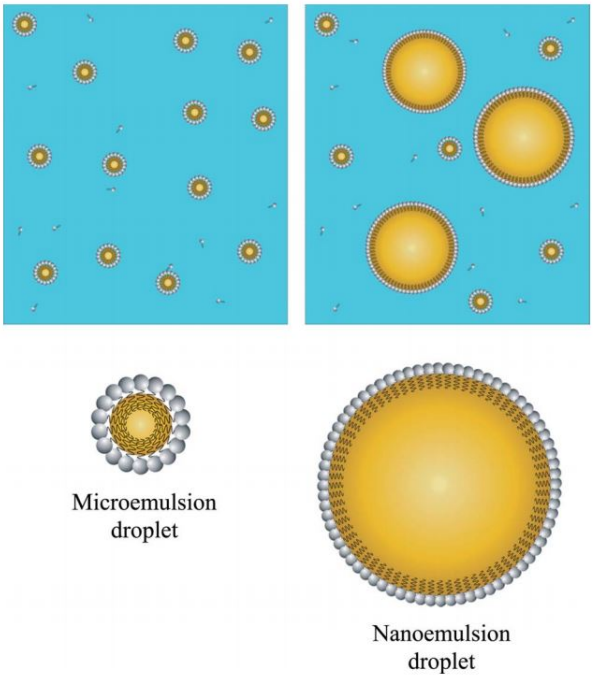

Figure 2.35. Schematic representation of microemulsions and nanoemulsions fabricated from oil, water and surfactant. The structure of the particles in both types of colloidal dispersion is fairly similar - a hydrophobic core of oil and surfactant tails and a hydrophobic shell of surfactant head groups [83].

In most applications of emulsion phase inversion, a surfactant and co-surfactant is used due to the enhanced stability it confers to the system. The presence of a complex surfactant system at the interface, Figure 2.36, yields greater strength and thus resistance to rupture. This makes the emulsion droplets less liable to coalescence, thereby making them more stable [87]. Greater emulsion stability was equally found to be associated to high surfactant packing at the interface, with the aforementioned best achieved with a complex film [87][88]. The method of preparation of phase inversion emulsions, involving complex surfactant films, involves the addition of the surfactant mixture to the dispersed phase [77].

The dispersed medium-surfactant mixture solution is then added to the continuous phase yielding what is commonly referred to as 'abnormal' emulsions [77].

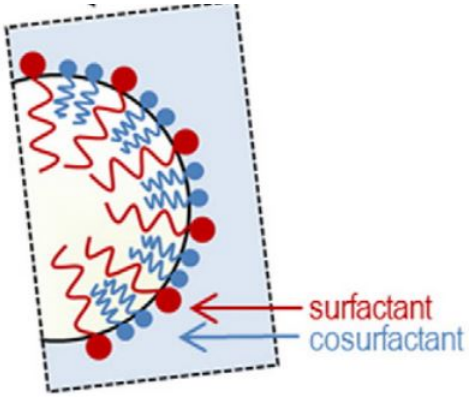

Figure 2.36. Complex surfactant film [78].

Figure 2.37 shows the effect of phase inversion on the apparent viscosity of an O/W emulsion system stabilized by a complex mixture of nonionic surfactants. The occurrence of phase inversion was observed to generate higher apparent viscosities (and thus shear stresses) in the emulsion system as well as rheopectic time-dependent behavior [89]. The formation of smaller dispersed droplets was found to account for the increase in viscosity (Figure 2.39b), while the onset of rheopexy was indicative of the occurrence of phase inversion [89][90].

Factors affecting the PIT at which inversion from one emulsion type to another occurs include (among others) the: O:W ratio and HLB of the emulsion system as shown in Figure 2.38 [89][91]. The polarity nature of the oil phase has been found to equally affect TIPI occurrence. Non-polar oils (e.g. paraffin oil) have been found to show distinct TIPI behavior as opposed to polar ones (e.g. isopropyl myristrate) [89].

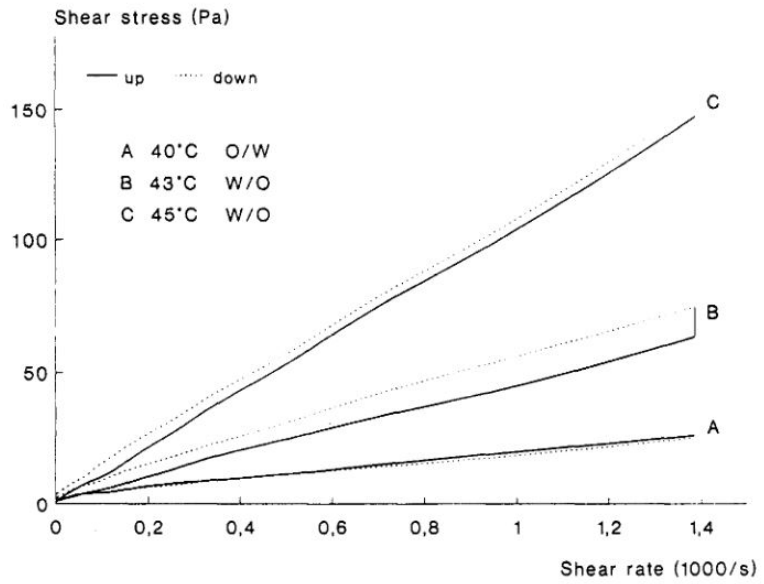

(a) The change in flow behavior with temperature from thixotropic (curves A) to negatively thixotropic (curves B) and (curves C) for an emulsion of liquid paraffin with 50 % (w/w) water and a 6 % (w/w) blend of Brij 92 and Brij 96 at an HLB of 6.5.

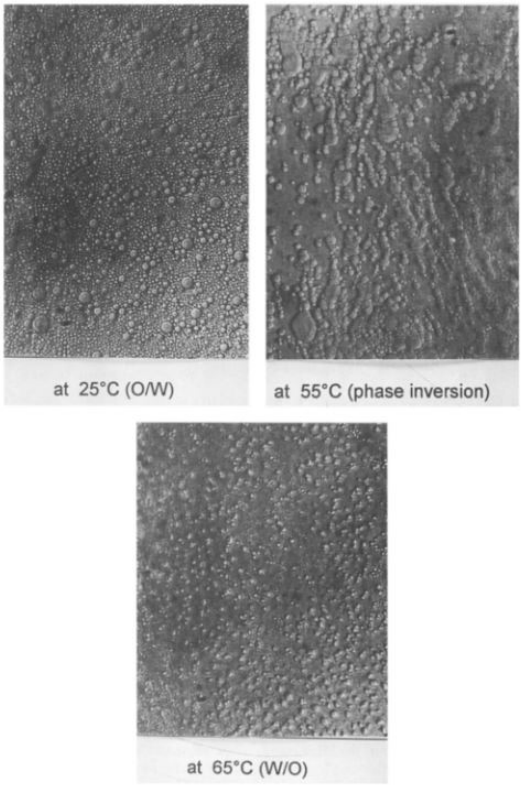

(b) Paraffin emulsion with 50 % (w/w) water and a 6% blend of Brij 92 and Brij 96 at an HLB of 7.5 at different temperatures (magnification, 400x).

Figure 2.37. Temperature-induced phase inversion [89].

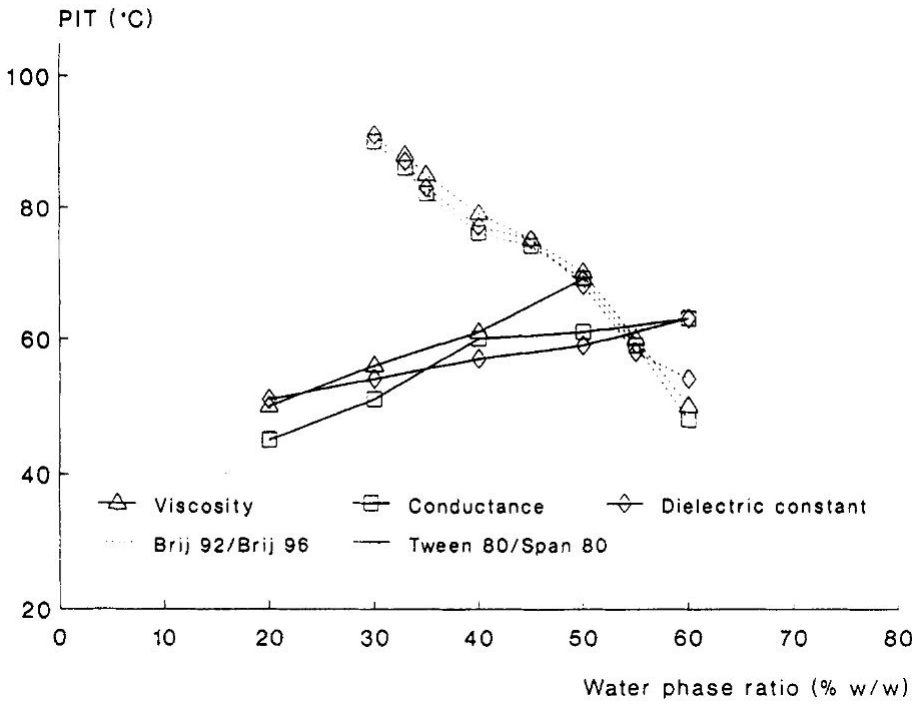

(a) Effect of O:W ratio: PIT versus water phase ratio for liquid paraffin emulsions stabilized by blends of Brij 92 + Brij 96, and Tween 80 + Span 80.

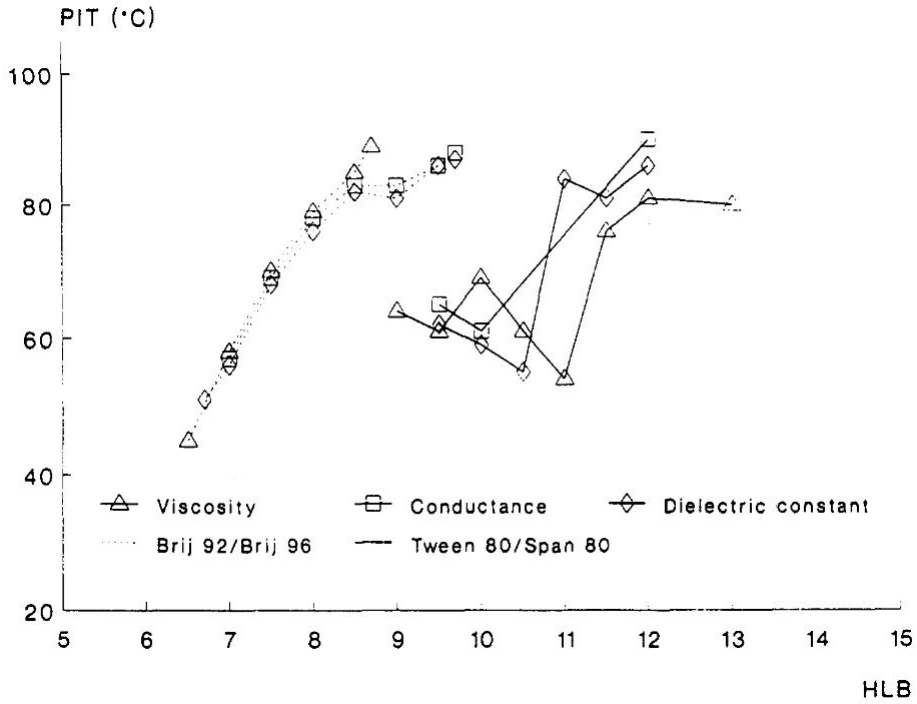

(b) Effect of HLB: influence of HLB on PIT for liquid paraffin emulsions stabilized by blends of Brij 92 + Brij 96, and Tween 80 + Span 80

Figure 2.38. Variables affecting phase inversion [89].

Application of transitional phase inversion of emulsion systems on the optimization of properties of drilling fluids has been investigated through the alteration of the affinity of nonionic surfactants components at 'constant temperature' [92]. Inversion of the drilling fluid was induced through the protonation and deprotonation of the nonionic surfactants. The study highlighted the maintenance and cost benefits for muds that could be inverted from one mud type to another through surfactant protonation and deprotonation for offshore operations. Protonation of the surfactant molecules in the presence of acids led to the stabilization of O/W emulsions, while transition to an W/O emulsion was obtained through the surfactants' de-protonation upon addition of a base [92].

Table 2.4: Typical Formulation (g) of Reversible Invert Drilling Fluid [92].

12.5 lb/gal, 70:30 O/W Ratio; 25 % $CaCl_2$	
oil	125
lime	1 - 2
organoclay	2 - 6
reversible emulsifier	8 - 12
wetting agent	1 - 3
brine	90
weight material	293

The advantages to drilling operations revolved around the respective beneficial properties of OBMs and WBMs during drilling and subsequently completion. As an OBM, the drilling fluid allowed higher ROPs, thinner filter cakes, good lubrication properties and excellent hole stability. On the other hand, the same mud as a WBM allowed excellent filtercake cleanups, better cementing, enhanced production in openhole completions and waste minimization [92]. Table 2.4 shows the formulation of the reversible invert drilling fluid that was investigated in the study, with an emulsifier concentration of 2.3 wt.%. Figure 2.39 on the other hand compares the return permeability between a conventional

drilling fluid and that of the invert emulsion drilling fluid.

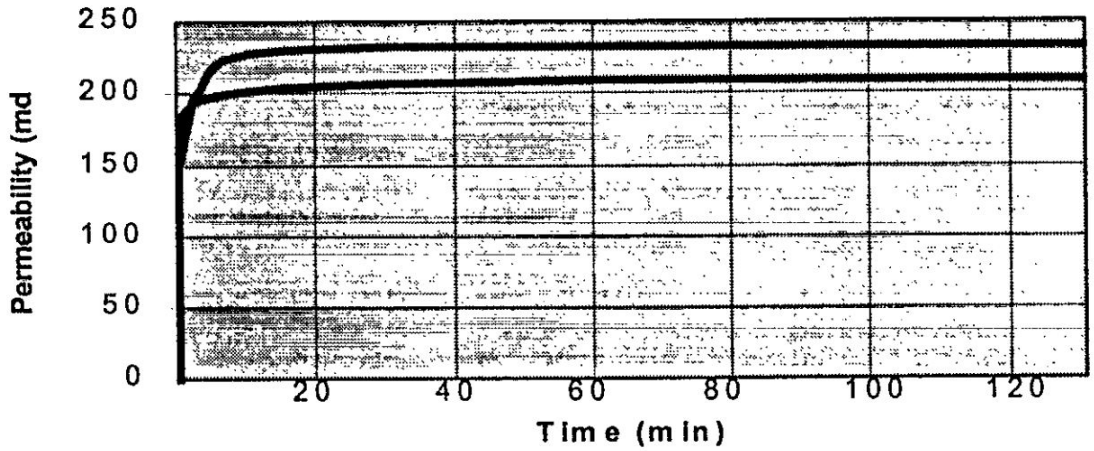

(a) Return permeability with a conventional synthetic-based mud.

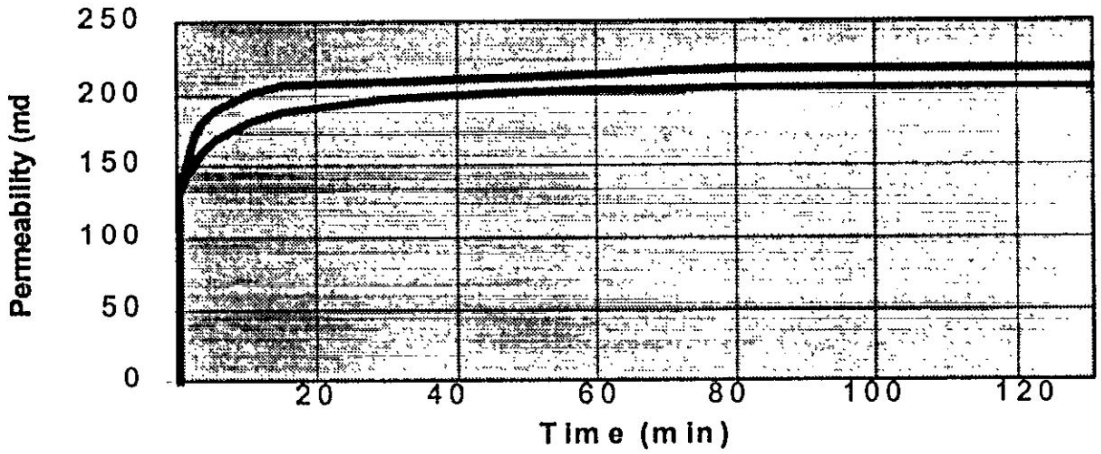

(b) Return permeability using a reversible invert emulsion mud.

Figure 2.39. Return permeability comparison between conventional and invert emulsion drilling fluids [92].

Although not the subject of a lot of studies in the drilling industry, catastrophic phase inversion (CPI), has been reported in other sectors of the oil and gas industry, specifically in the production and transportation sectors [74][75]. CPI involves the conversion of an emulsion from one type to another via the increment of the dispersed phase volume fraction or through continuous agitation of the emulsion mixture [76][77]. Figure 2.40 shows a schematic of the CPI process.

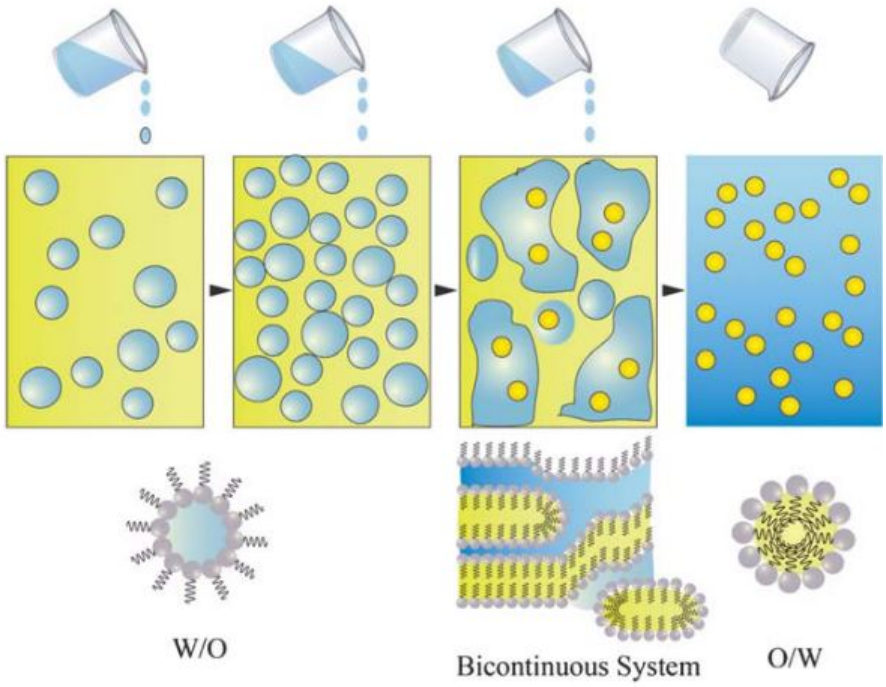

Figure 2.40. Schematic representation of the proposed mechanism for low-intensity emulsification by catastrophic phase inversion (CPI) method. The amount of water added to a W/O emulsion is progressively increased, until a phase inversion occurs and an O/W emulsion is formed [12].

2.6 Wall Slip & Jamming

The operating principle of all simple-shear rheometers involves the presence of solid boundaries against which the sample fluid is intended to adhere, while the neighboring fluid is set in motion by drag or pressure gradients [93]. The 'no-slip' condition remains valid in simple small-molecule liquids such as water [102]. The term 'wall slip' originates from the slip of one or both surfaces of solids when confined between two plates, with one of the plates set in motion [93][94].

It is therefore to be expected that complex fluids, such as drilling fluids, display wall slip at shear rates at which solid-like behavior prevails [93]. The term complex fluids refers to viscoelastic (non-Newtonian) systems, meaning they display flow behavior intermittent between solid-like and liquid-like based on the applied rate of deformation (shear rate), Figure 2.41. What may possibly be the most important thing from an engineering stand-

point is not to overcome the slippage but to characterize these effects in order to predict the flow in some applications [95].

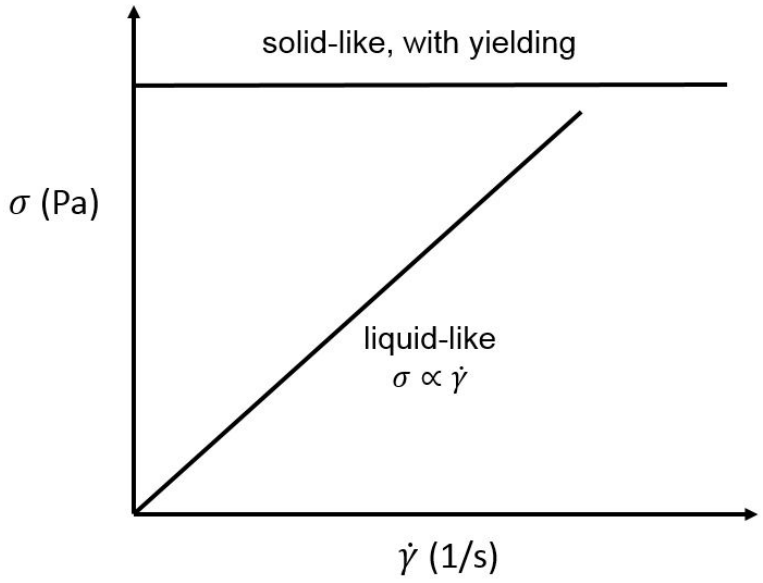

Figure 2.41. Illustration of shear-rate-dependent shear stress for prototypical 'liquid-like' and 'solid-like' materials [93].

Wall slip phenomenon is well established for viscoelastic (non-Newtonian) fluids like emulsions, suspensions, polymeric liquids, gels, and foams[13] which thus calls for special attention when understanding the flow behavior of these disperse systems under shear [95]-[99]. Wall slip can be sub-divided into three forms, namely; (i) true (wall) slip: in which a discontinuity exists at the boundary, (ii) cohesive slip: where the slip plane is found at a certain distance from the wall and (iii) wall depletion or lubrication: where the no-slip boundary condition is still valid but shear rate is enhanced at the wall [95][100]. See Figure 2.42.

For emulsion systems (soft particles), studies have found wall slip effects to be strongly dependent on the type (W/O or O/W) and composition of the emulsion [95][99]. For suspensions (hard particles), packing fraction particularly at values beyond 0.74 significantly affect their slip behavior, see Figure 2.43. Other contributing factors include the

shape, size and size distribution as well as volume fraction of particles, particle-particle and particle-matrix interactions as well as the continuous liquid matrix rheology [101].

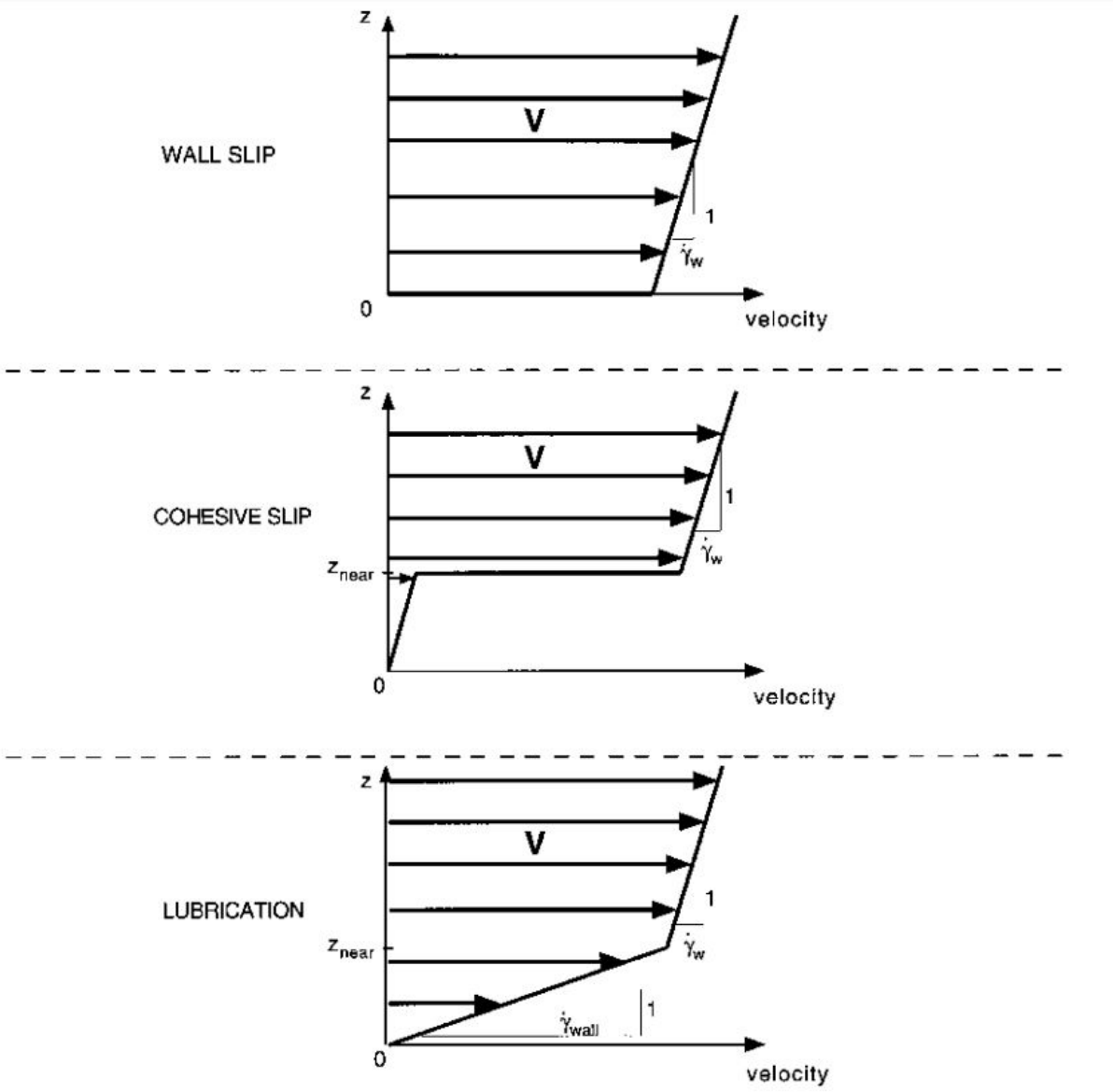

Figure 2.42. Near wall velocity profiles for wall, cohesive and lubrication slip [100].

For viscoelastic systems like emulsions and suspensions, that respectively have dispersed droplet and solids within a continuous liquid medium, lubrication slip occurs when the local concentration of particles is lower at the wall leading to the formation of a liquid slip layer. The aforementioned provides a lubrication effect and facilitates the flow of the bulk (core) fluid across the solid boundary [94]. Lubrication slip, Figure 2.44, is driven by chemical,

hydrodynamic, steric and viscoelastic forces [94].

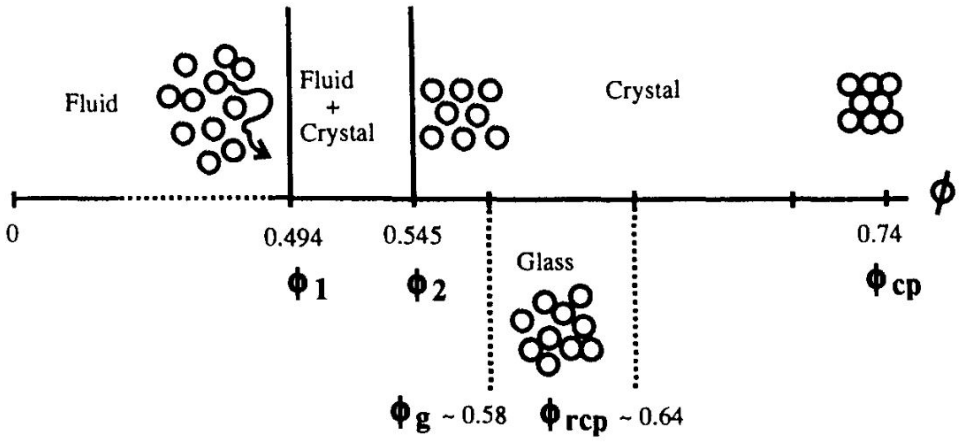

Figure 2.43. The hard sphere phase diagram. Below the volume fraction $\oslash < \oslash_1 = 0.494$, the suspension is a disordered fluid. Between $0.494 < \oslash < 0.545$, there is coexistence of the disordered phase with a colloidal crystalline phase with FCC (or HCP) order; the colloidal crystalline phase is the equilibrium one up to the maximum close-packing limit of $\oslash = 0.74$ [93].

Dispersed particles having (i) large dimensions (and/or flocs of smaller particles), (ii) elevated concentrations of dispersed phase ($\oslash_{disp}$) coupled with (iii) smooth walls are conditions that favor the occurrence of slip in general and lubrication slip in particular [94]. Its mitigation is driven by restoring osmotic forces, that increase particle concentration at the wall. Lubrication slip has equally been found to be suppressed when the slip layer thickness is comparable to the height of surface irregularities [101]. In other words, roughened surfaces prevent slip [94][101].

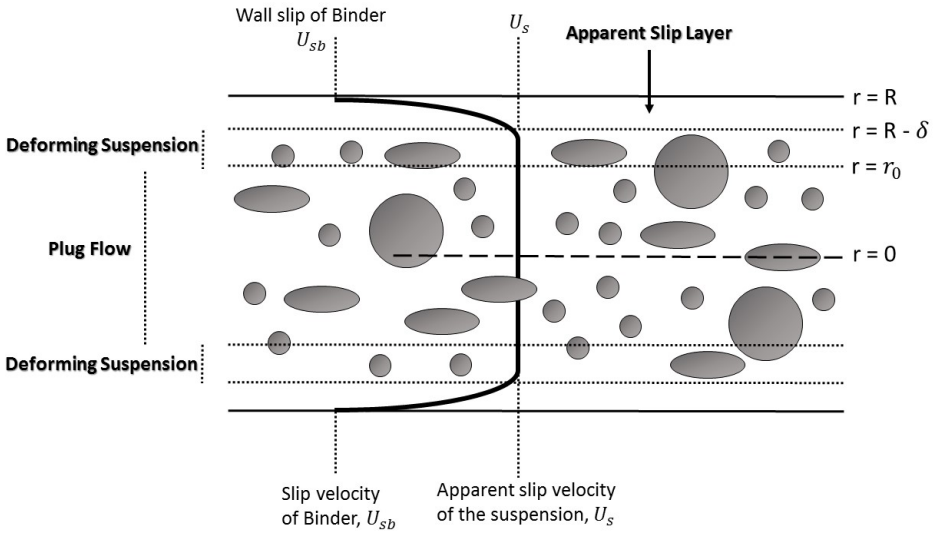

Figure 2.44. Schematics of the apparent slip mechanism of suspensions with the binder liquid exhibiting slip at the wall with slip velocity U_{sb} [105].

Determination of slip velocity and the true shear rate associated with lubrication slip in parallel disk experiments was outlined by Yoshimura and Prud'homme[106]. Their method was based on performing two measurements at two different gaps. Yilmazer and Kaylon[107] generalized this method by performing measurements at more than two gaps (H). They showed that when plotting apparent shear rate ($\dot{\gamma}_a$,)versus $1/H$ in Equation 2.20, straight lines would be obtained. Through extrapolation the intercept would thus be equal to the true shear rate, $\dot{\gamma}_t$. Where τ and U_s represent the measured shear stress and slip velocity respectively. The slip layer thickness, δ, is then determined by Equation 2.21 where μ_s represents the viscosity of the suspending liquid medium and T temperature. Equation 2.22 can be used to determine the true viscosity, μ, of the complex fluid [101].

$$\dot{\gamma}_a = \dot{\gamma}_t(\tau) + 2\frac{U_s(\tau)}{H} \tag{2.20}$$

$$U_s(\tau, T) = \frac{\delta}{\mu_s(T)}\tau \tag{2.21}$$

$$\mu = \frac{\tau}{\dot{\gamma}_t} \tag{2.22}$$

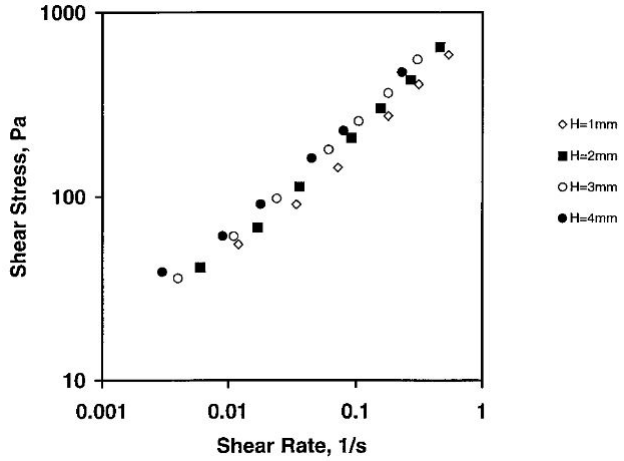

(a) Shear stress versus apparent shear rate at 21 °C at various gap heights.

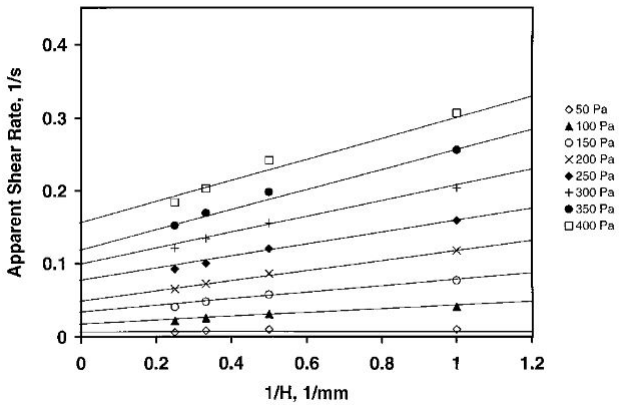

(b) Apparent shear rate versus $1/H$.

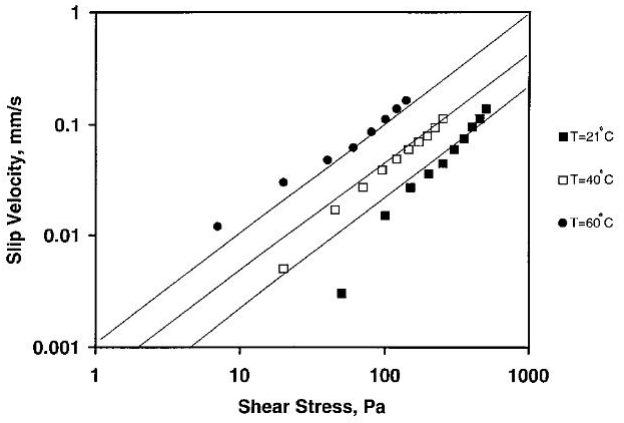

(c) Slip velocity versus shear rate at different temperatures.

Figure 2.45. 63 % glass beads (45.94 μm) suspension [101].

Figure 2.45 illustrates the application of Equations 2.20 and 2.21 to determine the slip layer thickness (δ) in a study investigating the effect of temperature on lubrication slip in suspensions of aluminium powder and glass beads [101]. The study found slip velocity to increase with temperature for a given shear stress value. The viscosity of the slip layer thickness was found to significantly affect the slip behavior of the suspension. Specifically, increasing temperatures were found to cause higher slip velocities as a result of decreasing slip layer viscosity with temperature, see Equation 2.21 [101]. The study equally found slip layer thickness to be independent of temperature, but to increase in value with increase in size of the dispersed particles [101].

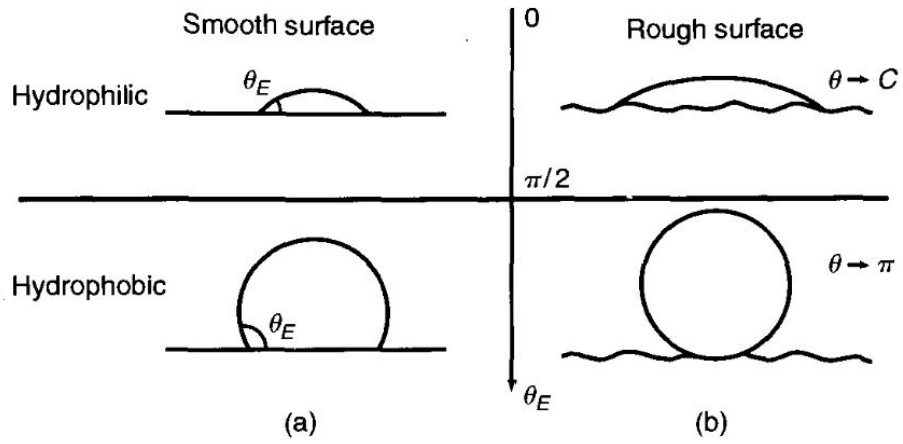

Figure 2.46. Controlling the wettability of a substrate through its roughness. (a) Smooth surface; (b) Rough surface. Hydrophilic substrate becoming even more hydrophilic with a rough surface (top); hydrophobic substrate becoming "super-hydrophobic" (bottom) [108].

Another factor affecting lubrication slip, is the wettability of continuous medium of the viscoelastic mixture. Mixtures whose continuous media show small contact angles on the solid surfaces are more likely to display lubrication slip. Figure 2.46 shows the effect of surface roughness of solid surfaces on the wettability of hydrophilic and hydrophobic substrates. It is has equally been found that plug flow behavior tends to be exhibited in viscoelastic mixtures experiencing lubrication slip [94].

In drilling fluids, the elevated concentration of dispersed particles either as part of their design (weight-additives and viscosifiers) and/or as a result of circulation (drill cuttings) create conditions favorable for the occurrence of slip (true, cohesive, and/or lubrication). The dimensions of these dispersed solid particles, Figure 2.47, when coupled with narrow and smooth conduits create conditions favorable for slip occurrence in drilling fluids.

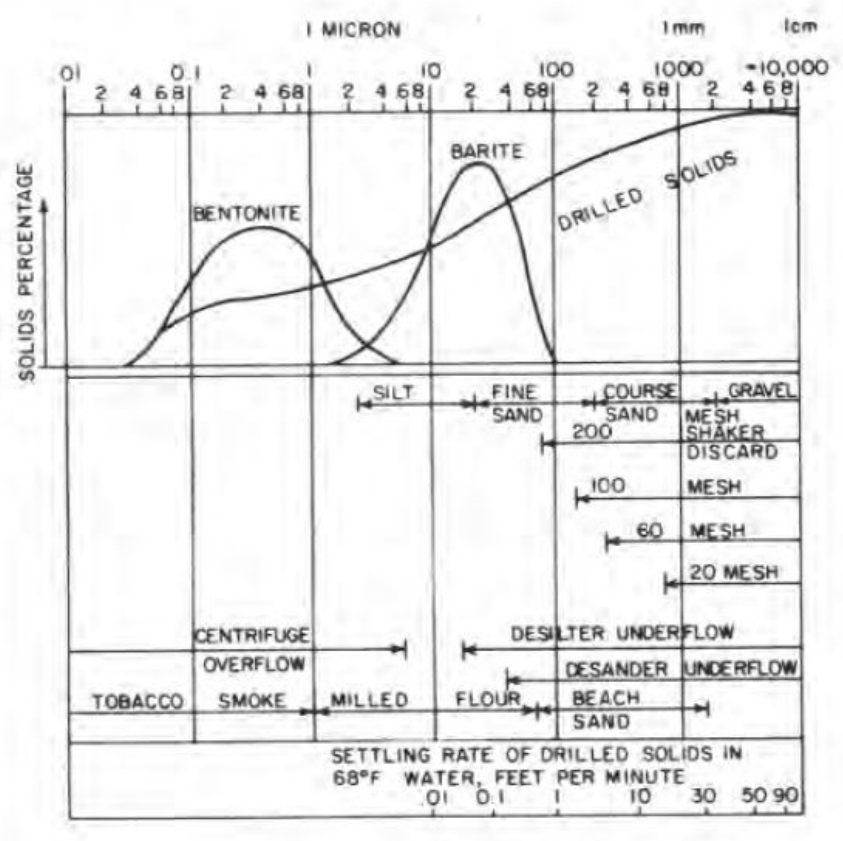

Figure 2.47. Particle size range for common solids found in weighted WBMs [16].

It is important to recall that large particles here refers to both individual and flocs of smaller particles [94]. Table 2.5 shows the absolute roughness of the different pipes commonly used in drilling operations. For instances where the dimensions of dispersed particles and thickness of the slip layer are significantly greater than the absolute roughness (ϵ), slip can be expected. The implications of the aforementioned are significantly both in terms of pump pressure requirements (cost, energy efficiency) but equally in terms of lower

than expected ECDs making the well more prone to kicks or blowouts (safety).

Table 2.5: Absolute Pipe Roughness for Several Types of Circular Pipes [16][104].

Pipe Type	Absolute Roughness, ϵ, $x10^{-3}$in	μm
riveted steel	0.250 - 2.50	6.35 - 63.50
concrete	0.083 - 0.830	2.11 - 21.10
cast iron	0.071	1.80
galvanized iron	0.042	1.07
asphalted cast Iron	0.033	0.84
commercial steel	0.013	0.33
drawn tubing	0.0004	0.01

A lot of emphasis has been laid so far on the lubrication form of slip. For true and cohesive slip dilatancy and hydroclustering, Figure 2.48, of the dispersed particles in non-Newtonian fluids play a significant role in the occurrence true and/or cohesive slip. Dilatancy is the generation of additional stresses from solid-solid friction as a result of the increase in the volume of particulate packing causing it to push against solid boundaries [110][111].

Hydroclustering on the other hand, is the mechanism by which dispersed particles push together into clusters under shear, thereby causing re-arrangements which lead to increase in the drag forces between particles [112][113]. In both semi-dilute and concentrated dispersions, formation of hydroclusters cause transient concentration fluctuations due to strong hydrodynamic coupling, Figure 2.49. The aforementioned are driven and sustained by the applied shear field due to strong hydrodynamic coupling between particles [113]. Severe anisotropy in the fluid's microstructure results and more importantly, leads to large stress fluctuation [113][115].

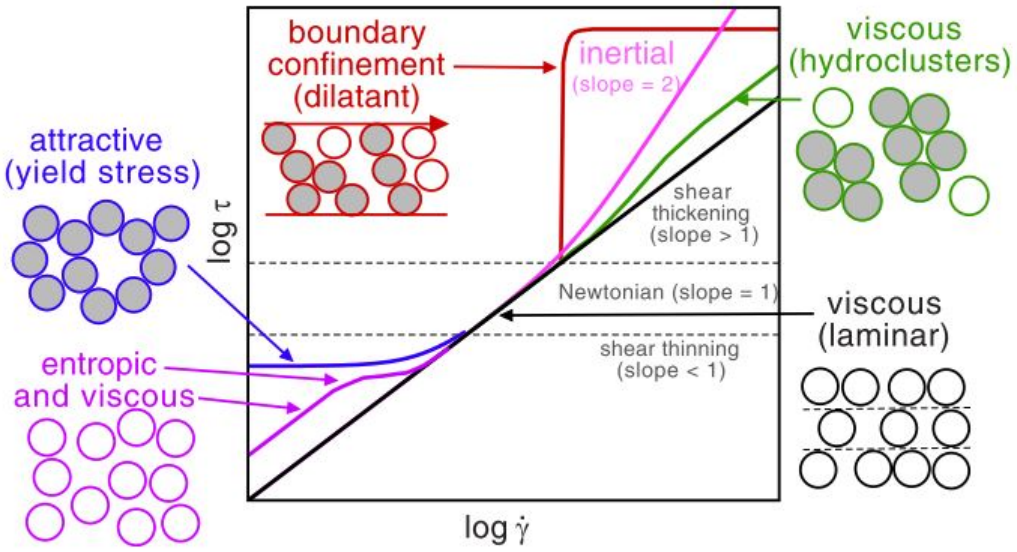

Figure 2.48. Sketch of different possible regimes of shear stress τ versus shear rate $\dot{\gamma}$ for suspensions, plotted on a log-log scale. Various contributions to stresses and their associated particle arrangements are indicated for different regimes of flow response to applied shear: shear thinning, Newtonian and shear thickening. A particular complex fluid may exhibit several of these regimes, depending on the material properties and dominant forces [114].

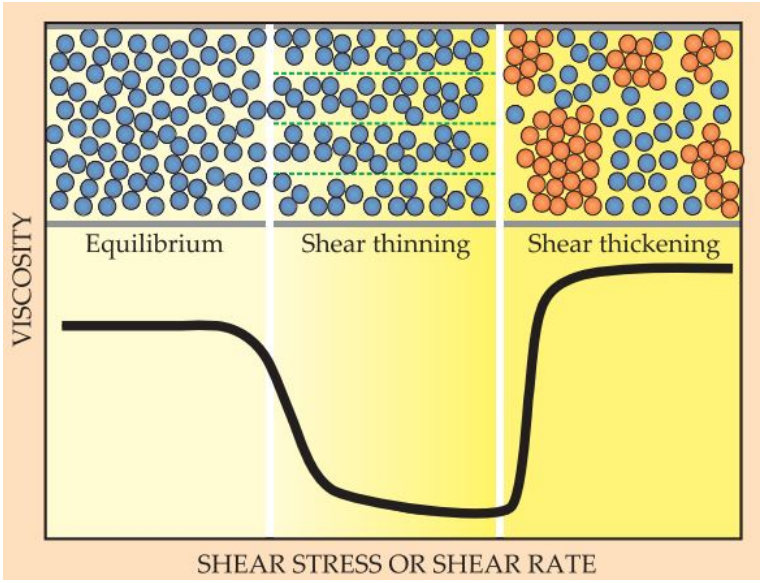

Figure 2.49. The change in the microstructure of colloidal dispersion explains the transitions to shear thinning and shear thickening. In equilibrium, random collisions among particles make them naturally resistant to flow. But as shear rate (shear stress) increases, particles becomes organized in flow, which lowers their viscosity. At yet higher shear rates hydrodynamic interactions between particles dominant over stochastic ones, a change that spawns hydroclusters (red) - transient fluctuations in particle concentration [113].

Anisotropy in the microstructure of semi-dilute and concentrated dispersion as a result of hydroclustering (and dilation) can result in variations in the shear rates experienced by the non-Newtonian mixture. This is typically the case for yield stress fluids where there appears to be no velocity gradient in the inner core. Pasty materials are examples of the aforementioned.

Figure 2.50 shows a kaolin suspensions with an unsheared (plug) region away from the wall and and a sheared region along it. The effect of the occurrence of shear rate gradients within complex fluids can be seen in Figure 2.51. At shear rates above the critical shear rate, $\dot{\gamma}_c$, the velocity profile of the mixture has an a slope that is almost constant over a significant distance. At rates below $\dot{\gamma}_c$, the velocity profile drops to almost zero and remains around this value over large distances [103].

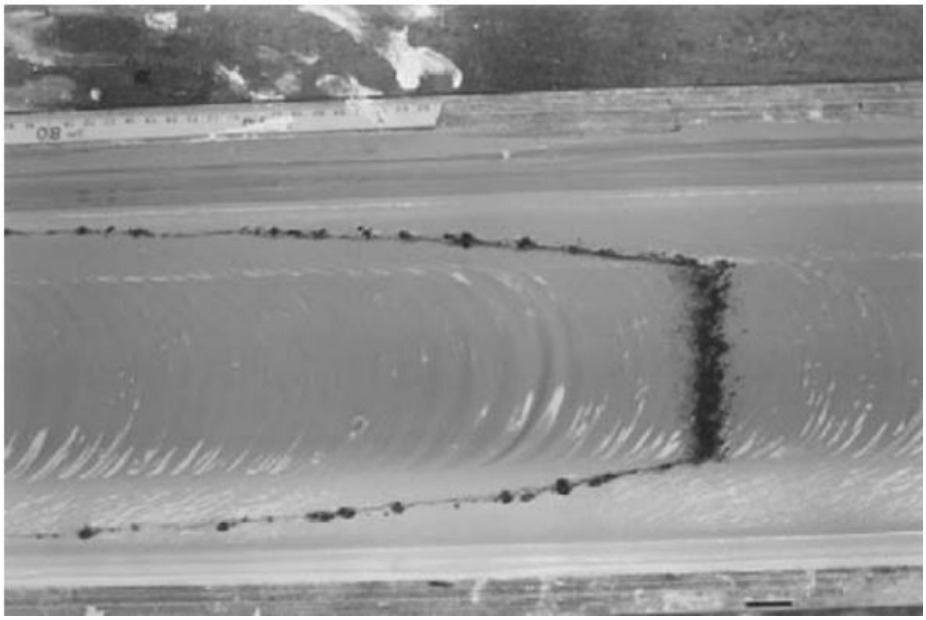

Figure 2.50. View from above the free surface of a kaolin suspension flowing (here from left to right) in a steady state in an inclined, rectangular open channel. A pepper line was dropped upstream perpendicularly to the flow direction. It now appears deformed due to shear along the walls and undeformed in the central plug region [109].

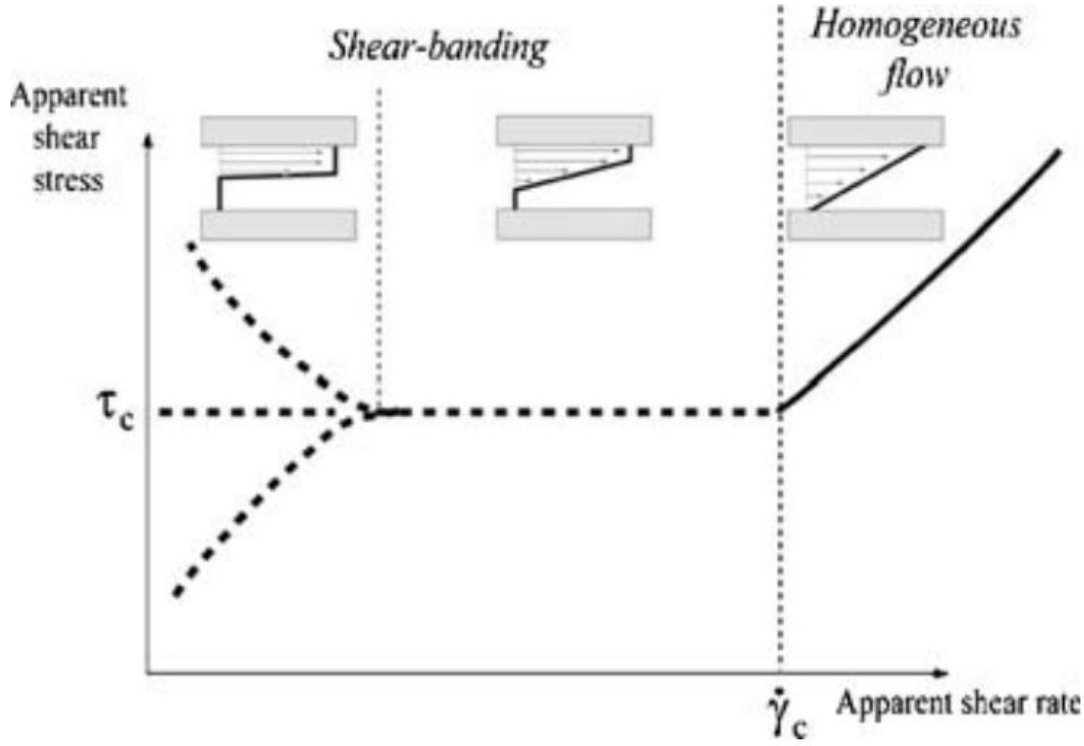

Figure 2.51. Typical flow curve obtained for some pasty material under imposed, apparent shear rate: the *solid line* corresponds to the rheological behavior of the material in steady-state homogeneous flow; the *dotted lines* correspond to the various apparent steady-state flow curves that can be observed in practice for shear rate below the critical value ($\dot{\gamma}$), but which do not correspond to an effective bulk behavior of the material. The drawings show the qualitative aspect of the velocity profile within the gap of the shear geometry in these apparent steady-state flows [103].

Although present, slip in one or all of its forms in the flow curves of drilling fluids as shown in Figures 2.52 - 2.53, has rarely been addressed in literature. Minute number of studies have looked into the effect of external conditions, particularly temperature, on the flow curves of drilling fluids. Although certain studies have made observations on slip occurrence in drilling fluids, fewer have dwelled on the mechanisms behind the results observed. As mentioned in the introduction, the most important from an engineering standpoint may possibly be characterizing the effects of slip in order to predict the flow in some applications rather than overcoming it [95].

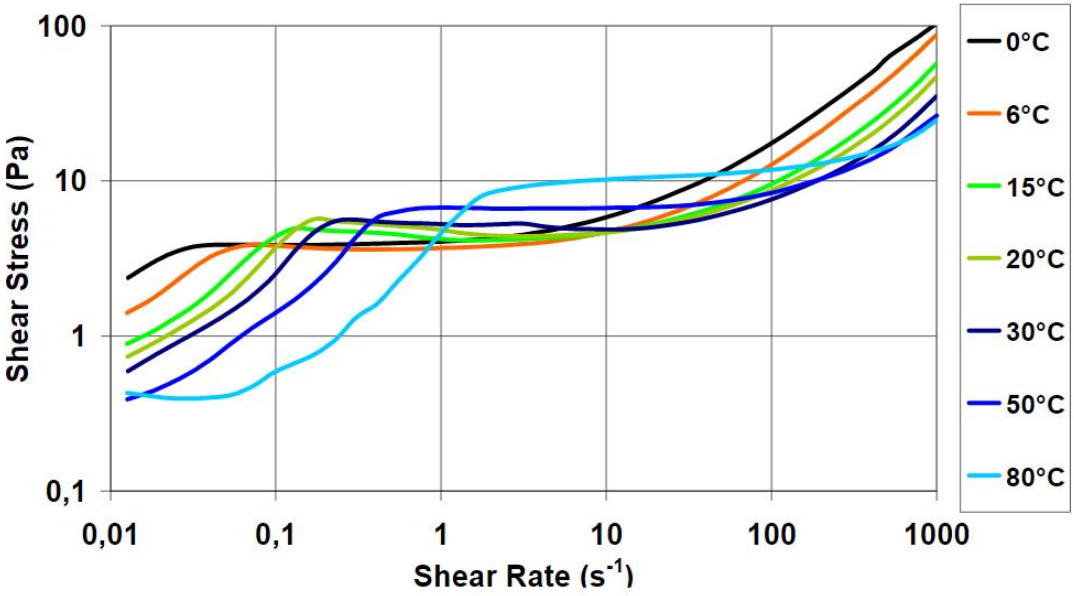

Figure 2.52. Flow curves of an OBM at different temperatures [123].

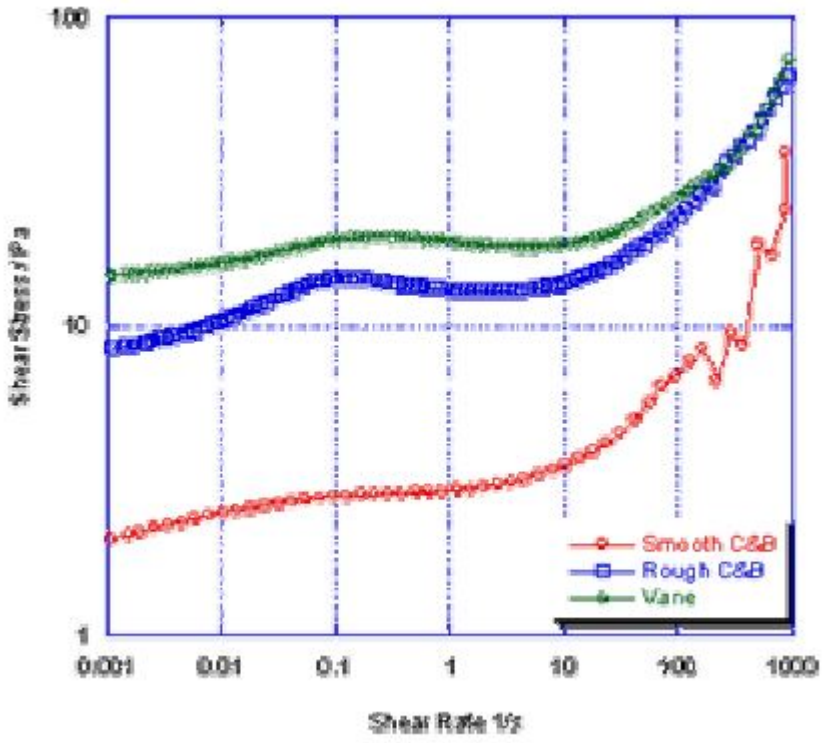

Figure 2.53. Wall slip in bentonite WBM [124].

Chapter 3
Project Variables & Experimental Procedure

3.1 Project Variables: Control & Performance

Rheology is the science of deformation and flow of matter under controlled testing conditions [93][116]. Flow is a special case of deformation and deformation is a special case of flow. The first goal of the research project was to experimentally determine the effect of surfactant polarity, concentration, Oil:Water ratio and temperature on the rheology i.e. flow curve and yield stress properties of oil-base complex fluids. Table 3.1 shows the control and performance variables of the project, while Table 3.2 enumerates the range of the control variables investigated.

Table 3.1: Control and Performance Variables

Control	Performance
surfactant polarity	flow curve
surfactant concentration	yield stress
Oil:Water ratio	fluid loss
temperature	phase inversion
	stability
	wall slip

Table 3.2: Control Variables

Conc. (wt.%)	HLB	OWR (vol.%)	T (^{o}C)
1	4.0	50:50	0
2	4.3	60:40	10
3	7.5	70:30	25
	11.5	80:20	50
		90:10	75
			90

3.2 Sample Components

Two types of emulsion-suspension complex fluids were prepared for experimental investigation, namely oil-base complex fluid (OCF) and water-base complex fluid (WCF) samples. The components used in preparing the samples were surfactants, deionized water, synethetic paraffin oil and Wyoming bentonite as viscosifier. Tables 3.3 and 3.4 show the relevant physical properties of the surfactants and other components.

The surfactants and paraffin oil were both purchased from Sigma Aldrich, while the deionized water and Wyoming bentonite were obtained from Lab Depot and Vermeer Texas respectively. The concentration of bentonite was kept constant at 9 wt.% with respect to the water volume fraction. It should be noted that the critical micelle concentration (CMC) of Brij 93 (Table 3.3) was not available neither from the supplier nor in literature.

Table 3.3: Surfactant Properties

Surfactant	Nature	HLB	CMC (g/L)
polyoxyethylene (2) oleyl ether (Brij 93)	nonionic	4.0	n/a
polyoxyethylene (10) oleyl ether (Brij O10)	nonionic	12.4	0.206
polyethylene glycol sorbitan monooleate (Tween 80)	nonionic	15.0	0.016
sorbitan monooleate (Span 80)	nonionic	4.3	0.008
sodium dodecyl sulfate (SDS)	anionic	40.0	2.88
cetyltrimethylammonium bromide (CTAB)	cationic	10.0	0.34

Table 3.4: Paraffin Oil, Water and Bentonite Properties

Property	Paraffin Oil	Water	Bentonite
dynamic viscosity (mPa.s)	110 - 230	0.89	n/a
density (g/cm^3)	0.83	0.99	2.46
dielectric constant	2.2	4 - 88 (80 @ 20 °C)	
particle size (μm)	n/a	n/a	< 44.0
boiling point (^{o}C)	260 - 450	100	n/a
shape	n/a	n/a	amorphous

Tables 3.5 and 3.6 show the different surfactants used to prepare the OCF and WCF samples. As a recall, surfactants with HLBs between 3 - 6 stabilize W/O emulsions while those having values between 8 - 18 stabilize O/W emulsion systems. The selection of two HLB values for the WCFs was done to assess the effect of HLB on temperature induced phase inversion (TIPI).

Table 3.5: Oil-base Complex Fluid (OCF) Samples

Surfactant	HLB	Nature	Sample
Span 80	4.3	nonionic	OCF S1
Brij 93	4.0	nonionic	OCF S2

Table 3.6: Water-base Complex Fluid (WCF) Samples

Surfactant	HLB	Nature	Mixture	Mixture HLB	Sample
Brij O10 Brij 93	12.4 4.0	nonionic nonionic	mixture 1 (M1)	7.5, 11.5	WCF M1
Tween 80 Span 80	15.0 4.3	nonionic nonionic	mixture 2 (M2)	7.5, 11.5	WCF M2
SDS CTAB	40.0 10.0	anionic cationic	mixture 3 (M3)	11.5	WCF M3

The rheology of the OCF samples was investigated and contrasted to that of oil-base mud (OBM) drilling fluid samples. The OBM samples were prepared using the components listed in Table 3.7. Duratone is a filtration control agent, while barite and sand are both weight additives. The surfactants used in preparing the OBMs were identical to those of OCF samples i.e. OBM S1 and OBM S2. As in the preparation of the OCF samples, the concentration of bentonite was kept constant at 9 wt.% with respect to the water volume fraction.

The water-base complex fluids (WCF) were investigated for transitional (temperature induced) phase inversion. WCF samples stabilized by ionic surfactant mixture were prepared to contrast the occurrence of phase inversion in their nonionic stabilized counterparts.

Table 3.7: Oil-based Mud Components

Oil-base Mud (OBM)
water
paraffin oil
surfactant
duratone
bentonite
barite

3.3 Sample Preparation

The OCF samples were prepared through direct emulsification, while abnormal emulsification was used in preparing the WCF samples to investigate TIPI. Abnormal emulsification involves homogenizing the surfactant(s) in the dispersed medium instead of the continuous one as outlined in Table 3.8. This emulsification procedure is the established method to initiate phase inversion via temperature variation for pure emulsion systems [77][78][89]. Direct (normal) emulsification procedure was used in the preparation of the OCF samples. The preparation of the OBM samples was done following the steps shown in Table 3.9.

Table 3.8: Complex Fluid Sample Preparation Procedure - MCR 52 (200 mL)

Step	WCF	OCF
1) addition of	surfactant mixture to oil phase	individual surfactant to oil phase
2) mixing at	900 rpm for 20 mins with magnetic blue stirrer	
3) addition to mixer cup	of water continuous phase	oil mixture continuous phase
4) addition of	bentonite to water	water to oil mixture
5) addition of	oil mixture to water phase	bentonite
6) mixing	at maximum speed for 3 mins with Hamilton beach mixer	
7) wait	24 hrs to ensure sample stability before measurement	

The weight concentration of bentonite was kept constant at 9 wt.% with respect to the volume fraction of water for all rheology measurements with the MCR 52 rheometer and Fann 35 viscometer. This value was lowered to 6 wt.% for microscope analysis to allow better visualization of the sample's microstructure variation with temperature.

Larger mixing times and speeds were used in the preparation of samples for measurements with Fann 35 viscometer. These were 1,400 rpm and 30 mins in step 2, and 5.5 mins in step 6. The protocol adjustment for the viscometer was because of the greater sample volume (350 mL) required for measurements in comparison to the rheometer ($\sim$ 3 mL). Thus the 200 mL sample volumes for the MCR 52 rheometer allowed repeated measurements, while single measurements were conducted with the Fann 35 viscometer.

Table 3.9: Drilling Fluid Sample Preparation Procedure

Step	OBM
1) addition of	individual surfactant to oil phase
2) mixing with	magnetic blue stirrer
3) addition of	duratone to oil-surfactant mixture
4) mixing with	Hamilton beach mixer
5) addition of	water
6) mixing with	Hamilton beach mixer
7) addition of	bentonite
8) mixing with	Hamilton beach mixer
9) addition of	barite
10) mixing with	Hamilton beach mixer
11) wait	24 hrs to ensure sample stability before measurement

3.4 Instruments & Equipment

The instruments used in the preparation of the complex and drilling fluid samples were the blue spin magnetic stirrer and Hamilton beach mixer, Figure 3.1. Their functions were to homogenize the surfactant(s) into the liquid medium for the former, and the entire sample components for the latter. Microstructure (as a function of temperature) and surface properties (contact angle, interfacial tension) of the samples were obtained using a DM6 Leica microscope and Thetha optical tensiometer, Figure 3.2.

(a) Magnetic blue stirrer

(b) Hamilton beach mixer

Figure 3.1. Mixing equipment.

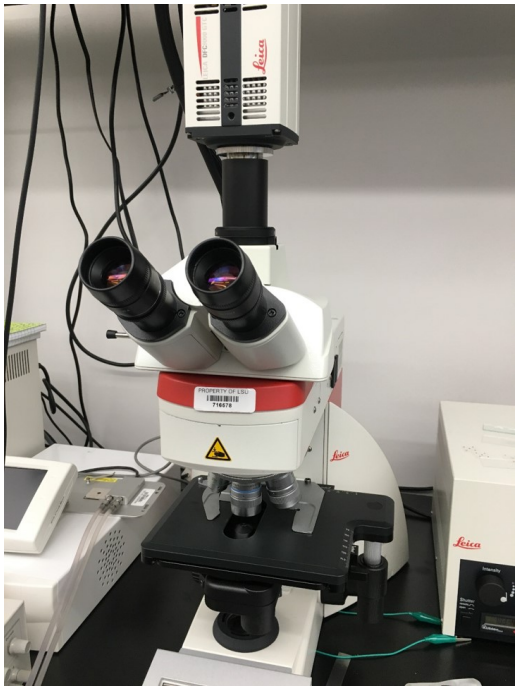

(a) Leica DM6 microscope

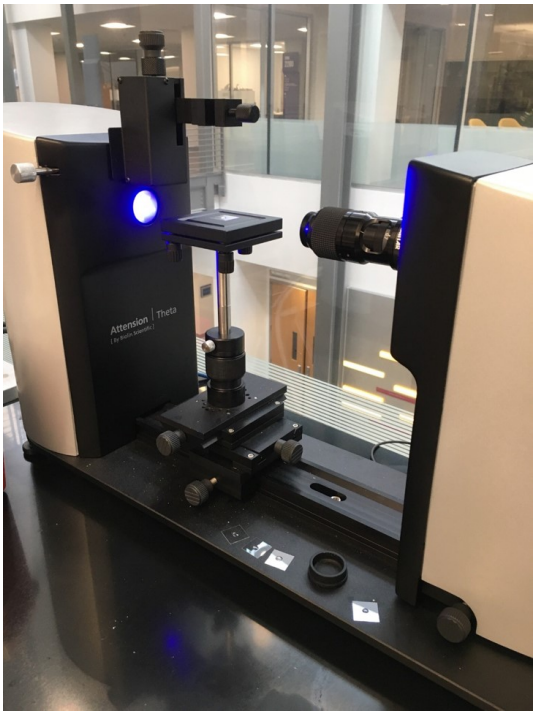

(b) Thetha optical tensiometer

Figure 3.2. Microstructure characterization and surface property measurement instruments.

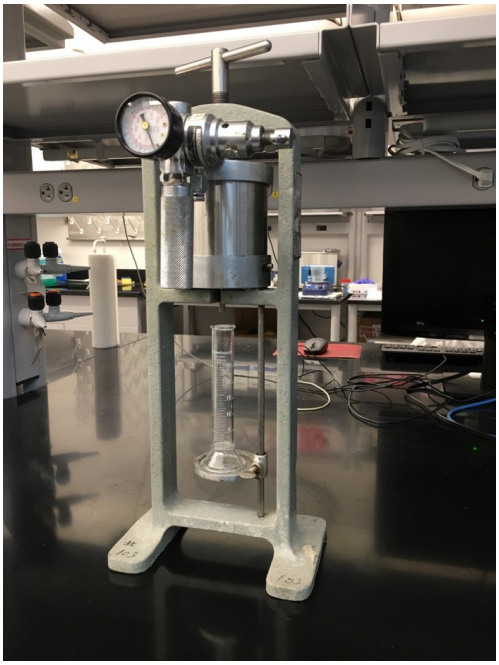

(a) Filter press

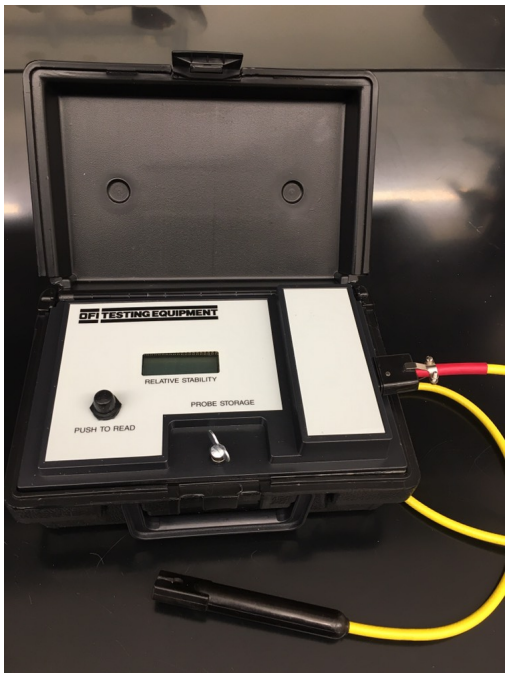

(b) OFI emulsion stability tester

Figure 3.3. Fluid loss and stability tester instruments.

(a) Conductivity meter

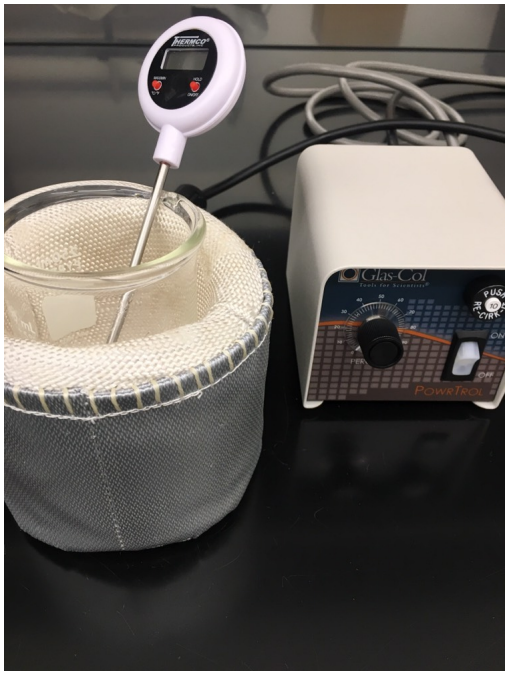

(b) Fabric mantle and power controller

Figure 3.4. Conductivity measurement instruments.

(a) MCR 52 rheometer

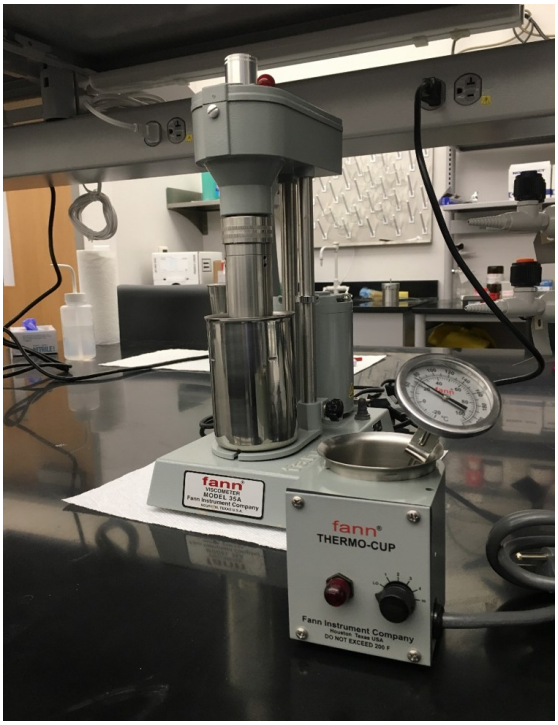

(b) Fann 35 viscometer

Figure 3.5. Flow characterization instruments.

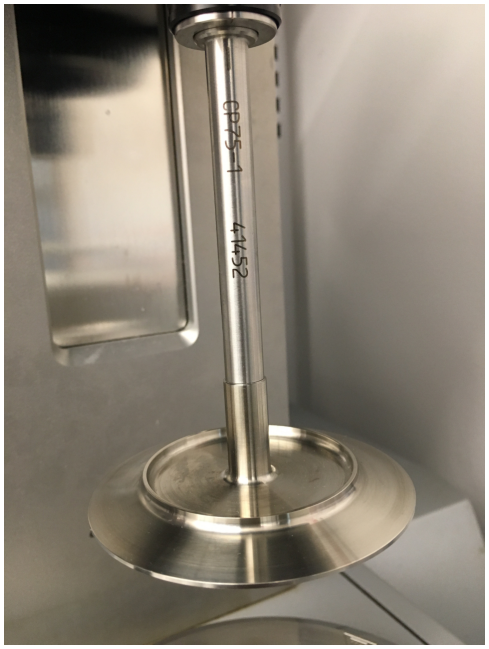

(a) MCR - Cone & Plate (CP) geometry

(b) MCR - Parallel Plate (PP) geometry

Figure 3.6. MCR measuring geometries.

Macroscopic characterization included measurements with a LPLT Fann filter press, Figure 3.3a, to quantify the fluid loss levels of the different emulsion-suspension complex fluid samples. An OFI emulsion stability tester, Figure 3.3b, was used in determining their

stability. A conductivity meter, in combination with a fabric mantle and power controller, Figure 3.4, was used to evaluate catastrophic and transitional (temperature) phase inversion of the samples.

Figure 3.5 shows the MCR 52 rheometer and Fann 35 viscometer which were used in characterizing the flow behavior of the different samples. Both instruments impose shearing through drag flow. The measuring geometry in the Fann 35 viscometer is a Couette geometry, while both cone & plate (CP) and parallel plate (PP) measuring geometries can be used in the MCR 52 rheometer. The CP geometry was used in flow curve and yield stress measurements of the samples, while the PP geometry was used for wall slip characterization.

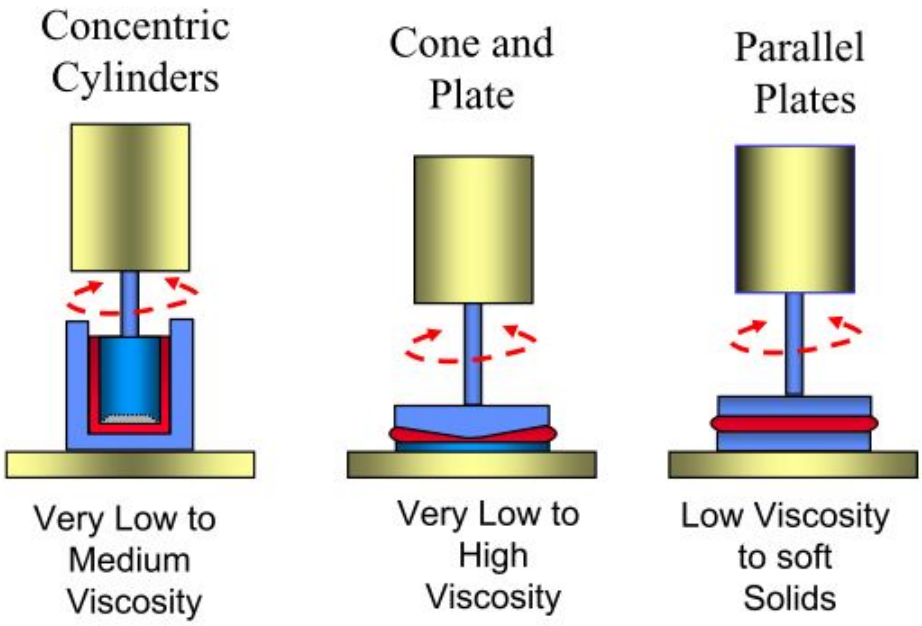

Figure 3.7. Measuring geometries [116].

The Couette flow geometry of the viscometer has a measuring gap of 1.17 mm, while that of the CP geometry (rheometer) is 0.15 mm. The PP geometry on the other hand has an adjustable measuring gap which makes it a popular geometry in slip assessment of non-Newtonian fluids. The main difference between the Fann viscometer and MCR rheometer lies in the limited shear rate range over which measurements can be carried in the former. This is 5.1 - 1,021.4 s^{-1} for the viscometer, in comparison to 0.1 - 3,000

s^{-1}. Furthermore, viscometers are intrinsically designed to measure the flow behavior of very low to medium viscosity materials, while CP and PP of rheometers can characterize materials having higher apparent viscosities, Figure 3.7.

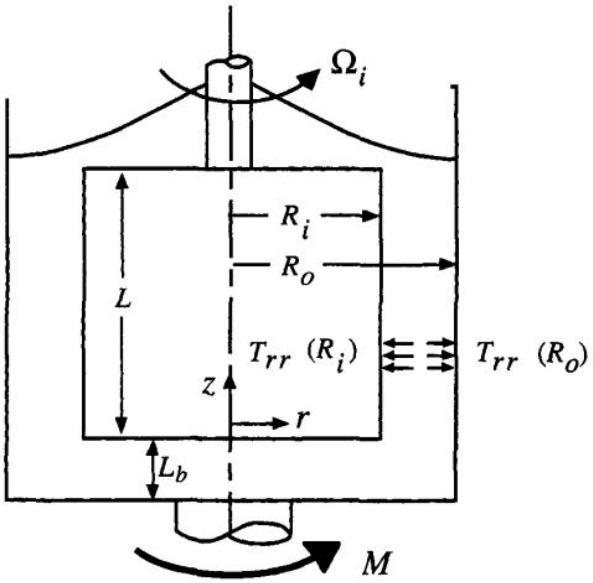

Figure 3.8. Working principle of Couette flow viscometers [117].

Below are the working equations of the Couette flow geometry of the Fann viscometer [117]:

Shear stress (Pa):

$$\tau_{21} = \tau_{r\theta}(R_i) = \frac{M_i}{2\pi R_i^2 L} \tag{3.1}$$

Shear strain:

$$\gamma = \frac{\theta \bar{R}}{R_o - R_i} or \frac{\Omega t \bar{R}}{R_o - Ri} \tag{3.2}$$

for narrow gaps, $k = \dfrac{R_i}{R_o} \geq 0.99$:

$$\frac{\Omega t \bar{R}}{R_o - Ri} \tag{3.3}$$

Where M_i is torque (Nm), θ is the angular displacement, $\theta = \Omega t$, for steady motion and $R = (R_o + R_i)/2$. Where R (mean radius), t and Ω have units of m, s and rad/s respectively.

Strain rate (1/s):

(i) for $k > 0.99$

$$\dot{\gamma}(R_i) \approx \dot{\gamma}(R_o) = \frac{\Omega \bar{R}}{R_o - R_i} = \frac{2\Omega_i}{1 - k^2} \tag{3.4}$$

(ii) for gaps $0.5 < k < 0.99$:

$$\begin{aligned} \dot{\gamma}(R_i) &= \frac{2\Omega_i}{n(1 - k^{2/n})} \\ \dot{\gamma}(R_o) &= \frac{-2\Omega_i}{n(1 - k^{-2/n})} \end{aligned} \tag{3.5}$$

where $n = (dInM_i)/(dIn\Omega_i)$.

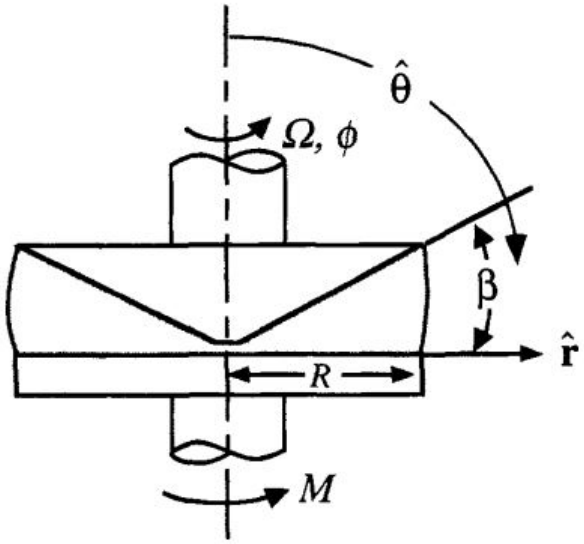

Figure 3.9. Working principle of rheometer cone & plate (CP) geometry [117].

Below are the working equations of the Cone & Plate (CP) geometry of the MCR rheometer [117]:

Shear stress (Pa):

$$\tau_{12} = \tau_{\phi\theta} = \frac{3M}{2\pi R^3} \tag{3.6}$$

Shear strain:

$$\gamma = \frac{\phi}{\beta} \tag{3.7}$$

Shear rate (1/s):

$$\dot{\gamma} = \frac{\Omega}{\beta} \tag{3.8}$$

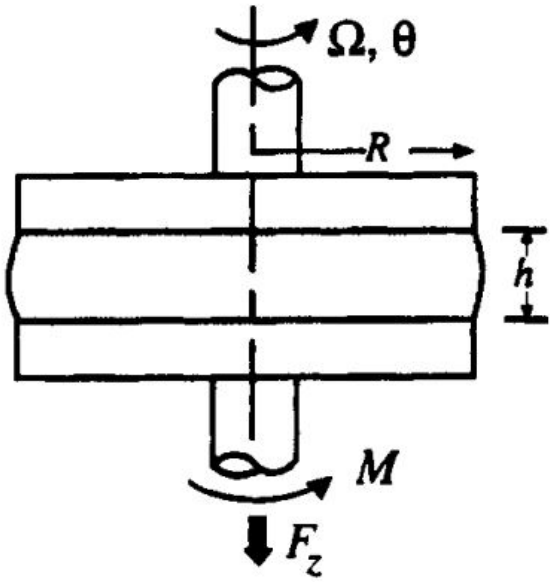

Figure 3.10. Working principle of rheometer parallel & plate (PP) geometry [117].

Below are the working equations of the Paralle Plate (PP) geometry of the MCR rheometer [117]:

Shear strain:

$$\gamma = \frac{\theta r}{h} \tag{3.9}$$

Shear rate at r = R (1/s):

$$\dot{\gamma}_R = \frac{R\Omega}{h} \tag{3.10}$$

Shear stress (Pa):

$$\tau_{12} = \tau_{\theta z} = \frac{M}{2\pi R^3}[3 + \frac{dInM}{dIn\dot{\gamma}_R}] \tag{3.11}$$

3.5 Measurement Procedure

3.5.1 Microstructure Characterization

- Characterization of the microstructure of all samples was conducted using a Leica DM6 microscope equipped with a heatable sample holder. Images were acquired using a 63x (and 100x) magnification lens at temperatures ranging from 0 - 90 °C. The temperature was ramped as follows 25 °C → 0 °C → 10 °C → 50 °C → 75 °C → 90 °C. A drop of the sample was placed on a slide and then fitted on a heatable sample holder under the microscope lens.

- Contact angles of deionzed water and paraffin oil were acquired, as well as those of the aforementioned in the presence of the different individual surfactant and surfactant mixtures using a Thetha optical tensionmeter on a borosilicate glass surface.

- The same instrument was used in determining the interfacial properties of the oil-water base emulsion of the complex fluids in the presence (and absence) of the different surfactant(s). The lighter (oil) fluid was placed in a cubic receptacle while a drop of the denser (water) fluid was suspended within it. The contour formed by the oil droplet was fitted using the Laplace equation to determine the interfacial tension.

3.5.2 Macroscopic Characterization

- Flow curve measurements with the MCR 52 rheometer were acquired over shear rates spanning four orders of magnitude, 0.1 - 3,000 s^{-1} at temperatures ranging from 0 - 90 °C. The measuring geometry used in these measurements was a Cone & Plate (PP) measuring geometry. All samples were pre-sheared at a constant shear rate of 50 s^{-1} for 1 min to homogenize the mixture. An equilibration time of 5 mins was observed at each temperature to ensure the samples reached thermal steady-state. Sample volume used per measurement in the MCR was $\sim$ 3 mL.

- Measurements with the Fann 35 were acquired over shear rates ranging from 5.1 -

1,021.4 s^{-1} and were pre-sheared at 1,021.4 s^{-1} for 10 mins for homogenization of the mixture. The pre-shear value and duration were scaled-up from that set for the MCR. Due to the limitations on its scope of temperature variation, flow curve measurements with the Fann 35 viscometer were performed at temperatures of 25, 50 and 75 °C.

- All flow curve measurements with the rheometer were repeated thrice with fresh samples at each run to ensure reproducibility, single runs were performed with the viscometer due to the larger volume requirements (350 mL).

- Stress sweeps to determine yield stress of the samples were performed at the lowest (0 °C) and highest (90 °C) temperature of investigation as well as room temperature (25 °C). These measurements were performed with the rheometer. Shear stresses ranging from 0 - 50 Pa were applied to the samples to determine their yield properties via their strain deformation profile. Measurements were repeated twice to ensure reproducibility. Yielding of the samples was indicated by an inflection in their strain vs stress profile as shown in Figure 3.11.

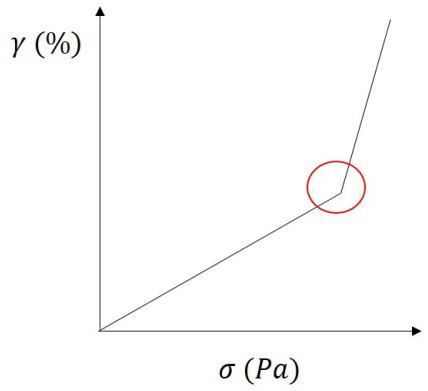

Figure 3.11. Yield stress.

- Fluid loss tests were conducted at room temperature for all samples. 100 psig (ΔP) was applied and the filtrate volume (V_f), described by Darcy's equation (Equation 3.12) [16], was recorded over time (t). Where k represent the permeability of the mudcake, A the filter paper cross-sectional area, μ_f the filtrate volume viscosity and

h_{mc} the mudcake thickness.

The test was carried over 7.5 mins ($V_{7.5}$) and the total filtrate volume (V_{30}) was calculated using Equation 3.13, based on the relationship between filtrate volume and measurement time ($V_f \propto \sqrt{t}$). Spurt volume losses (V_{sp}) observed at the beginning of measurements were accounted for by the equation. Only the total filtrate volume and mudcake thickness were measured.

The surfactant concentration was set to the maximum value of 3 wt.% for all samples and bentonite concentration reduced to 6 wt.% with respect to the volume fraction of the water phase. This was done to highlight the effect of surfactant chemistry on fluid loss. 150 mL sample volume was used for each measurement.

$$\frac{dV_f}{dt} = \frac{kA\Delta P}{\mu_f h_{mc}} \tag{3.12}$$

$$V_{30} = 2(V_{7.5} - V_{sp}) + V_{sp} \tag{3.13}$$

- Wall slip assessment and analysis was conducted using the parallel plate (PP) measuring geometry. Measurements were conducted at temperatures of 10, 25, 50 and 75 °C at three different gaps of 0.5, 1.17 and 2.0 mm. Shear rates ranging from 0.1 - 1,020 s^{-1} were applied to the samples to characterize their slip properties. Measurements were repeated twice to ensure reproducibility.

- Sample stability was determined using an OFI emulsion stability tester. Per the instrument guidelines, the samples were pre-heated to 48 °C. They were then stirred for 10 seconds using the electrode probe to reduce gradients in composition and temperature, after which the electrical stability (ES) value is recorded. Hard, not deionized, water was used for these measurements because of their higher electrical conductivity.

- Catastrophic and transitional phase inversion via conductivity measurements was

investigated. The first step consisted of inducing inversion of the oil-base complex fluid (OCF) to a water-base complex fluid (WCF) via catastrophic phase inversion (CPI). This step was carried out by adding 10 mL of water to the sample and mixing it for 20 seconds using the Hamilton beach mixer, after which the conductivity value was recorded.

This was repeated till a significant increase in conductivity was observed, indicative of the inversion of the sample to a WCF. Following CPI, the sample was then heated using a heatable fabric mantle from 25 to 100 °C and the conductivity recorded at 10 °C intervals. Hard, not deionized, water was used for these measurements because of their higher electrical conductivity.

3.5.3 Sample Spectrum

Figure 3.12 shows the spectrum of the samples prepared. Measurements were conducted only in samples that were stable following an observation time of 24 hrs. As shown in the figure all samples at the O:W of 90:10 were unstable, while those at O:W of 70:30 and 80:20 showed stability that varied based on the surfactant type, HLB and concentration.

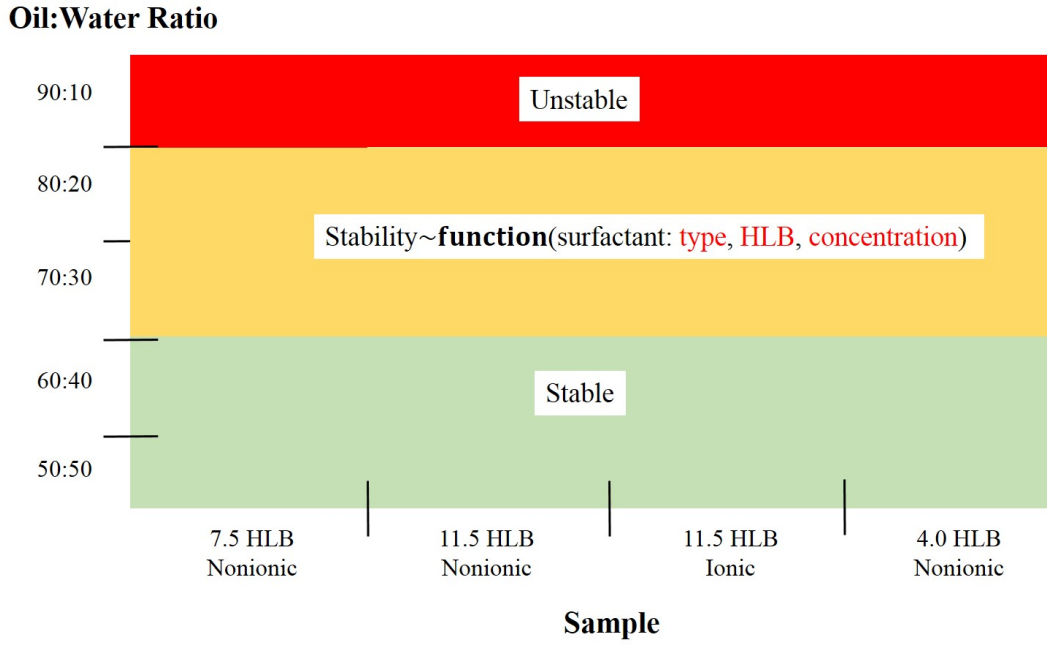

Figure 3.12. Sample spectrum.

Chapter 4
Experimental Results & Discussion: Oil-base Complex Fluids

4.1 Effect of Surfactant Polarity

4.1.1 Flow Curve

In this section results of the investigation of the effect of the control variable polarity (HLB) on the performance variable flow curve of oil-base complex fluid samples OCF S1 and OCF S2 is discussed. These samples were respectively stabilized by Span 80 and Brij 93 nonionic surfactants, see Table 3.5. Span 80 has an HLB value of 4.3, while that of Brij 93 is 4.0. Figures 4.1 to 4.11 show the difference in flow curve profiles between the two samples at room temperature (25 °C) and maximum surfactant concentration of 3 wt.% at different O:W ratios. Included in Appendix A are the comparison between the samples at all other temperatures and surfacant concentrations.

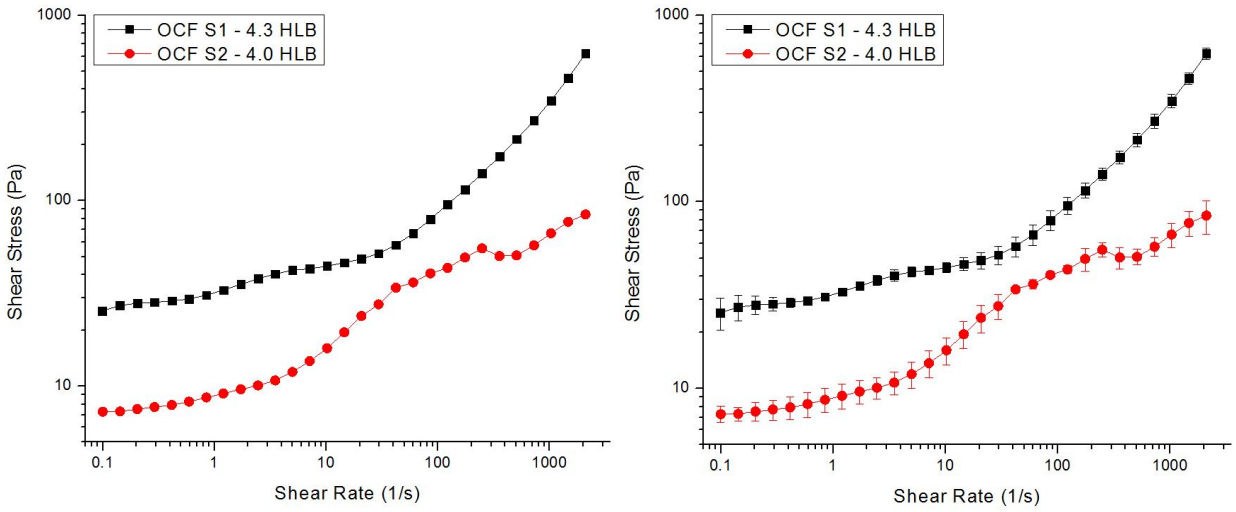

(a) Average Values (b) with Standard Deviation

Figure 4.1. O:W = 50:50, T = 25 °C, C_{surf} = 3 wt.%.

OCF S1 is observed to holistically display higher shear stresses than OCF S2 at O:W ratios going up to 80:20. This can be explained in terms of the difference in (i) polarity (dipole moment) of the surfactants as well as their differing (ii) critical micelle concentrations (CMC). Figures 4.2 and 4.3 show the chemical structure of Span 80 and Brij 93, respective surfactant components of OCF S1 and OCF S2. Span 80 has a greater dipole

moment than Brij 93 due to its greater number of electron withdrawing atoms (oxygen).

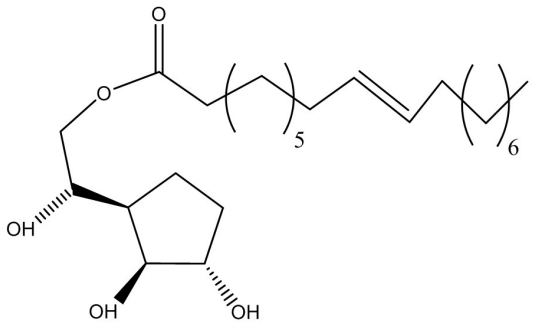

Figure 4.2. Span 80 (sorbitan monooleate).

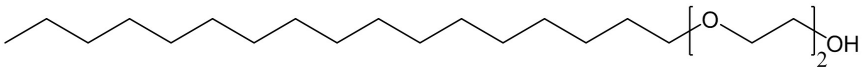

Figure 4.3. Brij 93 (polyoxyethylene (2) oleyl ether).

The concept of dipole moment is best illustrated with the compound, carbon monoxide (CO). Oxygen is a highly electronegative atom, significantly greater than carbon is for that matter. As a result, the former pulls the electron cloud of carbon towards itself, creating a charge imbalance as shown in Figure 4.4. This charge imbalance creates a dipole moment, Figure 4.5, which enables nonionic surfactants to interact with charged surfaces. This interaction is important, given that bentonite used as viscosifier in the samples has a net electrostatic charge on its surfaces.

Figure 4.4. Carbon monoxide.

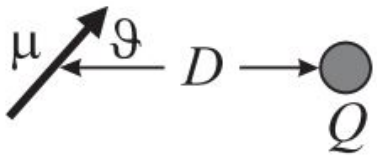

Figure 4.5. Dipole moment of non-charged molecules. It is a vector that points from the more negative side of a molecule to its more positive side. Where u is the dipole moment, Q is a single net charge and D is the distant between the polar molecule and net charge [50].

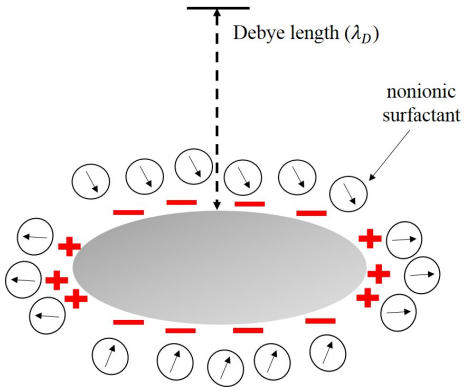

Figure 4.6. Weakening of the electrostatic field of bentonite particles due to adsorption of surfactant molecules, reduction of Debye length.

In the case of nonionic surfactants, they adsorb on the surface of bentonite particles reducing their Debye length (λ_D), Equation 4.1 [50]. Where $\dot{A}$ represents the unit length Armstrong (10^{-10} m) and c_0 salt concentration, which for the case under consideration represents nonionic surfactants having large dipole moments.

$$\lambda_D = \frac{3.04\dot{A}}{\sqrt{c_0}} \tag{4.1}$$

The greater the number of electron-withdrawing atoms present in the structure of non-ionic surfactants, the greater is their dipole moment. The greater is their dipole moment, the greater is their adsorption on the surface of the charged bentonite particles, weakening their electrostatic field, Figure 4.6, which prevents edge-to-face or edge-to-edge linkage of

the particles. Thus, bentonite particles are prone to display better linkage in OCF S2 than OCF S1. This has implication on the degree of emulsification of these emulsion-suspension samples, as shown in Figure 4.7.

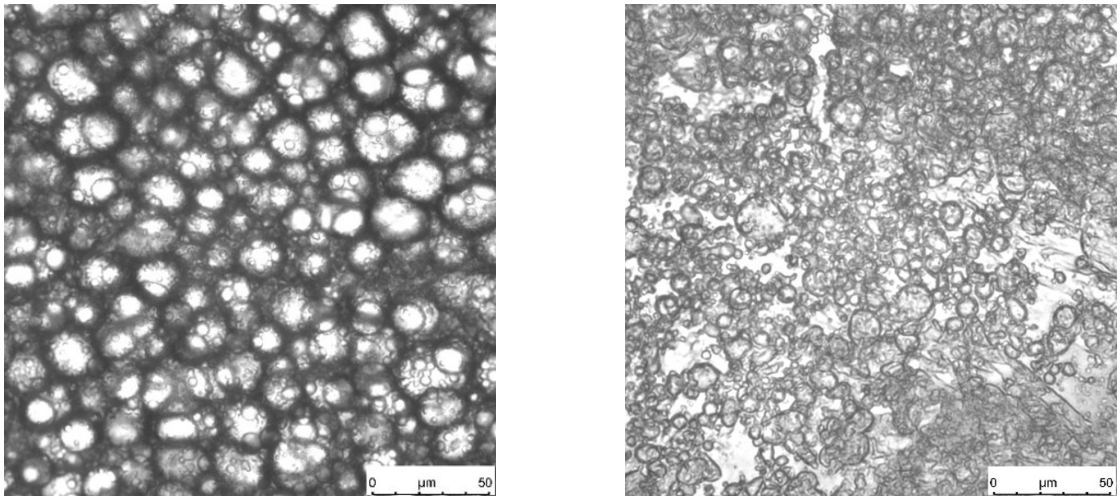

(a) OCF S1 (b) OCF S2

Figure 4.7. O:W = 60:40, T = 25 °C, C_{surf} = 3 wt.%.

In addition to dipole moment, the greater degree of emulsification seen in the microstructure of OCF S1 accounting for the greater shear stress level observed in its flow curve over OCF S2 can further be explained by their differing CMCs. As indicated in Table 3.3, Span 80 has a CMC of 0.008 g/L and it is assumed that of Brij 93 is greater implying a higher mitigation of bentonite particle linkage in OCF S1.

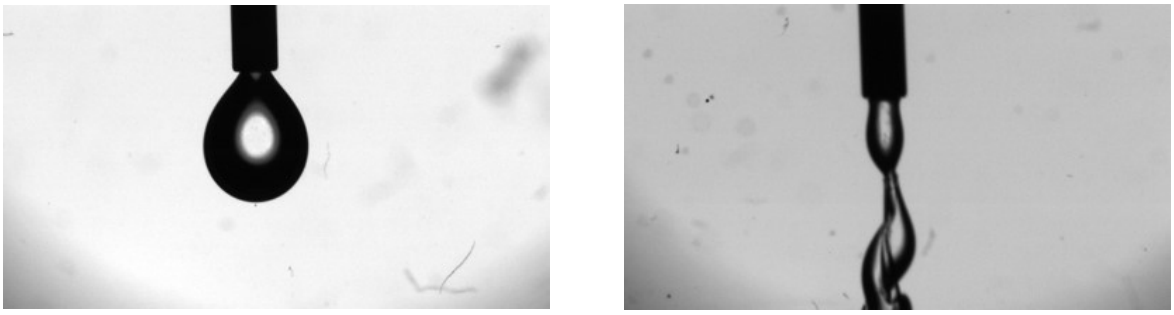

(a) Oil + Water + S1: 3.52 mN/m (b) Oil + Water + S2: very low

Figure 4.8. Interfacial tension: T = 25 °C, C_{surf} = 3 wt.%.

Figure 4.8 shows the difference in interfacial tension between OCF S1 and OCF S2.

The higher interfacial tension of OCF S1 in comparison to OCF S2 accounts for the large dispersed droplets observed in the microstructure of the former. The aforementioned makes the jamming, Figure 4.9, of the dispersed emulsion droplets an additional contributor to the shear stresses observed in the flow curve of OCF S1.

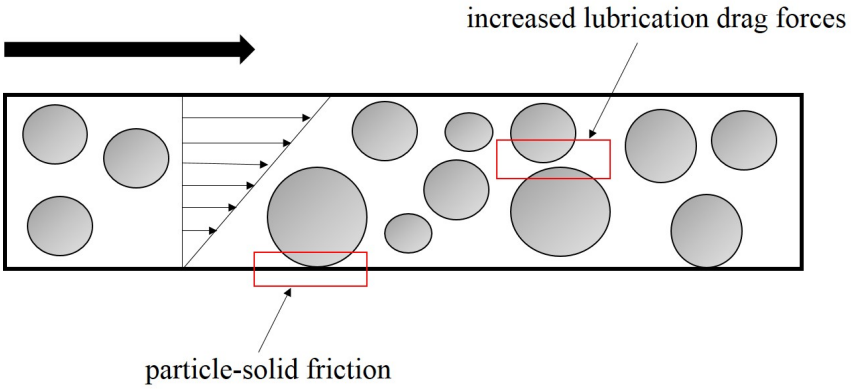

Figure 4.9. Jamming of dispersed particles.

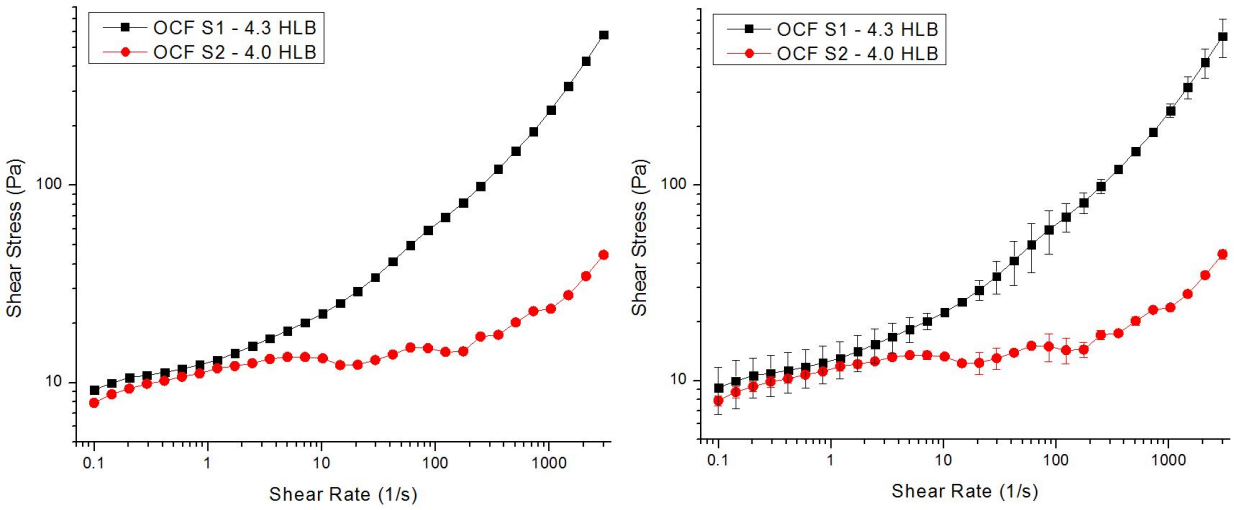

(a) Average Values

(b) with Standard Deviation

Figure 4.10. O:W = 60:40, T = 25 °C, C_{surf} = 3 wt.%.

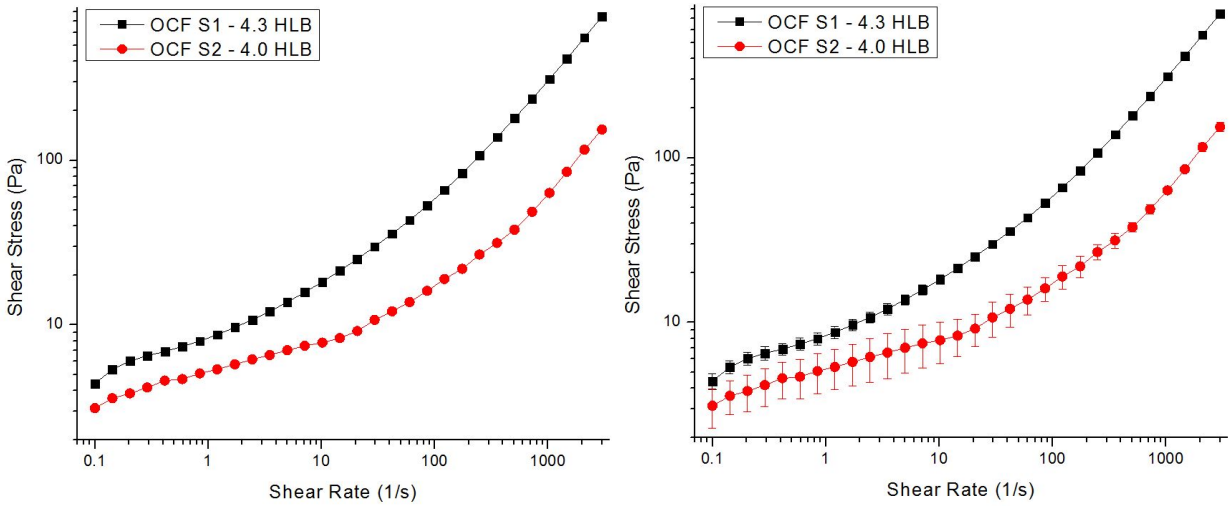

(a) Average Values (b) with Standard Deviation

Figure 4.11. O:W = 70:30, T = 25 °C, C_{surf} = 3 wt.%.

At O:W ratios of 60:40 and 70:30, Figures 4.10 and 4.11, the greater shear stress in the flow curve OCF S1 due to its greater dipole moment, lower CMC and higher interfacial tension can be observed. At 80:20 O:W ratio however, OCF S1 was found to be unstable as opposed to OCF S2. The instability observed at this O:W ratio, plausibly results from depletion flocculation (see Section 2.3 of Chapter 2) where the very high micelle concentration drives the coalescence of the 20 vol.% dispersed water phase, Figure 4.12.

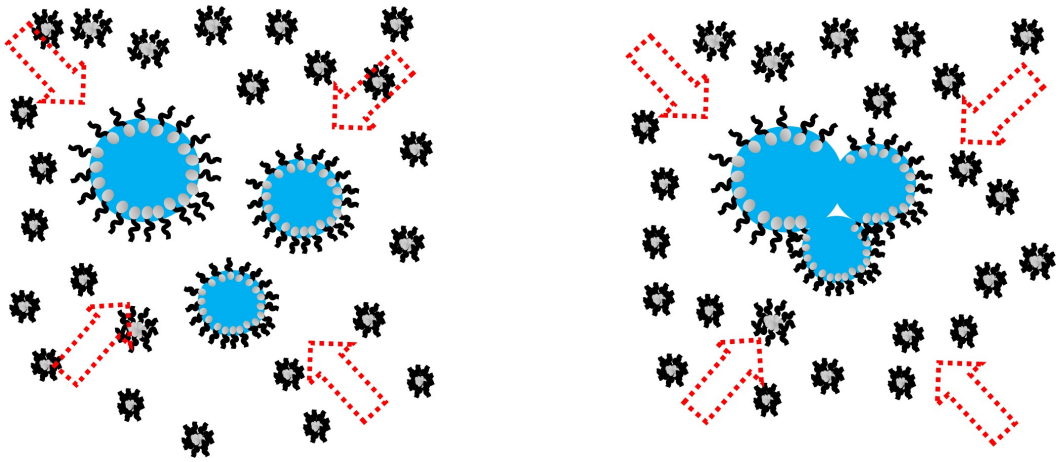

(a) Depletion flocculation (b) Droplet coalescence

Figure 4.12. Instability driven by flocculation of dispersed droplets due to elevaed micelle concentration.

4.1.2 Yield Stress

Discussed in this section is the effect of the control variable polarity (HLB) on the performance variable yield stress of the oil-base complex fluid samples: OCF S1 and OCF S2. Figures 4.13 to 4.15 show the strain response of the OCF samples to applied shear stress at room temperature and maximum surfactant concentration of 3 wt.%. Included in Appendix A are the stress sweep responses of the samples at all other temperatures and concentrations.

With the exception of 50:50 O:W ratio, OCF S1 is holistically observed to display higher structuration (ability to support or transmit loads) as opposed to OCF S2 as shown by the lower shear stain observed in Figures 4.14 and 4.15. At 60:40 O:W ratio, both samples are observed to yield around 30 Pa, but the strain deformation of OCF S2 is significantly greater than that of OCF S1.

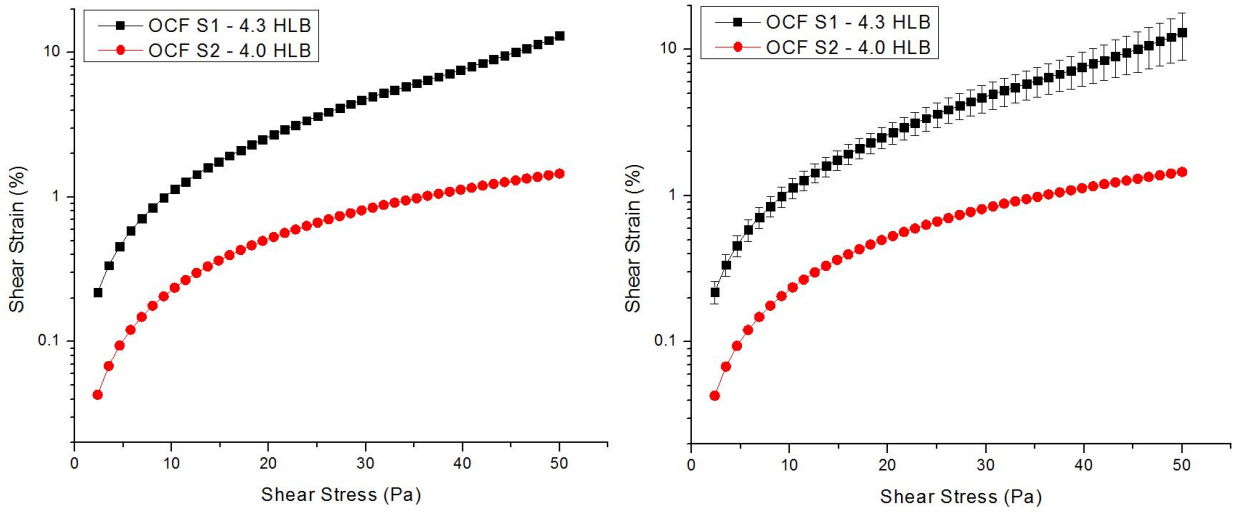

(a) Average Values (b) with Standard Deviation

Figure 4.13. O:W = 50:50, T = 25 °C, C_{surf} = 3 wt.%.

This difference in strain deformation level is accentuated at 70:30 O:W ratio, where differences in shear strain of almost 4 orders of magnitude is observed. This difference is driven by the higher dipole moment and lower CMC of Span 80 over Brij 93, which mitigates interaction between bentonite particles that would otherwise stifle droplet formation. The

lower CMC of Span 80, implies for a given surfactant concentration there is a significantly higher micelle concentration to favor emulsion formation.

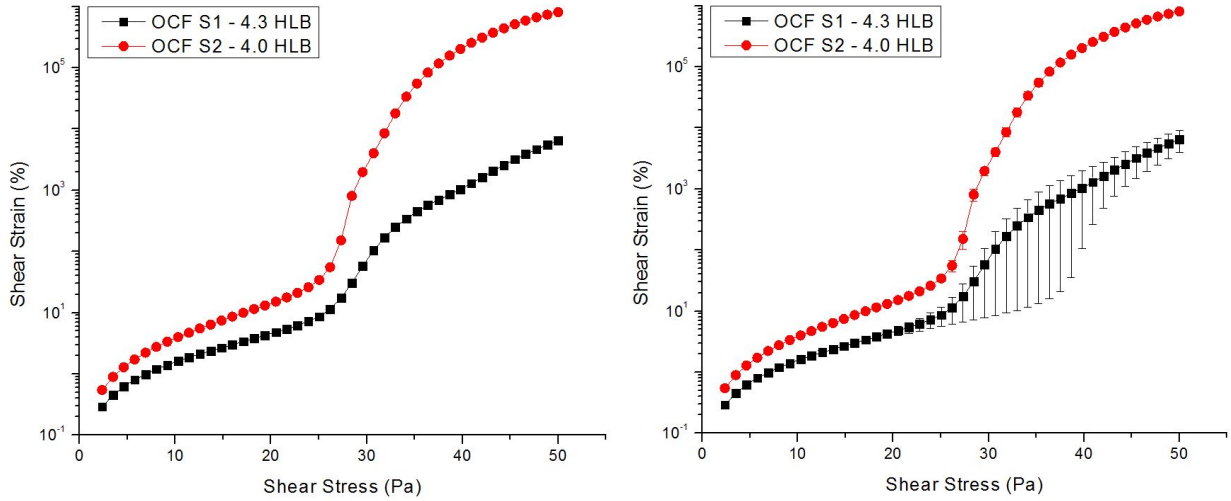

(a) Run 1 (b) Run 2

Figure 4.14. O:W = 60:40, T = 25 °C, C_{surf} = 3 wt.%.

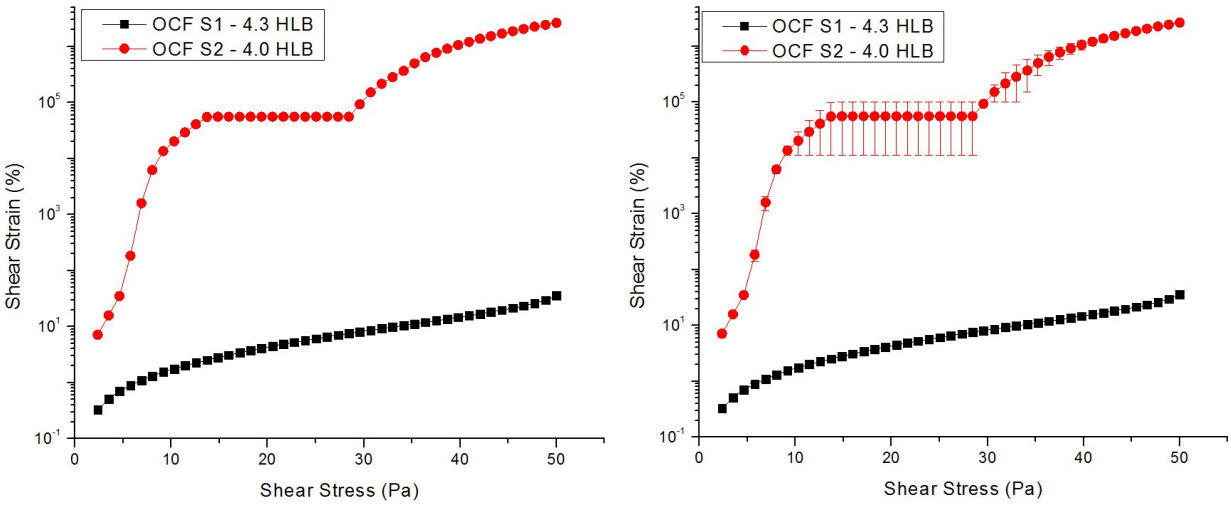

(a) Average Values (b) with Standard Deviation

Figure 4.15. O:W = 70:30, T = 25 °C, C_{surf} = 3 wt.%.

At 80:20 O:W ratio, OCF S1 is unstable and large deformations are observed in OCF S2 due to the lower amount of bentonite (viscosifier) present within its structure. As a recall, bentonite concentration is kept constant with respect to water volume fraction.

4.1.3 Fluid loss

In this section the effect of the control variable polarity (HLB) on the performance variable fluid loss is investigated in the oil-base complex fluid samples: OCF S1 and OCF S2. Figures 4.16 and 4.17 compare the filtrate volumes and associated mudcake thickness of the oil-base complex fluids at room temperature, maximum surfactant concentration of 3 wt.% and O:W ratios ranging from 50:50 to 80:20.

The effect of differing dipole moment and CMC between OCF S1 and OCF S2 is reflected in their filtrate volumes and mudcake thickness. Due to the lower dipole moment and higher CMC of OCF S2, bentonite contribution to fluid loss mitigation is greater than in OCF S2.

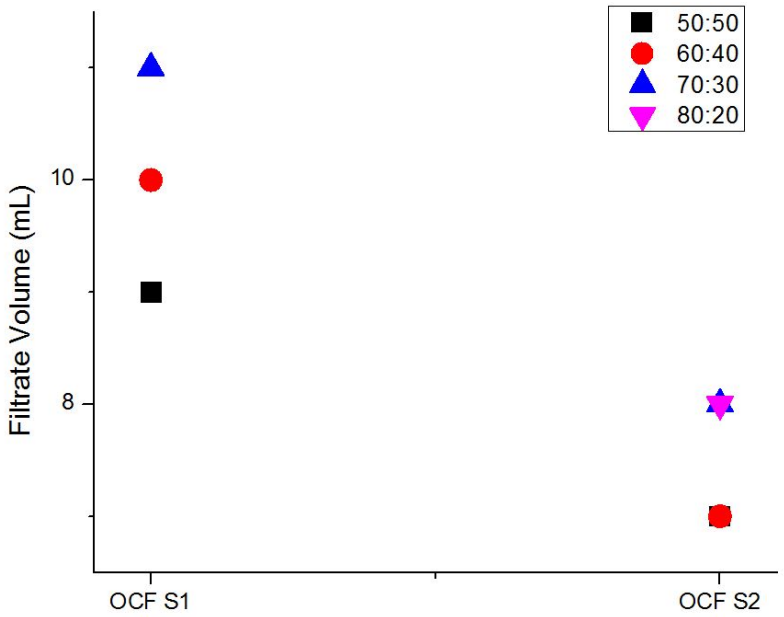

Figure 4.16. Filtrate volume (mL): T = 25 °C, C_{surf} = 3 wt.%.

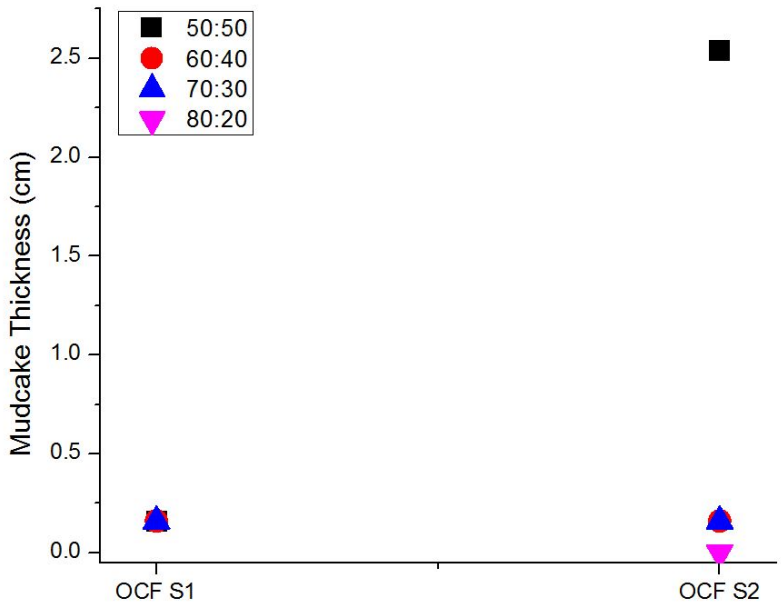

Figure 4.17. Mudcake Thickness (cm): T = 25 °C, C_{surf} = 3 wt.%.

4.1.4 Stability

In this section the effect of the control variable polarity (HLB) on the performance variable stability is investigated in the oil-base complex fluid samples: OCF S1 and OCF S2. Table 4.1 shows the electrical stability test results of the oil-base complex fluids at different O:W ratios and surfactant concentrations. The results are clearly indicative of the larger stability of OCF S2 over OCF S1. The greater inhibition of linkage of bentonite particles (i.e. deflocculation) and degree of emulsification in OCF S1 (see Figure 4.7), makes it more prone to instability due to a higher tendency of the dispersed droplets to flocculate and ultimately coalesce.

The higher CMC of the surfactant component of OCF S2, equally makes the possibility of depletion flocculation phenomenon less pronounced as opposed to OCF S1. The samples with the mention 'unstable' are those that were found to demulsify after the 24 hr observation time following preparation.

Table 4.1: Electrical Stability

O:W Ratio	C_{surf} (wt.%)	OCF S1 (volts)	OCF S2 (volts)
50:50	1	1	1
50:50	3	1	1
60:40	1	1	1
60:40	3	1	35
70:30	1	unstable	unstable
70:30	3	3	62
80:20	1	unstable	unstable
80:20	3	unstable	96

4.2 Effect of Oil:Water Ratio

4.2.1 Flow Curve

In this section the effect of the control variable O:W ratio on the performance variable flow curve is investigated in the oil-base complex fluid samples: OCF S1 and OCF S2. Shown in Figures 4.18 and 4.19 are the flow curves of these complex fluids at room temperature and maximum surfactant concentration of 3 wt.%. Included in Appendix A, are the flow curves of the samples at all other temperatures and surfactant concentrations.

OCF S1 is observed to show an increase in shear stress with increasing O:W ratio, this can be explained by a greater contribution to the fluid's apparent viscosity from emulsion formation and amount of viscosifier (bentonite). As opposed to OCF S1, OCF S2 (Figure 4.19) is observed to show in its flow curve alternating instances of shear stress increase and decrease. This flow behavior can be attributed to wall slip, which is discussed in Chapter 5. Table 3.5 shows the composition of both OCF S1 and OCF S2.

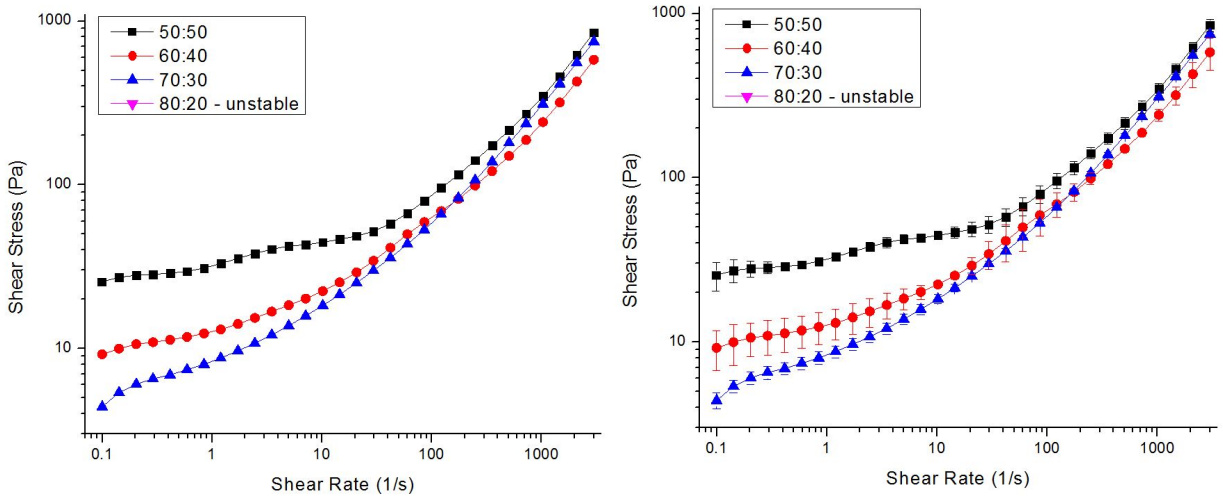

(a) Average Values (b) with Standard Deviation

Figure 4.18. OCF S1: T = 25 °C, C_{surf} = 3 wt.%.

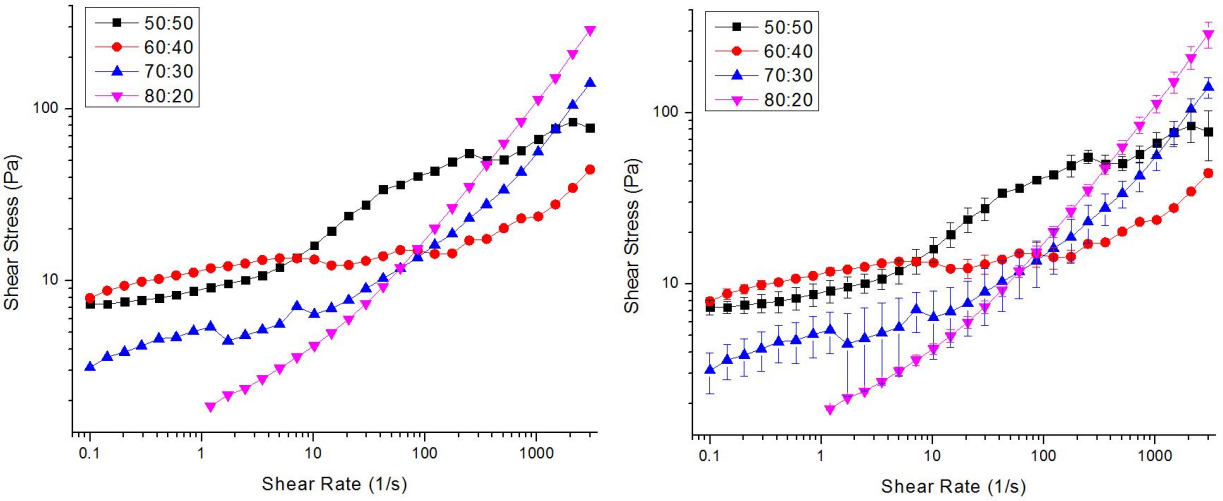

(a) Average Values (b) with Standard Deviation

Figure 4.19. OCF S2: T = 25 °C, C_{surf} = 3 wt.%.

Two factors account for the greater slip behavior in OCF S2 as opposed to OCF S1, namely: (i) the lower dipole moment of Brij 93 (S2) allows linkage of bentonite particles, however given (ii) Brij 93's higher CMC the amount of surfactant molecules (and micelles) at given surfactant concentration is lower than that of Span 80 (S1). In other words, OCF S2 has a heterogeneous internal structure resulting from the combination of the two aforementioned factors resulting in slip, see Figures 2.49, 2.51 and 4.7b. The topic of wall

slip will be further discussed in Chapter 5.

4.2.2 Yield Stress

In this section the effect of the control variable O:W ratio on the performance variable yield stress is investigated in the oil-base complex fluid samples: OCF S1 and OCF S2. Figures 4.20 and 4.21 show the strain response of the complex fluids OCF S1 and OCF S2 to the stress sweep at room temperature and maximum surfactant concentration of 3 wt.%.

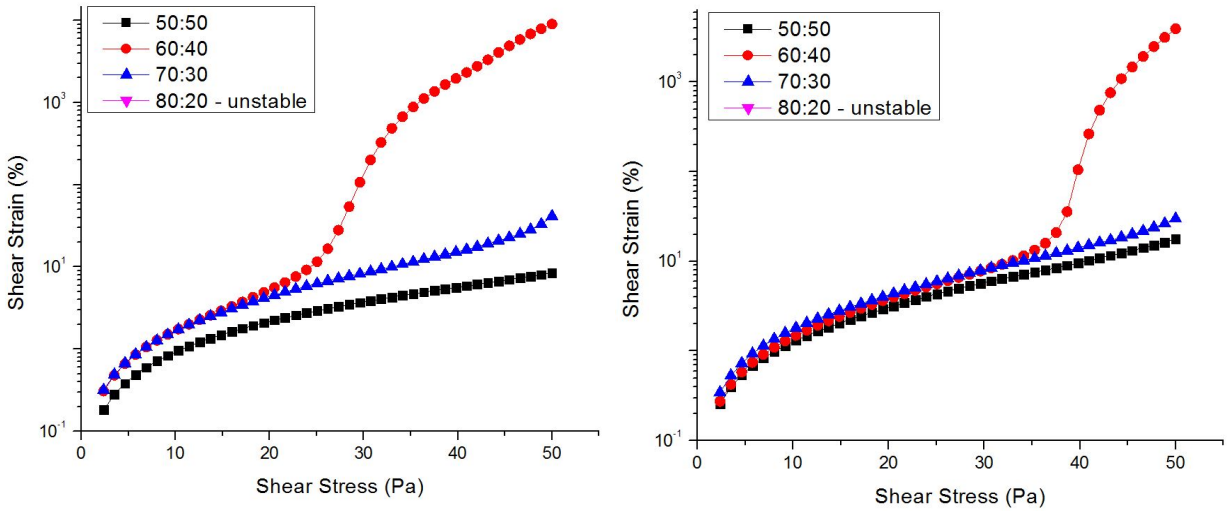

(a) Run 1

(b) Run 2

Figure 4.20. OCF S1: T = 25 °C, C_{surf} = 3 wt.%.

Bentonite contribution to the internal structure of the samples of both OCF S1 and OCF S2 decreases with increasing O:W ratio. OCF S1 was observed to display an abnormal trend in its yield properties, with the yield of the sample at 60:40 O:W ratio. Further study is recommended to assess this behavior. OCF S2 on the other hand was observed to display a more normal trend in its yield properties with respect to O:W ratio. Depletion flocculation can possibly account for the instability of the OCF S1 at 80:20 O:W ratio (see Figures 2.28 and 2.29 in Section 2.3).

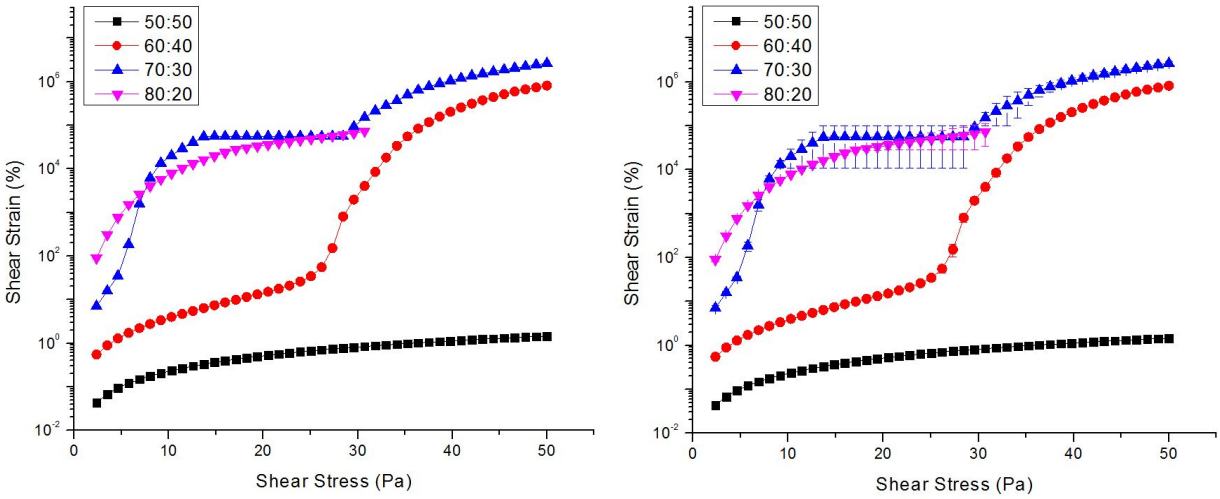

(a) Average Values (b) with Standard Deviation

Figure 4.21. OCF S2: T = 25 °C, C_{surf} = 3 wt.%.

4.2.3 Fluid loss

In this section the effect of the control variable O:W ratio on the performance variable fluid loss is investigated in the oil-base complex fluid samples: OCF S1 and OCF S2. Figure 4.22 shows the filtrate volumes of the different oil-base complex fluids at O:W ratios ranging from 50:50 to 80:20. Fluid loss in OCF S1 is observed to slightly increase with O:W ratio. The slight increase can be attributed to the increase in volume fraction of the oil continuous phase that facilitates fluid passage through the filter.

OCF S2 on the other hand, was equally found to show a slight increase in fluid loss with increasing O:W ratio as a result of the increase of the volume fraction of the oil continuous phase and decrease in bentonite amount. Holistically, no significant effect of O:W ratio was seen for either type of OCF. It should further be noted this was not a study but a single test, thus further investigation is recommended.

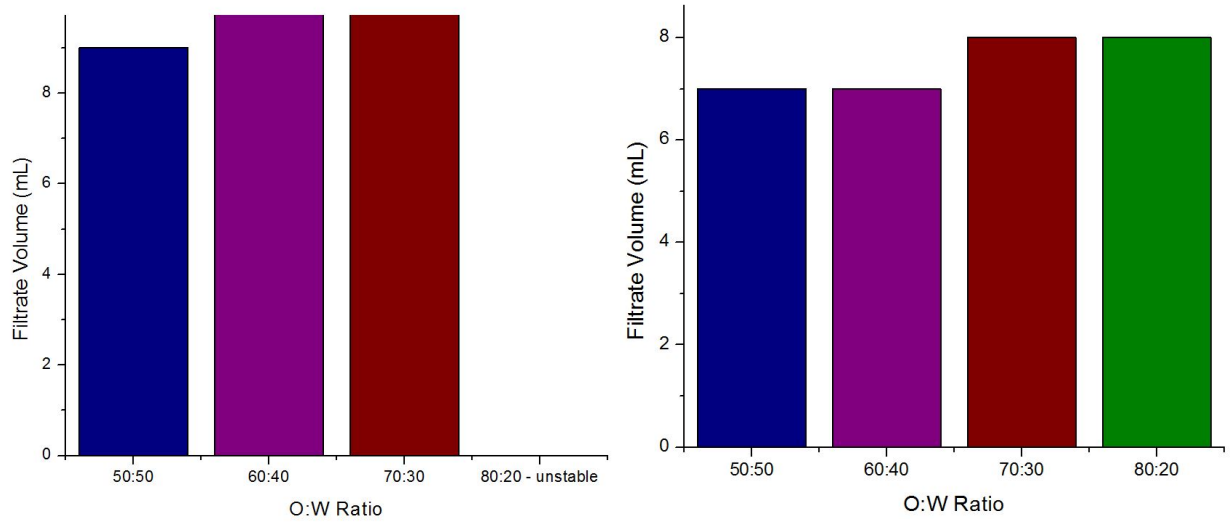

(a) OCF S1 (b) OCF S2

Figure 4.22. O:W Ratio Effect, T = 25 °C, C_{surf} = 3 wt.%.

4.2.4 Stability

In this section the effect of the control variable O:W ratio on the performance variable stability is investigated in the oil-base complex fluid samples: OCF S1 and OCF S2. Table 4.2 shows the electrical stability of the oil-base complex fluids as a function of O:W ratio. It can be seen that the stability of the samples increases with O:W ratio, which is an expected trend given that the higher is the dispersed phase volume fraction, the greater is the probability of it to coalesce and demulsify. This trend can clearly be seen in OCF S2.

In the case of OCF S1 however, additional parameters play an important role namely the CMC of its surfactant (Span 80). The very low CMC of Span 80, makes the concentration of micelles within the oil continuous medium greater with increasing O:W ratio. This implies the driving force bringing the dispersed droplets together increases with O:W ratio (see Figure 4.12), which explains the instability observed at 80:20 O:W ratio. Further study is however recommended as the analysis conducted was a test.

Table 4.2: Electrical Stability: 3 wt.% concentration

O:W Ratio	OCF S1 (volts)	OCF S2 (volts)
50:50	1	1
60:40	1	35
70:30	3	62
80:20	unstable	96

4.3 Effect of Temperature

4.3.1 Flow Curve

In this section the effect of the control variable temperature on the performance variable flow curve is investigated in the oil-base complex fluid samples: OCF S1 and OCF S2. Figures 4.23 to **??** show the flow curves of the oil-base complex fluid samples as a function of temperature at the maximum surfactant concentration of 3 wt.%. Included in Appendix A, are the flow curve measurements at all other O:W ratios and surfactant concentrations.

At 50:50 O:W ratio, Figure 4.23, the flow behavior of OCF S1 can be seen to progressively move towards profiles with increasing and decreasing shear stresses with increasing temperatures (> 25 °C). The aforementioned is the result of wall slip. With temperature increase, thermal fluctuations of dispersed particles within the sample increases its heterogeneity in its internal structure (see Figure 2.51, causing it to have greater anisotropy in its flow curve properties).

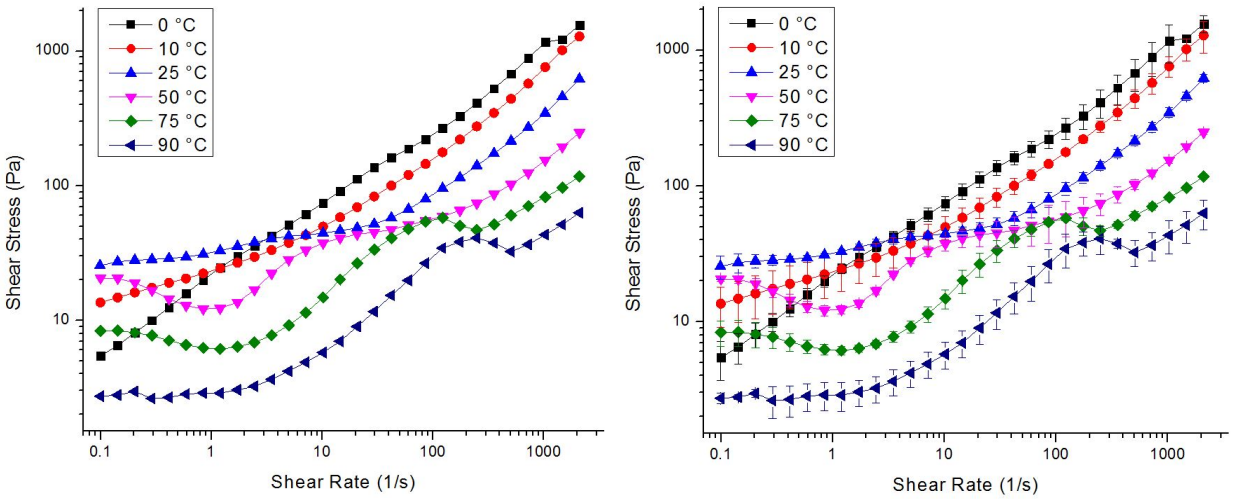

(a) Average Values (b) with Standard Deviation

Figure 4.23. OCF S1: O:W Ratio = 50:50, C_{surf} = 3 wt.%.

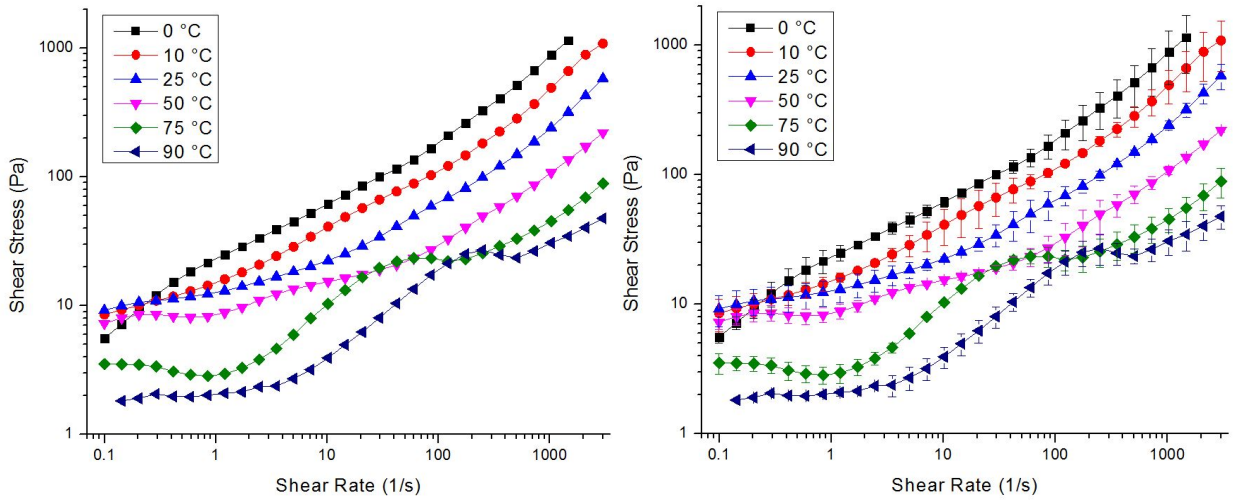

(a) Average Values (b) with Standard Deviation

Figure 4.24. OCF S1: O:W Ratio = 60:40, C_{surf} = 3 wt.%.

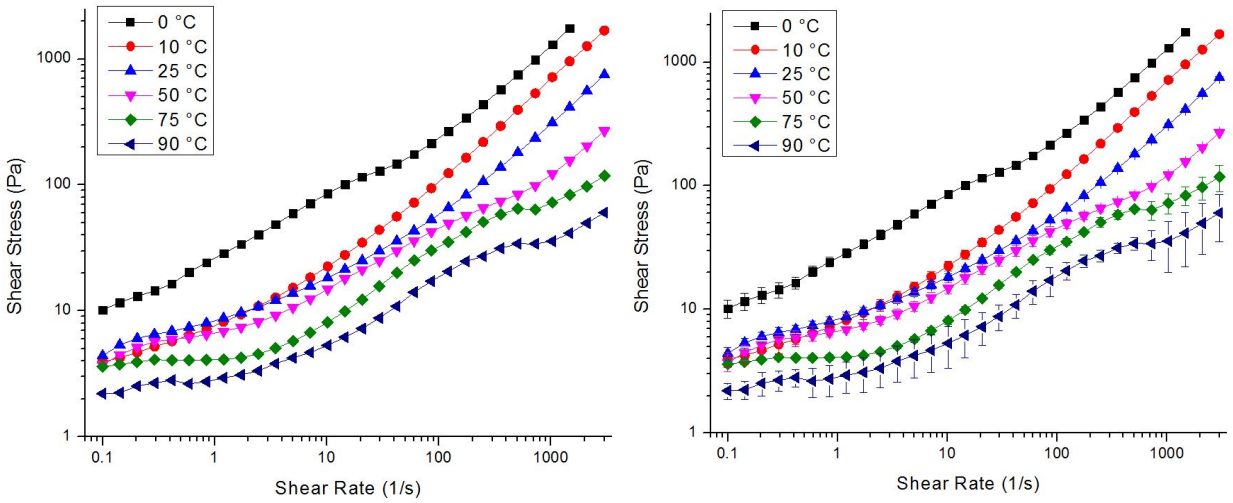

(a) Average Values (b) with Standard Deviation

Figure 4.25. OCF S1: O:W Ratio = 70:30, C_{surf} = 3 wt.%.

With increasing O:W ratio, the amount of dispersed particles (droplets, bentonite) decreases reducing the level of heterogeneity of the sample's internal structure. This explains the less pronounced level of decreasing and increasing shear stress profiles observed at 70:30 O:W ratio, Figure 4.25. It can further be seen that with increasing O:W ratio, there is a reduced level of intersection of the flow curves, Figures 4.23 to 4.25. As a recall, OCF S1 was found to be unstable at 80:20 O:W ratio following the 24 hr observation time.

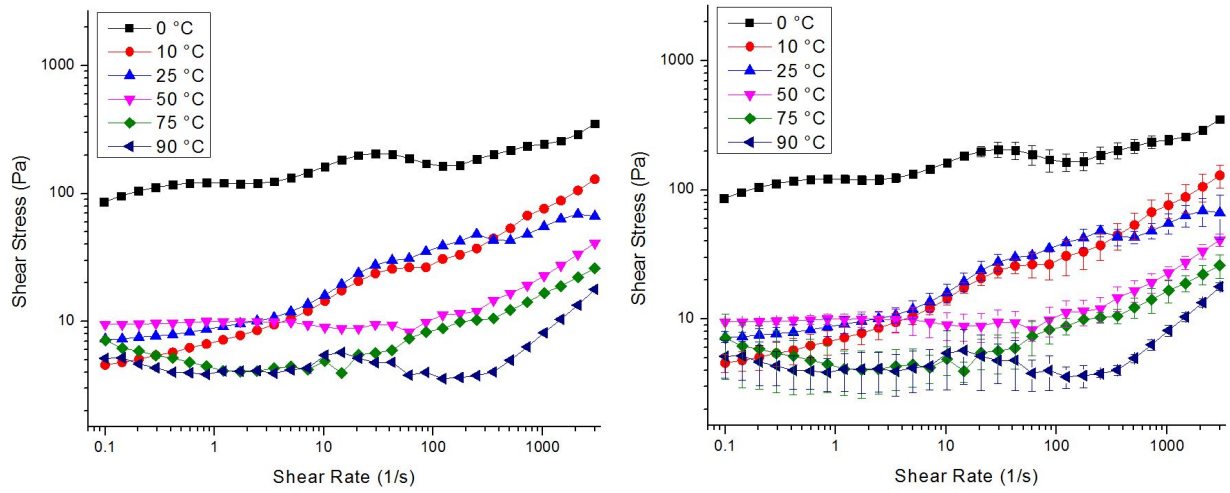

(a) Average Values (b) with Standard Deviation

Figure 4.26. OCF S2: O:W Ratio = 50:50, C_{surf} = 3 wt.%.

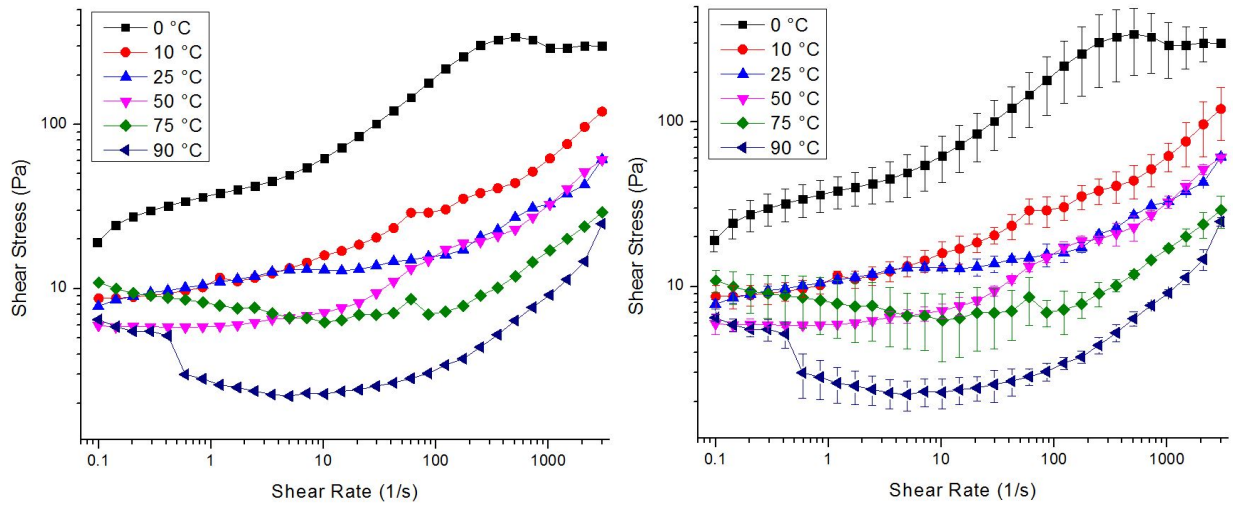

(a) Average Values (b) with Standard Deviation

Figure 4.27. OCF S2: O:W Ratio = 60:40, C_{surf} = 3 wt.%.

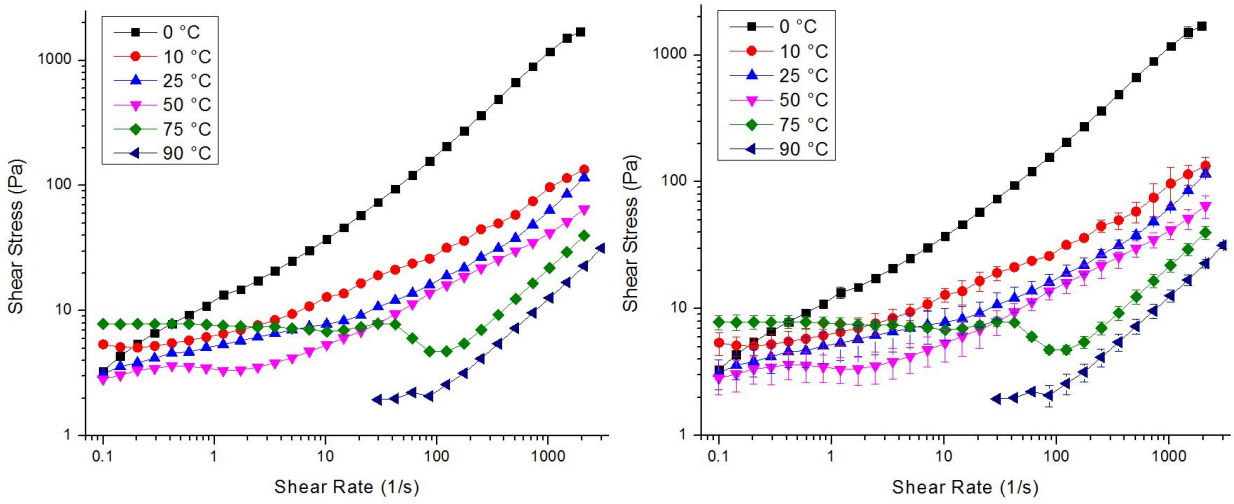

(a) Average Values (b) with Standard Deviation

Figure 4.28. OCF S2: O:W Ratio = 70:30, C_{surf} = 3 wt.%.

Figures 4.26 to **??** show the flow curves of OCF S2 at O:W ratios of 50:50 to 70:30. An identical trend to that of OCF S1 at 50:50 O:W ratio can be observed in OCF S2, Figure 4.26, where shear stress is observed to decrease and increase indicating wall slip. The main difference however, is that this profile can be seen at temperatures as low as 0 °C.

Here again, the lower dipole moment of the surfactant component of OCF S2 (Brij 93) and its higher CMC account for the larger level of heterogeneity in the sample microstruc-

ture. With increasing O:W ratios and with surfactant concentration remaining constant, higher structure homogeneity of the sample accounts for the absence of slip in the flow curve of OCF S2 with increasing O:W ratio despite increasing temperatures.

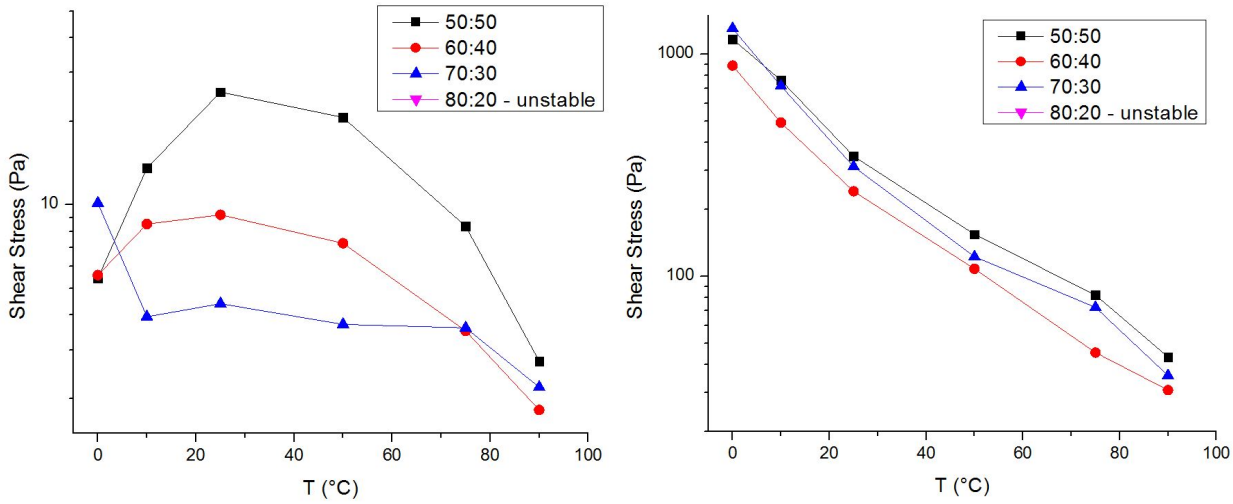

(a) 0.1 s^{-1} (b) 1,000 s^{-1}

Figure 4.29. OCF S1: C_{surf} = 3 wt.%.

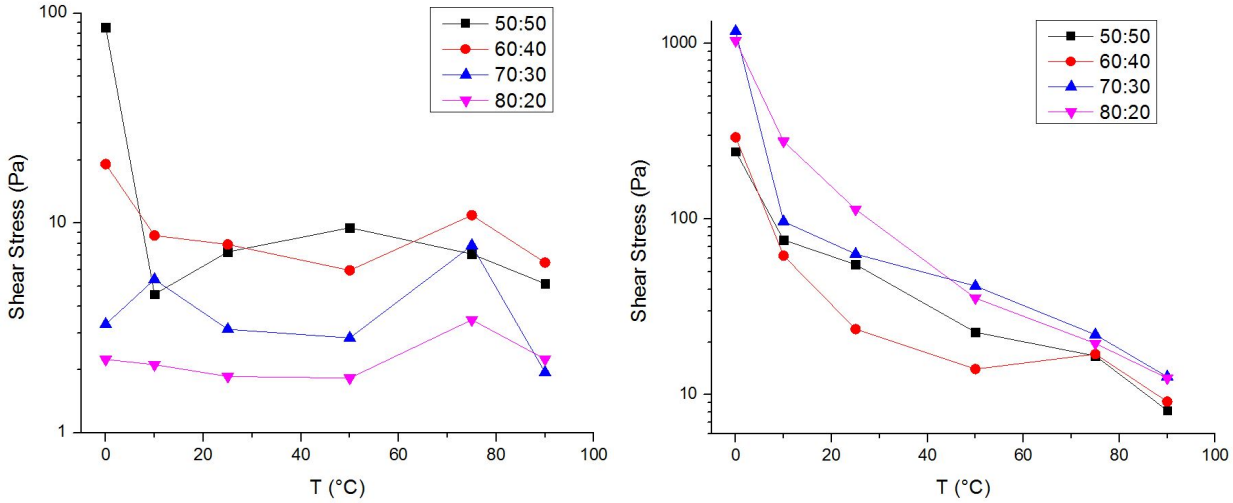

(a) 0.1 s^{-1} (b) 1,000 s^{-1}

Figure 4.30. OCF S2: C_{surf} = 3 wt.%.

Figures 4.29 and 4.30 show the shear stress of the OCF fluid samples at 0.1 and 1,000 s^{-1}. At the high shear rate, both types of complex fluids, OCF S1 and OCF S2, can be seen to show a decrease in shear stress with increasing temperature. The aforementioned

is driven by the decrease in apparent viscosity of the fluid with increasing temperature at elevated shear rates. At low shear rate however, 0.1 s^{-1}, no distinct trend can be observed particularly at low O:W ratios. Further study is thus required to assess the contribution of other phenomena on the abnormal trend observed at low shear rates.

4.3.2 Yield Stress

In this section the effect of the control variable temperature on the performance variable yield stress is investigated in the oil-base complex fluid samples: OCF S1 and OCF S2. The effect of temperature on the yield properties of the oil-base complex fluids is illustrated in Figures 4.31 to 4.36. Included in Appendix A are the stress sweep measurements at all other O:W ratios and surfactant concentrations. At 50:50 O:W ratio, Figure 4.31, OCF S1 is observed to display high structuration (ability to support or transmit loads) at all temperatures. The aforementioned is driven by the contributions of bentonite (viscosifier) and emulsification to its internal structure.

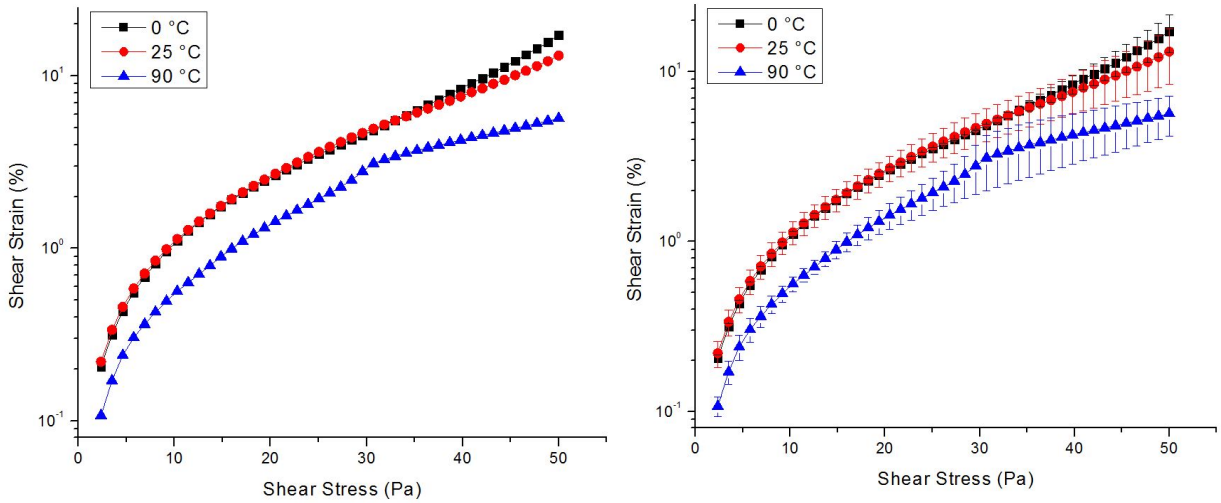

(a) Average Values (b) with Standard Deviation

Figure 4.31. OCF S1: O:W Ratio = 50:50, C_{surf} = 3 wt.%.

With increasing O:W ratio, depletion flocculation is observed to possibly contribute to the elastic properties of the sample (see Figures 2.27 to 2.29 in Chapter 2). This can

be seen at 60:40 and 70:30 O:W ratios (Figures 4.32 and 4.33), where OCF S1 yields at low but not high temperatures. The thickening of the sample as a result of floccualtion of bentonite particles which is enhanced at high temperatures, can plausibly be another contributing factor to the non-yielding behavior observed at elevated temperatures.

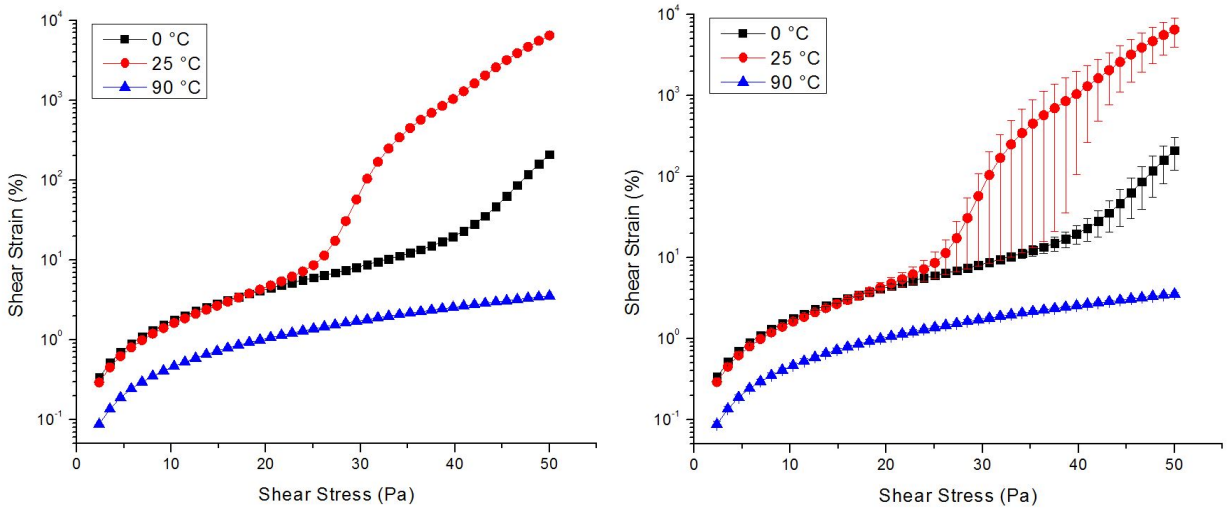

(a) Average Values (b) with Standard Deviation

Figure 4.32. OCF S1: O:W Ratio = 60:40, C_{surf} = 3 wt.%.

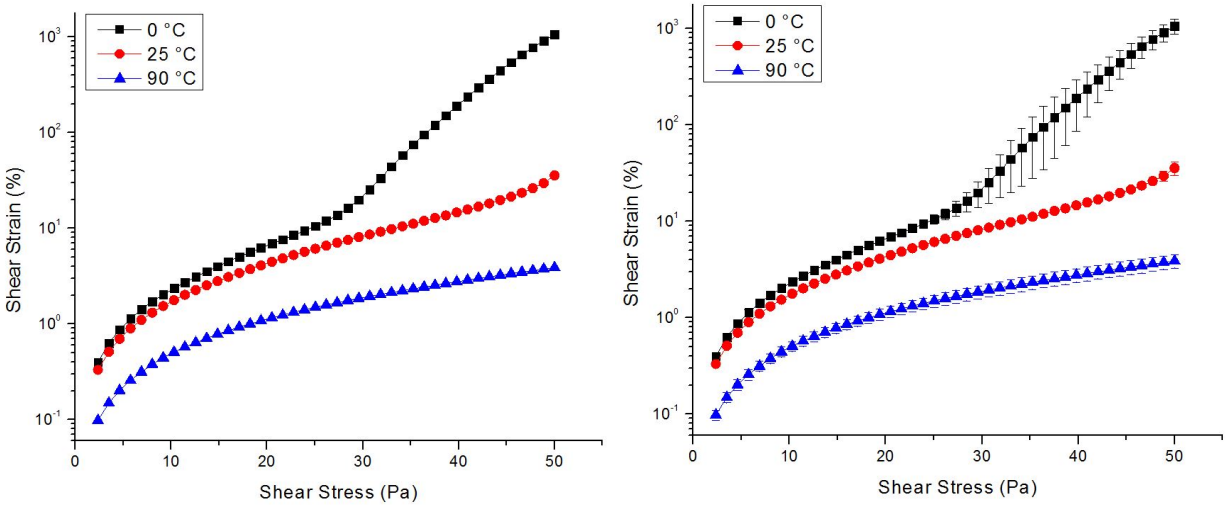

(a) Average Values (b) with Standard Deviation

Figure 4.33. OCF S1: O:W Ratio = 70:30, C_{surf} = 3 wt.%.

At 50:50 O:W ratio, Figure 4.34, a behavior similar to that of OCF S1 can be observed for OCF S2. The absence of yield in this case however is to a larger extent attributed to the

greater interaction between bentonite particles. With increasing temperatures, this interaction becomes more important due to the greater aggregation of the bentonite particles.

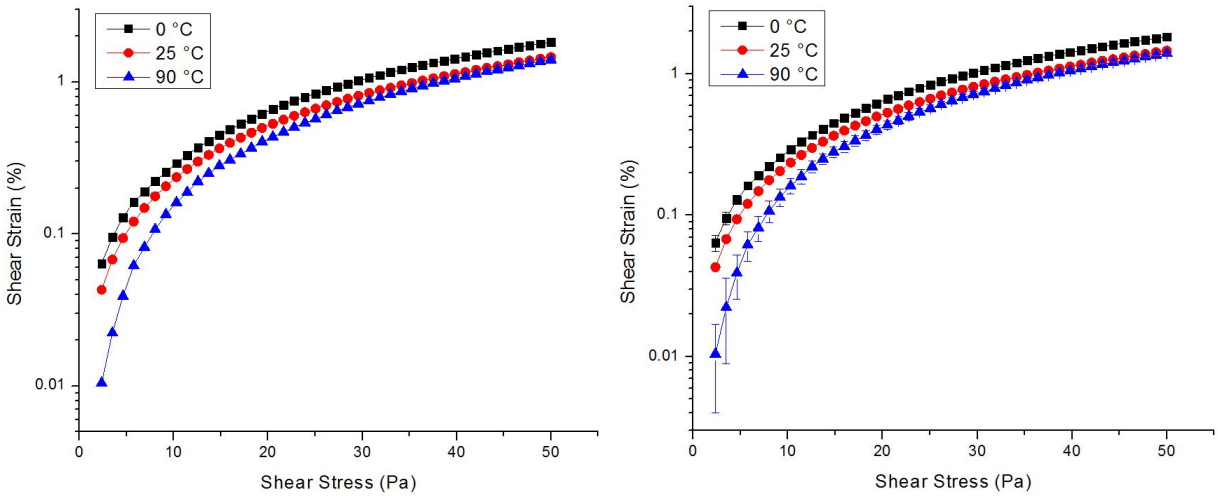

(a) Average Values (b) with Standard Deviation

Figure 4.34. OCF S2: O:W Ratio = 50:50, C_{surf} = 3 wt.%.

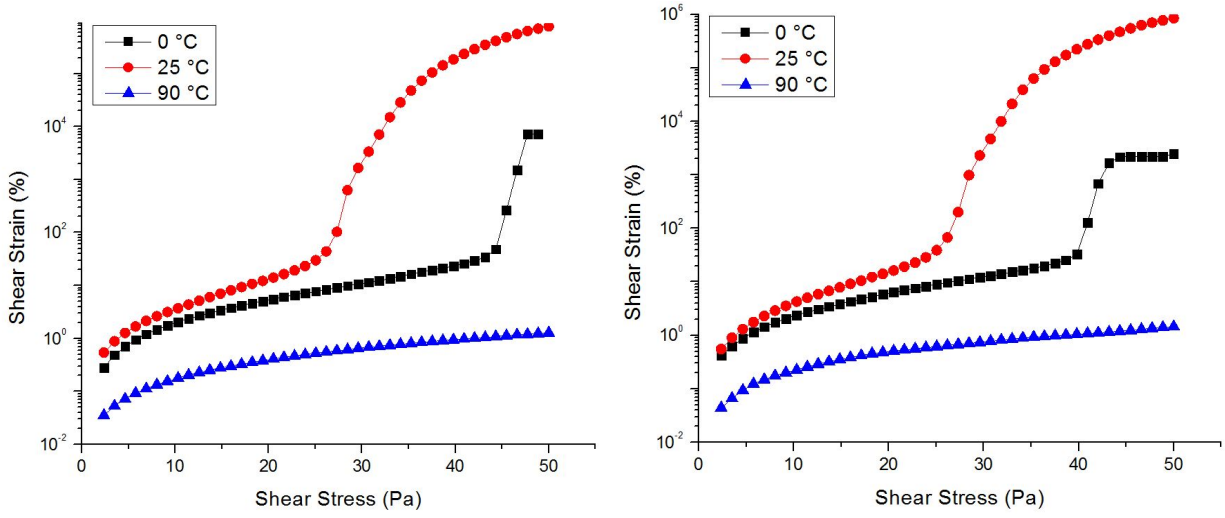

(a) Run 1 (b) Run 2

Figure 4.35. OCF S2: O:W Ratio = 60:40, C_{surf} = 3 wt.%.

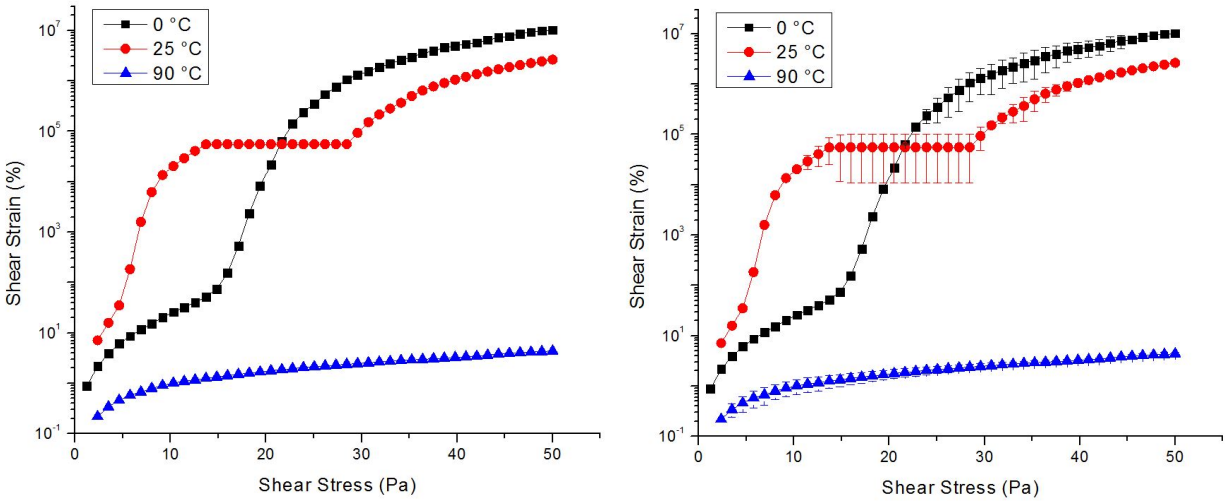

(a) Average Values (b) with Standard Deviation

Figure 4.36. OCF S2: O:W Ratio = 70:30, C_{surf} = 3 wt.%.

This aggregation has been reported in literature to lead to an increase in yield stress in bentonite dispersions [120]. This explains the increase in elastic properties of OCF S2 at elevated temperatures, Figures 4.34 to 4.36. It is important to recall that the lower dipole moment and higher CMC of the surfactant component (Brij 93) of OCF S2 allows greater interaction between bentonite particles as opposed to OCF S1.

4.3.3 Stability

In this section the effect of the control variable temperature on the performance variable stability is investigated in the oil-base complex fluid samples: OCF S1 and OCF S2. Figures 4.37 and 4.38 show the variation in the microstructure of the oil-base complex fluid samples with temperature. Included are the microstructure images of the samples at 25, 75 and 90 °C, the temperature variation they were subjected to was ramped from 25 °C → 0 °C → 10 °C → 50 °C → 75 °C → 90 °C. Included in Appendix A, are the microstructure images of the samples at all temperatures and O:W ratios.

Exemplified at 60:40 O:W ratio, Figures 4.37 and 4.38, are the microstructure images of OCF S1 and OCF S2. They were both observed to remain stable till 90 °C where ultimately

demulsification of the samples occurred. This is particularly noticeable in OCF S1, where the flocculation and coalescence of the dispersed droplets is driven by their greater kinetic energy.

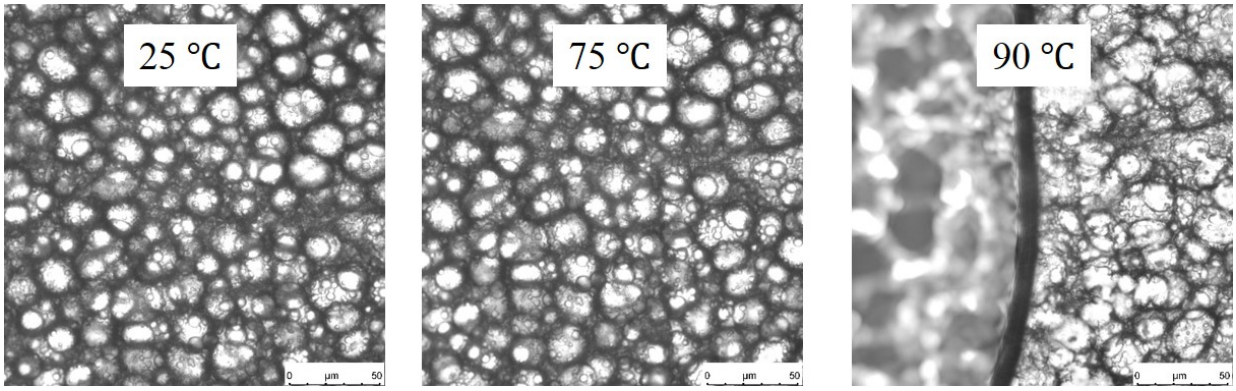

Figure 4.37. OCF S1: O:W Ratio = 60:40, C_{surf} = 3 wt.%.

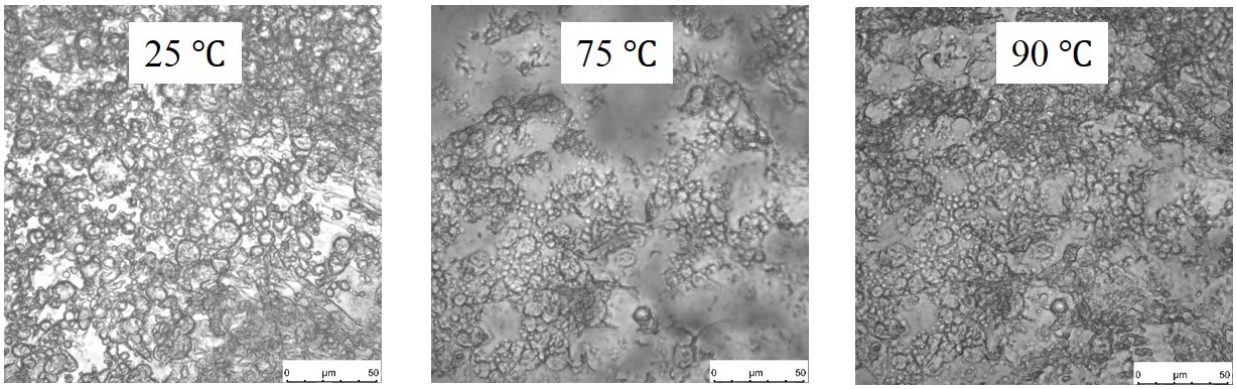

Figure 4.38. OCF S2: O:W Ratio = 60:40, C_{surf} = 3 wt.%.

Thermal instability in OCF S2 is less pronounced as is showed by its microstructure at 90 °C, Figure 4.38. This is because of the greater contribution of bentonite particles to its stability. To recall, linkage of bentonite particles is more significant in OCF S2 due to the lower dipole moment of its surfactant component. This particular O:W ratio was chosen to illustrate the effect of temperature on stability of oil-base complex fluids because of the higher clarity of the images.

4.4 Phase Inversion

4.4.1 Oil-base Complex Fluids

In this section the effect of the control variables O:W ratio and temperature on the performance variable phase inversion is investigated in the oil-base complex fluid samples: OCF S1 and OCF S2. Figures 4.39 and 4.40 show the effect of O:W ratio on catastrophic and transitional phase inversion on oil-base complex fluids at the maximum surfactant concentration of 3 wt.%. OCF S1 was found invert to a water-base complex fluid between 50 - 60 vol.% of water at all O:W ratios, Figure 4.39a. Inversion to a water-base complex fluid was indicated by a significant change of slope of conductivity with respect to water fraction.

The relative constant value of OCF S1 following inversion to a water-complex fluid is due to the very low CMC of its surfactant component, which translates to a very high concentration of surfactant molecules (and micelles) that saturate the aqueous medium. Following catastrophic phase inversion (CPI), the now water-base complex fluid was subjected to temperatures ranging from 0 - 100 °C, Figure 4.39b, to assess transitional phase inversion (TPI).

The conductivity profile shown by the sample was indicative of the occurrence of temperature induced phase inversion (TIPI), though not at a significant level at temperatures < 50 °C as is reflected by the instances of conductivity increase. TIPI was observed to be pronounced at temperatures > 70 °C. It should be noted that the O:W ratio in the legend of Figure 4.39b is that of samples before CPI.

Shown in Figure 4.40 is the phase inversion behavior of OCF S2. Similar to OCF S1, OCF S2 was observed to invert catastrophically to a water-base complex fluid at water volume fractions between 50 - 60 vol.%. The change of slope of conductivity with respect to water fraction indicative of phase inversion was however different from that of OCF S1, as shown in Figure 4.40a. This is due to the higher CMC of Brij 93 of OCF S2, thereby saturating the water continuous medium following inversion to a lesser degree.

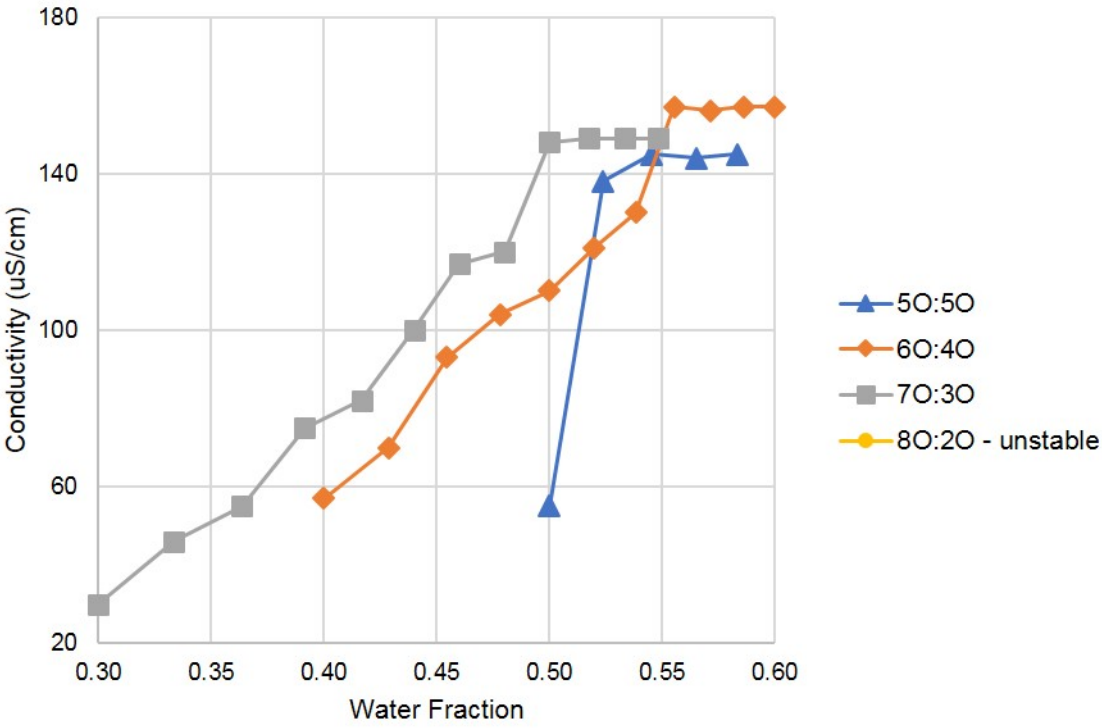

(a) Catastrophic

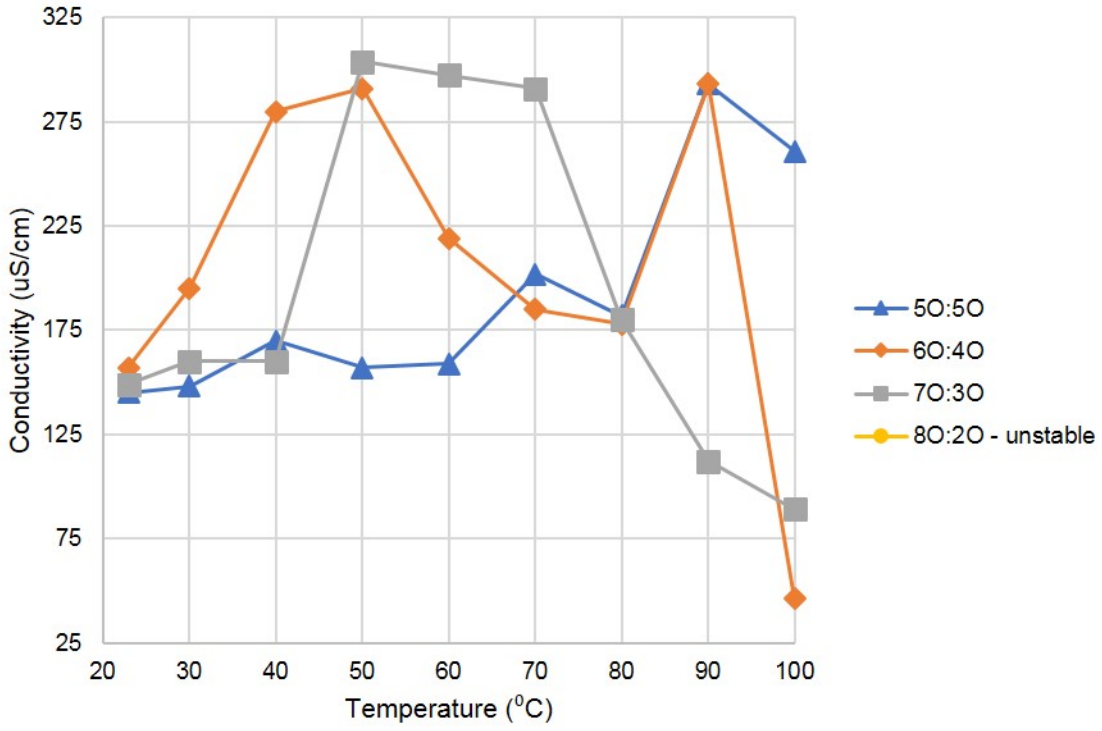

(b) Transitional

Figure 4.39. OCF S1 - Phase inversion, C_{surf} = 3 wt.%.

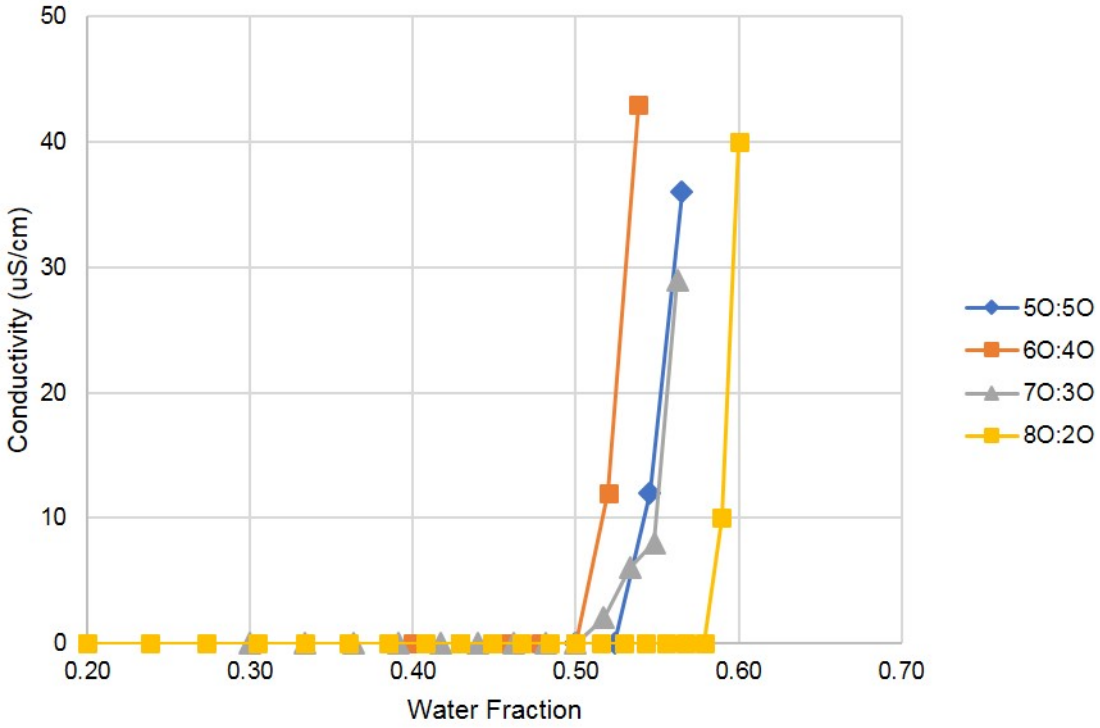

(a) Catastrophic

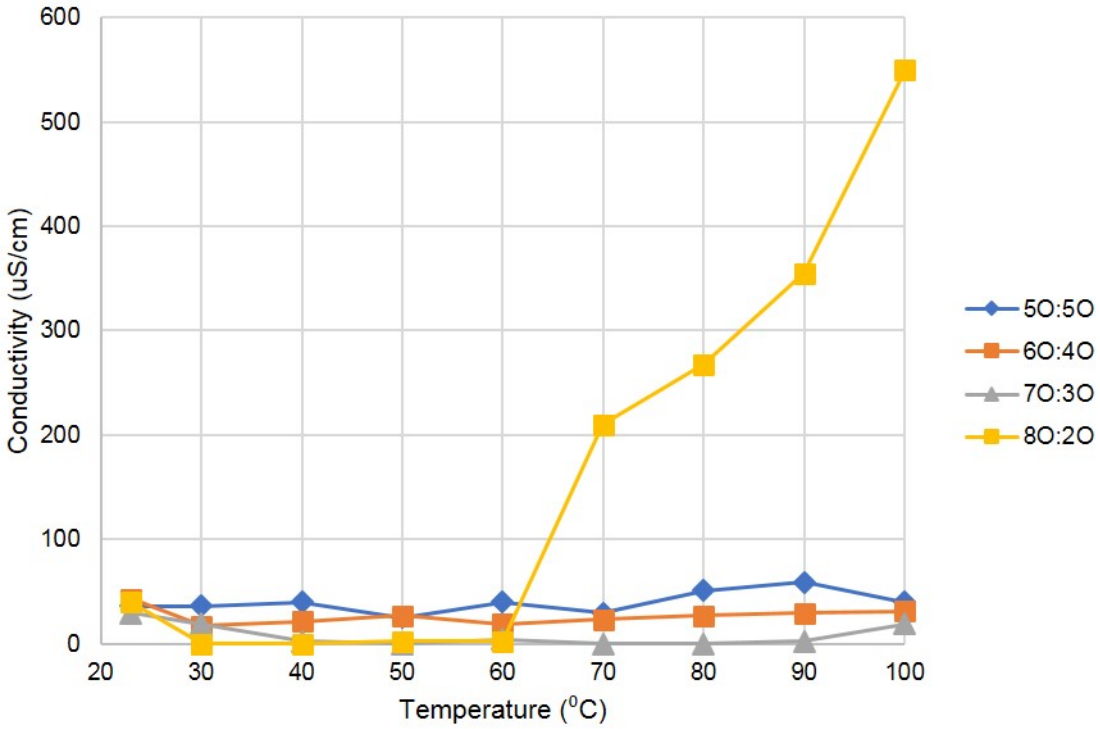

(b) Transitional

Figure 4.40. OCF S1 - Phase inversion, C_{surf} = 3 wt.%.

Following CPI, a trend in TPI identical to that of OCF S1 was displayed by OCF S2, Figure 4.40b. Shown in Figure 4.41 is the same figure without the 80:20 O:W ratio for a better visualization of the conductivity variation with temperature at lower (initial) O:W ratios. Following inversion to a water-base complex fluid, OCF S2 was observed to undergo TIPI as is indicated by instances of conductivity decrease at 50:50 and 60:40 O:W ratios.

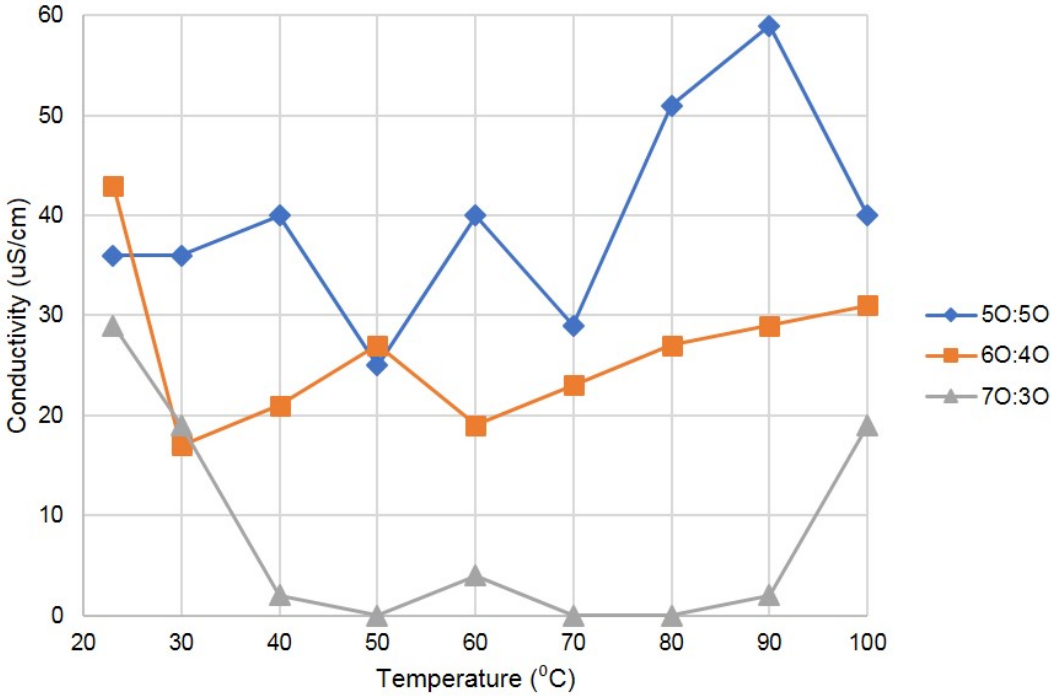

Figure 4.41. OCF S2 - Transitional phase inversion, C_{surf} = 3 wt.%.

Significant TIPI can be seen at 70:30 O:W ratio, as shown by the drastic drop and relative constant conductivity observed. The substantial increase in conductivity displayed by the sample at 80:20 O:W ratio, Figure 4.40, at around 60 °C is due to the phase separation (demulsification) of the sample.

4.4.2 Water-base Complex Fluids

In this section the effect of the control variable polarity (HLB) on the performance variable phase inversion is investigated in the water-base complex fluid (WCF) samples. Phase inversion was observed only in the nonionic-stabilized WCF samples, which is in

agreement with literature [12][78][89]. Figures 4.42 and 4.43, respectively show the flow curves and microstructure of WCF M1 at 11.5 HLB as a function of temperature. A decrease in its apparent viscosity (shear stress) is observed with increasing temperature till 75 °C, where an increase in its low-shear viscosity occurs at 90 °C.

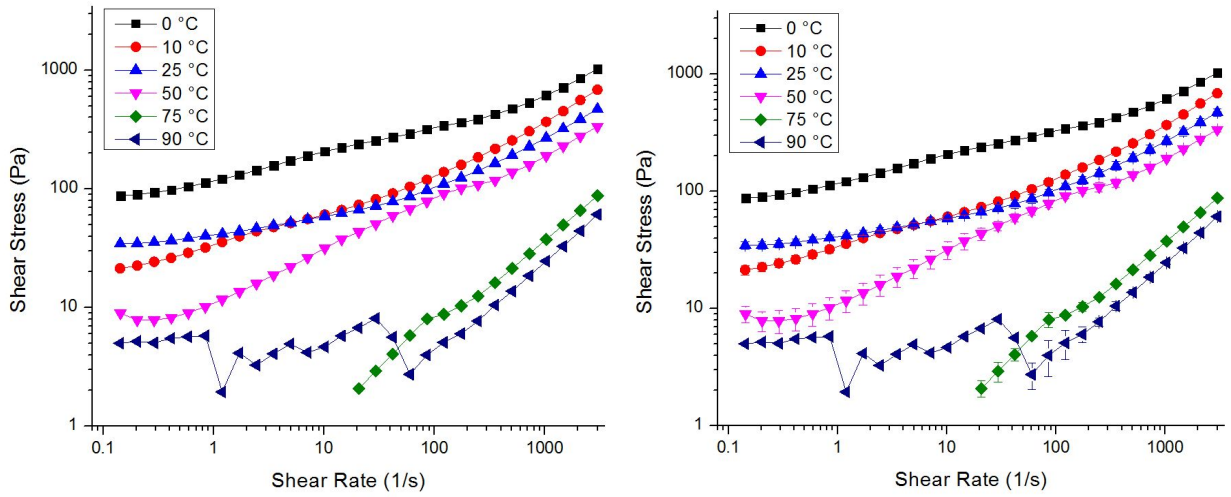

(a) Average Values (b) with Standard Deviation

Figure 4.42. WCF M1: O:W = 60:40, HLB = 11.5, C_{surf} = 3 wt.%.

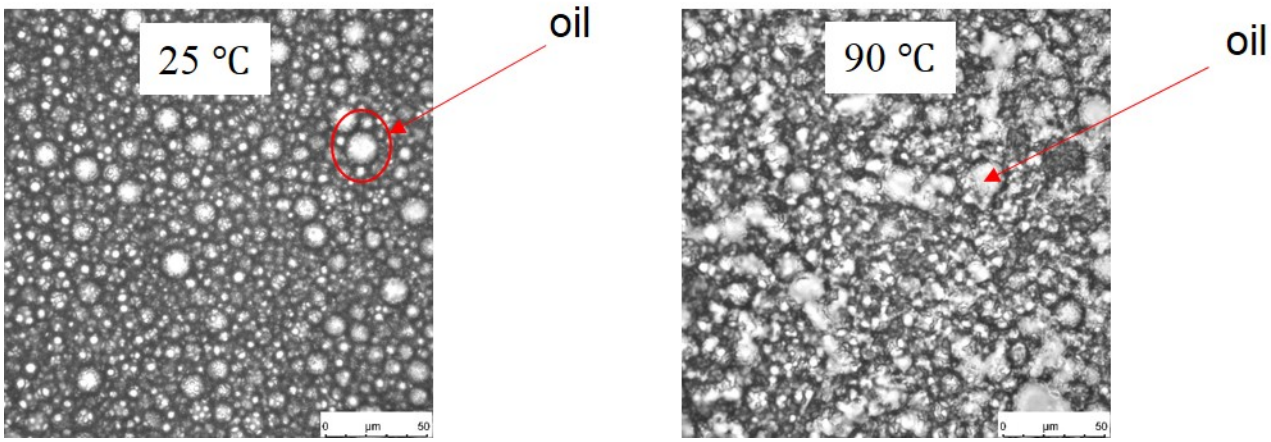

Figure 4.43. WCF M1: O:W = 60:40, HLB = 11.5, C_{surf} = 3 wt.% (63x lens).

The microstructure of the sample can be seen to change at 90 °C, as a result of phase inversion. As shown in the phase inversion schematic, Figure 4.44, at the phase inversion temperature (PIT) the droplets in the emulsion breakdown due to ultralow interfacial tension leading to the formation of a bicontinuous phase. This explains the microstructure

of WCF M1 at 90 °C. Thus, phase inversion as a result of temperature was shown to occur in nonionic-stabilized water-base complex fluids.

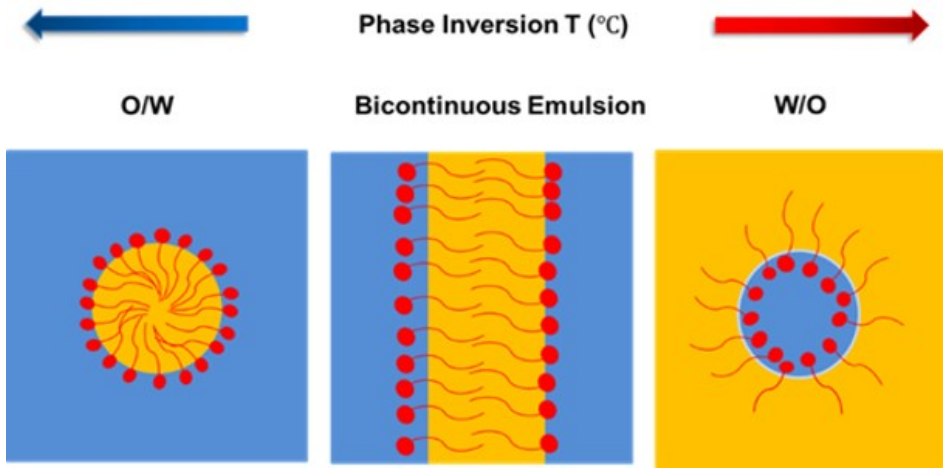

Figure 4.44. Phase inversion process [78].

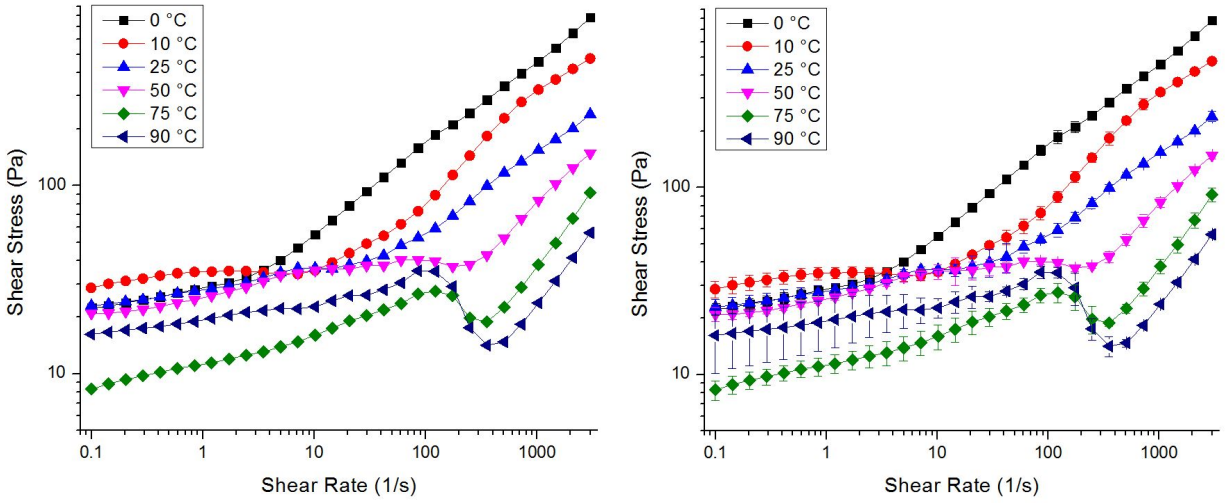

(a) Average Values

(b) with Standard Deviation

Figure 4.45. Phase Inversion - WCF M1: O:W = 60:40, HLB = 7.5, C_{surf} = 3 wt.%.

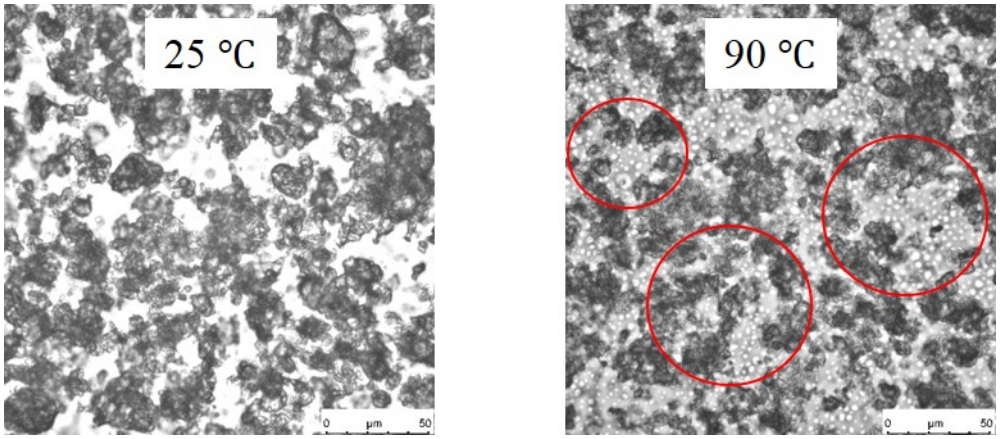

Figure 4.46. WCF M1: O:W = 60:40, HLB = 7.5, C_{surf} = 3 wt.% (63x lens).

A dependence of phase inversion on HLB was also found, which showed a consistent trend to phase inversion studies for pure emulsion systems [89]. Figures 4.45 and 4.46 show the flow curve and microstructure, as function of temperature, of WCF M1 at the lower HLB of 7.5. The low shear rheology of the sample shows a buildup in apparent viscosity when temperature increases from 75 to 90 °C. The occurrence of phase inversion accounts for the observed increase.

Shown in Figure 4.46, is the formation of nano-sized water dispersed droplets at 90 °C. The large Laplace pressure of these droplets accounts for the change in rheology observed with temperature increase to 90 °C. The greater distinction of these droplets at 7.5 HLB as opposed to 11.5, can further be explained by the dependence of phase inversion on HLB, see Figure 2.38 in Chapter 2. Figure 4.47, shows the substantial buildup in the low-shear apparent viscosity of WCF M1 at 7.5 HLB as a result of phase inversion.

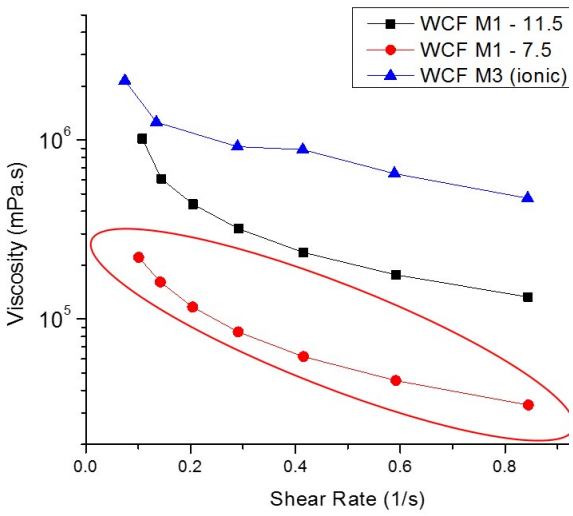

(a) 0 °C

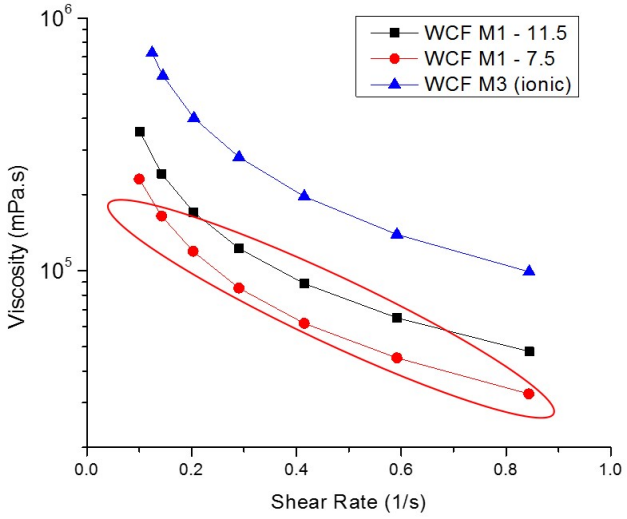

(b) 25 °C

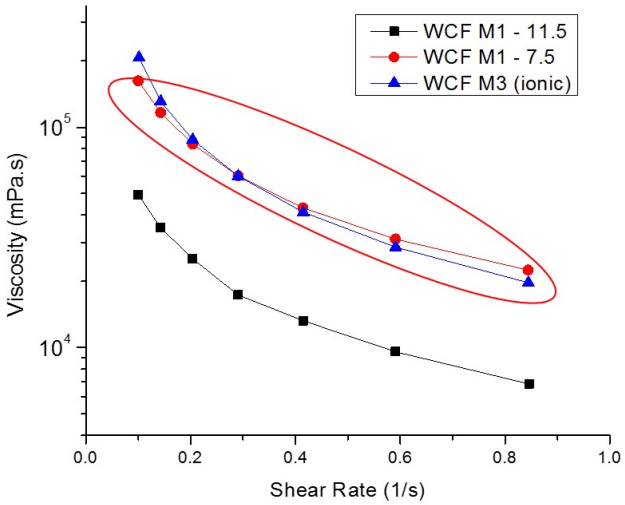

(c) 90 °C

Figure 4.47. Low-shear viscosity: O:W = 60:40, C_{surf} = 3 wt.%.

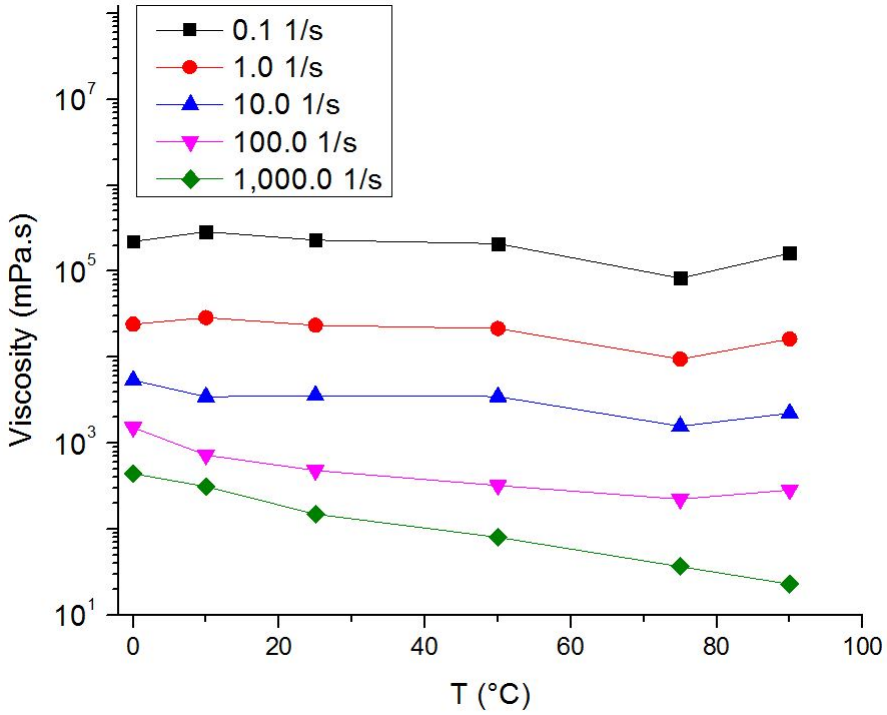

Figure 4.48. WCF M1: HLB = 7.5, O:W = 60:40, C_{surf} = 3 wt.%.

Figure 4.48 shows the variation of the apparent viscosity of WCF M1 (7.5 HLB) as a function of temperature at different shear rates. It can be seen that the increase in apparent viscosity following phase inversion is most noticeable at $\dot{\gamma} < 100$ s^{-1}. At higher shear rates, the breakdown of the complex fluid's internal structure is more substantial that its structure buildup as a result of phase inversion.

Not all nonionic stabilized WCF samples were however found to undergo phase inversion. WCF samples stabilized by polyoxyethylene surfactants, M1 surfactants, displayed phase inversion which is in agreement with literature studies [78][89]. However M2 surfactant components were not observed to 'distinctly' display phase inversion.

The flow curves of WCF M2 at both 7.5 and 11.5 HLB, Figures 4.49 and 4.51, did not display any substantial build-up in apparent viscosity with increasing temperature. It should however be pointed out that the microstructure of WCF M2 at 7.5 HLB, Figure 4.52, appeared to show the formation of dispersed water droplets at high temperatures.

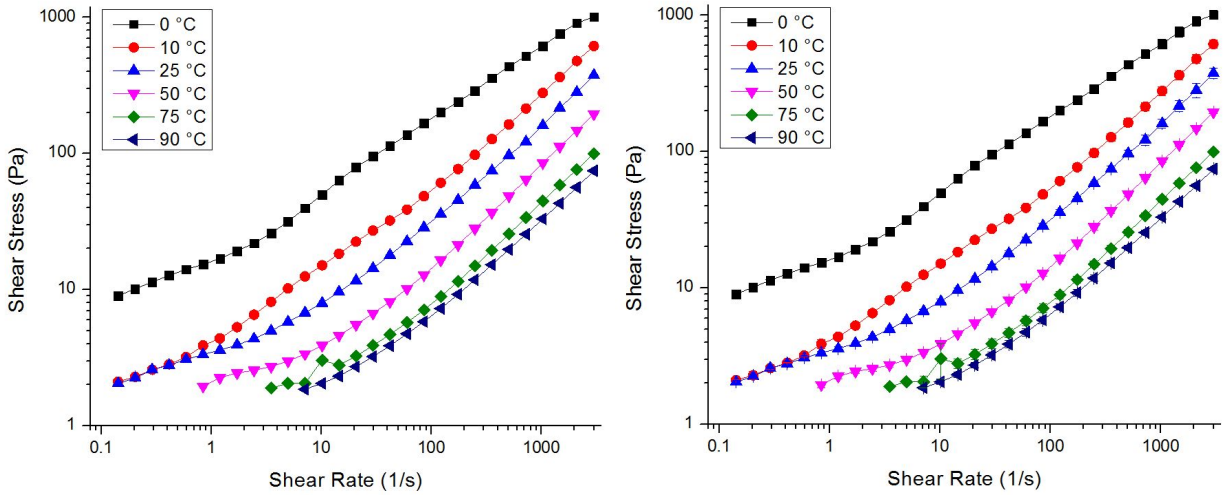

(a) Average Values (b) with Standard Deviation

Figure 4.49. WCF M2: O:W = 60:40, HLB = 11.5, C_{surf} = 3 wt.%.

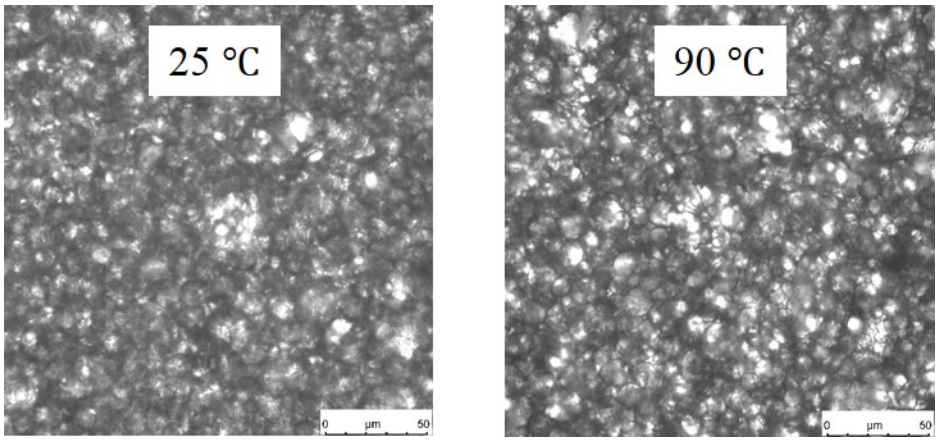

Figure 4.50. WCF M2: O:W = 60:40, HLB = 11.5, C_{surf} = 3 wt.% (63x lens).

Clear visualization of the microstructure variation of WCF M2 with temperature, Figures 4.50 and 4.52, was not possible with the 63x lens used with the heatable sample holder of the Leica DM6 microscope. The ionic stabilized WCF M3 was not observed to display phase inversion, Figure 4.54, confirming the phenomenon is peculiar to nonionic stabilized water-base complex fluids.

Figures 4.53 shows the flow curve of WCF M3 (ionic) as a function of temperature. The aforementioned was observed to display, for the most part, decreasing apparent viscosity with increasing temperatures driven by the decrease in viscosity of the liquid media. The

increase in apparent viscosity (shear stress) observed at 90 °C was driven by the 'further' aggregation of the already flocculated particles, which is consistent with literature studies of water-bentonite mixtures [120].

The enhanced aggregation of particles with temperature increase is driven by the greater Brownian motion of the particles, enhancing their collisions and linkage. This increase in aggregation of the bentonite particles due to their greater kinetic energy, ultimately leads to the instability (phase separation) of the sample as shown in Figure 4.54.

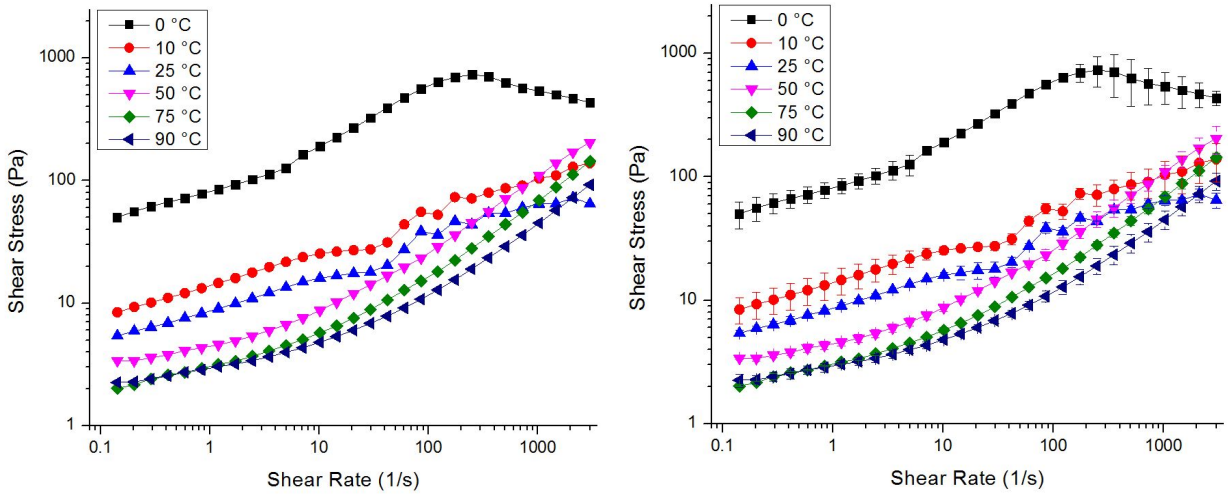

(a) Average Values (b) with Standard Deviation

Figure 4.51. WCF M2: O:W = 60:40, HLB = 7.5, C_{surf} = 3 wt.%.

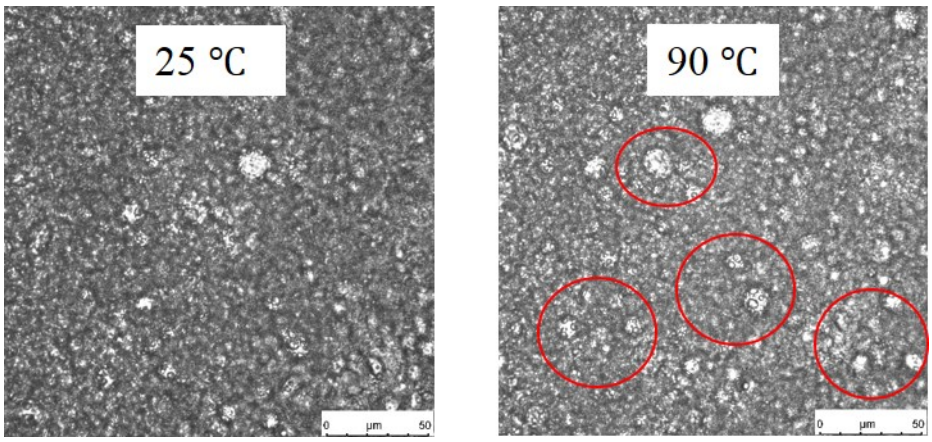

Figure 4.52. WCF M2: O:W = 60:40, HLB = 7.5, C_{surf} = 3 wt.% (63x lens).

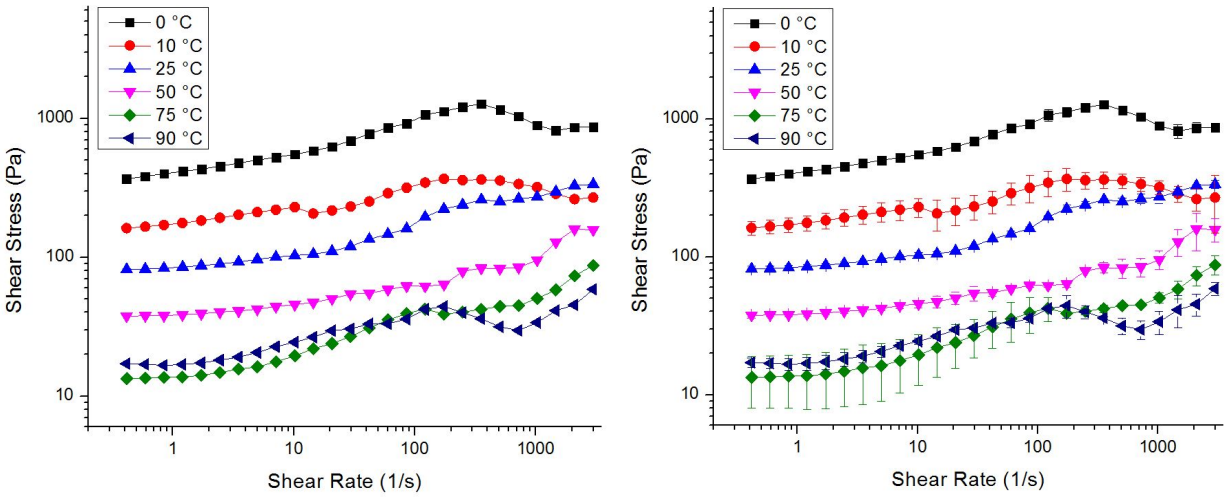

(a) Average Values (b) with Standard Deviation

Figure 4.53. WCF M3 (ionic): O:W = 60:40, HLB = 11.5, C_{surf} = 3 wt.%.

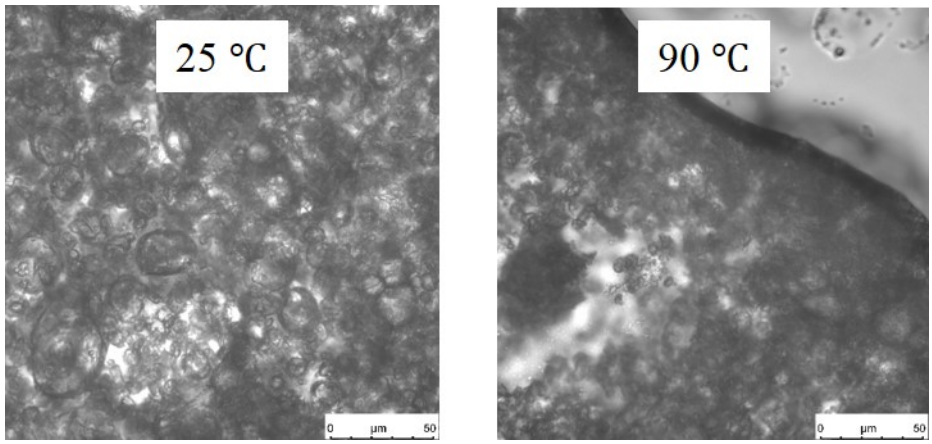

Figure 4.54. WCF M3 (ionic): O:W = 60:40, HLB = 11.5, C_{surf} = 3 wt.% (63x lens).

4.5 Drilling Muds

4.5.1 Flow Curve

In this section the effect of the control variable polarity (HLB) on the performance variable flow curve is investigated for the oil-based mud (OBM) samples. Figures 4.55 to 4.57 show the flow behavior of the oil-based mud OBM S1 at different temperatures and O:W ratios at the maximum surfactant concentration of 3 wt.%. The mud sample can be observed to display a smooth decrease in its shear stress profile with temperature increase

at any given O:W ratio. Wall slip in the form of decreasing shear stress is not observed except at 70:30 O:W ratio, Figure 4.57, at 0 and 90 °C.

This otherwise slip-free flow curve profile can be explained by its homogeneous microstructure as shown in Figure 4.58. Thus, the presence of fluid loss reducer (duratone) and weight additive (barite) components in presence of Span 80 (S1) surfactant contributes in reducing the anisotropy in the mechanical properties of the sample.

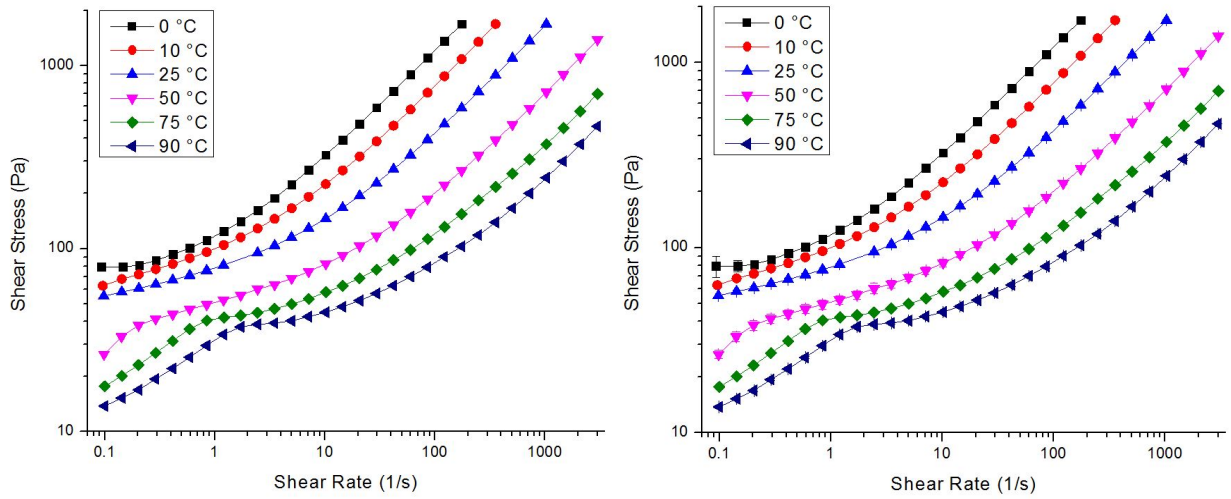

(a) Average Values (b) with Standard Deviation

Figure 4.55. OBM S1: O:W = 50:50, C_{surf} = 3 wt.%.

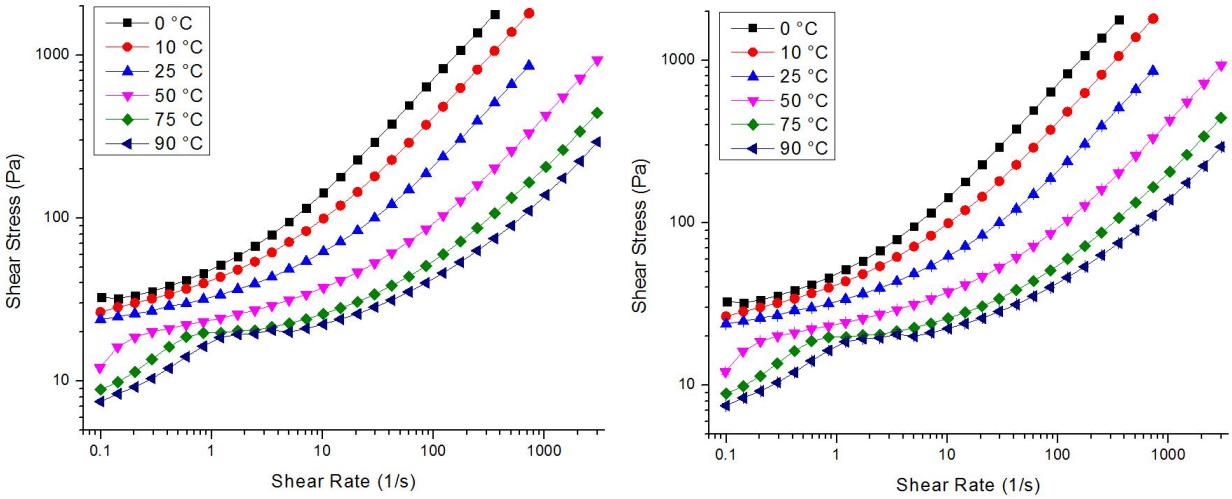

(a) Average Values (b) with Standard Deviation

Figure 4.56. OBM S1: O:W = 60:40, C_{surf} = 3 wt.%.

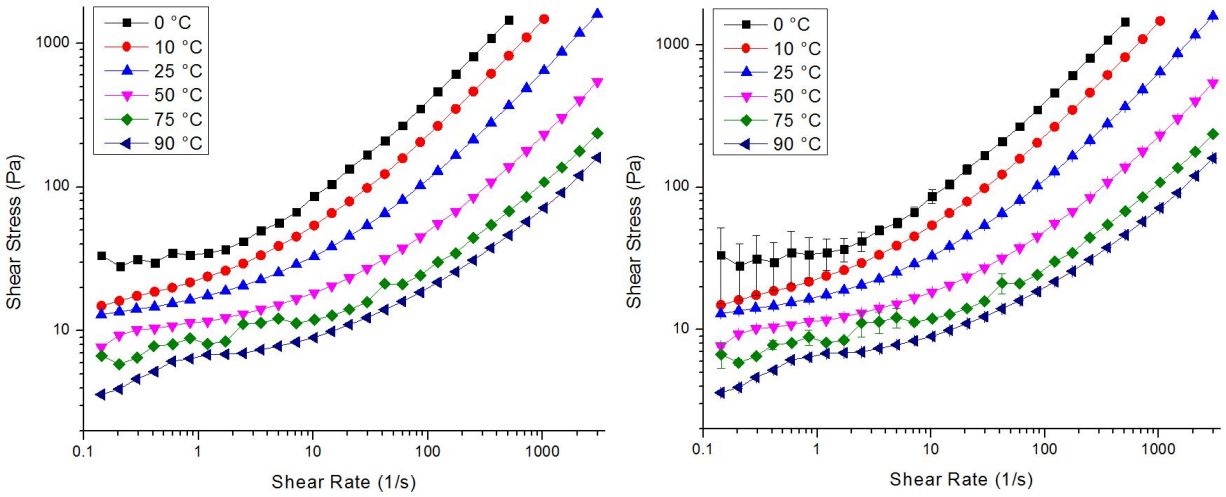

(a) Average Values (b) with Standard Deviation

Figure 4.57. OBM S1: O:W = 70:30, C_{surf} = 3 wt.%.

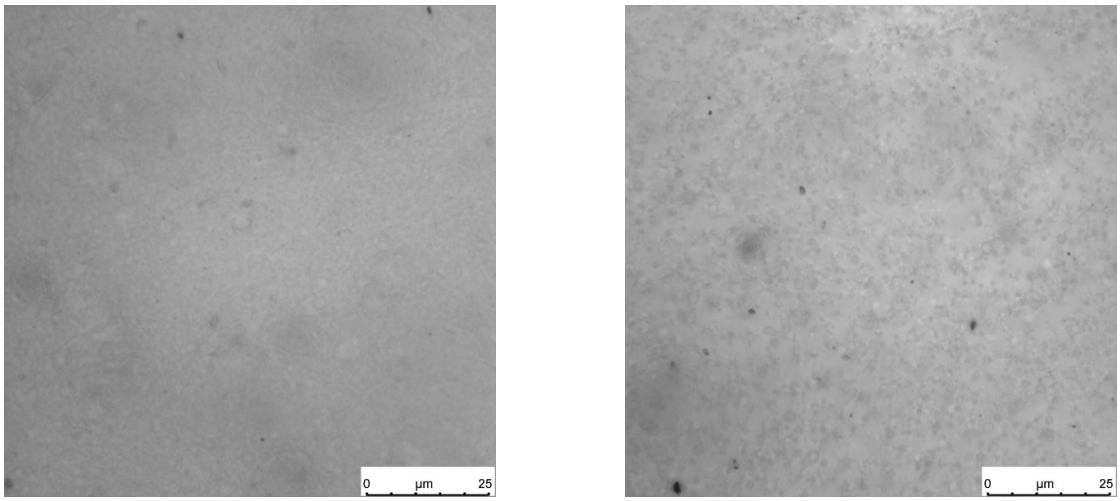

(a) O:W = 50:50 (b) O:W = 70:30

Figure 4.58. OBM S1: T = 25 °C, C_{surf} = 3 wt.%.

This was however observed to not be the case for the oil-base mud sample OBM S2. Figures 4.59 to 4.61 show the flow curves of OBM S2 at different temperatures and O:W ratios at the maximum surfactant concentration of 3 wt.%. OBM S2 can be seen to display a drastic difference in its flow behavior in comparison to OBM S1. At 50:50 O:W ratio, Figure 4.59, significant slip can be seen at almost all temperatures, particularly at 0 °C. As discussed in Section 4.1, surfactants having different dipole moments (polarity) and CMCs

define the end structure of non-Newtonian fluids differently.

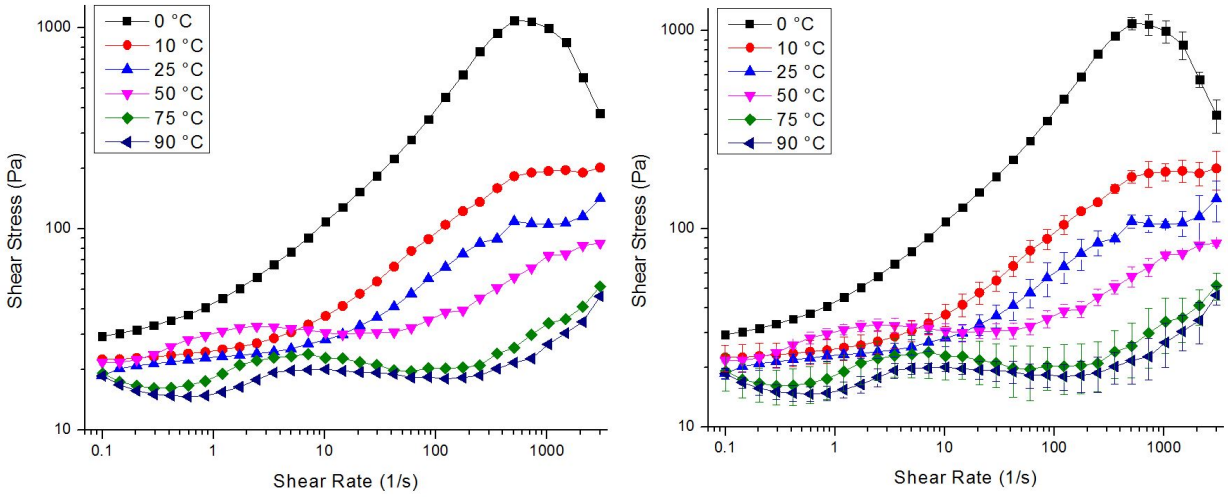

(a) Average Values (b) with Standard Deviation

Figure 4.59. OBM S2: O:W = 50:50, C_{surf} = 3 wt.%.

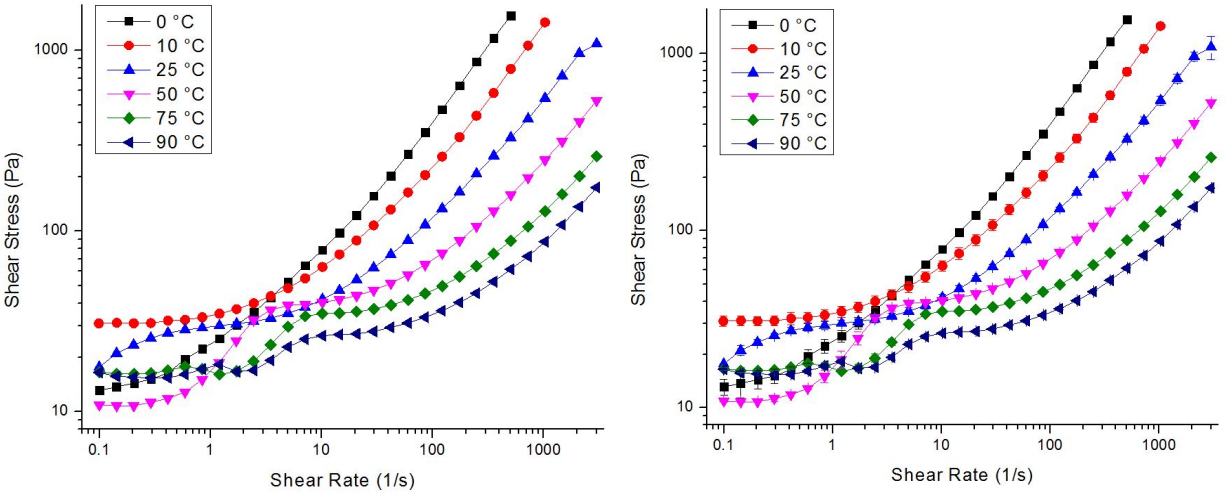

(a) Average Values (b) with Standard Deviation

Figure 4.60. OBM S2: O:W = 60:40, C_{surf} = 3 wt.%.

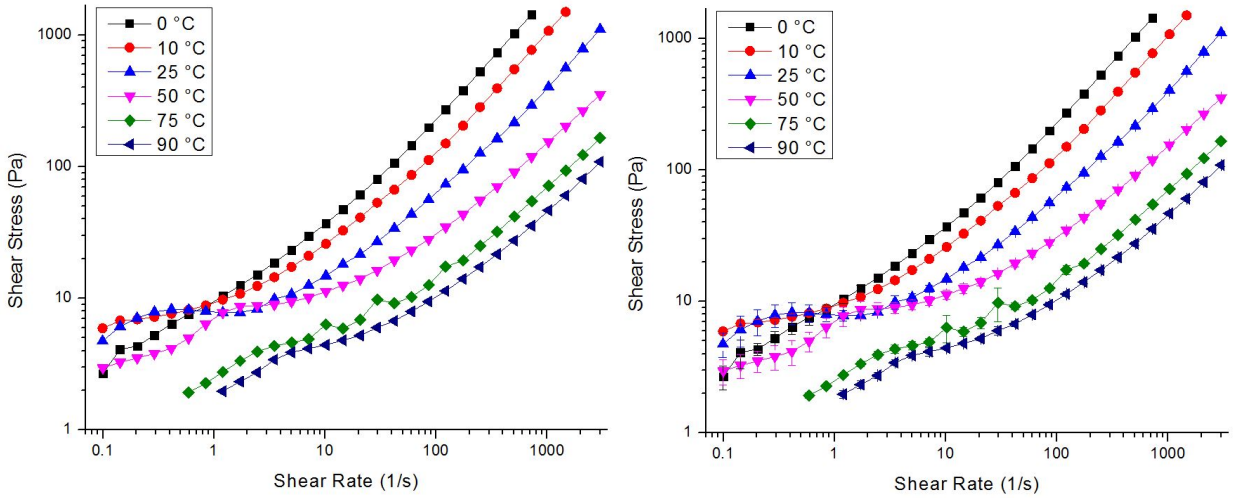

(a) Average Values

(b) with Standard Deviation

Figure 4.61. OBM S2: O:W = 70:30, C_{surf} = 3 wt.%.

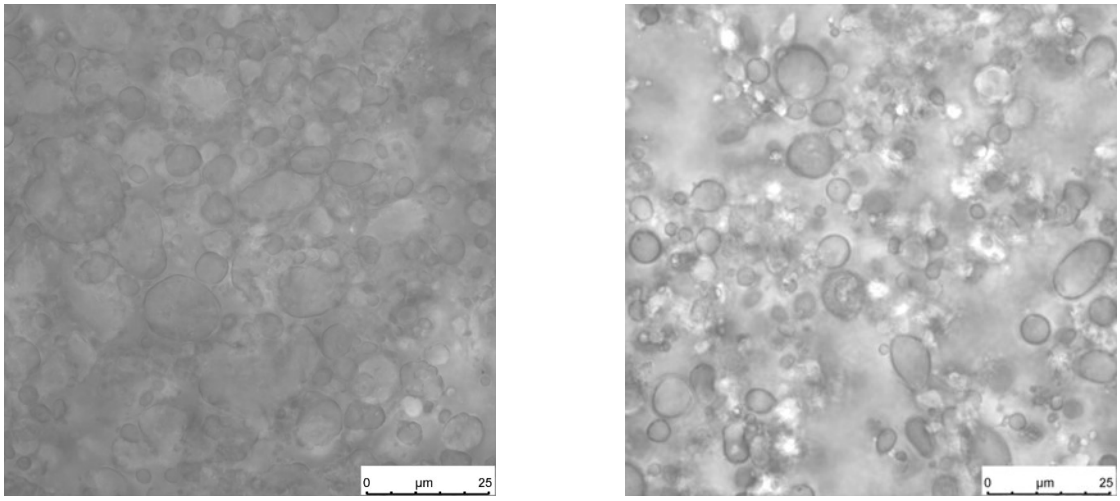

(a) O:W = 50:50

(b) O:W = 70:30

Figure 4.62. OBM S2: T = 25 °C, C_{surf} = 3 wt.%.

Shown in Figure 4.62 are the microstructure images of OBM S2 at 50:50 and 70:30 O:W ratios. The presence of particles of different dimensions and shapes are distinguishable as opposed to OBM S1 (see Figure 4.58). The pronounced slip behavior present in OBM S2 is driven by the flocculation of bentonite particles in the presence of other solids that are duratone and barite. The resulting heterogeneity in the mud's structure leads to slip behavior. With increasing O:W ratio the level slip behavior reduces, Figure 4.61, due to

the lower amount of solids within the mud sample.

4.5.2 Comparison to Oil-base Complex Fluids

Figures 4.63 to 4.68 compare the flow curves of the oil-base complex fluid (OCF) to the oil-based mud (OBM) samples. OCF and OBM samples stabilized by surfactant S1 (Span 80) showed almost identical profiles in their flow curves, Figures 4.63 to 4.65. The OBM however displayed higher shear stresses, which is due to the higher concentration of solids in the OBM (duratone, bentonite, barite) as compared to the OCF (bentonite). With increasing O:W ratio, the difference in shear stress level can be seen to decrease due to the lower concentration of bentonite (based on volume fraction of water phase).

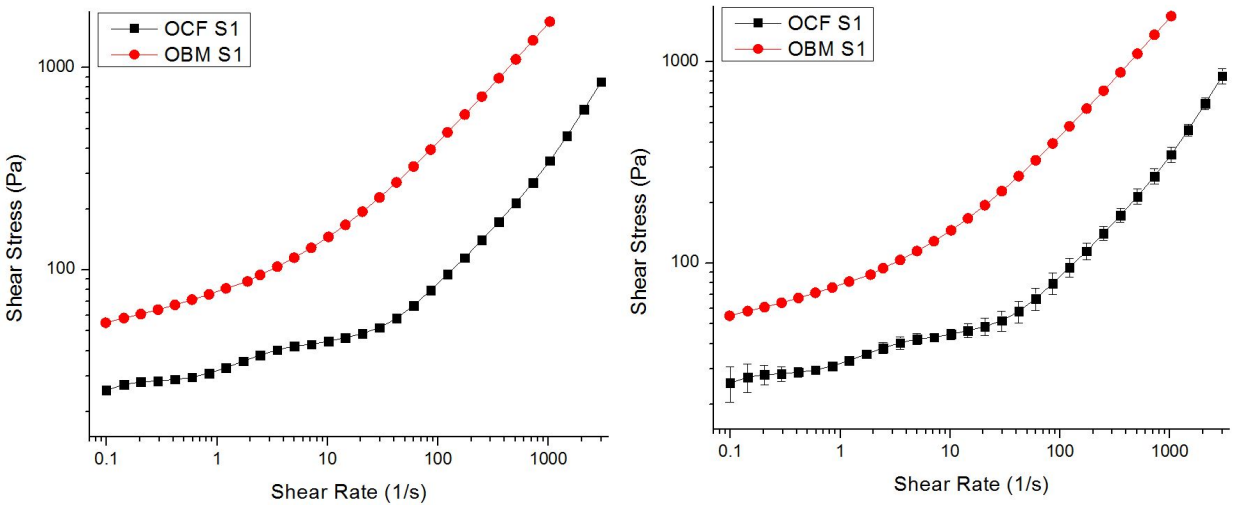

(a) Average Values (b) with Standard Deviation

Figure 4.63. S1: O:W Ratio = 50:50, T = 25 °C, C_{surf} = 3 wt.%.

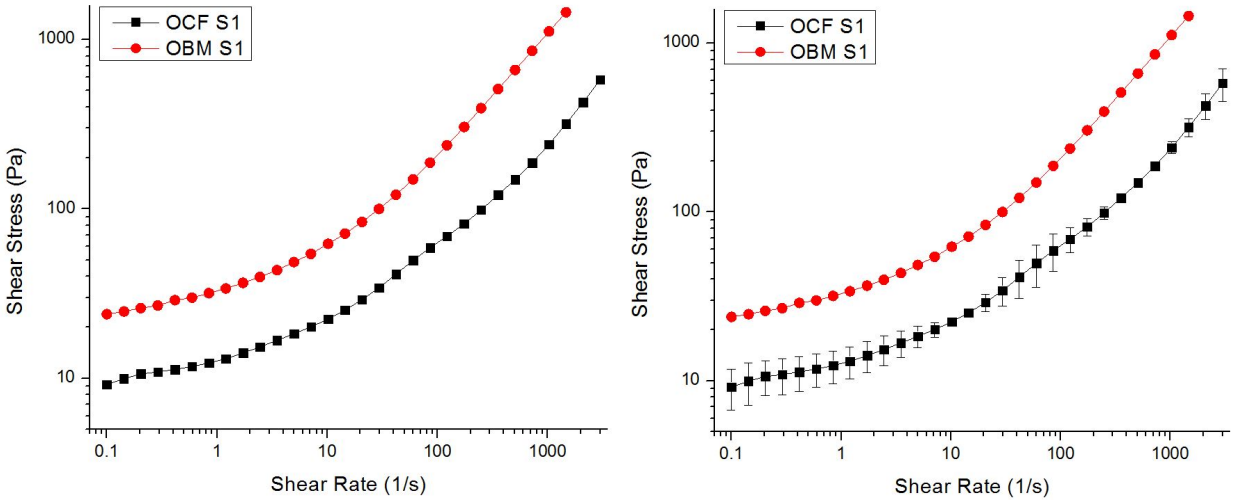

(a) Average Values (b) with Standard Deviation

Figure 4.64. S1: O:W Ratio = 60:40, T = 25 °C, C_{surf} = 3 wt.%.

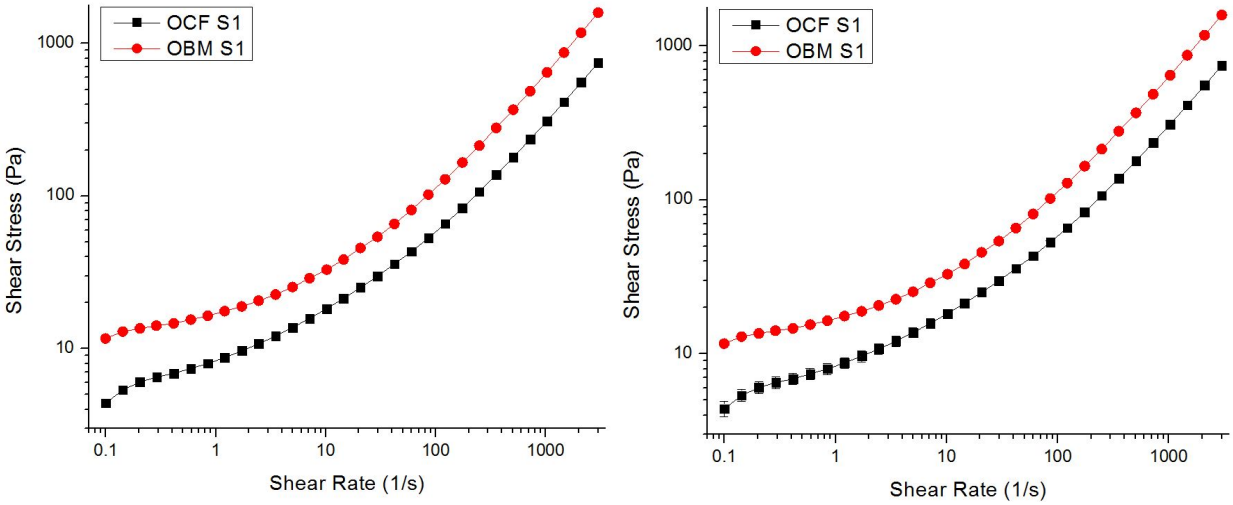

(a) Average Values (b) with Standard Deviation

Figure 4.65. S1: O:W Ratio = 70:30, T = 25 °C, C_{surf} = 3 wt.%.

OCF and OBM samples stabilized by surfactant 2 (Brij 93) were observed to display similar trends in their flow curve profiles, Figures 4.66 to 4.68, particularly with respect to their slip behavior tendency. Although OCF S2 is seen to experience wall slip, a trend can be seen in slip mitigation with increasing O:W ratio. The main reason (as mentioned in earlier sections) being that the flocculation of particles, particularly bentonite, reduces

because of its lower amount at high O:W ratios, Figure 4.68. It can also be seen that OCF S2 displays an apparent yield stress at low shear rates not present in OBM S2 at 60:40 O:W ratio.

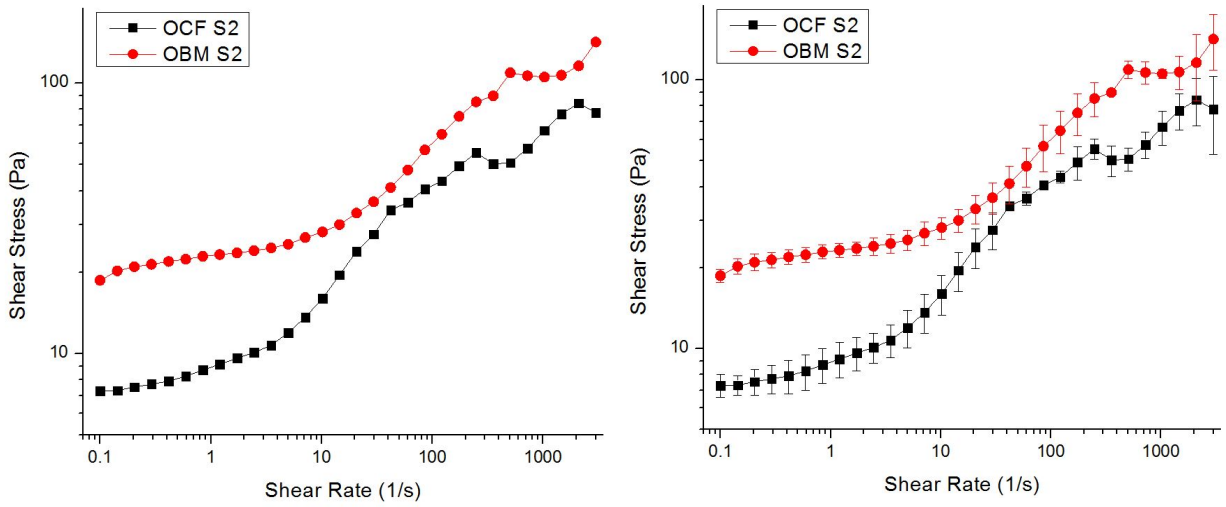

(a) Average Values (b) with Standard Deviation

Figure 4.66. S2: O:W Ratio = 50:50, T = 25 °C, C_{surf} = 3 wt.%.

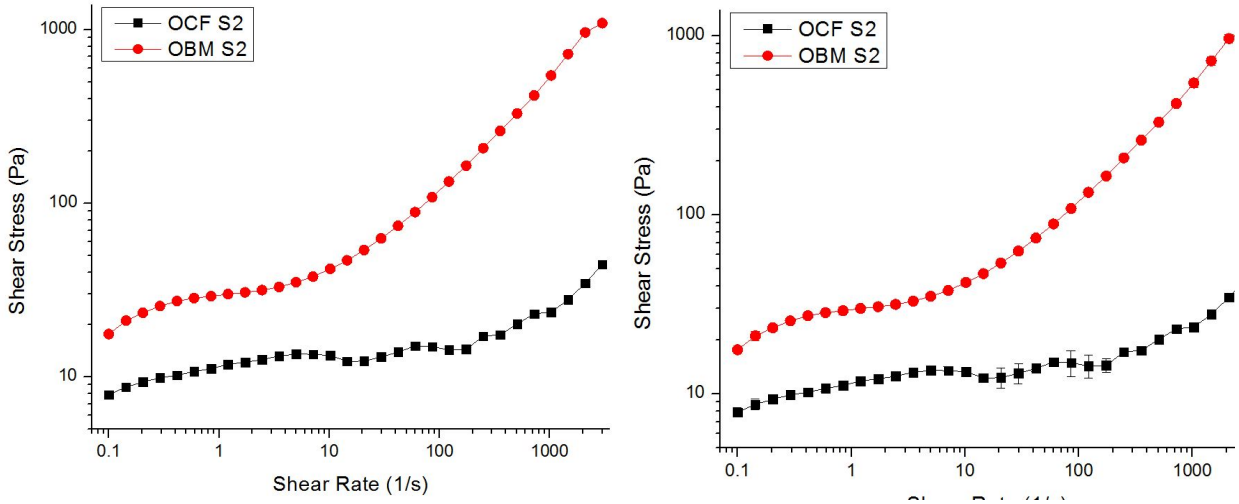

(a) Average Values (b) with Standard Deviation

Figure 4.67. S2: O:W Ratio = 60:40, T = 25 °C, C_{surf} = 3 wt.%.

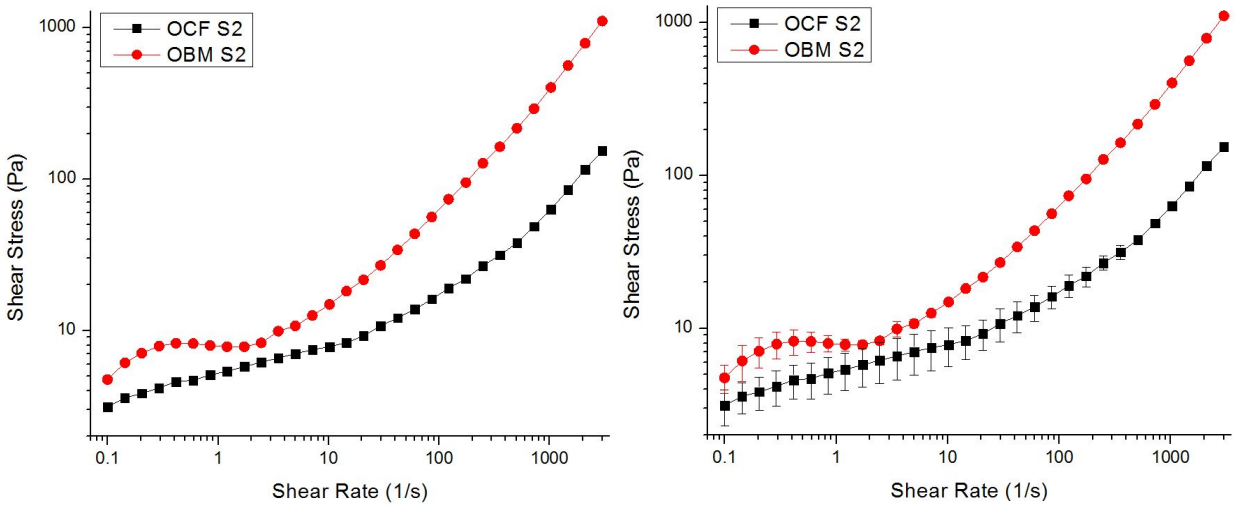

(a) Average Values (b) with Standard Deviation

Figure 4.68. S2: O:W Ratio = 70:30, T = 25 °C, C_{surf} = 3 wt.%.

4.5.3 Yield Stress

Figures 4.69 to 4.74 compare the yield properties of the oil-base complex fluids (OCF) and drilling mud (OBM) samples stabilized by the two surfactants Span 80 (S1) and Brij 93 (S2). As shown in Figures 4.69 and 4.70, OBM S1 has a higher structuration level than OCF S1. This is reflected by the lower strain deformation displayed at 50:50 and 60:40 O:W ratios. The higher concentration of solids in OBM S1, because of the presence of additional additives, confers it higher elastic properties (see Figure 2.43). At 70:30 O:W ratio, the samples show comparable strain deformation levels due to reduced amount of solids (bentonite), Figure 4.71.

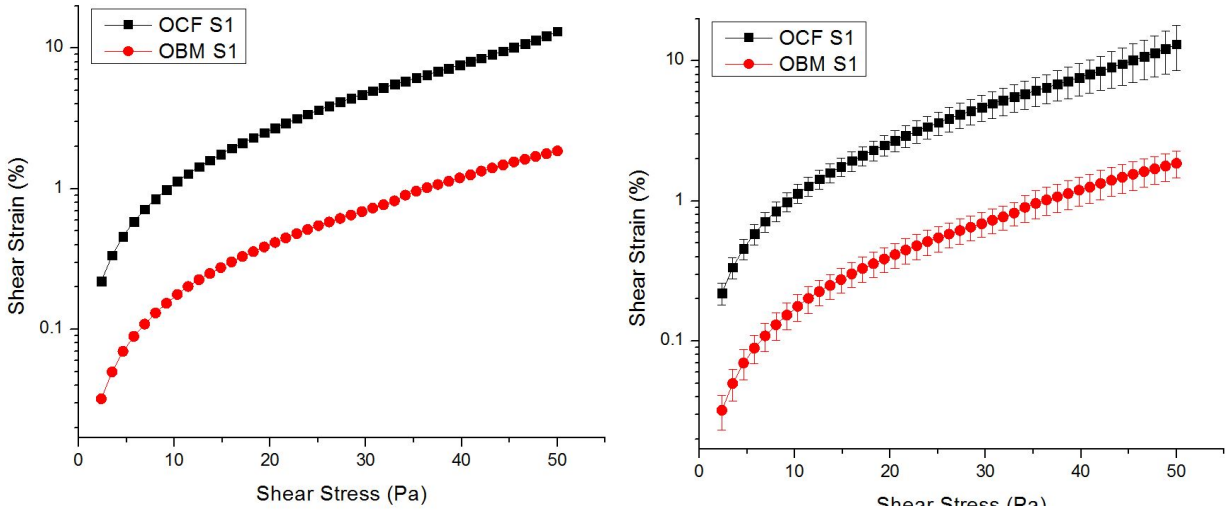

(a) Average Values (b) with Standard Deviation

Figure 4.69. S1: O:W Ratio = 50:50, T = 25 °C, C_{surf} = 3 wt.%.

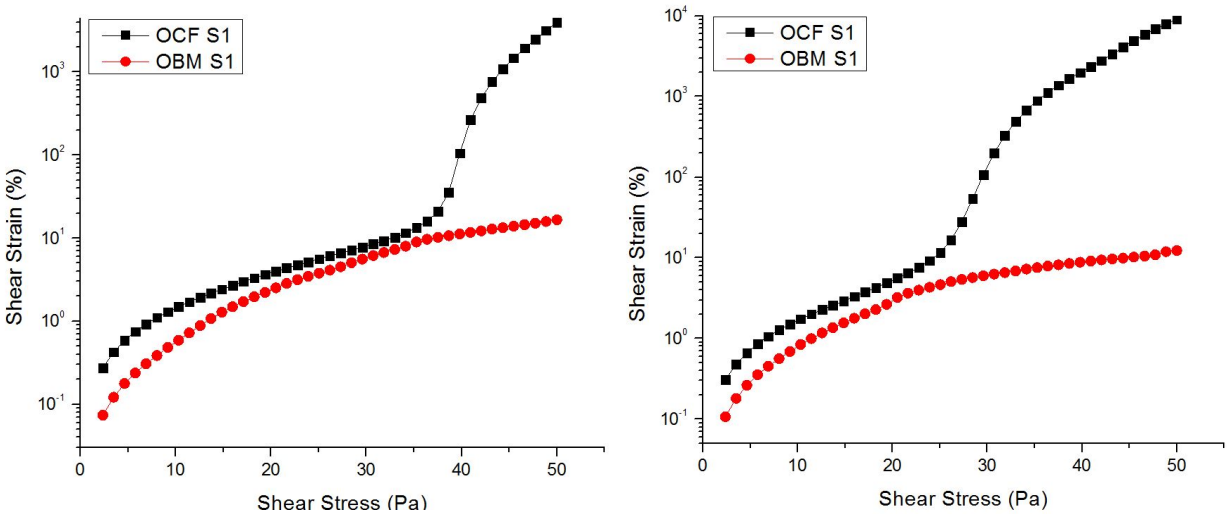

(a) Run 1 (b) Run 2

Figure 4.70. S1: O:W Ratio = 60:40, T = 25 °C, C_{surf} = 3 wt.%.

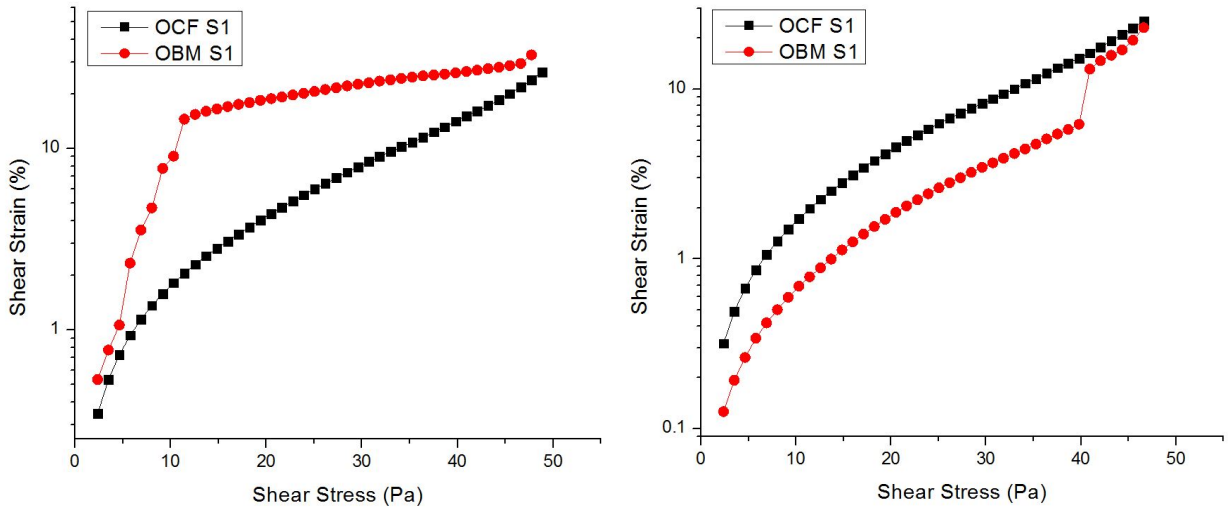

(a) Run 1 (b) Run 2

Figure 4.71. S1: O:W Ratio = 70:30, T = 25 °C, C_{surf} = 3 wt.%.

Comparison between the OCF and OBM stabilized by Brij 93 (S2) is shown in Figures 4.72 to 4.74. OBM S2 is seen to have higher elastic properties in comparison to OCF S2. This is once more due to the presence of additional additives (duratone, barite) in OBM S2, conferring it a more rigid internal structure.

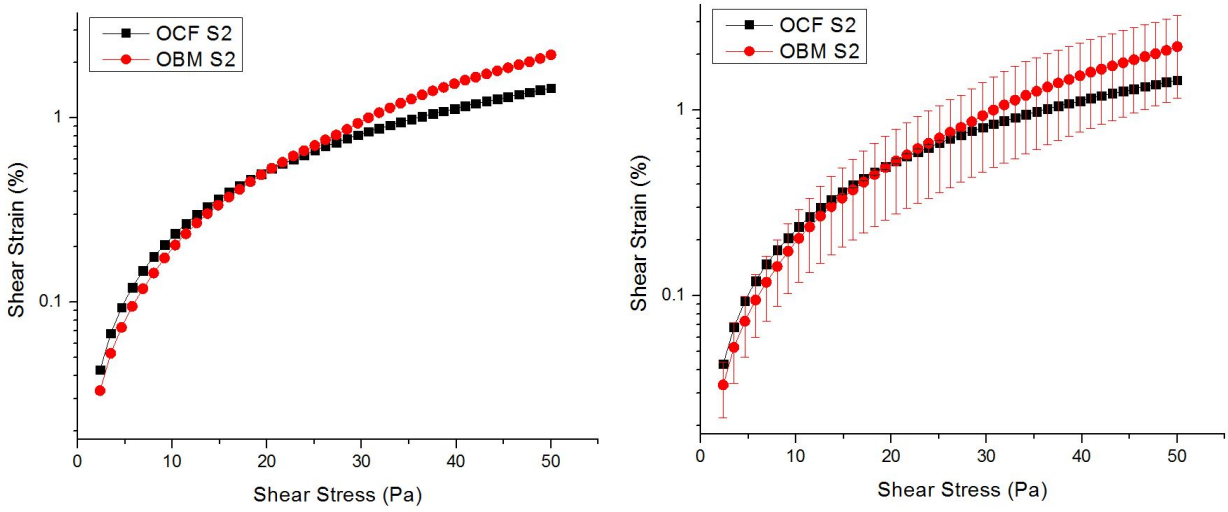

(a) Average Values (b) with Standard Deviation

Figure 4.72. S2: O:W Ratio = 50:50, T = 25 °C, C_{surf} = 3 wt.%.

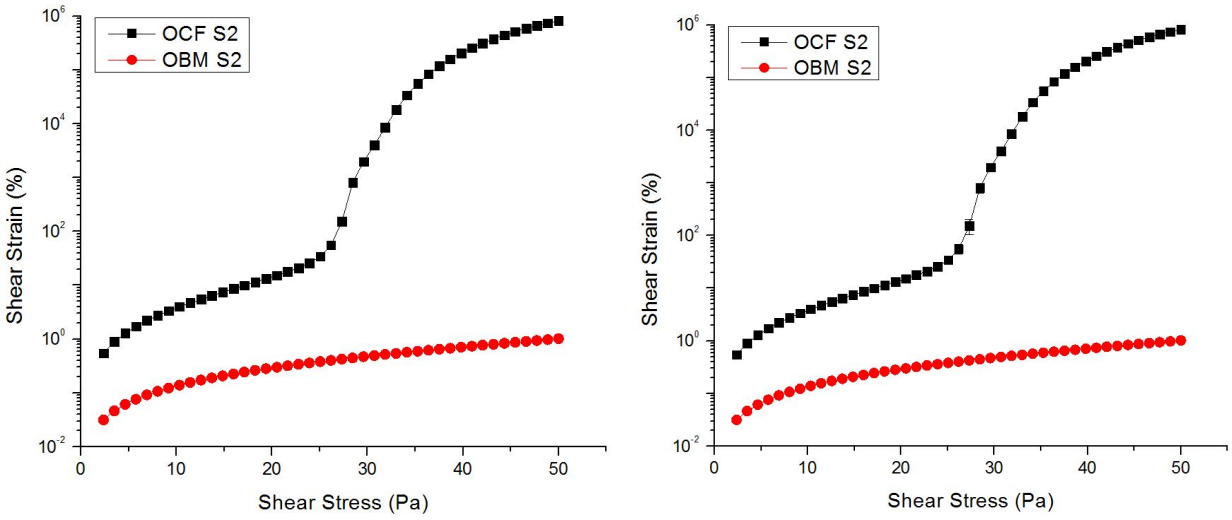

(a) Average Values (b) with Standard Deviation

Figure 4.73. S2 O:W Ratio = 60:40, T = 25 °C, C_{surf} = 3 wt.%.

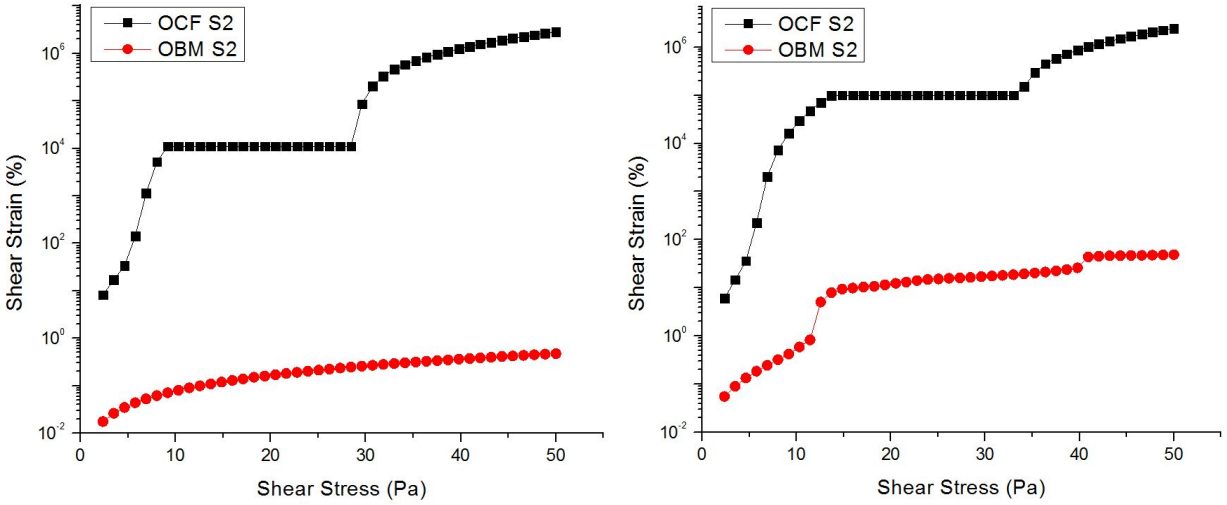

(a) Run 1 (b) Run 2

Figure 4.74. S1: O:W Ratio = 70:30, T = 25 °C, C_{surf} = 3 wt.%.

4.5.4 Industry Field Muds

Figures 4.75 and 4.76 show the flow curves at different temperatures of two field drilling muds provided to us by industry. The exact composition of these drilling muds cannot be provided for confidentiality purposes. The apparent viscosity (shear stress) of these drilling muds can be seen to smoothly decrease with increasing temperatures. Wall slip

i.e. decreasing shear stress with increasing shear rate is for the most part absent in both drilling muds. This can be explained by the relative homogeneity of their microstructure as shown in Figure 4.77.

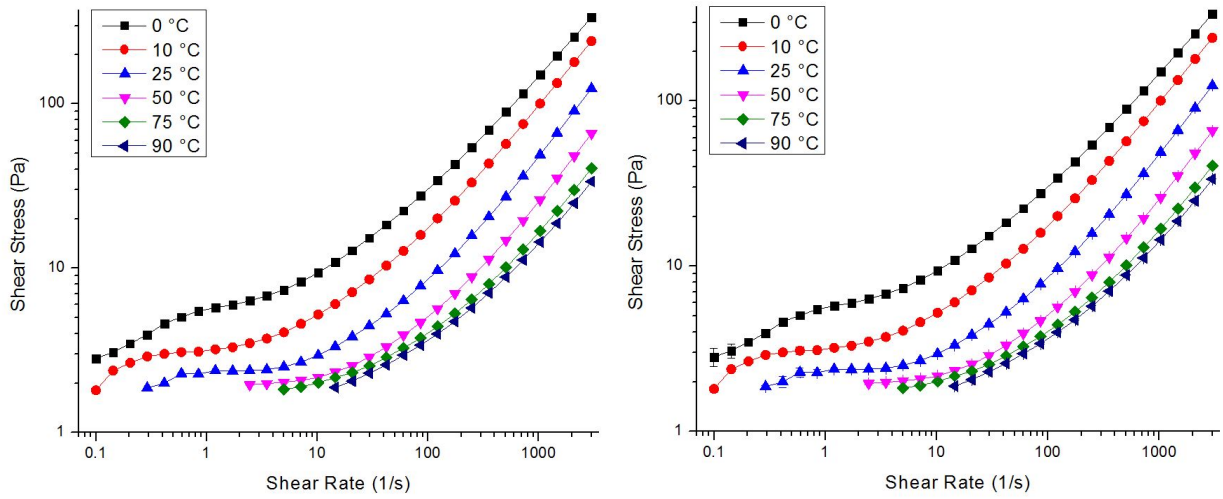

(a) Average Values (b) with Standard Deviation

Figure 4.75. Field OBM 1

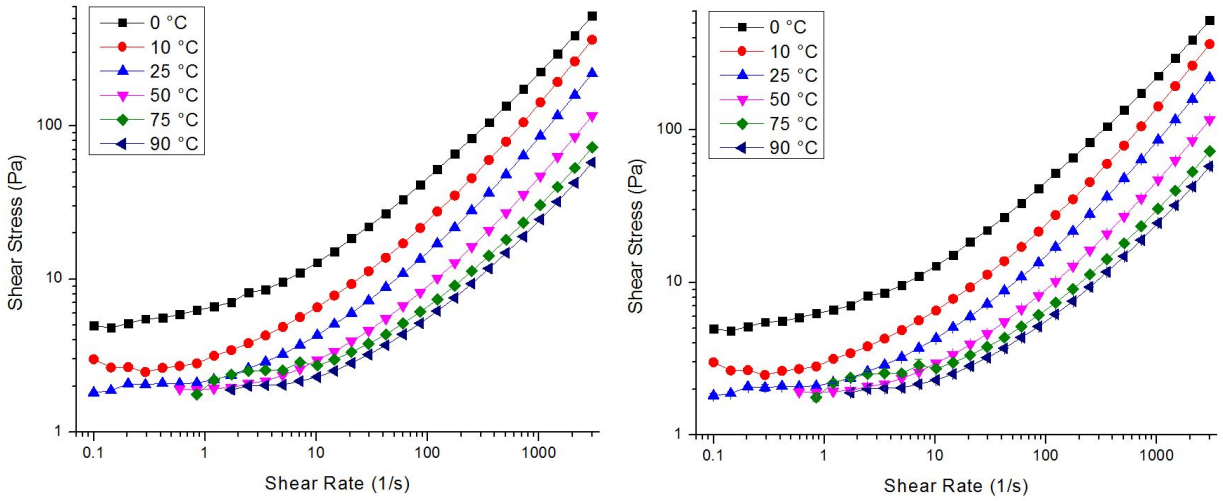

(a) Average Values (b) with Standard Deviation

Figure 4.76. Field OBM 2

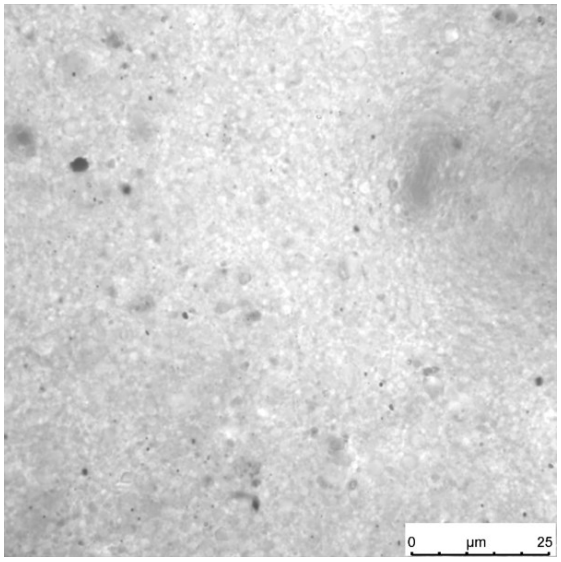

(a) Field OBM 1

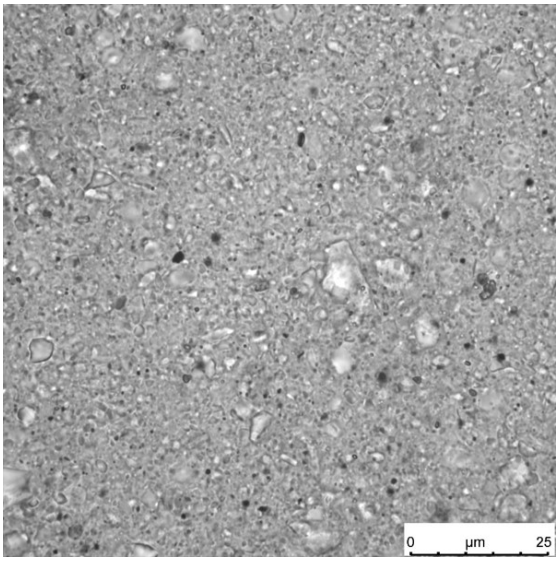

(b) Field OBM 2

Figure 4.77. T = 25 °C.

Chapter 5
Experimental Results & Discussion: Wall Slip Occurrence

In many instances in the previous chapter did we encounter samples having flow curves with decreasing and increasing shear stress i.e. wall slip. In this chapter, wall slip will be investigated as function of surfactant concentration, polarity, O:W ratio and temperature.

The rheology measurements of all samples conducted in the previous chapter was entirely done using the Cone & Plate (CP) measuring geometry of the MCR 52 rheometer that has a gap of 0.15 mm (see Figure 3.6a). In this chapter, analysis of slip will involve measurements performed with the Parallel Plate (PP) geometry (see Figure 3.6b) of the MCR and those conducted with the Couette flow geometry of the Fann 35 viscometer (see Figure 3.5b).

The experimental investigation in this chapter was set to the determine the effect of surfactant concentration and polarity, temperature and O:W ratio on the occurrence of slip. Only lubrication form of slip was quantified, further study is recommended on quantifying the other forms of slip (true and cohesive).

- MCR PP: 0.5, 1.17 and 2.0 mm
- Fann 35: 1.17 mm

To recall, the peculiarity of the PP geometry is that it allows measurements at different gaps to be conducted. As shown above, the gap selection of the PP geometry was as such to allow comparison with the Fann 35 viscometer at the gap of 1.17 mm, in order to observe trends 'independent' of the measuring instrument. See Figure 3.7 for difference in configuration of these three geometries.

Three types of slip behavior can be displayed by non-Newtonian fluids namely: wall (true), cohesive and lubrication slip. See Figure 2.42. It was found that complex fluids can exhibit all forms of slip depending on their composition and the magnitude of external variables such as temperature.

As it has been reported in literature, it is possible for very viscous mixtures to lose complete adhesion with respect to the wall and slide along them leading to true slip [94][125]. The aforementioned is identified by the occurrence of *jumps* or abrupt *slope changes* in curves of shear stress versus shear rate, driven by alternating periods of 'stick-slip' [93][126].

Cohesive slip on the other hand results from the presence of shear rate or stress gradients within the probed material. This tends to be the case of fluids highly heterogeneous with respect to their microstructure, see Figure 2.50. The aforementioned can also occur due to the clumping of dispersed particles in emulsions (and suspensions) driven by thermodynamics [93] and often enhanced by flow, see Figure 2.49.

Finally, lubrication slip is favored when complex fluids have: large individual dispersed particles (and/or flocs of particles), high dependence of the fluid on the dispersed phase volume fraction (concentration) and flow over smooth and narrow surfaces [94]. Viscoelastic, hydrodynamic and steric forces and constraints acting on the dispersed phase drives them away from the solid boundary leading to the formation of a slip layer (δ), see Figure 2.44. Lubrication slip is always limited by the reverse osmotic forces that causes an increase in concentration of particles near the solid boundary [94].

Ultimately, for all these different forms of slip, what may possibly be the most important thing from an engineering standpoint is not to overcome the slippage but to characterize these effects in order to predict the flow in some applications as they will occur in smooth pipes and conduits [94][95].

- **Slip Diagnosis**

Below are the flow curves corresponding to the different types of slips. These flow curves can serve as diagnostic tools in identifying the form of slip undergone by non-Newtonian fluids. With respect to true and cohesive slip, this is particularly important for drilling fluids where very low shear rates are experienced during pump startups following a trip or connection and when the fluid is being circulated through large annuli.

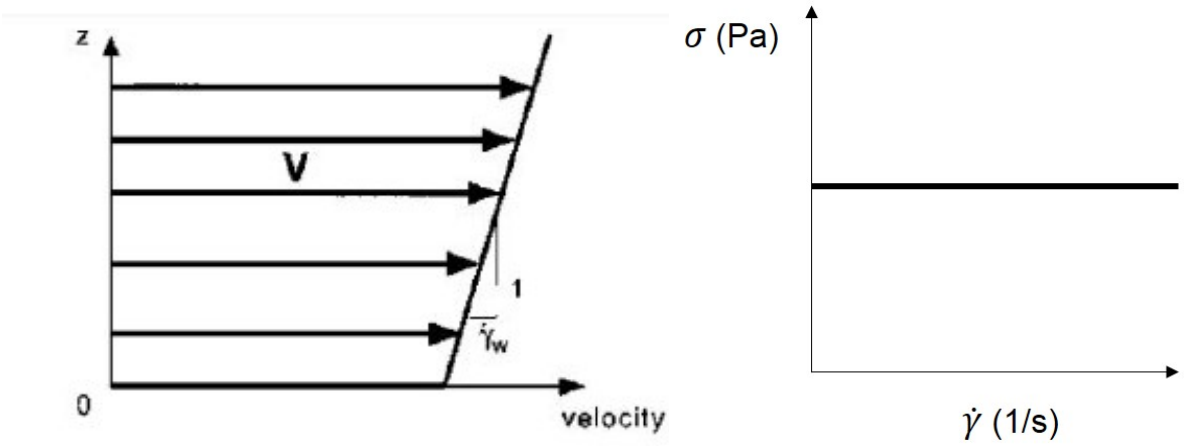

(a) Velocity profile [100]

(b) Diagnostic flow curve

Figure 5.1. Wall (true) slip.

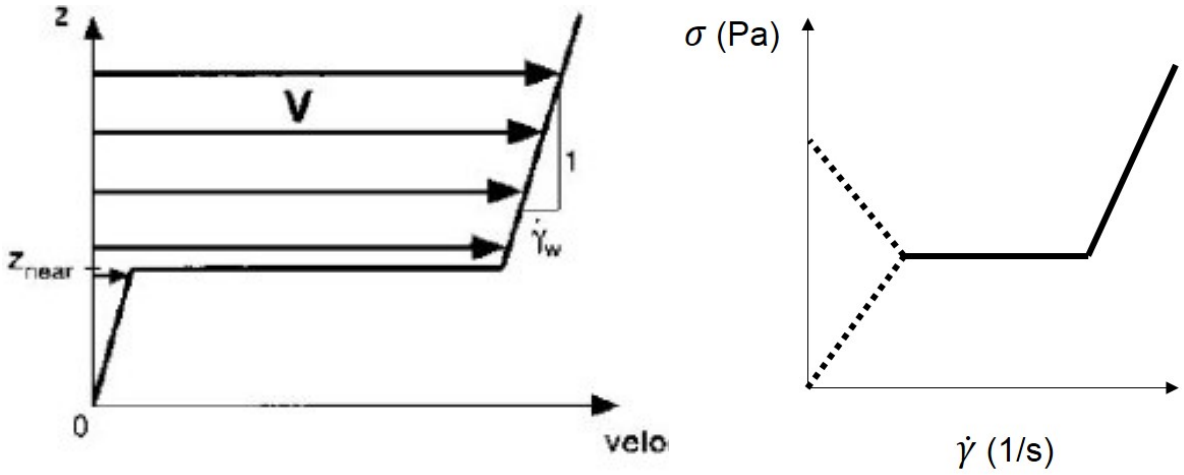

(a) Velocity profile [100]

(b) Diagnostic flow curve [103]

Figure 5.2. Cohesive slip.

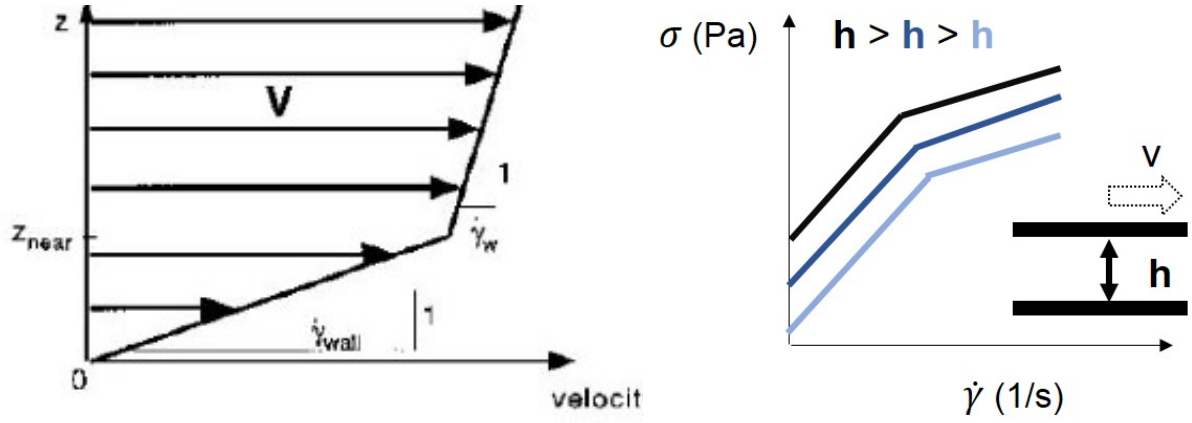

(a) Velocity profile [100]

(b) Diagnostic flow curve

Figure 5.3. Lubrication slip.

5.1 Effect of Surfactant Concentration

This section will highlight the effect of surfactant concentration (C_{surf}) on slip behavior on oil-base complex fluids. The flow curve measurements obtained with PP measuring geometry of the MCR rheometer are contrasted with those of the Fann viscometer to discern slip patterns independent of instrument type.

Results in this chapter will be shown in the following manner: (i) for instrument comparison, all repeated runs for the MCR PP geometry are shown when comparing it with that obtained with the Fann measurement at the same gap of 1.17 mm, (ii) for slip layer (δ) determination, average values of measurements conducted at different gaps (H) will be shown. In Appendix B are these measurements, and all others, with their standard deviations included.

Figures 5.4 shows the flow curves of the OCF sample, OCF S1, at 1 and 3 wt.% surfactant concentration. Cohesive slip can be seen to occur at very low shear rates from the MCR measurement at 1 wt.% concentration. This form of slip cannot be seen in the Fann instrument as it occurs at shear rates that fall out of its range of measurement.

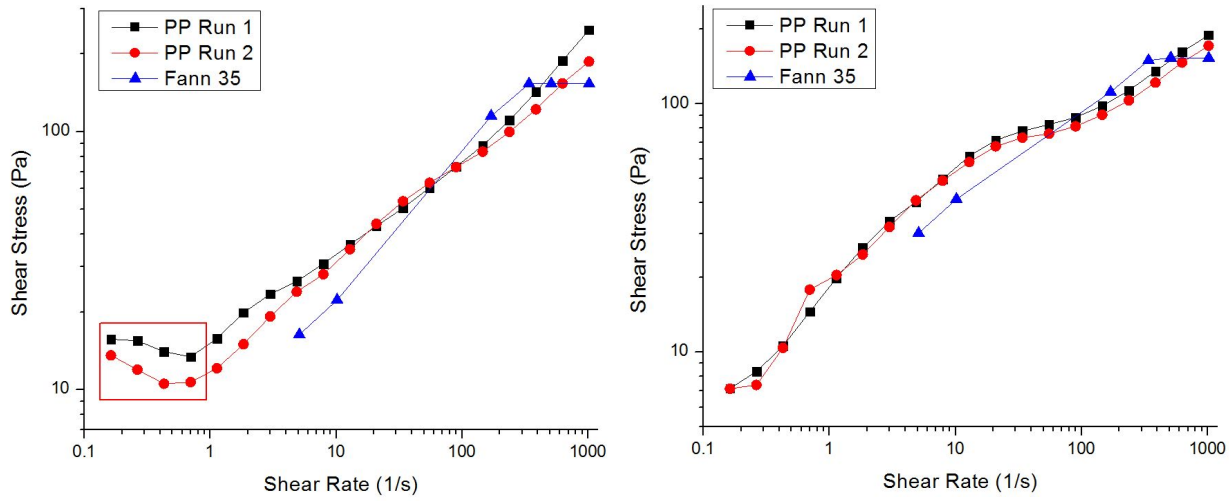

(a) 1 wt.%

(b) 3 wt.%

Figure 5.4. Fann vs MCR - OCF S1: HLB = 4.3, O:W = 60:40, T = 25 °C.

With increase in surfactant concentration to 3 wt.%, Figure 5.4b, cohesive slip was found to be suppressed. The next step was to determine if the third form of slip, lubrication slip, was present. The procedure and equations (Equations 2.20 and 2.21) established by Yilmazer & Kaylon [107] based off Yoshimura & Prud'homme's method [106] were used to identify this form of slip and its associated slip layer thickness (δ).

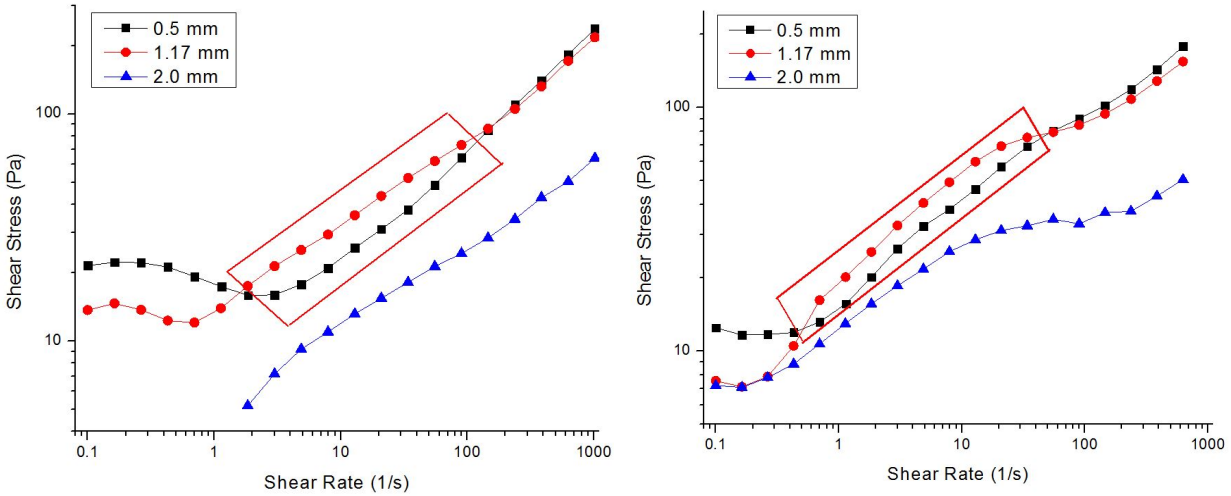

(a) 1 wt.%

(b) 3 wt.%

Figure 5.5. MCR PP - OCF S1: HLB = 4.3, O:W = 60:40, T = 25 °C.

The presence of a slip layer in non-Newtonian fluids is done by conducting measure-

ments at different gaps (H) and assessing whether there is an increase in shear stress with measuring gap. Figure 5.5 shows flow curve measurements at different gaps for the same sample. At both 1 and 3 wt.% surfactant concentration, measurements at 1.17 mm can be seen to be greater than those at 0.5 mm over a given shear rate interval, this is indicative of the presence of a slip layer.

The next step was to determine the thickness of the slip layer at both surfactant concentrations. This was done as shown in Figure 5.6 using Yilmazer & Kaylon's equations, see Equations 2.20 and 2.21. Only the shear rate region in which shear stresses at 1.17 mm gap were greater than 0.5 mm was used in determining the slip layer. Table 5.1 summarizes the slip layer thickness determined at 1 and 3 wt.%. It can be seen that increase in surfactant concentration reduces slip layer thickness which is in agreement with literature [94][95][101].

Jamming of the dispersed particles in OCF S1 explains the 'increase' in shear stress with 'decreasing' measuring gap. As shown in Figure 4.9, the increase in drag forces between particles causes them to dilate under shear leading to additional stresses from solid-solid friction [110][111]. The aforementioned explains the increase in shear stress with decreasing gap in the absence of lubrication slip.

Table 5.1: OCF S1: O:W = 60:40, HLB = 4.3, T = 25 °C.

Surf. Conc. (wt.%)	δ (μm)
1	52.77
3	29.04

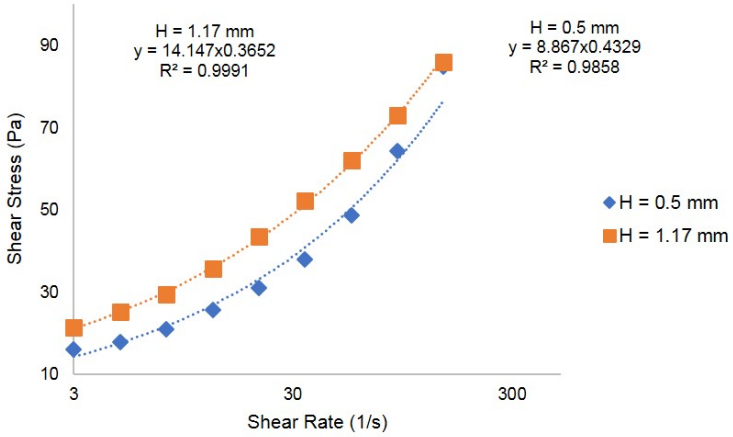

(a) Curve fitting

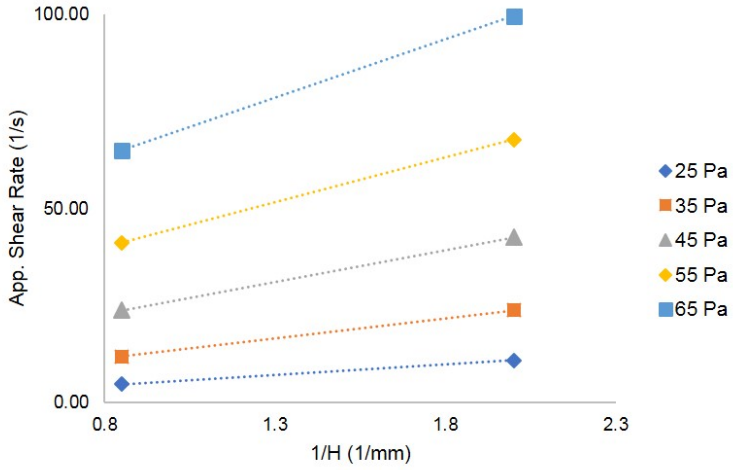

(b) Slip velocity

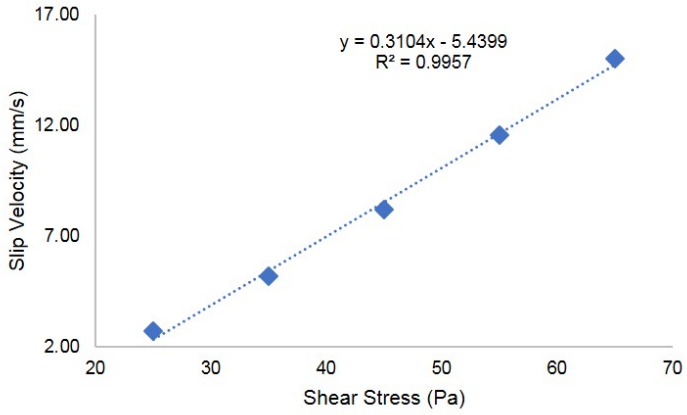

(c) Slip layer

Figure 5.6. Lubrication slip analysis: OCF S1 - 1 wt.%, O:W Ratio = 60:40.

fluids assume no-slip boundary conditions at the wall of solid boundaries, $v_w = 0$. The slip velocity equation shown in Figure 5.6 for OCF S1 at 1 wt.% surfactant concentration will be used to determine if the presence of a slip layer invalids the aforementioned assumption, and if yes to what extent. This is done by using the highest shear stress for which the slip velocity equation, Figure 5.6c, is valid i.e. 65 Pa.

The results gives a slip velocity of 14.73 mm/s or 0.015 m/s, thus the presence of a slip layer for the sample considered does not invalid the no-slip boundary condition. However, depending on how thick the slip layer can possibly get and its interval of occurrence (low or high shear rates) the validity of the no-slip condition may possibly decrease.

Shown in Figures 5.7 and 5.8 is the effect of surfactant concentration on the different forms of slip on the oil-base complex fluid OCF S2 at 60:40 O:W ratio. From Figure 5.7, it can be seen that OCF S2 displays cohesive slip at very low shear rates. Upon increase in surfactant concentration however, this slip behavior is seen to be suppressed.

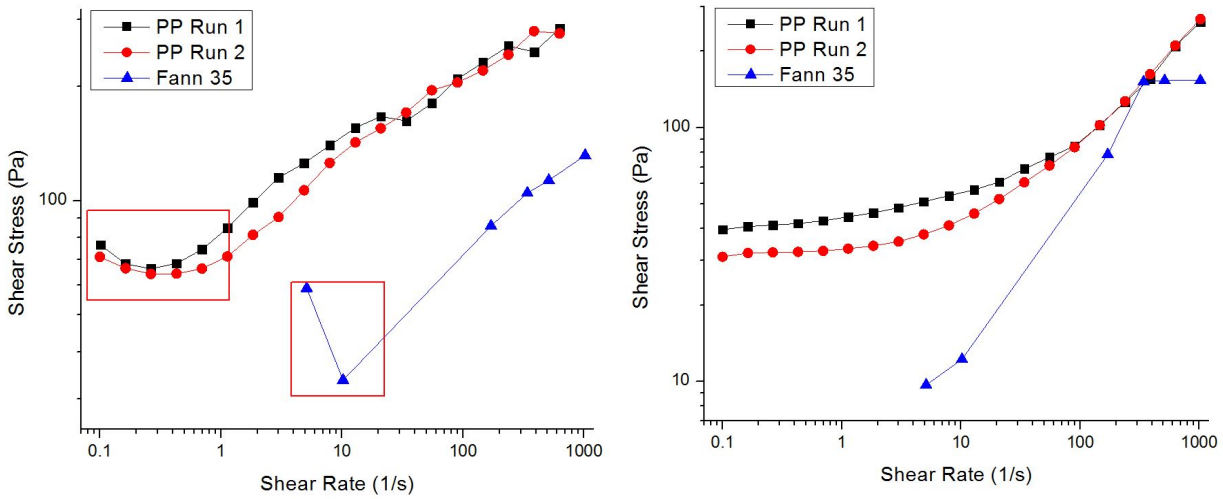

(a) 1 wt.%

(b) 3 wt.%

Figure 5.7. Fann vs MCR - OCF S2: HLB = 4.0, O:W = 60:40, T = 25 °C.

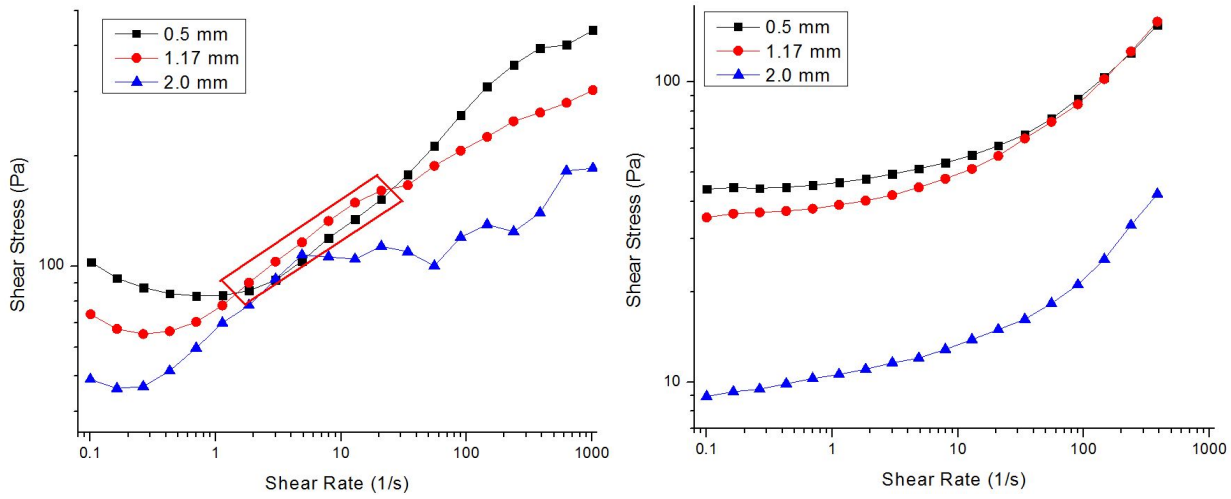

(a) 1 wt.% (b) 3 wt.%

Figure 5.8. MCR PP - OCF S2: HLB = 4.0, O:W = 60:40, T = 25 °C.

The presence of a slip layer at either concentration was determined by measurements at different gaps shown in Figure 5.8. A 7.06 μm thick slip layer was determined at 1 wt.% surfactant concentration. This slip layer was however observed to be suppressed at 3 wt.% concentration, which is once more in agreement with literature.

Table 5.2: OCF S2: O:W = 60:40, HLB = 4.0, T = 25 °C.

Surf. Conc. (wt.%)	δ (μm)
1	7.06
3	nil

5.2 Effect of Surfactant Polarity

Figures 5.9 and 5.10 highlight the effect of surfactant polarity on the slip behavior of oil-base complex fluids at 3 wt.% surfactant concentration and different O:W ratios. True (wall) and cohesive slip can both be seen to be absent from the flow curves of OCF S1 and OCF S2. Included in Appendix B are slip behavior comparison for all other composition and temperature variables.

Lubrication slip, is the form of slip for which a distinct difference could be seen between

both types of complex fluids based on surfactant polarity. OCF S1 was associated with thicker slip layers over OCF S2, see Table 5.3.

This is driven by the presence of (large) dispersed droplets in OCF S1, see Figure 4.7. The aforementioned being one of the major conditions favoring lubrication slip. The greater linkage of bentonite particles in OCF S2 minimizes the formation of a slip layer due to the lower sphericity of individual or aggregation of particles.

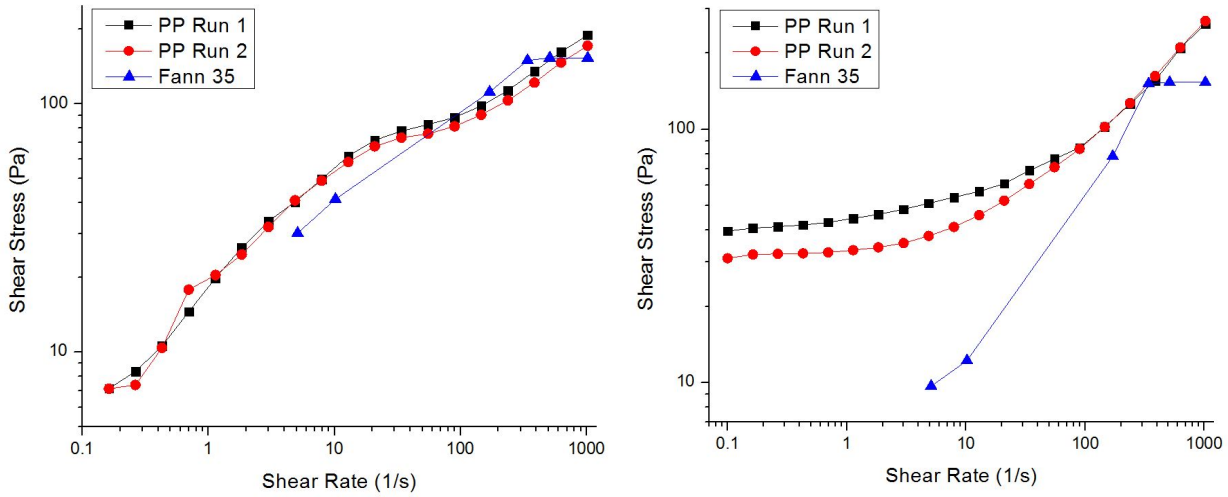

(a) OCF S1 (b) OCF S2

Figure 5.9. O:W = 60:40, C_{surf} = 3 wt.%, T = 25 °C.

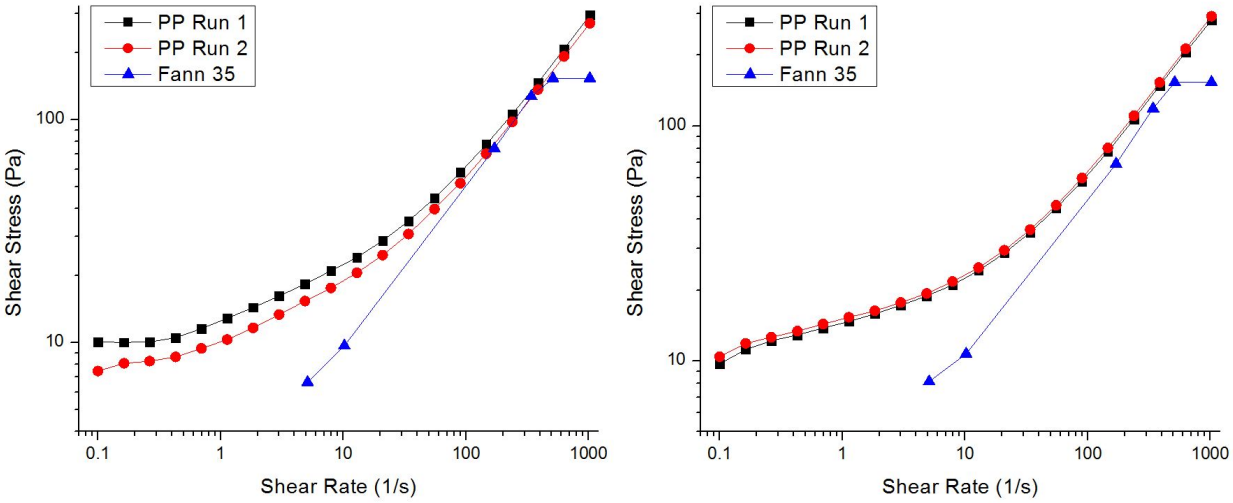

(a) OCF S1 (b) OCF S2

Figure 5.10. O:W = 70:30, C_{surf} = 3 wt.%, T = 25 °C.

Table 5.3: C_{surf} = 3 wt.%, T = 25 °C.

O:W Ratio	OCF S1	OCF S2
60:40	29.04 μm	nil
70:30	92.58 μm	0.56 μm

5.3 Effect of Temperature

In this section the effect of temperature on the slip behavior of oil-base complex fluids is assessed at 3 wt.% surfactant concentration for OCF S1 and OCF S2. From Figure 5.11, it can be seen that cohesive slip is induced by temperature increase as is reflected from the low shear stress profile at 75 °C.

Lubrication slip was equally found to be exacerbated from temperature increase, as shown in Figure 5.12. The slip layer thickness was found to increase from 29.04 to 323.37 μm, as shown in Table 5.4. Additionally, it can be seen that the degree of cohesive slip displayed by the sample increases at each measuring gap at 75 °C.

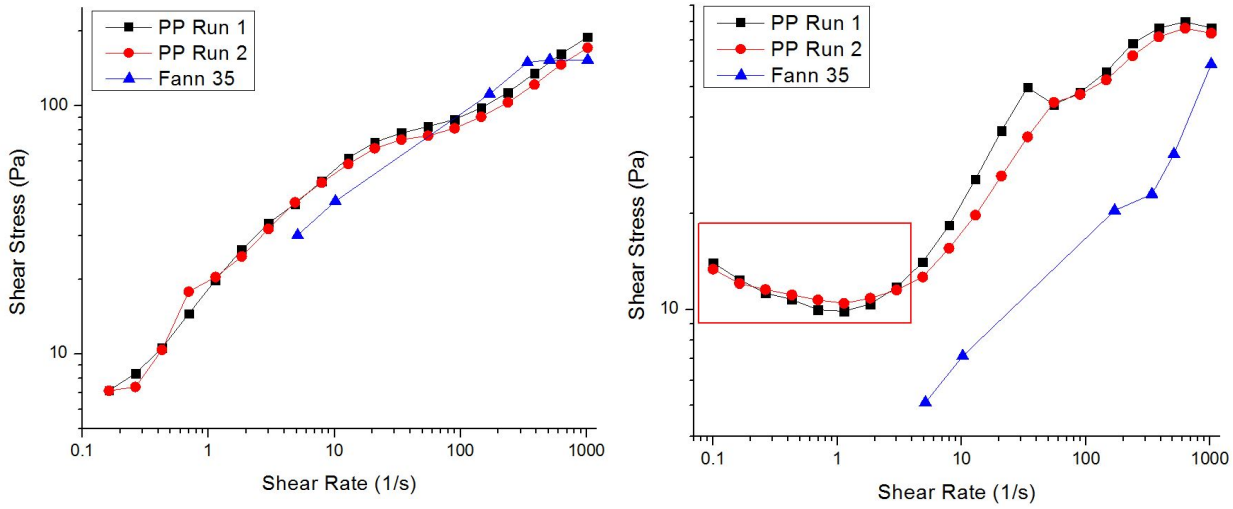

(a) 25 °C

(b) 75 °C

Figure 5.11. Fann vs MCR - OCF S1: C_{surf} = 3 wt.% , O:W = 60:40.

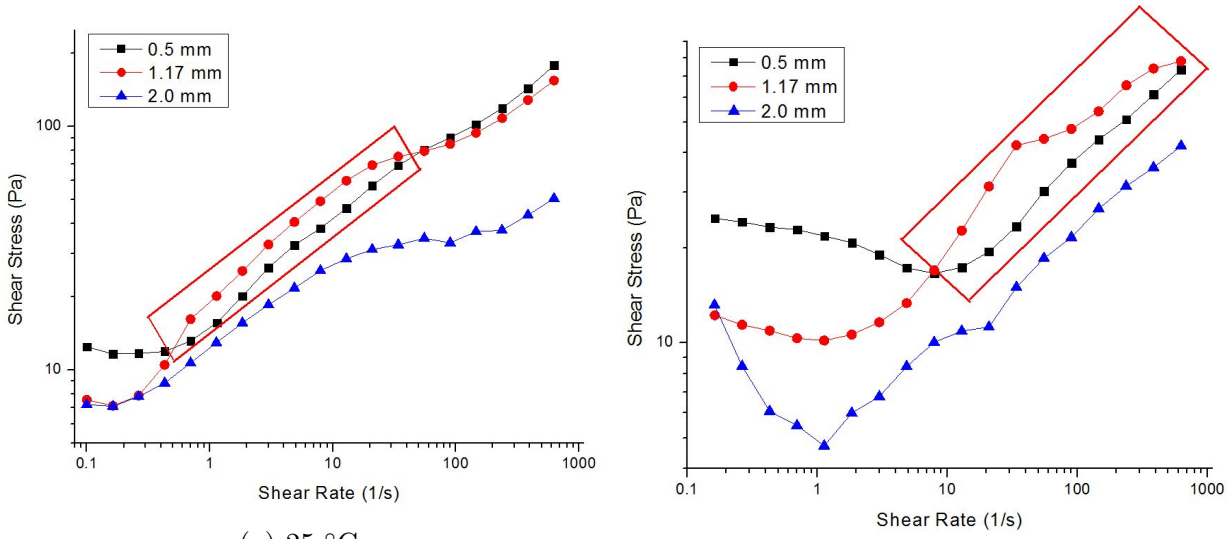

(a) 25 °C

(b) 75 °C

Figure 5.12. MCR PP - OCF S1: C_{surf} = 3 wt.%, O:W = 60:40.

Table 5.4: OCF S1: O:W = 60:40, C_{surf} = 3 wt.%.

Temp. (°C)	δ (μm)
25	29.04
75	323.37

Figures 5.13 and 5.14 shows the effect of temperature on the slip behavior of the oil-base complex fluid OCF S2. The different forms of slip can be seen to be induced as a result of temperature increase. True slip as can be seen to occur upon temperature increase to 75 °C, as is shown by the low shear profile in Figure 5.13. Slip layer thickness, indicative of lubrication slip, was further found to increase from a value of nil to 407.80 μm as determined from Figure 5.14.

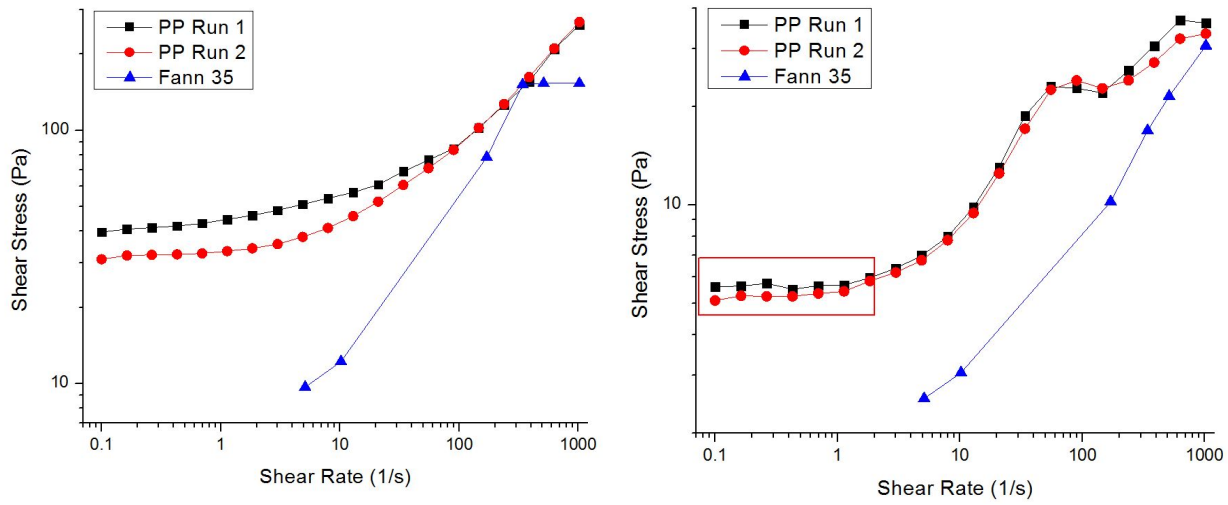

(a) 25 °C (b) 75 °C

Figure 5.13. Fann vs MCR - OCF S2: C_{surf} = 3 wt.%, O:W = 60:40.

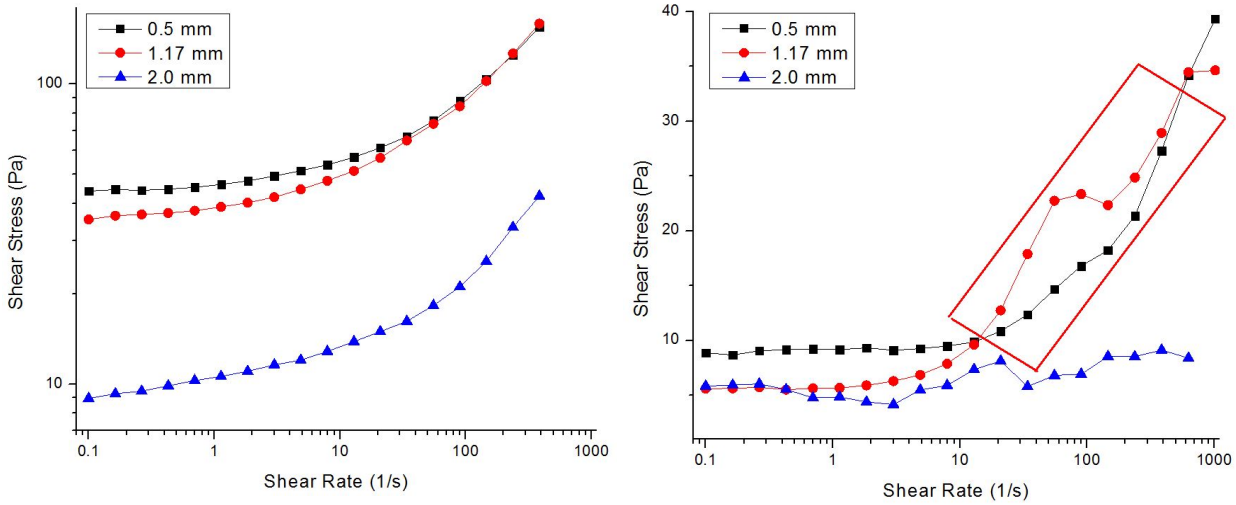

(a) 25 °C (b) 75 °C

Figure 5.14. MCR PP - OCF S2: C_{surf} = 3 wt.%, O:W = 60:40.

Table 5.5: OCF S2: O:W = 60:40, C_{surf} = 3 wt.%.

Temp. (°C)	δ (μm)
25	0
75	407.80

5.4 Effect of Oil:Water Ratio

This section assesses the effect of O:W ratio on slip occurrence on complex fluids with no surfactants (0 wt.%). The effect of dispersed phase volume fraction on slip was assessed by conducting flow curve measurements with 0, 50 and 60 vol.% oil dispersed phase volume fractions in a water-bentonite continuous medium. Measurements at volume fractions greater than 60 vol.% were not possible due to the instability of the sample at such elevated volume fractions in the absence of surfactants. Included in Appendix B are the results of O:W ratio effect on slip in the presence of surfactants.

Figures 5.15 to 5.17 show the lubrication slip analysis of the samples at different measuring gaps conducted with the MCR PP geometry. It can be seen that with increase in volume fraction of the dispersed phase, lubrication slip becomes more pronounced. This can be seen through the increase in slip layer thickness from nil at 0 vol.% dispersed phase, to 0.04 μm at 60 vol.% dispersed phase.

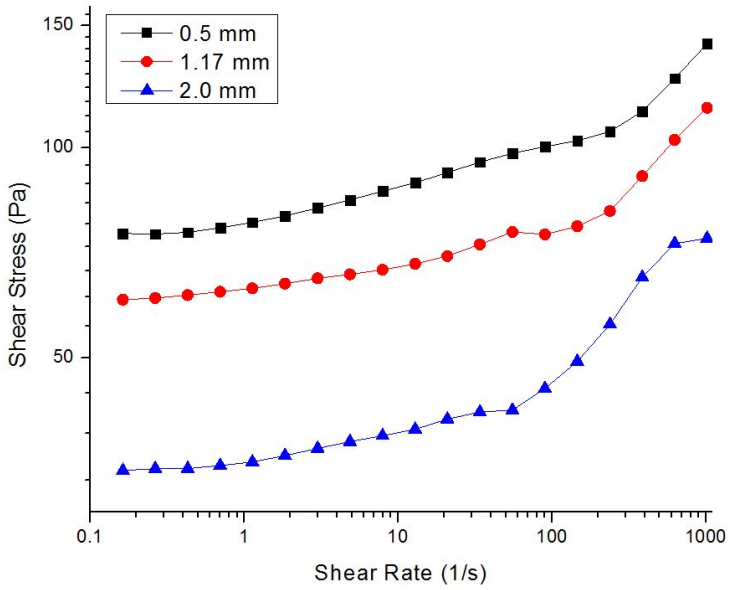

Figure 5.15. Water + bentonite

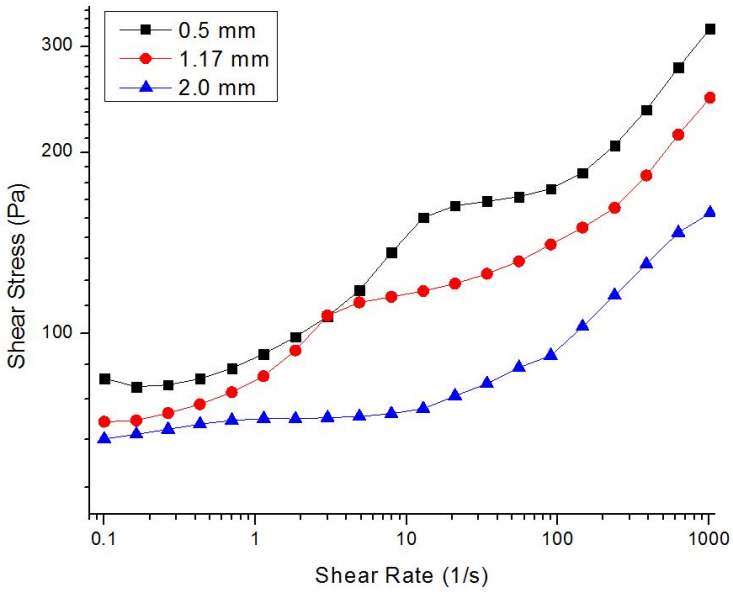

Figure 5.16. Water + oil + bentonite - O:W = 50:50

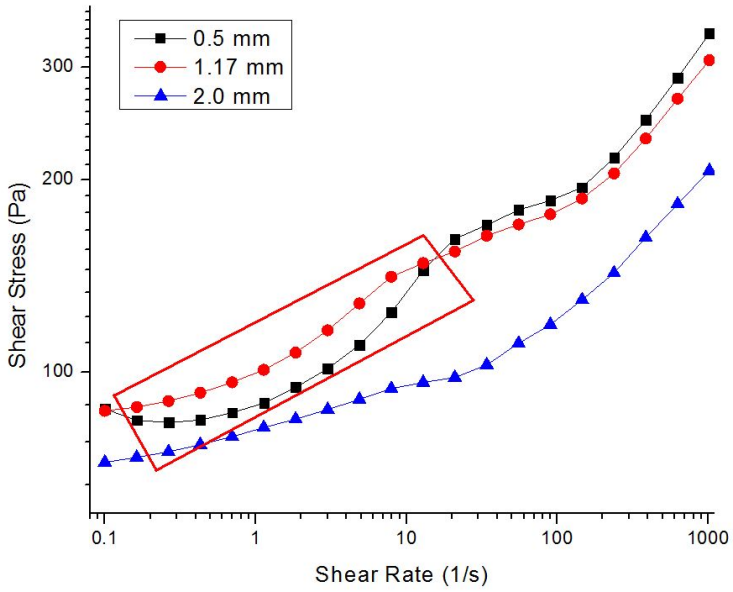

Figure 5.17. Water + oil + bentonite - O:W = 60:40

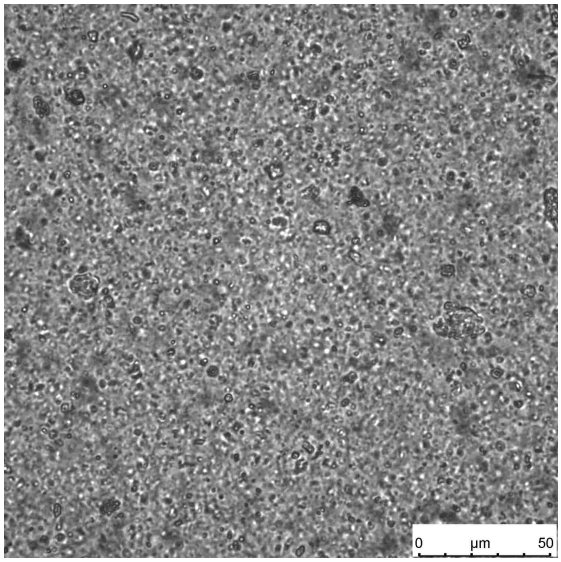

Figure 5.18. Water + bentonite: T = 25 °C (63x lens).

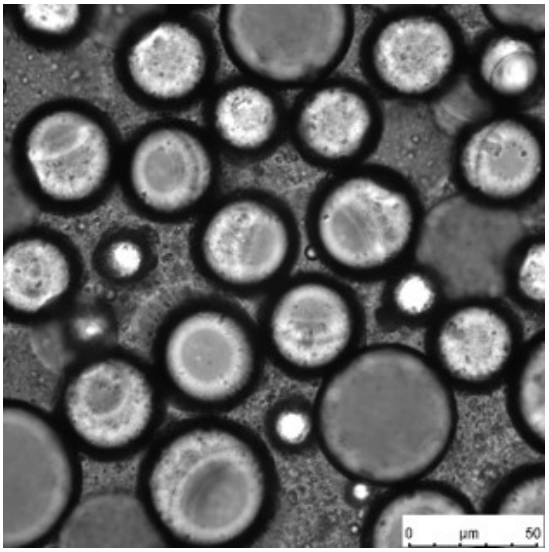

Figure 5.19. Water + oil + bentonite: O:W = 50:50, T = 25 °C (63x lens).

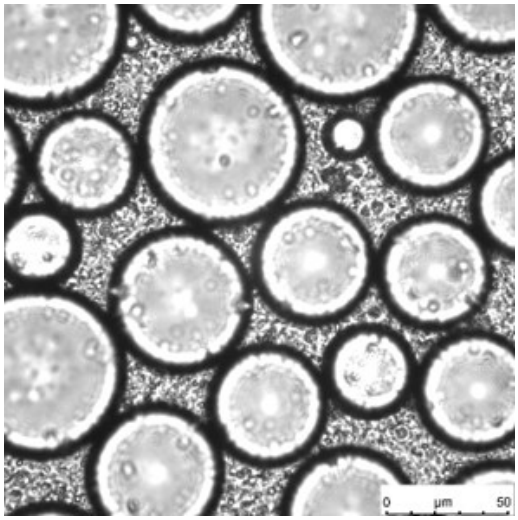

Figure 5.20. Water + oil + bentonite: O:W = 60:40, T = 25 °C (63x lens).

Table 5.6: Effect of Oil:Water Ratio: no surfactant.

Sample	Oil Vol. Frac.	δ (μm)
water + bentonite	0	nil
water + bentonite + oil	50	nil
water + bentonite + oil	60	0.04

This trend can be explained by the greater steric and hydrodynamics forces acting on the dispersed oil droplets that drive them away from the solid boundaries leading to the formation of a slip layer. The aforementioned is in agreement with conditions favorable to lubrication slip occurrence which are: (i) the presence of large individual or flocs of particles and (ii) high dependence of viscosity on volume fraction (or concentration) of the dispersed phase. Figures 5.18 to 5.20 show the microstructures of these samples.

5.5 Comparison to Drilling Muds

In this section, the effect of additives present in drilling fluids on slip behavior will be assessed by comparing the oil-base complex fluid (OCF) to the oil-base muds (OBM)

samples. As can be seen from Figures 5.21 to 5.24, the presence of fluid loss and weight additives present in the OBM samples do not induce true nor cohesive slip. The aforementioned observation is the case at all ratios. The main difference between the OCF and OBM samples was in lubrication form of slip.

This was particularly the case for those stabilized by surfactant S1 (Span 80). The presence of additives in the OBM led to the suppression of the slip layer, Table 5.7. This result is in agreement with literature, that reports increase in concentration of dispersed particle decrease slip layer thickness [94][95][101]. Absence of a distinct trend of the effect of additives on lubrication slip for the OCF and OBM samples stabilized by surfactant S2 (Brij 93) was found. Included in Appendix B are the slip type determination from flow curves of all OCF and OBM samples.

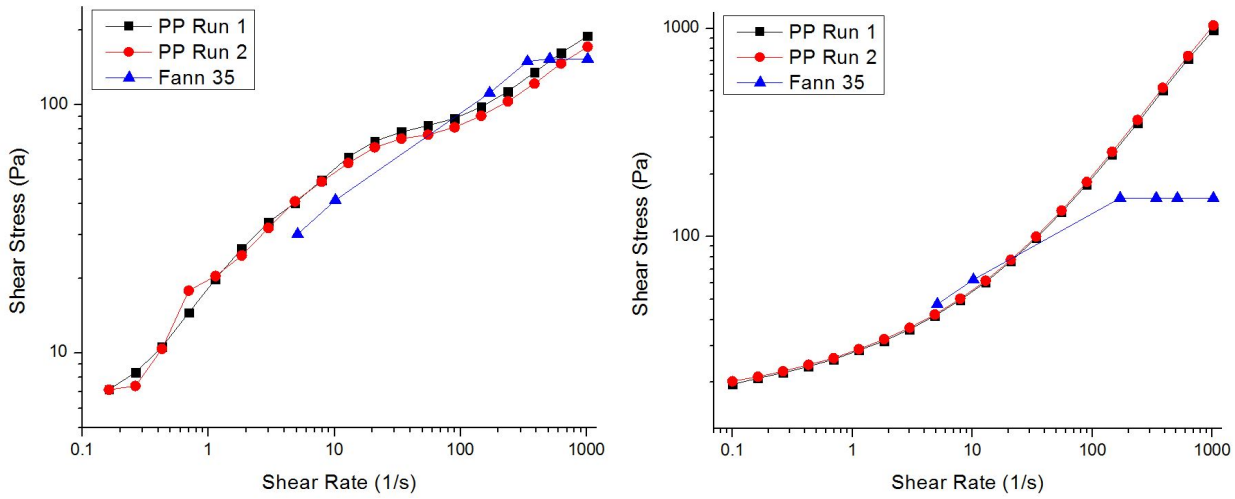

(a) OCF S1 (b) OBM S1

Figure 5.21. O:W = 60:40, C_{surf} = 3 wt.%, T = 25 °C.

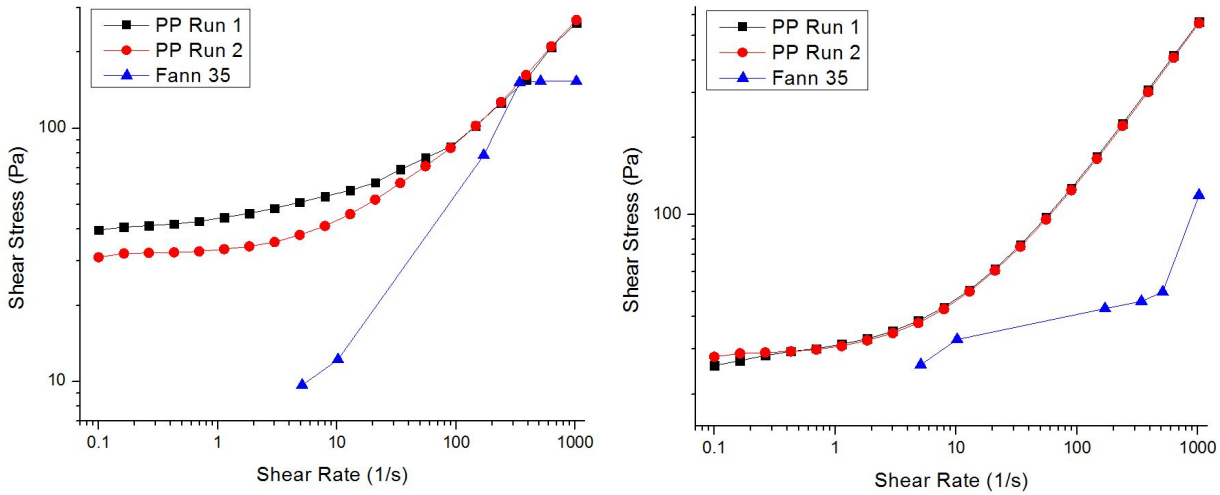

(a) OCF S2 (b) OBM S2

Figure 5.22. O:W = 60:40, C_{surf} = 3 wt.%, T = 25 °C.

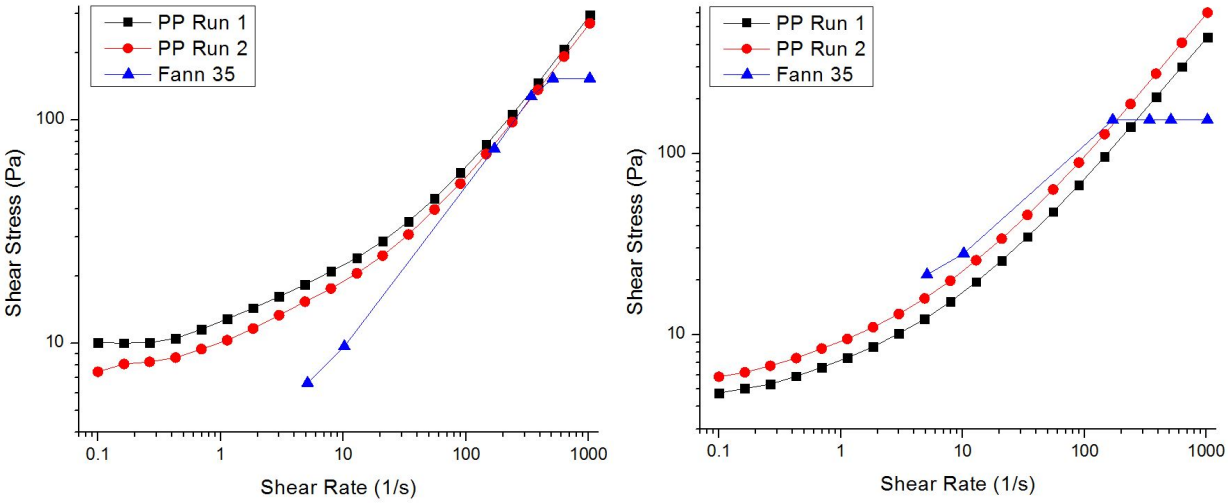

(a) OCF S1 (b) OBM S1

Figure 5.23. O:W = 70:30, C_{surf} = 3 wt.%, T = 25 °C.

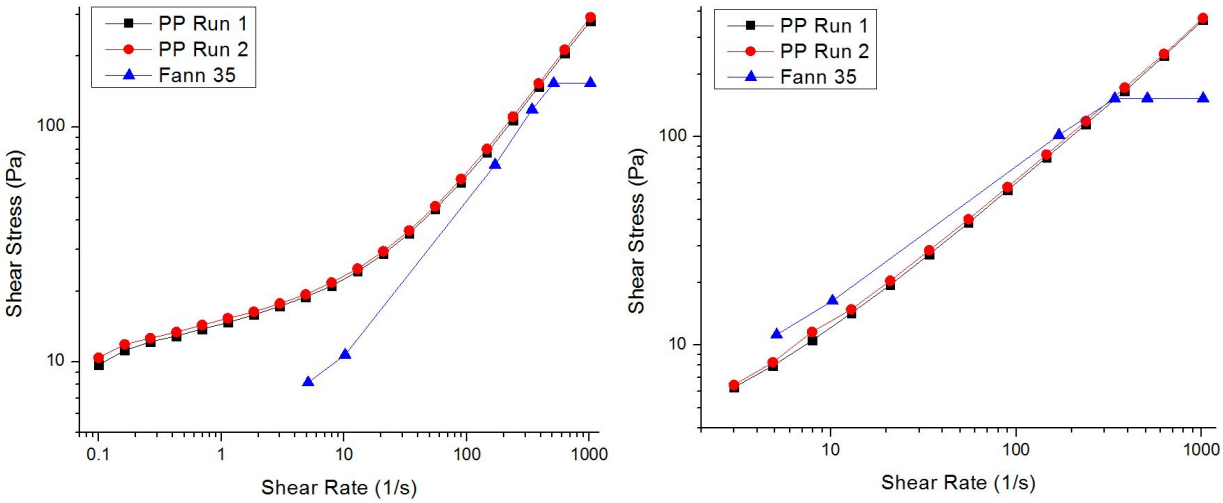

(a) OCF S2

(b) OBM S2

Figure 5.24. O:W = 70:30, C_{surf} = 3 wt.%, T = 25 °C.

Table 5.7: S1: C_{surf} = 3 wt.%, T = 25 °C.

O:W Ratio	OCF S1	OBM S1
60:40	52.77 μm	nil
70:30	92.58 μm	nil

Table 5.8: S2: C_{surf} = 3 wt.%, T = 25 °C.

O:W Ratio	OCF S2	OBM S2
60:40	nil	1.75 μm
70:30	0.56 μm	nil

Chapter 6
Conclusions

6.1 Effect of Surfactant Polarity

- Oil-base complex fluids (OCF) were found to display differing flow curve and yield properties based on the dipole moment (HLB) of the stabilizing surfactant. Difference in HLB as small as 0.3, as is the case between Span 80 and Brij 93 were found to lead to different outcomes in the flow curve and yield stress properties of the OCF samples. Samples stabilized by Span 80 displayed higher apparent viscosity than their counterparts stabilized by Brij 93. This was in great part due to the greater mitigation of linkage between bentonite particles, thereby facilitating emulsification.

- The difference in critical micelle concentration (CMC) between both surfactants, also contributed to the difference in flow curve and yield properties observed between both OCFs. The very low CMC of Span 80 translated to a greater concentration of surfactant molecules and micelles over Brij 93 at a fixed surfactant concentration. This made the plausible occurrence of depletion flocculation, driving of dispersed particles together, more prominent in Span 80 stabilized samples.

- Difference in dipole moment and CMC observed between complex fluids stabilized by the Span 80 (S1) and Brij 93 (S2) was also reflected in their fluid loss and stability properties. Lower fluid losses and higher stability were observed in OCFs stabilized by Brij 93. The aforementioned was driven by the greater contribution of bentonite to the end structure of the complex fluid.

6.2 Effect of Oil:Water Ratio

- Differences in flow curve and yield properties as a result of O:W ratio, were observed particularly for oil-base complex fluids stabilized by Span 80 (S1). Increase in O:W ratio, was associated to a decrease in apparent viscosity of the samples due to a reduction in the contribution of bentonite to its end structure. Effect of O:W ratio in

samples stabilized by Brij 93 was not distinct due to the contribution of other effects such as wall slip.

- The lower dipole moment of Brij 93 in comparison to Span 80, facilitates linkage between bentonite particles. This linkage however is not identical throughout the fluid's structure, resulting in anisotropy in its flow properties due to a heterogeneous microstructure. Thereby accounting for the more pronounced slip behavior in the flow curves of Brij 93 OCF samples as opposed to those of Span 80.

- No significant effect on fluid loss due to varying O:W ratio was found to occur samples stabilized by either surfactant. Stability of both type of oil-base complex fluids was found to increase with O:W ratio. This can be explained by the lower volume fraction of the conductive aqueous phase with increasing O:W ratio.

6.3 Effect of Temperature

- The apparent viscosity of all complex fluids was found to decrease with increasing temperature. This was driven by the weakening of the cohesive forces between liquid molecules with temperature increase.

- An increase in the trend of slip behavior was also observed with temperature increase for all samples. This stemmed from the increase in thermal fluctuations of dispersed particles with temperature increase, resulting in anisotropy of the fluid's mechanical properties i.e. flow curve.

- Increase in the elastic properties of the samples as a result of the flocculation of bentonite particles, and thus thickening of the complex fluid, was observed with temperature increase. This was particularly the case of samples stabilized by Brij 93.

- OCFs stabilized by Span 80 were found to be more prone to complete demulsification at high temperatures, due to the lower contribution of bentonite to their end structure.

This is accounted for by the greater dipole moment and lower CMC of Span 80 in comparison to Brij 93.

6.4 Phase Inversion

- Oil-base complex fluids were all found to undergo catastrophic phase inversion (CPI) to water-base complex fluids at O:W ratios between 40:60 - 50:50 (i.e. 50 - 60 vol.% water). This range of inversion was found to be independent of surfactant polarity. Subsequent transitional phase inversion (TPI) back to an oil-base fluid was also found to occur in all samples, albeit to different extents based on surfactant polarity. Oil-base complex fluids stabilized by Brij 93 were found to undergo TPI to a greater extent as a opposed to their Span 80 counterparts.

- The separate investigation on water-base complex fluids for transitional phase inversion, showed complex fluids stabilized by polyoxyethylene oleyl ether (nonionic) surfactants underwent distinct phase inversion to oil-base complex fluids. This was particularly the case at 7.5 HLB, where buildup in the apparent viscosity of the samples following temperature increase was significant.

- Phase inversion was not distinctly observed in sorbitan monooleate (nonionic) surfactant stabilized fluid samples, and did not occur at all in ionic surfactant stabilized samples.

6.5 Comparison to Drilling Muds

- Comparison between oil-base complex fluids (OCF) and oil-base muds (OBM) showed the latter to display higher apparent viscosity in their flow curve measurements. This observation was found to be independent of the stabilizing surfactant's polarity. The increase in dispersed particle concentration, due to the presence of fluid loss and weight additives, accounted for the larger apparent viscosity of the OBM samples.

- OCF and OBM stabilized by surfactant Span 80 were observed to display identical flow curve profiles, although higher shear stresses were observed for OBM.

- OCF and OBM stabilized by Brij 93 surfactant stabilized samples did not display identical flow curve profiles. It was further observed when comparing the flow curves, that greater slip behavior was displayed by OCF over OBM samples.

- Yield properties of the OBM samples were equally found to be superior to those of the OCFs, with lower strain deformation levels observed in the former. This observation was independent of surfactant polarity.

6.6 Wall Slip

- Investigation of the different forms of slip: true (wall), cohesive and lubrication slip in oil-base complex fluids, showed composition and temperature to significantly affect the occurrence of either slip form and its extent.

- Increase in surfactant concentration was found to mitigate or suppress the occurrence of all forms of slip. This observation was independent of surfactant polarity, and was driven by the reduction of particle clusters and droplet size with increase in surfactant concentration.

- Surfactant polarity was not observed to affect the occurrence of true and cohesve slip, however lubrication slip was found to be more prominent in Span 80 (S1) stabilized fluid samples. The lower CMC and higher dipole moment of Span 80 over Brij 93 allows the formation of emulsion droplets which get depleted from the wall boundary of solids surfaces, thereby facilitating the formation of slip layers.

- Increasing temperatures was found to exacerbate all forms of slip behavior irrespective of the stabilizing surfactant. This was accounted for by the increase in thermal fluctuation of dispersed particles, as well as the enhanced aggregation of bentonite particles.

Both of the aforementioned increase the level of heterogeneity of the complex fluids making them prone to exhibit slip. The increase in the depletion of dispersed particles away from solid boundaries as a result of thermal fluctuations equally increases slip.

- Oil:Water ratio was found to primarily affect lubrication slip. Increase in Oil:Water ratio was observed to lead to an increase in slip layer thickness.

- Comparison between OCFs and OBMs found lubrication slip to be the main form of slip where a significant difference existed between both types of fluid. This was particularly the case of Span 80 (S1) stabilized samples, where no slip layer was associated to OBM as opposed to OCF.

References

[1] Jha, P. V., V. Mahto and V. K. Saxena. 2014. "Emulsion Based Drilling Fluids: An Overview." *International Journal of ChemTech Research.*

[2] Hilfiger, Matthew G., Thaemlitz, Carl J., and Mollendick, Eric. 2016. "Investigating the Chemical Nature of Flat Rheology." *SPE Deepwater Drilling & Completion Conference, SPE-180320-MS, SPE Galvestone*

[3] Dekker, Martijn and David Reid. 2014. "Deepwater Development Strategy." *Offshore Technology Conference, OTC-25135, Houston*

[4] Charnvit, K., F. Huadi, C. Promkhote, C. Aldea, D. Power, N. Kongpat, and S. Gilles. 2014. "Meeting Drilling Fluid Challenges in the Gulf of Thailand Ultra-High Temperature Exploration Wells." *IADC/SPE Asia Drilling Technology Conference, IADC/SPE-170514-MS, Bangkok.*

[5] Souders, Paul. *http://fortune.com/2012/05/10/the-coming-arms-race-for-arctic-oil/.*

[6] Zamora, M., P. N. Broussard and M. P. Stephens. 2000. "The Top 10 Mud-Related Concerns in Deepwater Drilling Operations." *SPE International Petroleum Conference and Exhibition, SPE-59019, Villahermosa.*

[7] McLean, A., A. Wilde, M. Zamora and M. Rafferty. 2010. "The Top 10 Mud-Related Concerns in Deepwater Drilling Operations - Revisited after 10 Years." *2010 AADE Fluids Conference and Exhibition, AADE-10-DF-HO-04, Houston.*

[8] Fereday, Kelli. 2012. "Downhole Drilling Problems: Drilling Mysteries Revealed!." *2012 AAPL Annual Meeting Sponsors, San Francisco.*

[9] Young, S., J. Friedheim, J. Lee and O. I. Prebensen. 2012. "A New Generation of Flat Rheology Invert Drilling Fluids." *SPE Oil and Gas India Conference and Exhibition, SPE-154682, Mumbai.*

[10] Leaper, R., N. Hansen, M. Otto, L. Moroni and B. Dye. 2006. "Meeting Deepwater Challenges with High Performance Water Based Muds." *AADE Drilling Fluids Technical Conference, AADE-06-DF-HO-31, Houston.*

[11] Scott, Katherine. 2013. "Can't Keep the Offshore Industry Down." *http://www.drillingcontractor.org/cant-keep-the-offshore-industry-down-22460.*

[12] McClements, David J. 2011. "Edible Nanoemulsions: Fabrication, Properties, and Functional Performance." *The Royal Society of Chemistry, Soft Matter, vol. 7, pp. 2297-2316.*

[13] Sadeghy, K. 2001. "Wall Slip Effects of Water-Based Bentonite Drilling Muds at High Pressures and Temperatures." *IADC/SPE Middle East Technology, SPE/IADC-72326, Bahrain*

[14] BSEE per Holland. 2017. "Loss of Well Control Occurrence and Size Estimators, Phase I and II." *BSEE Report Nº. ES201471/2.*

[15] M-I LLC. 2002. "Drilling Fluids Engineering Manual." *Houston, TX.*

[16] Bourgoyne Jr., A. T., K. K. Millheim, M. E. Chenevert, and F. S. Young Jr. 1991. "Applied Drilling Engineering." *Second Printing Society of Petroleum Engineers; Richardson, TX.*

[17] ASME. 2005. "Drilling Fluids Processing Handbook." *Gulf Professional Publishing: Burlington.*

[18] Oil & Gas UK. $https : //www.rigzone.com/training/insight.asp?insight_id = 291\&c_id =$.

[19] Quintero, Lirio. 2002. "An Overview of Surfactant Applications in Drilling Fluids for the Petroleum Industry." *J. Dispersion Science and Technology, vol. 23 (1-3), pp. 393-404.*

[20] Schlumberger Oilfield Glossary. January 2019. $https : //www.glossary.oilfield.slb.com/en/Terms/d/differential_sticking.aspx$.

[21] Al-Riyamy, K. and M. M. Sharma. 2004. "Filtration Properties of Oil-in-Water Emulsions containing Solids." *SPE Drilling & Completion, SPE-89015.*

[22] Perkins, H. W. 1951. "A Report on Oil-Emulsion Drilling Fluids." *Spring Meeting, Southwestern District.*

[23] Griffin, W. C. 1949. "Classification of Surface-Active Agents by HLB." *Journal of Cosmetic Science, vol. 1, no.5, pp. 311-326.*

[24] Davies, H. T. 1994. "Factors Determining Emulsion Type: Hydrophile-Lipophile Balance and Beyond." *Colloids and Surfaces A: Physicochemical and Engineering Aspects, vol. 91, pp. 9 - 24.*

[25] Becher, P. 1985. "Hydrophile-Lipophile Balance: An Updated Bibliography." *Encyclopedia of Emulsion Technology, vol. 2, pp. 425 - 512.*

[26] Quintero, L., E. Lujano and J. Blanco. 1995. "Formulation of Diesel-in-Water Emulsions as Drilling Fluids." *IX European Conference on Colloid and Interfacial Science, Barcelona.*

[27] Blanco, J. and L. Quintero. 1998. "Oil-in-Water Emulsion Well Servicing Fluids." *U. S. Patent No. 5,783,525, July 21, 1998.*

[28] Salager, J. L. 1996. "Guidelines to Attain Desired Emulsion Properties. In Surfactant in Solutions, Surfactant Science Series." *New York, vol. 64, 261 - 295.*

[29] Lummus, J. L. and J. J. Azar. 1953. "The Effects of use of Oil in Drilling Muds." *Spring meeting of the Midcontinent District, Division of Production, Tulsa.*

[30] Lawhon, C. P., W. M. Evans, and J. P. Simpson. 1967. "Laboratory drilling rate and filtration studies of emulsion drilling fluids." *Journal of Petroleum Technology, pp. 943 - 948.*

[31] Caenn, R., H. C. H. Darley and G. R. Gray. 2011. "Composition and Properties of Drilling and Completion Fluids." *6th Edition, Elsevier Inc, pp. 92 - 101.*

[32] Caenn, R. and G. V. Chillingar. 1996. "Drilling fluids: State of the Art." *Journal of Petroleum Science and Engineering, vol. 14, pp. 221 - 230.*

[33] Wunderlich, R. W. 1991. "Obtaining Samples with Preserved Wettability." *In Interfacial Phenomena in Petroleum Recovery, Surfactant Science Series, vol. 36, pp. 289 - 317.*

[34] Kulkami, P. 2010. "India's First Deepwater Offshore Field Showcases Ingenuity." *Journal of Petroleum Technology.*

[35] Sheplyakova Helen. 2017. "Deepwater Oil Drilling: Discovering Pros and Cons of a Controversial Industry." *https : //medium.com/@helen.sheplyakova/deepwater − oil − drilling − discovering − pros − and − cons − of − a − controversial − industry −* 35436*e*1161*b*5.

[36] van Oort, E., J. Lee, J. Friedheim, and B. Toups. 2004. "New Flat-Rheology Synthetic-Based Mud for Improved Deepwater Drilling." *SPE Annual Technical Conference & Exhibition, SPE-90987, Houston.*

[37] Aadnoy, B., I. Cooper, S. Miska, R. F. Mitchell, and M. L. Payne. 2009. "Advanced Drilling and Well Technology." *Society of Petroleum Engineers, ISBN: 978-1-55563-145-1.*

[38] Saasen Arild. 2014. "Annular Frictional Pressure Losses during Drilling - Predicting the Effect of Drillstring Rotation." *Journal of Energy Resources Technology, vol. 136.*

[39] Kelessidis, V. C., R. Maglione, C. Tsamantaki and Y. Aspirtakis. 2006. "Optimal Determination of Rheological Parameters for Herschel-Bulkley Drilling Fluids and Impact on Pressure Drop, Velocity Profiles and Penetration Rates during Drilling." *Journal of Petroleum Science and Engineering vol.53, pp. 203 - 224.*

[40] Khodja, M., M. Khoda-Saber, J.P. Canselier, N. Cohaut and F. Bergaya. 2010. "Drilling Fluid Technology: Performances and Environmental Considerations." *Products and Services from R and D to Final Solutions, 10.5772/10393.*

[41] Haldenwang Rainer. 2003. "Flow of Non-Newtonian Fluids in Open Channels." *Dissertation Department of Civil Engineering, Cape Technikon.*

[42] Sayindla, S., B. Lund, J. D. Ytrehus and A. Saasen. 2017. "CFD Modelling of Observed Cuttings Transport in Oil-Based and Water-Based Drilling Fluids." *SPE/IADC Drilling Conference and Exhibition, SPE/IADC-184660-MS, The Hague.*

[43] Rooki, R., F. D. Ardejani, A. Moradzadeh and M. Norouzi. 2015. "CFD Simulation of Rheological Model Effect of Cuttings Transport." *Journal of Dispersion Science and Technology, vol. 36, pp. 402 - 410.*

[44] Versteeg, H. K. and W. Malalasekera. 1995. "An Introduction to Computational Fluid Dynamics, the Finite Volume Method." *Upper Saddle River, NJ: Prentice Hall.*

[45] Cho, H., S. N. Shah and S. O. Osisanya. 2000. "A Three-Segment Hydraulic Model for Cuttings Transport in Horizontal and Deviated Wells." *Proceedings of the SPE/Petroleum Society of CIM International Conference on Horizontal Well Technology, Calgary.*

[46] Adari, R. B., S. Miska, E. Kuru, P. Bern and A. Saasen. 2000. "Selecting Drilling Fluid Properties and Flow Rates for Effective Hole Cleaning in High-Angle and Horizontal Wells." *Proceedings of the SPE Annual Technical Conference and Exhibition, Dallas, pp. 273 - 281.*

[47] Valluri, S. G., S. Z. Miska, R. Ahmed, M. Yu and N. Takach. 2006. "Experimental Study of Effective Hole Cleaning using 'Sweep' in Horizontal Wellbores." *SPE Annual Technical Conference and Exhibition, SPE-101220, San Antonio.*

[48] Mohammadsalehi, M. and N. Malekzadeh. 2011. "Optimization of Hole Cleaning and Cutting Removal in Vertical, Deviated and Horizontal Wells." *Proceedings of the Asia Pacific Oil and Gas Conference and Exhibition, SPE-143675, Jakarta.*

[49] Ofei T. N. 2016. "Effect of Yield Power Law Fluid Rheological Properties on Cuttings Transport in Eccentric Horizontal Narrow Annulus." *Journal of Fluids, vol. 2016, pp. 10.*

[50] Butt, H. J., K. Graf and M. Kappl. 2003. "Physics and Chemistry of Interfaces." *Weinheim: Wiley-VcH.*

[51] Laughlin, R. G. 1996. "The Aqueous Phase Behavior of Surfactants." *Academic Press, London.*

[52] Gelbart, W. M., A. Ben-Shaul, and D. Roux. 1994. "Micelles, Membranes, Microemulsions and Monolayers." *Springer, New York.*

[53] Tanford, C. 1980. "The Hydrophobic Effect." *Wiley, New York.*

[54] Bancroft, W. D. J. 1913. "The Theory of Emulsification." *Journal of Physical Chemistry, 17:501*

[55] Clowes, G. H. A. 1916. "The Protoplasmic Equilibrium." *The Journal of Physical Chemistry, vol. 20, pp. 407 - 451.*

[56] Al-Sabagh, A. M. 2002. "The Relevance HLB of Surfactants on the Stability of Asphalt Emulsions." *Colloid and Surfaces A: Physicochemical and Engineering Aspects, vol. 204, pp. 73 - 83.*

[57] Preziosi, V., A. Perazzo, S. Caserta, G. Tomaiuolo and S. Guido. 2013. "Phase Inversion Emulsification." *Chemical Engineering Transactions, vol. 32, pp. 1585-1590.*

[58] Mason, T. G. 1999. "New Fundamental Concepts in Emulsion Rheology." *Current Opinion in Colloid and Interface Science, vol. 4, pp. 231-238.*

[59] Tadros, T. F. 1994. "Fundamental Principles of Emulsion Rheology and their Application." *Colloids and Surfaces Physicochemical and Engineering Aspects, vol. 91, pp. 39-55.*

[60] Sherman, P. 1968. "Rheology of Emulsions." *Emulsion Science, Chapter 4, Academic Press, London.*

[61] Bibette, J., and F. Leal-Calderon. 1996. "Surfactant Stabilized Emulsions." *Current Opinion in Colloid Interface Science, vol. 1, pp. 746-751.*

[62] Lequeux, F. 1998. "Emulsion Rheology." *Current Opinion in Colloid and Interface Science, vol. 3, pp. 408-411.*

[63] Dimitrova, T. D., L. Calderon, T. D. Gurkov and B. Campbell. 2004. "Surface Forces in Model Oil-in-Water Emulsions stabilized by Proteins Oil." *Advanced Colloid Interface Science, vol. 108 - 109, pp. 73 - 86.*

[64] Russev, S. C., T. V. Arguirov and T. D. Gurkov. 2000. "Beta-Cassein Adsorption Kinetics on Air-Water and Oil-Water Interfaces studied by Ellipsometry." *Colloids Surfaces, vol. 19, pp. 89 - 100.*

[65] Einstein, A. 1906. "Investigations on the Theory of Brownian Movement." *Dover, New York.*

[66] Taylor, G. I. 1932. "The Viscosity of a Fluid Containing Small Drops of Another Fluid." *Proceedings of the Royal Society, vol. 138, issue 834.*

[67] Richardson, E. G. 1950. "The formation and flow of emulsion." *Journal of Colloid Science, vol. 5, pp. 404 - 413.*

[68] Packman, M. K. and Th. F. Tadros. 1992. "Depletion Flocculation of Concentrated Latex Suspensions by Surfactant Micelles." *Colloids and Surfaces, vol. 67, pp. 265 - 272.*

[69] Rommetveit, R., and K. S. Bjorkevoll. 1997. "Temperature and Pressure Effects on Drilling Fluid Rheology and ECD in very Deep Well." *SPE/IADC Middle East Drilling Technology Conference, SPE/IADC-39282.*

[70] Lee, J., A. Shadravan and S. Young. 2012. "Rheological Properties of Invert Emulsion Drilling Fluid under Extreme HPHT Conditions." *IADC/SPE Drilling Conference and Exhibition, SPE/IADC-151413.*

[71] Chen, G. and D. Tao. 2005. "An Experimental Study of the Stability of Oil-Water Emulsions." *Fuel Processing Technology,vol. 86, pp. 499 - 508.*

[72] James, R. P. and R. P. Charles. 1985. *Petroleum Spills.*

[73] Oltedal, V. M., B. Werner, B. Lund, A. Saasen and J. D. Ytrehus. 2015. "Rheological Properties of Oil Based Drilling Fluids and Base Oils." *Proceedings of the ASME 2015 34th International Conference on Ocean, Offshore and Artic Engineering, OMAE2015-41911, Newfoundland.*

[74] Duan, L., J. Jing, J. Wang, X. Huang, x. Qin and Y. Qiu. 2010. "Study on Phase Inversion Characteristics of Heavy Oil Emulsions." *Internation Society of Offshore and Polar Engineers, ISOPE-I-10-364.*

[75] Plasencia, J., and O. J. Nydal. 2014. "Phase Inversion in Dispersed Two Phase Oil-Water Pipe Flow." *9th North American Conference on Multiphase Technology, BHR-2014-E2.*

[76] Sajjadi, S., M. Zerfa and B. W. Brooks. 2000. "Morphological Change in Drop Structure with Time for Abnormal Polymer/Water/Surfactant Dispersions." *Langmuir Vol. 16, pp. 100015-10019.*

[77] Jahanzad, F., G. Crombie, R. Innes, and S. Sajjadi. 2009. "Catastrophic Phase Inversion via Formation of Multiple Emulsions: A Prerequisite for Formation of Fine Emulsions." *Chemical Engineering Research and Design, vol. 87, pp. 492-498.*

[78] Solans, C. and I. Sole. 2012. "Nano-Emulsions: Formation by Low-Energy Methods." *Current Opinion in Colloid and Interface Science, vol. 17, pp. 246-254.*

[79] Anton, N., P. Gayet, J. P. Benoit, and P. Saulnier. 2007. "Nano-Emulsions and Nanocapsules by the PIT method: An Investigation on the Role of the Temperature Cycling on the Emulsion Phase Inversion." *Int. J. Pharm., vol. 344, pp. 44-52.*

[80] Anton, N., and T.F. Vandamme. 2009. "The Universality of Low-Energy Nano-Emulsification." *International Journal of Pharmaceutics, vol. 377, pp. 142-147.*

[81] Gutierrez, J. M., C. Gonzalez, A. Maestro, I. Sole, C. M. Pey and J. Nolla. 2008. "Nano-Emulsions: New Applications and Optimization of their Preparation." *Current Opinion in Colloid and Interface Science, vol. 13, pp. 245-251.*

[82] Israelachvili, J. 1992. "Intermolecula and Surface Forces." *Academic Press, 2nd Edition, London, UK.*

[83] McClements, J. David. 2012. "Nanoemulsions versus microemulsions: terminology, differences and similarities." *Soft Matter, vol. 8, pp. 1719 - 1729.*

[84] Tadros, T., R. Izquierdo, J. Esquena and C. Solans. 2004. "Formation and stability of nano-emulsions." *Advances in Colloid and Interface Science, vol. 108 - 410, pp. 303 - 318.*

[85] Mason, T. G., J. N. Wilking, K. Meleson, C. B. Chang and S. M. Graves. 2006. "Nanoemulsions: formation, structure and physical properties." *Journal of Physics: Condensed Matter, vol. 19, pp. R635 - R666.*

[86] Sonneville-Auburn, O., J. T. Simonnet and F. L'Alloret. 2004. "Nano-emulsions: a new vehicle for skincare products." *Advances in Colloid and Interface Science, vol. 108 - 109, pp. 145 - 149.*

[87] Becher, P. 2001. "Emulsions: Theory and Practice." *American Chemical Society, Washington, DC.*

[88] Alexander, A. E. and J. H. Schulman. 1949. "Molecular interactions at oil-water interfaces. Part III. Interfacial tension measurements." *Transactions of the Faraday Society, vol. 36, pp. 960 - 964.*

[89] Lehnert, S., H. Tarabishi, and H. Leuenberger. 1994. "Investigation of Thermal Phase Inversion in Emulsions." *Physicochemical and Engineering Aspects, vol. 91, pp. 227-235.*

[90] Dahms, G. 1991. "Rheology of Cosmetic Water-in-Oil Formulations." *Seifen Oele Fette Wachse, vol. 117(4), pp. 145 - 150*

[91] Shinoda, K., and H. Saito. 1969. "The Stability of O/W Type of Emulsions as Functions of Temperature and the HLB of Emulsifiers: The Emulsification by the PIT-Method." *Journal of Colloid and Interface Science, vol. 30, pp. 258-263.*

[92] Patel, A. D. 1998. "Reversible Invert Emulsion Drilling Fluids - A Quantum Leap in Technology." *IADC/SPE Asia Pacific Drilling Technology, SPE-47772-MS, Jakarta.*

[93] Larson, G. Ronald. 1999. "The Structure and Rheology of Complex Fluids." *Oxford University Press, Inc.*

[94] Barnes, H. 1995. "A Review of the Slip of Polymer Solutions, Emulsions and Suspensions in Viscometers." *Journal of Non-Newtonian Fluid Mechanics, vol. 56, p. 221.*

[95] Sanchez, M. C., C. Valencia, J. M. Franco, and C. Gallegos. 2001. "Wall Slip Phenomena in Oil-in-Water Emulsions: Effect of some Structural Parameters." *Journal of Colloid and Interface Science, vol. 241, pp. 226-232.*

[96] Ma, L. and G. V. Barbosa-Canovas. 1995. "Rheological Characterization of Mayonnaise. Part II: Flow of Viscoelastic Properties at Different Oil and Xanthan Gum Concentrations." *Journal of Rheology, vol. 25, pp. 397.*

[97] Goshawk, J. A., D. M. Binding, D. B. Kell and R. J. Goodacre. 1998. "Rheological Phenomena occurring during the the Shearing Flow of Mayonnaise." *Journal of Rheology, vol. 42, pp. 1537.*

[98] Plucinski, J., R. K. Gupta and S. Chakrabart. 1998. "Wall slip of Mayonnaises in Viscometers." *Rheologica Acta, vol. 37, issue 3, pp. 256 - 269.*

[99] Franco, J. M., C. Galllegos and H. A. Barnes. 1998. "On Slip Effects in Steady-State Flow Measurements of Oil-in-Water Food Emulsions." *Journal of Food Engineering, vol. 36, issue 1, pp. 89 - 102.*

[100] Wise, G. M., M. M. Denn, A. T. Bell, J. W. Mays, K. Hong and H. Iatrou. 2000. "Surface Mobility and Slip of Polybutadiene Melts in Shear Flow." *Journal of Rheology, vol. 44, pp. 549.*

[101] Soltani, F., and U. Yilmazer. 1998. "Slip Velocity and Slip Layer Thickness in Flow of Concentrated Suspensions." *Journal of Applied Polymer Science, vol. 70, pp. 515-522.*

[102] McDonough, J. M. 2009. "Lectures in Elementary Fluid Dynamics". *Department of Mechanical Engineering and Mathematics, University of Kentucky.*

[103] Ovarlez, G., S. Rodts, X. Chateau and P. Coussot. 2009. "Phenomenology and Physical Origin of Shear Localization and Shear Banding in Complex Fluids." *Rheologica Acta, vol. 48, pp. 831 - 844.*

[104] Warren, T. M. 1984. "Factors Affecting Torque for a Roller Cone Bit." *Journal of Petroleum Technology, pp. 1500 - 1508.*

[105] Tang, H. S., and D. M. Kalyon. 2008. "Time-dependent Tube Flow of Compressible Suspensions subject to Pressure Dependent Wall Slip: Ramifications on Development of Flow Instabilities." *Journal of Rheology, vol. 52, 1069.*

[106] Yoshimura, A. and R. K. Prud'homme. 1988. "Wall Slip Corrections for Couette and Parallel Disk Viscometers." *Journal of Rheology, vol. 32, pp. 53 - 67.*

[107] Yilmazer, U. and D. M. Kaylon. 1989. "Slip Effects in Capillary and Parallel Disk Torsional Flows of Highly Filled Suspensions." *Journal of Rheology, vol. 33, pp. 1197 - 1212.*

[108] de Gennes, P.-G., F. Brochard-Wyart, and D. Quere. 2004. "Capillarity and Wetting Phenomena". *Springer-Verlag New York, Inc.*

[109] Coussot, P., J. S. Raynaud, F. Bertrand, P. Moucheront, J. P. Guilbaud, H. T. Huynh, S. Jarny and D. Lesueur. 2002. "Coexistence of Liquid and Solid Phases in Flowing Soft-Glassy Materials." *Phys. Rev. Lett., vol. 88.*

[110] Brown, E. and H. M. Jaeger. 2012. "The Role of Dilation and Confining Stress in Shear Thickening of Dense Suspensions." *J. Rheol., vol. 56, pp. 875 - 923.*

[111] Brown, E. and H. Jaeger. 2014. "Shear Thickening in Concentrated Suspensions: Phenomenology, Mechanisms and Relations to Jamming." *Rep. Prog. Phys., vol. 77.*

[112] Brady, J. F. and G. Bossis. 1985. "The Rheology of Concentrated Suspensions of Spheres in Simple Shear Flow by Numerical Simulations." *Journal of Fluid Mechanics, vol. 155, pp. 105.*

[113] Wagner, N. J. and J. F. Brady. 2009. "Shear Thickening in Colloidal Dispersions." *Phys. Today, vol. 62, pp. 27 - 32.*

[114] Brown, E. and H. M. Jaeger. 2011. "Through Thick and Thin." *Science, vol. 333, pp. 1230.*

[115] Melrose, J. R. and R. C. Ball. 2004. "Continuous Shear Thickening Transitions in Model Concentrated Colloids - The Role of Interparticle Forces." *Journal of Rheology, vol. 48, pp. 937.*

[116] Somwangthanaroj, A. 2010. "Rheology and Polymer Characterization." *htttp://pioneer.netserve.chula.ac.th/ sanongn1/course.html*

[117] Macosko, C. W. 1994. "Rheology: Principles, Measurements and Applications." *Wiley-VcH, New York.*

[118] Do Nascimento, G. M. 2016. "Structure of Clays and Polymer Composites Studied by X-ray Absorption Spectroscopies." *Clay, Clay Minerals and Ceramic Materials Based on Clay Minerals, Intechopen.*

[119] Wilson, G. J. 1968. "An Improved Method for Computing Directional Survey." *Journal of Petroleum Technology, pp. 871-876, AIME, 243.*

[120] Vryzas, Z., V. C. Kelessidis, L. Nalbantian, V. Zaspalis, D. I. Gerogiorgis and Y. Wubulikasimu. 2017. "Effect of Temperature on the Rheological Properties of Neat Aqueous Wyoming Sodium Bentonite Dispersions." *Applied Clay Science, vol. 469, pp. 26 - 36.*

[121] van Olphen, H. "Introduction to Clay Colloidal Chemistry." *2nd edition, Wiley N. Y.*

[122] Chhabra, R. P. 2010. "Non-Newtonian Fluids: An Introduction." *SERC Schooll-cum-Symposium on Rheology of Complex Fluids, Chennai.*

[123] Herzhaft, B., L. Rousseau, L. Neau, M. Moan and F. Frederic. 2002. "Influence of Temperature and Clays/Emulsion Microstructure on Oil-Based Low Shear Rate Rheology." *SPE Annual Technical Conference and Exhibition, SPE 77818, San Antonio.*

[124] Tehrani, Ahmadi. 2007. "Behavior of Suspensions and Emulsions in Drilling Fluids." *Annual Transactions of the Nordic Rheology Society, vol. 15.*

[125] Lim, F. J. and W. R. Schowalter. 1989. "Wall Slip of Narrow Molecular Weight Distribution Polybutadienes." *Journal of Rheology, vol. 33, pp. 1395.*

[126] Benbow, J. J. and P. Lamb. 1963. "New aspects of melt fracture." *Polymer Science and Engineering.*

Appendix A
Oil-base Complex Fluids
A.1 Effect of Surfactant Polarity

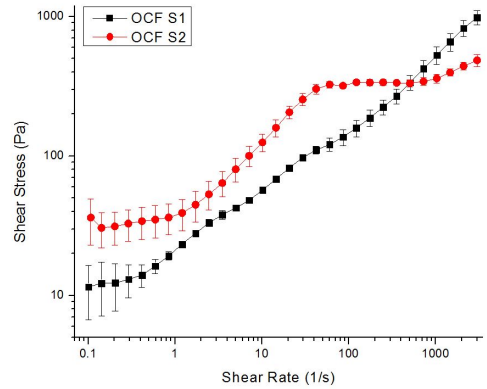

(a) T = 0 °C

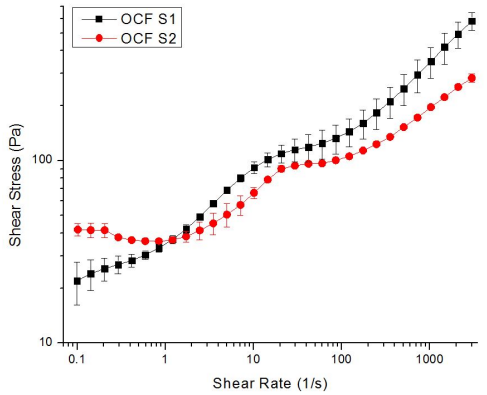

(b) T = 10 °C

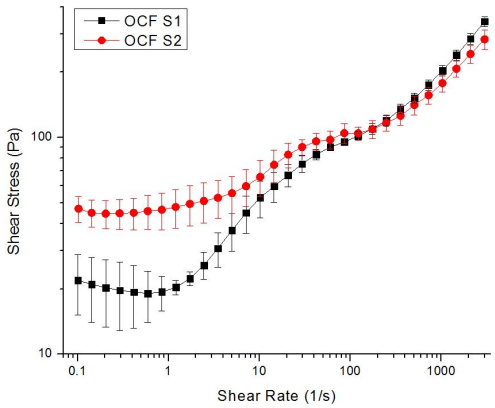

(c) T = 25 °C

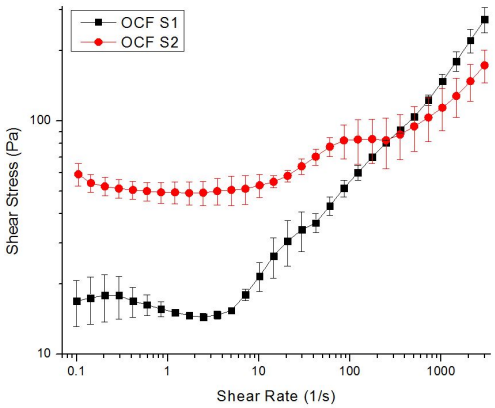

(d) T = 50 °C

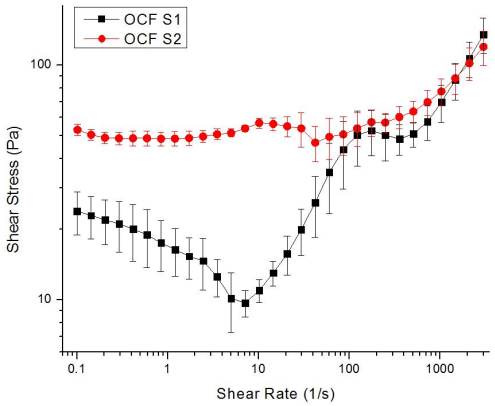

(e) T = 75 °C

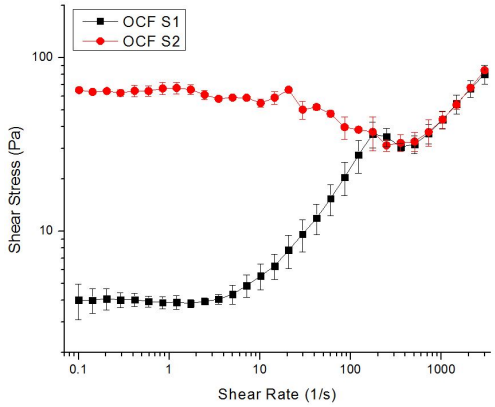

(f) T = 90 °C

Figure A.1. Flow Curve: O:W = 50:50, C_{surf} = 1 wt.%.

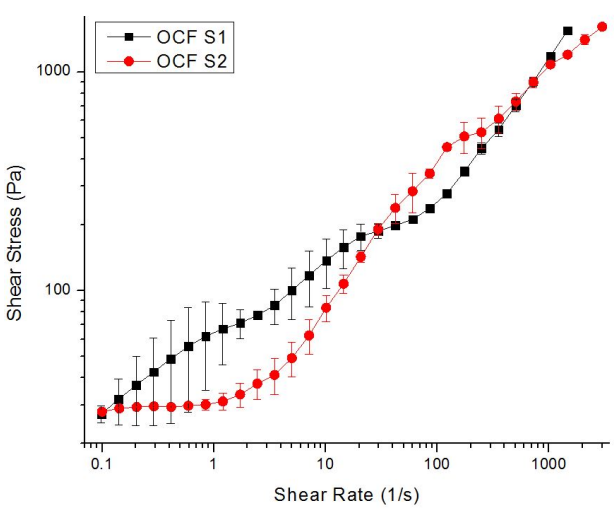

(a) T = 0 °C

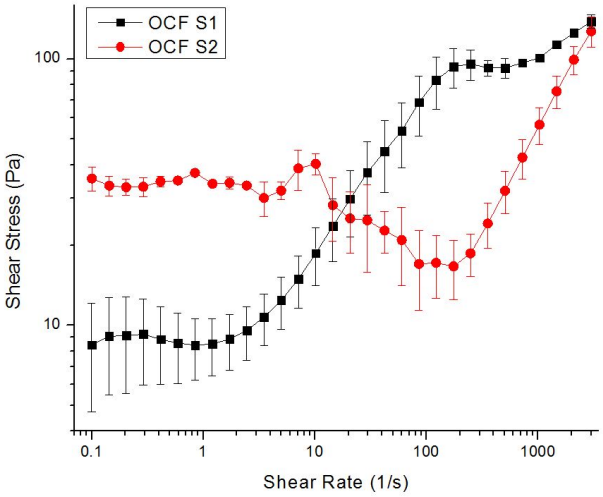

(d) T = 50 °C

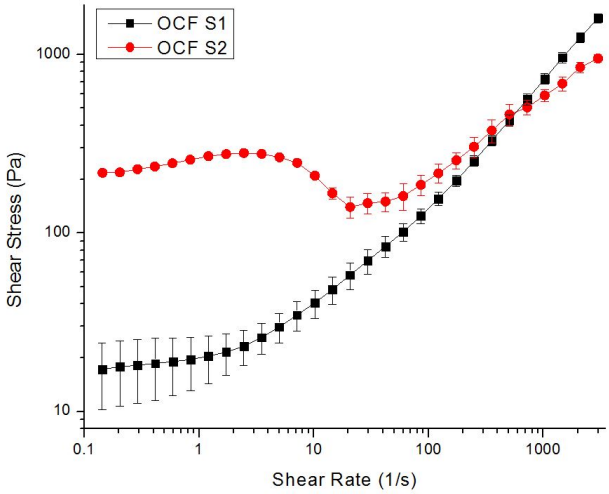

(b) T = 10 °C

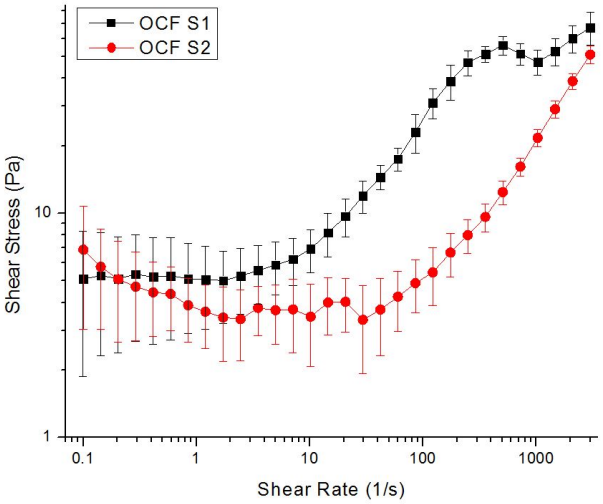

(e) T = 75 °C

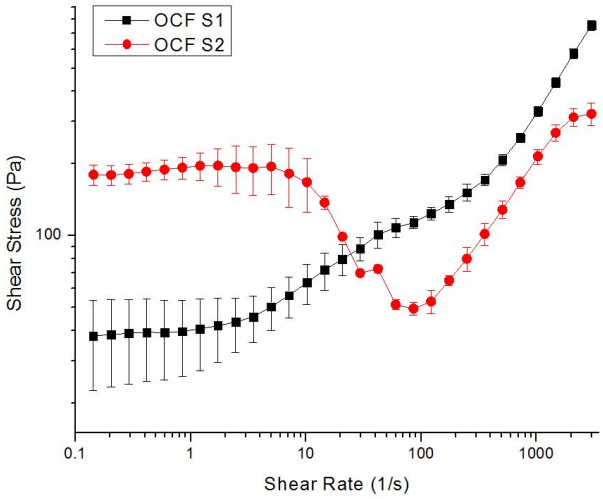

(c) T = 25 °C

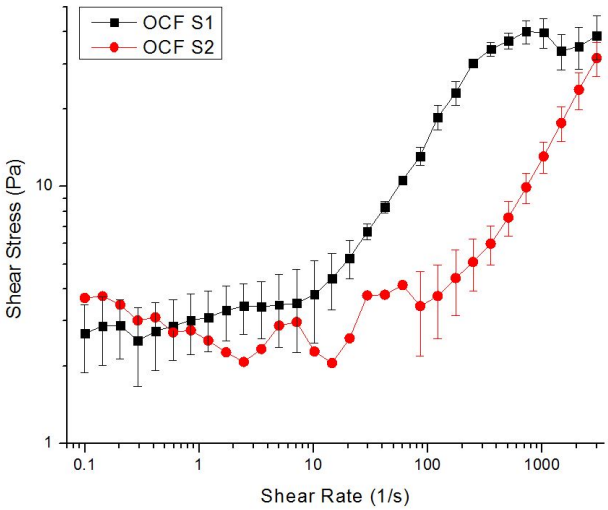

(f) T = 90 °C

Figure A.2. Flow Curve: O:W = 60:40, C_{surf} = 1 wt.%.

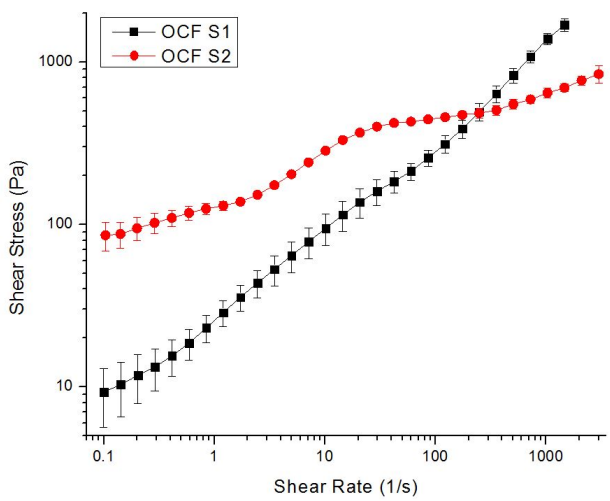

(a) T = 0 °C

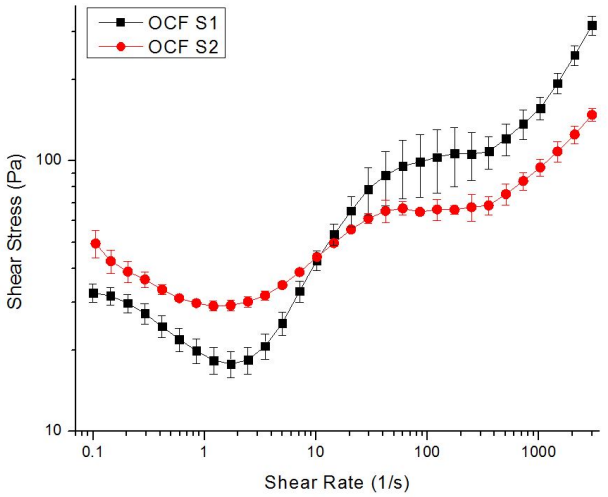

(d) T = 50 °C

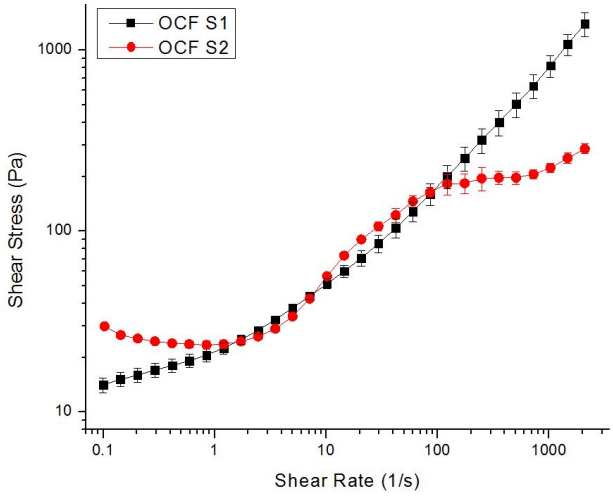

(b) T = 10 °C

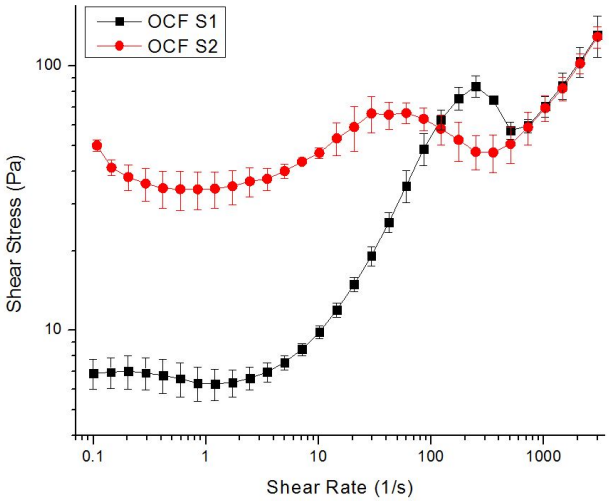

(e) T = 75 °C

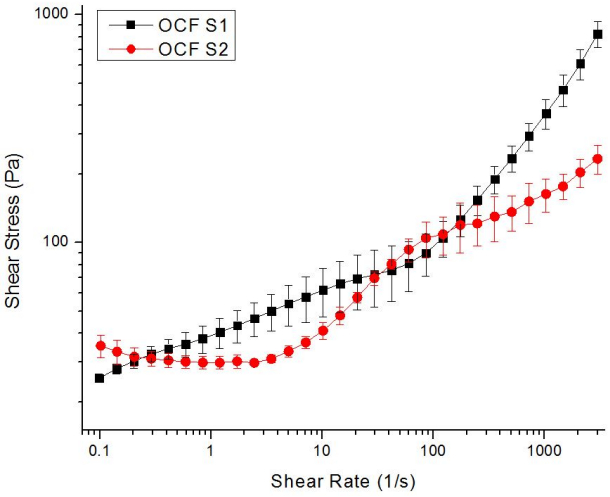

(c) T = 25 °C

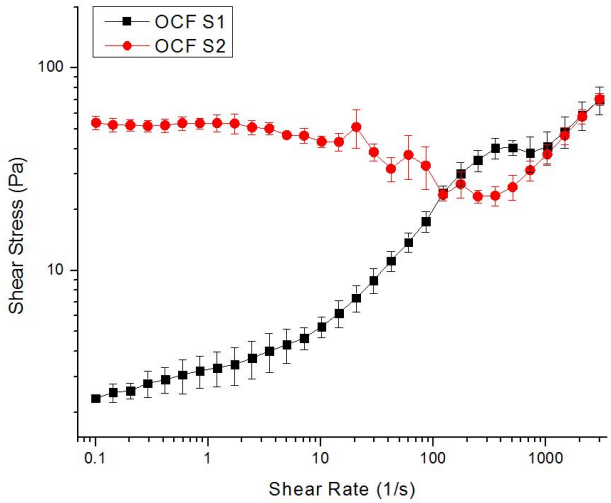

(f) T = 90 °C

Figure A.3. Flow Curve: O:W = 50:50, C_{surf} = 2 wt.%.

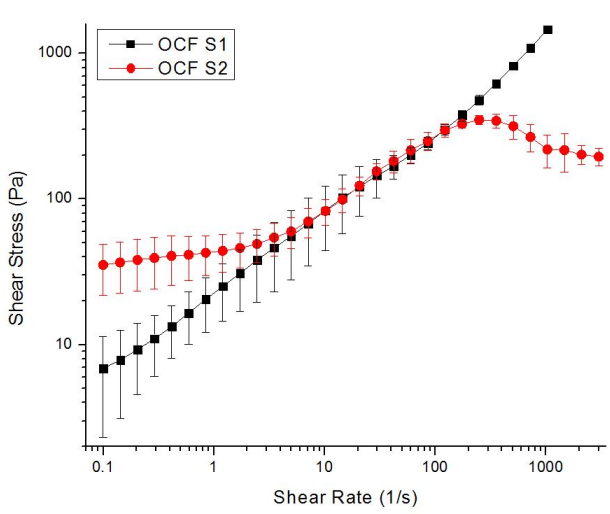

(a) T = 0 °C

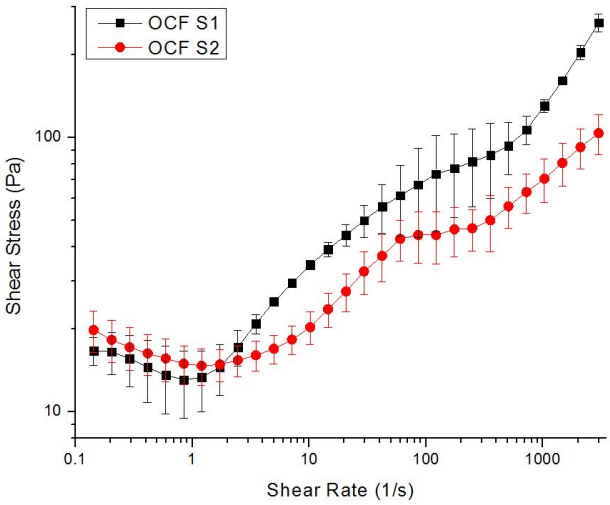

(d) T = 50 °C

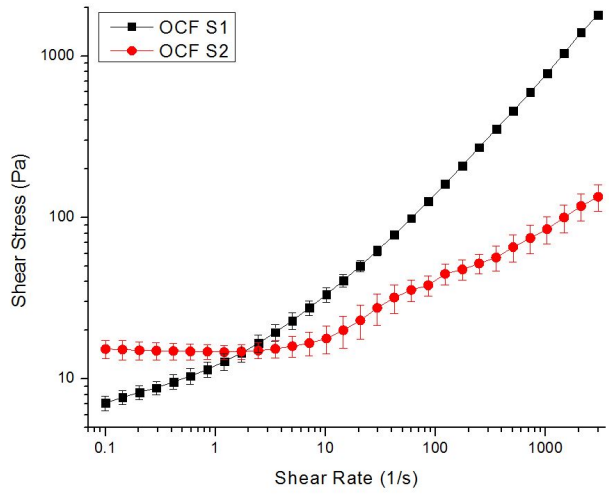

(b) T = 10 °C

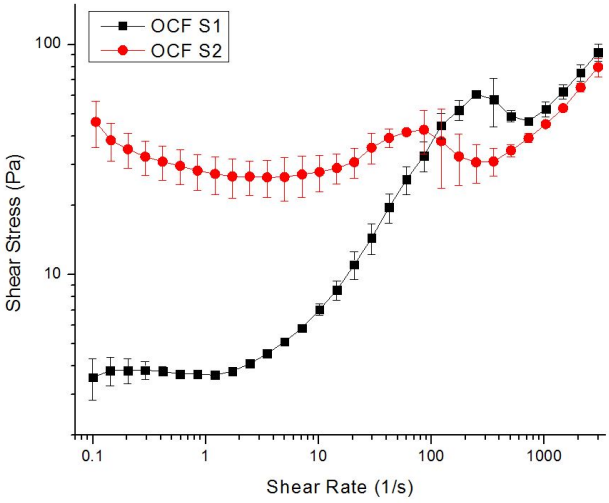

(e) T = 75 °C

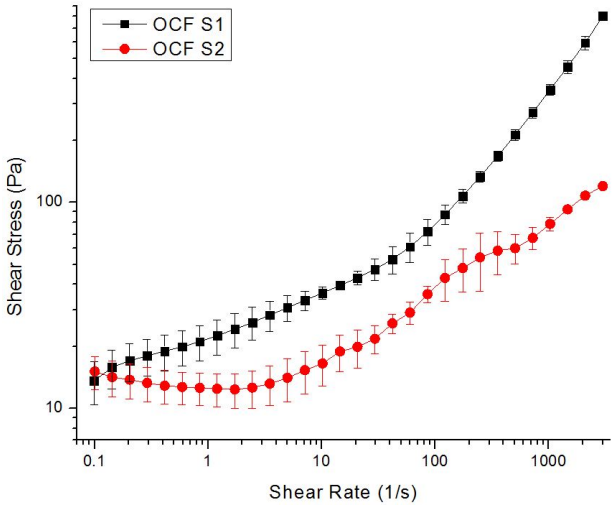

(c) T = 25 °C

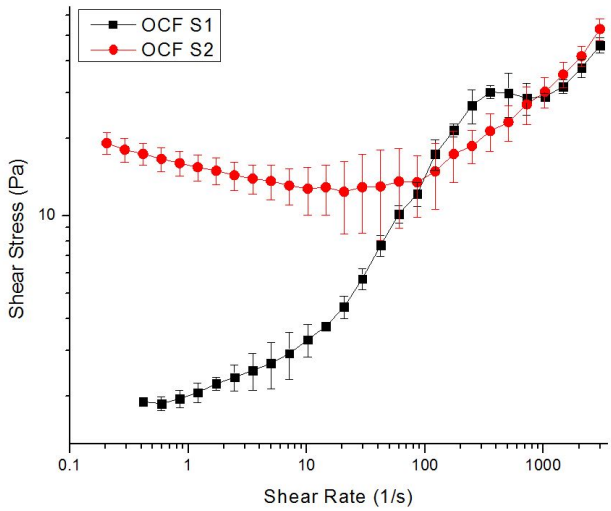

(f) T = 90 °C

Figure A.4. Flow Curve: O:W = 60:40, C_{surf} = 2 wt.%.

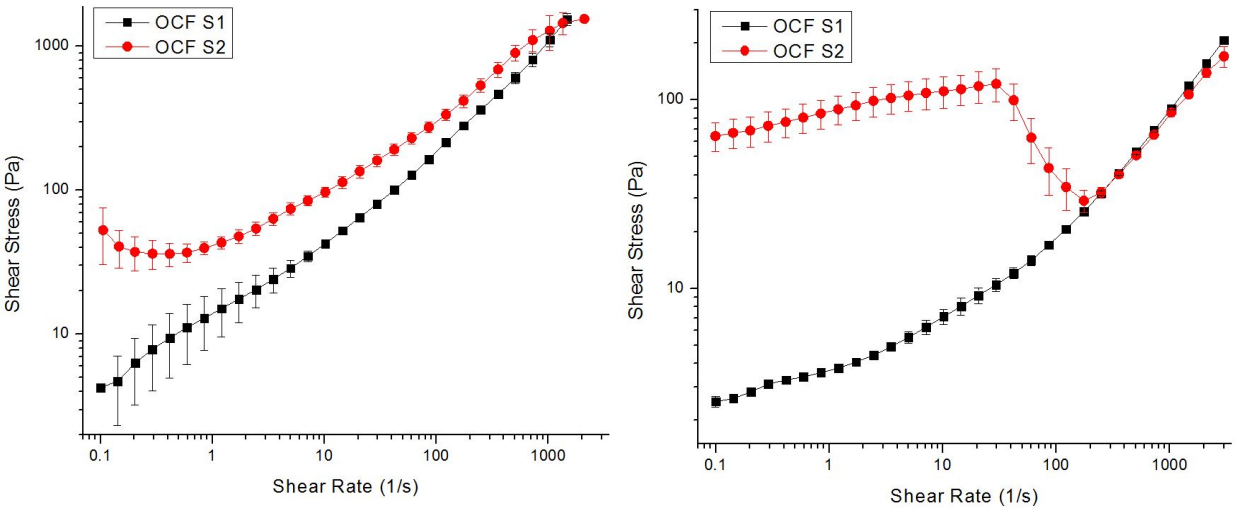

(a) T = 0 °C

(d) T = 50 °C

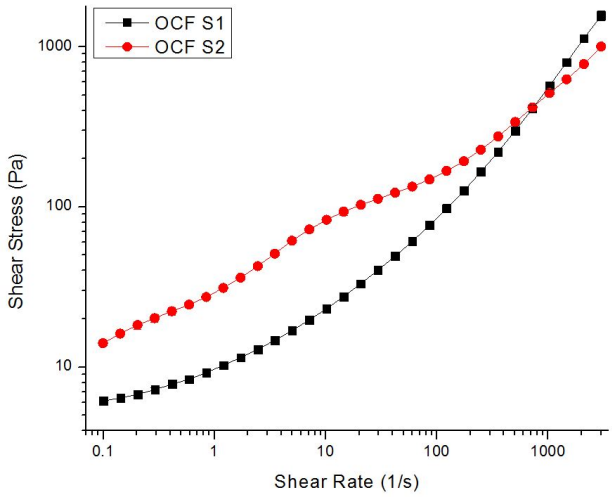

(b) T = 10 °C

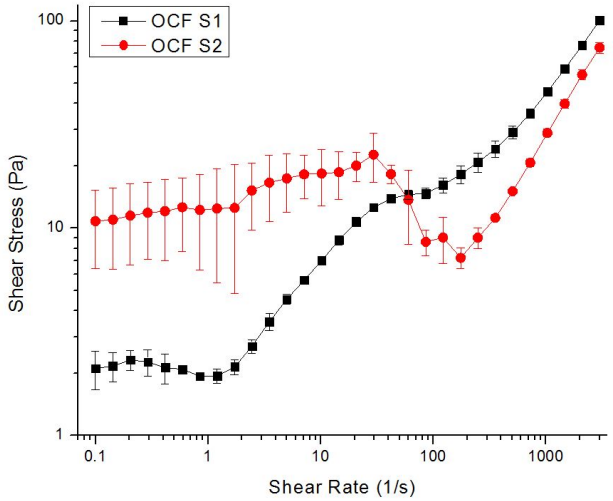

(e) T = 75 °C

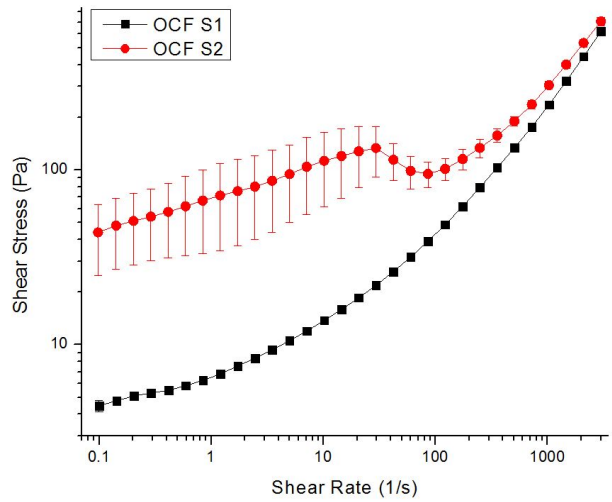

(c) T = 25 °C

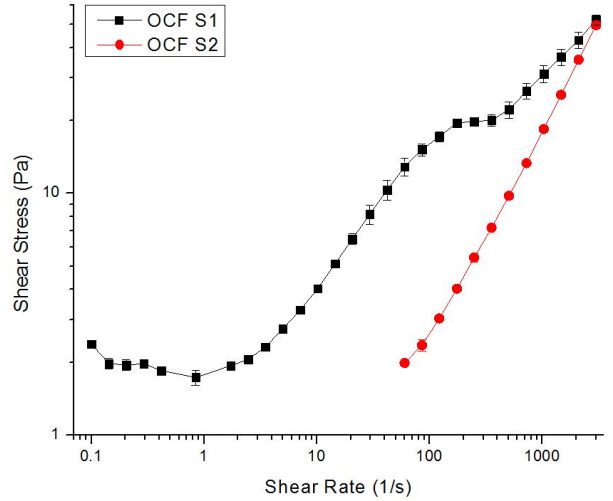

(f) T = 90 °C

Figure A.5. Flow Curve: O:W = 70:30, C_{surf} = 2 wt.%.

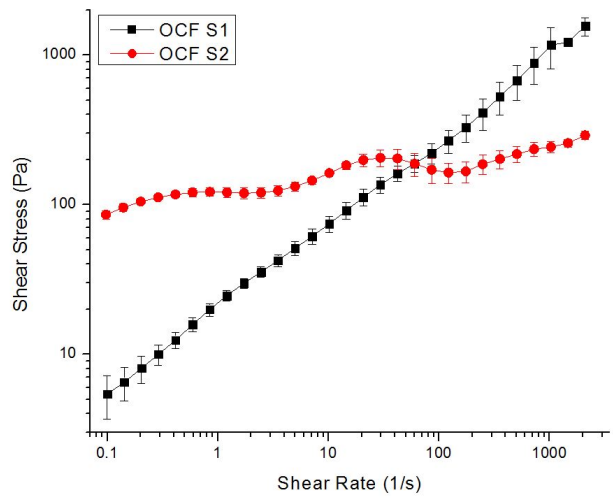

(a) T = 0 °C

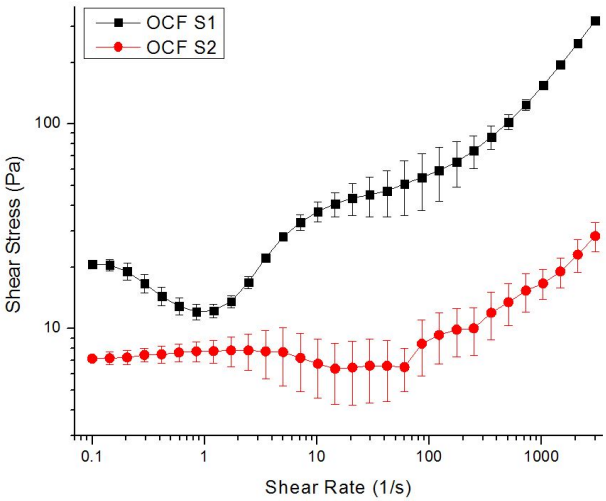

(d) T = 50 °C

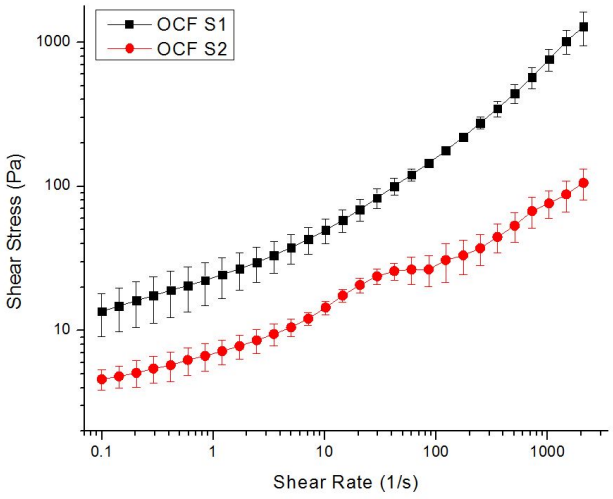

(b) T = 10 °C

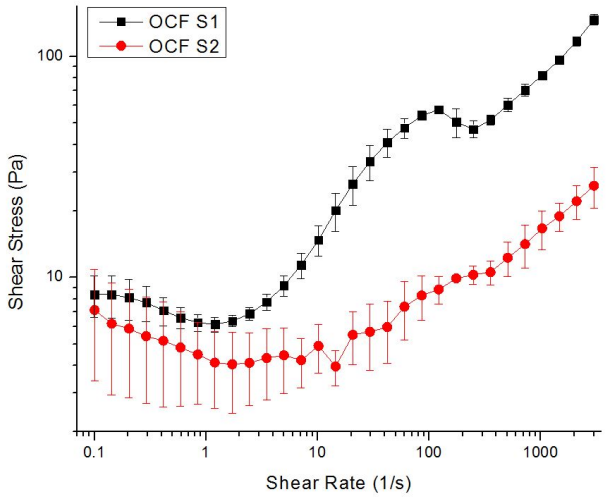

(e) T = 75 °C

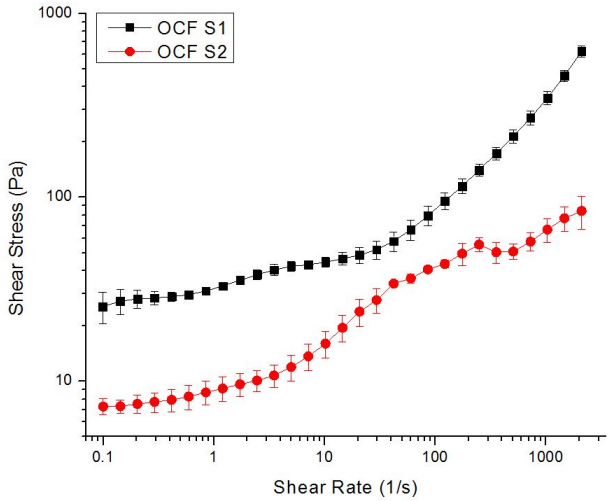

(c) T = 25 °C

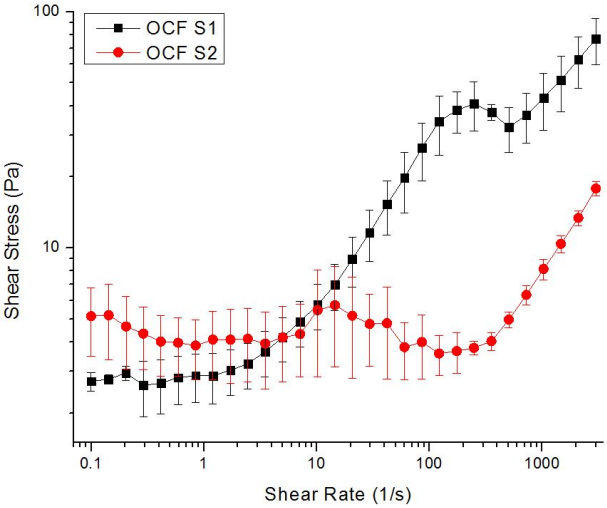

(f) T = 90 °C

Figure A.6. Flow Curve: O:W = 50:50, C_{surf} = 3 wt.%.

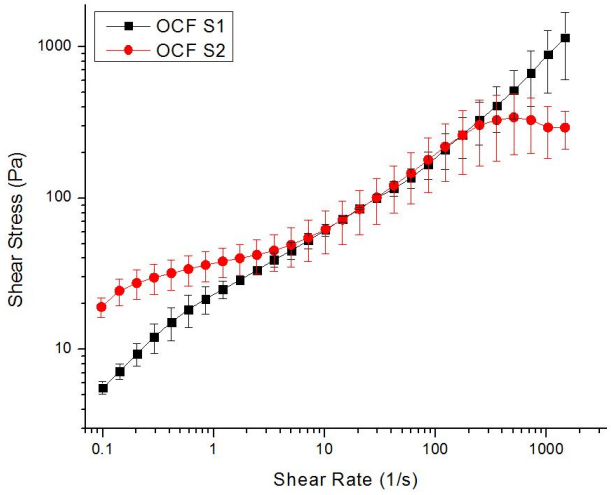

(a) T = 0 °C

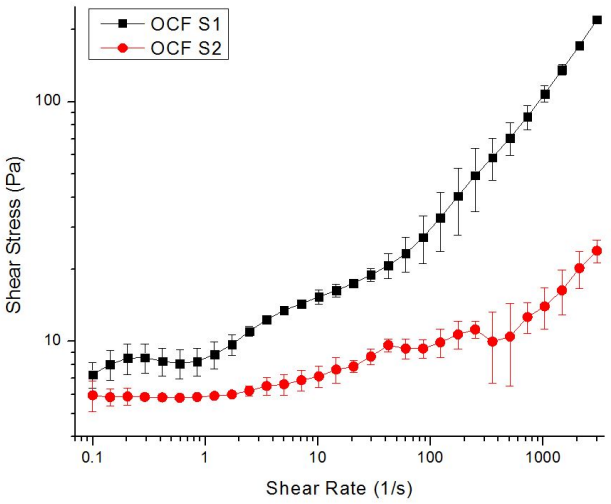

(d) T = 50 °C

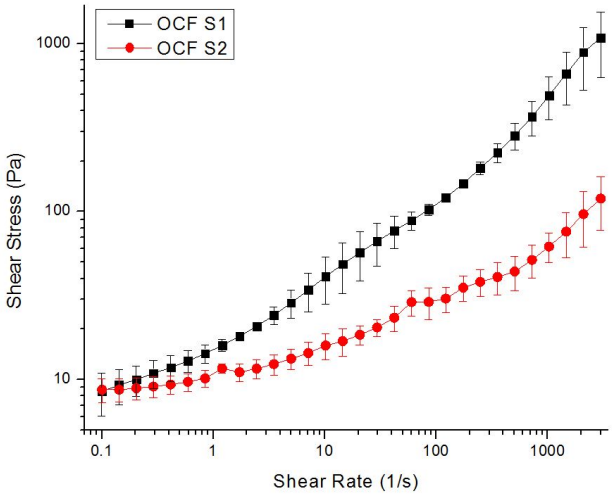

(b) T = 10 °C

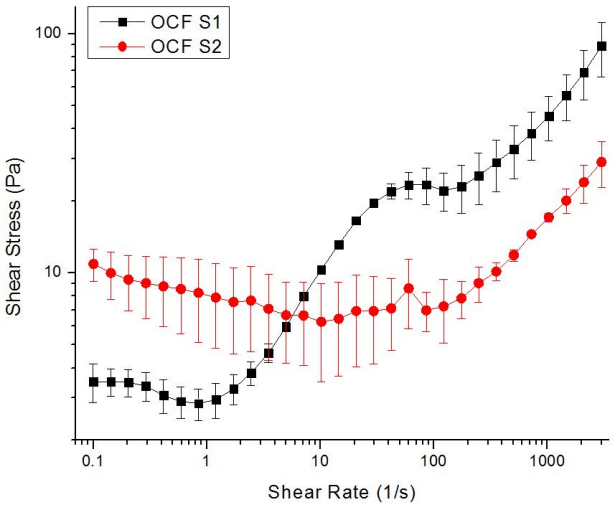

(e) T = 75 °C

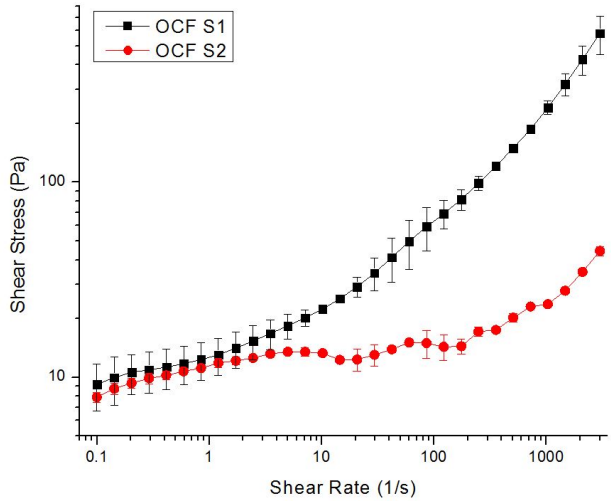

(c) T = 25 °C

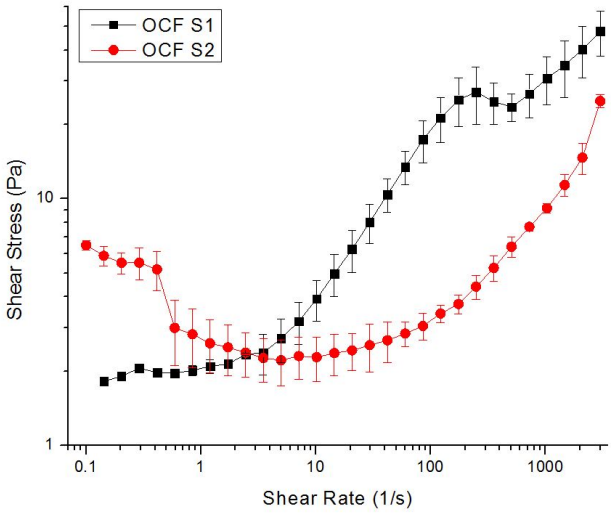

(f) T = 90 °C

Figure A.7. Flow Curve: O:W = 60:40, C_{surf} = 3 wt.%.

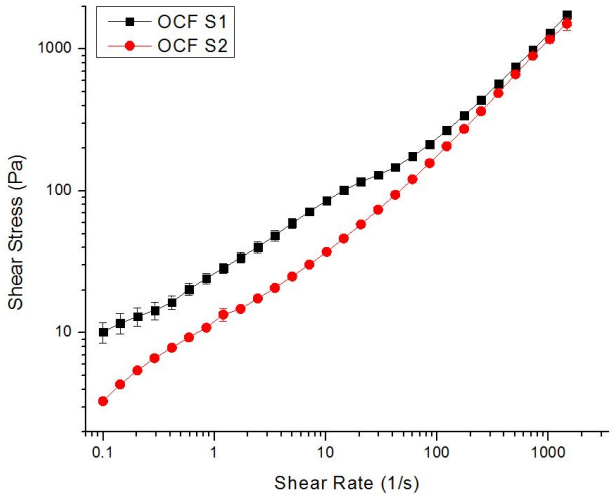

(a) T = 0 °C

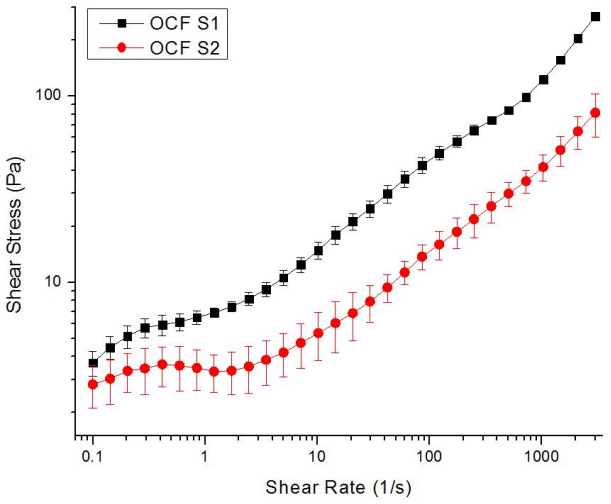

(d) T = 50 °C

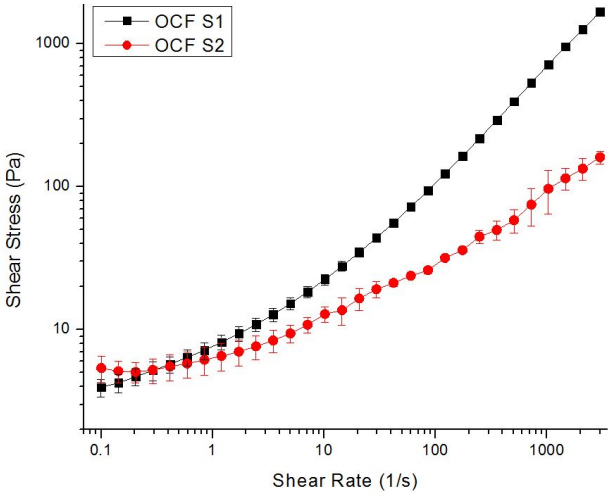

(b) T = 10 °C

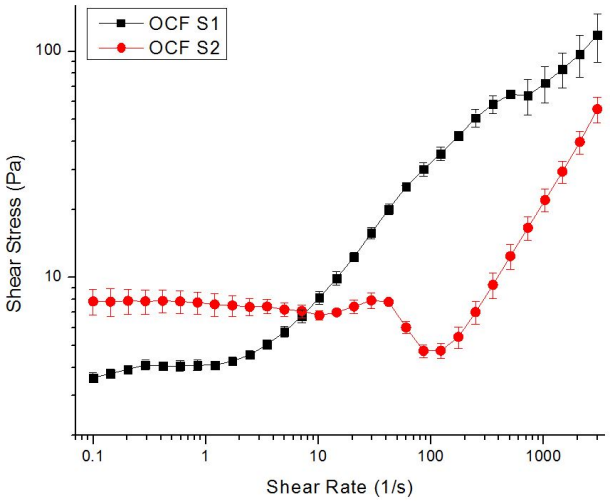

(e) T = 75 °C

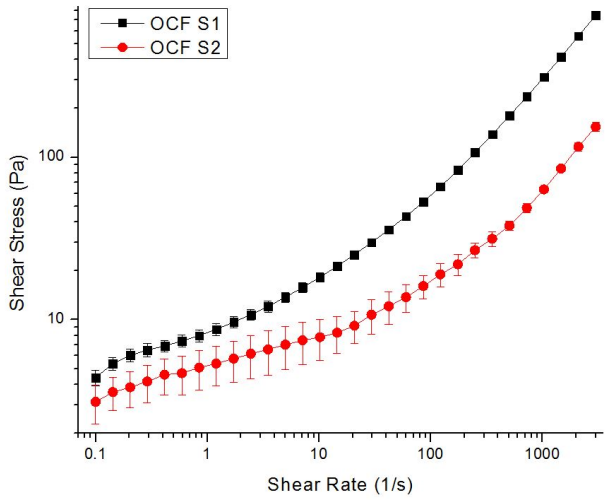

(c) T = 25 °C

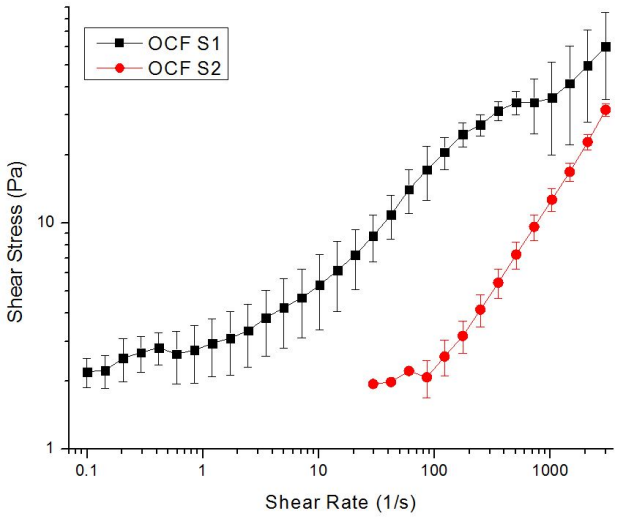

(f) T = 90 °C

Figure A.8. Flow Curve: O:W = 70:30, C_{surf} = 3 wt.%.

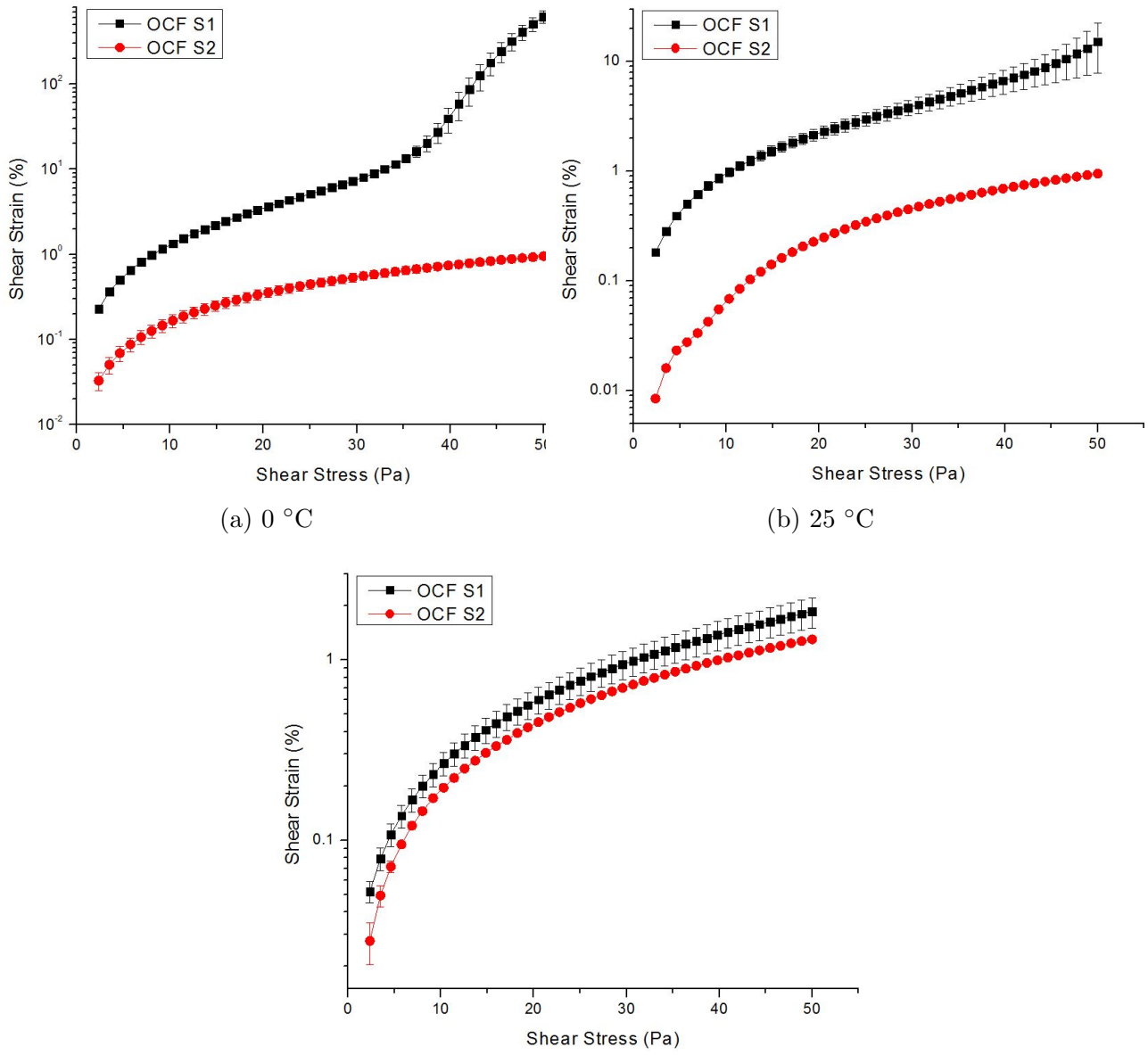

(a) 0 °C

(b) 25 °C

(c) 90 °C

Figure A.9. Stress Sweep: O:W = 50:50, $C_{surf.}$ = 1 wt.%.

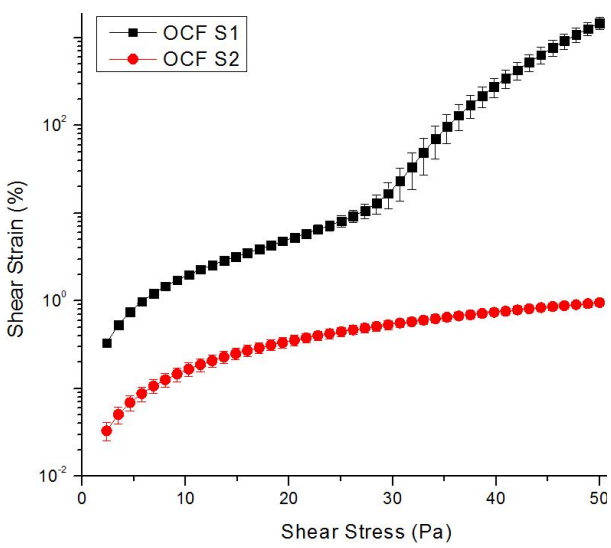

(a) 0 °C

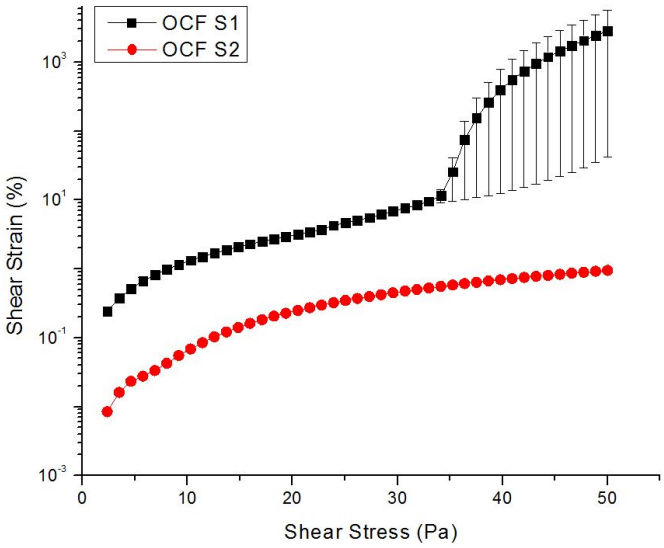

(b) 25 °C

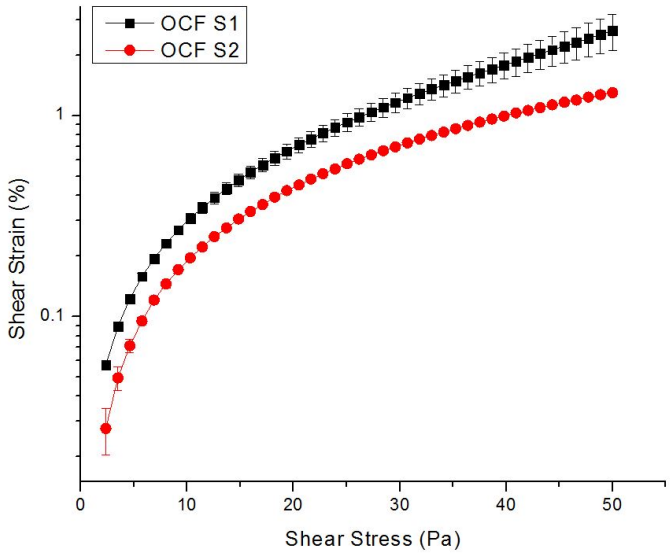

(c) 90 °C

Figure A.10. Stress Sweep: O:W = 60:40, $C_{surf.}$ = 1 wt.%.

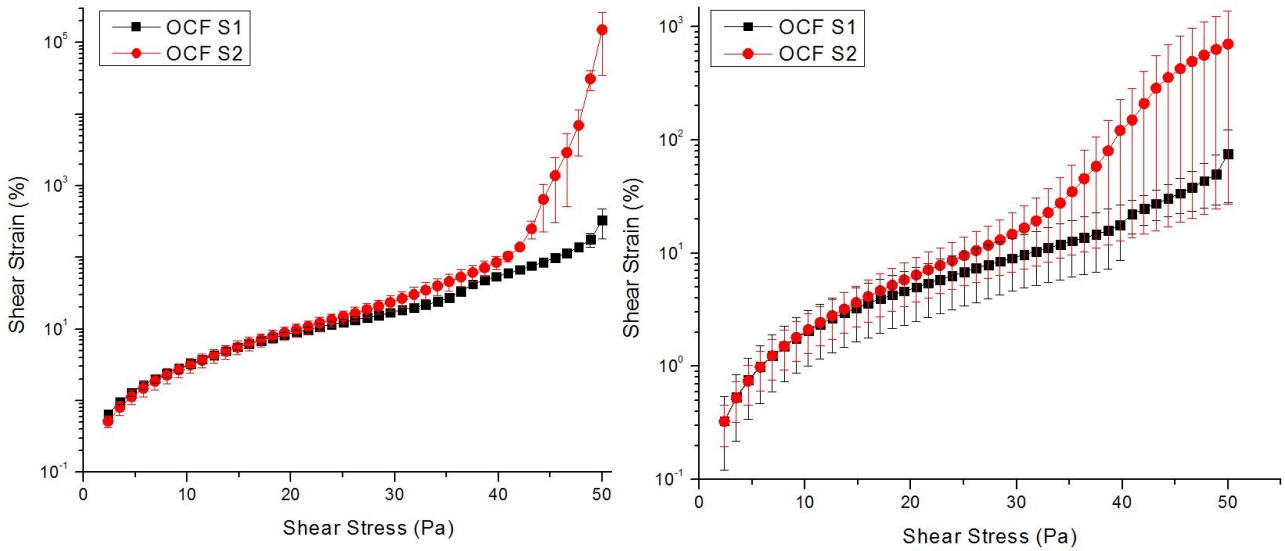

(a) 0 °C

(b) 25 °C

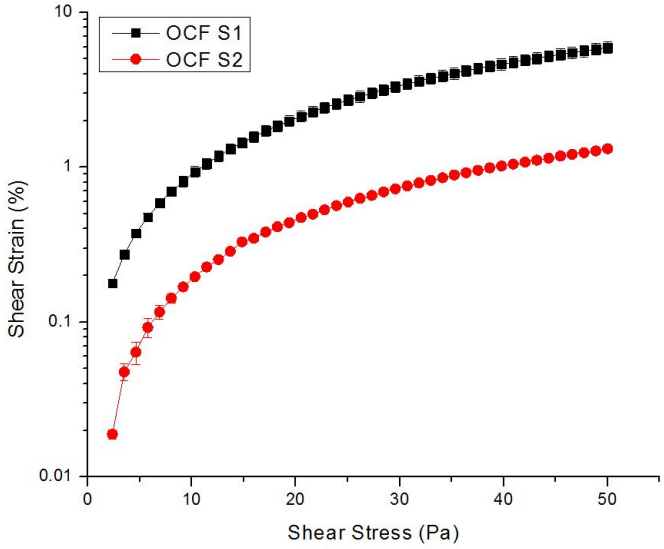

(c) 90 °C

Figure A.11. Stress Sweep: O:W = 70:30, $C_{surf.}$ = 2 wt.%.

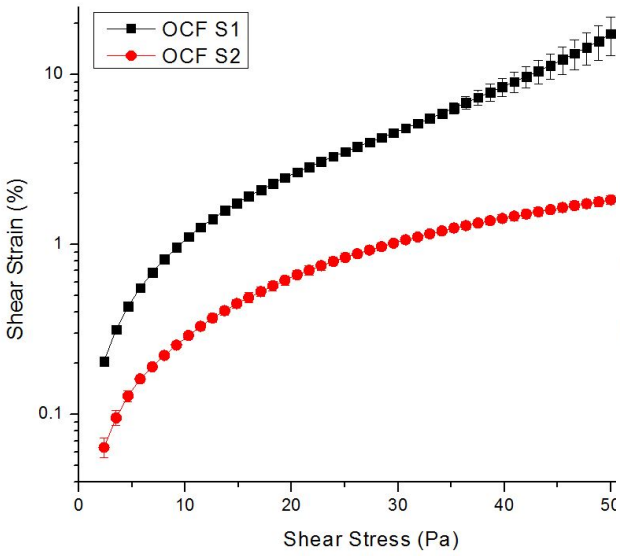

(a) 0 °C

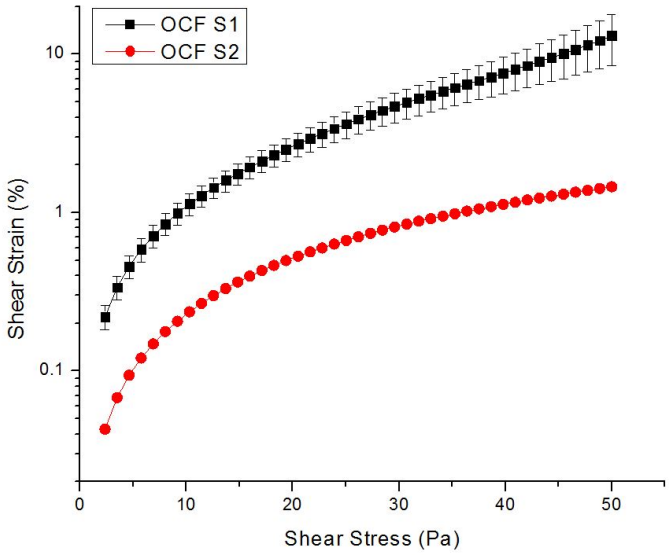

(b) 25 °C

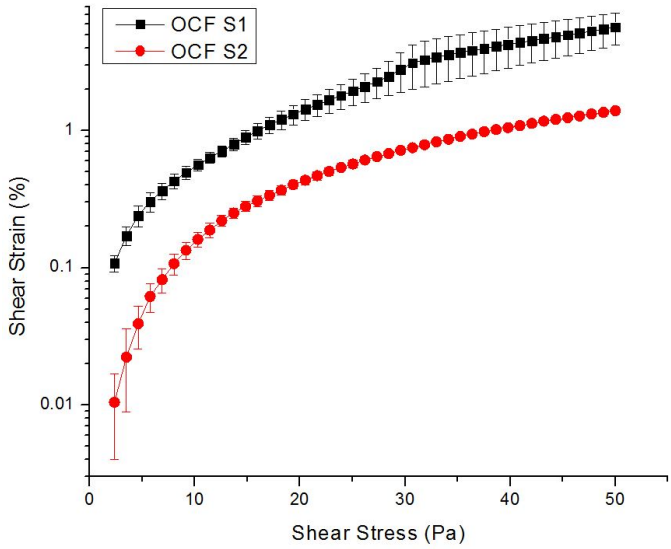

(c) 90 °C

Figure A.12. Stress Sweep: O:W = 50:50, $C_{surf.}$ = 3 wt.%.

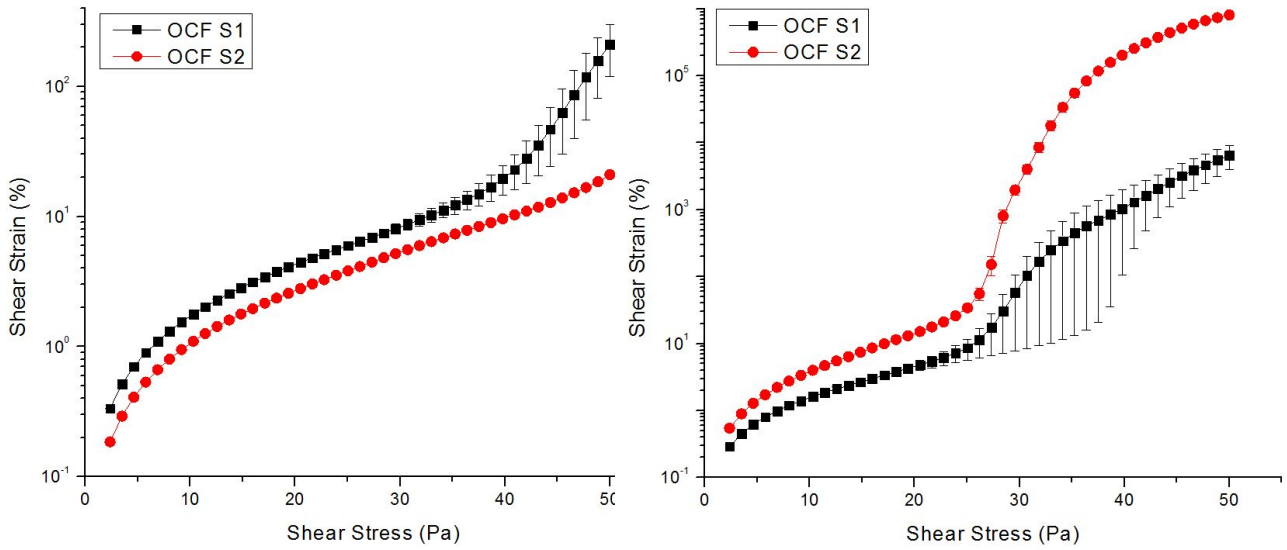

(a) 0 °C

(b) 25 °C

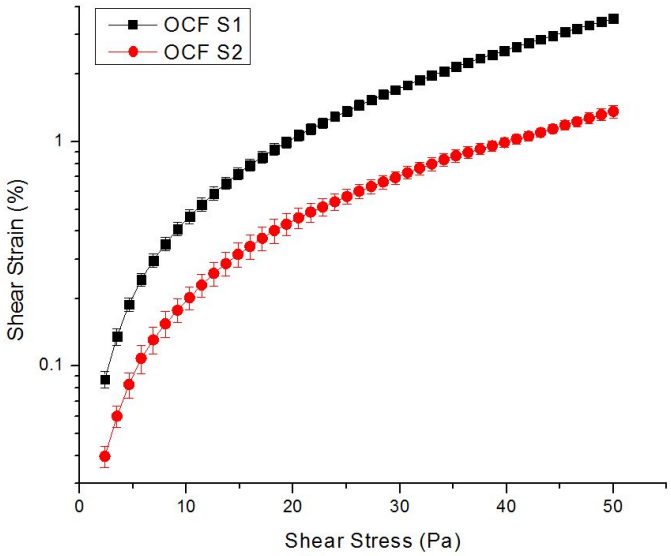

(c) 90 °C

Figure A.13. Stress Sweep: O:W = 60:40, $C_{surf.}$ = 3 wt.%.

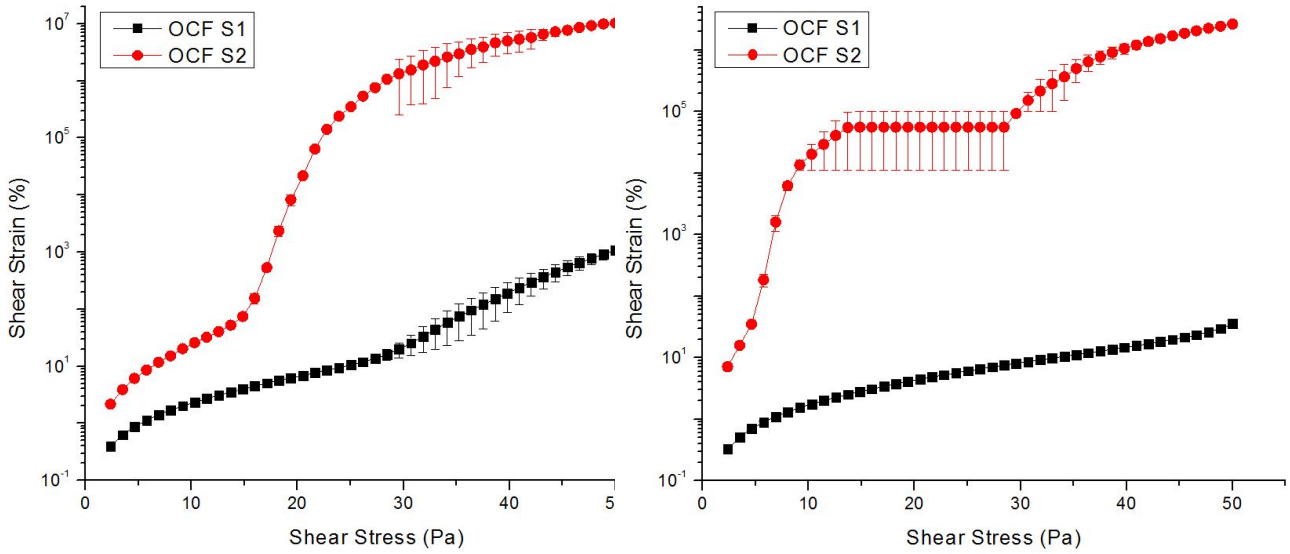

(a) 0 °C

(b) 25 °C

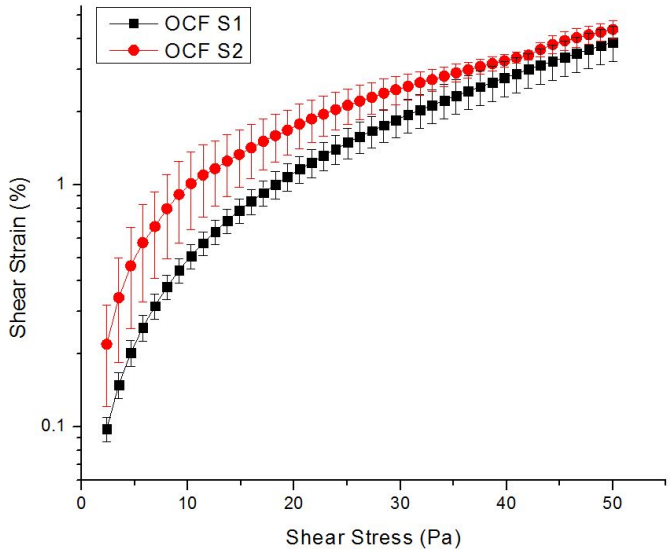

(c) 90 °C

Figure A.14. Stress Sweep: O:W = 70:30, $C_{surf.}$ = 3 wt.%.

.

A.2 Effect of Surfactant Concentration

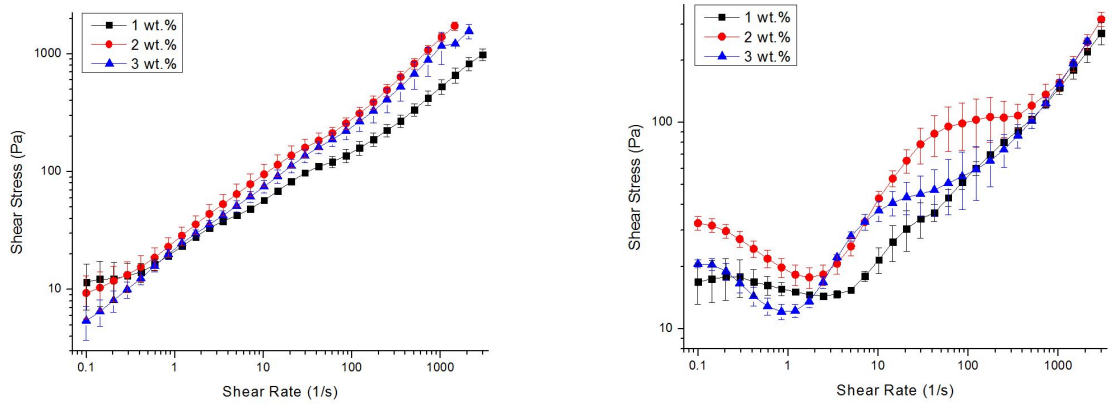

(a) T = 0 °C

(d) T = 50 °C

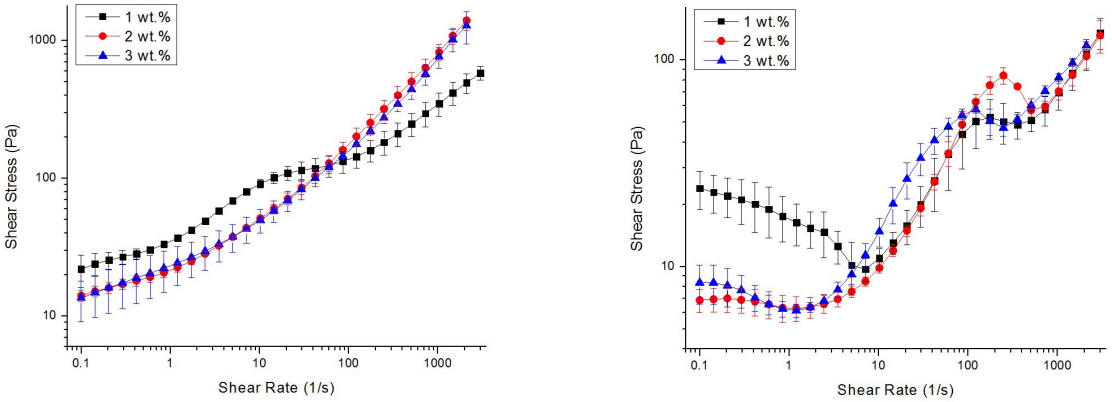

(b) T = 10 °C

(e) T = 75 °C

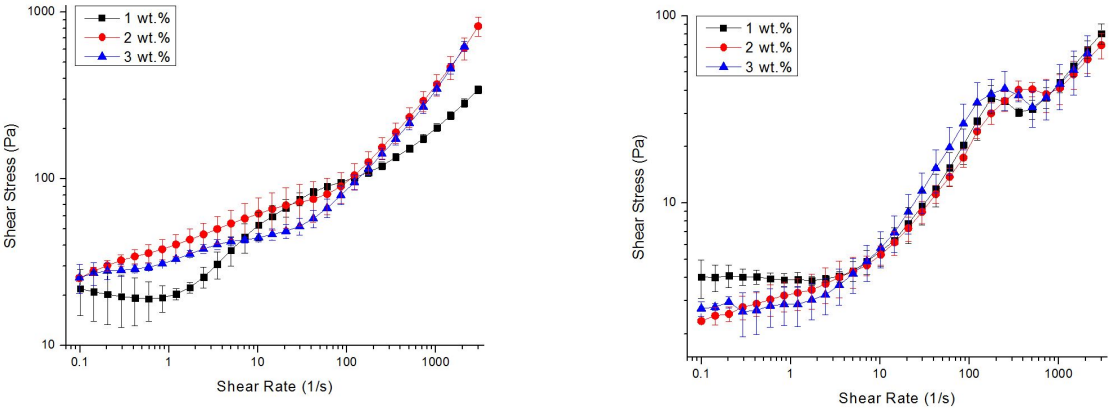

(c) T = 25 °C

(f) T = 90 °C

Figure A.15. Flow Curve: OCF S1, O:W = 50:50.

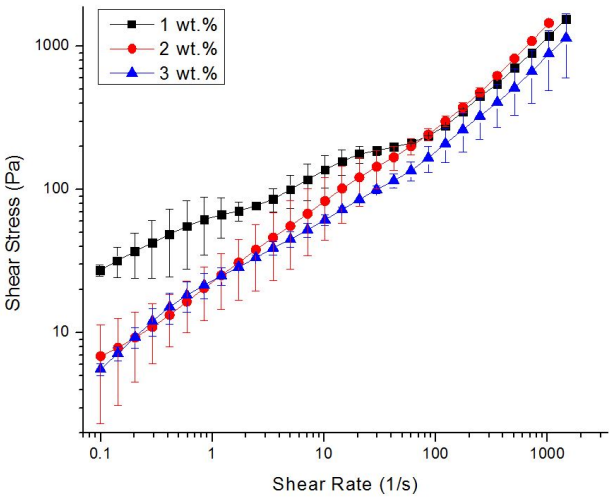

(a) T = 0 °C

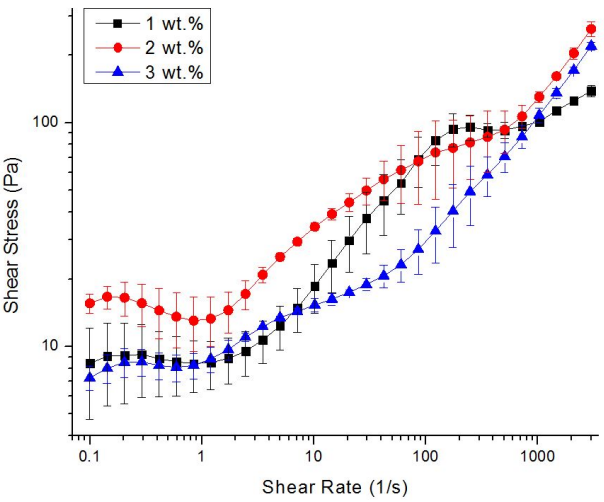

(d) T = 50 °C

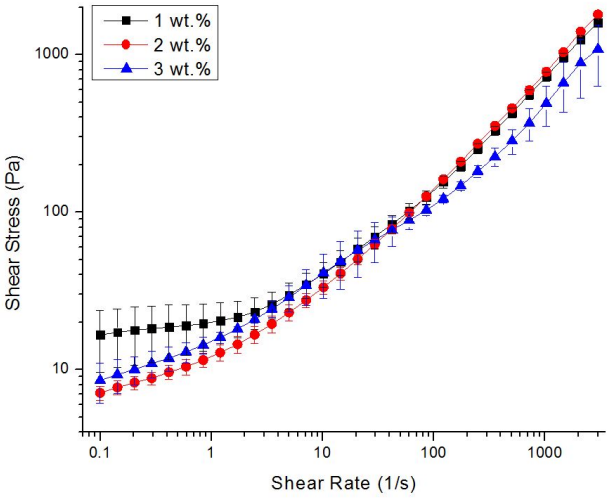

(b) T = 10 °C

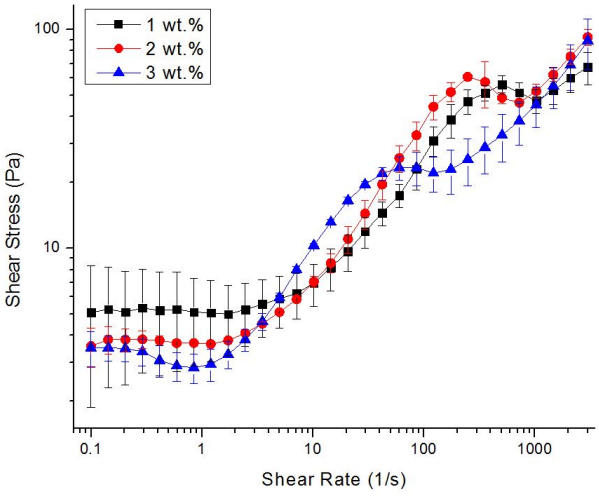

(e) T = 75 °C

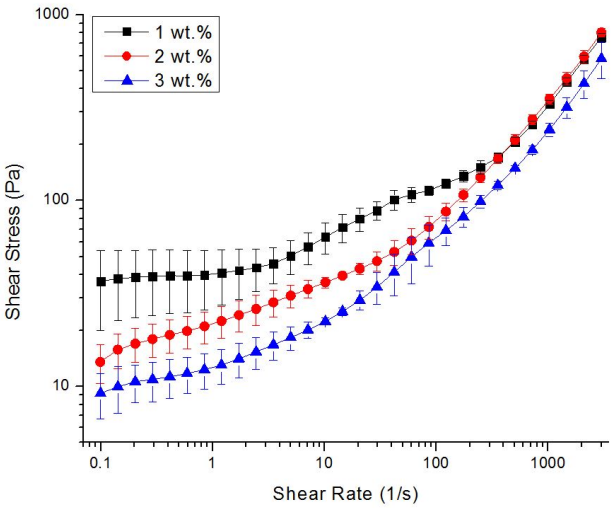

(c) T = 25 °C

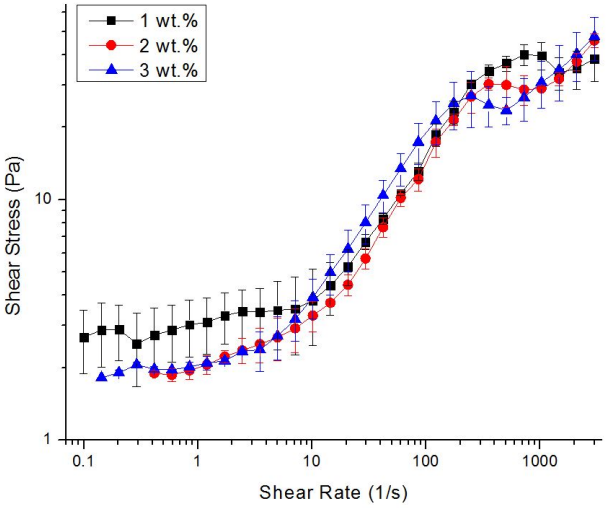

(f) T = 90 °C

Figure A.16. Flow Curve: OCF S1, O:W = 60:40.

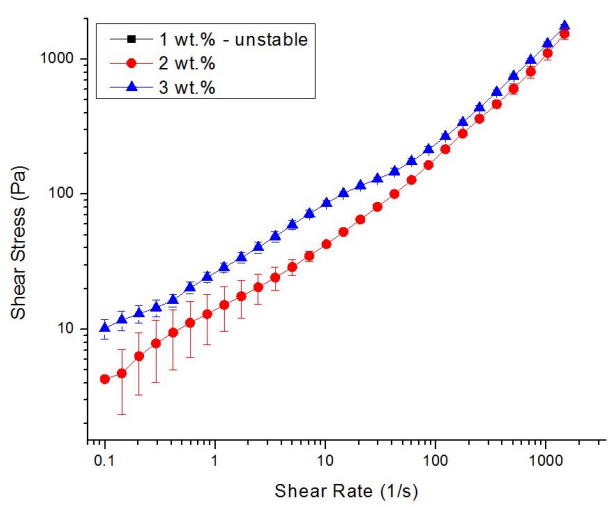

(a) T = 0 °C

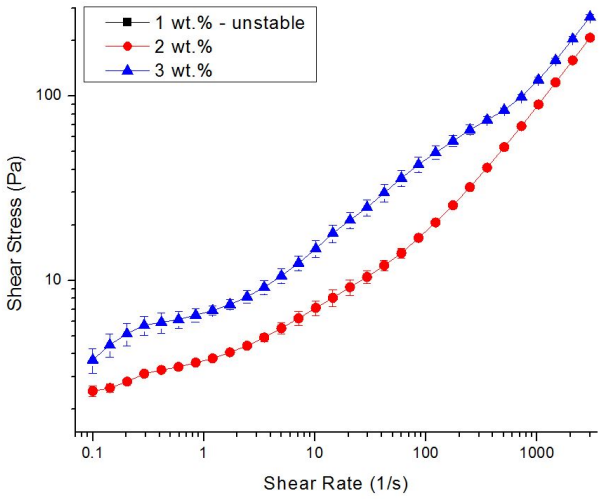

(d) T = 50 °C

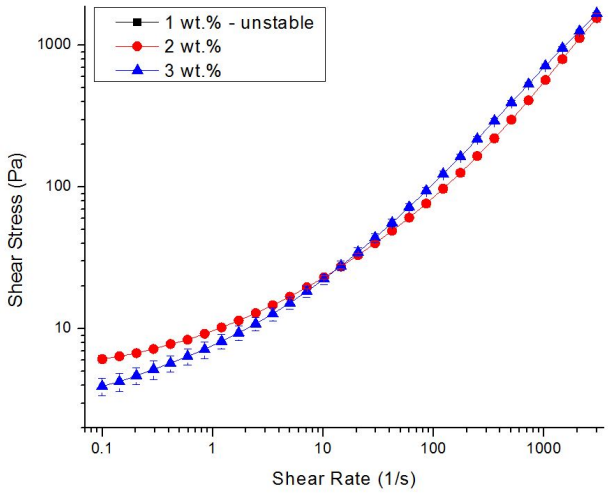

(b) T = 10 °C

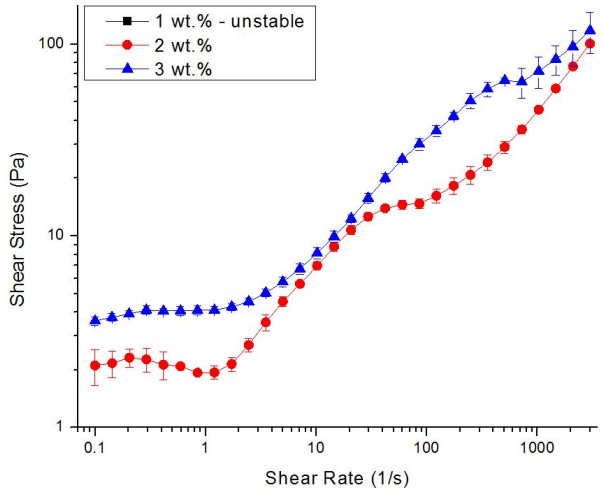

(e) T = 75 °C

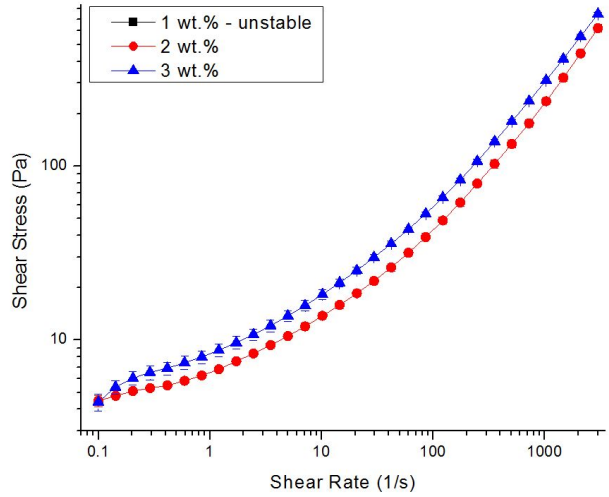

(c) T = 25 °C

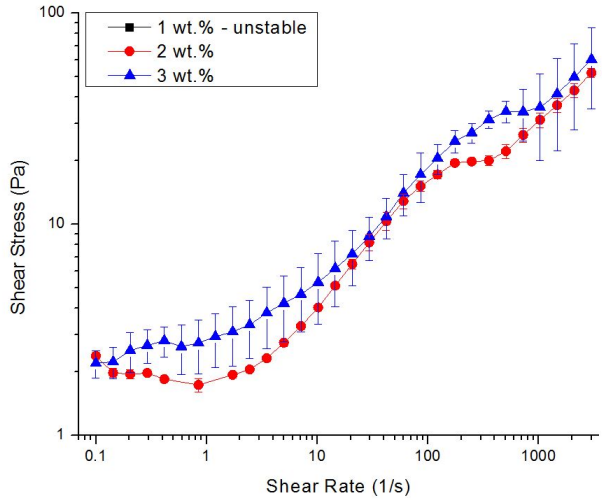

(f) T = 90 °C

Figure A.17. Flow Curve: OCF S1, O:W = 70:30.

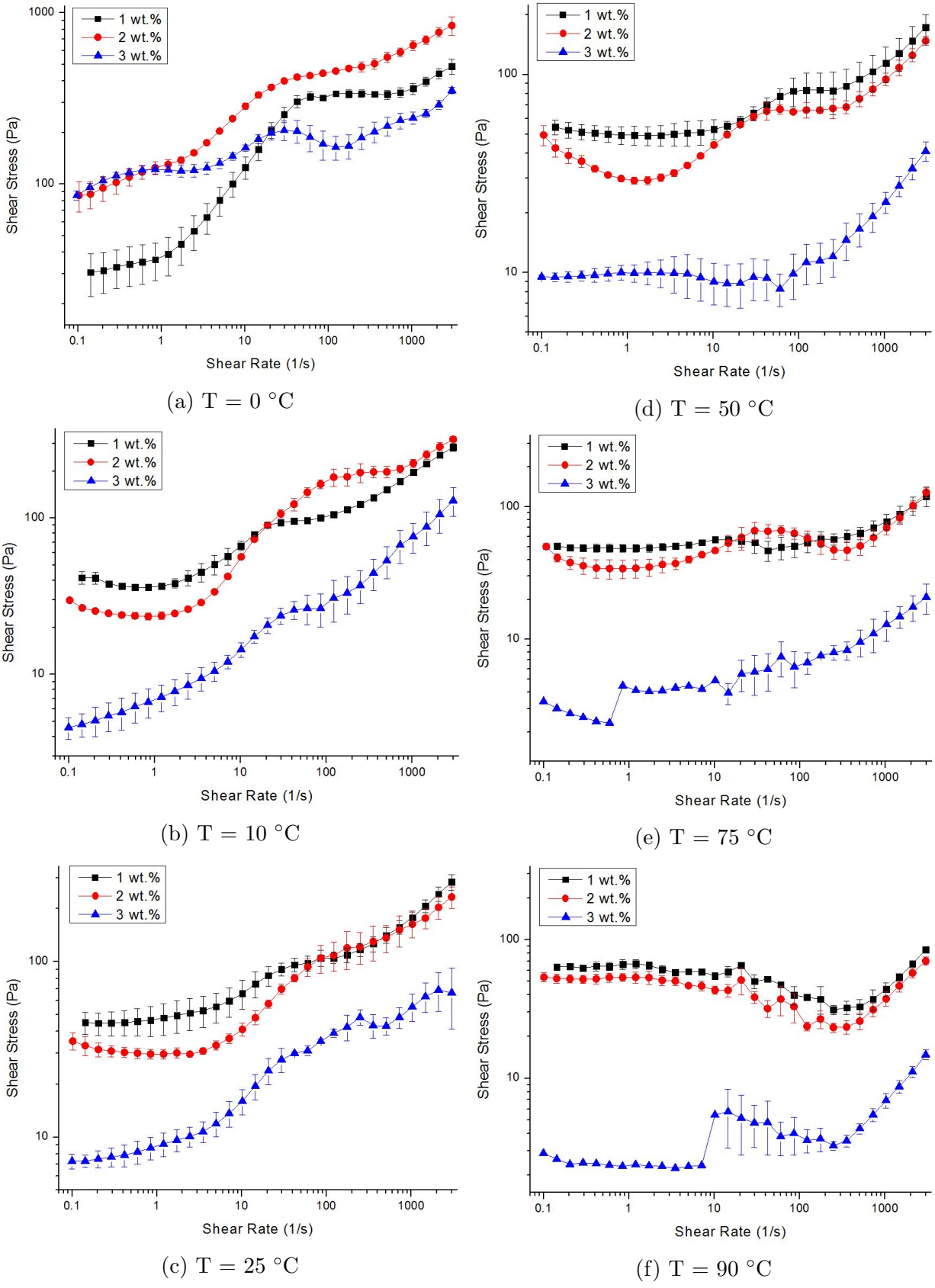

(a) T = 0 °C

(d) T = 50 °C

(b) T = 10 °C

(e) T = 75 °C

(c) T = 25 °C

(f) T = 90 °C

Figure A.18. Flow Curve: OCF S2, O:W = 50:50.

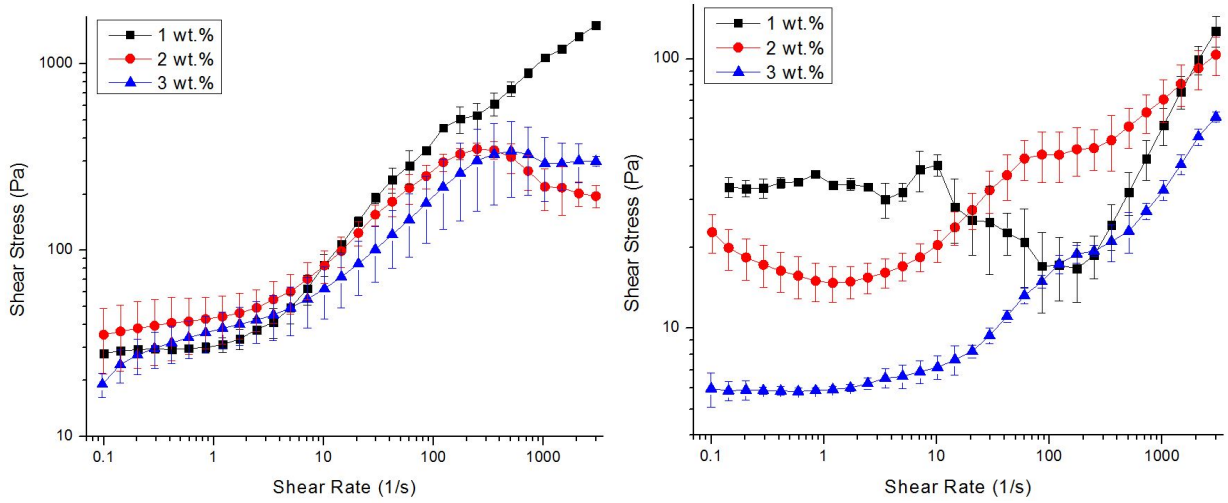

(a) T = 0 °C

(d) T = 50 °C

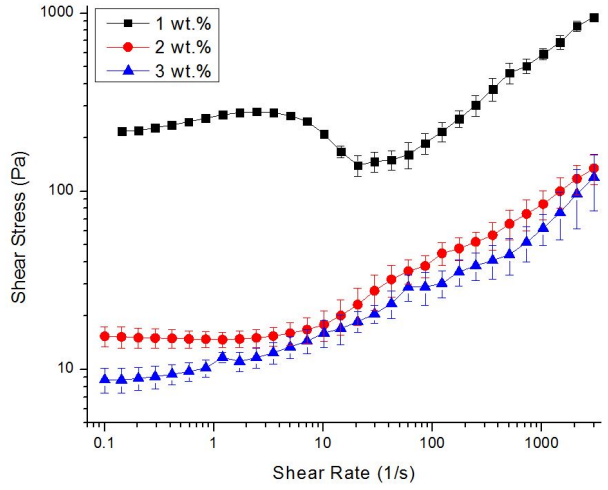

(b) T = 10 °C

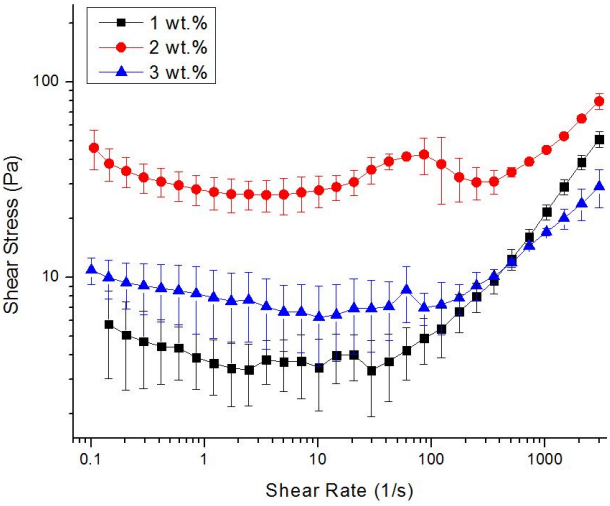

(e) T = 75 °C

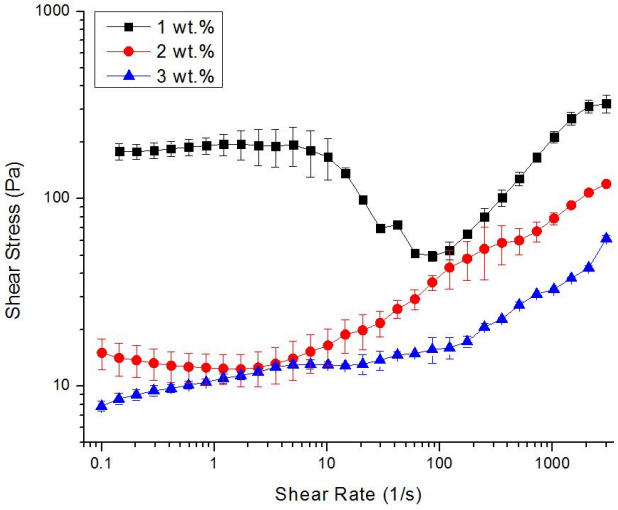

(c) T = 25 °C

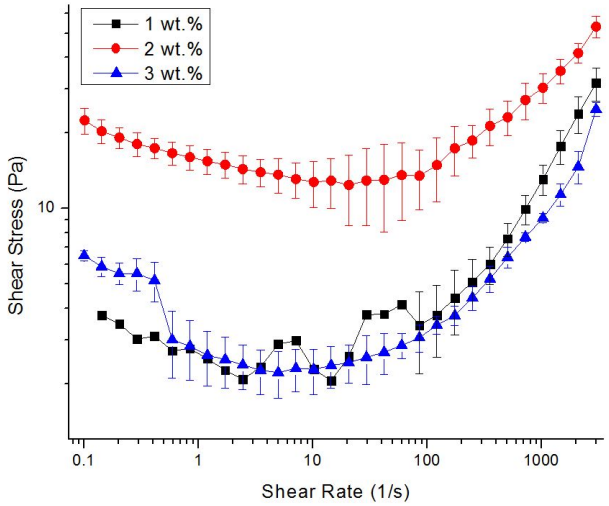

(f) T = 90 °C

Figure A.19. Flow Curve: OCF S2, O:W = 60:40.

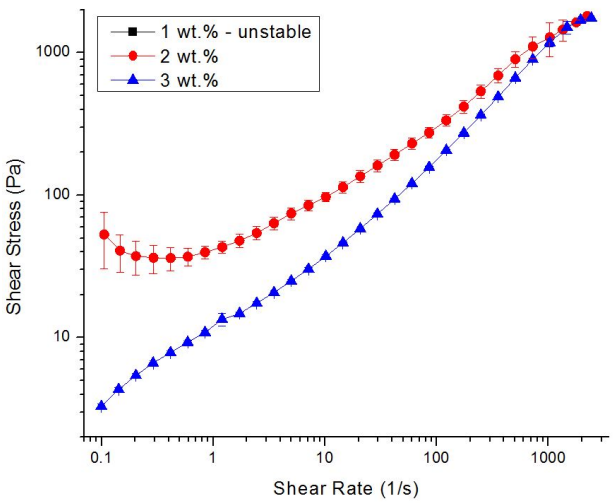

(a) T = 0 °C

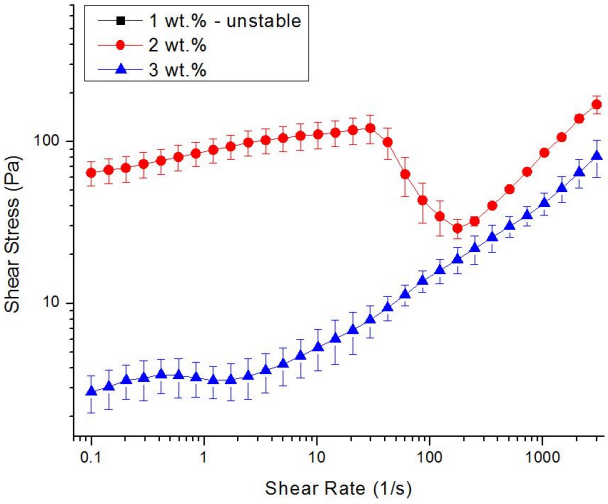

(d) T = 50 °C

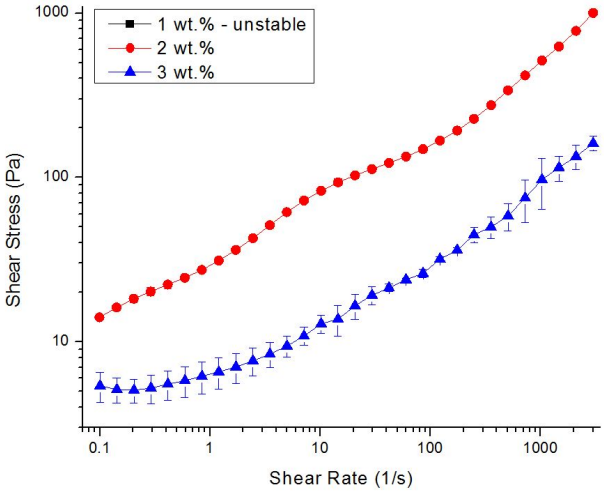

(b) T = 10 °C

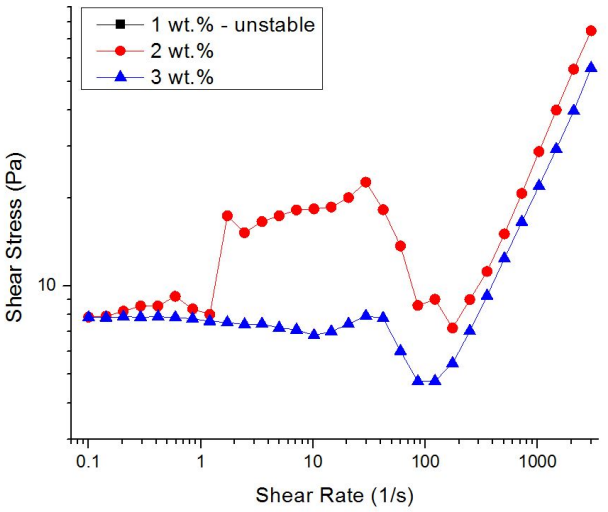

(e) T = 75 °C

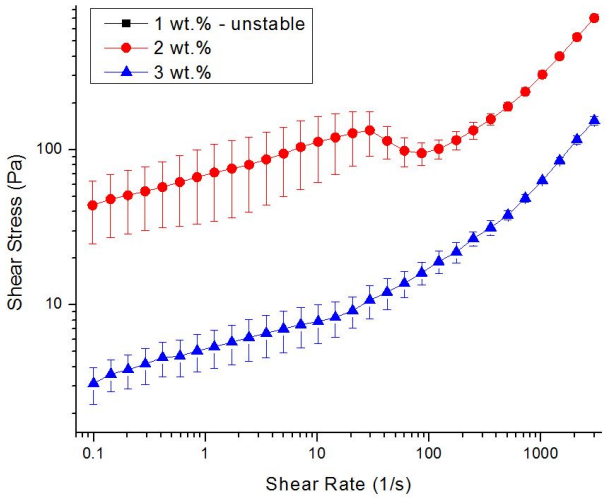

(c) T = 25 °C

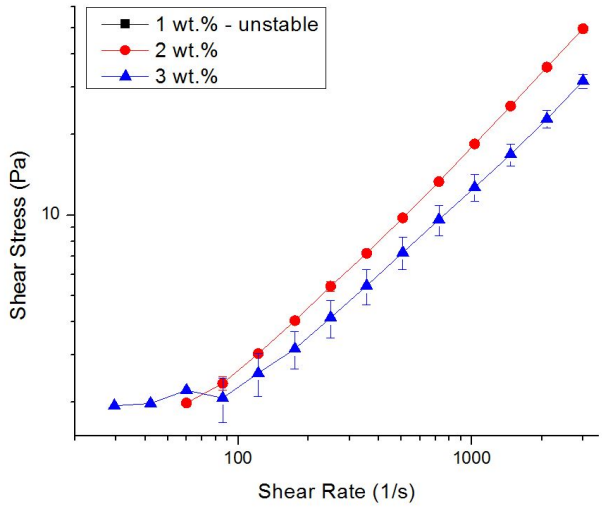

(f) T = 90 °C

Figure A.20. Flow Curve: OCF S2, O:W = 70:30.

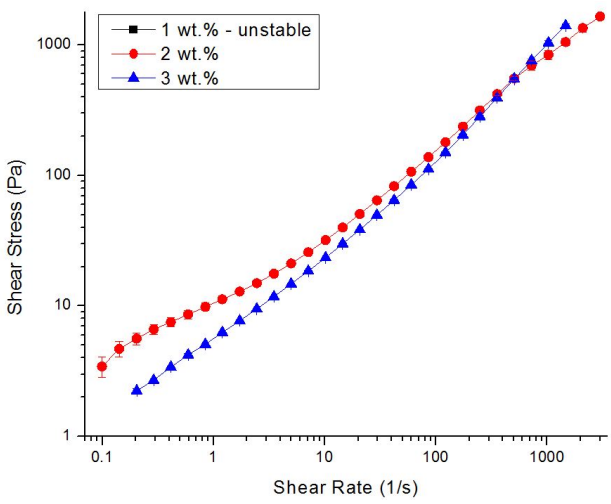

(a) T = 0 °C

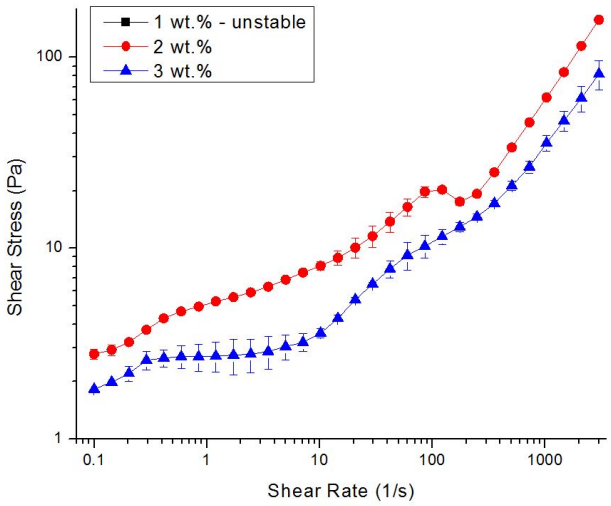

(d) T = 50 °C

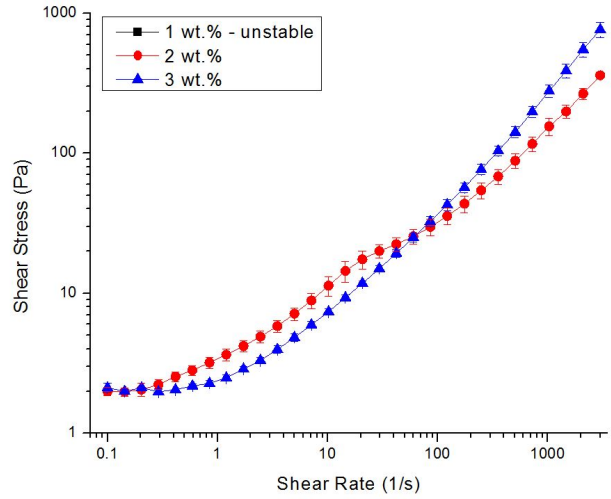

(b) T = 10 °C

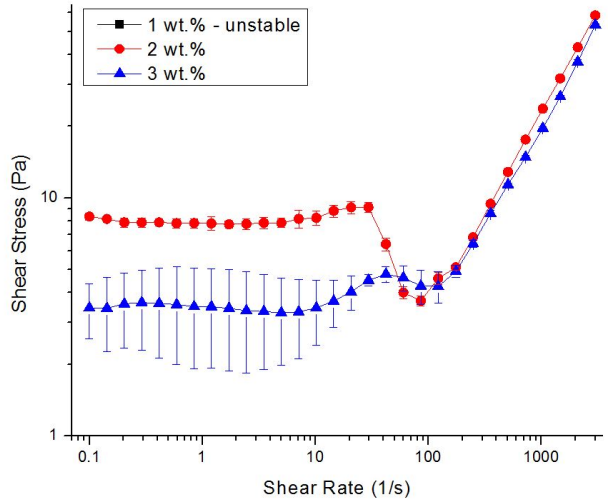

(e) T = 75 °C

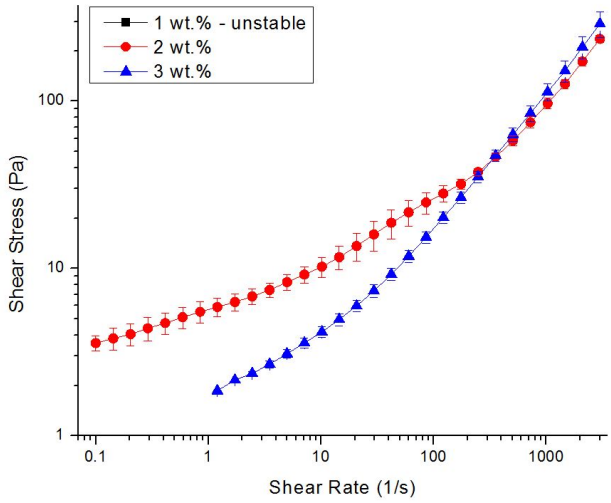

(c) T = 25 °C

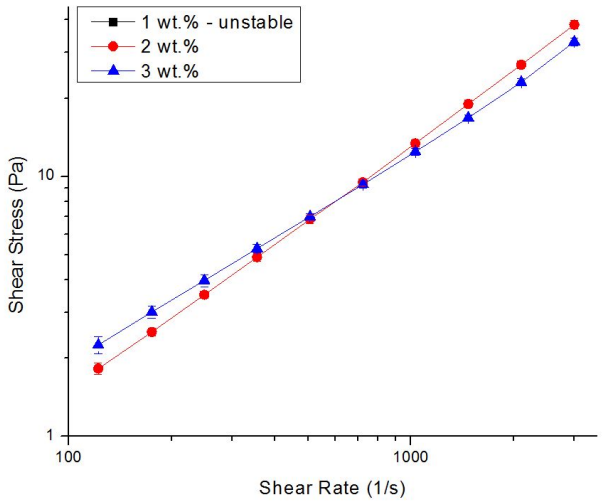

(f) T = 90 °C

Figure A.21. Flow Curve: OCF S2, O:W = 80:20.

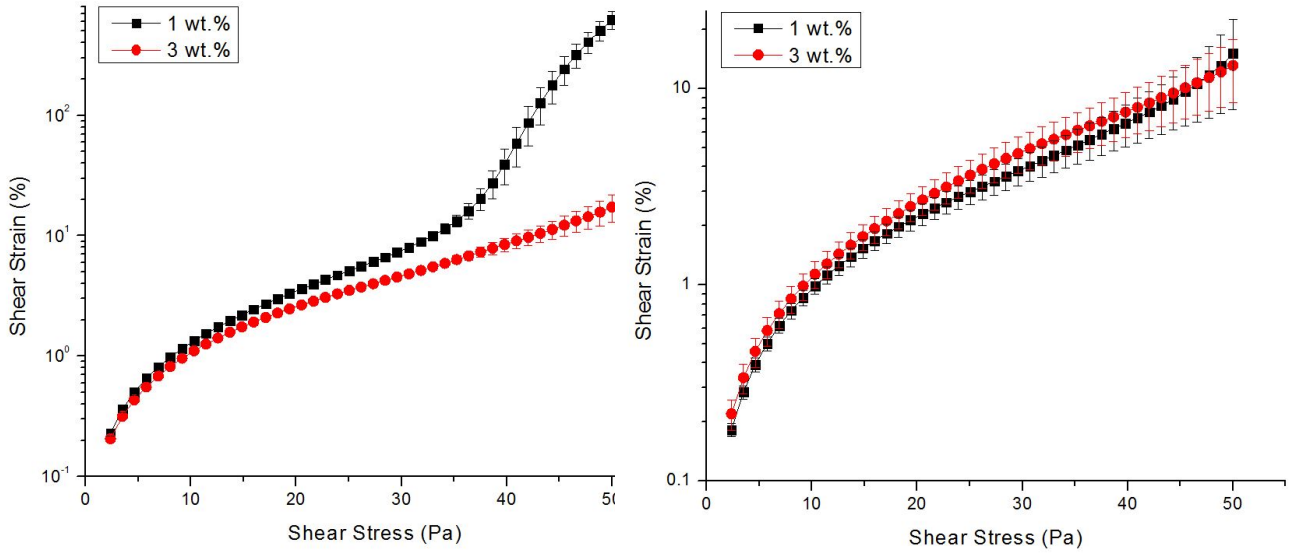

(a) 0 °C

(b) 25 °C

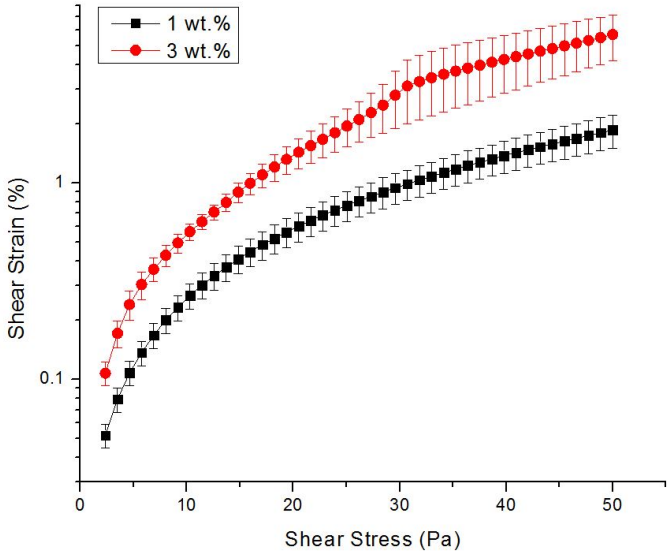

(c) 90 °C

Figure A.22. Stress Sweep: OCF S1, O:W = 50:50.

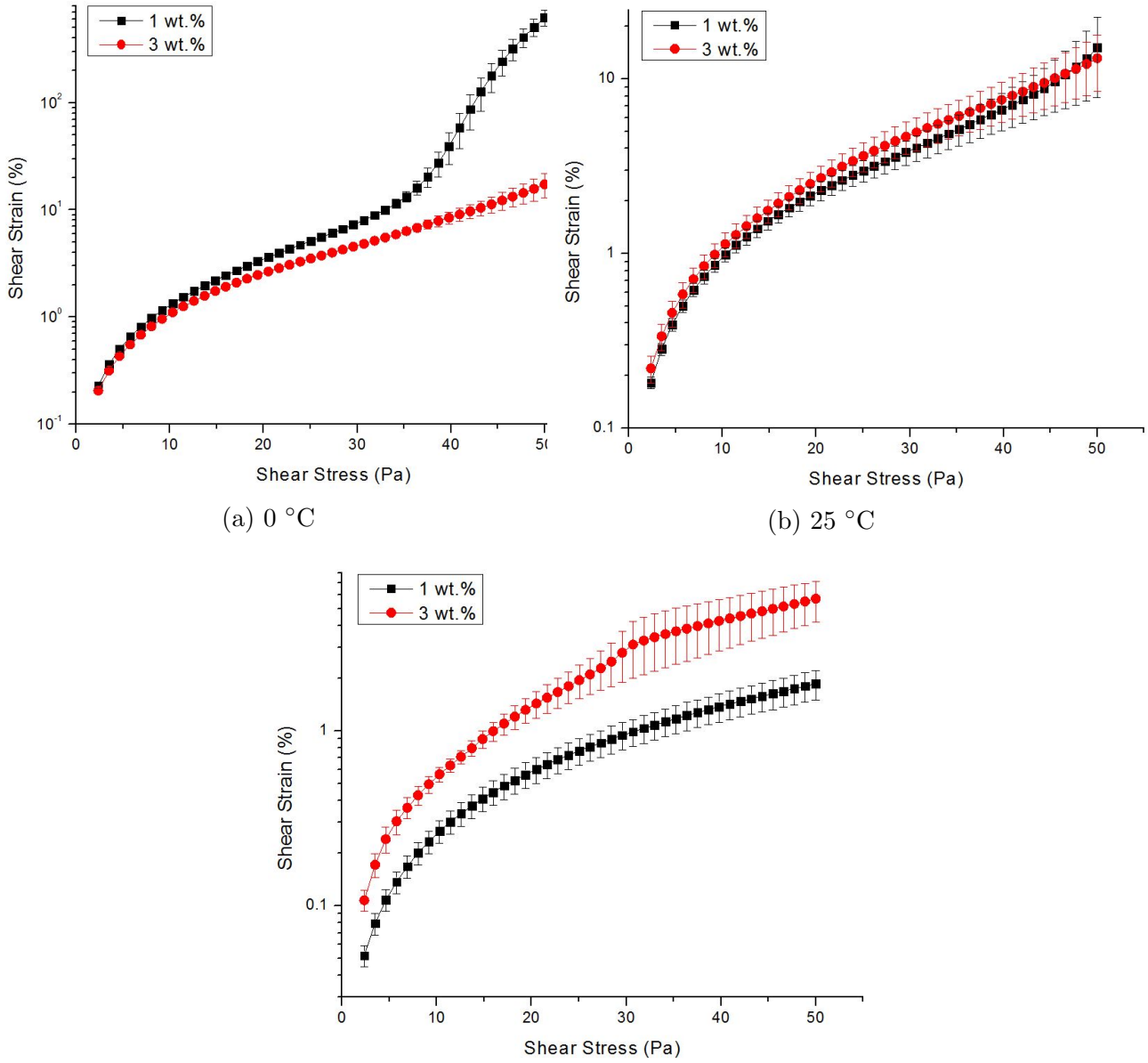

(a) 0 °C

(b) 25 °C

(c) 90 °C

Figure A.23. Stress Sweep: OCF S1, O:W = 60:40.

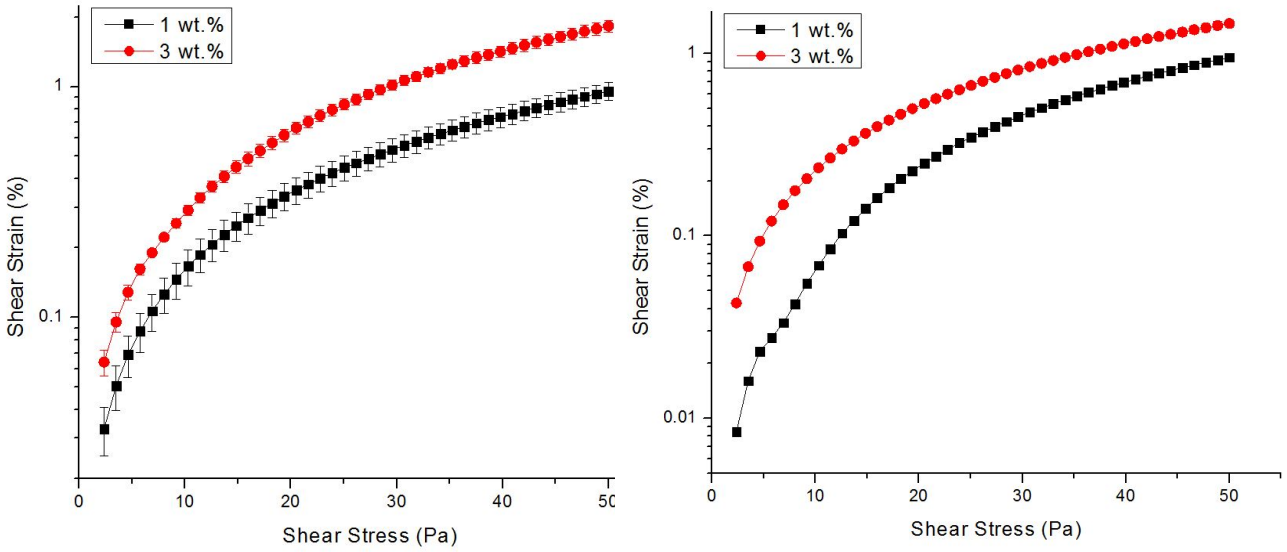

(a) 0 °C

(b) 25 °C

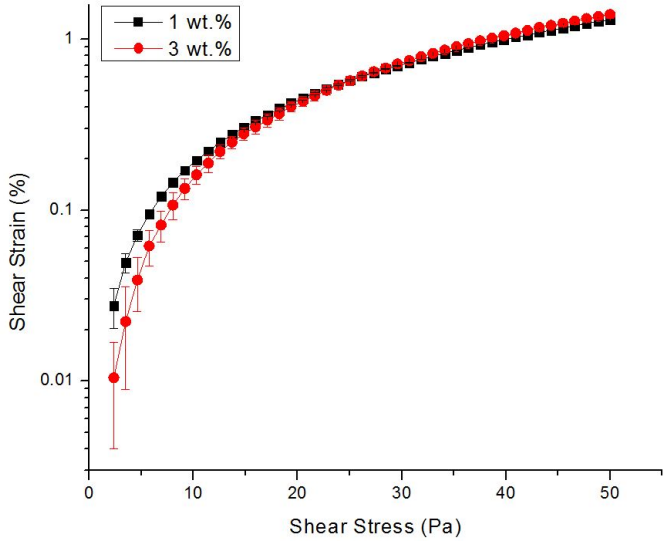

(c) 90 °C

Figure A.24. Stress Sweep: OCF S2, O:W = 50:50.

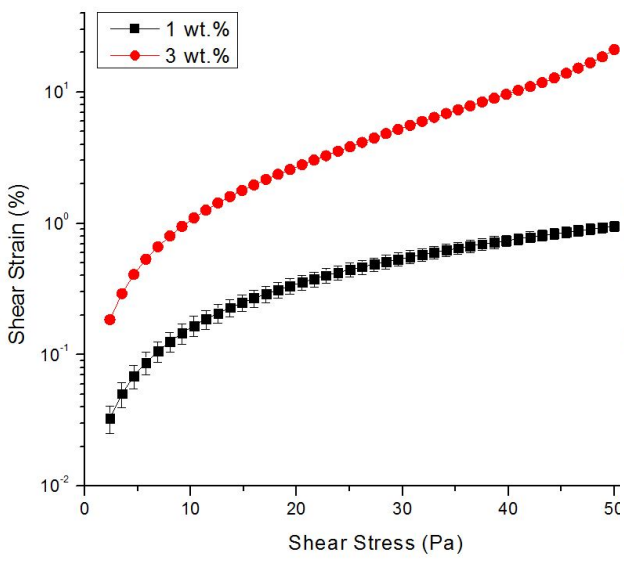

(a) 0 °C

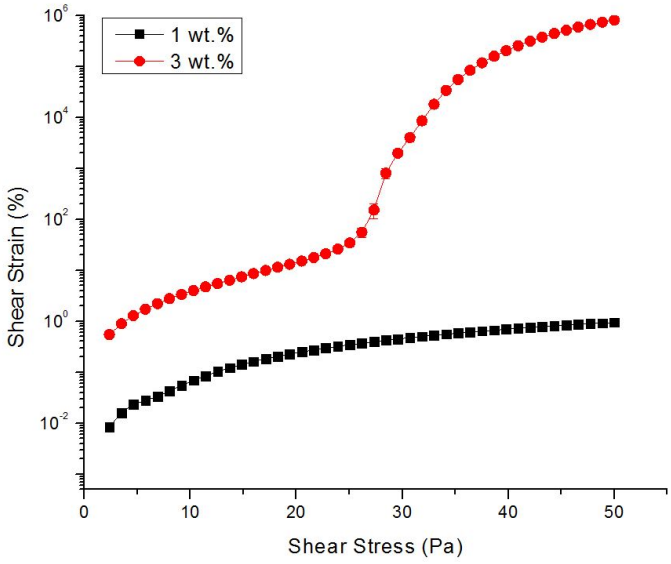

(b) 25 °C

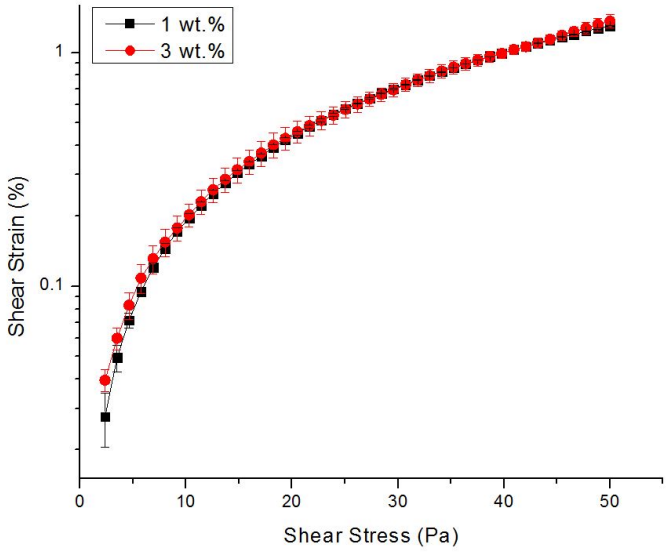

(c) 90 °C

Figure A.25. Stress Sweep: OCF S2, O:W = 60:40.

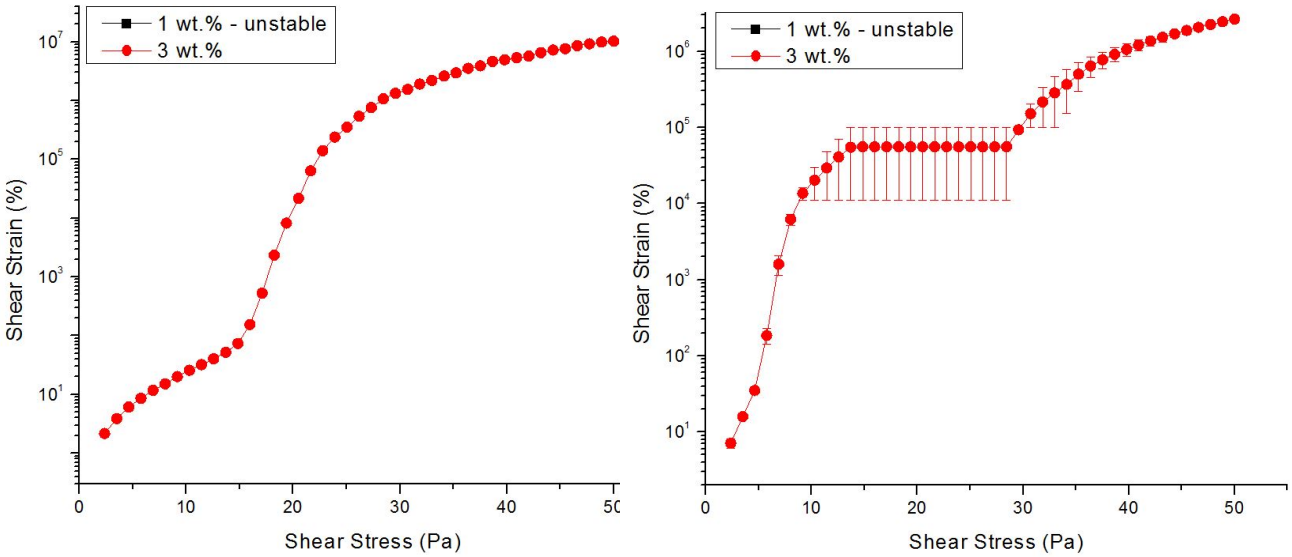

(a) 0 °C

(b) 25 °C

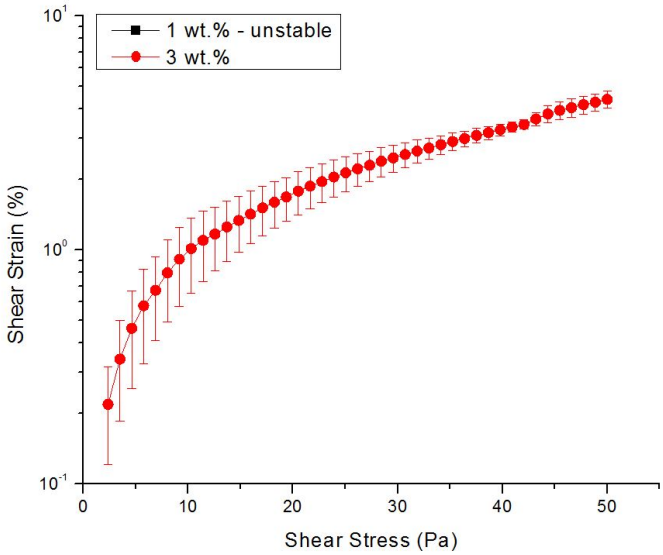

(c) 90 °C

Figure A.26. Stress Sweep: OCF S2, O:W = 70:30.

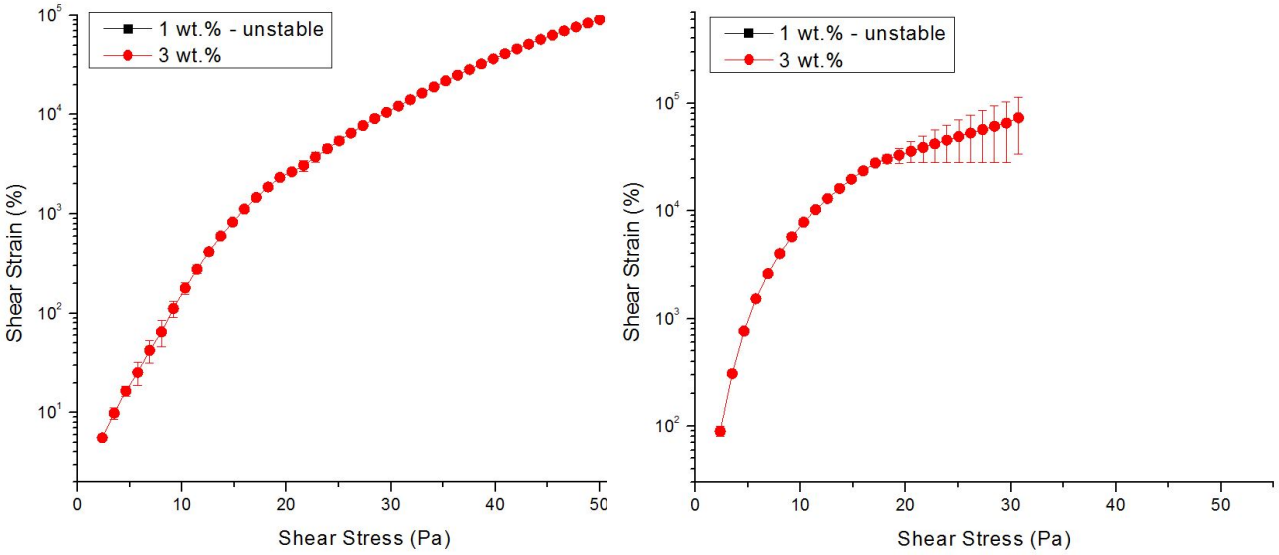

(a) 0 °C

(b) 25 °C

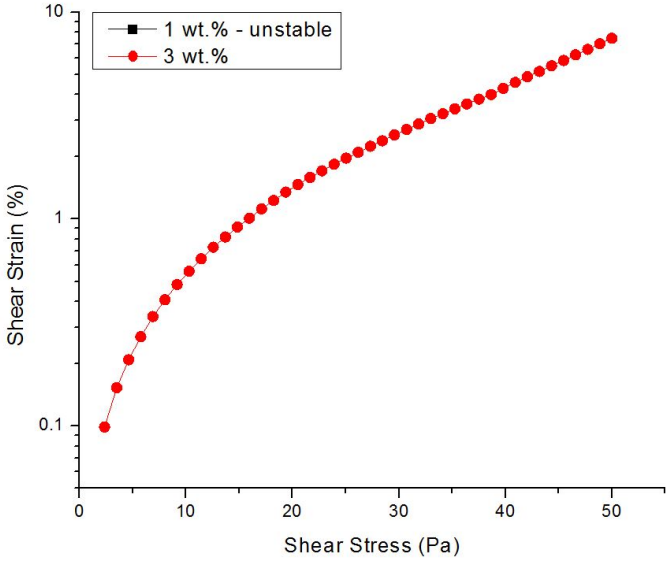

(c) 90 °C

Figure A.27. Stress Sweep: OCF S2, O:W = 80:20.

A.3 Effect of Oil:Water Ratio

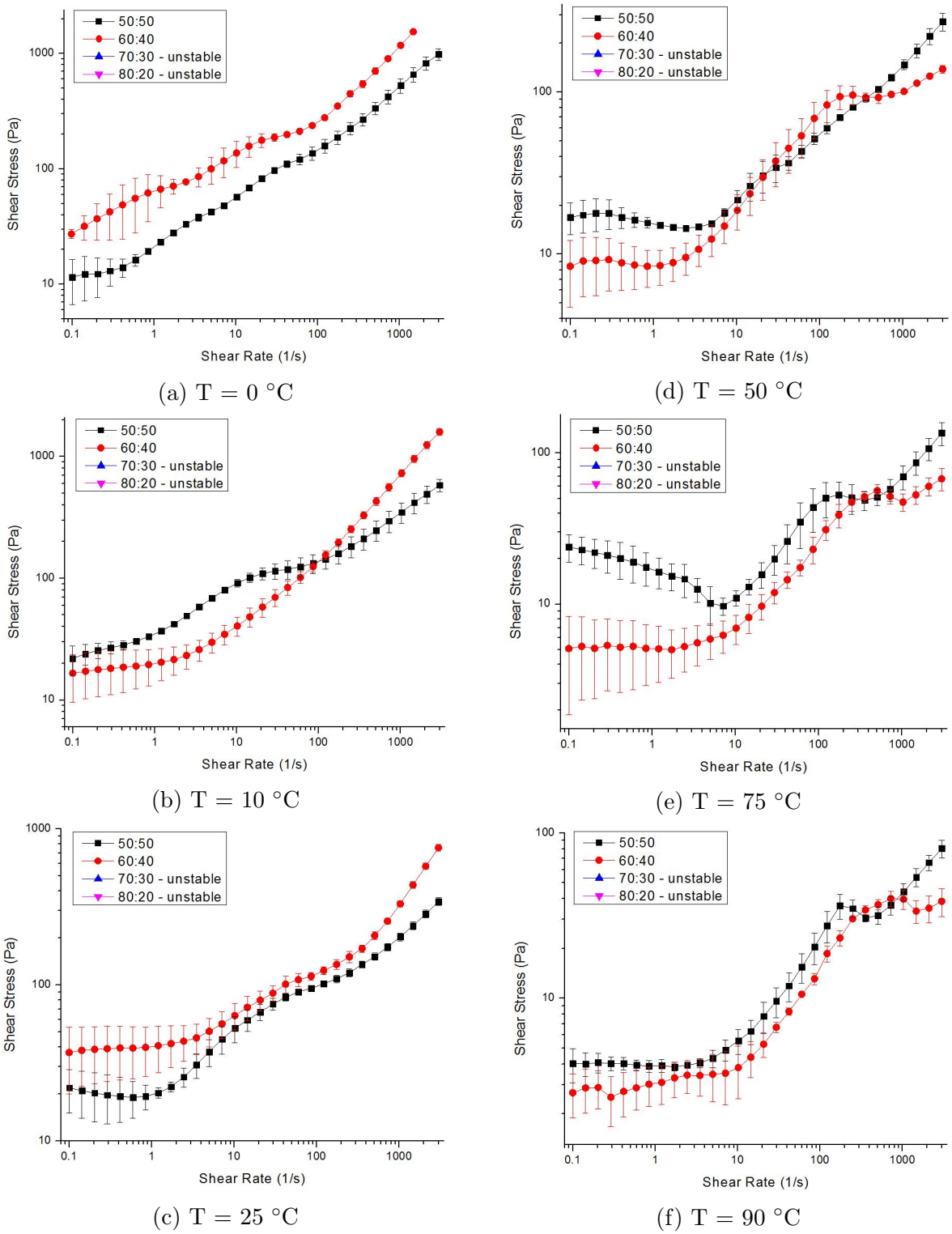

(a) T = 0 °C

(d) T = 50 °C

(b) T = 10 °C

(e) T = 75 °C

(c) T = 25 °C

(f) T = 90 °C

Figure A.28. Flow Curve: OCF S1, C_{surf} = 1 wt.%.

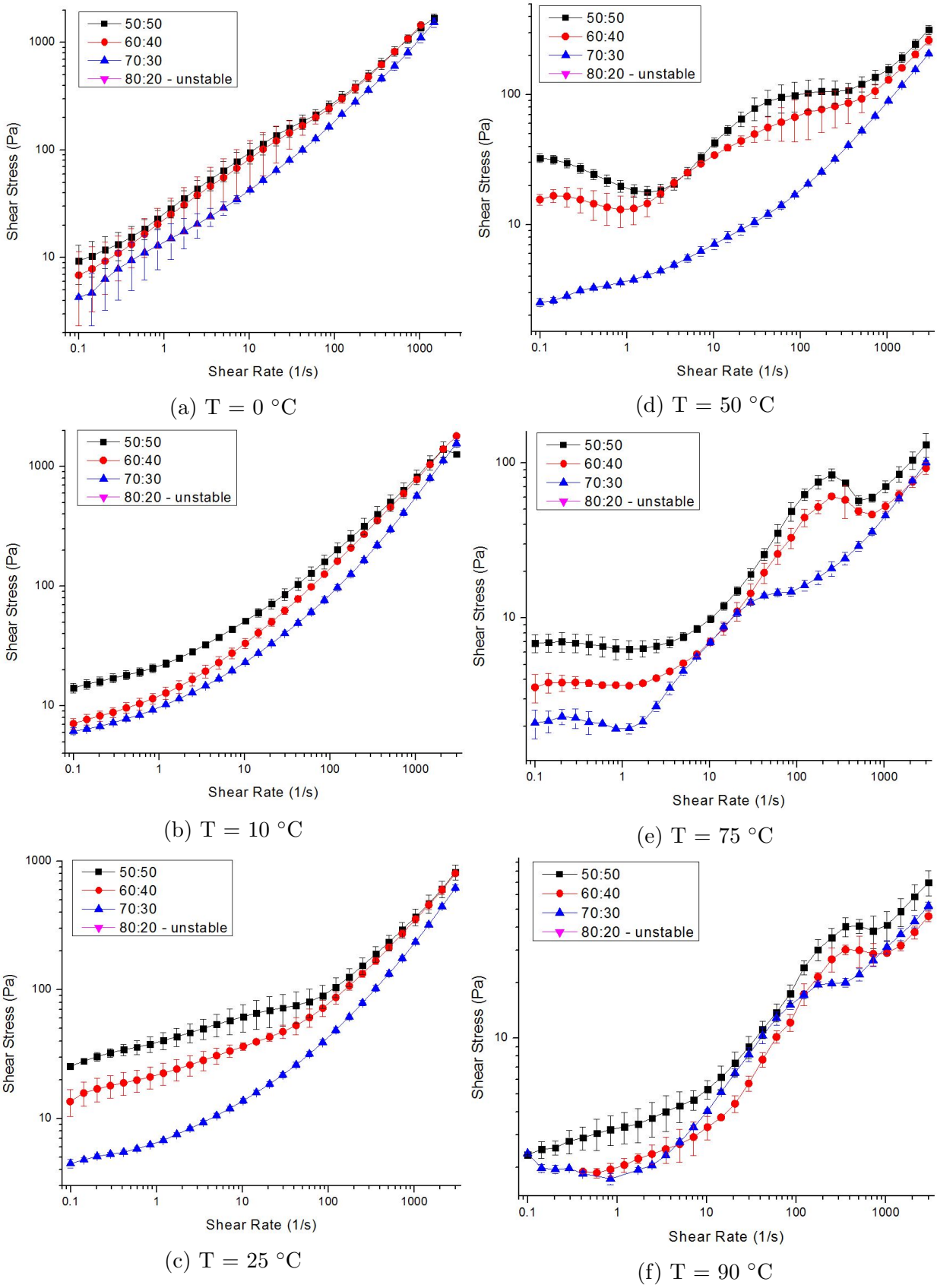

(a) T = 0 °C

(d) T = 50 °C

(b) T = 10 °C

(e) T = 75 °C

(c) T = 25 °C

(f) T = 90 °C

Figure A.29. Flow Curve: OCF S1, C_{surf} = 2 wt.%.

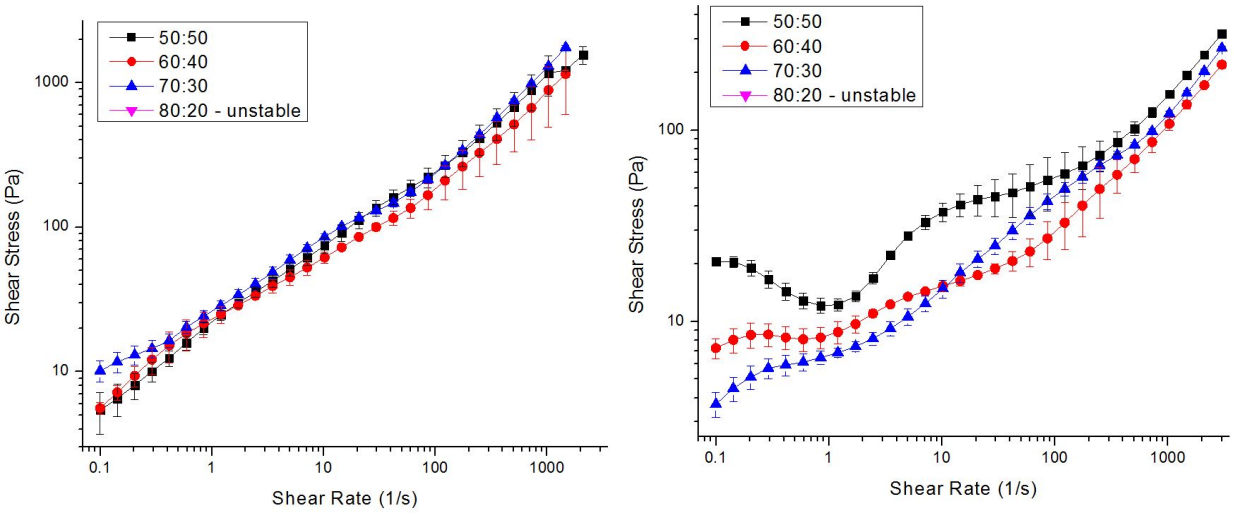

(a) T = 0 °C

(d) T = 50 °C

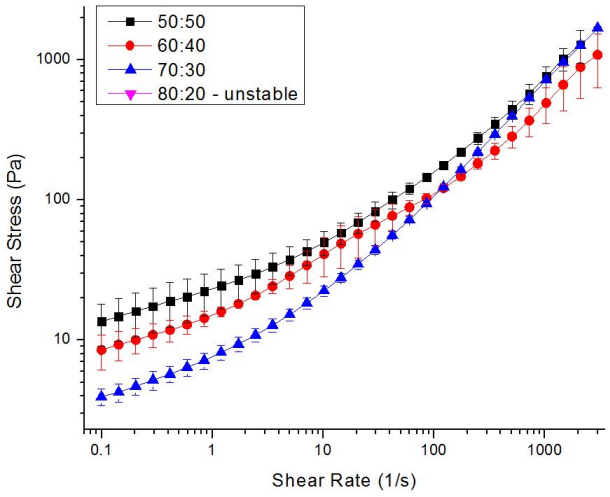

(b) T = 10 °C

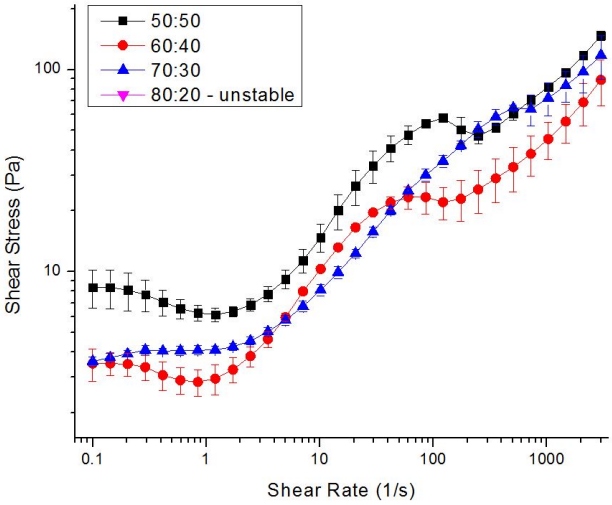

(e) T = 75 °C

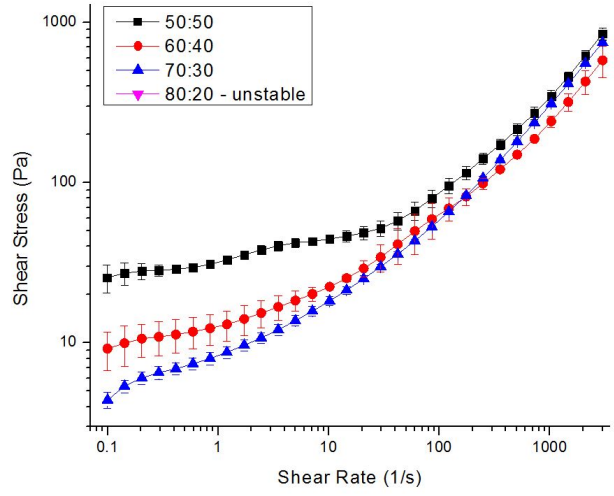

(c) T = 25 °C

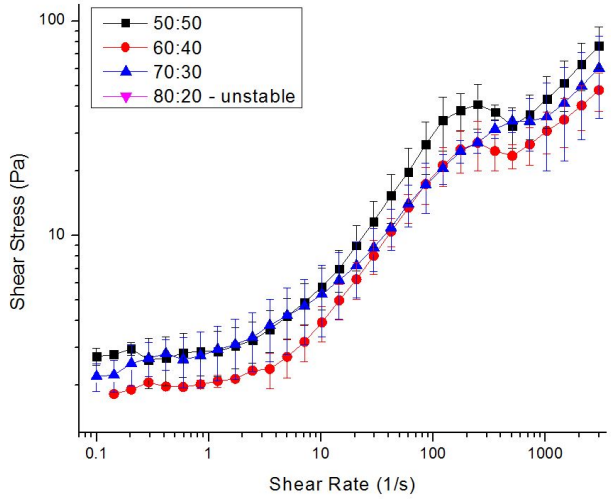

(f) T = 90 °C

Figure A.30. Flow Curve: OCF S1, C_{surf} = 3 wt.%.

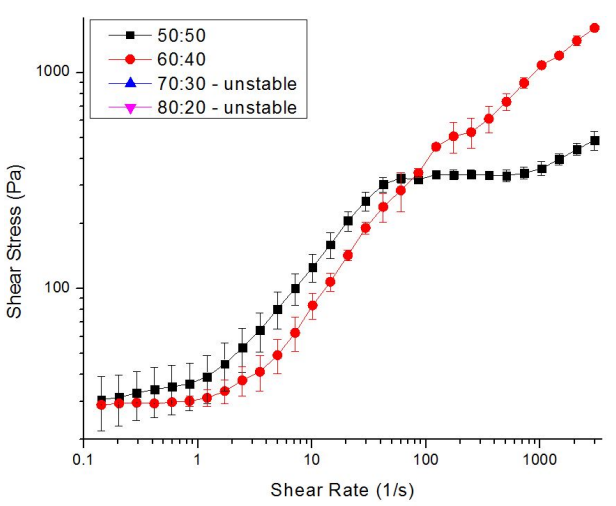

(a) T = 0 °C

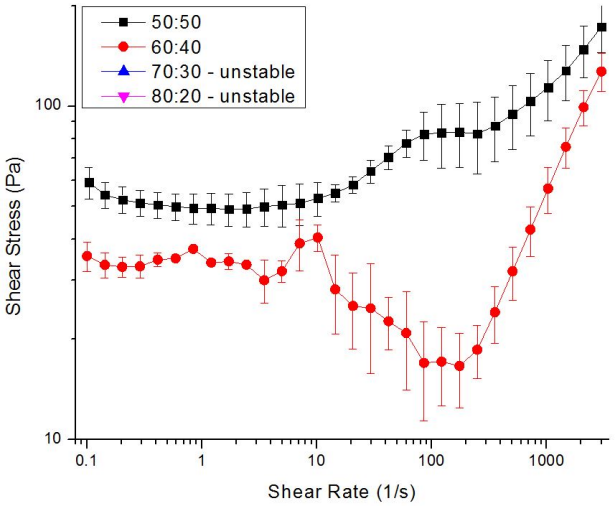

(d) T = 50 °C

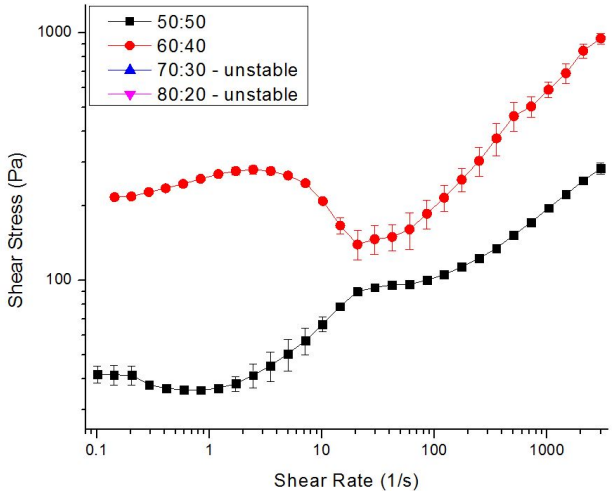

(b) T = 10 °C

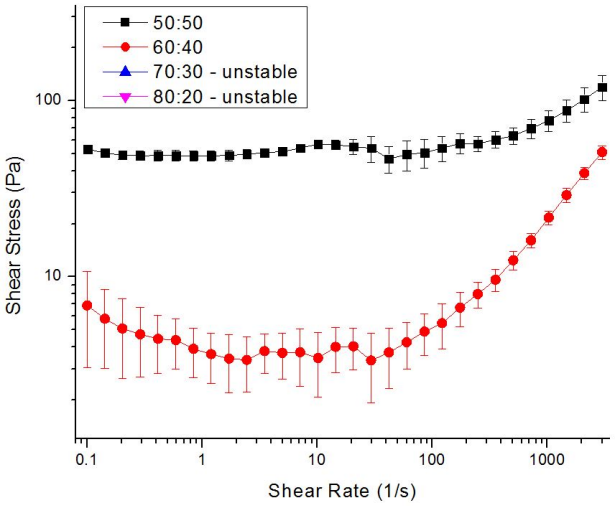

(e) T = 75 °C

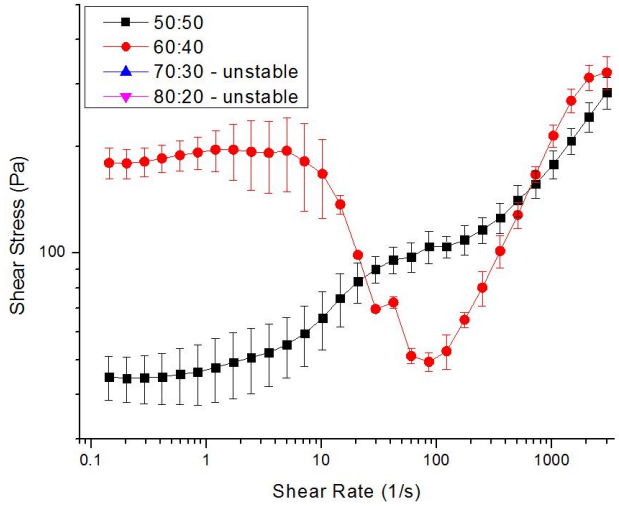

(c) T = 25 °C

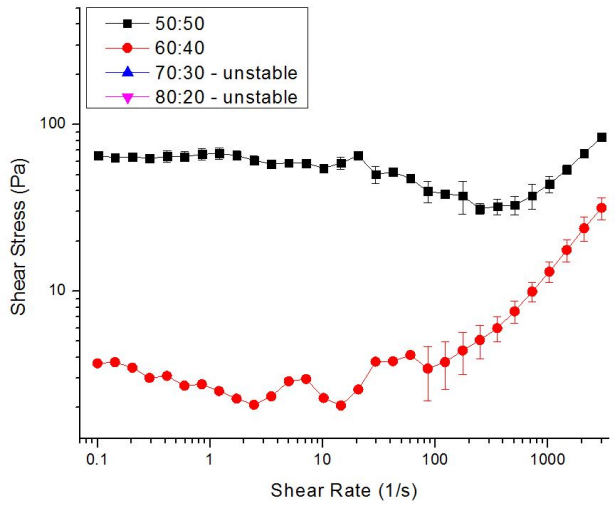

(f) T = 90 °C

Figure A.31. Flow Curve: OCF S1, C_{surf} = 1 wt.%.

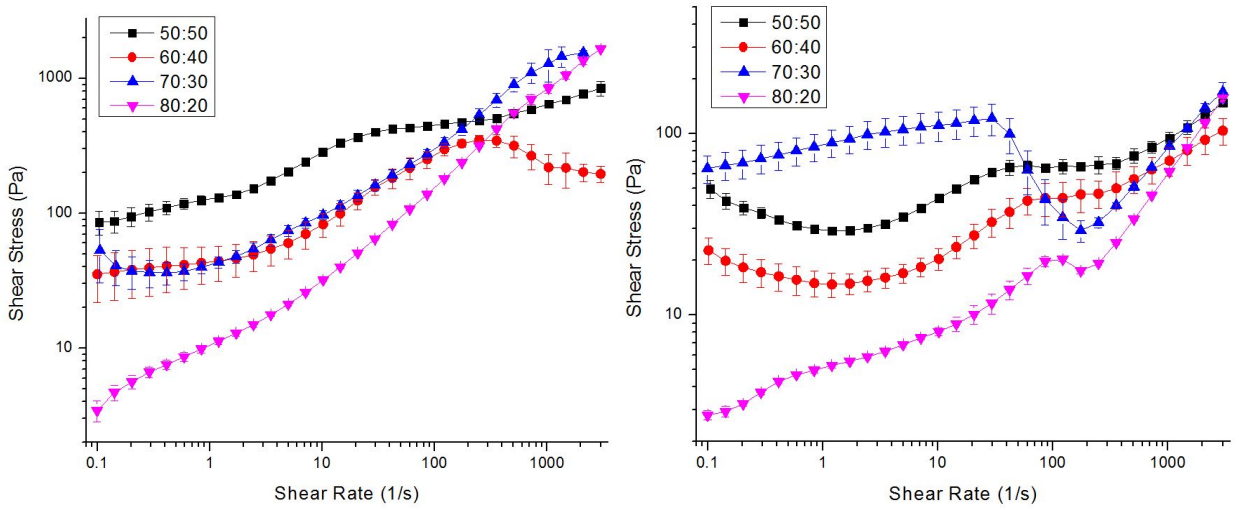

(a) T = 0 °C

(d) T = 50 °C

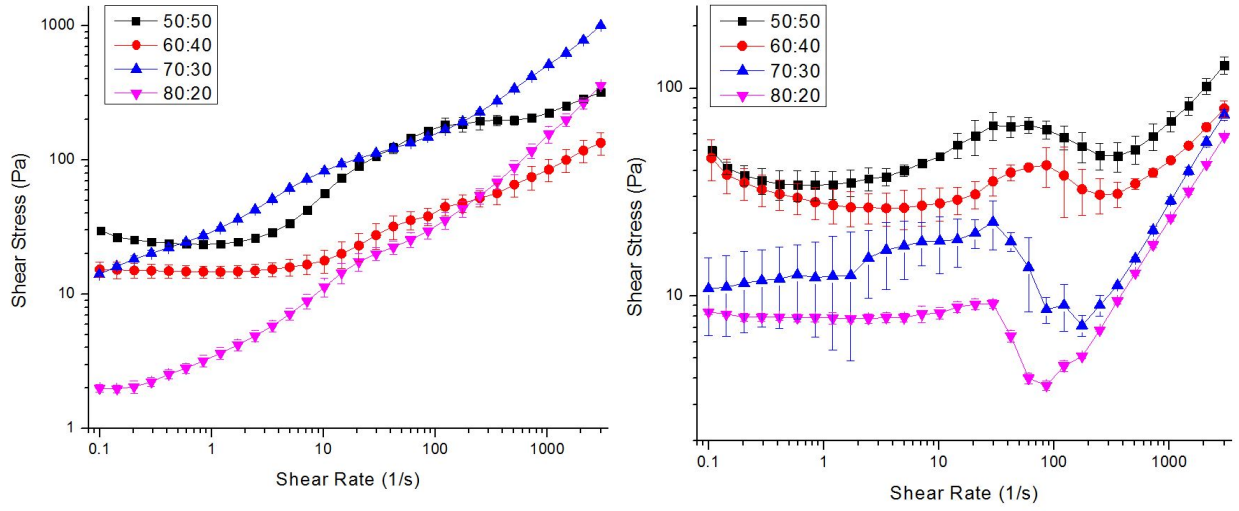

(b) T = 10 °C

(e) T = 75 °C

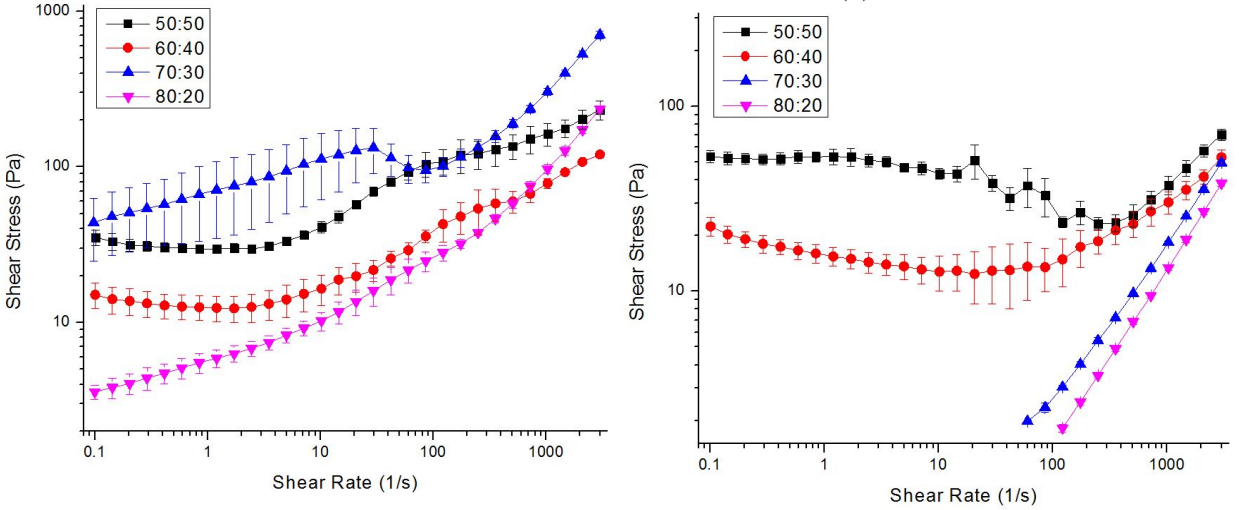

(c) T = 25 °C

(f) T = 90 °C

Figure A.32. Flow Curve: OCF S1, C_{surf} = 2 wt.%.

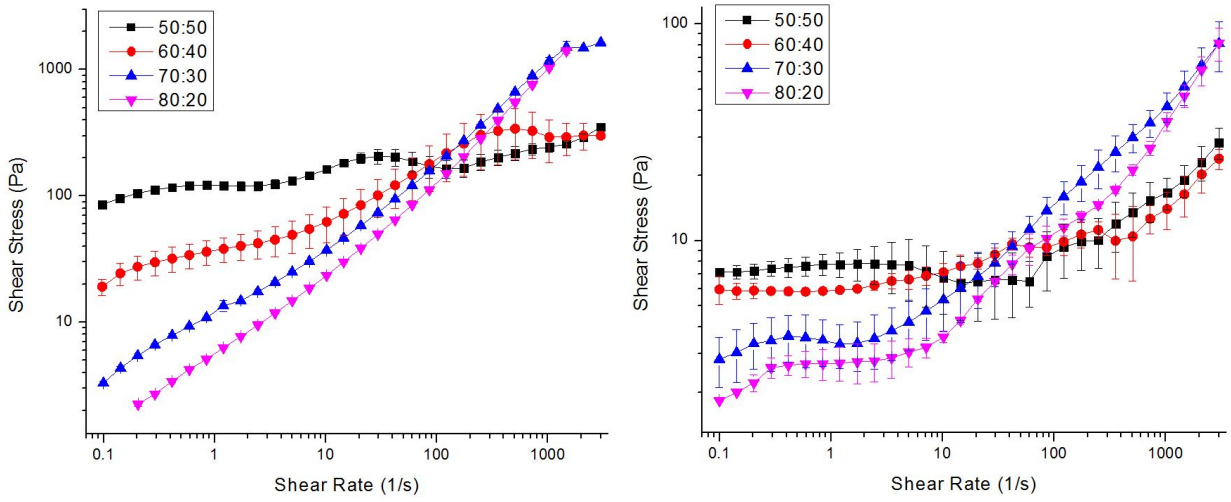

(a) T = 0 °C

(d) T = 50 °C

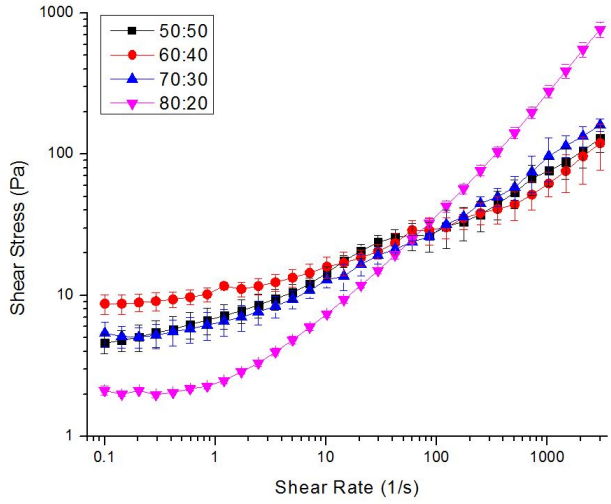

(b) T = 10 °C

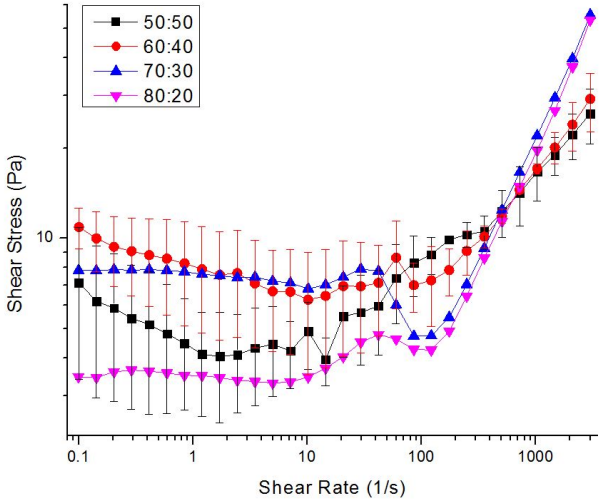

(e) T = 75 °C

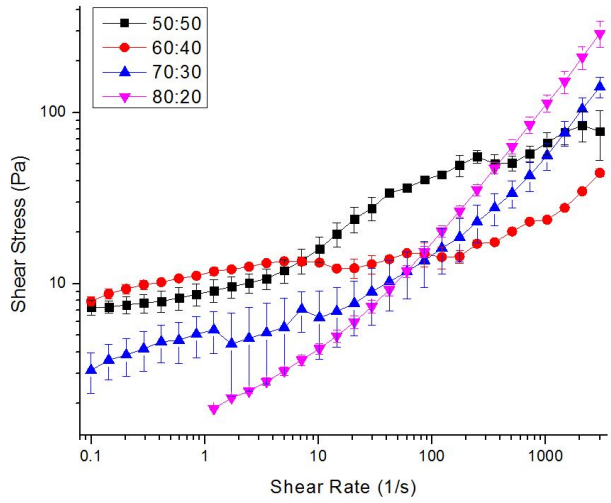

(c) T = 25 °C

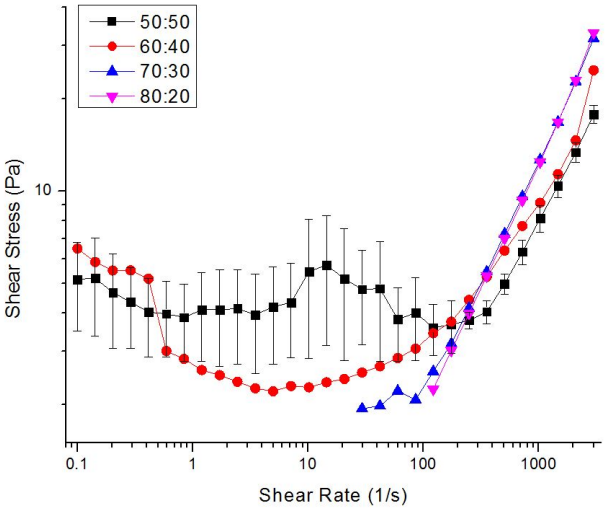

(f) T = 90 °C

Figure A.33. Flow Curve: OCF S1, $C_{surf.}$ = 3 wt.%.

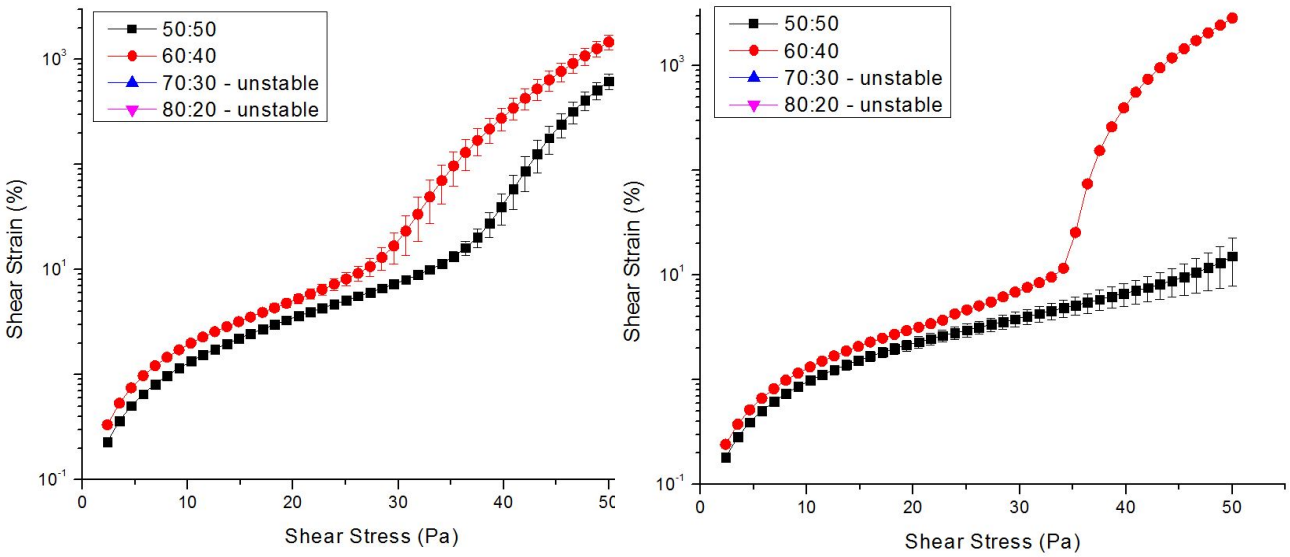

(a) 0 °C

(b) 25 °C

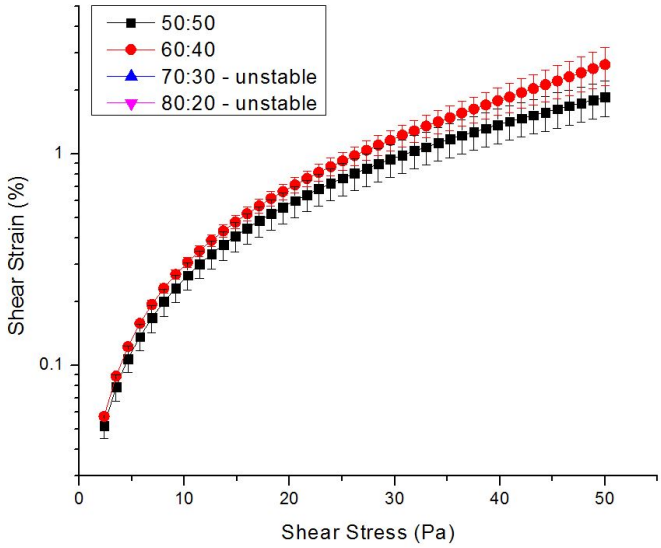

(c) 90 °C

Figure A.34. Stress Sweep: OCF S1, C_{surf} = 1 wt.%.

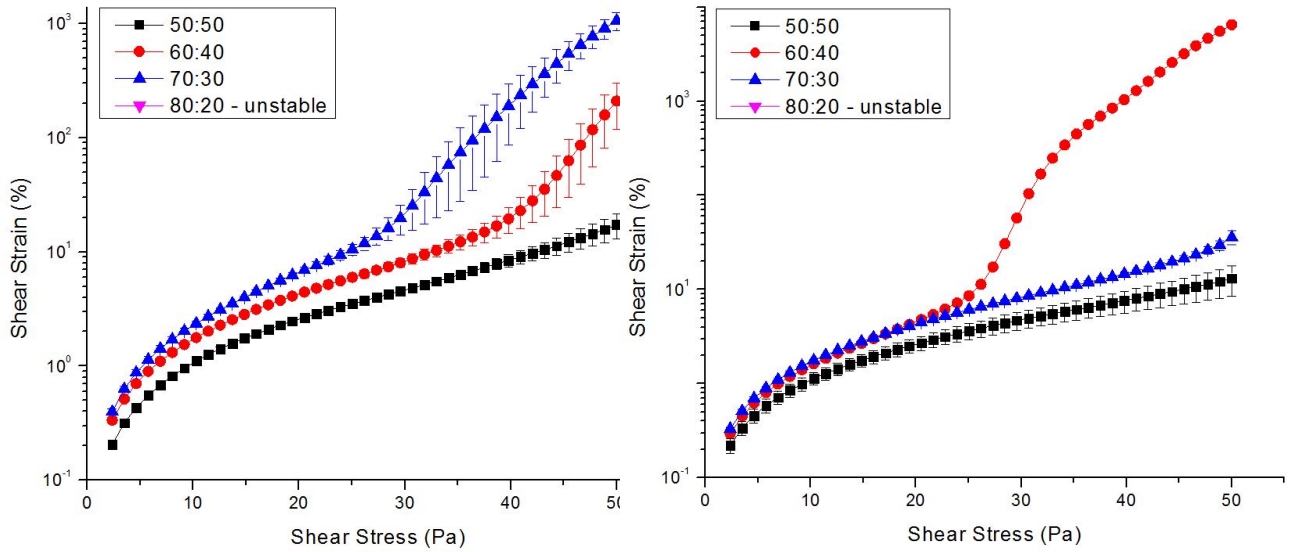

(a) 0 °C

(b) 25 °C

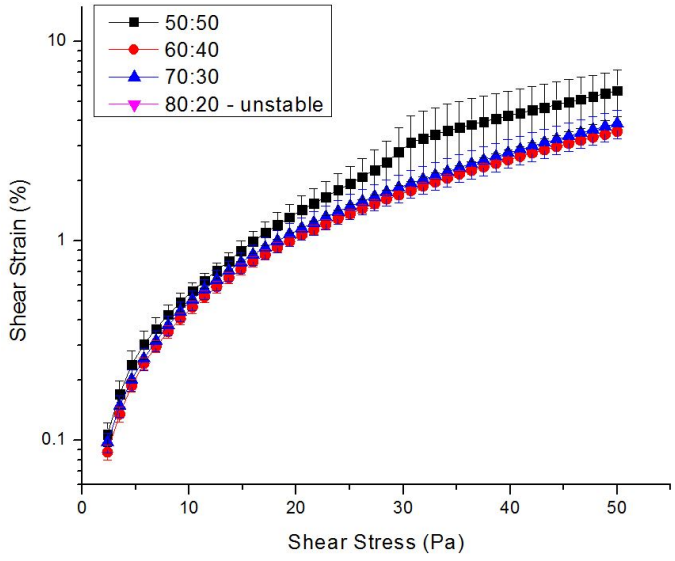

(c) 90 °C

Figure A.35. Stress Sweep: OCF S1, C_{surf} = 3 wt.%.

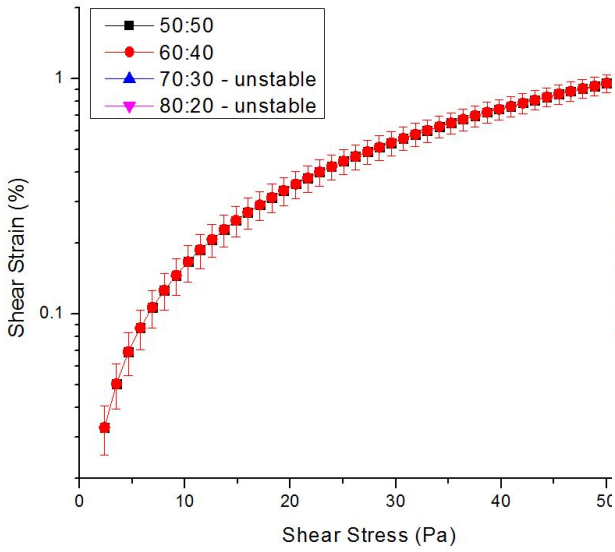

(a) 0 °C

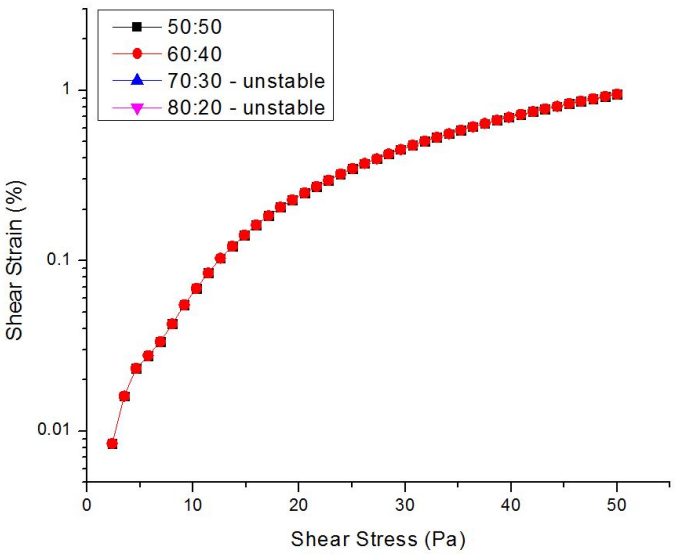

(b) 25 °C

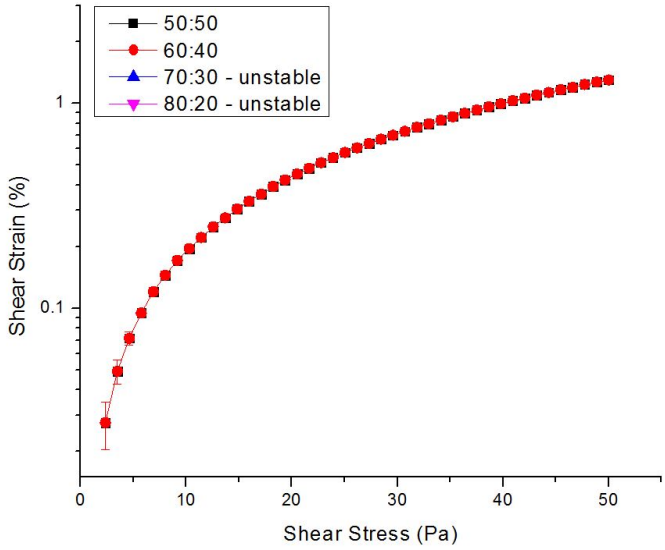

(c) 90 °C

Figure A.36. Stress Sweep: OCF S2, C_{surf} = 3 wt.%.

A.4 Effect of Temperature

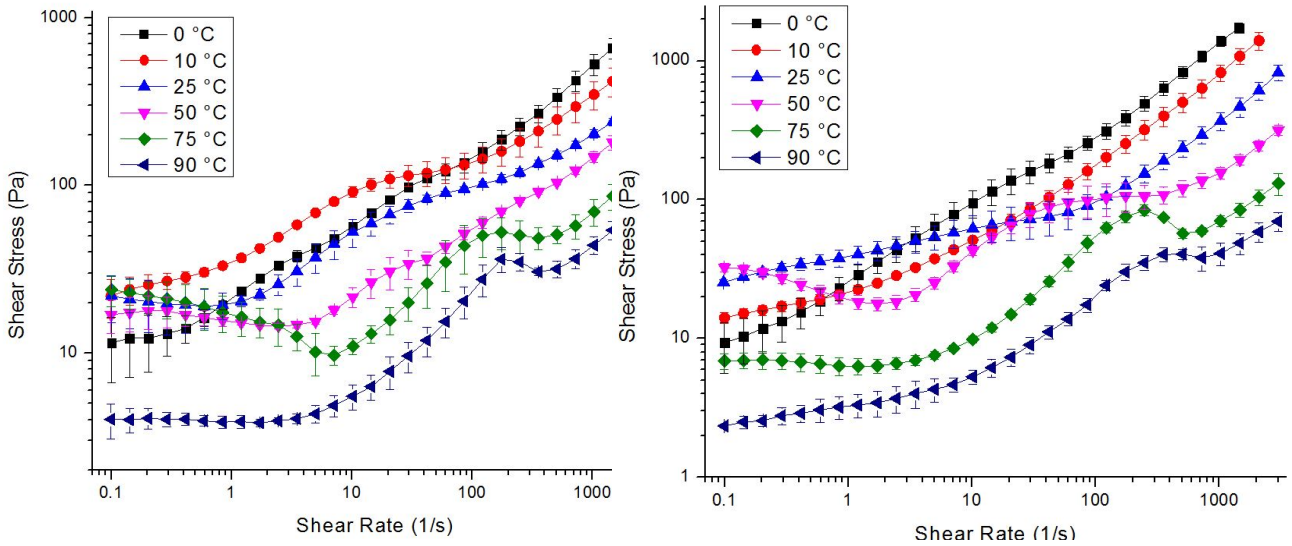

(a) 1 wt.%

(b) 2 wt.%

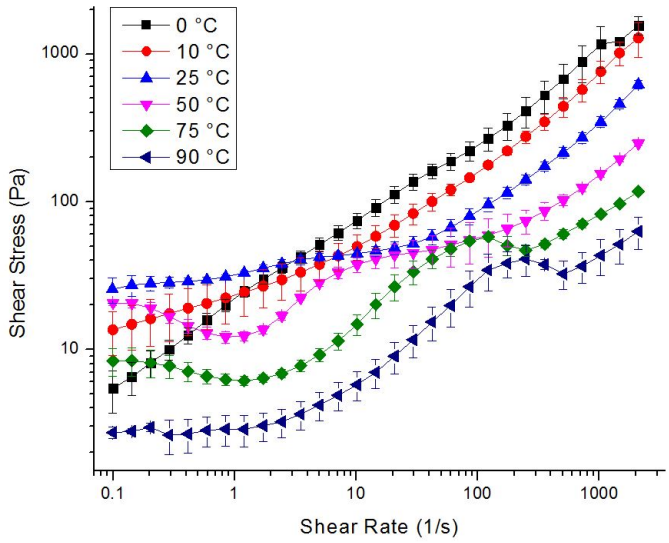

(c) 3 wt.%

Figure A.37. Flow Curve: OCF S1, O:W = 50:50.

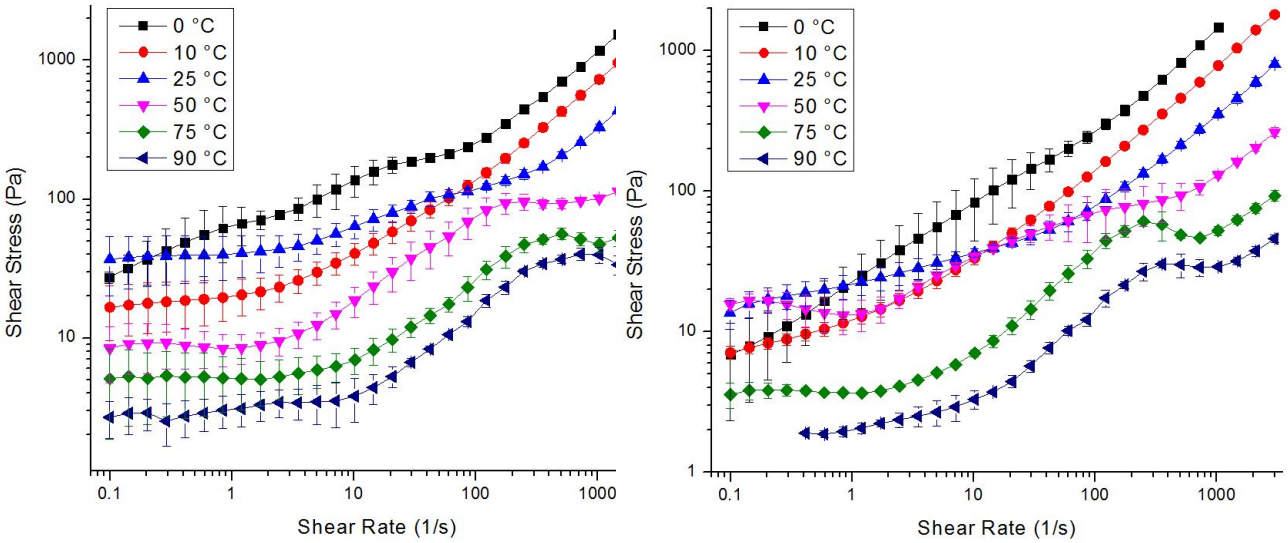

(a) 1 wt.%

(b) 2 wt.%

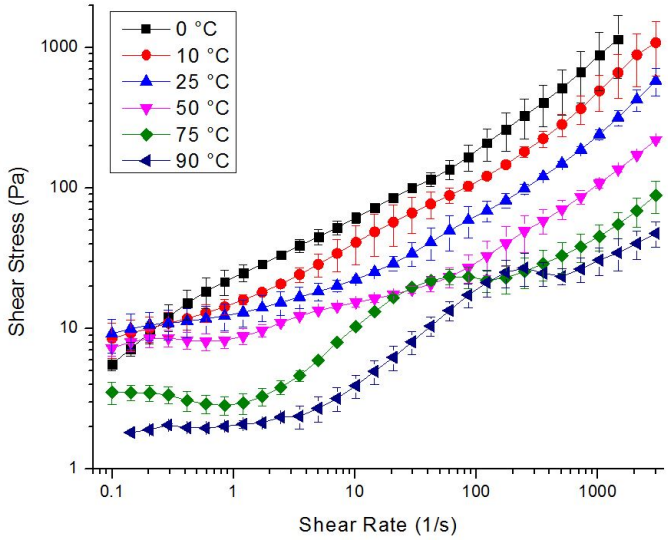

(c) 3 wt.%

Figure A.38. Flow Curve: OCF S1, O:W = 60:40.

unstable

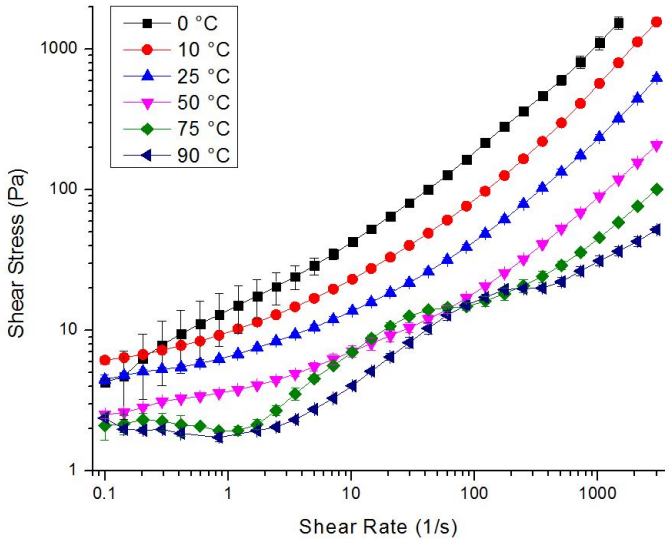

(a) 1 wt.%

(b) 2 wt.%

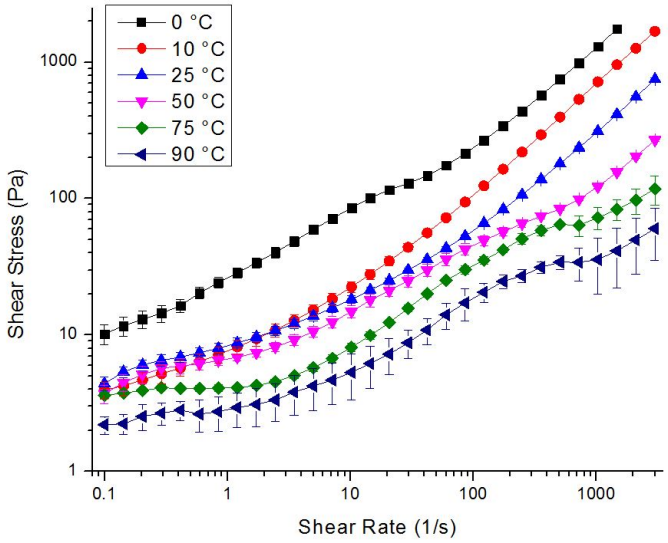

(c) 3 wt.%

Figure A.39. Flow Curve: OCF S1, O:W = 70:30.

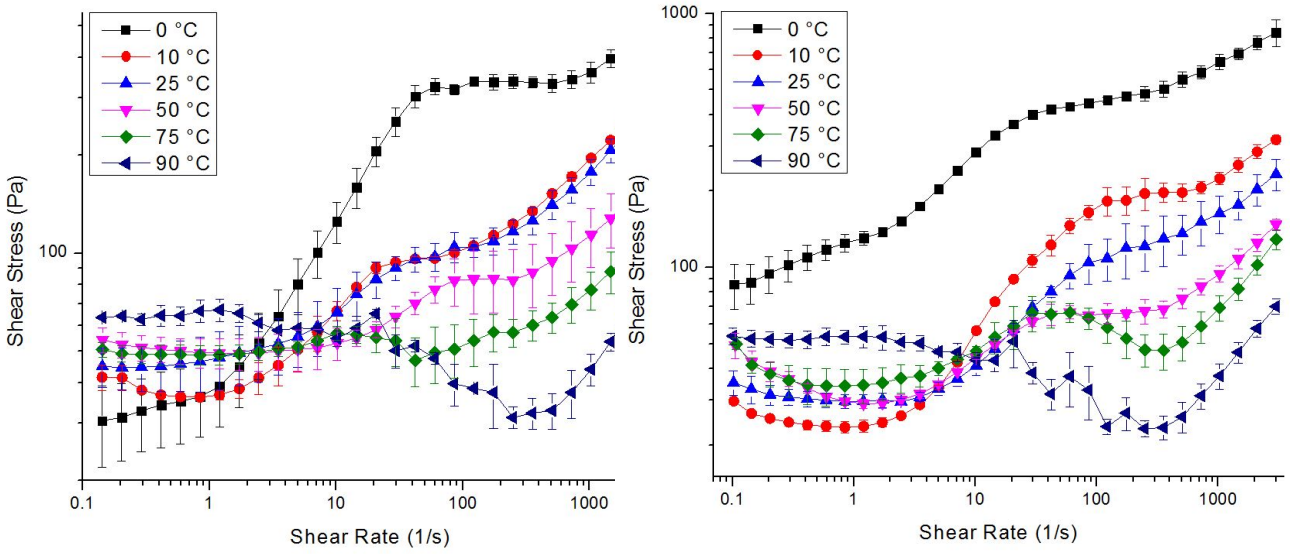

(a) 1 wt.%

(b) 2 wt.%

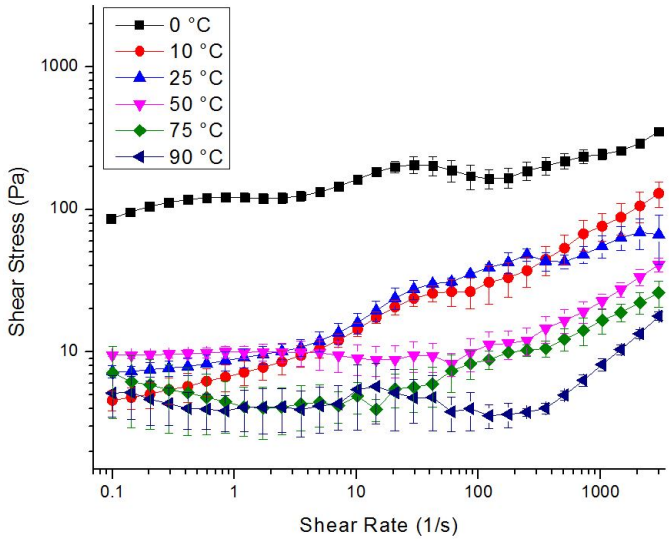

(c) 3 wt.%

Figure A.40. Flow Curve: OCF S2, O:W = 50:50.

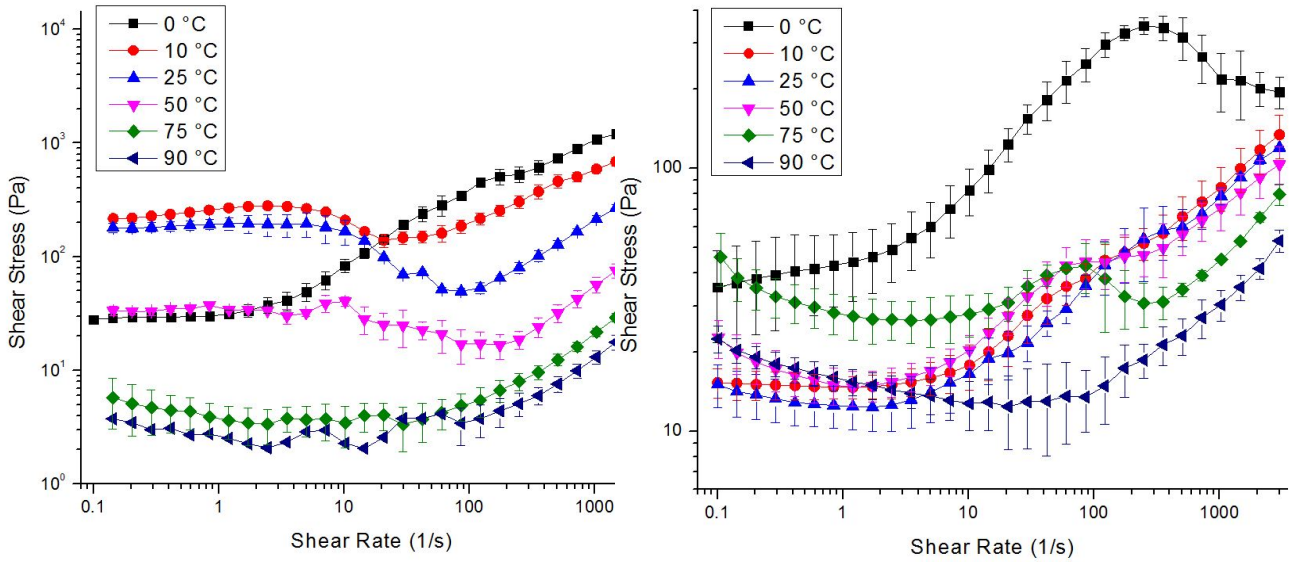

(a) 1 wt.%

(b) 2 wt.%

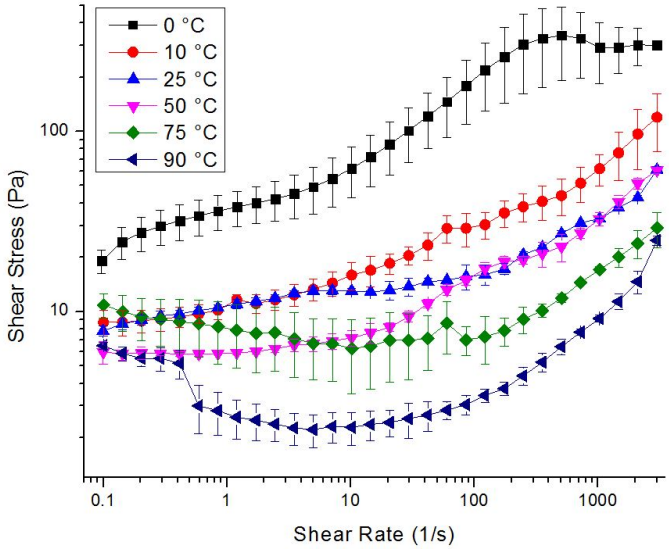

(c) 3 wt.%

Figure A.41. Flow Curve: OCF S2, O:W = 60:40.

unstable

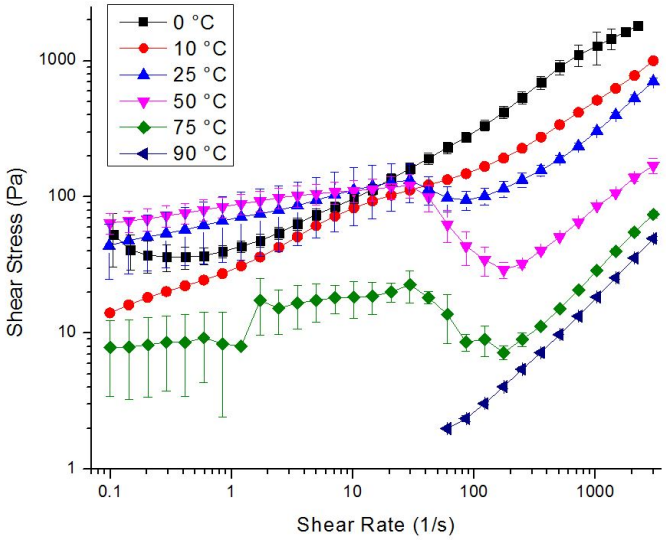

(a) 1 wt.%

(b) 2 wt.%

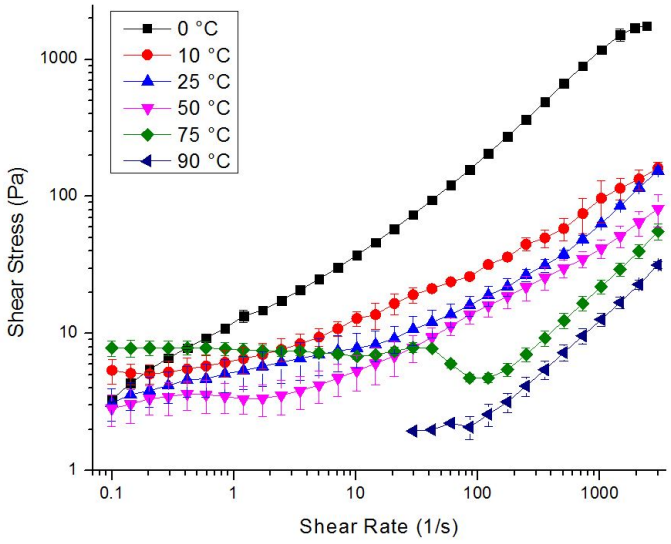

(c) 3 wt.%

Figure A.42. Flow Curve: OCF S2, O:W = 70:30.

unstable

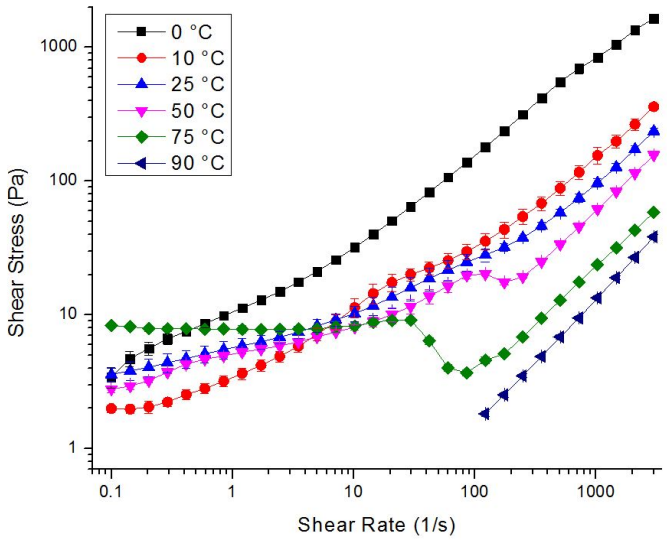

(a) 1 wt.%

(b) 2 wt.%

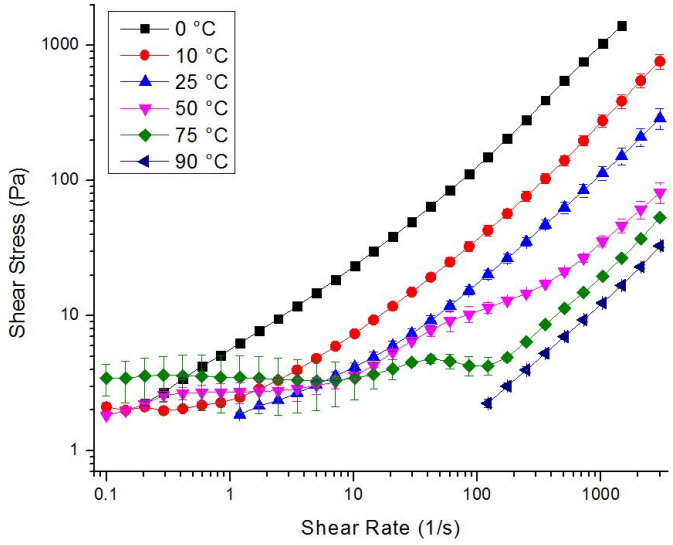

(c) 3 wt.%

Figure A.43. Flow Curve: OCF S2, O:W = 80:20.

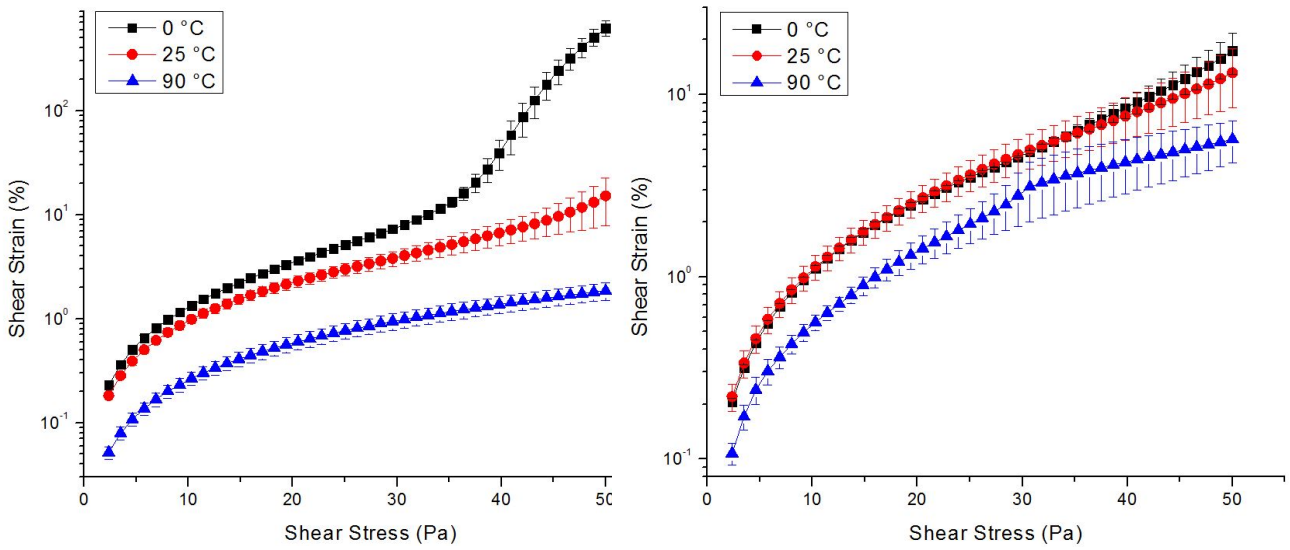

(a) 1 wt.% (b) 3 wt.%

Figure A.44. Stress Sweep: OCF S1, O:W = 50:50.

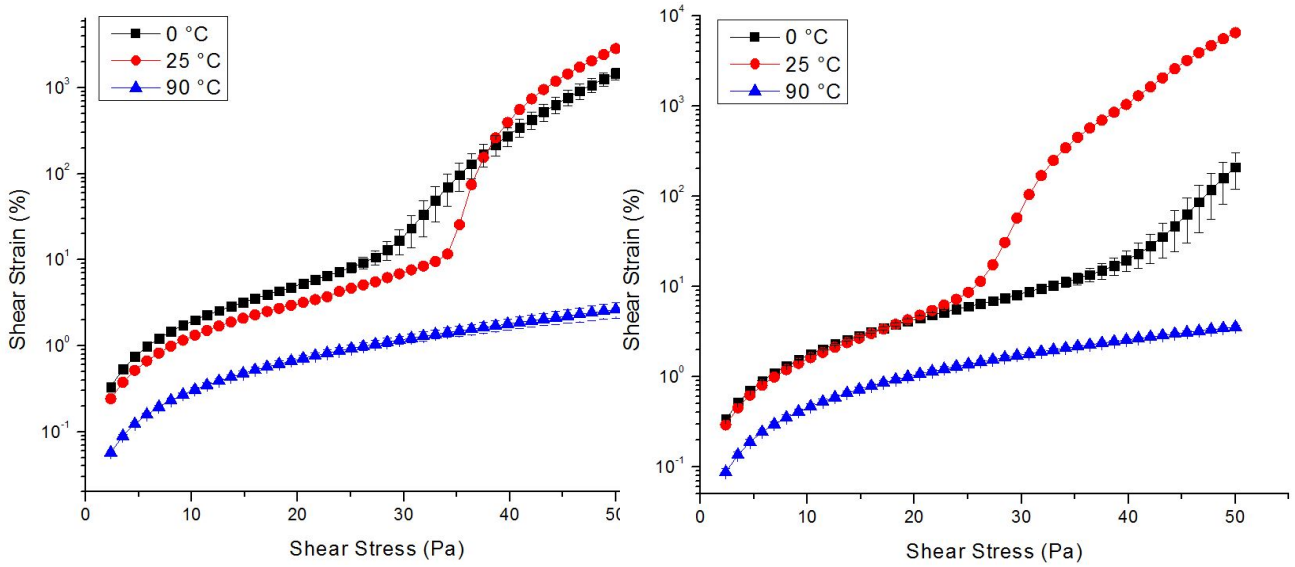

(a) 1 wt.% (b) 3 wt.%

Figure A.45. Stress Sweep: OCF S1, O:W = 60:40.

unstable

(a) 1 wt.%

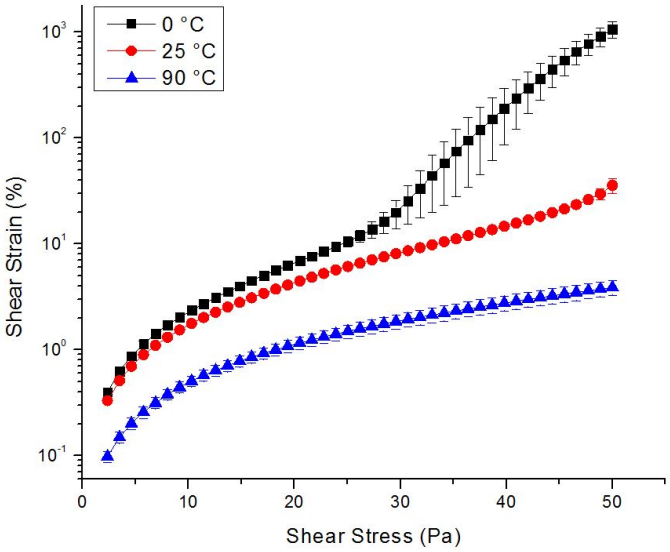

(b) 3 wt.%

Figure A.46. Stress Sweep: OCF S1, O:W = 70:30.

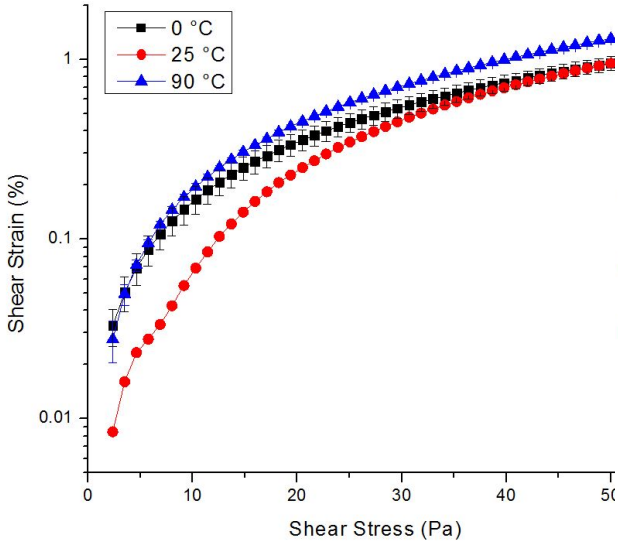

(a) 1 wt.%

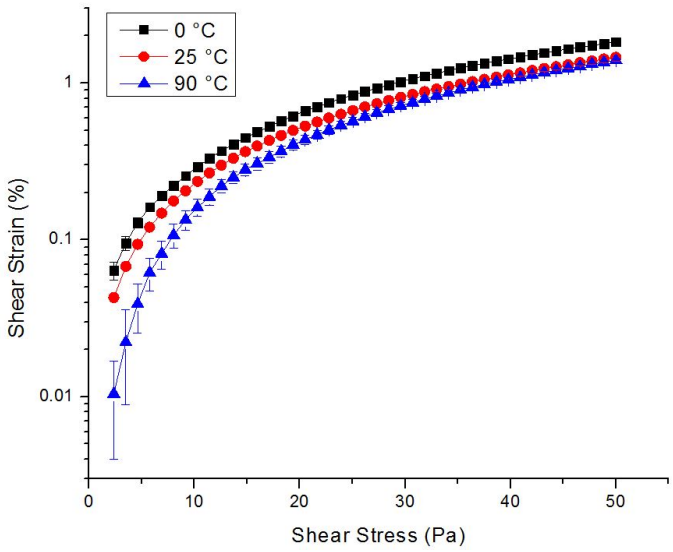

(b) 3 wt.%

Figure A.47. Stress Sweep: OCF S2, O:W = 50:50.

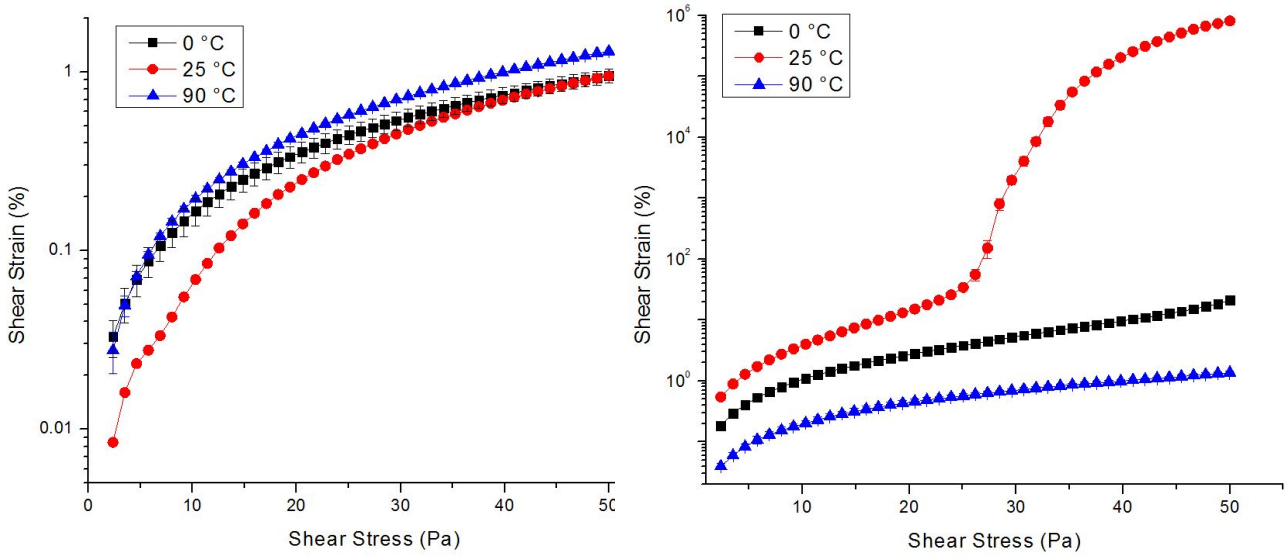

(a) 1 wt.%

(b) 3 wt.%

Figure A.48. Stress Sweep: OCF S2, O:W = 60:40.

unstable

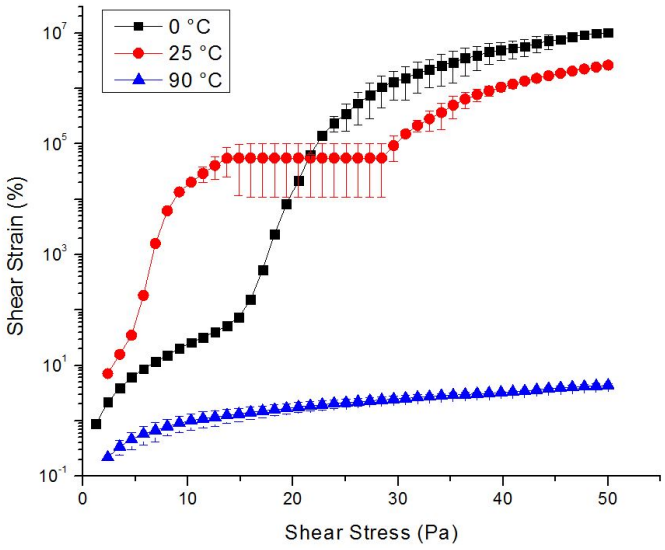

(a) 1 wt.%

(b) 3 wt.%

Figure A.49. Stress Sweep: OCF S2, O:W = 70:30.

unstable

(a) 1 wt.%

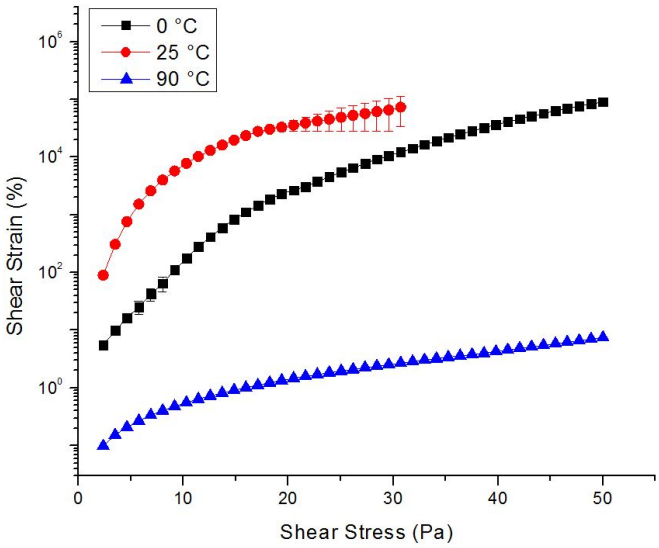

(b) 3 wt.%

Figure A.50. Stress Sweep: OCF S2, O:W = 80:20.

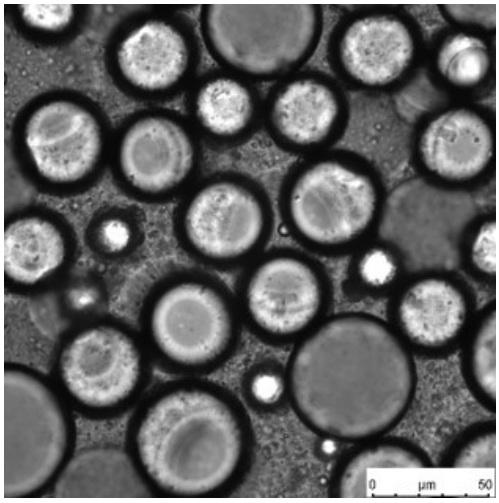

(a) 25 °C

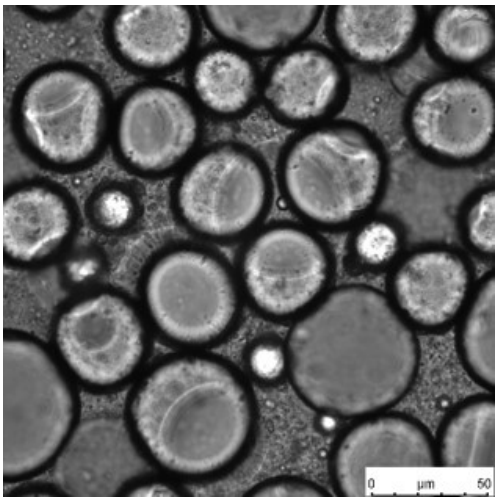

(d) 50 °C

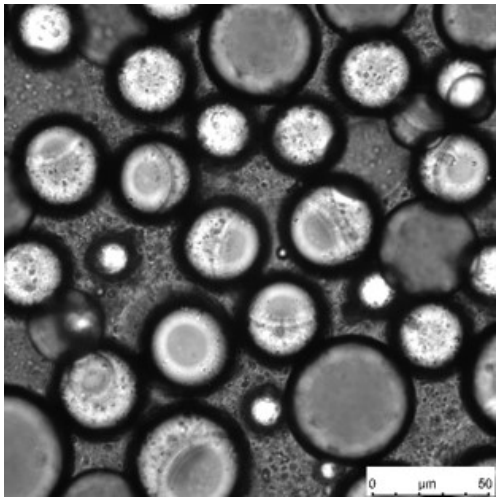

(b) 0 °C

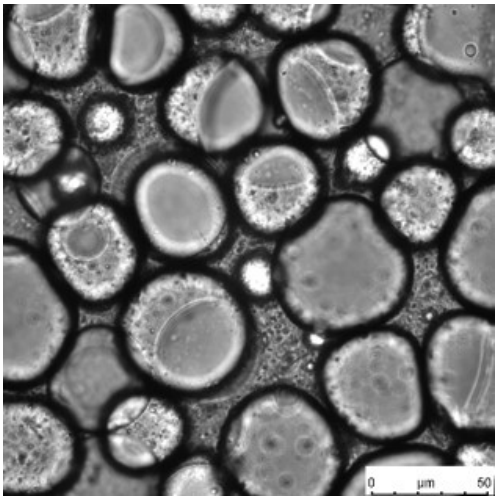

(e) 75 °C

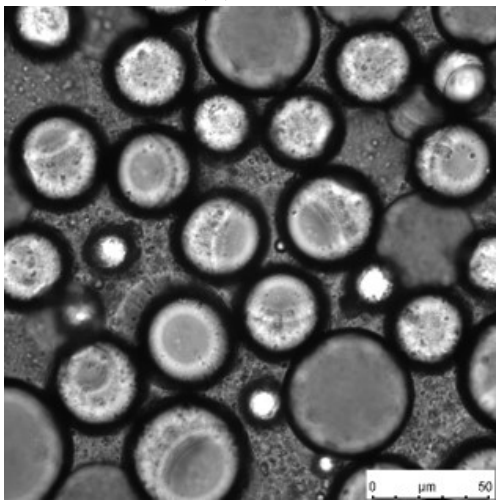

(c) 10 °C

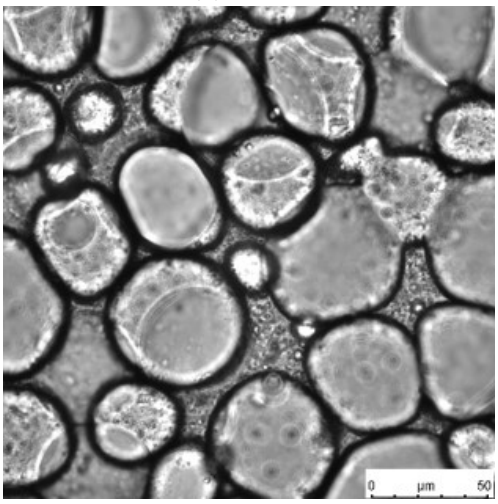

(f)

Figure A.51. No surfactant: O:W = 50:50.

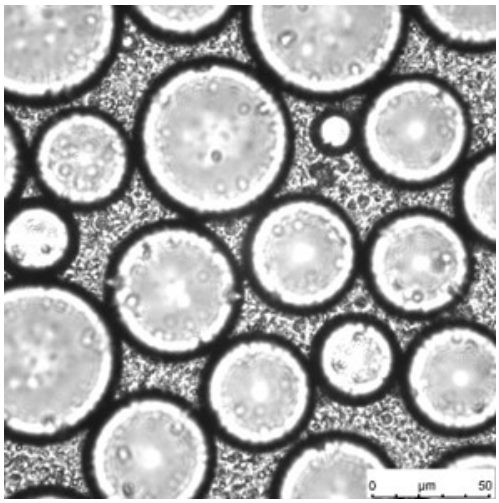

(a) 25 °C

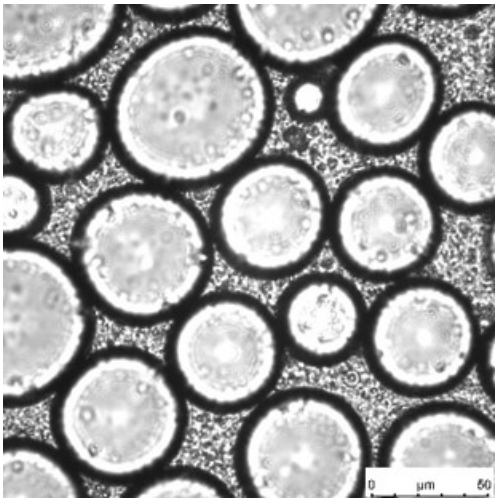

(d) 50 °C

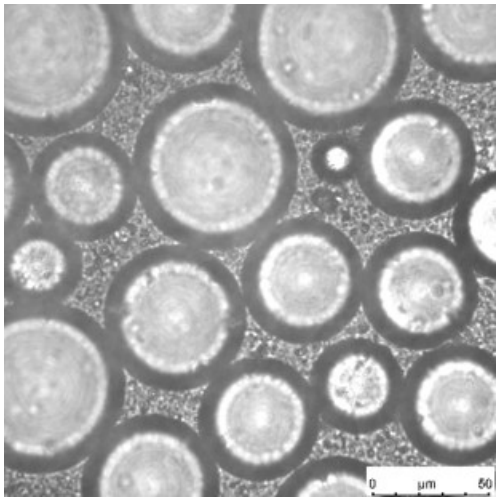

(b) 0 °C

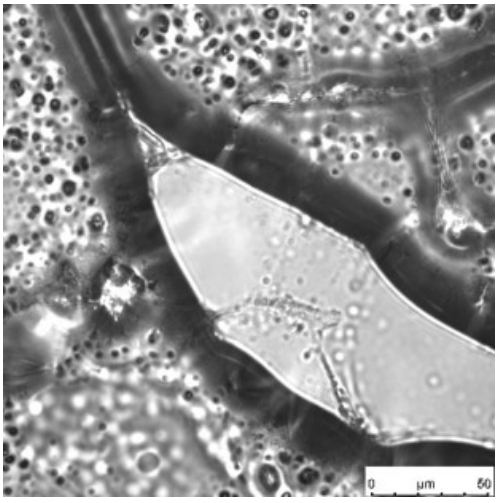

(e) 75 °C - Demulsification

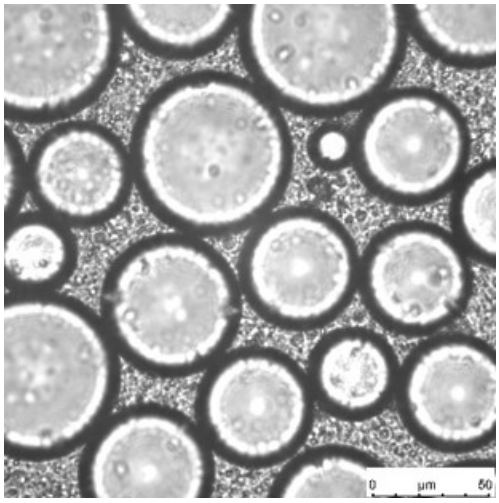

(c) 10 °C

(f)

Figure A.52. No surfactant: O:W = 60:40.

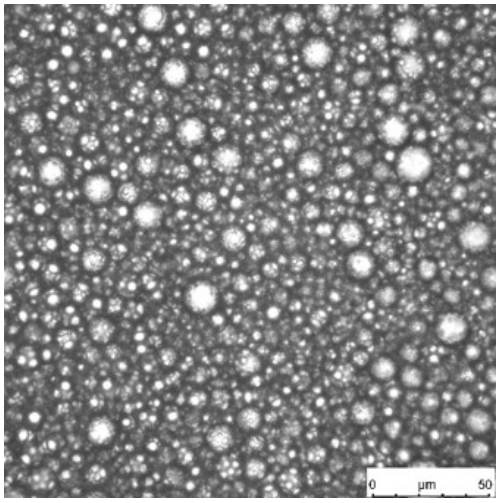

(a) 25 °C

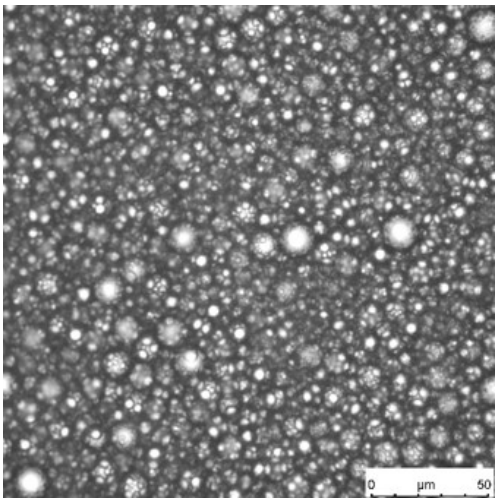

(d) 50 °C

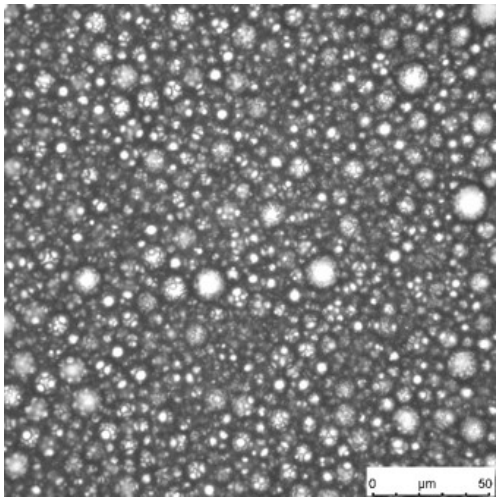

(b) 0 °C

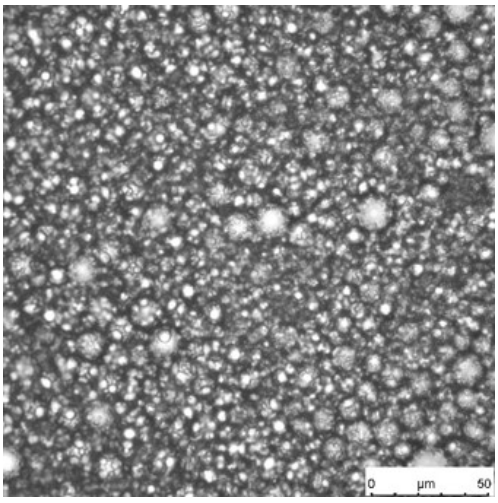

(e) 75 °C

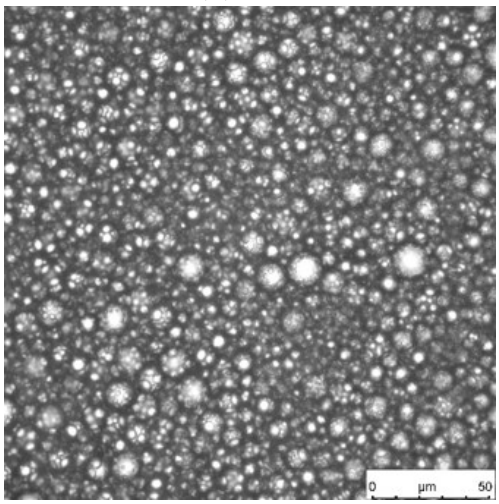

(c) 10 °C

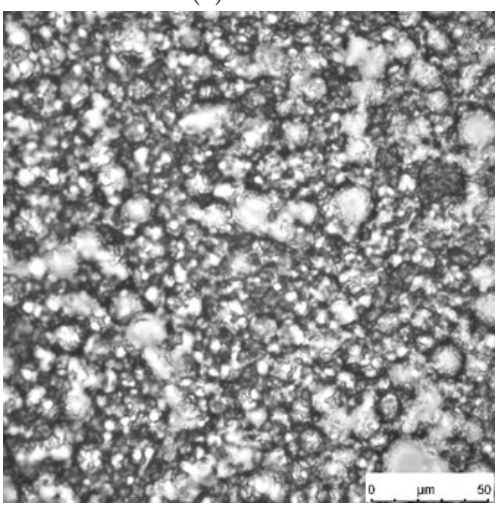

(f) 90 °C - Phase Inversion

Figure A.53. WCF M1: O:W = 60:40, C_{surf} = 3 wt.%, HLB = 11.5.

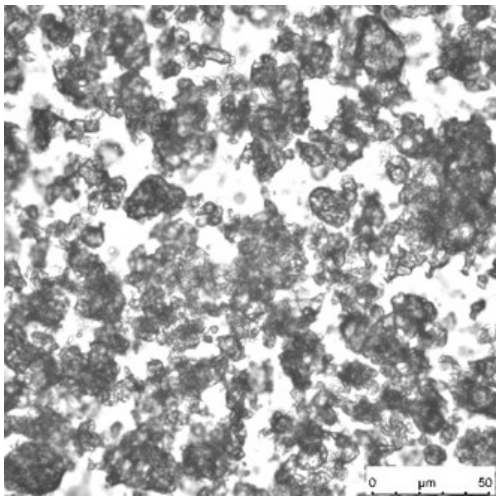

(a) 25 °C

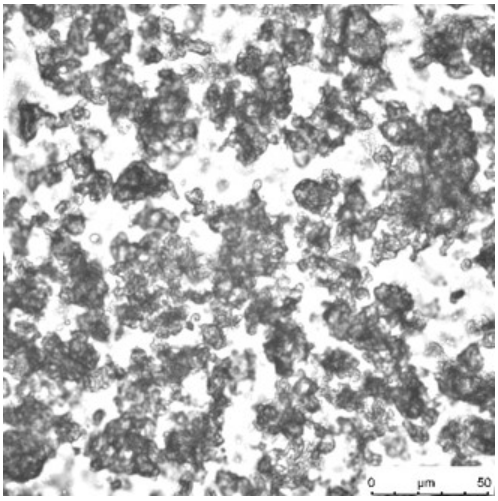

(d) 50 °C

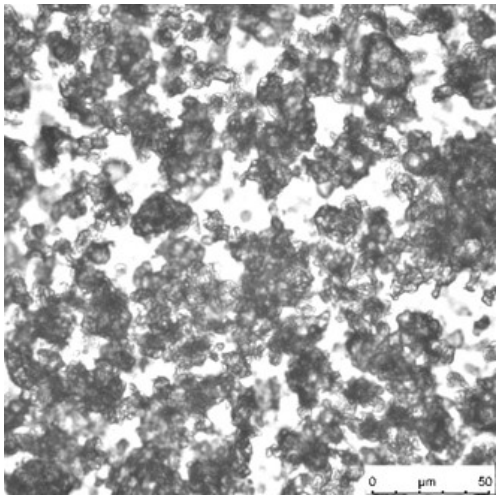

(b) 0 °C

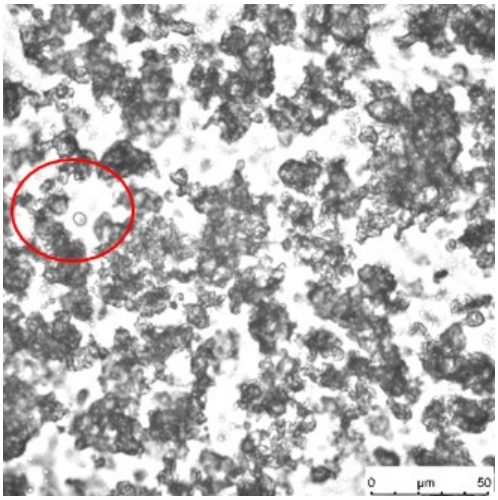

(e) 75 °C

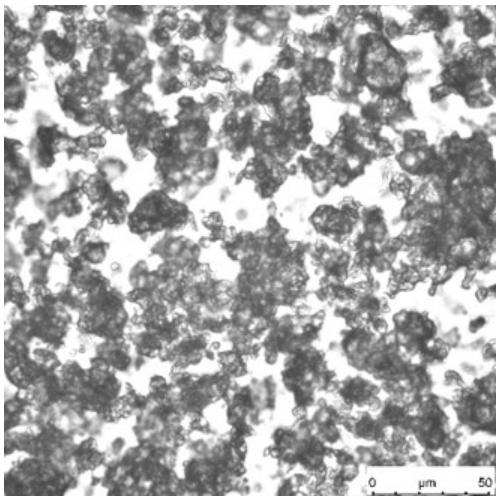

(c) 10 °C

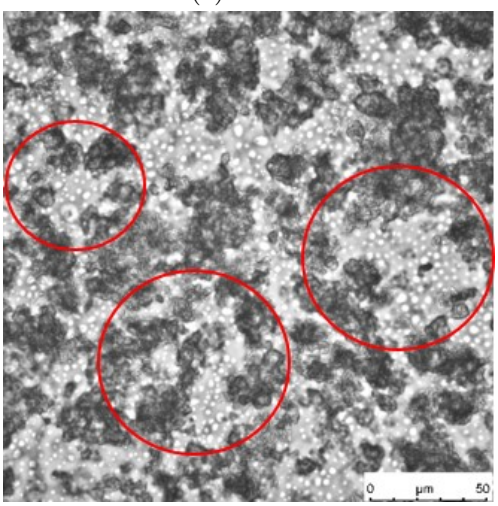

(f) 90 °C - Phase Inversion

Figure A.54. WCF M1: O:W = 60:40, C_{surf} = 3 wt.%, HLB = 7.5.

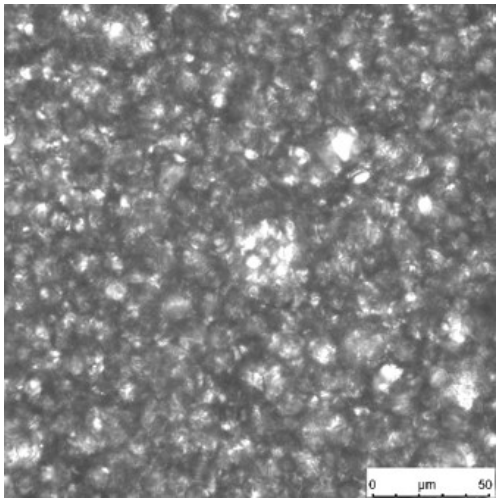

(a) 25 °C

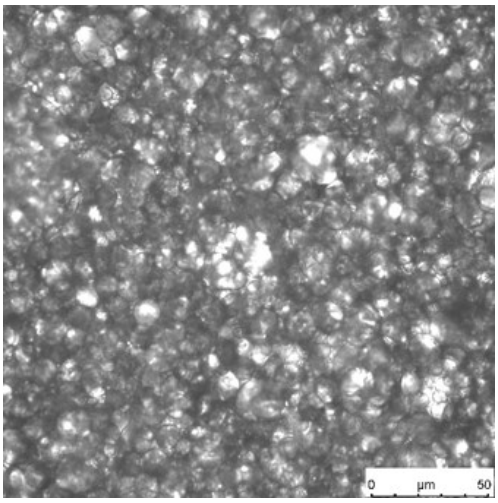

(d) 50 °C

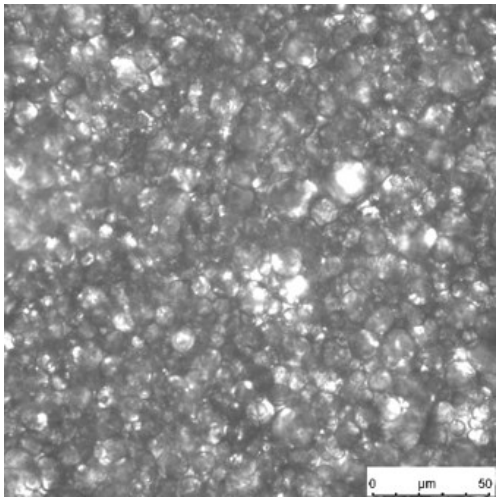

(b) 0 °C

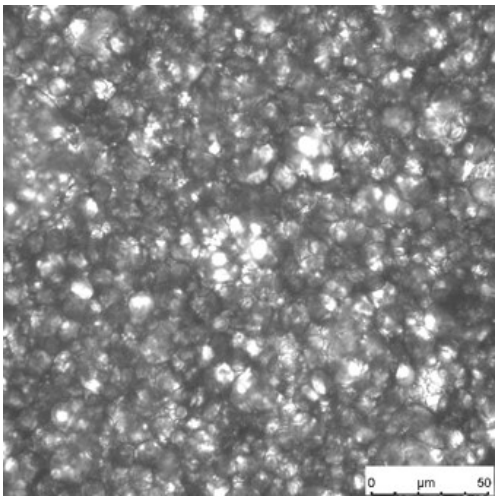

(e) 75 °C

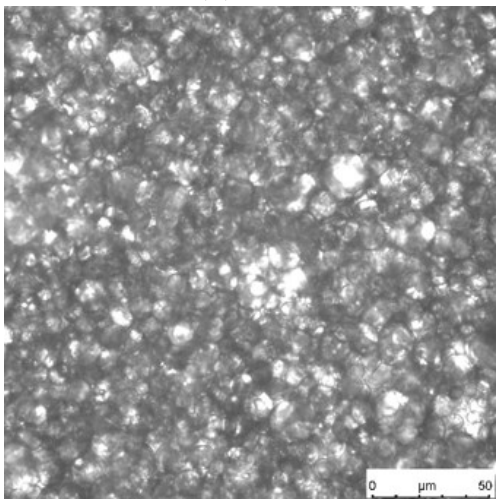

(c) 10 °C

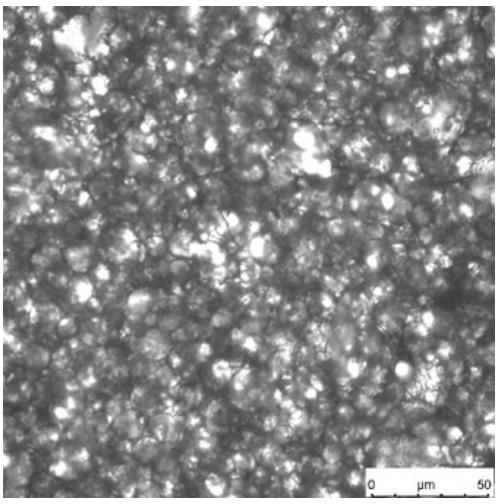

(f) 90 °C

Figure A.55. WCF M2: O:W = 60:40, C_{surf} = 3 wt.%, HLB = 11.5.

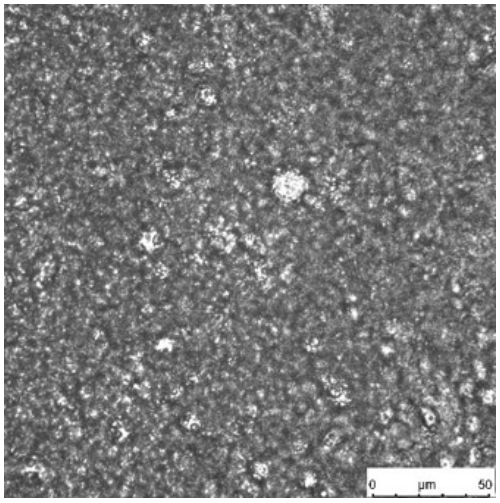

(a) 25 °C

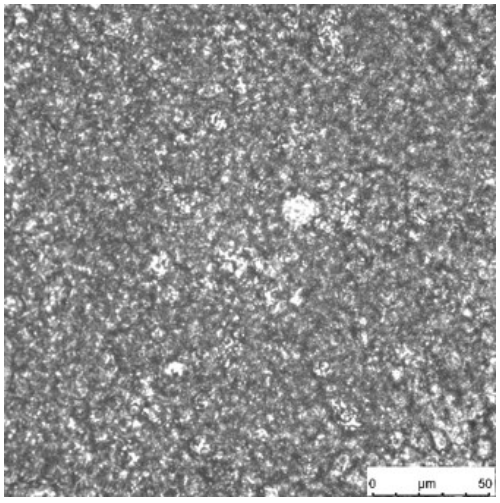

(b) 0 °C

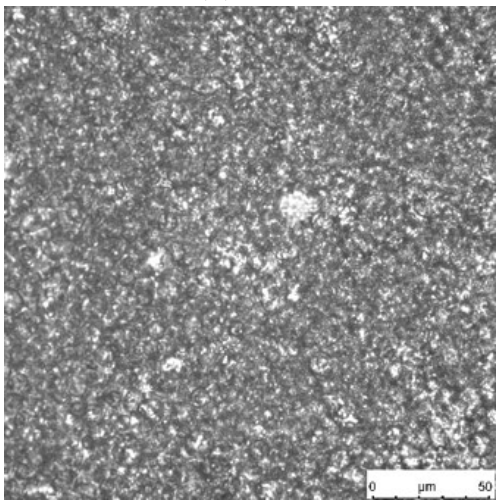

(c) 10 °C

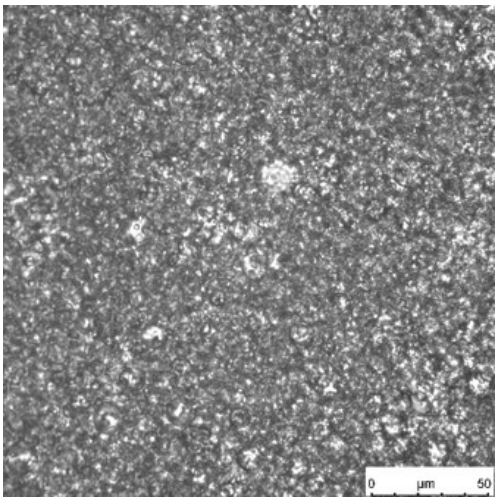

(d) 50 °C

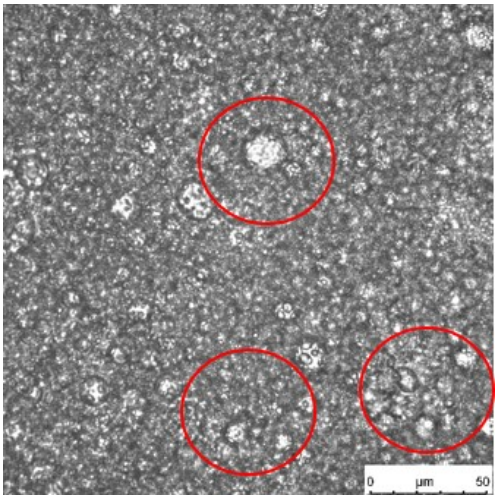

(e) 75 °C

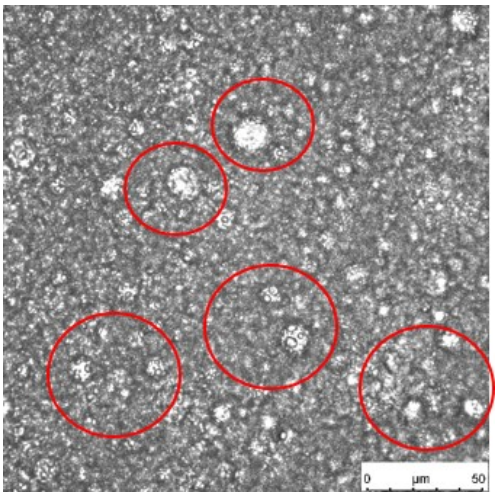

(f) 90 °C

Figure A.56. WCF M2: O:W = 60:40, C_{surf} = 3 wt.%, HLB = 7.5.

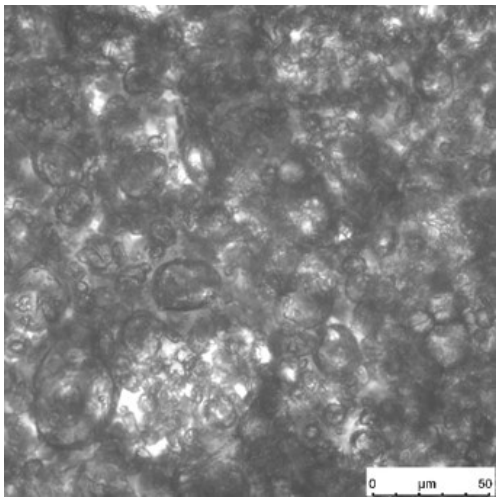

(a) 25 °C

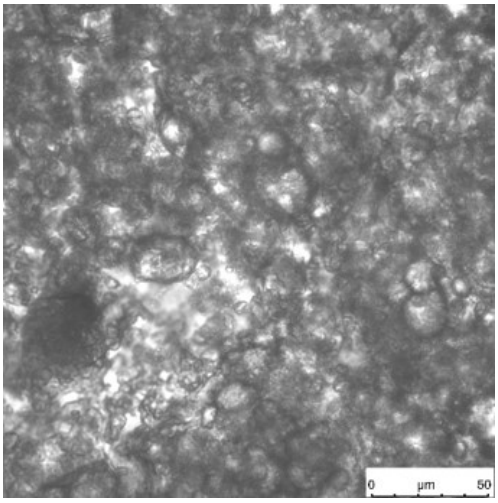

(d) 50 °C

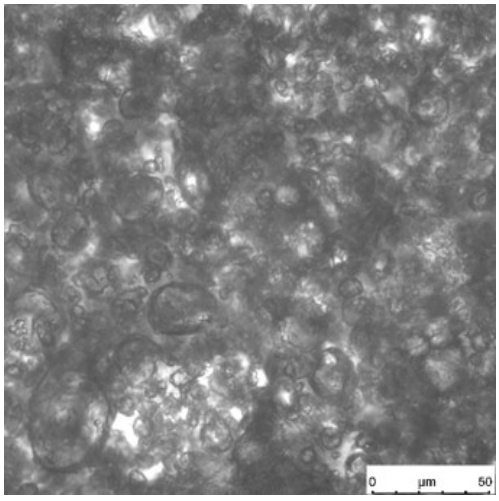

(b) 0 °C

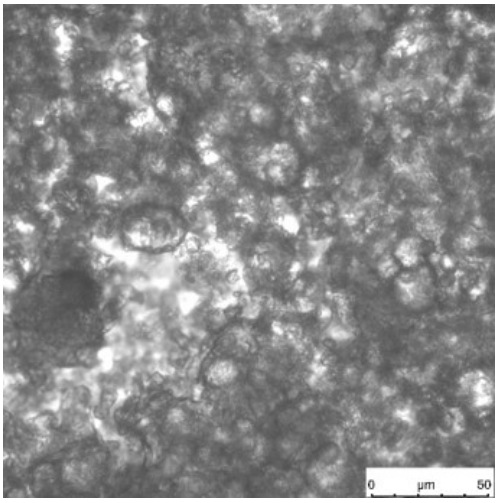

(e) 75 °C

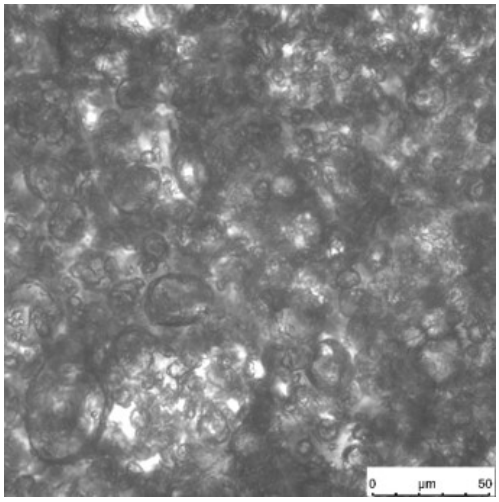

(c) 10 °C

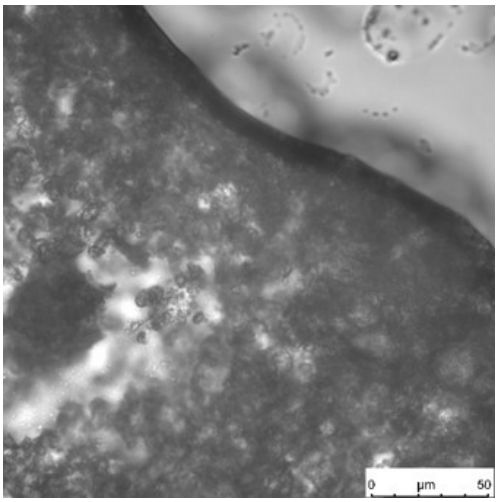

(f) 90 °C - Demulsification

Figure A.57. WCF M3 (ionic): O:W = 60:40, C_{surf} = 3 wt.%, HLB = 11.5.

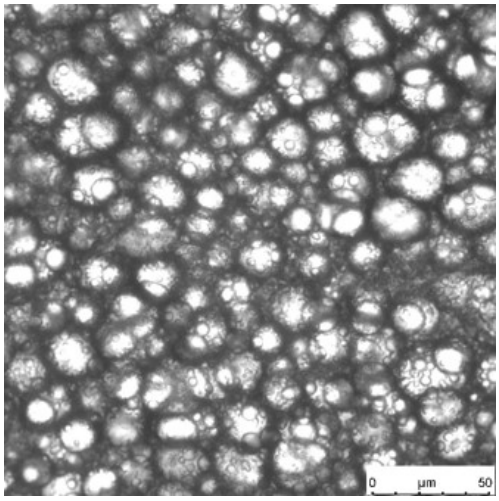

(a) 25 °C

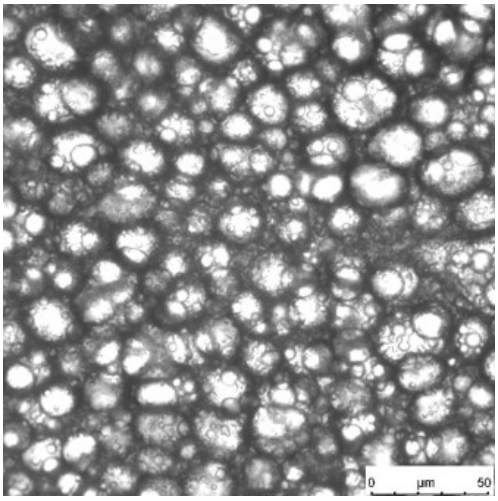

(d) 50 °C

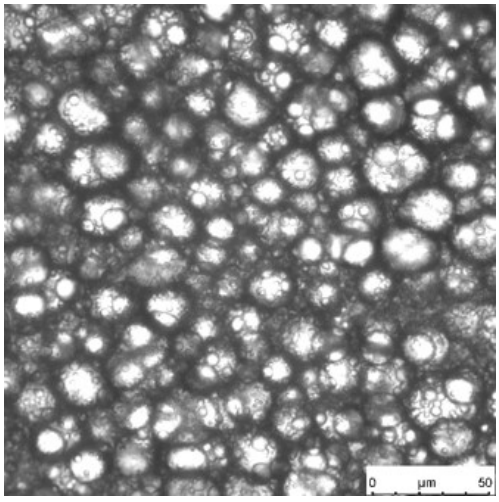

(b) 0 °C

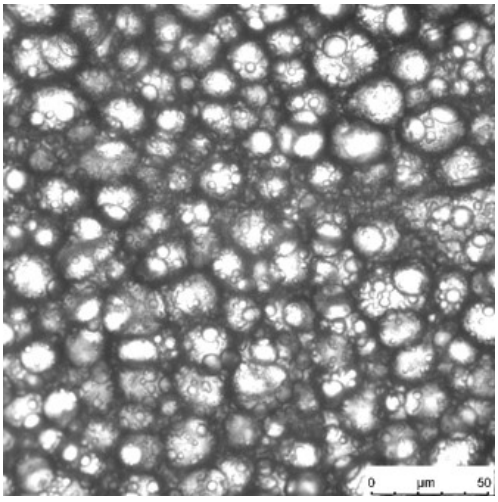

(e) 75 °C

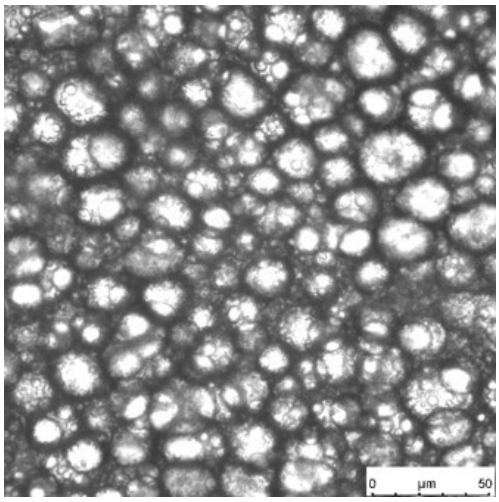

(c) 10 °C

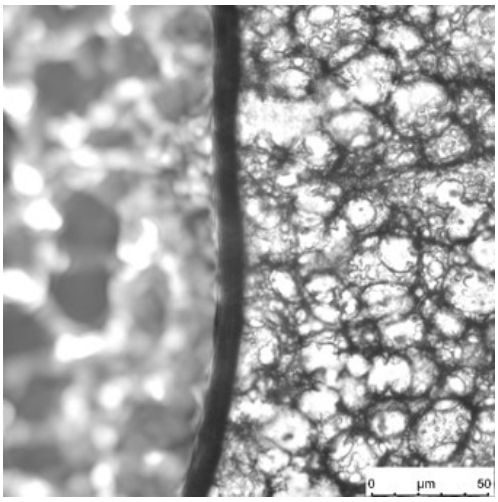

(f) 90 °C - Demulsification

Figure A.58. OCF S1: O:W = 60:40, C_{surf} = 3 wt.%, HLB = 4.3.

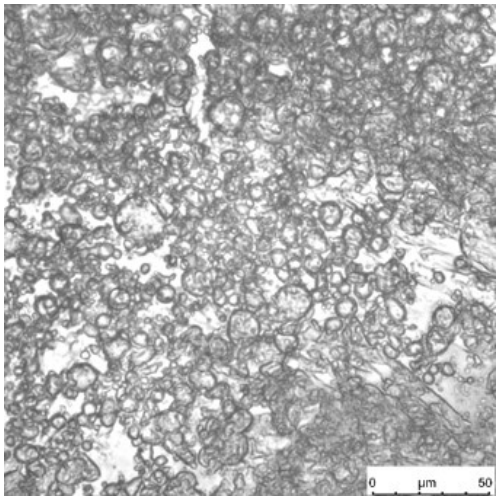

(a) 25 °C

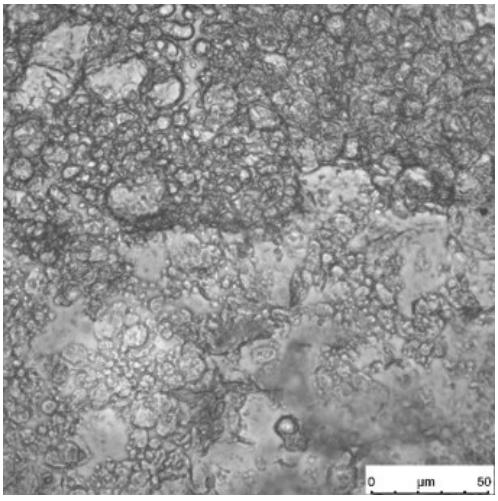

(d) 50 °C - Demulsification

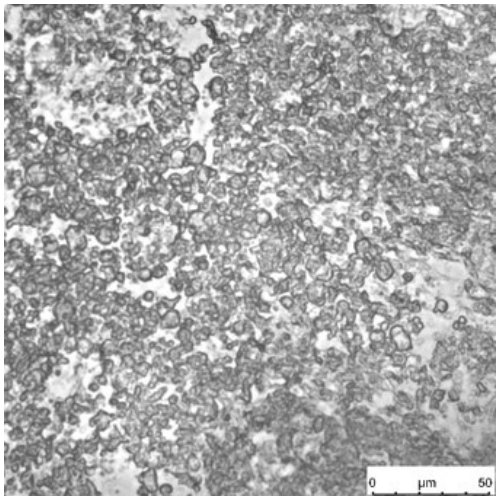

(b) 0 °C

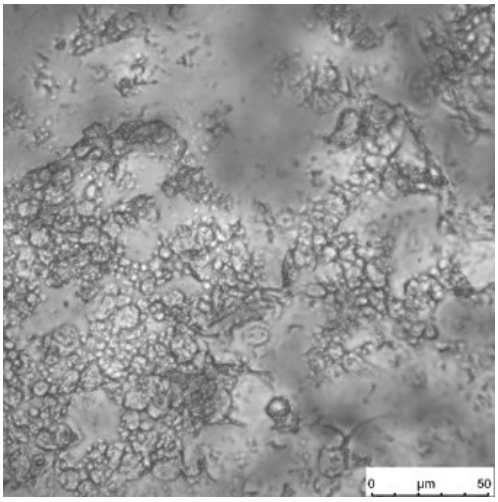

(e) 75 °C

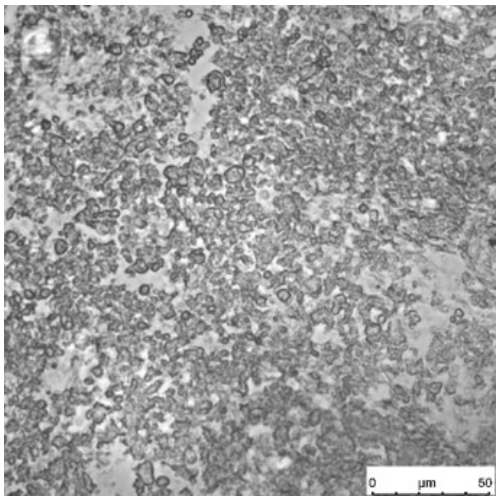

(c) 10 °C

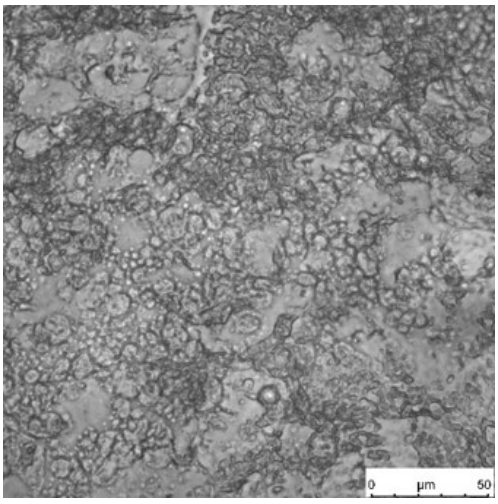

(f) 90 °C

Figure A.59. OCF S2: O:W = 60:40, C_{surf} = 3 wt.%, HLB = 4.0.

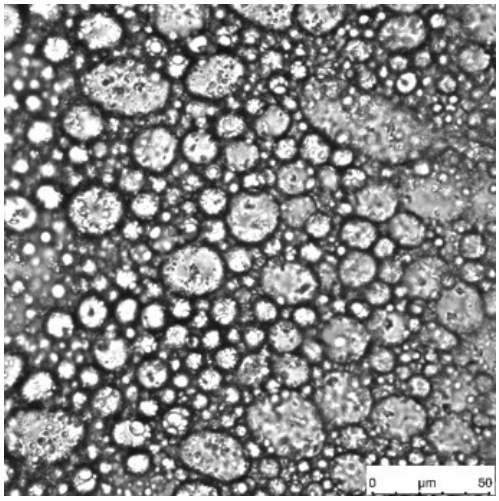

(a) 25 °C

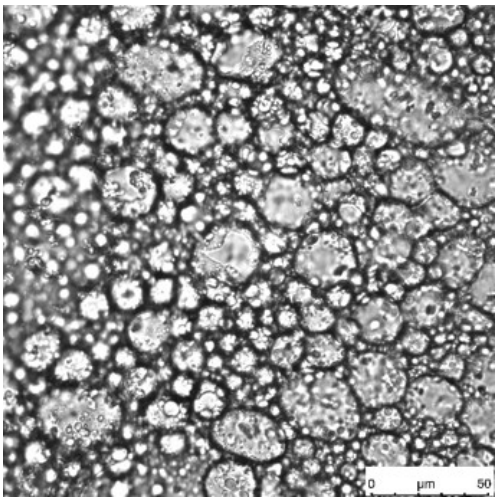

(d) 50 °C

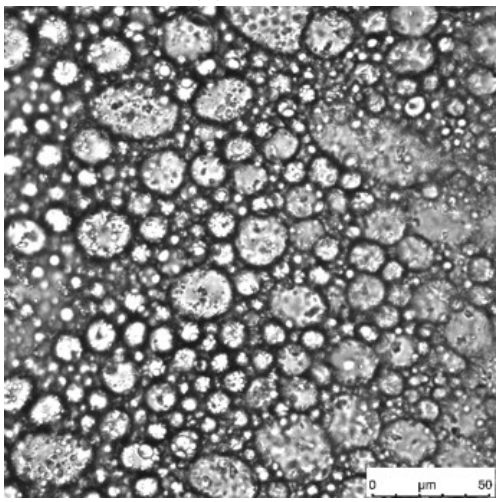

(b) 0 °C

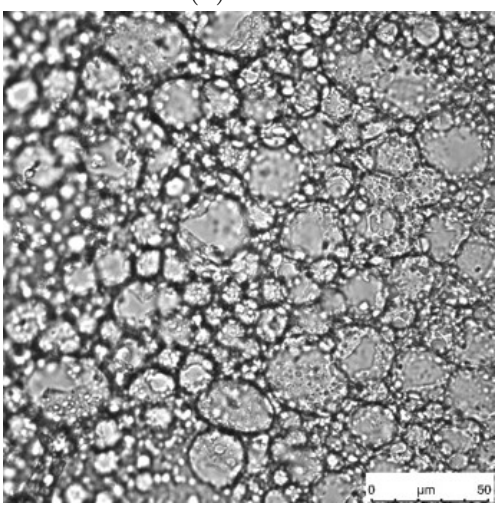

(e) 75 °C

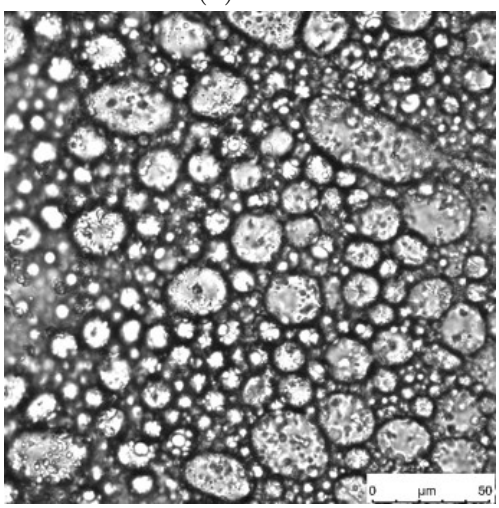

(c) 10 °C

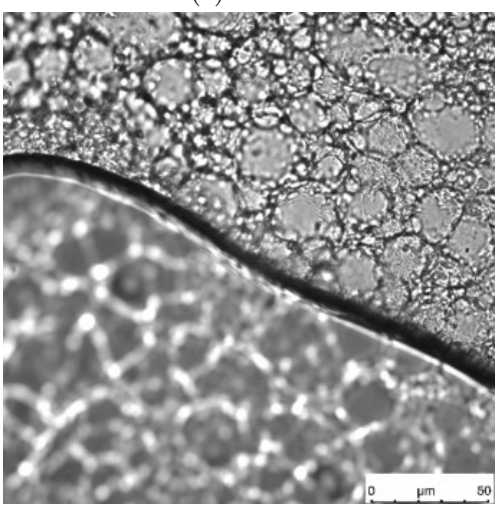

(f) 90 °C - Demulsification

Figure A.60. OCF S1: O:W = 70:30, C_{surf} = 3 wt.%, HLB = 4.3.

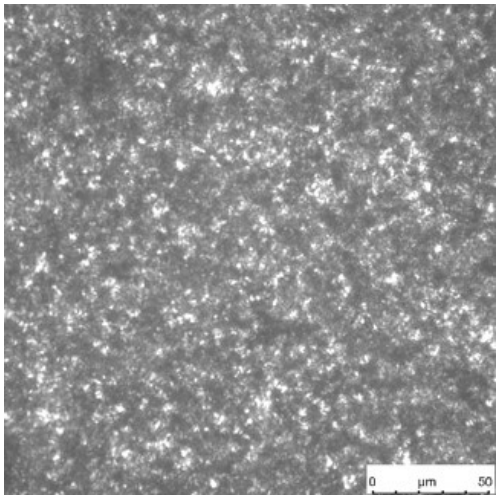

(a) 25 °C

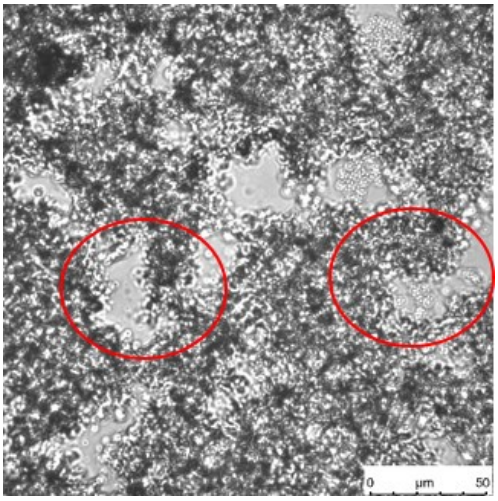

(d) 50 °C

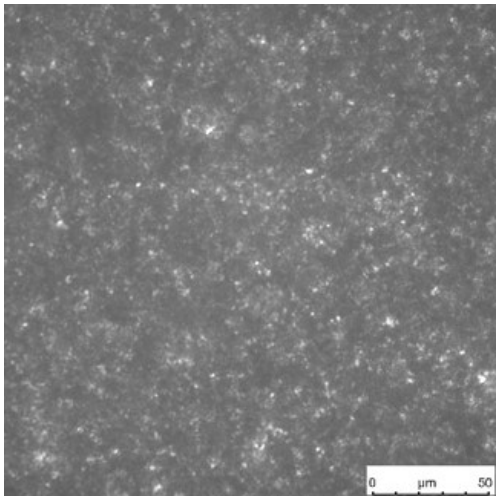

(b) 0 °C

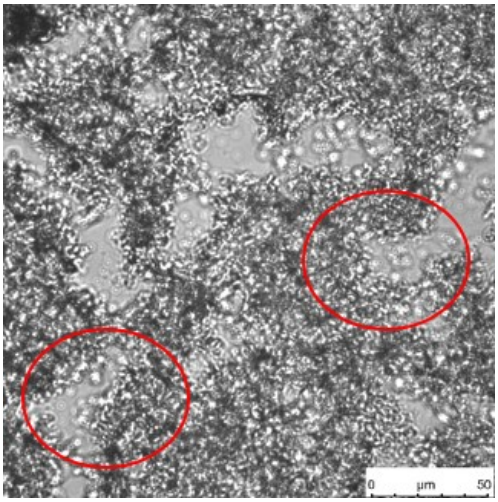

(e) 75 °C

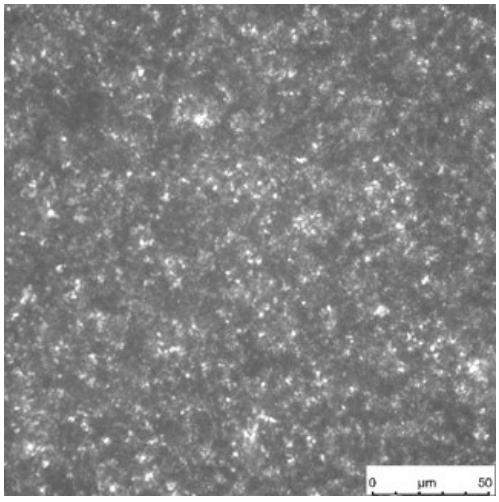

(c) 10 °C

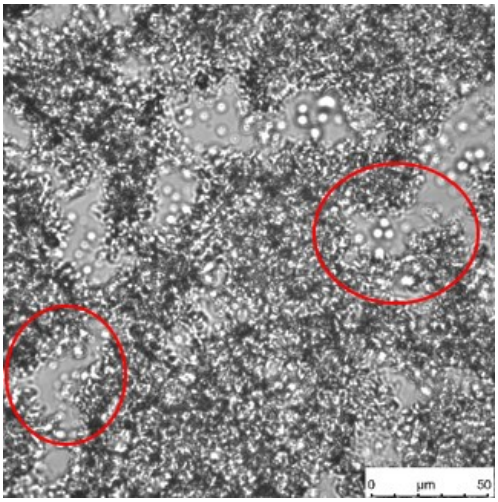

(f) 90 °C

Figure A.61. WCF M1: O:W = 70:30, C_{surf} = 3 wt.%, HLB = 7.5.

A.5 Comparison to Drilling Muds

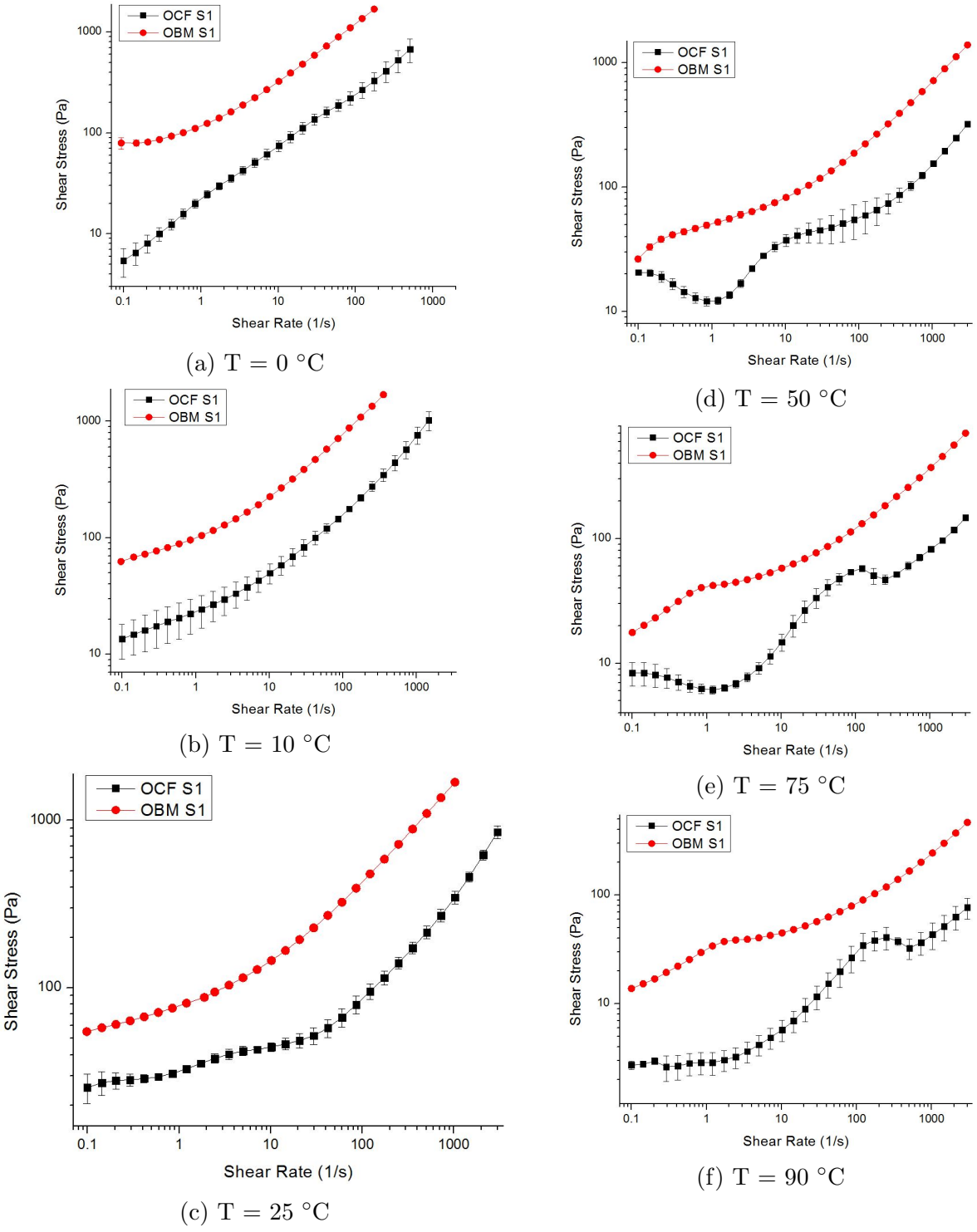

(a) T = 0 °C

(b) T = 10 °C

(c) T = 25 °C

(d) T = 50 °C

(e) T = 75 °C

(f) T = 90 °C

Figure A.62. Flow Curve: Surfactant S1 (Span 80) - O:W = 50:50, C_{surf} = 3 wt.%.

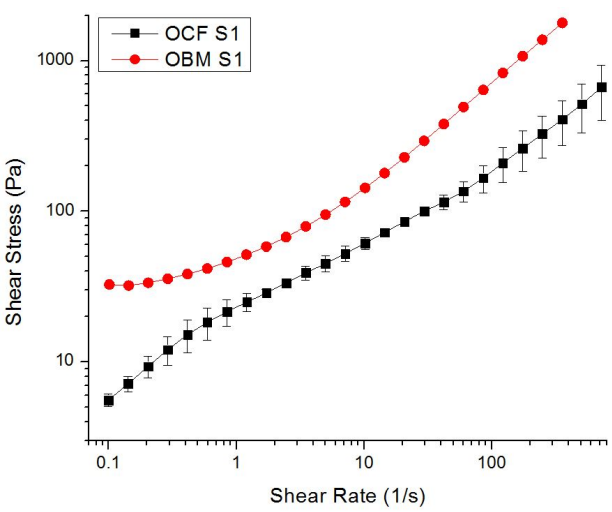

(a) T = 0 °C

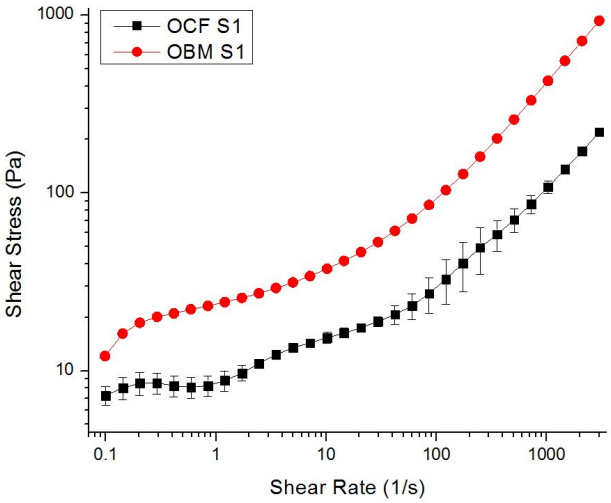

(d) T = 50 °C

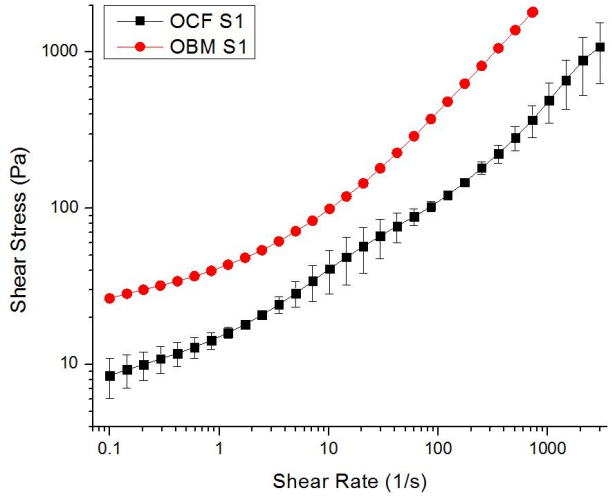

(b) T = 10 °C

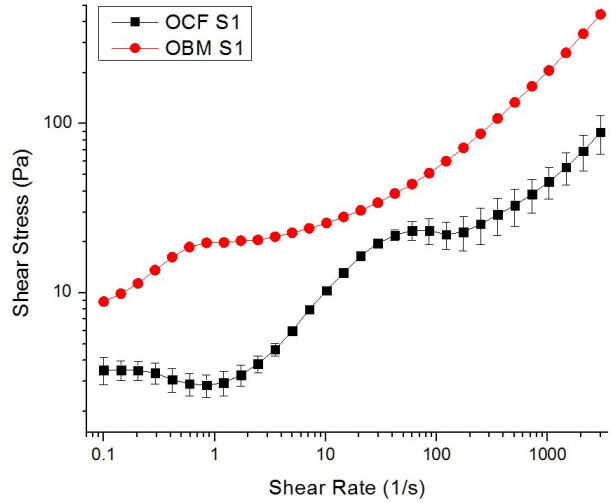

(e) T = 75 °C

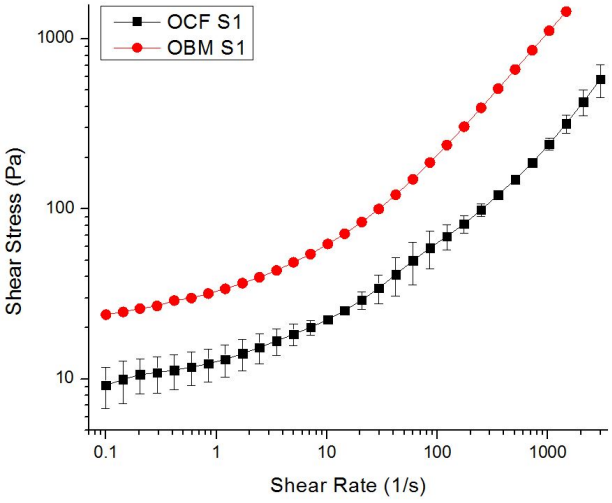

(c) T = 25 °C

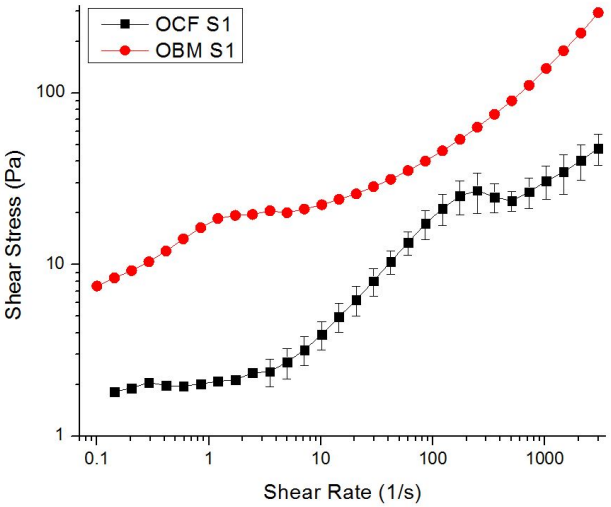

(f) T = 90 °C

Figure A.63. Flow Curve: Surfactant S1 (Span 80) - O:W = 60:40, C_{surf} = 3 wt.%.

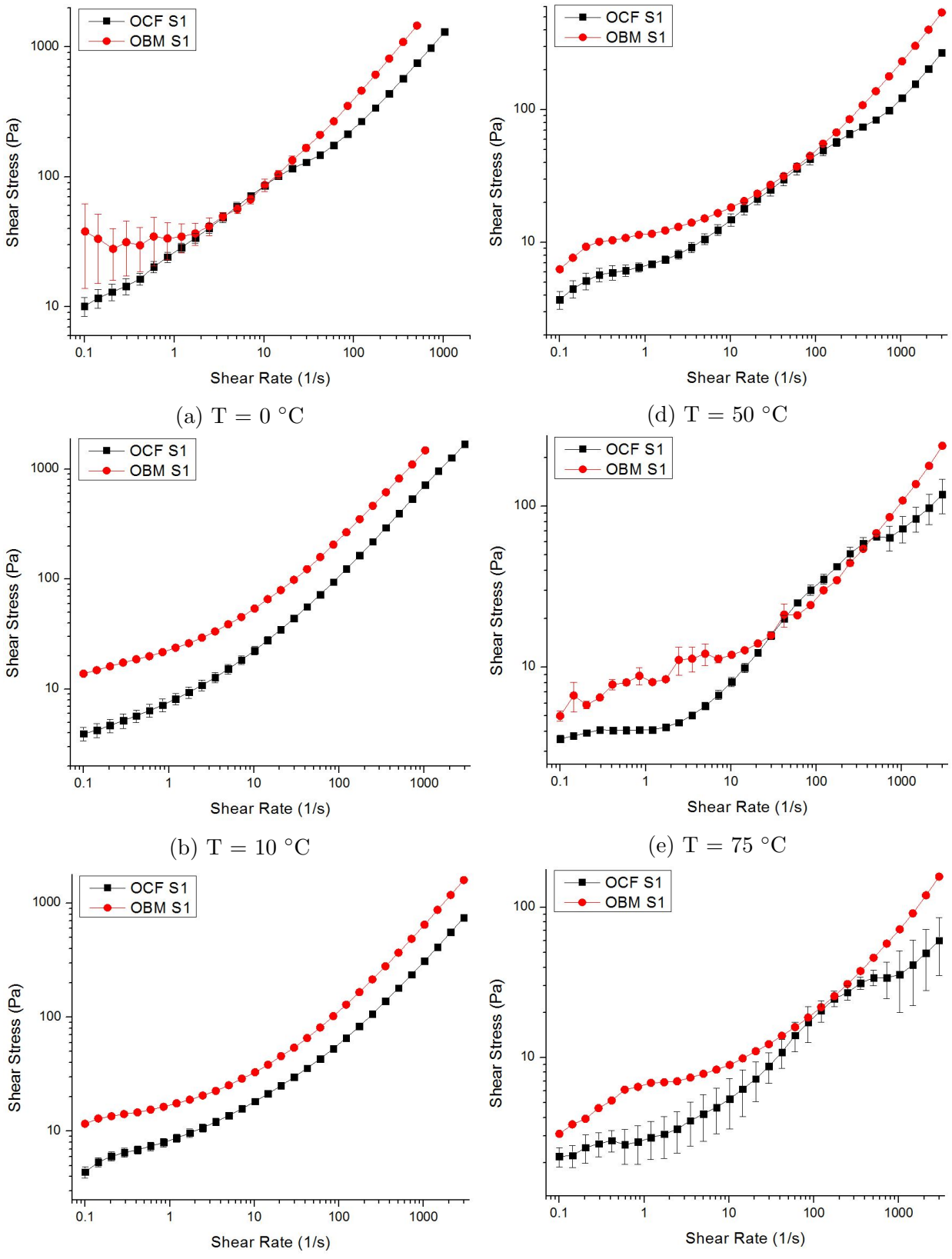

(a) T = 0 °C

(d) T = 50 °C

(b) T = 10 °C

(e) T = 75 °C

(c) T = 25 °C

(f) T = 90 °C

Figure A.64. Flow Curve: Surfactant S1 (Span 80) - O:W = 70:30, C_{surf} = 3 wt.%.

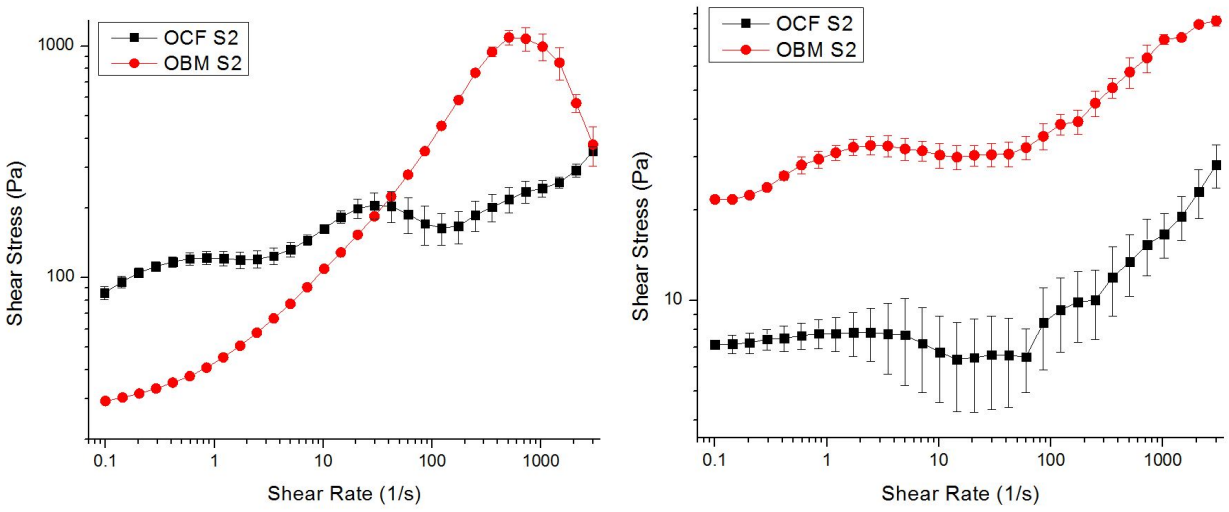

(a) T = 0 °C

(d) T = 50 °C

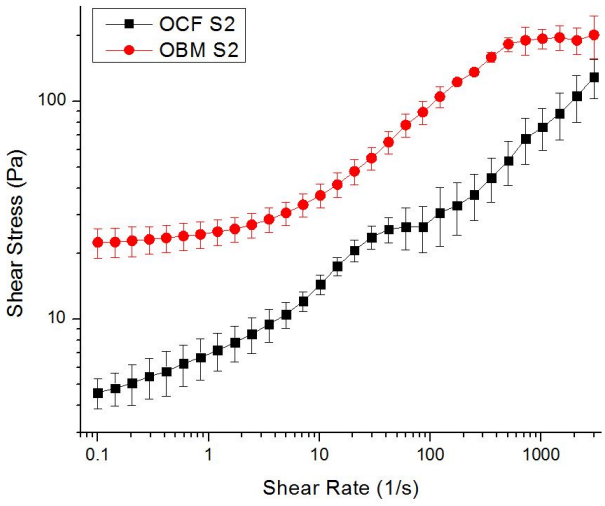

(b) T = 10 °C

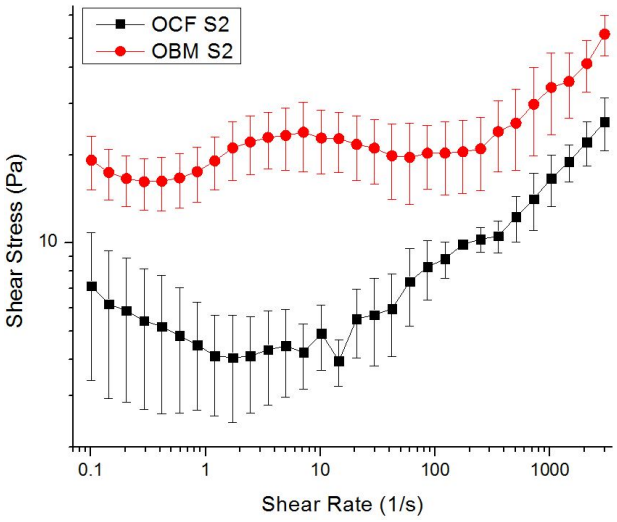

(e) T = 75 °C

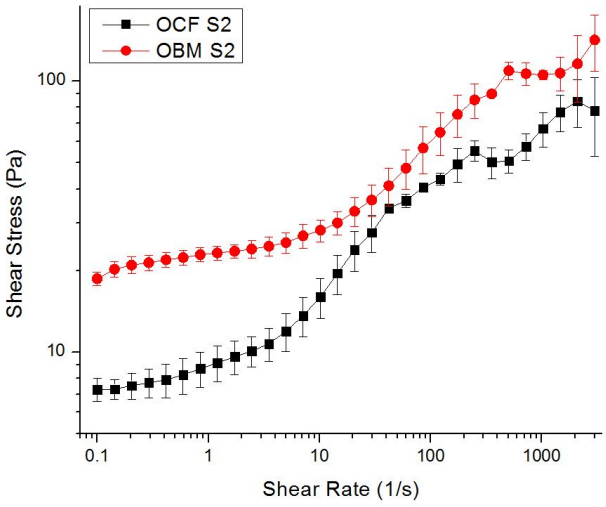

(c) T = 25 °C

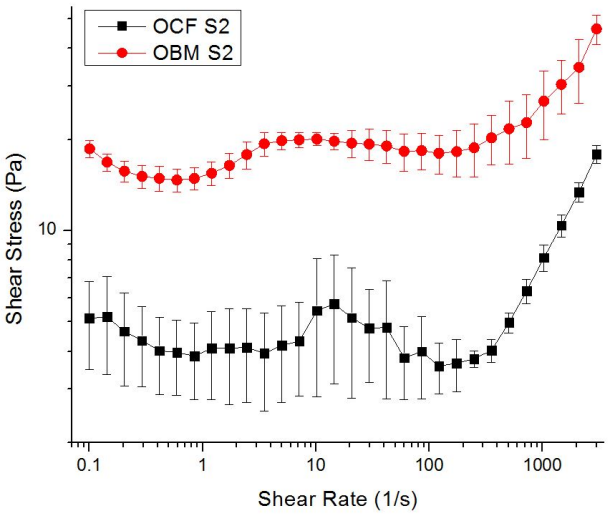

(f) T = 90 °C

Figure A.65. Flow Curve: Surfactant S2 (Brij 93) - O:W = 50:50, C_{surf} = 3 wt.%.

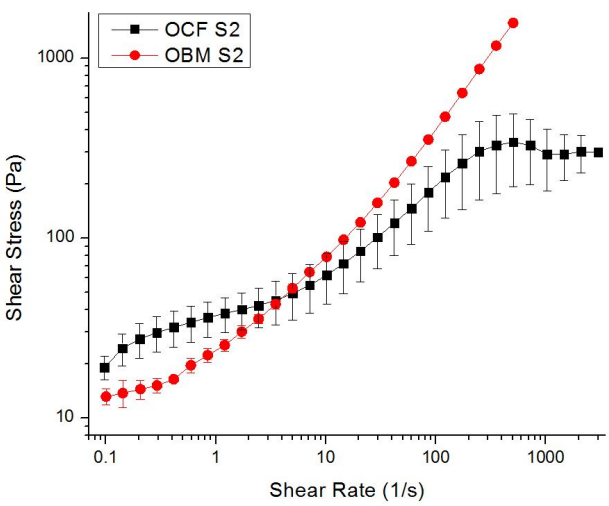

(a) T = 0 °C

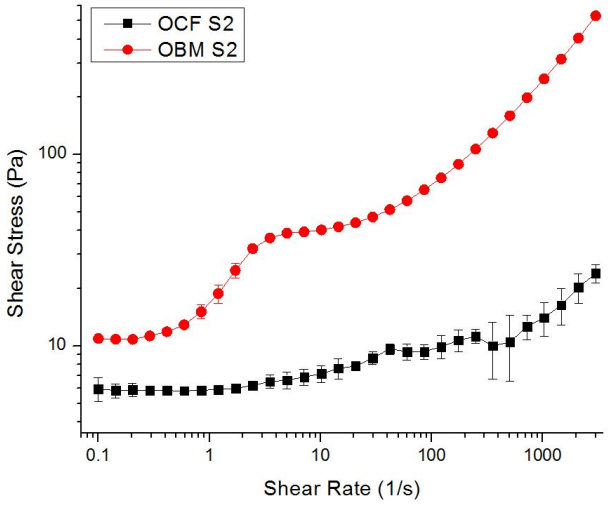

(d) T = 50 °C

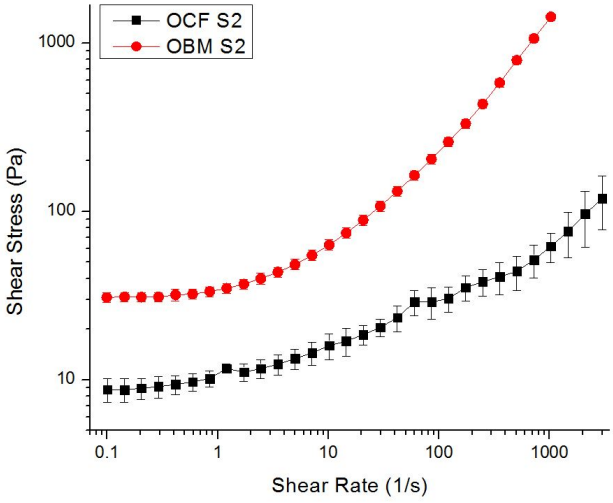

(b) T = 10 °C

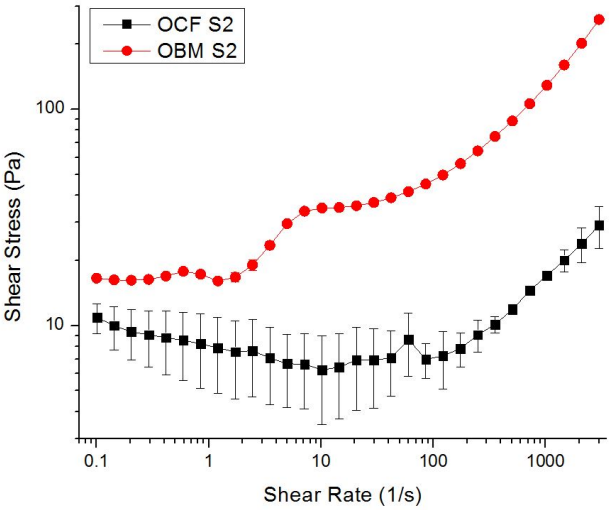

(e) T = 75 °C

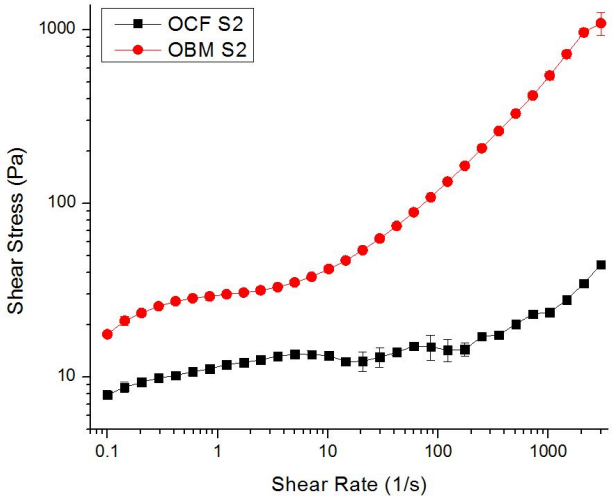

(c) T = 25 °C

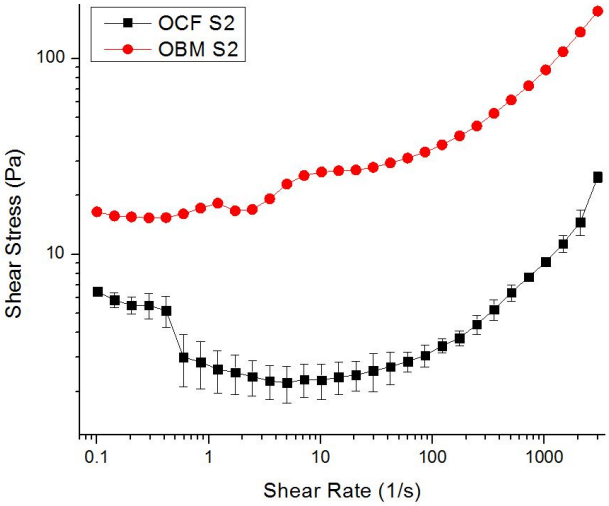

(f) T = 90 °C

Figure A.66. Flow Curve: Surfactant S2 (Brij 93) - O:W = 60:40, C_{surf} = 3 wt.%.

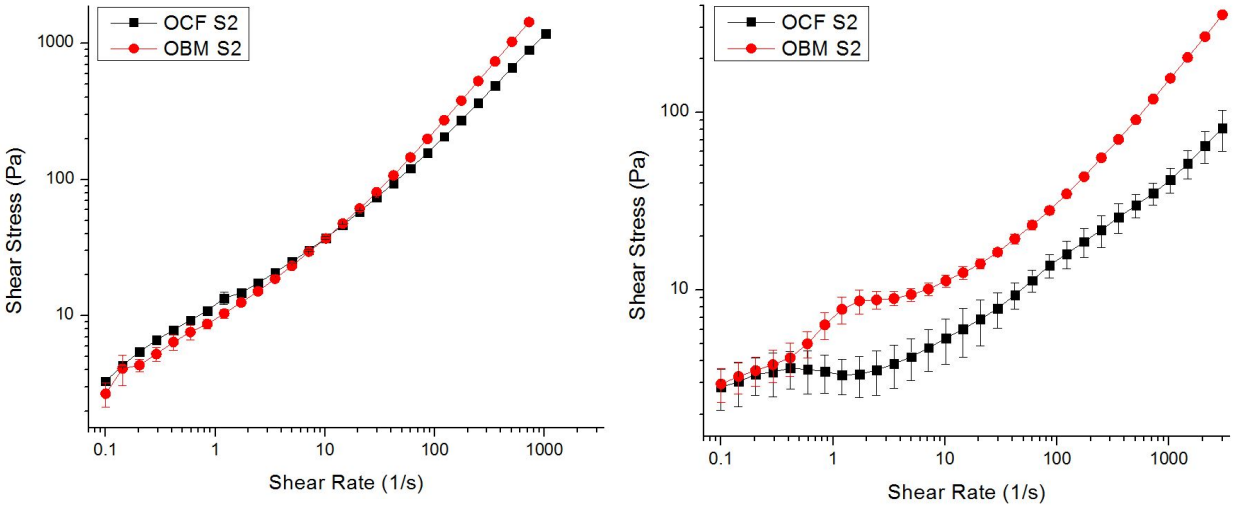

(a) T = 0 °C

(d) T = 50 °C

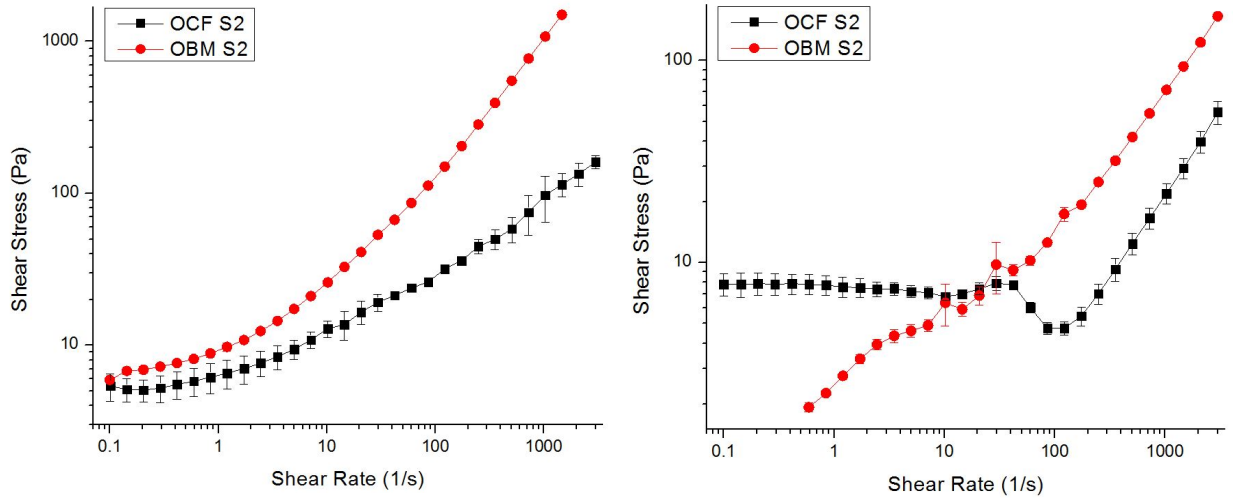

(b) T = 10 °C

(e) T = 75 °C

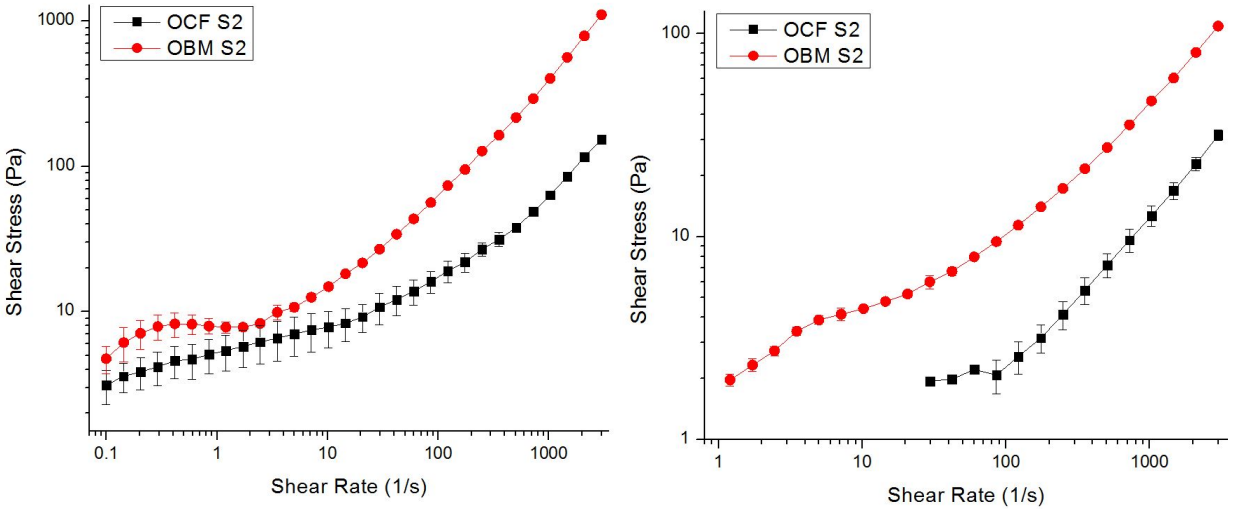

(c) T = 25 °C

(f) T = 90 °C

Figure A.67. Flow Curve: Surfactant S2 (Brij 93) - O:W = 70:30, C_{surf} = 3 wt.%.

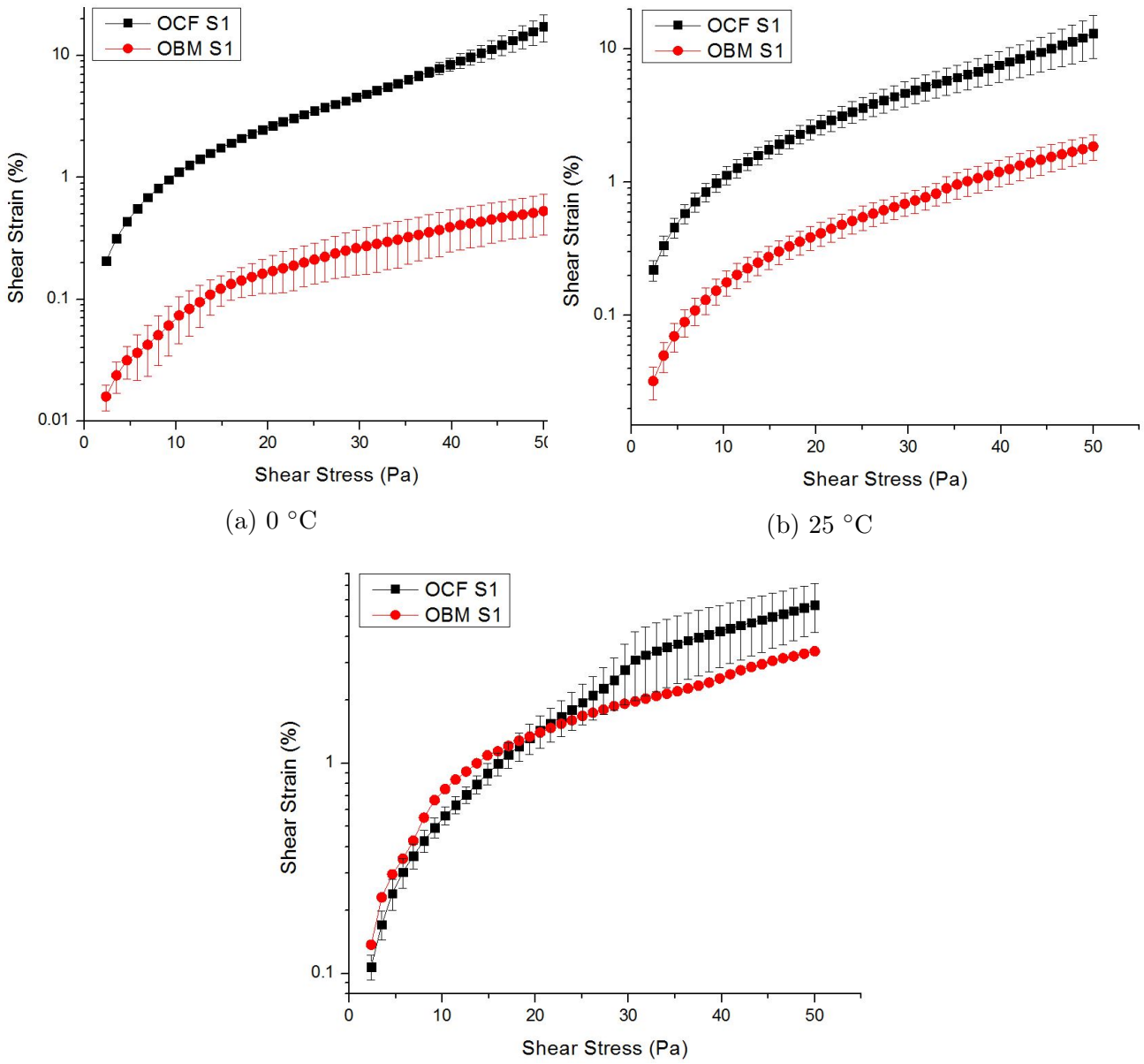

(a) 0 °C

(b) 25 °C

(c) 90 °C

Figure A.68. Stress Sweep: Surfactant S1 (Span 80) - O:W = 50:50, $C_{surf.}$ = 3 wt.%.

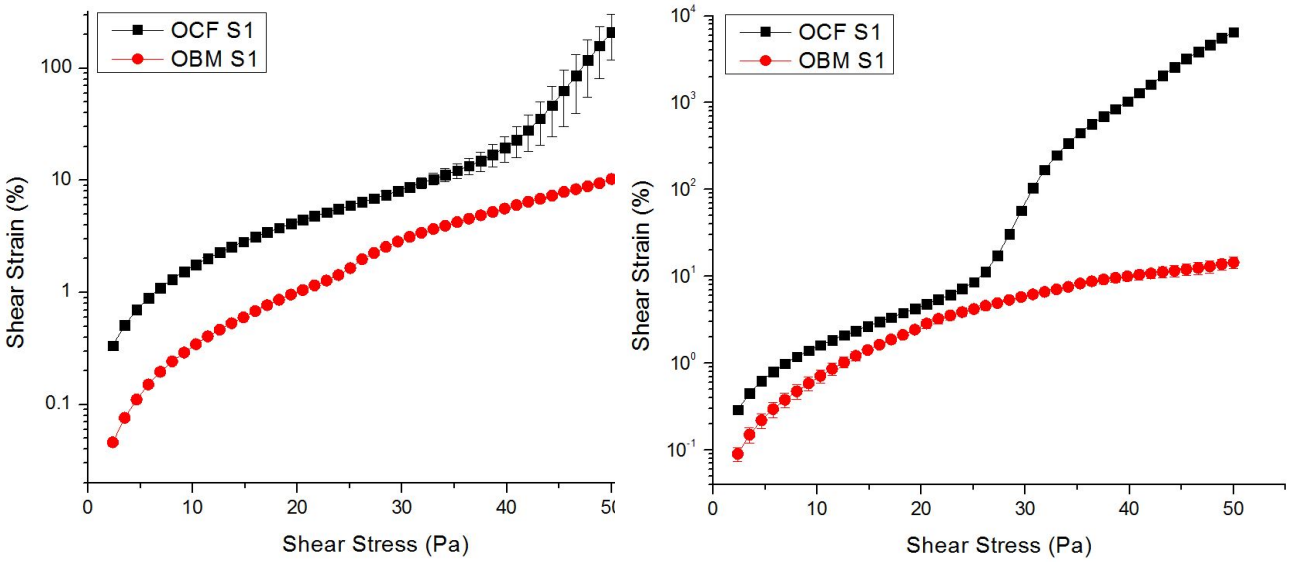

(a) 0 °C

(b) 25 °C

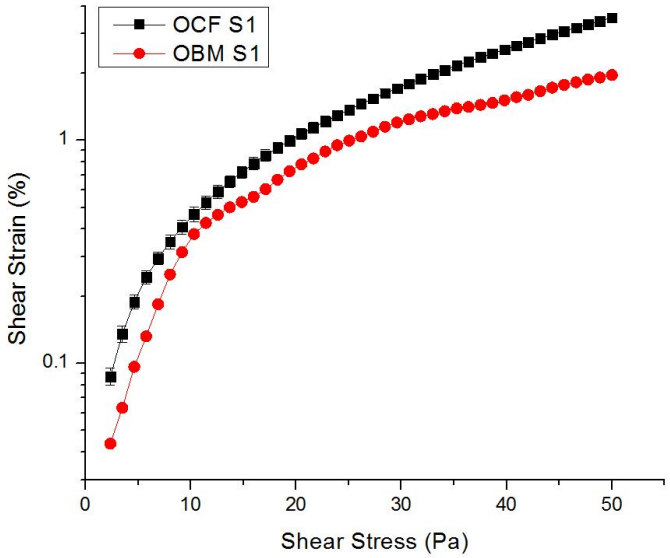

(c) 90 °C

Figure A.69. Stress Sweep: Surfactant S1 (Span 80) - O:W = 60:40, $C_{surf.}$ = 3 wt.%.

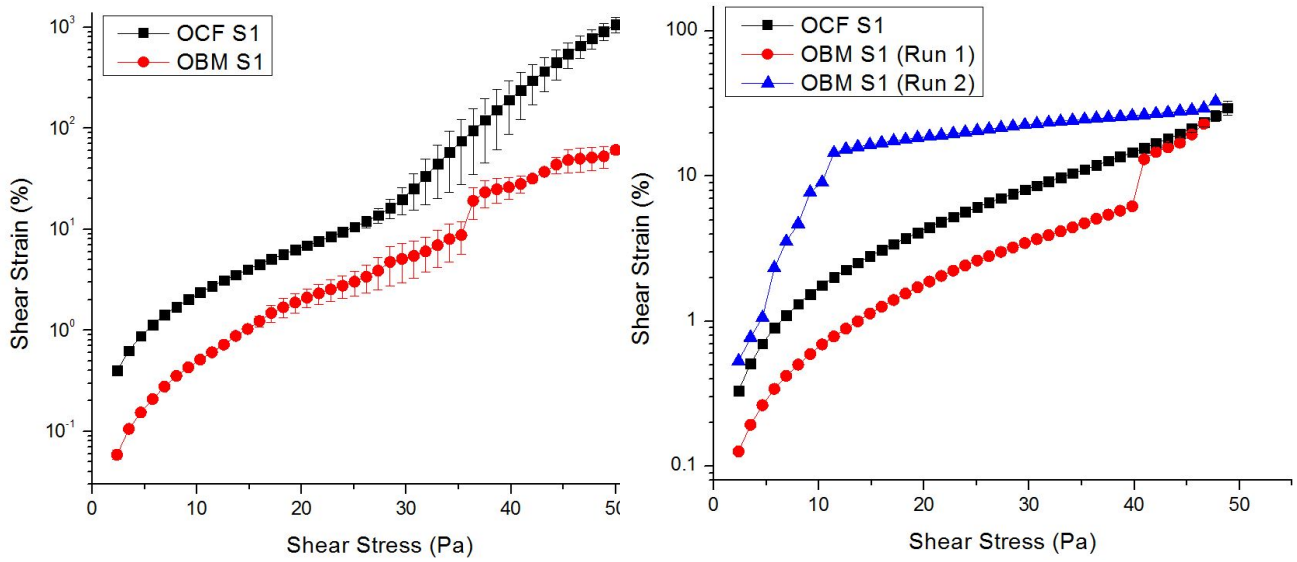

(a) 0 °C

(b) 25 °C

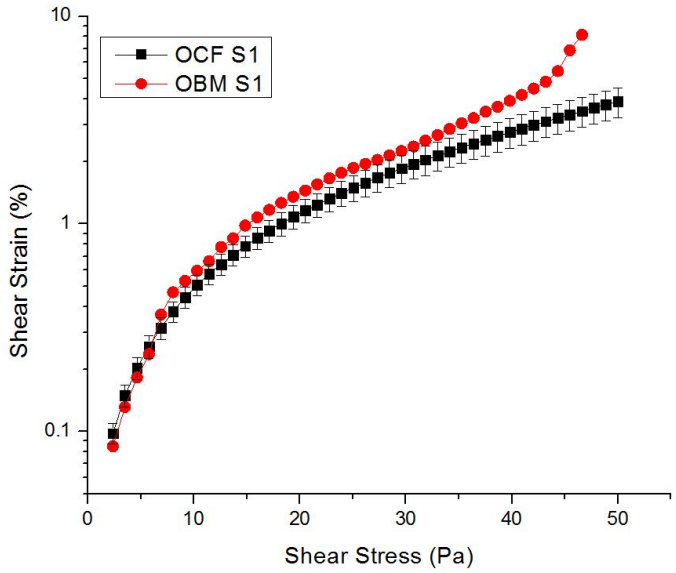

(c) 90 °C

Figure A.70. Stress Sweep: Surfactant S1 (Span 80) - O:W = 70:30, $C_{surf.}$ = 3 wt.%.

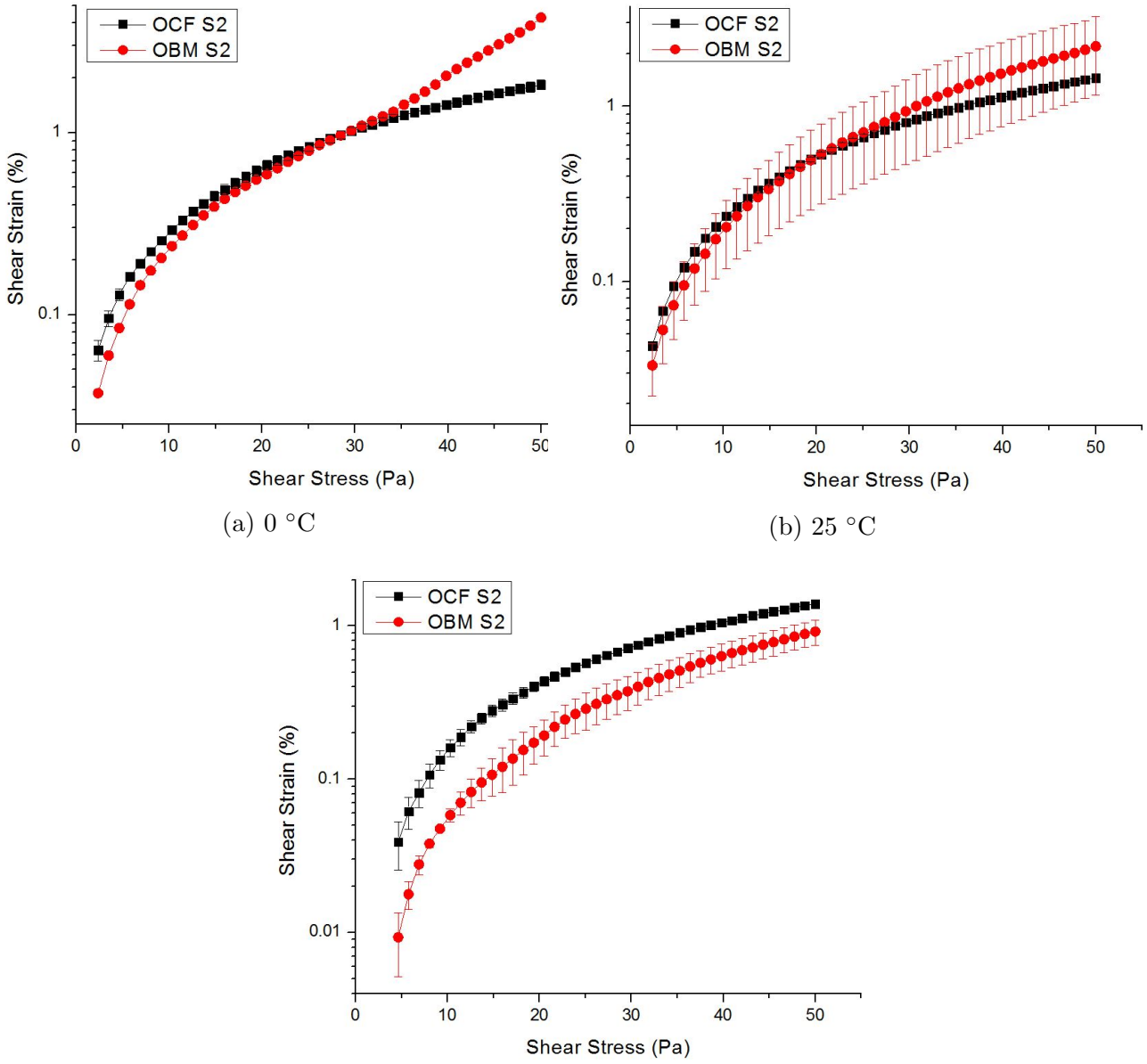

(a) 0 °C

(b) 25 °C

(c) 90 °C

Figure A.71. Stress Sweep: Surfactant S2 (Brij 93) - O:W = 50:50, $C_{surf.}$ = 3 wt.%.

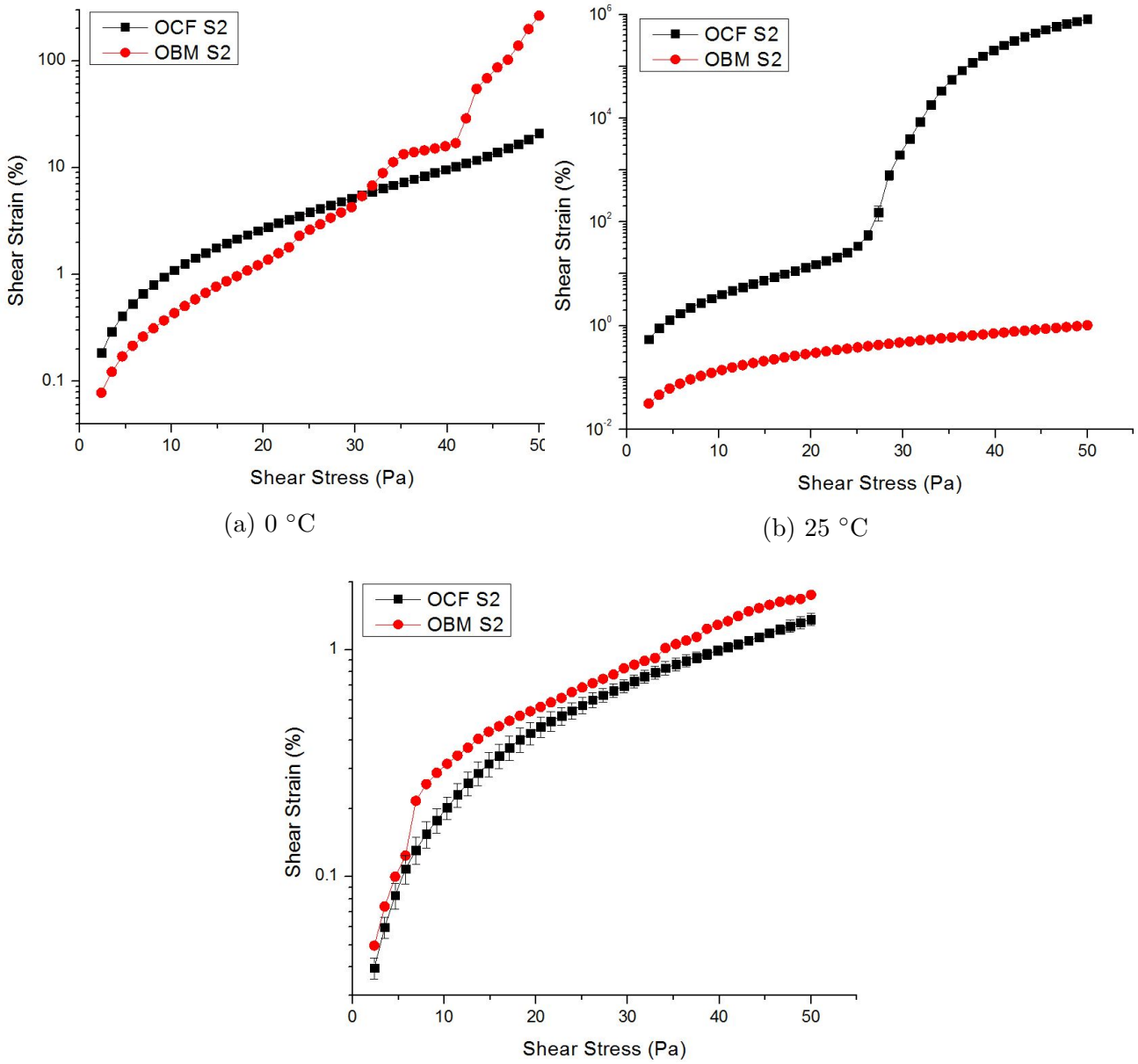

(a) 0 °C

(b) 25 °C

(c) 90 °C

Figure A.72. Stress Sweep: Surfactant S2 (Brij 93) - O:W = 60:40, $C_{surf.}$ = 3 wt.%.

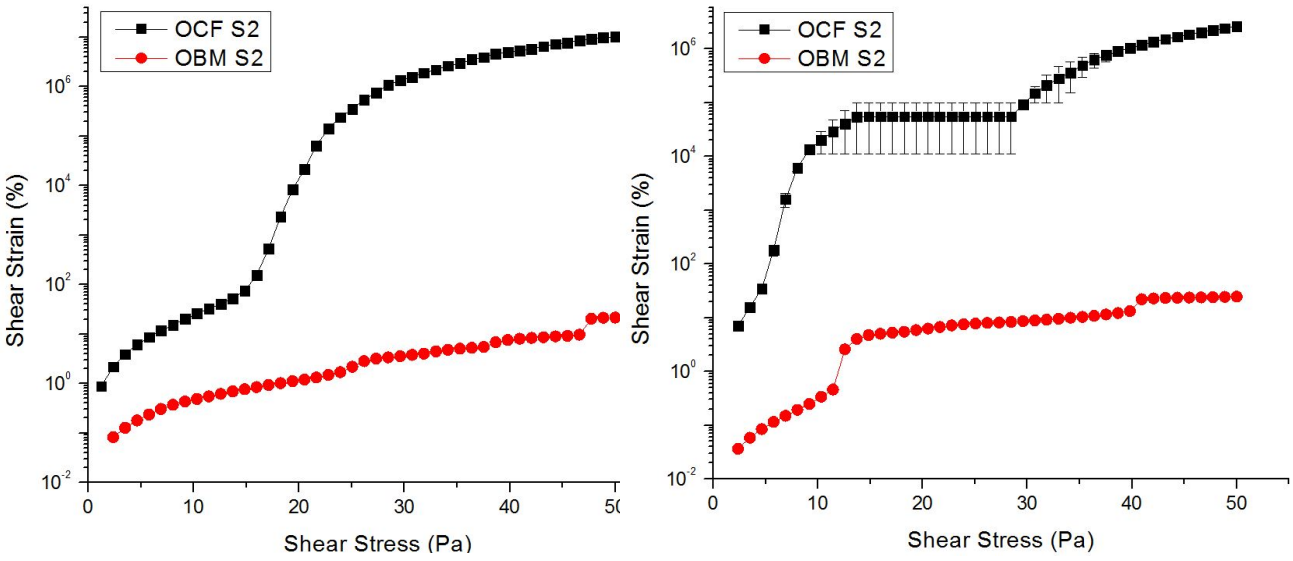

(a) 0 °C

(b) 25 °C

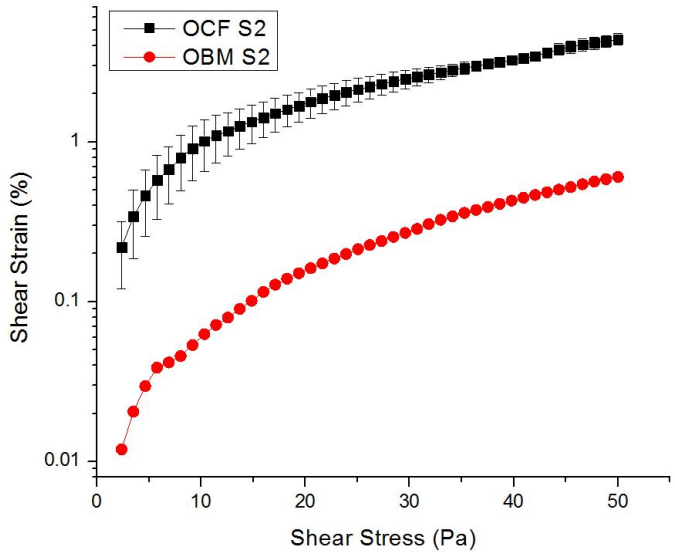

(c) 90 °C

Figure A.73. Stress Sweep: Surfactant S2 (Brij 93) - O:W = 70:30, $C_{surf.}$ = 3 wt.%.

Appendix B
Wall Slip
B.1 Effect of Surfactant Concentration

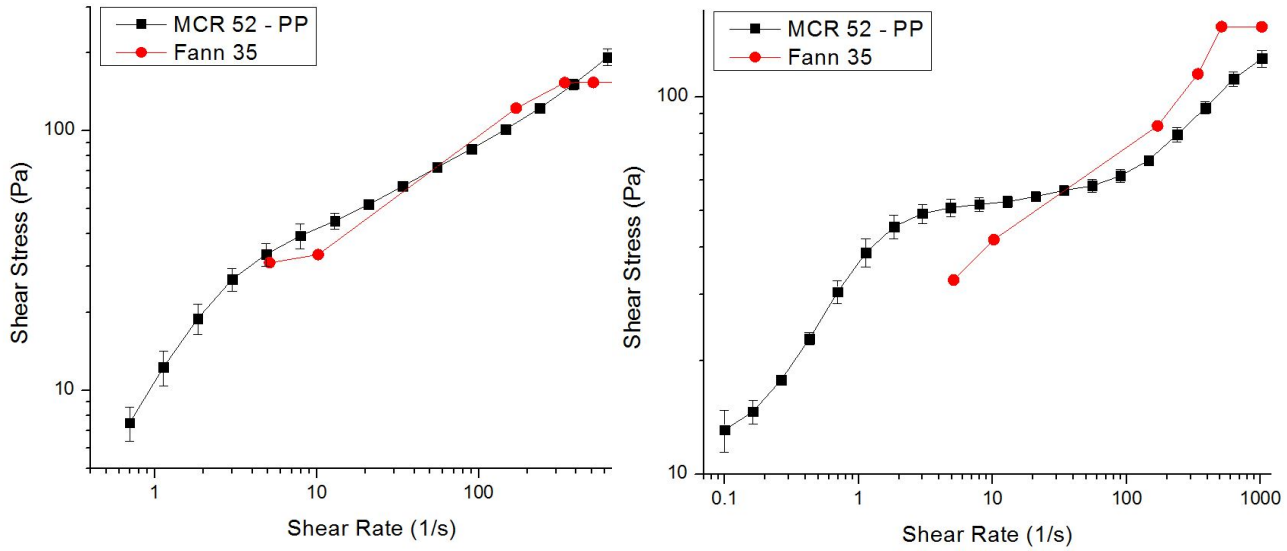

(a) 1 wt.% (b) 3 wt.%

Figure B.1. True & Cohesive Slip Determination: OCF S1, O:W = 50:50, T = 25 °C.

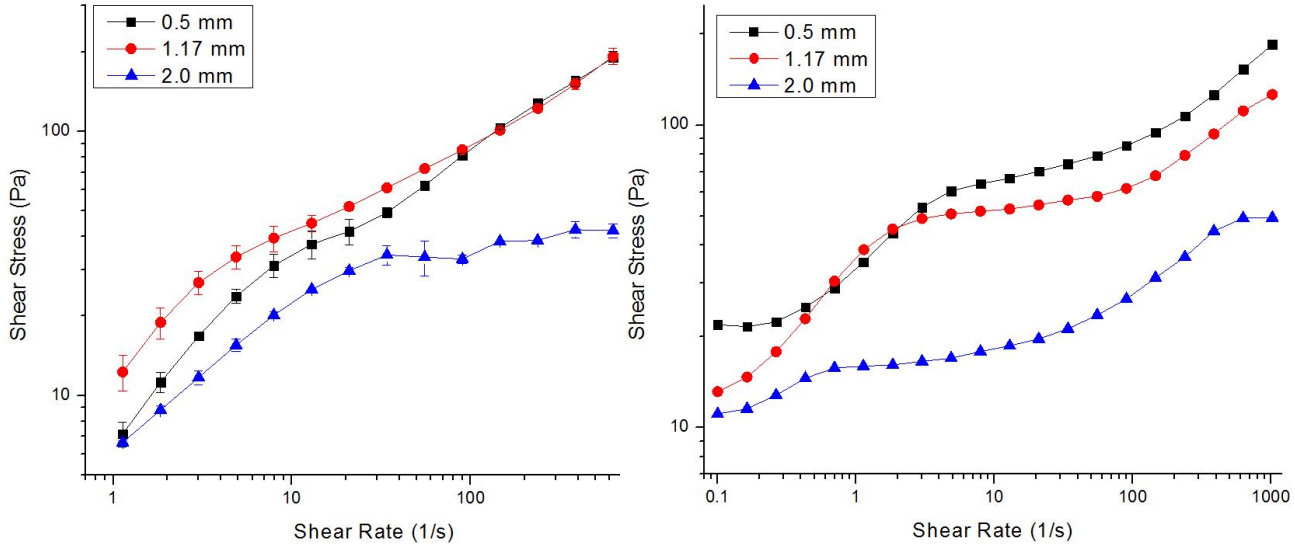

(a) 1 wt.% (b) 3 wt.%

Figure B.2. Lubrication Slip Determination: OCF S1, O:W = 50:50, T = 25 °C.

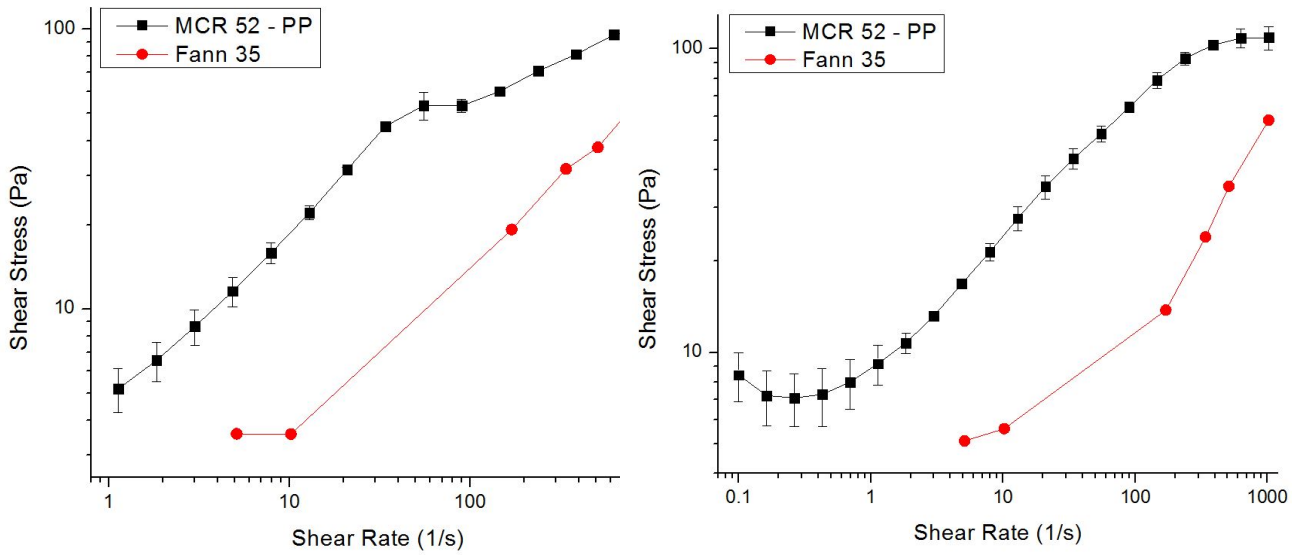

(a) 1 wt.% (b) 3 wt.%

Figure B.3. True & Cohesive Slip Determination: OCF S1, O:W = 50:50, T = 75 °C.

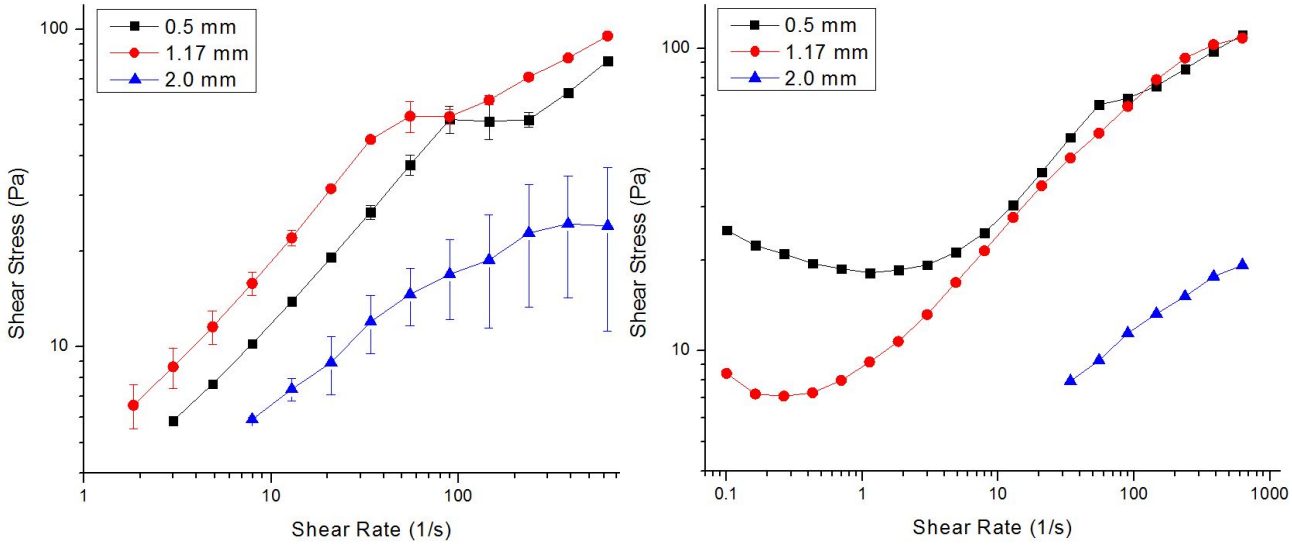

(a) 1 wt.% (b) 3 wt.%

Figure B.4. Lubrication Slip Determination: OCF S1, O:W = 50:50, T = 75 °C.

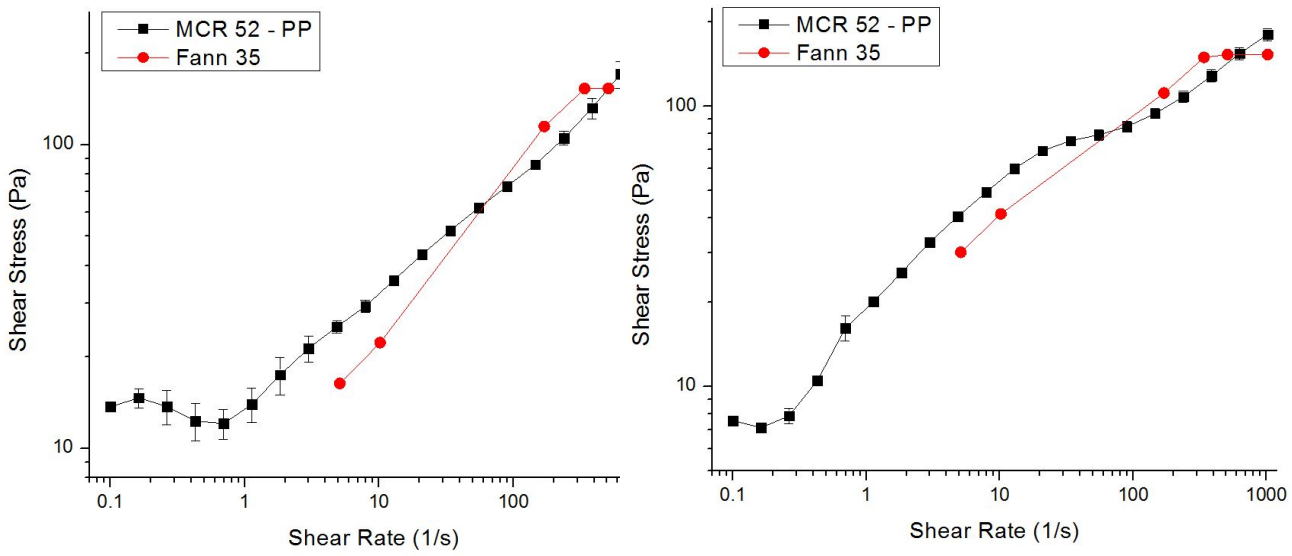

(a) 1 wt.% (b) 3 wt.%

Figure B.5. True & Cohesive Slip Determination: OCF S1, O:W = 60:40, T = 25 °C.

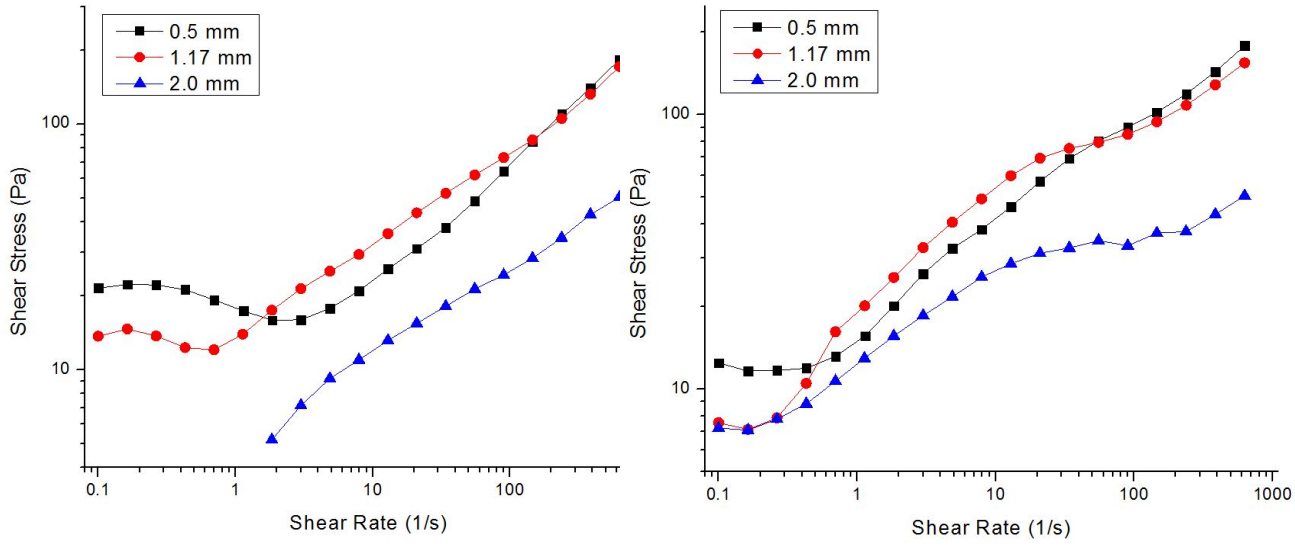

(a) 1 wt.% (b) 3 wt.%

Figure B.6. Lubrication Slip Determination: OCF S1, O:W = 60:40, T = 25 °C

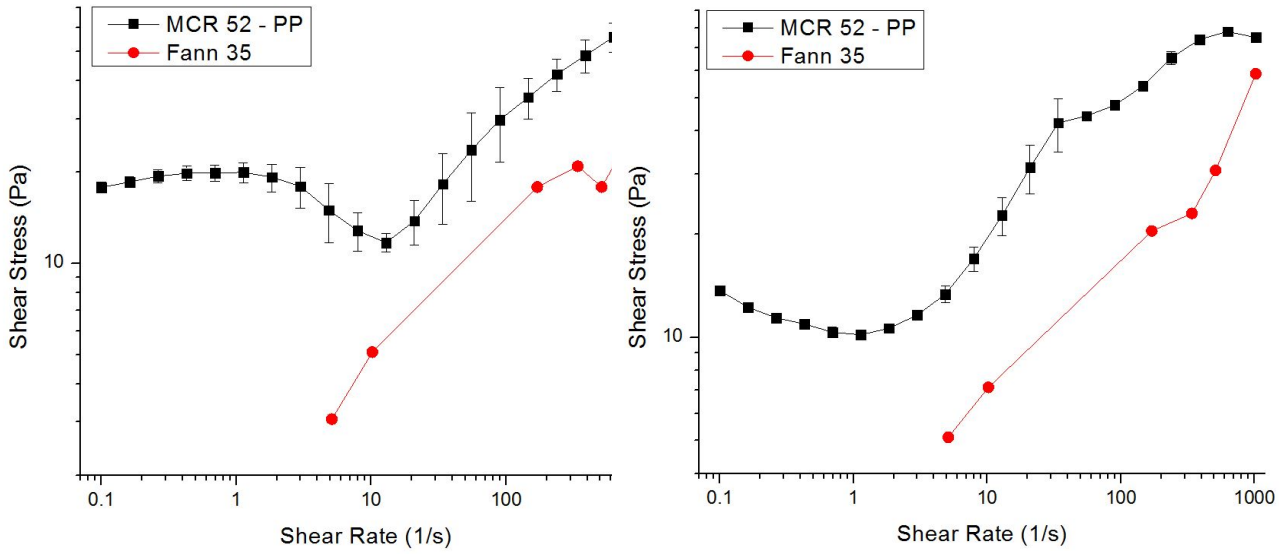

(a) 1 wt.% (b) 3 wt.%

Figure B.7. True & Cohesive Slip Determination: OCF S1, O:W = 60:40, T = 75 °C.

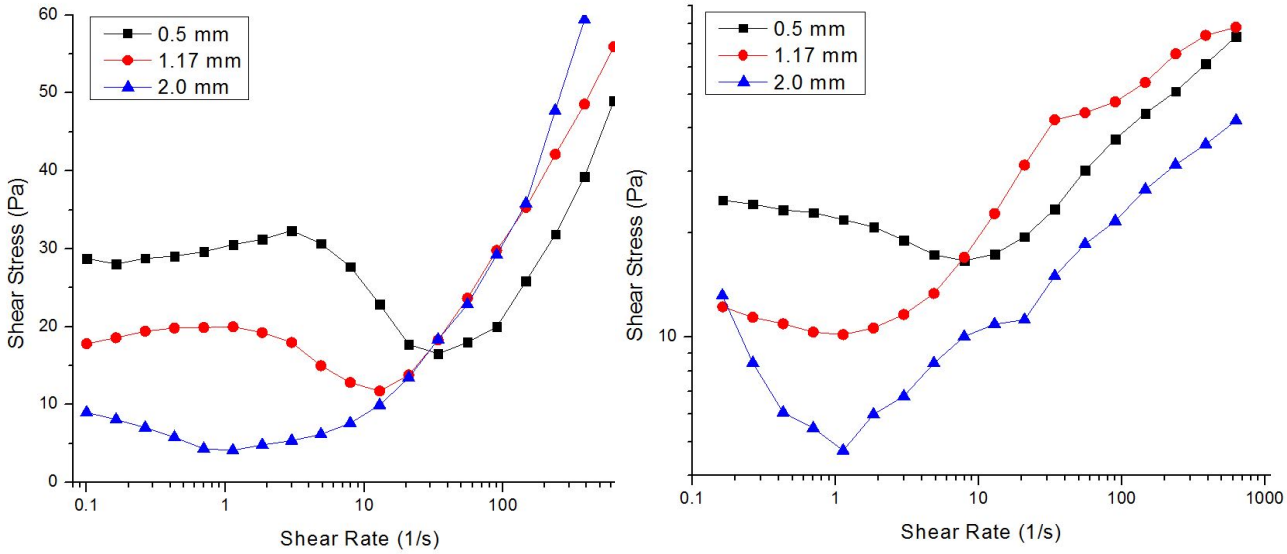

(a) 1 wt.% (b) 3 wt.%

Figure B.8. Lubrication Slip Determination: OCF S1, O:W = 60:40, T = 75 °C.

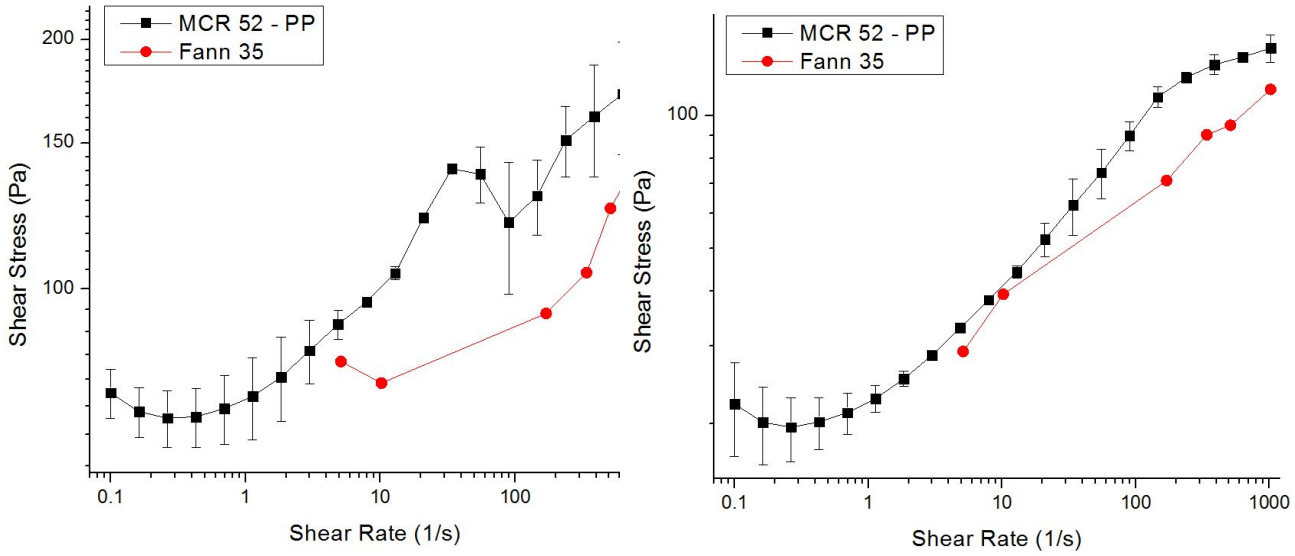

(a) 1 wt.% (b) 3 wt.%

Figure B.9. True & Cohesive Slip Determination: OCF S2, O:W = 50:50, T = 25 °C.

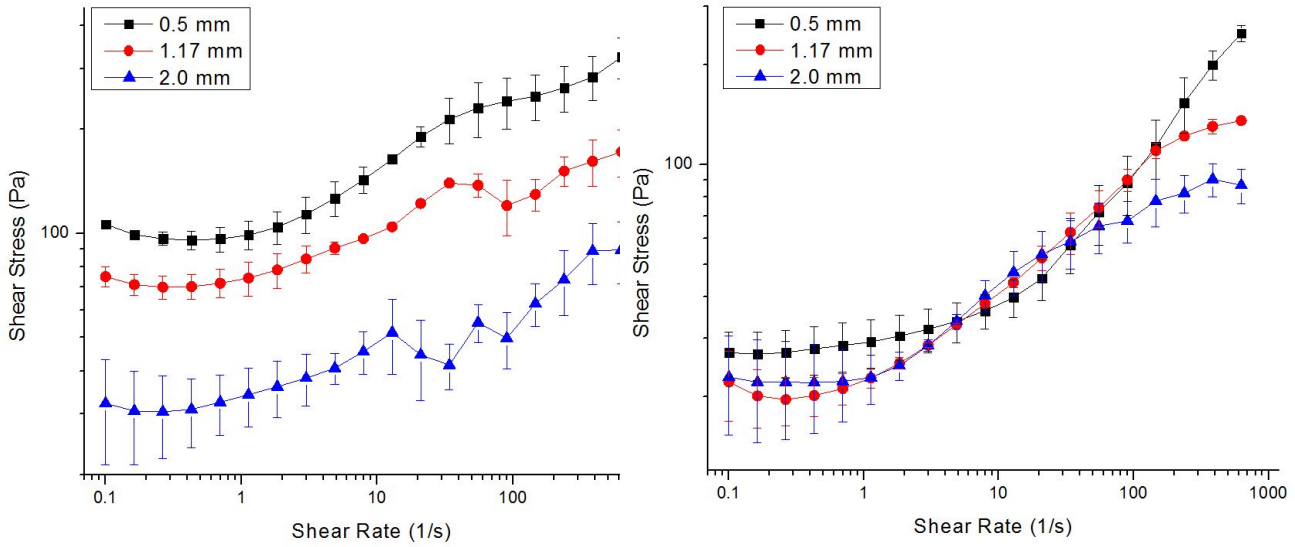

(a) 1 wt.% (b) 3 wt.%

Figure B.10. Lubrication Slip Determination: OCF S2, O:W = 50:50, T = 25 °C.

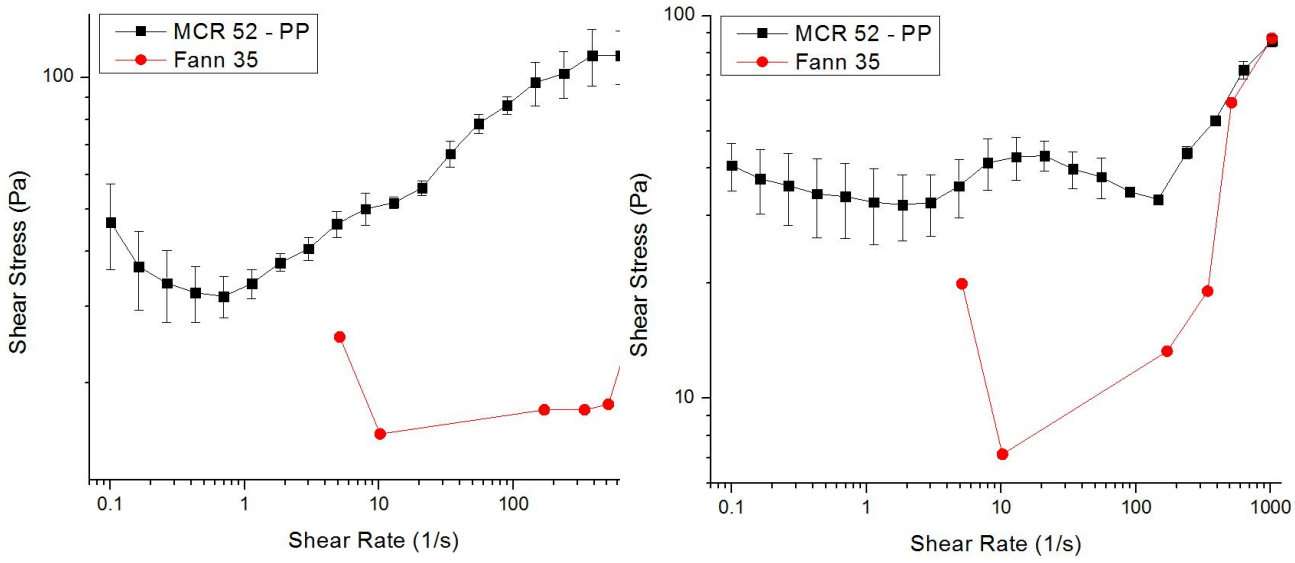

(a) 1 wt.%

(b) 3 wt.%

Figure B.11. True & Cohesive Slip Determination: OCF S2, O:W = 50:50, T = 75 °C.

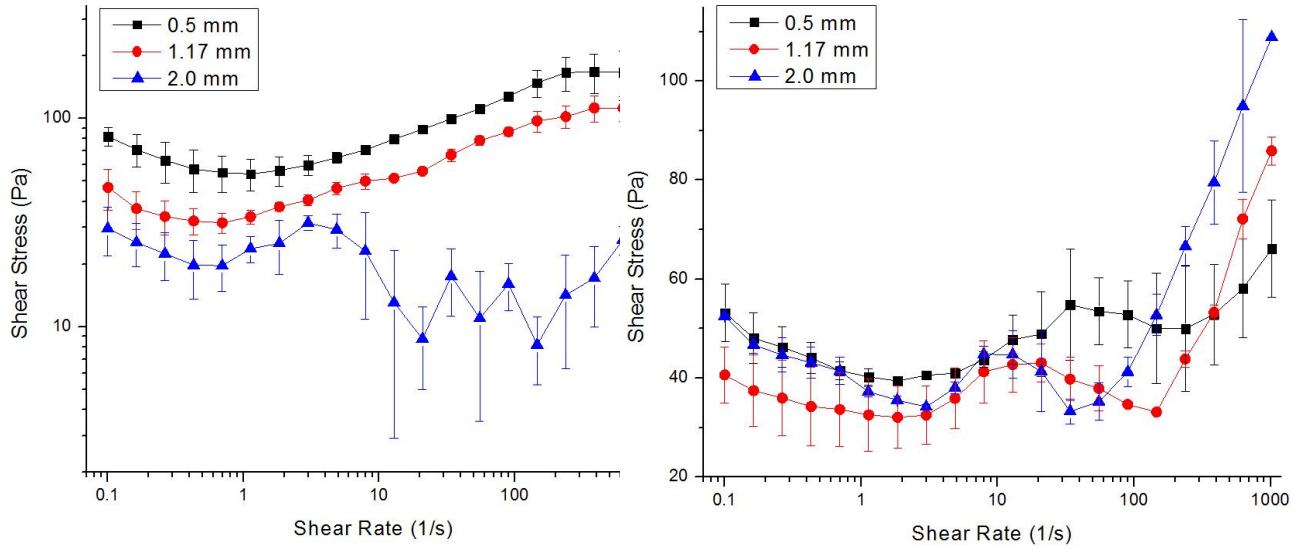

(a) 1 wt.%

(b) 3 wt.%

Figure B.12. Lubrication Slip Determination: OCF S2, O:W = 50:50, T = 75 °C.

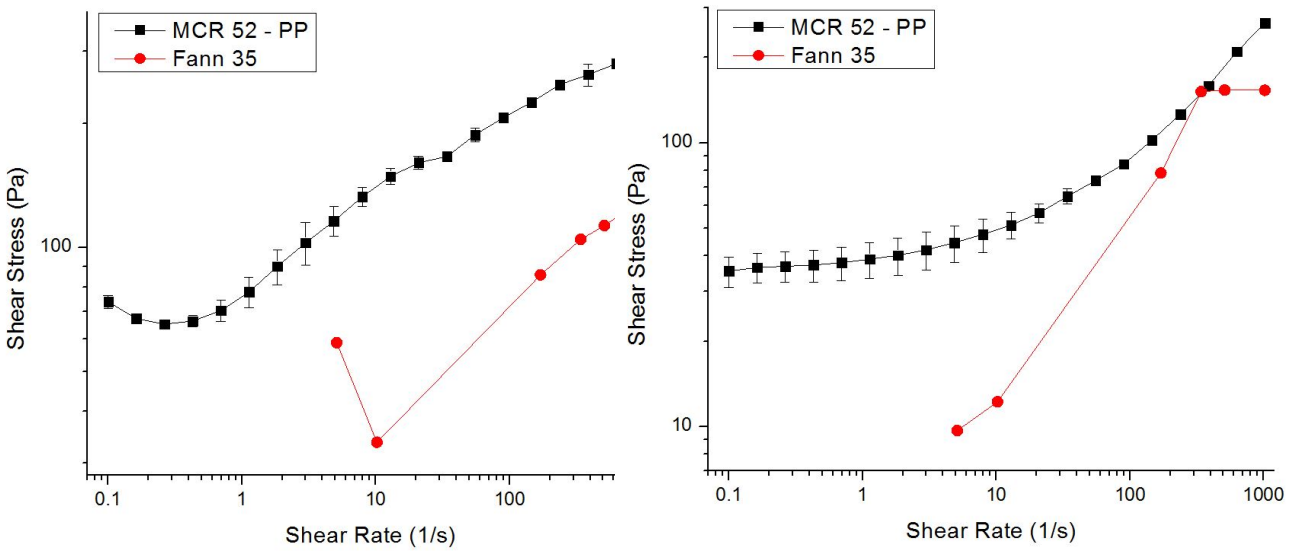

(a) 1 wt.% (b) 3 wt.%

Figure B.13. True & Cohesive Slip Determination: OCF S2, O:W = 60:40, T = 25 °C.

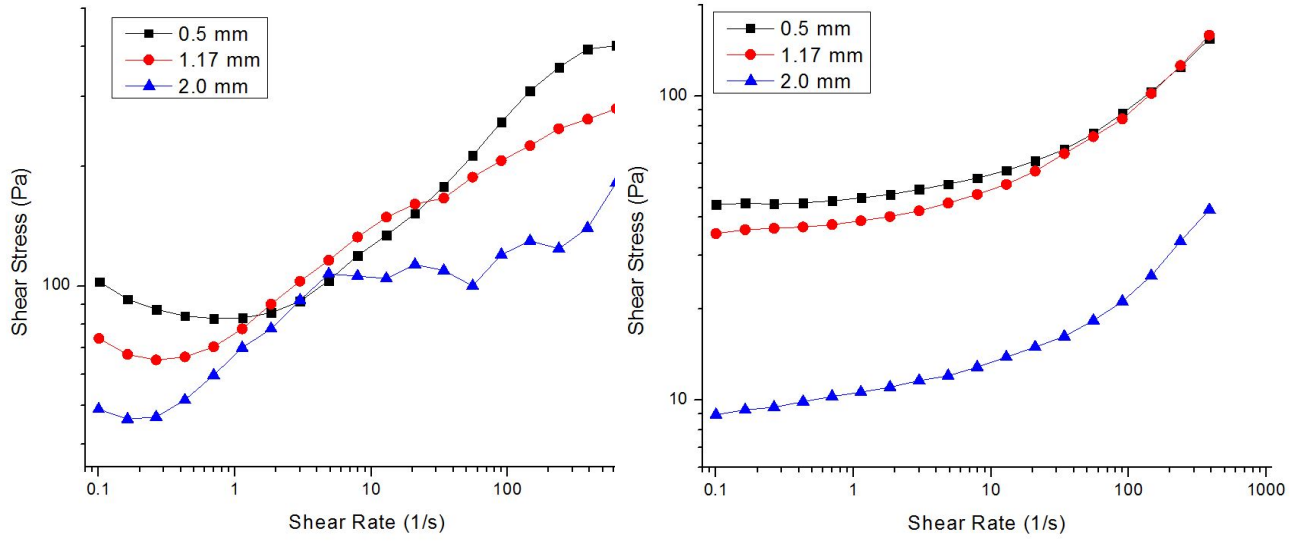

(a) 1 wt.% (b) 3 wt.%

Figure B.14. Lubrication Slip Determination: OCF S2, O:W = 60:40, T = 25 °C.

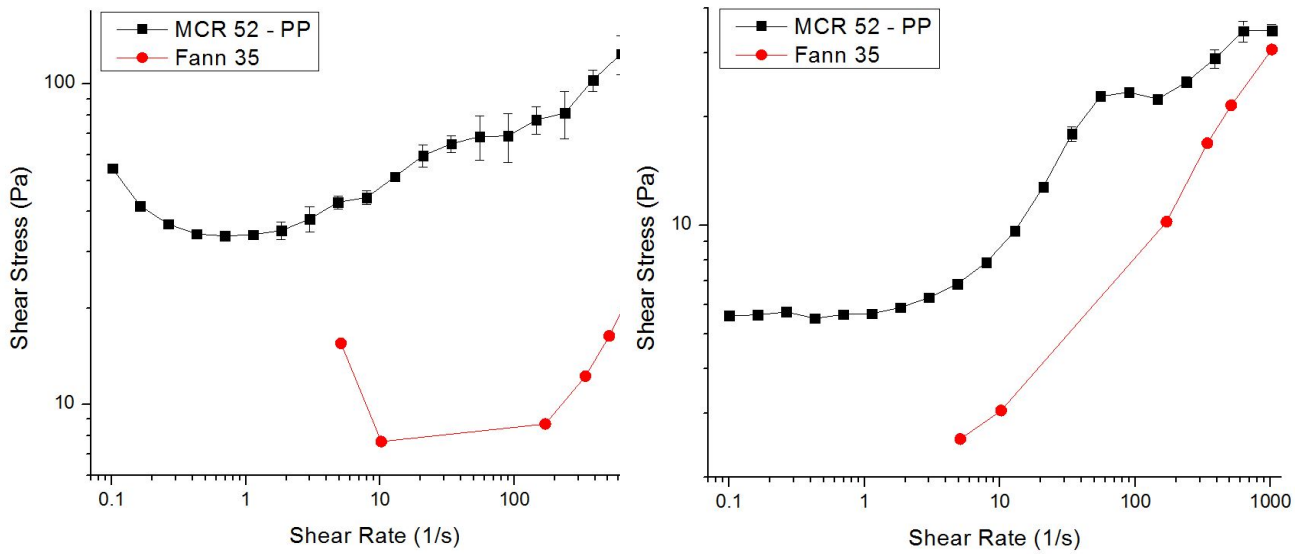

(a) 1 wt.% (b) 3 wt.%

Figure B.15. True & Cohesive Slip Determination: OCF S2, O:W = 60:40, T = 75 °C.

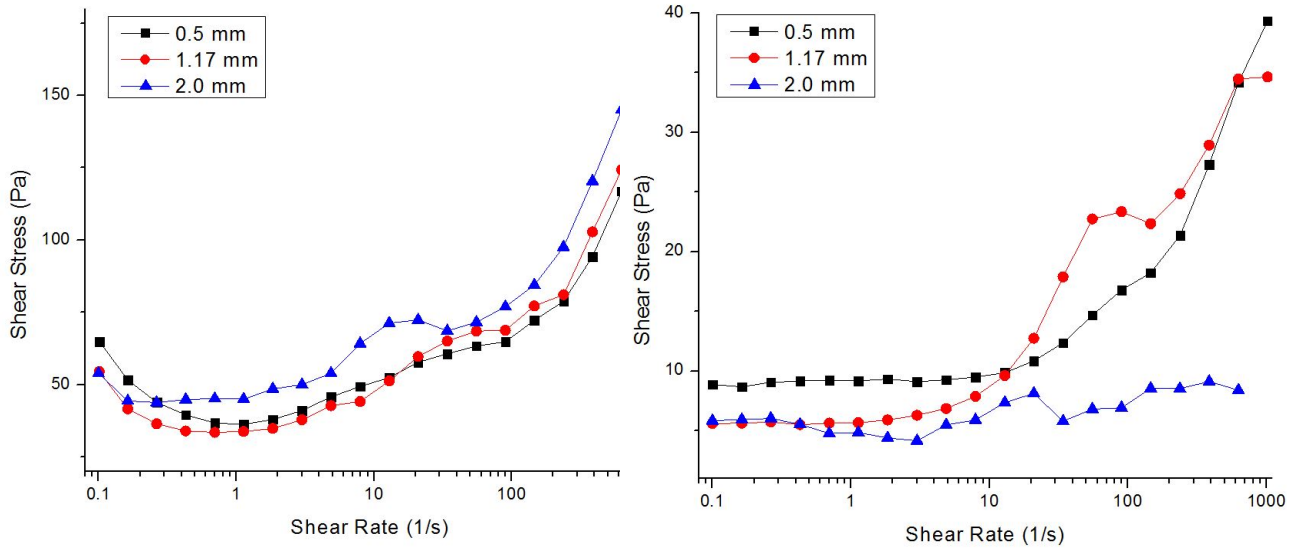

(a) 1 wt.% (b) 3 wt.%

Figure B.16. Lubrication Slip Determination: OCF S2, O:W = 60:40, T = 75 °C.

B.2 Effect of Surfactant Polarity

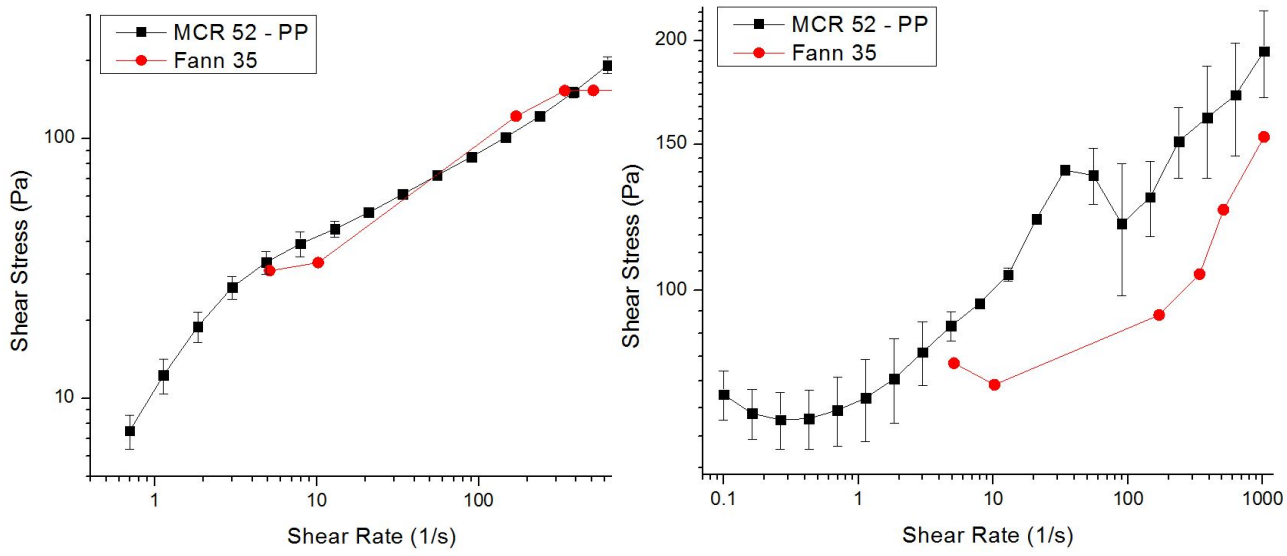

(a) OCF S1 (b) OCF S2

Figure B.17. True & Cohesive Slip Determination: O:W = 50:50, C_{surf} = 1 wt.%, T = 25 °C.

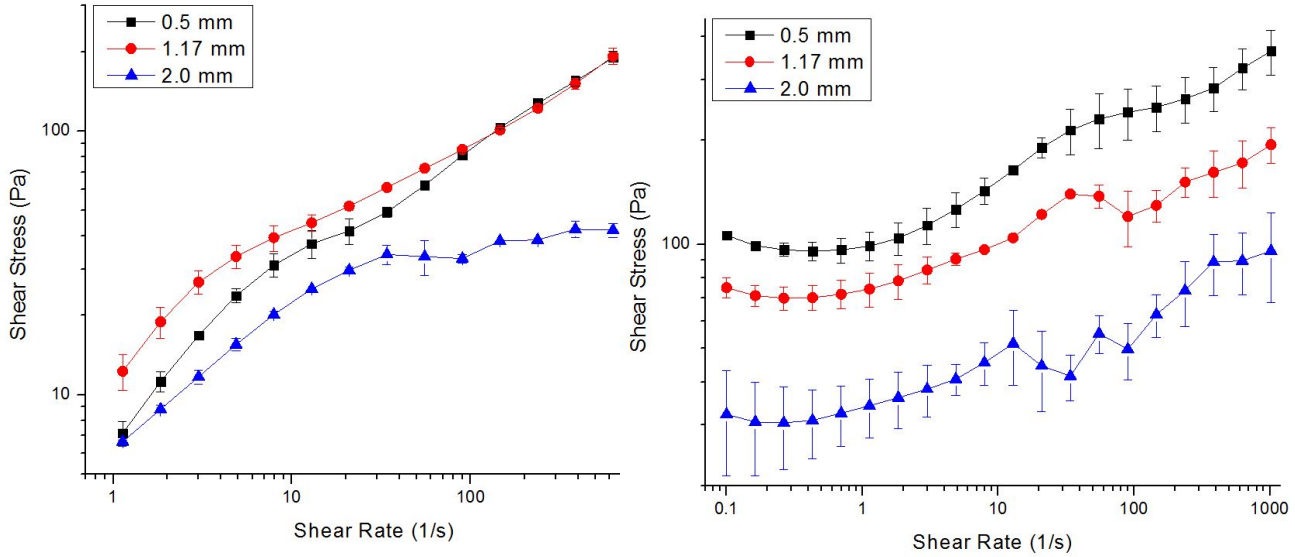

(a) OCF S1 (b) OCF S2

Figure B.18. Lubrication Slip Determination: O:W = 50:50, C_{surf} = 1 wt.%, T = 25 °C.

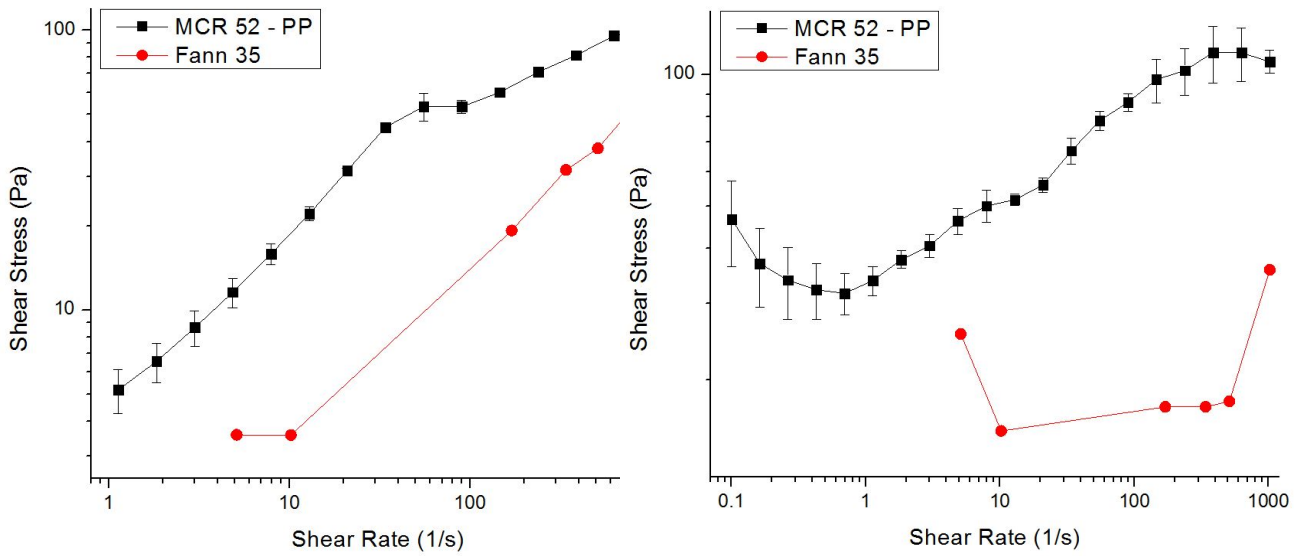

(a) OCF S1 (b) OCF S2

Figure B.19. True & Cohesive Slip Determination: O:W = 50:50, C_{surf} = 1 wt.%, T = 75 °C.

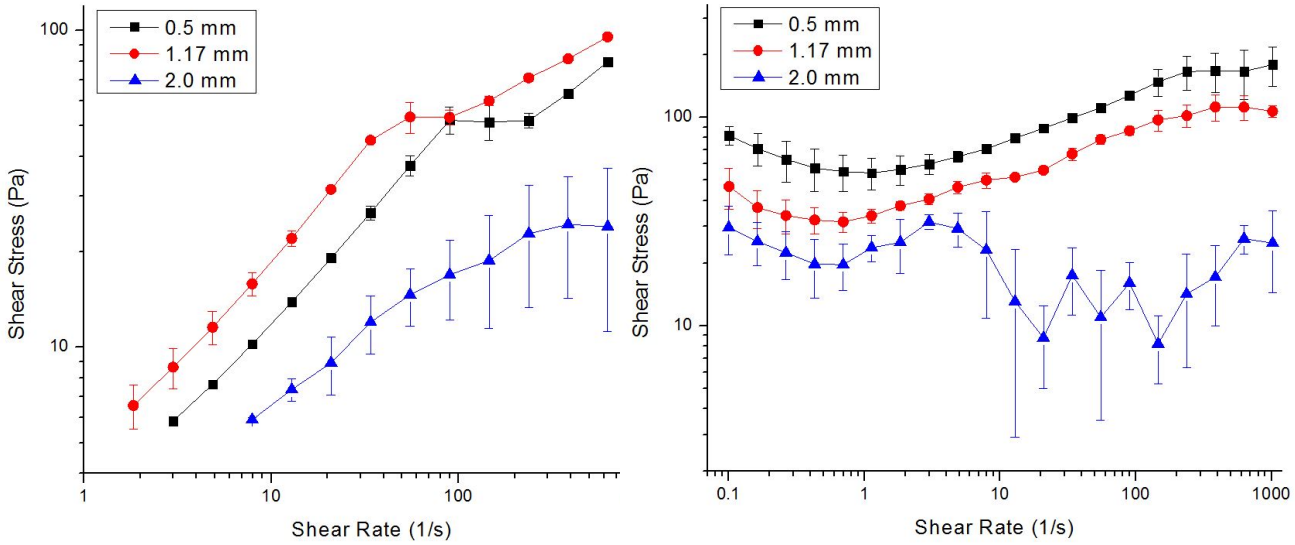

(a) OCF S1 (b) OCF S2

Figure B.20. Lubrication Slip Determination: O:W = 50:50, C_{surf} = 1 wt.%, T = 75 °C.

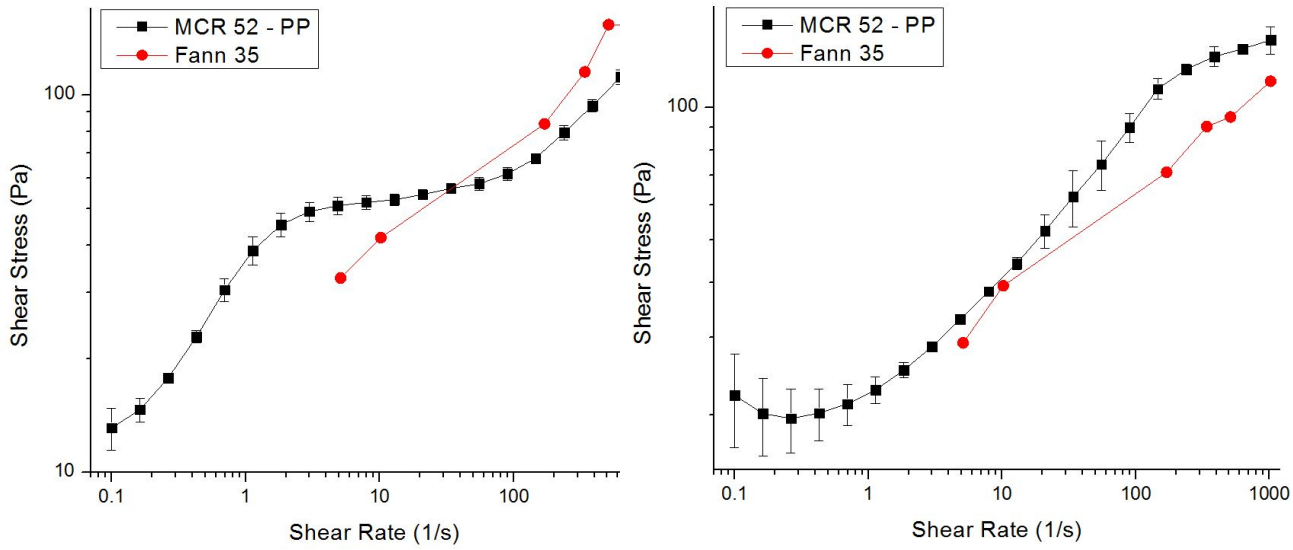

(a) OCF S1 (b) OCF S2

Figure B.21. True & Cohesive Slip Determination: O:W = 50:50, C_{surf} = 3 wt.%, T = 25 °C.

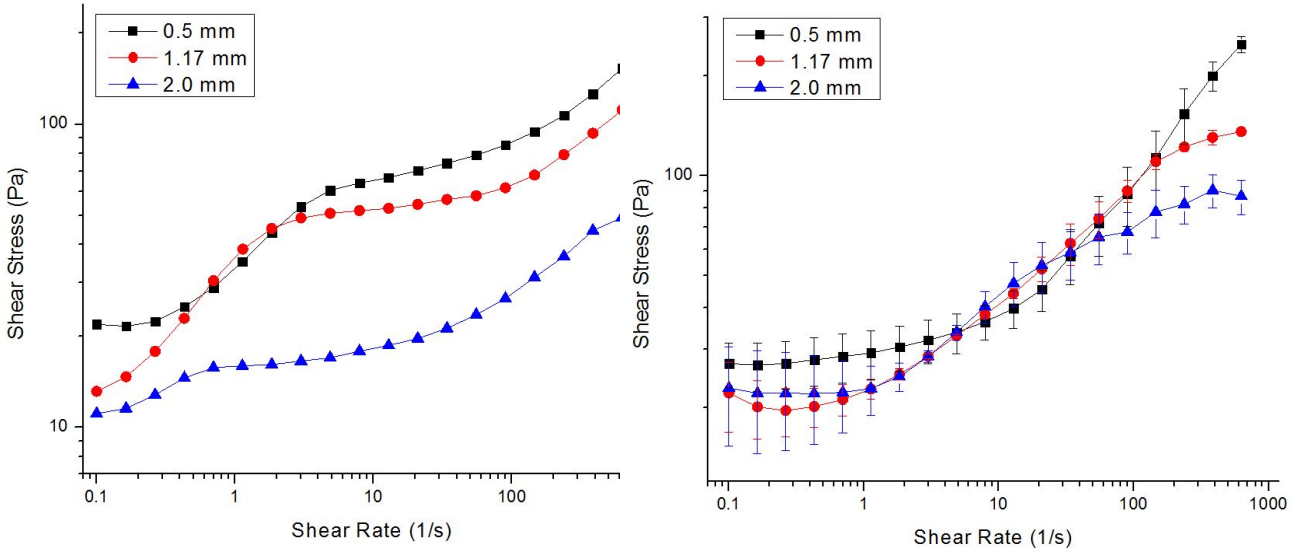

(a) OCF S1 (b) OCF S2

Figure B.22. Lubrication Slip Determination: O:W = 50:50, C_{surf} = 3 wt.%, T = 25 °C.

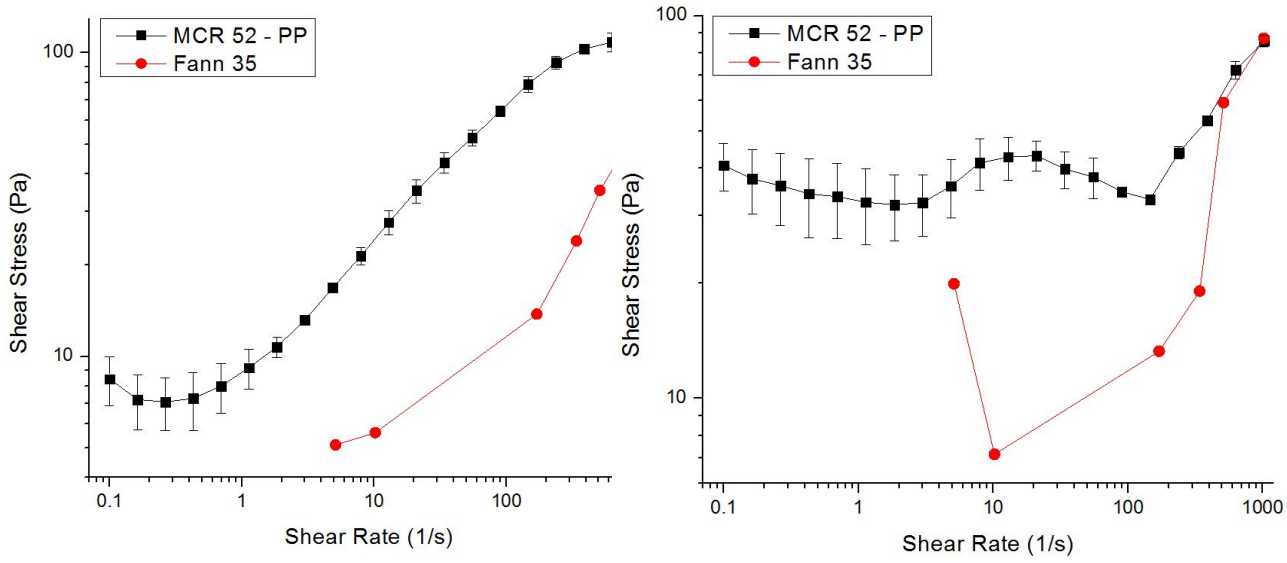

(a) OCF S1

(b) OCF S2

Figure B.23. True & Cohesive Slip Determination: O:W = 50:50, C_{surf} = 3 wt.%, T = 75 °C.

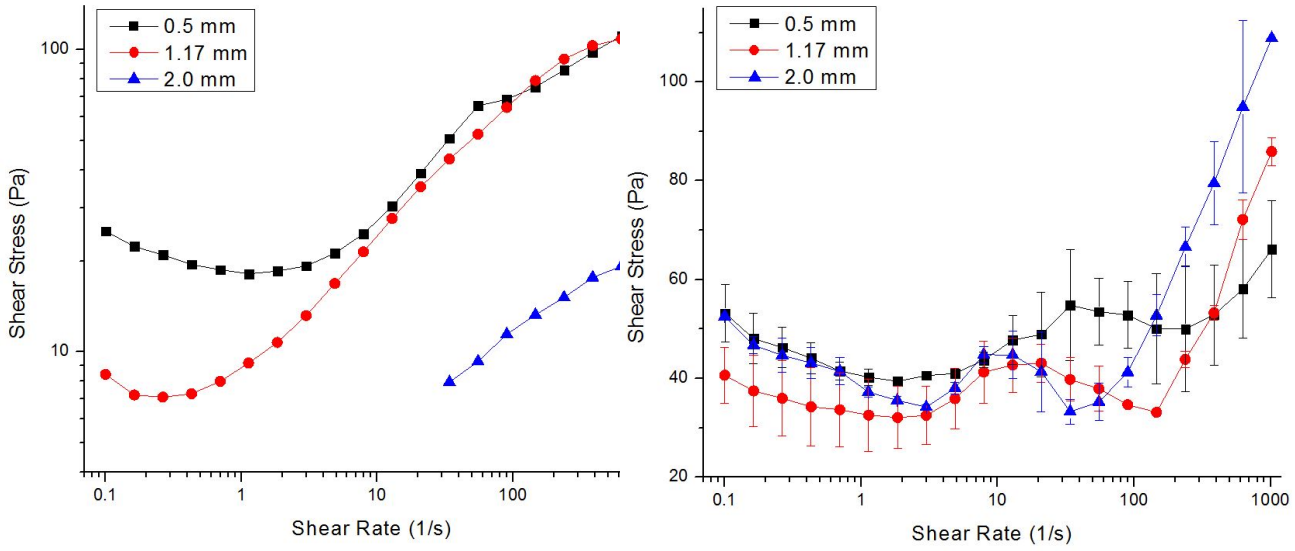

(a) OCF S1

(b) OCF S2

Figure B.24. Lubrication Slip Determination: O:W = 50:50, C_{surf} = 3 wt.%, T = 75 °C.

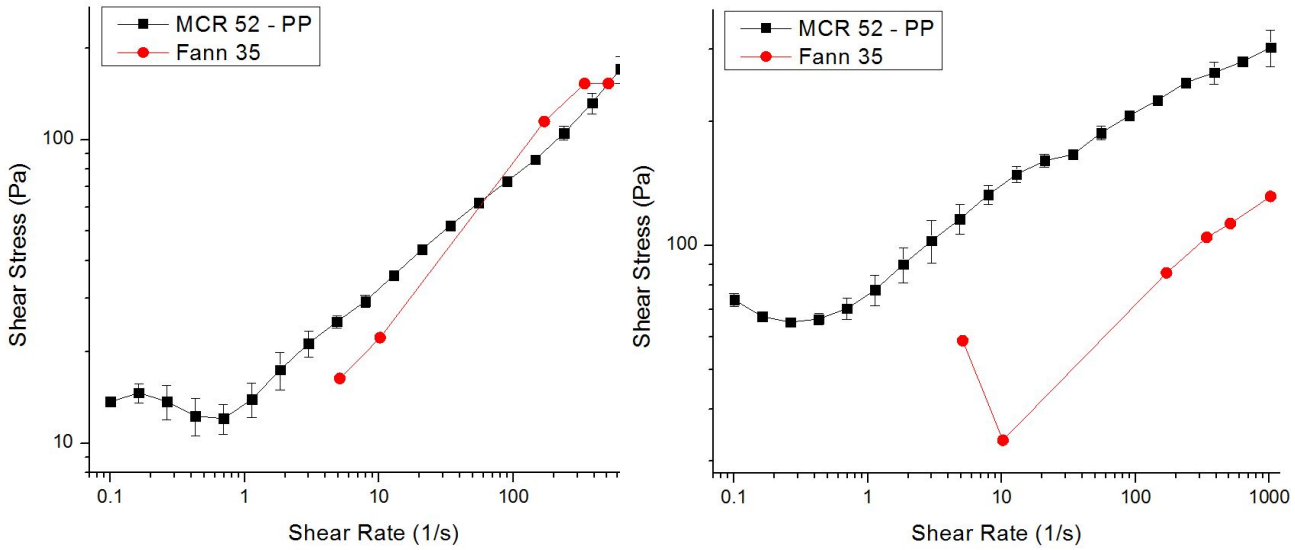

(a) OCF S1 (b) OCF S2

Figure B.25. True & Cohesive Slip Determination: O:W = 60:40, C_{surf} = 1 wt.%, T = 25 °C.

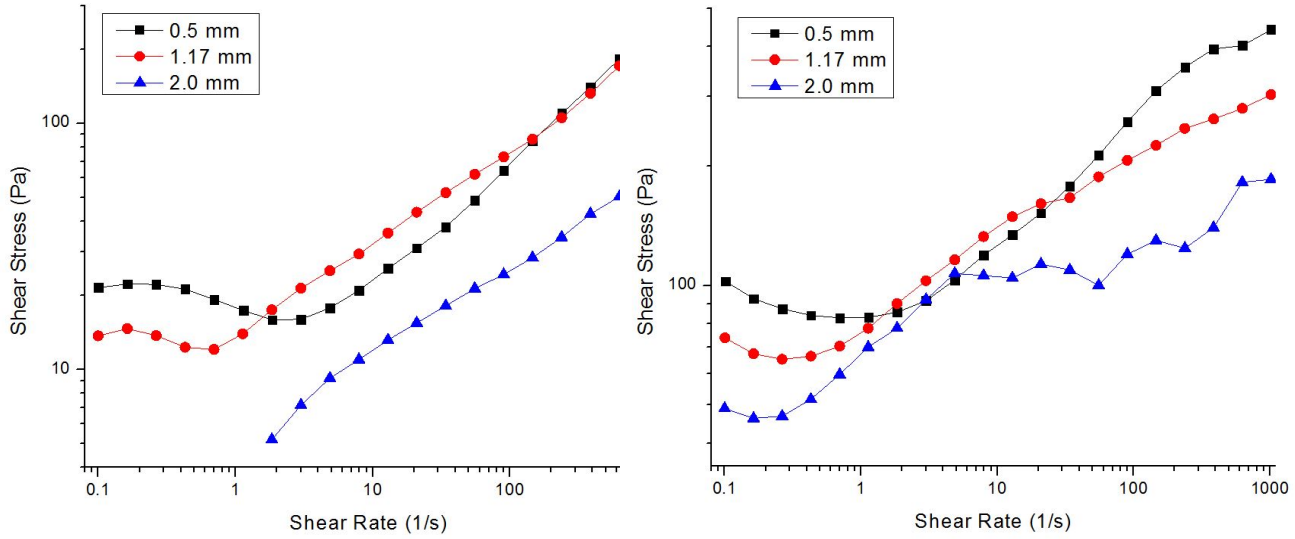

(a) OCF S1 (b) OCF S2

Figure B.26. Lubrication Slip Determination: O:W = 60:40, C_{surf} = 1 wt.%, T = 25 °C.

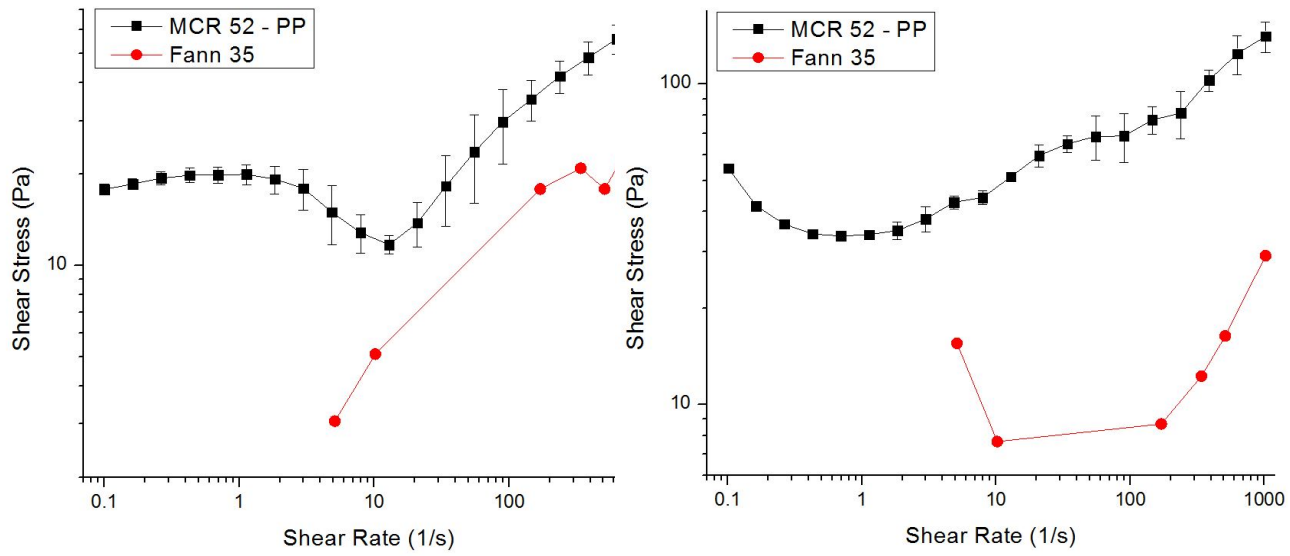

(a) OCF S1 (b) OCF S2

Figure B.27. True & Cohesive Slip Determination: O:W = 60:40, C_{surf} = 1 wt.%, T = 75 °C.

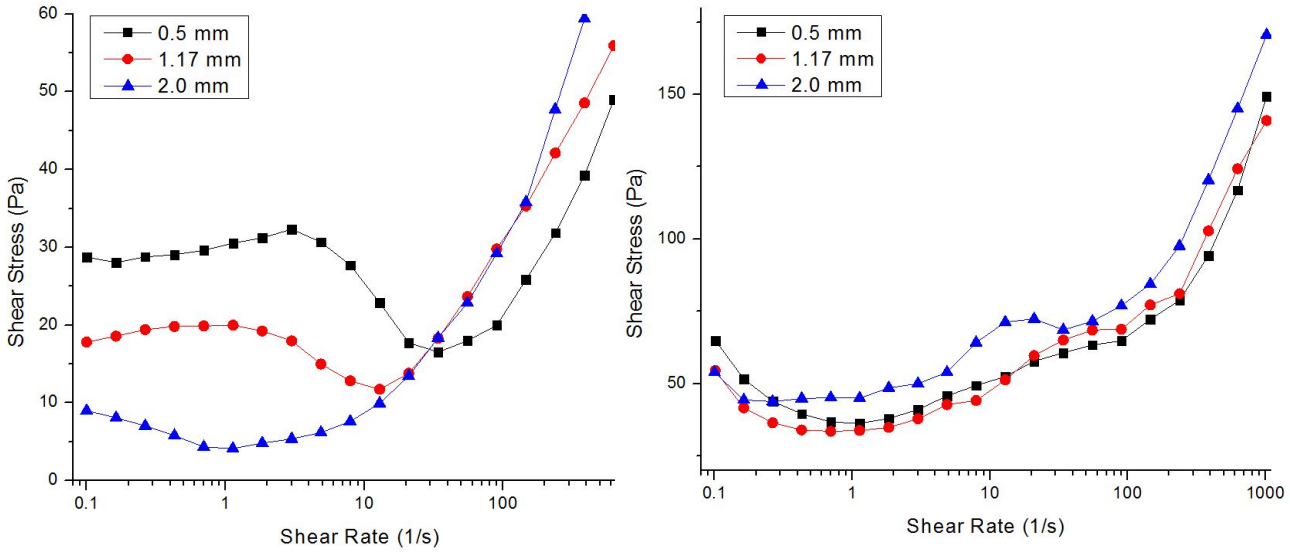

(a) OCF S1 (b) OCF S2

Figure B.28. Lubrication Slip Determination: O:W = 60:40, C_{surf} = 1 wt.%, T = 75 °C.

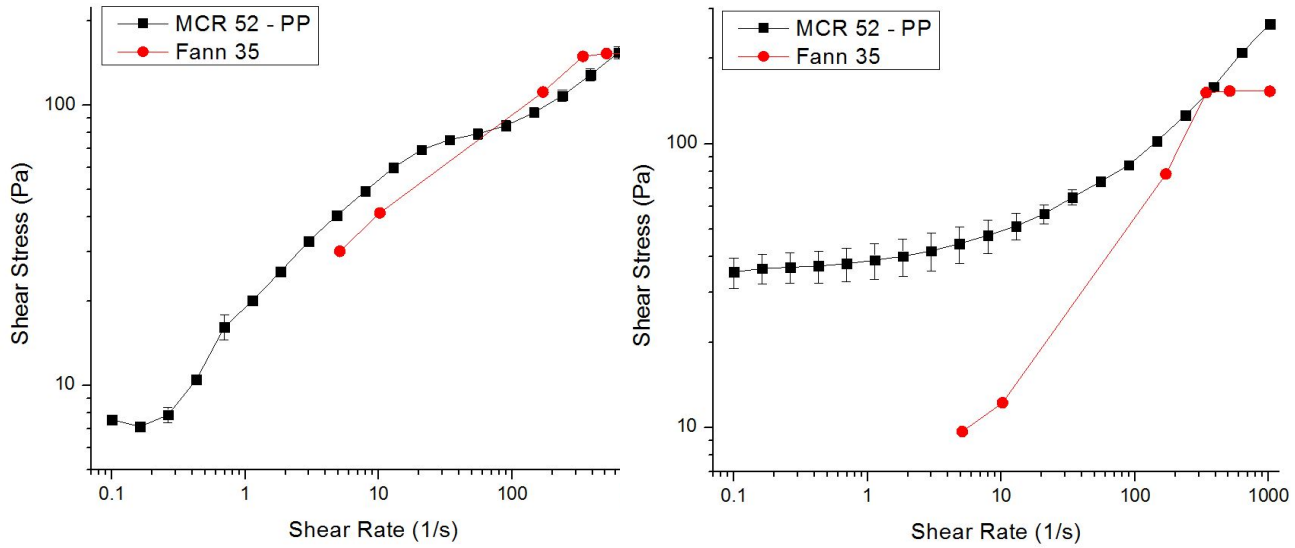

(a) OCF S1 (b) OCF S2

Figure B.29. True & Cohesive Slip Determination: O:W = 60:40, C_{surf} = 3 wt.%, T = 25 °C.

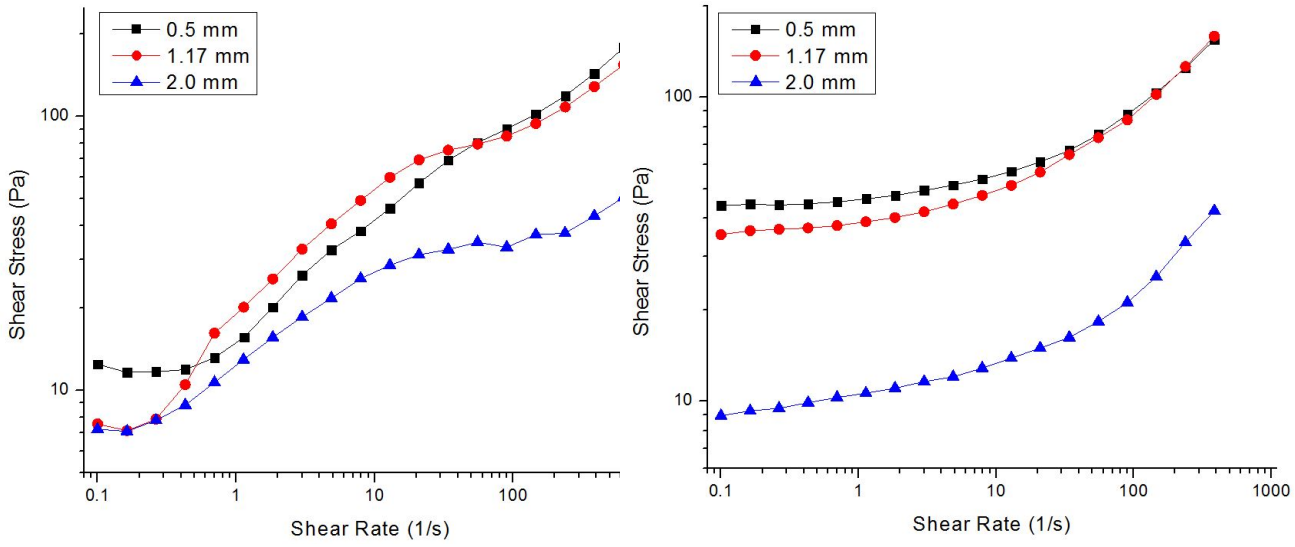

(a) OCF S1 (b) OCF S2

Figure B.30. Lubrication Slip Determination: O:W = 60:40, C_{surf} = 3 wt.%, T = 25 °C.

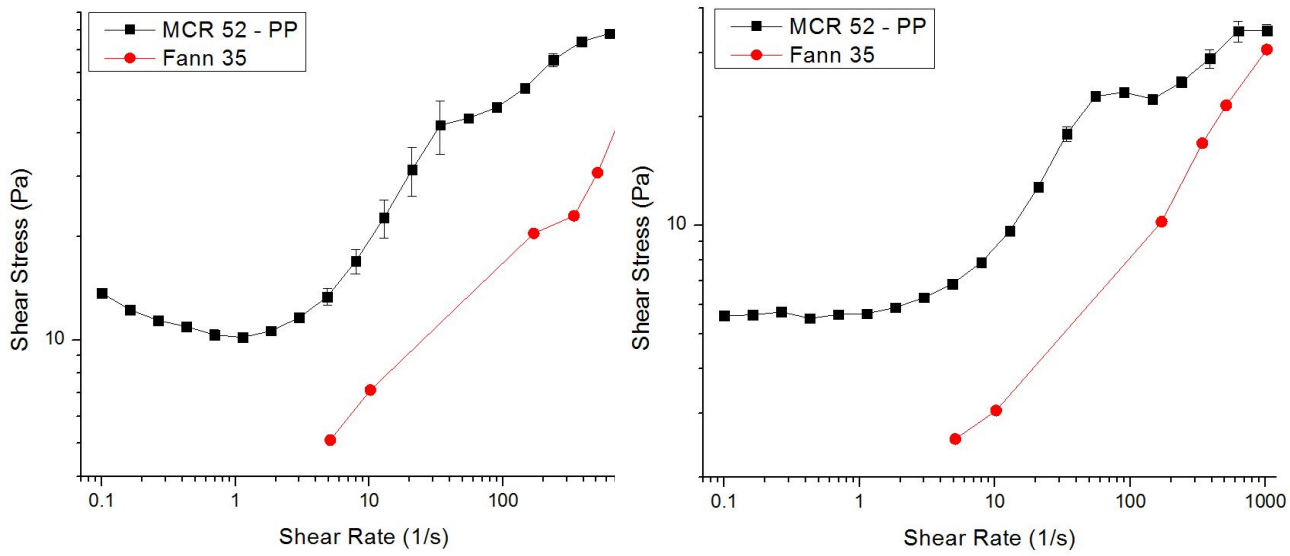

(a) OCF S1 (b) OCF S2

Figure B.31. True & Cohesive Slip Determination: O:W = 60:40, C_{surf} = 3 wt.%, T = 75 °C.

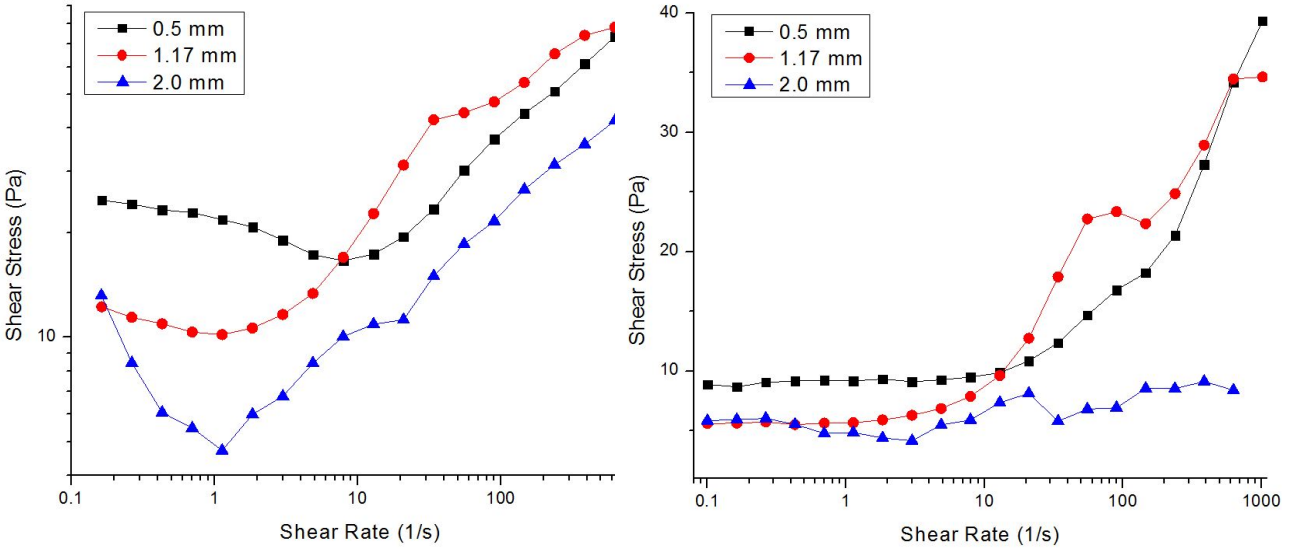

(a) OCF S1 (b) OCF S2

Figure B.32. Lubrication Slip Determination: O:W = 60:40, C_{surf} = 3 wt.%, T = 75 °C.

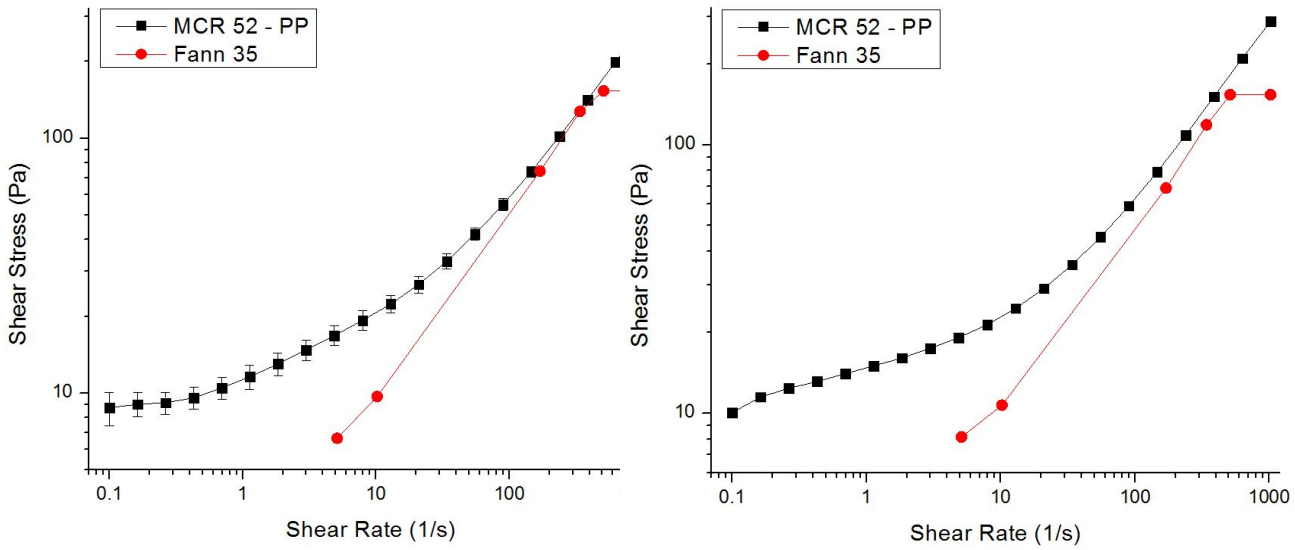

(a) OCF S1 (b) OCF S2

Figure B.33. True & Cohesive Slip Determination: O:W = 70:30, C_{surf} = 3 wt.%, T = 25 °C.

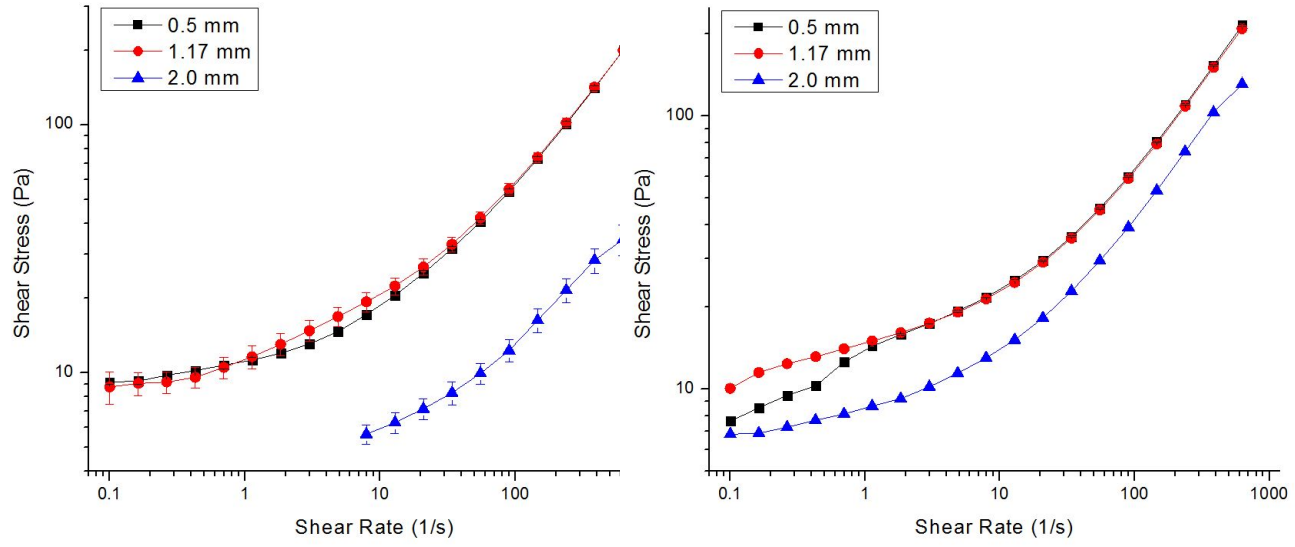

(a) OCF S1 (b) OCF S2

Figure B.34. Lubrication Slip Determination: O:W = 70:30, C_{surf} = 3 wt.%, T = 25 °C.

B.3 Effect of Temperature

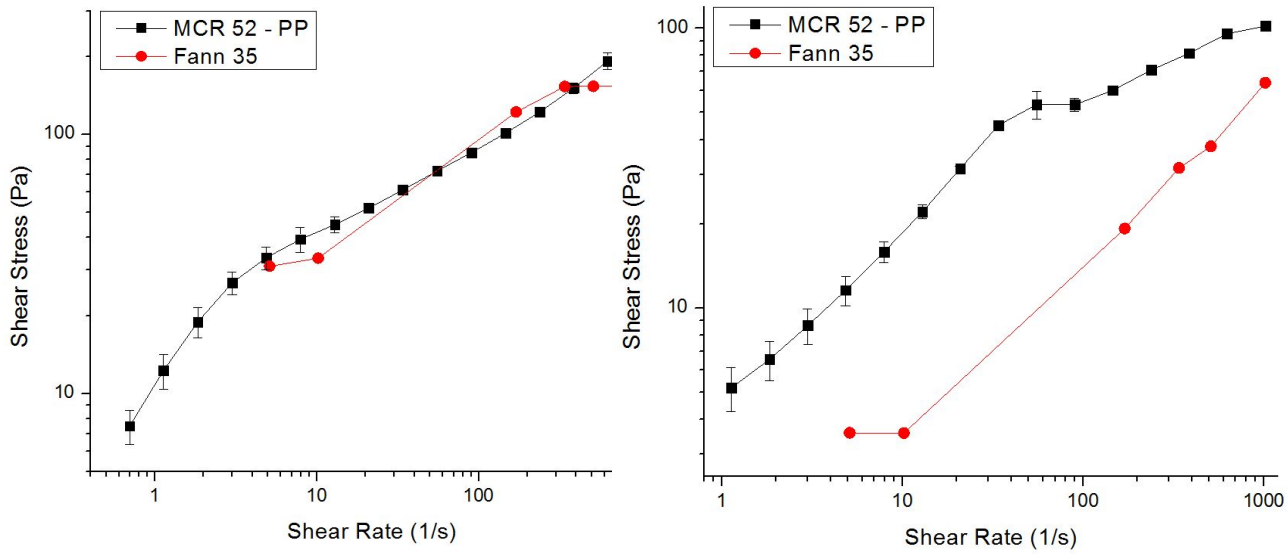

(a) 25 °C (b) 75 °C

Figure B.35. True & Cohesive Slip Determination: OCF S1, O:W = 50:50, C_{surf} = 1 wt.%

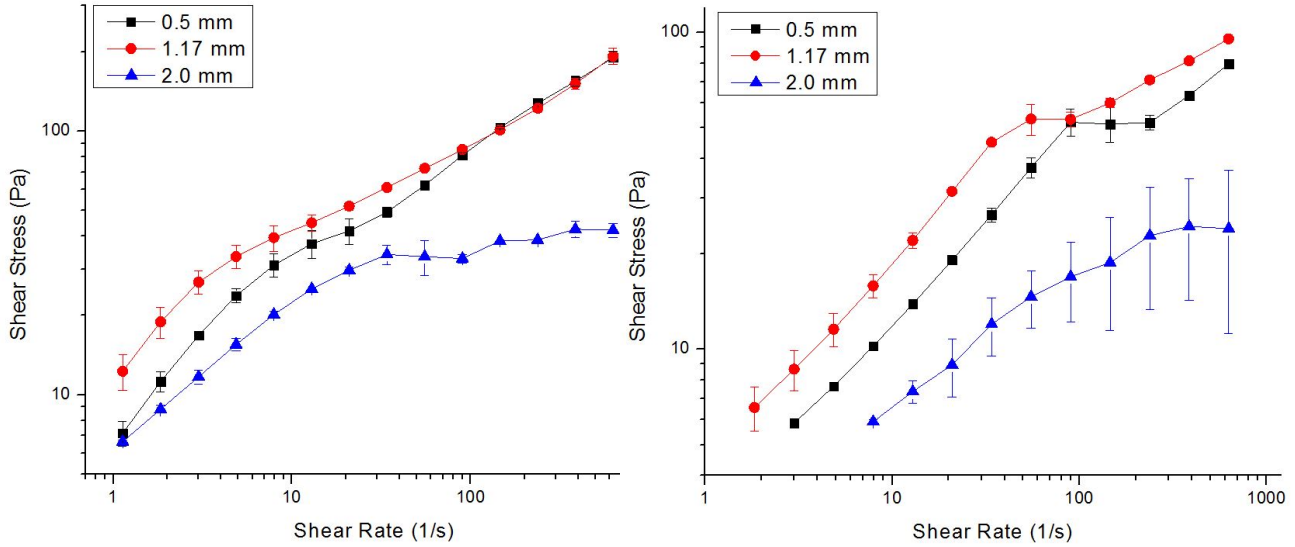

(a) 25 °C (b) 75 °C

Figure B.36. Lubrication Slip Determination: OCF S1, O:W = 50:50, C_{surf} = 1 wt.%.

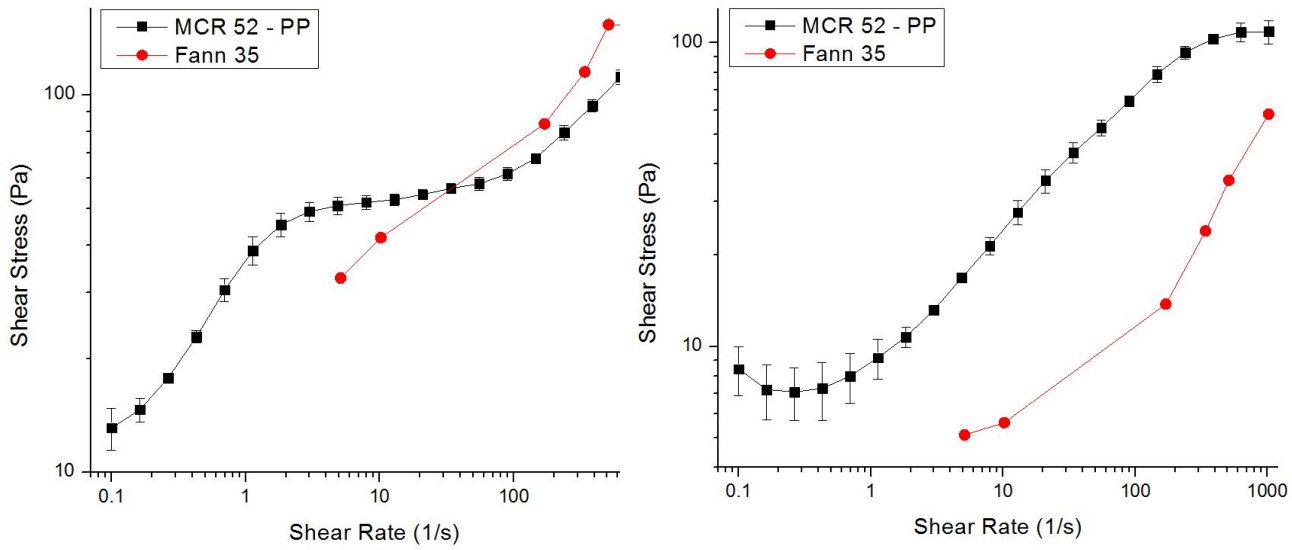

(a) 25 °C (b) 75 °C

Figure B.37. True & Cohesive Slip Determination: OCF S1, O:W = 50:50, C_{surf} = 3 wt.%.

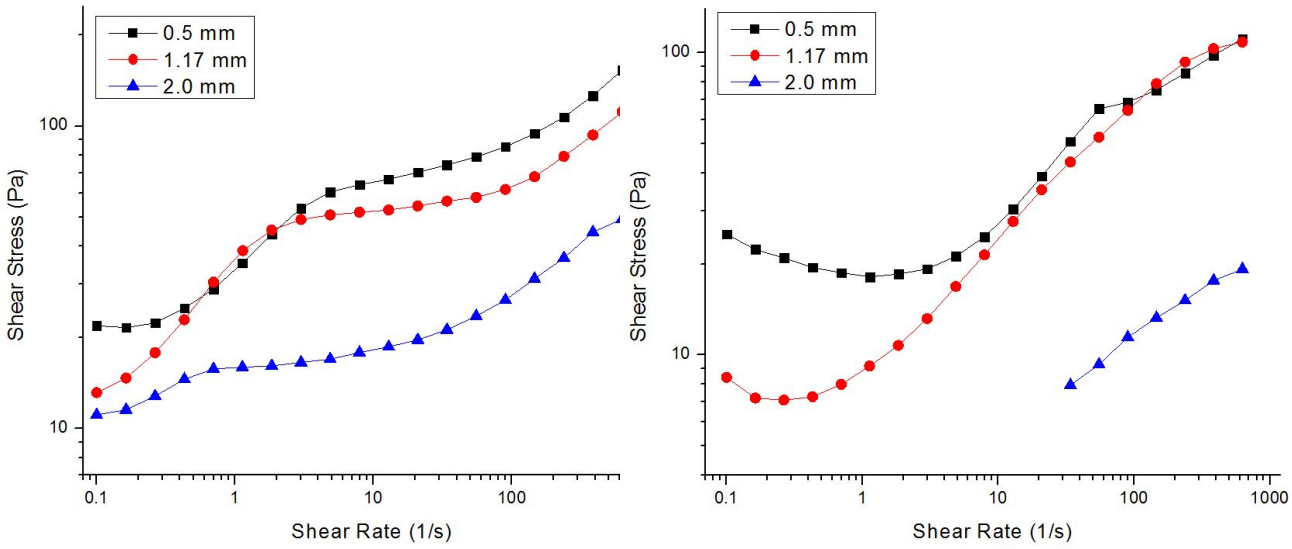

(a) 25 °C (b) 75 °C

Figure B.38. Lubrication Slip Determination: OCF S1, O:W = 50:50, C_{surf} = 3 wt.%.

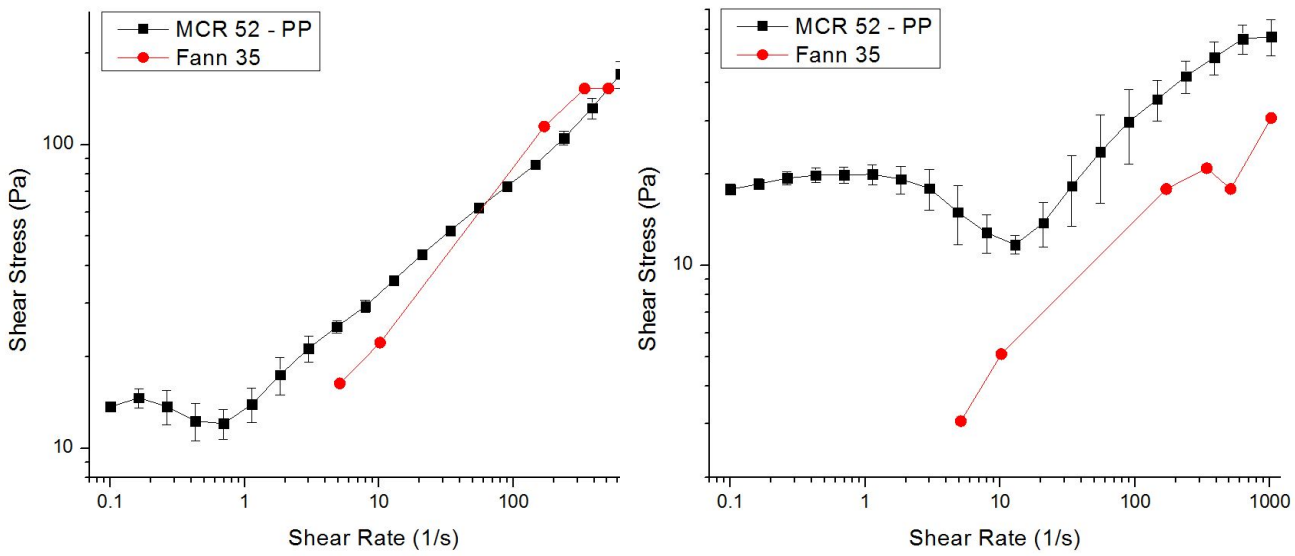

(a) 25 °C (b) 75 °C

Figure B.39. True & Cohesive Slip Determination: OCF S1, O:W = 60:40, C_{surf} = 1 wt.%.

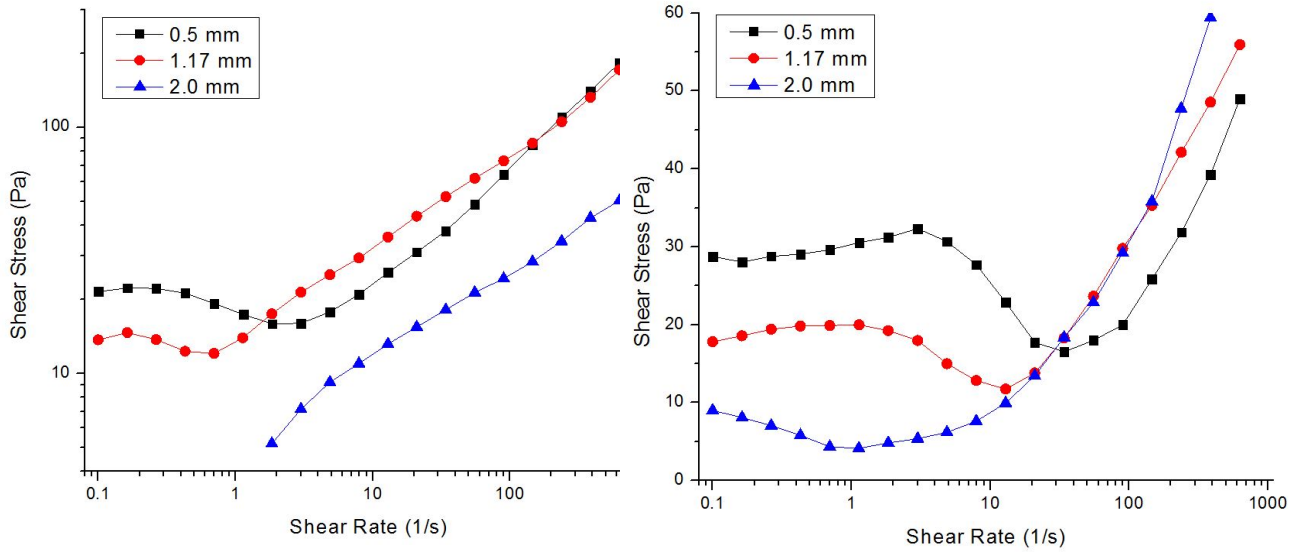

(a) 25 °C (b) 75 °C

Figure B.40. Lubrication Slip Determination: OCF S1, O:W = 60:40, C_{surf} = 1 wt.%.

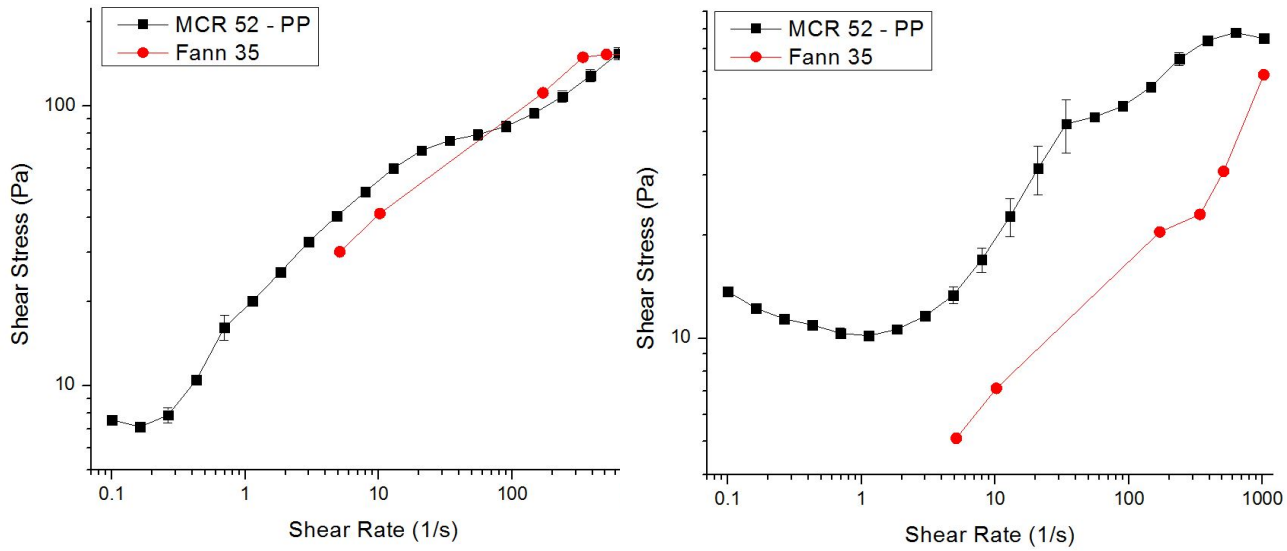

(a) 25 °C (b) 75 °C

Figure B.41. True & Cohesive Slip Determination: OCF S1, O:W = 60:40, C_{surf} = 3 wt.%.

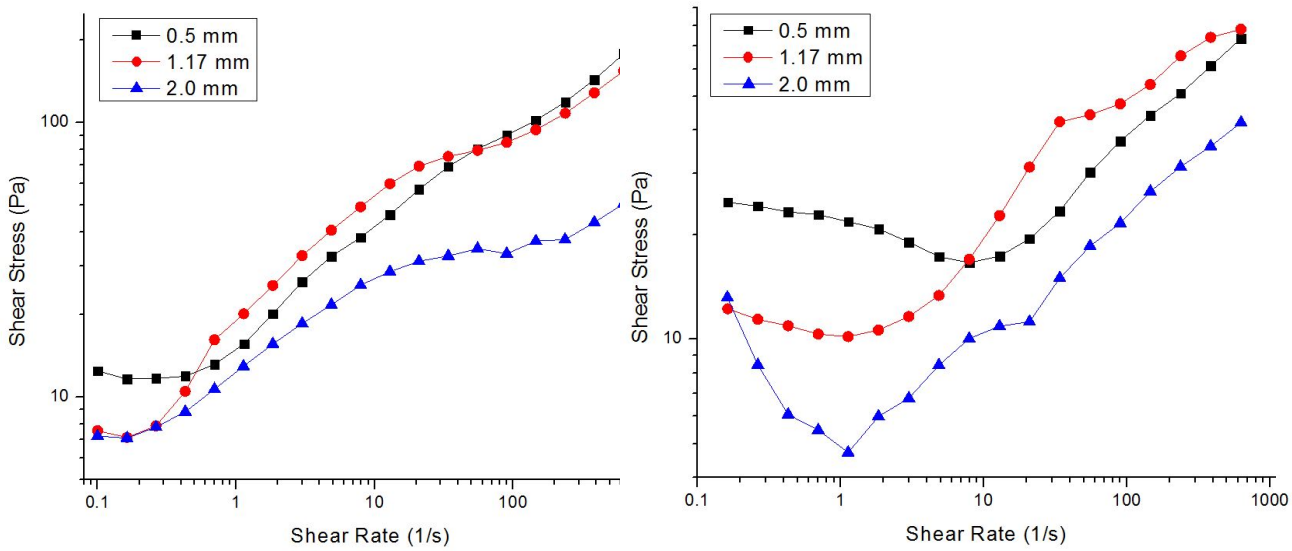

(a) 25 °C (b) 75 °C

Figure B.42. Lubrication Slip Determination: OCF S1, O:W = 60:40, C_{surf} = 3 wt.%.

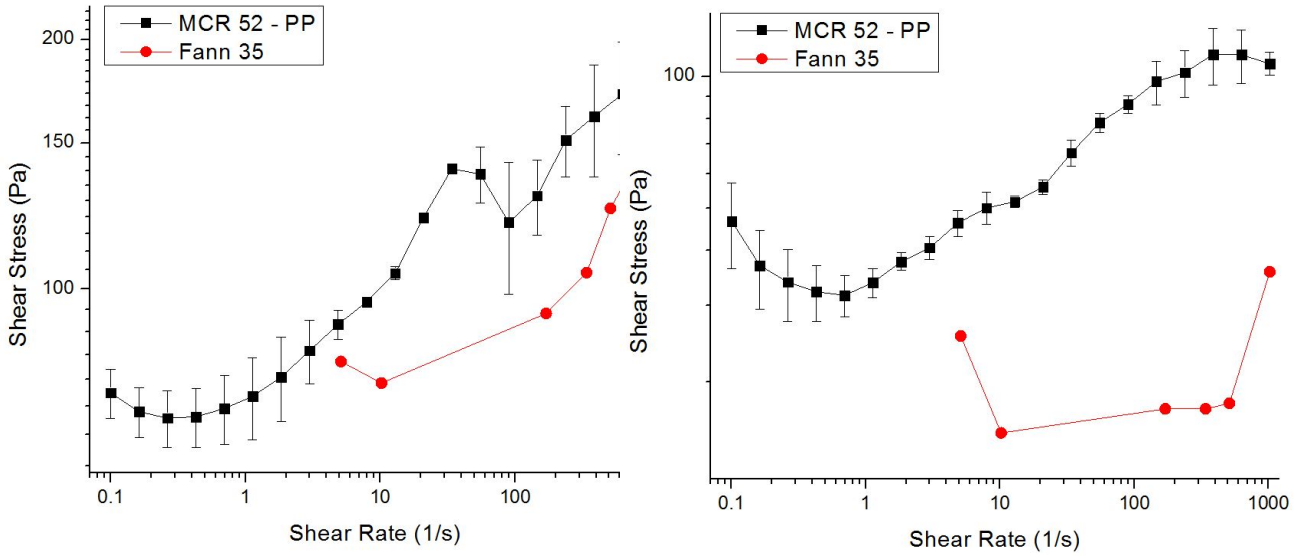

(a) 25 °C (b) 75 °C

Figure B.43. True & Cohesive Slip Determination: OCF S2, O:W = 50:50, C_{surf} = 1 wt.%.

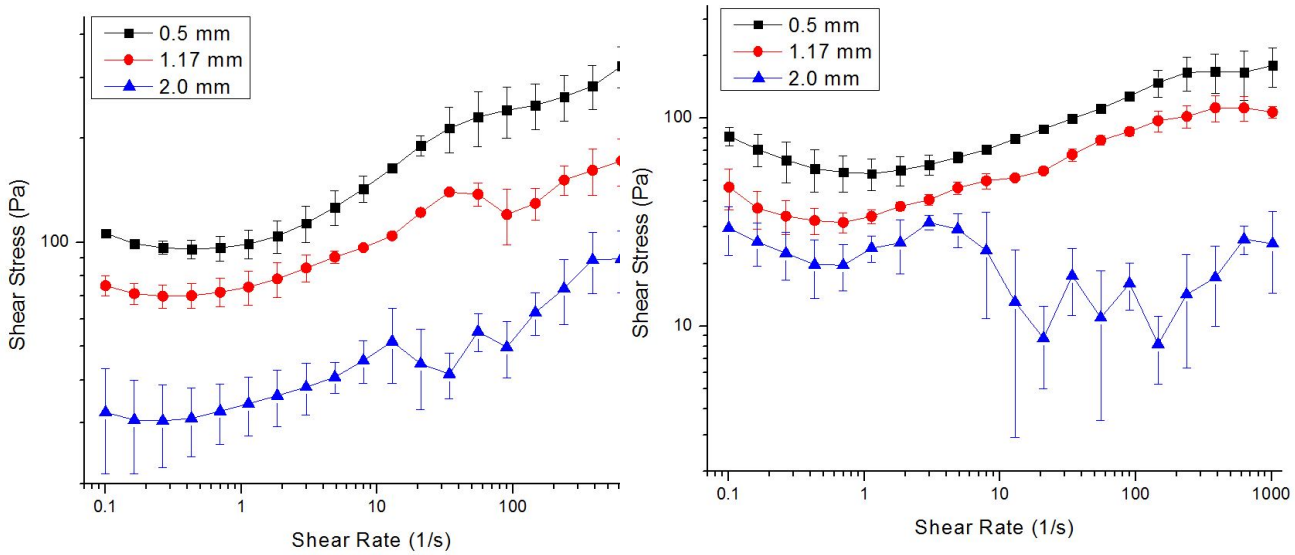

(a) 25 °C (b) 75 °C

Figure B.44. Lubrication Slip Determination: OCF S2, O:W = 50:50, C_{surf} = 1 wt.%.

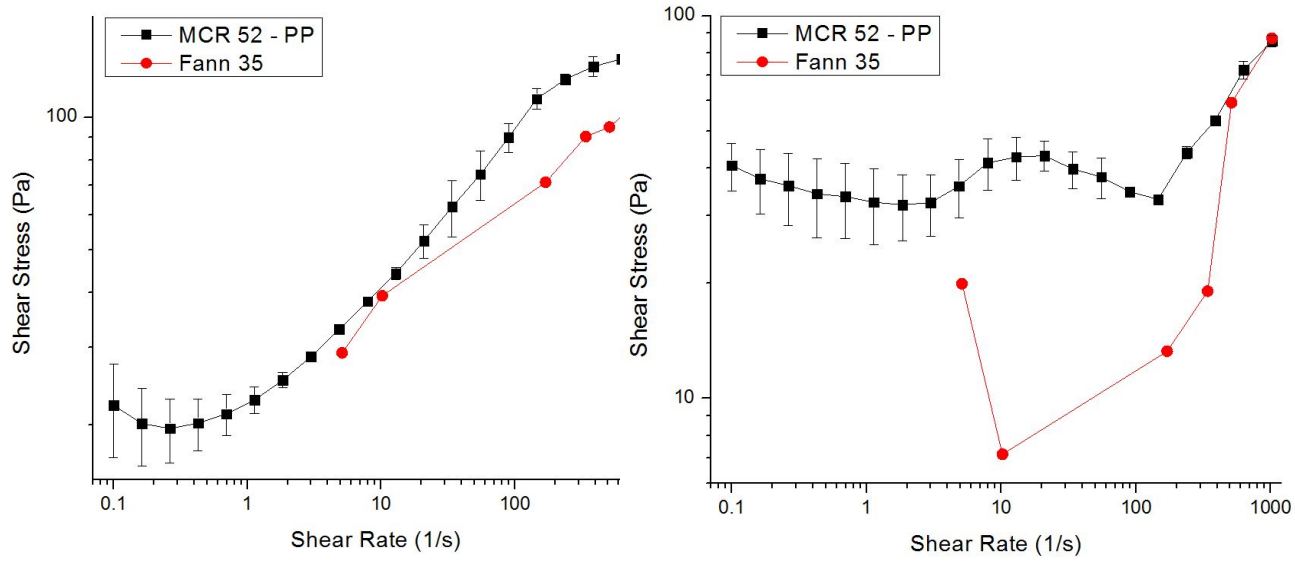

(a) 25 °C (b) 75 °C

Figure B.45. True & Cohesive Slip Determination: OCF S2, O:W = 50:50, C_{surf} = 3 wt.%.

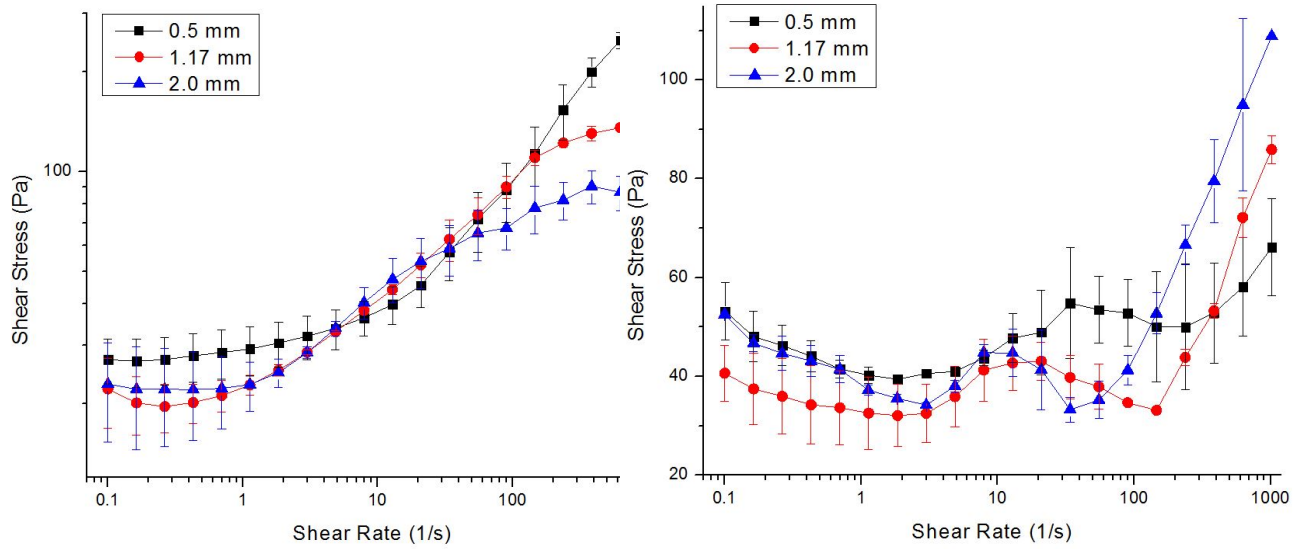

(a) 25 °C (b) 75 °C

Figure B.46. Lubrication Slip Determination: OCF S2, O:W = 50:50, C_{surf} = 3 wt.%.

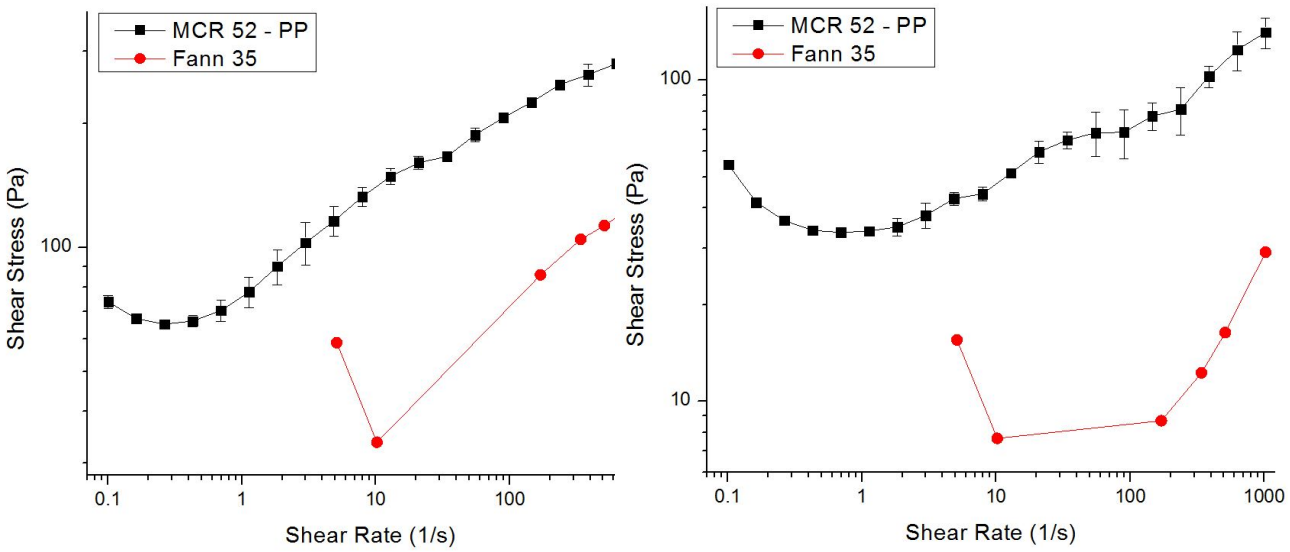

(a) 25 °C (b) 75 °C

Figure B.47. True & Cohesive Slip Determination: OCF S2, O:W = 60:40, C_{surf} = 1 wt.%.

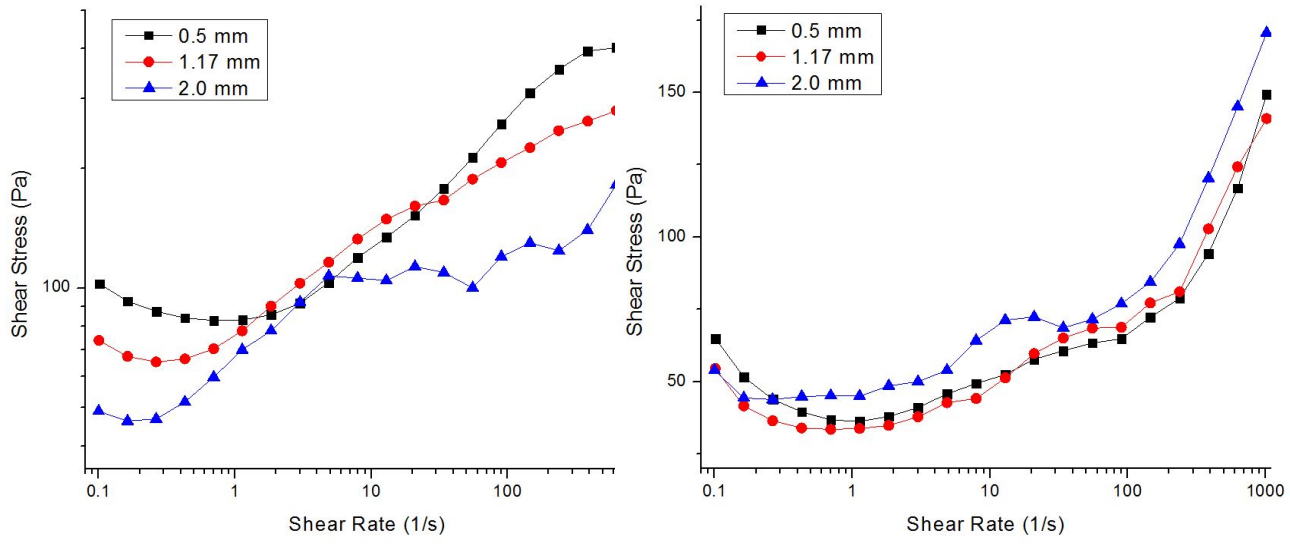

(a) 25 °C (b) 75 °C

Figure B.48. Lubrication Slip Determination: OCF S2, O:W = 60:40, C_{surf} = 1 wt.%.

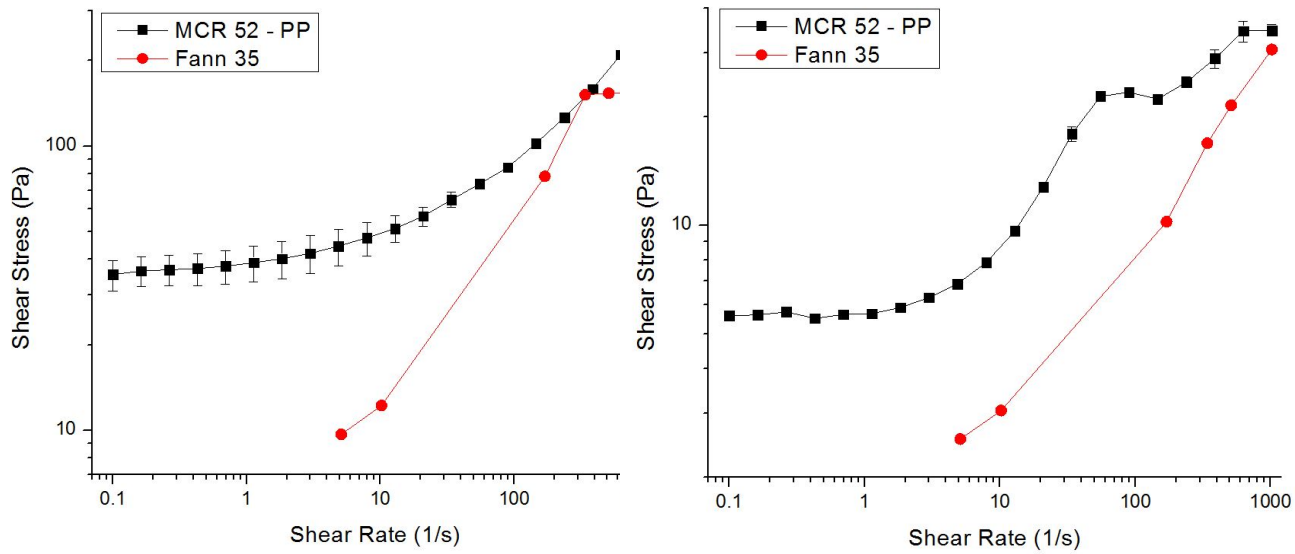

(a) 25 °C (b) 75 °C

Figure B.49. True & Cohesive Slip Determination: OCF S2, O:W = 60:40, C_{surf} = 3 wt.%.

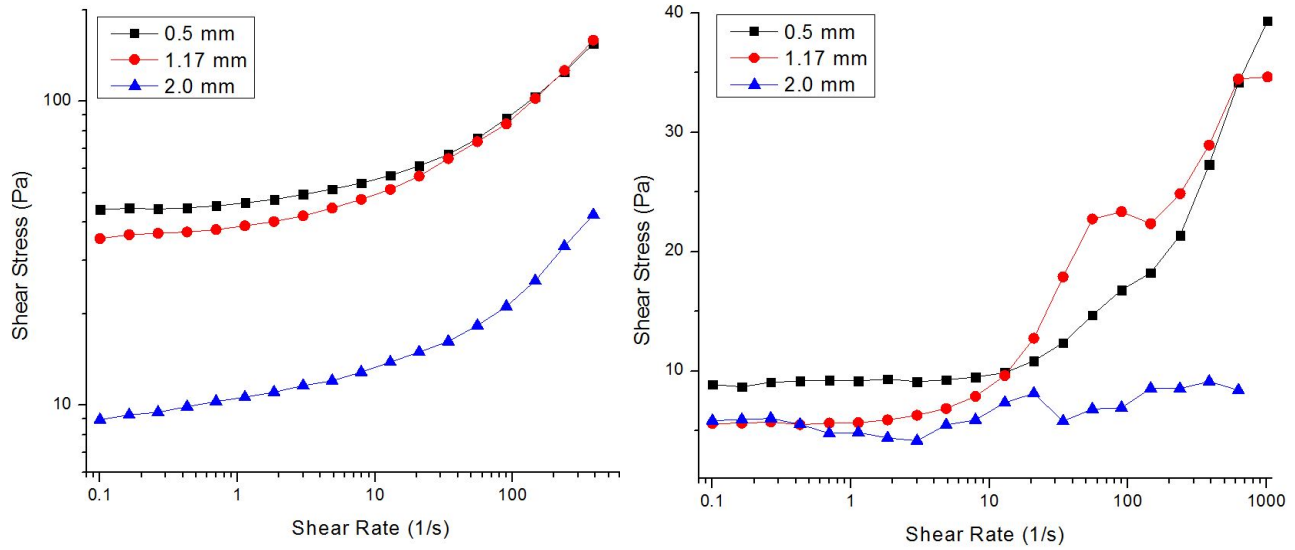

(a) 25 °C (b) 75 °C

Figure B.50. Lubrication Slip Determination: OCF S2, O:W = 60:40, C_{surf} = 3 wt.%.

B.4 Effect of Oil:Water Ratio

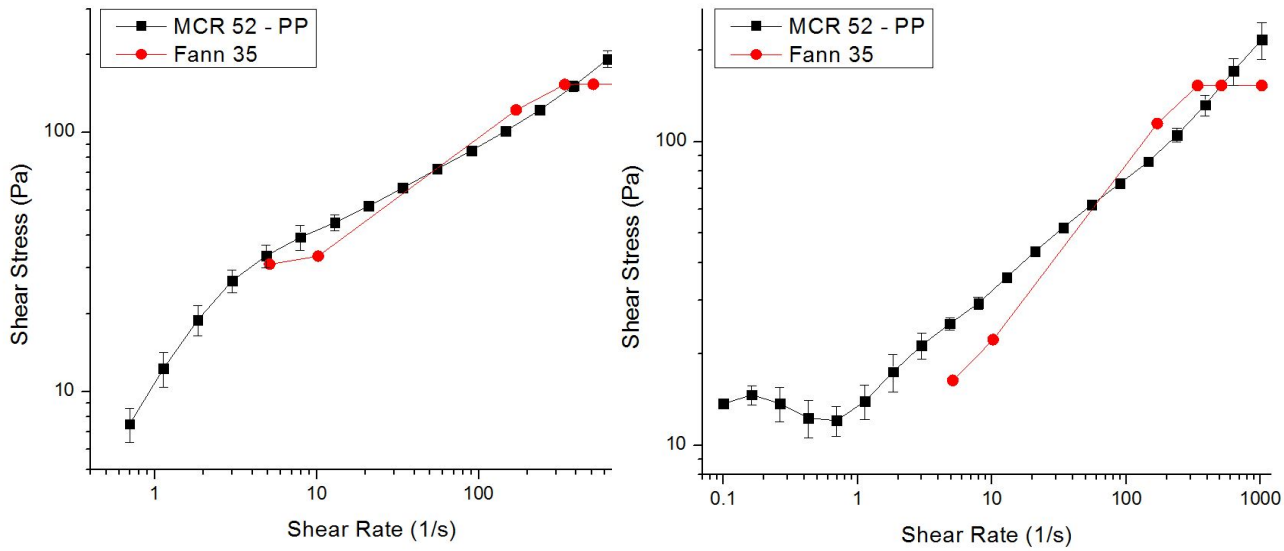

(a) O:W = 50:50 (b) O:W = 60:40

Figure B.51. True & Cohesive Slip Determination: OCF S1, C_{surf} = 1 wt.%, T = 25 °C.

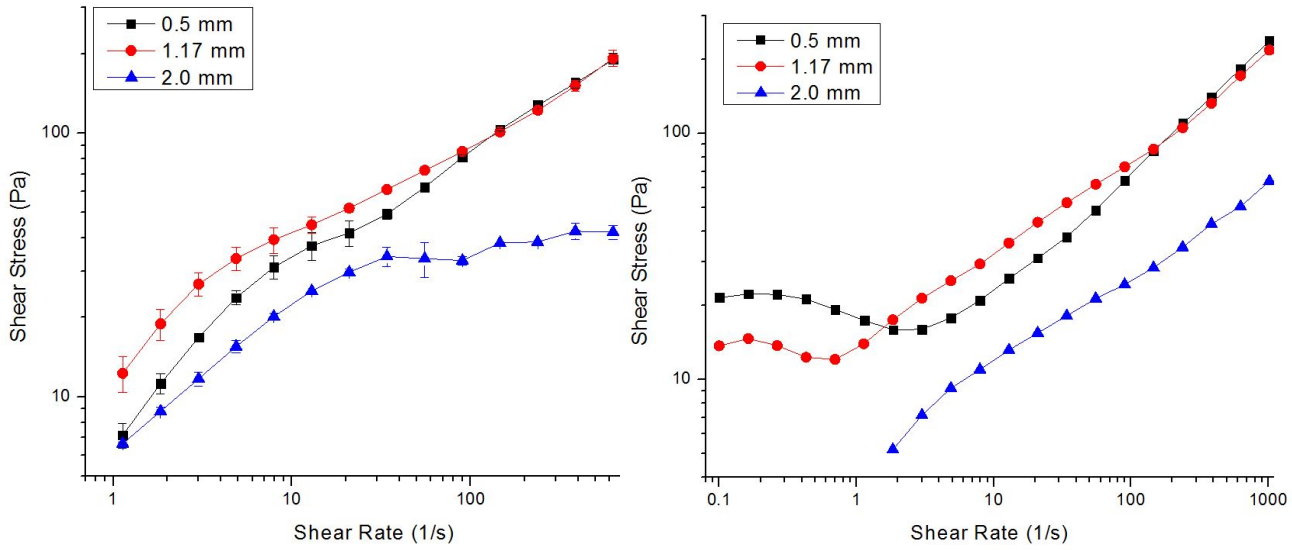

(a) 50:50 (b) 60:40

Figure B.52. Lubrication Slip Determination: OCF S1, C_{surf} = 1 wt.%, T = 25 °C.

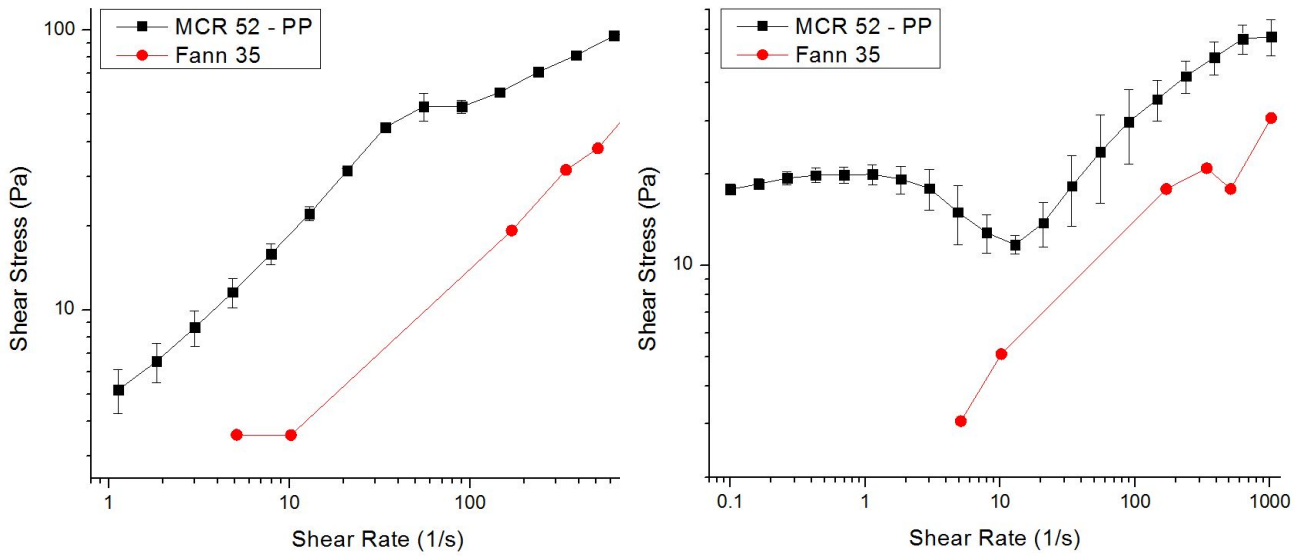

(a) O:W = 50:50 (b) O:W = 60:40

Figure B.53. True & Cohesive Slip Determination: OCF S1, C_{surf} = 1 wt.%, T = 75 °C.

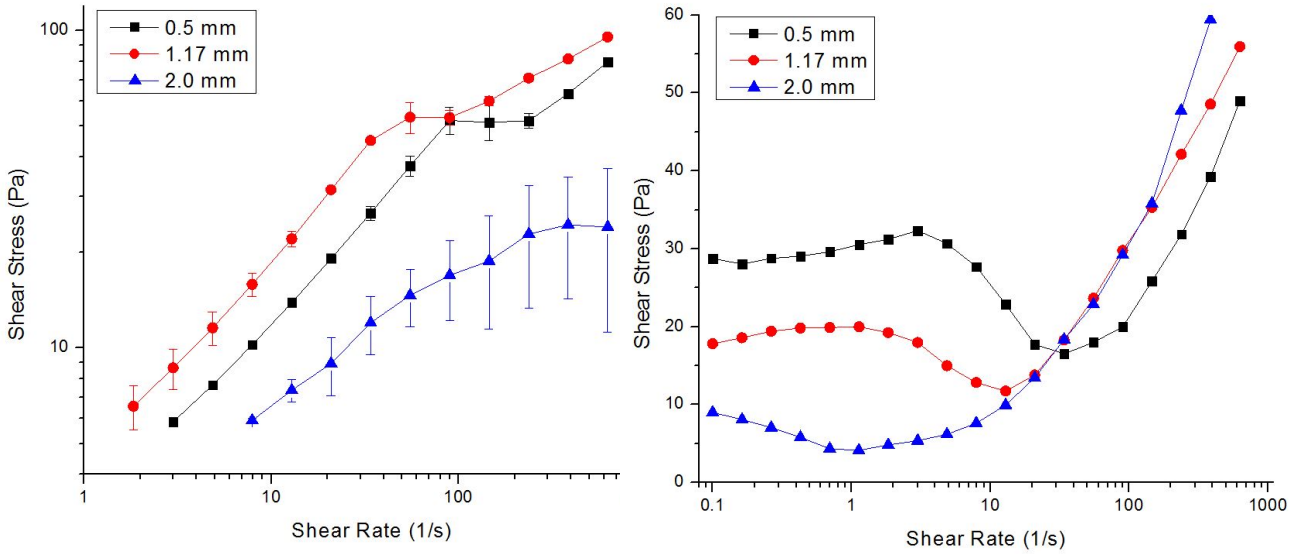

(a) 50:50 (b) 60:40

Figure B.54. Lubrication Slip Determination: OCF S1, C_{surf} = 1 wt.%, T = 75 °C.

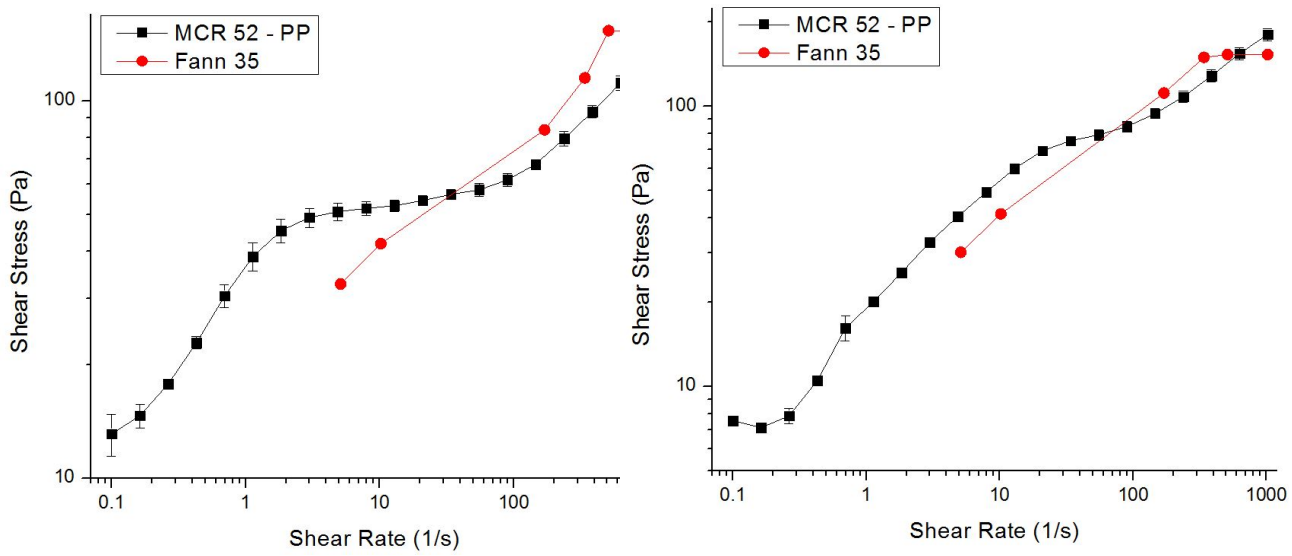

(a) O:W = 50:50 (b) O:W = 60:40

Figure B.55. True & Cohesive Slip Determination: OCF S1, C_{surf} = 3 wt.%, T = 25 °C.

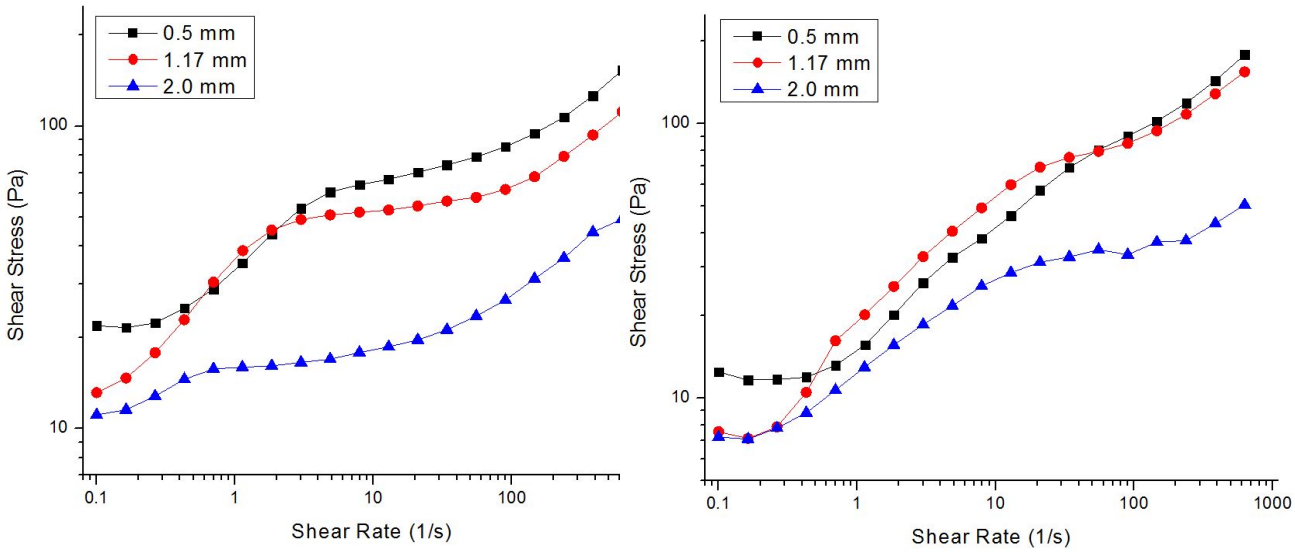

(a) 50:50 (b) 60:40

Figure B.56. Lubrication Slip Determination: OCF S1, C_{surf} = 3 wt.%, T = 25 °C.

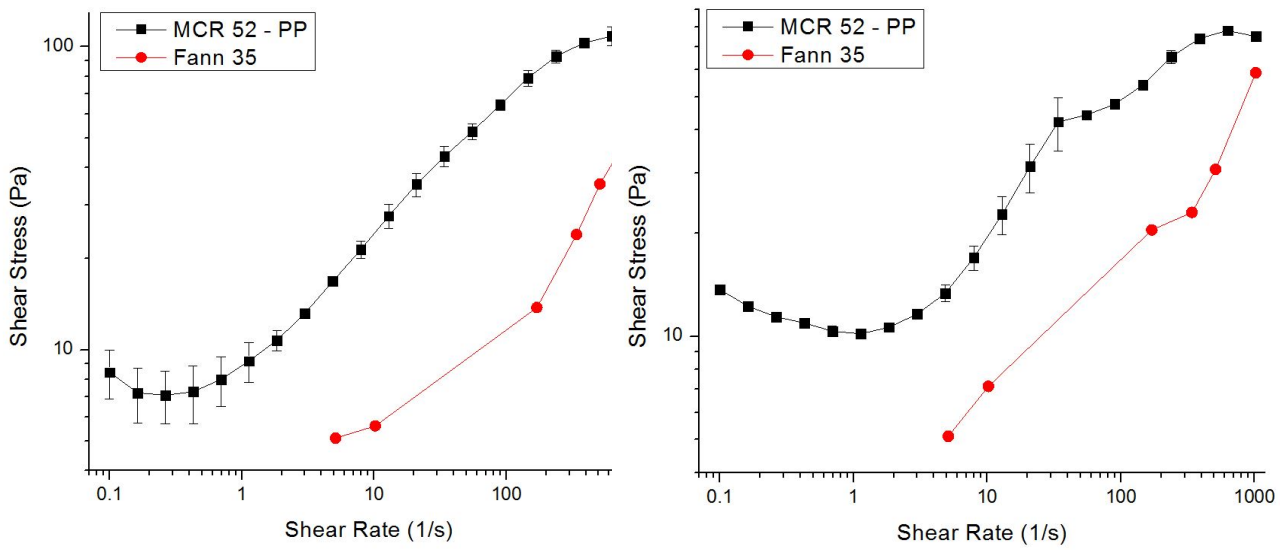

(a) O:W = 50:50 (b) O:W = 60:40

Figure B.57. True & Cohesive Slip Determination: OCF S1, C_{surf} = 3 wt.%, T = 75 °C.

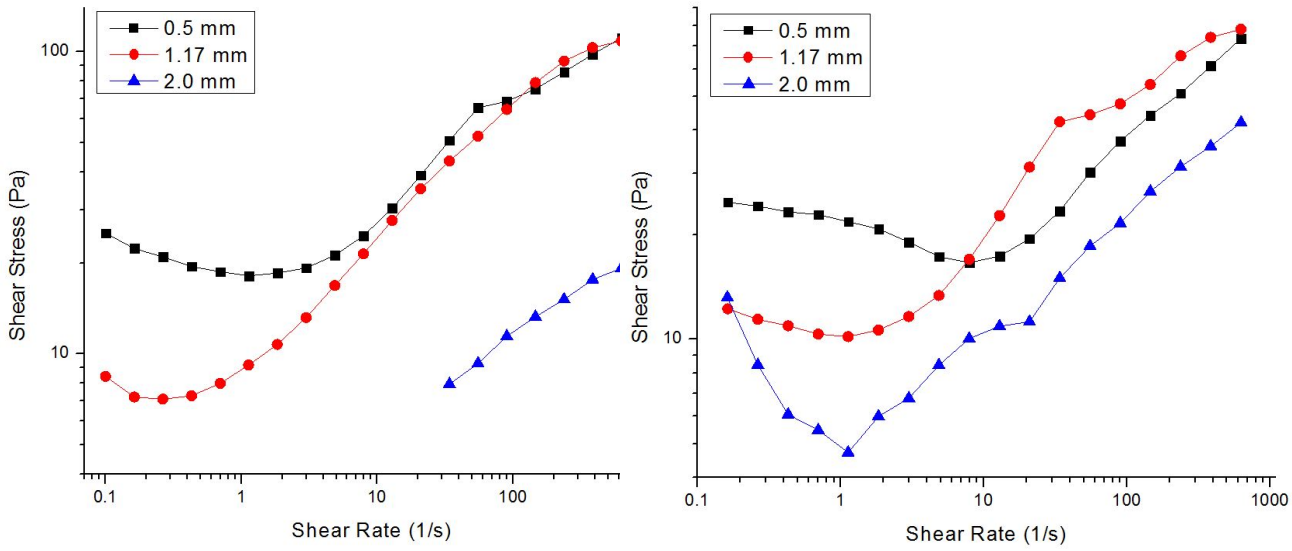

(a) 50:50 (b) 60:40

Figure B.58. Lubrication Slip Determination: OCF S1, C_{surf} = 3 wt.%, T = 75 °C.

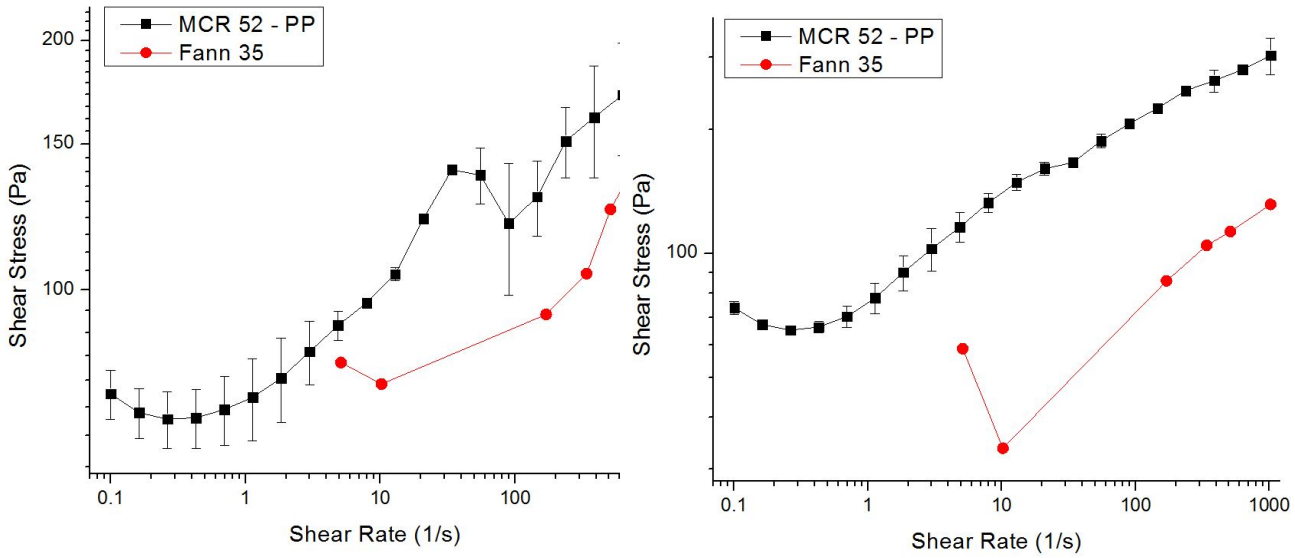

(a) O:W = 50:50 (b) O:W = 60:40

Figure B.59. True & Cohesive Slip Determination: OCF S2, C_{surf} = 1 wt.%, T = 25 °C.

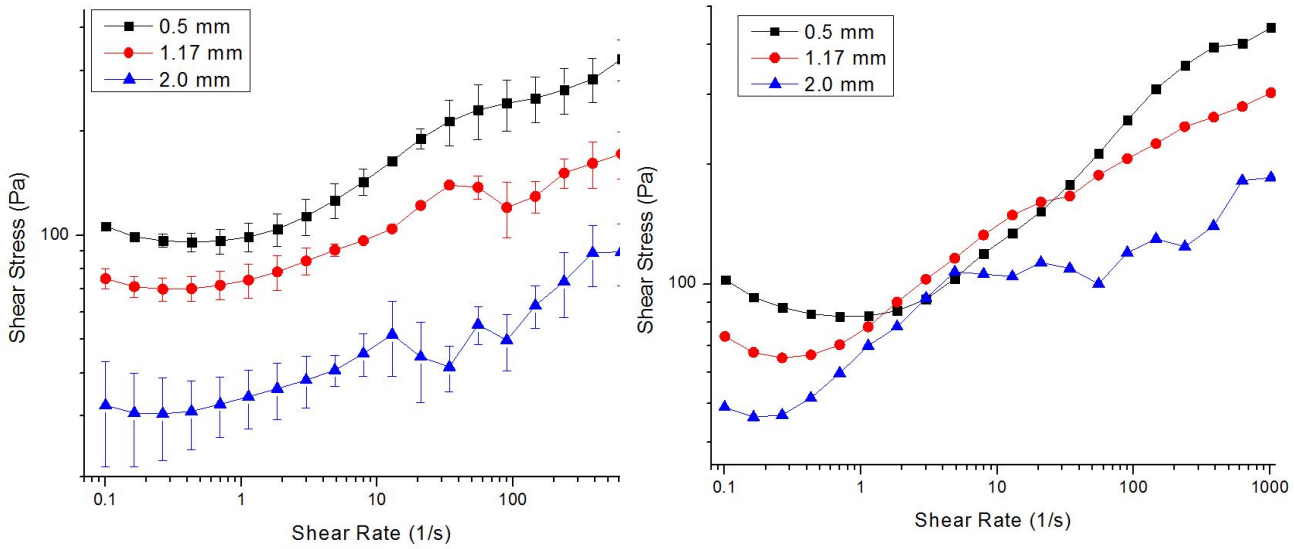

(a) 50:50 (b) 60:40

Figure B.60. Lubrication Slip Determination: OCF S2, C_{surf} = 1 wt.%, T = 25 °C.

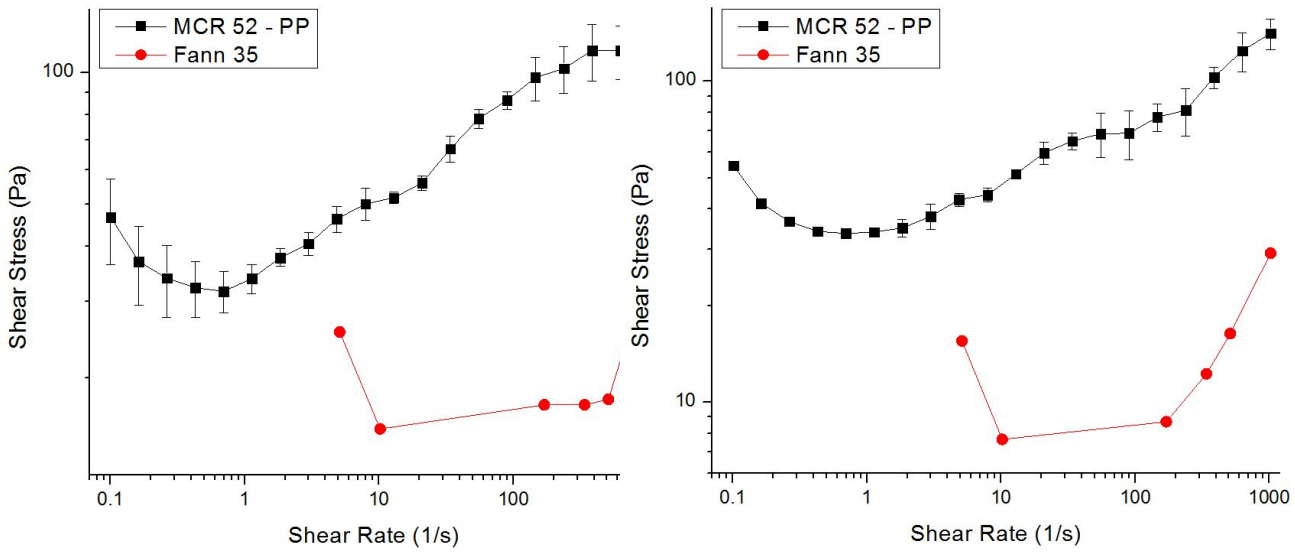

(a) O:W = 50:50 (b) O:W = 60:40

Figure B.61. True & Cohesive Slip Determination: OCF S2, C_{surf} = 1 wt.%, T = 75 °C.

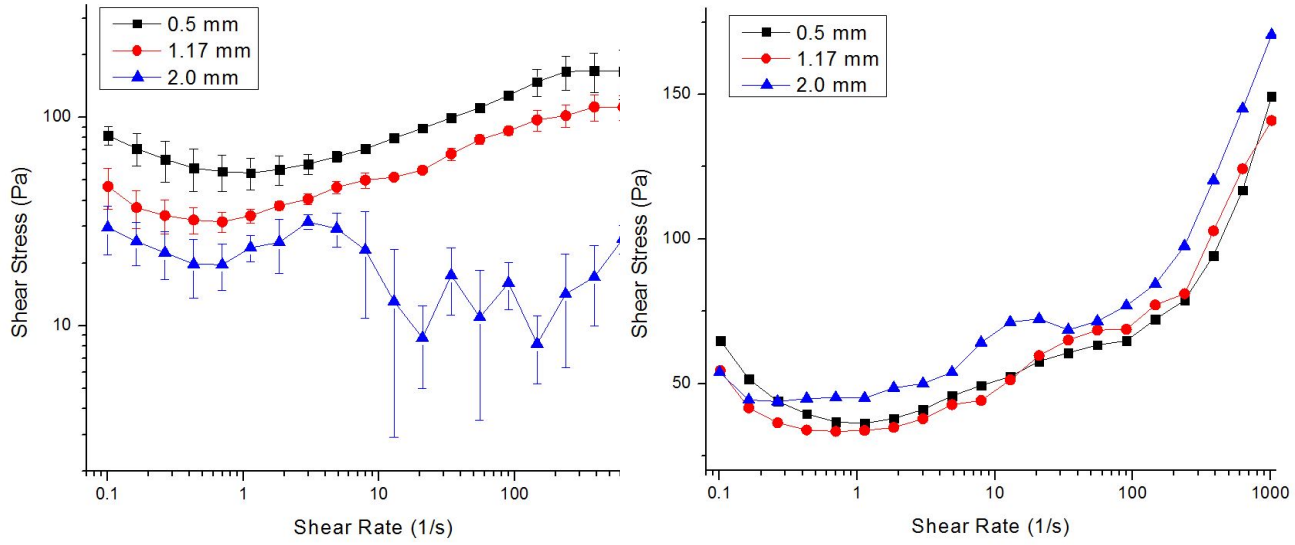

(a) 50:50 (b) 60:40

Figure B.62. Lubrication Slip Determination: OCF S2, C_{surf} = 1 wt.%, T = 75 °C.

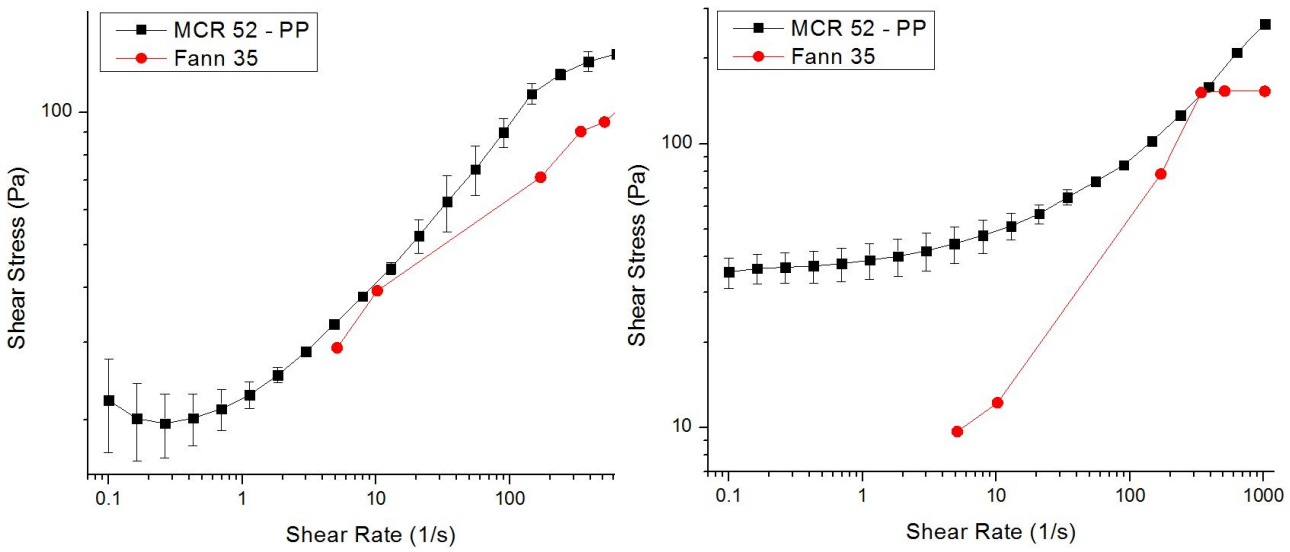

(a) O:W = 50:50 (b) O:W = 60:40

Figure B.63. True & Cohesive Slip Determination: OCF S2, C_{surf} = 3 wt.%, T = 25 °C.

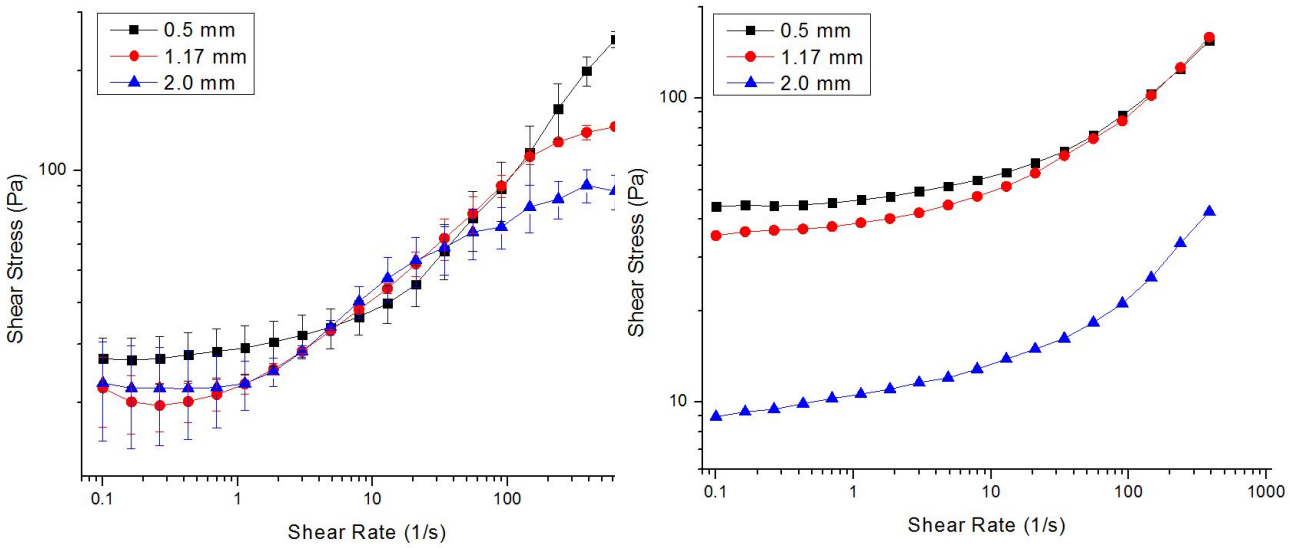

(a) 50:50 (b) 60:40

Figure B.64. Lubrication Slip Determination: OCF S2, C_{surf} = 3 wt.%, T = 25 °C.

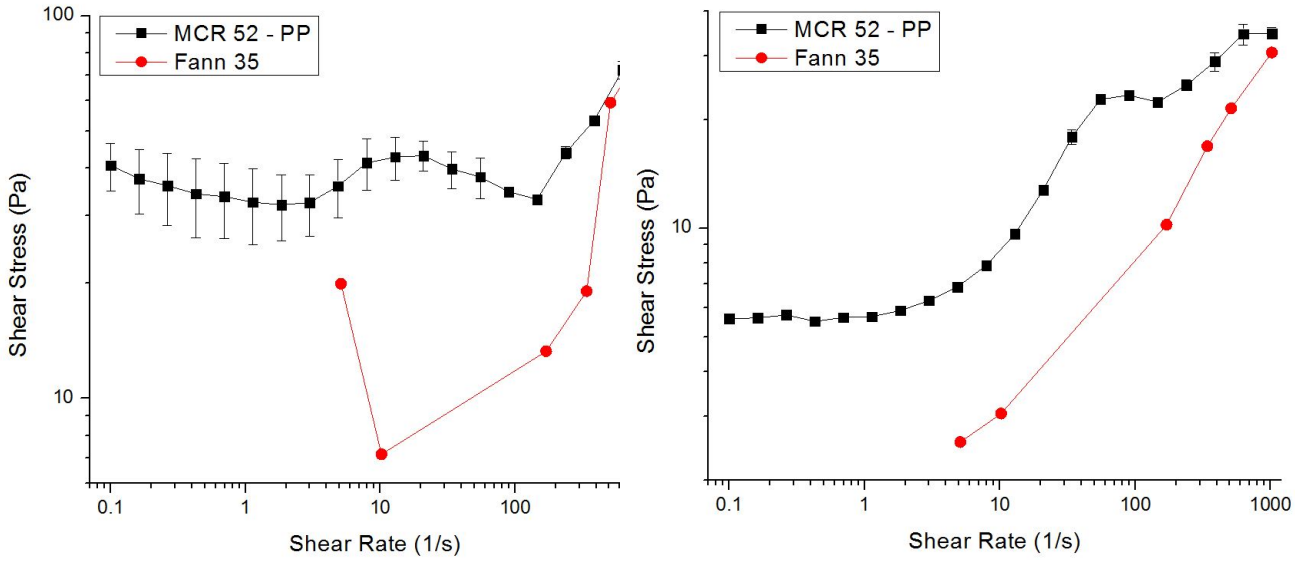

(a) O:W = 50:50 (b) O:W = 60:40

Figure B.65. True & Cohesive Slip Determination: OCF S2, C_{surf} = 3 wt.%, T = 75 °C.

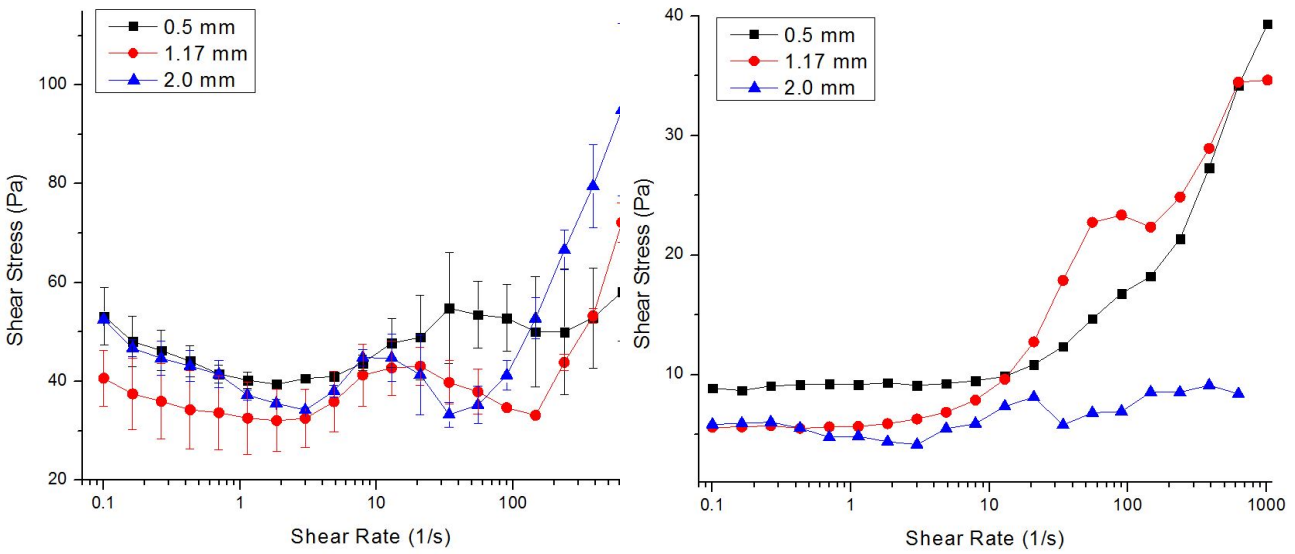

(a) 50:50 (b) 60:40

Figure B.66. Lubrication Slip Determination: OCF S2, C_{surf} = 3 wt.%, T = 75 °C.

B.5 Comparison to Drilling Muds

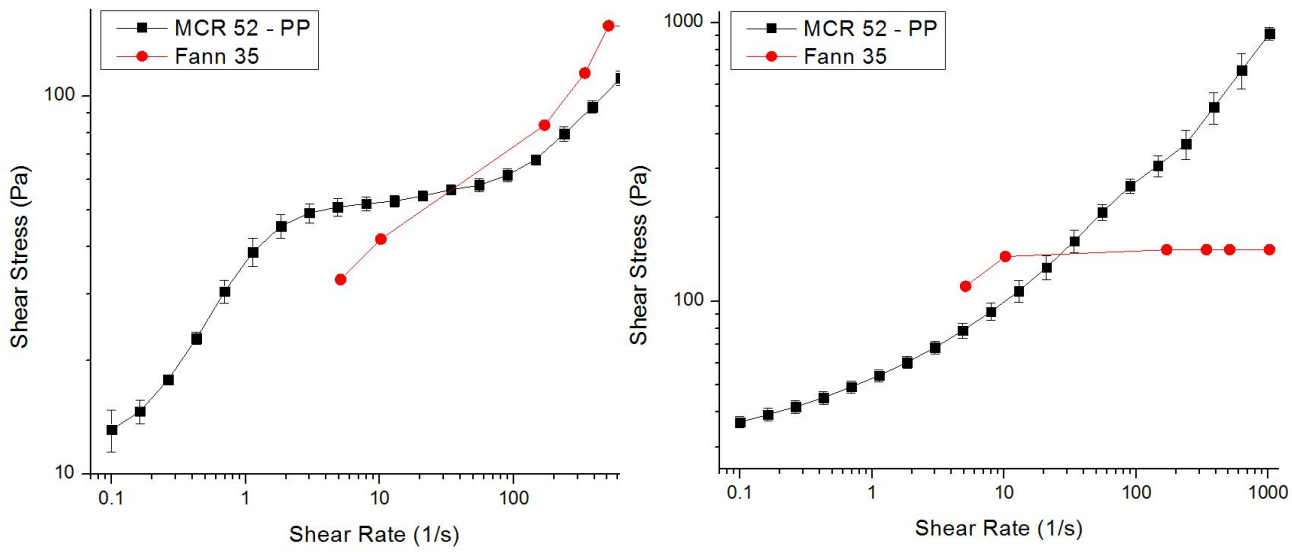

(a) OCF S1 (b) OBM S1

Figure B.67. True & Cohesive Slip Determination: O:W = 50:50, C_{surf} = 3 wt.%, T = 25 °C.

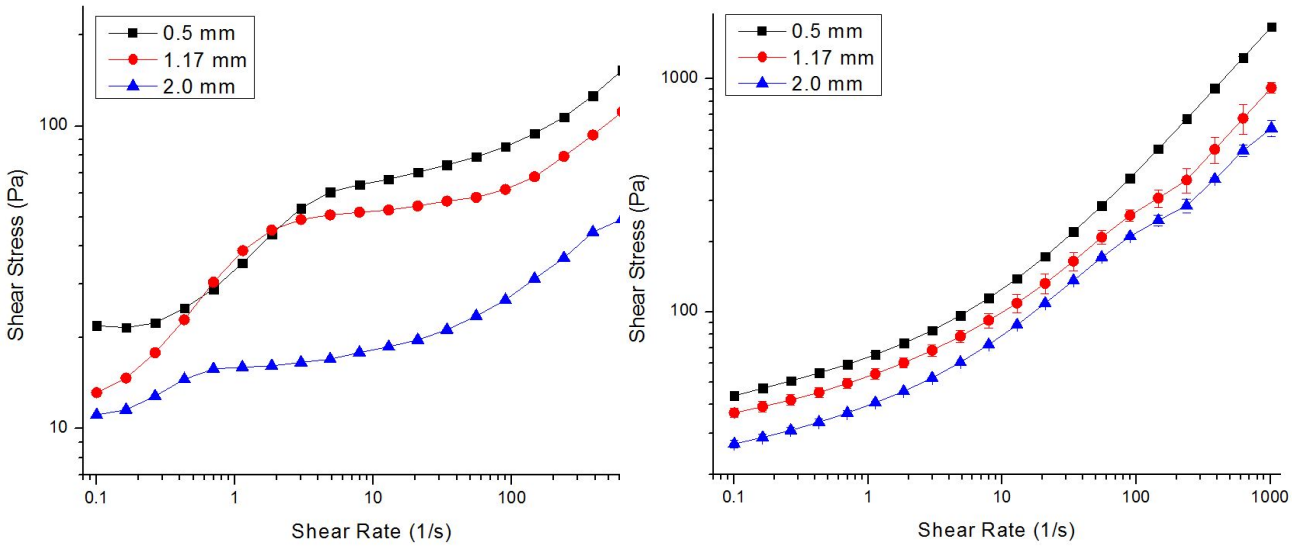

(a) OCF S1 (b) OBM S1

Figure B.68. Lubrication Slip Determination: O:W = 50:50, C_{surf} = 3 wt.%, T = 25 °C.

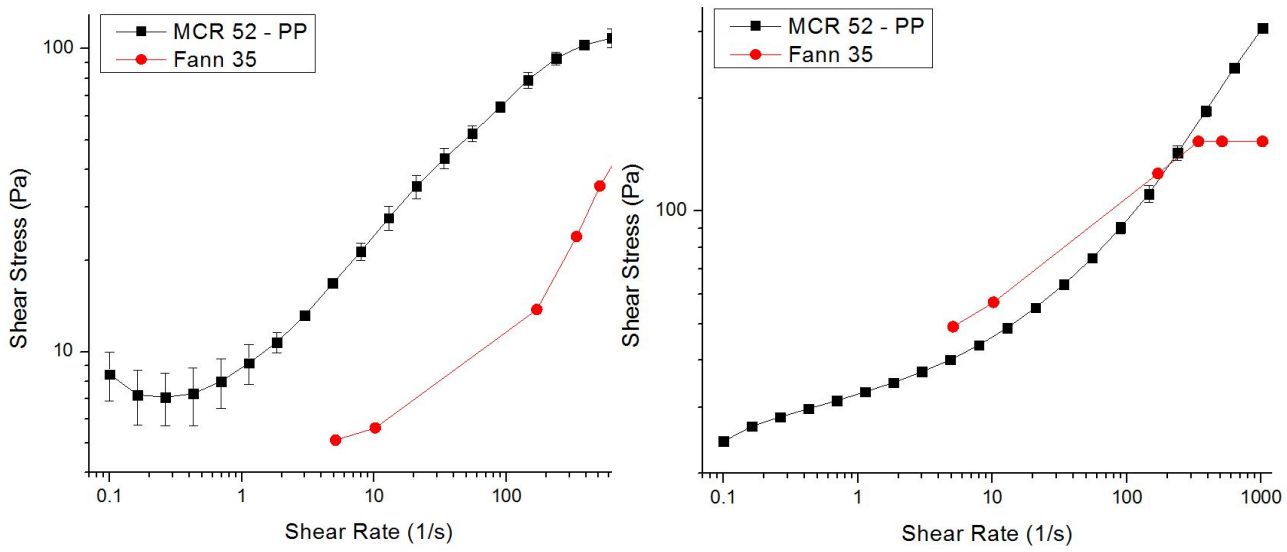

(a) OCF S1 (b) OBM S1

Figure B.69. True & Cohesive Slip Determination: O:W = 50:50, C_{surf} = 3 wt.%, T = 75 °C.

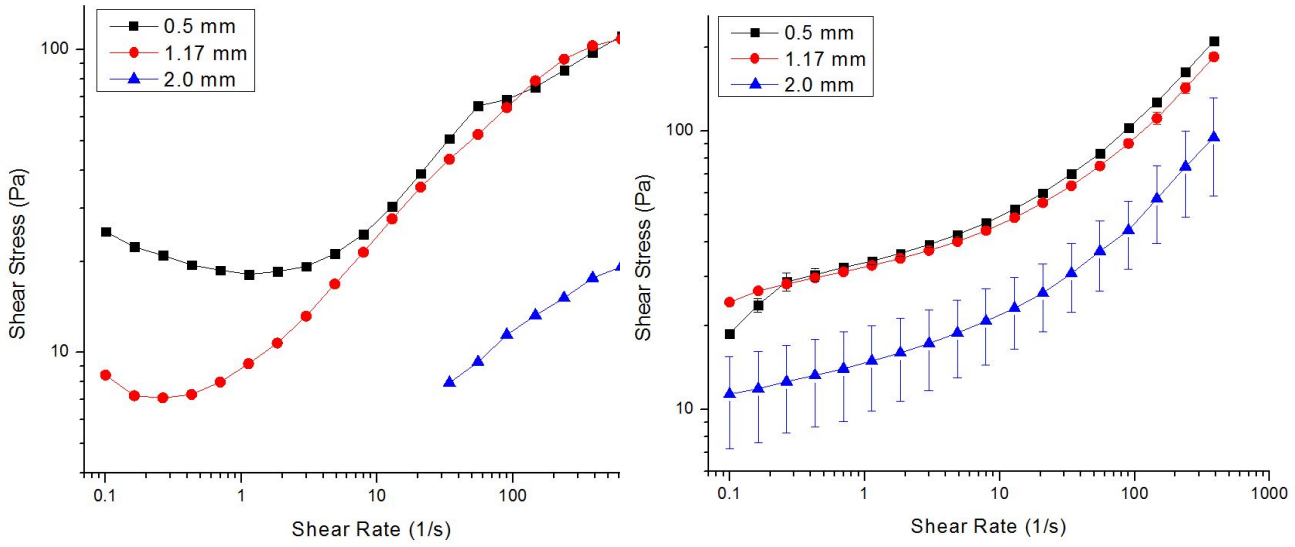

(a) OCF S1 (b) OBM S1

Figure B.70. Lubrication Slip Determination: O:W = 50:50, C_{surf} = 3 wt.%, T = 75 °C.

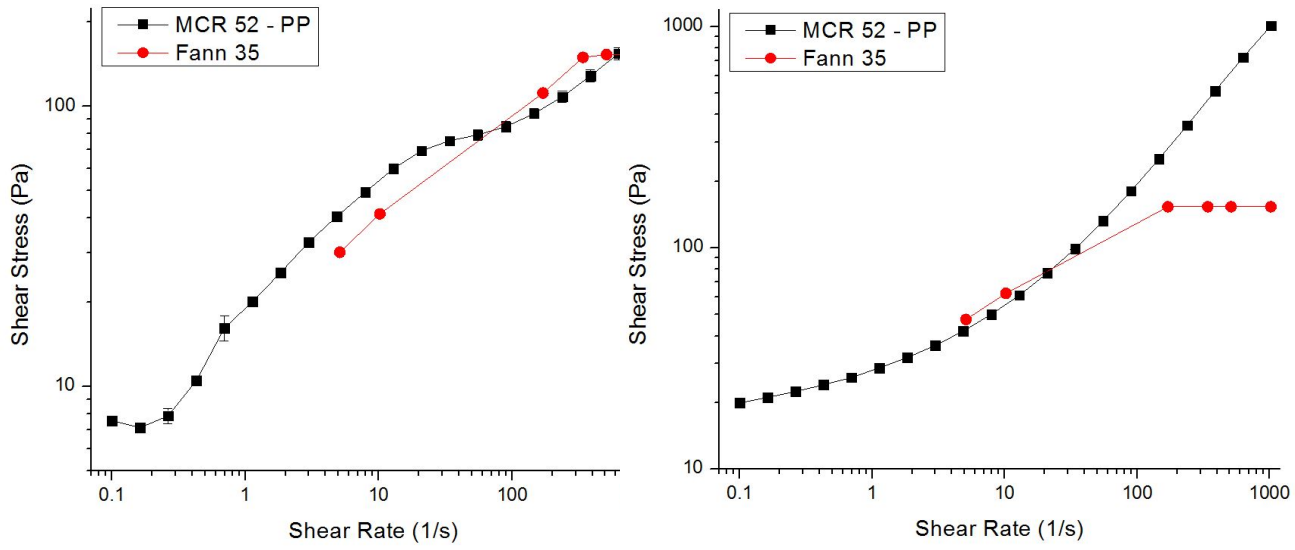

(a) OCF S1 (b) OBM S1

Figure B.71. True & Cohesive Slip Determination: O:W = 60:40, C_{surf} = 3 wt.%, T = 25 °C.

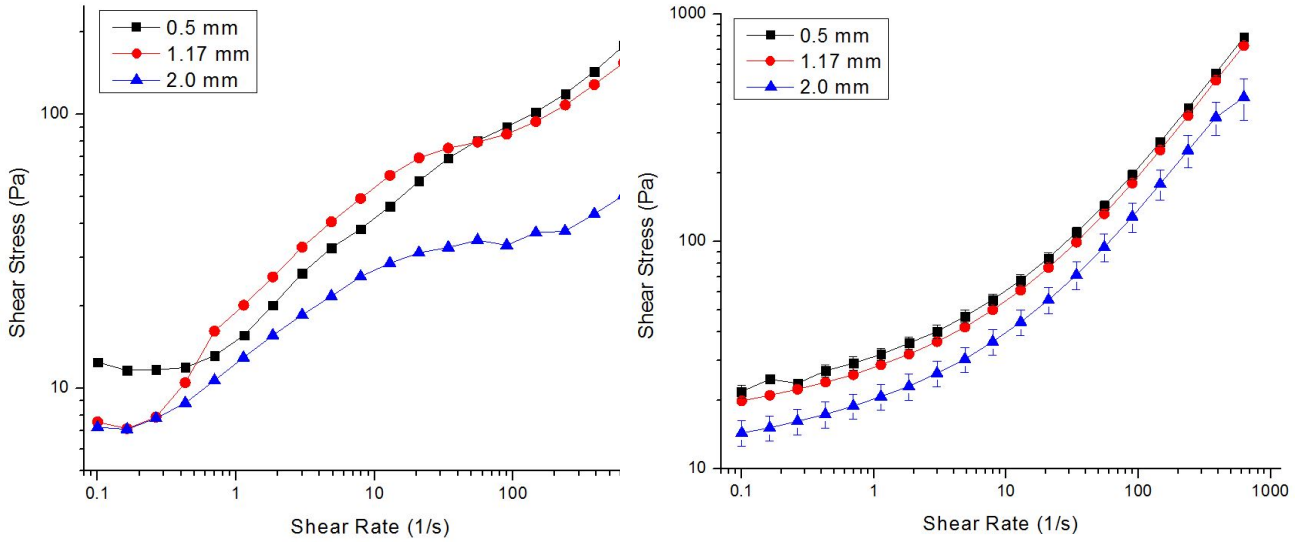

(a) OCF S1 (b) OBM S1

Figure B.72. Lubrication Slip Determination: O:W = 60:40, C_{surf} = 3 wt.%, T = 25 °C.

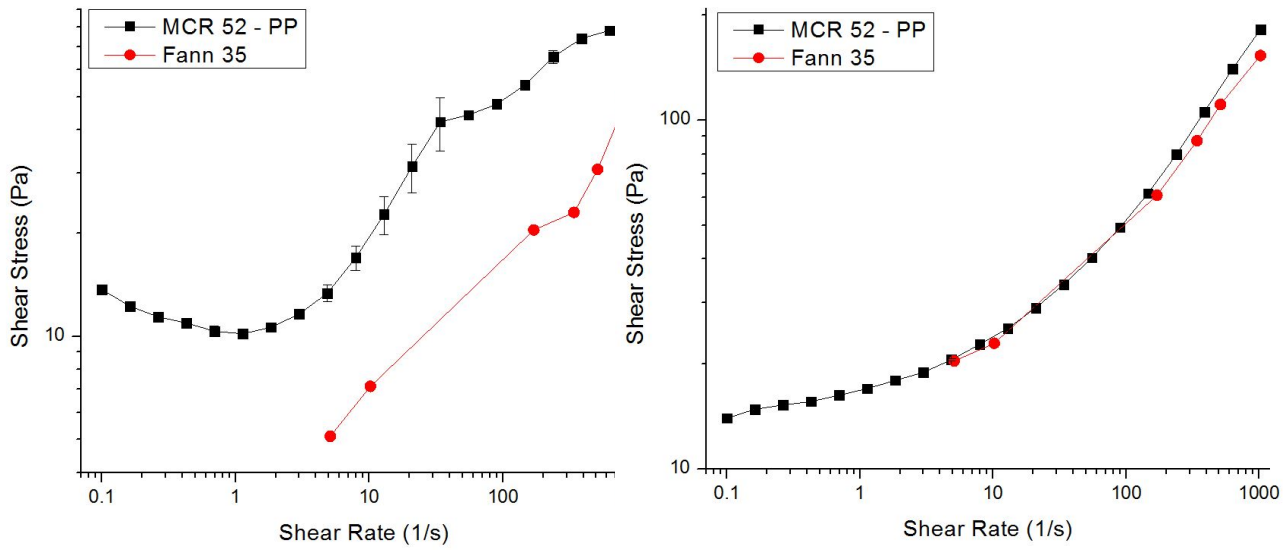

(a) OCF S1 (b) OBM S1

Figure B.73. True & Cohesive Slip Determination: O:W = 60:40, C_{surf} = 3 wt.%, T = 75 °C.

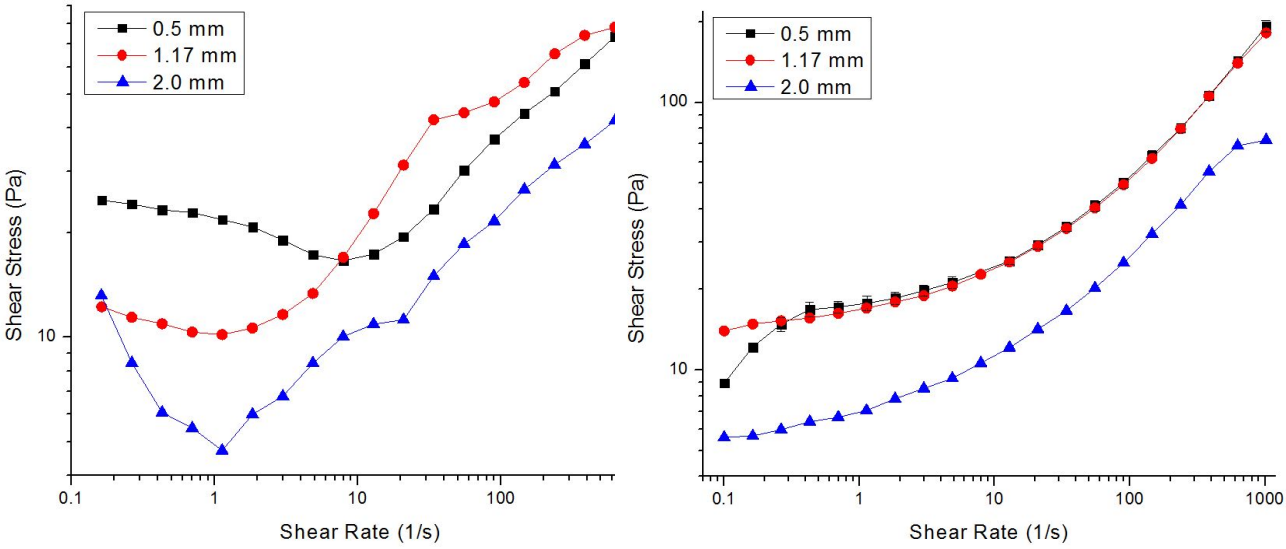

(a) OCF S1 (b) OBM S1

Figure B.74. Lubrication Slip Determination: O:W = 60:40, C_{surf} = 3 wt.%, T = 75 °C.

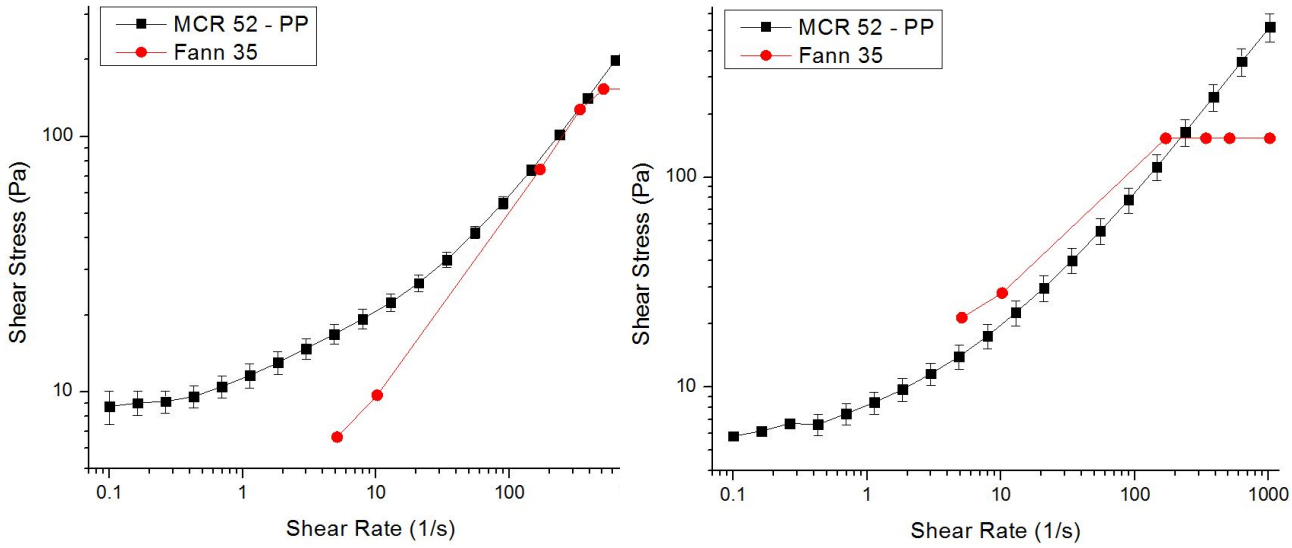

(a) OCF S1 (b) OBM S1

Figure B.75. True & Cohesive Slip Determination: O:W = 70:30, C_{surf} = 3 wt.%, T = 25 °C.

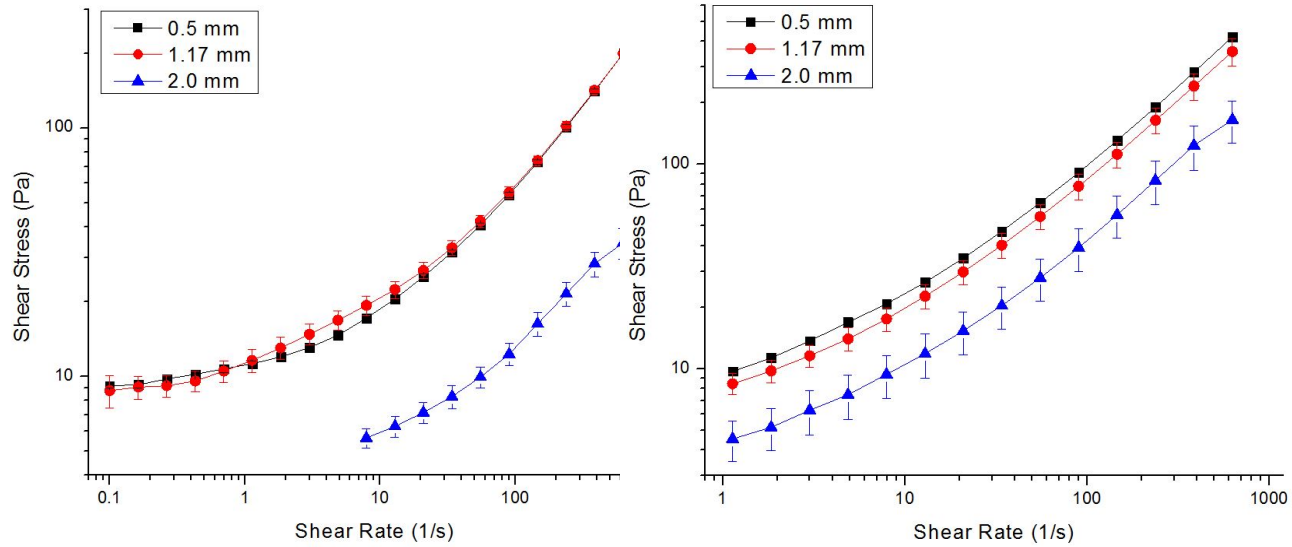

(a) OCF S1 (b) OBM S1

Figure B.76. Lubrication Slip Determination: O:W = 70:30, C_{surf} = 3 wt.%, T = 25 °C.

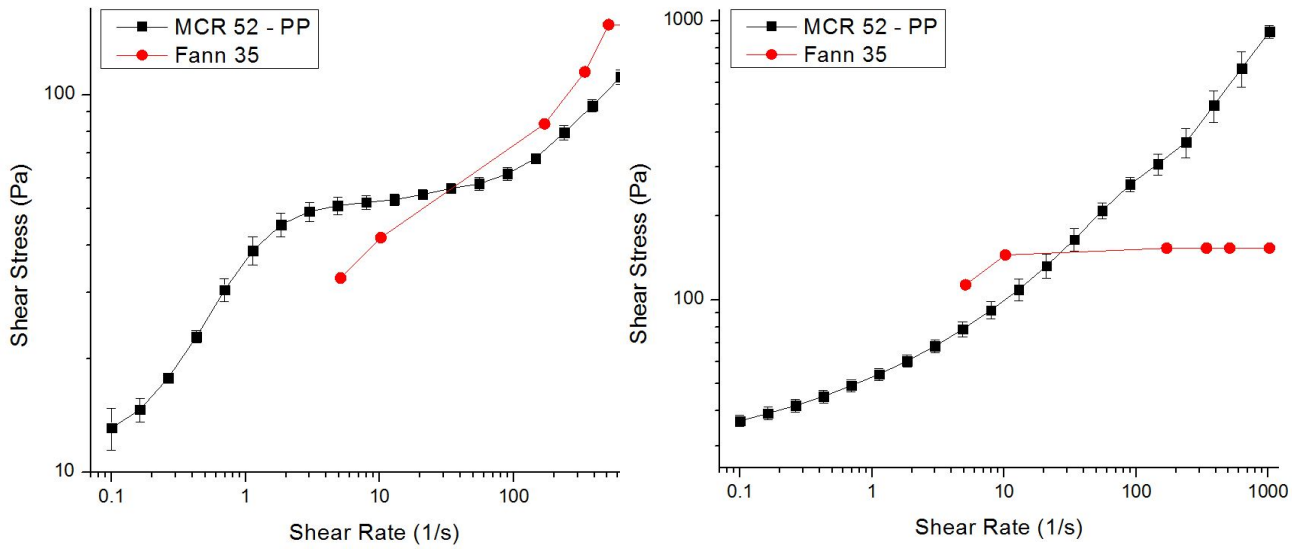

(a) OCF S1 (b) OBM S1

Figure B.77. True & Cohesive Slip Determination: O:W = 50:50, C_{surf} = 3 wt.%, T = 25 °C.

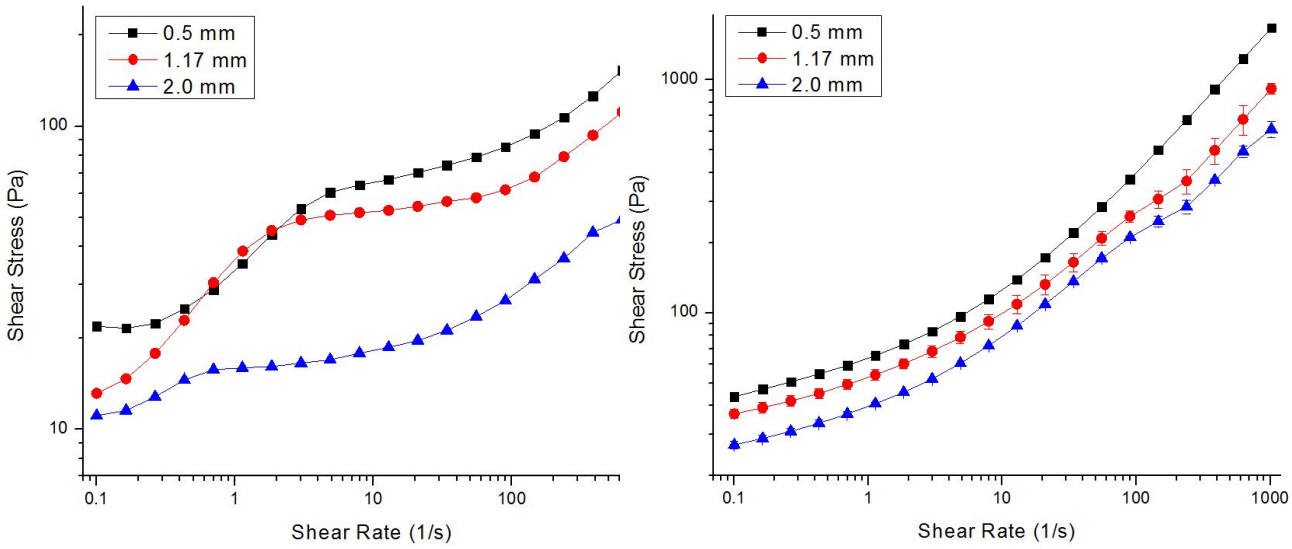

(a) OCF S1 (b) OBM S1

Figure B.78. Lubrication Slip Determination: O:W = 50:50, C_{surf} = 3 wt.%, T = 25 °C.

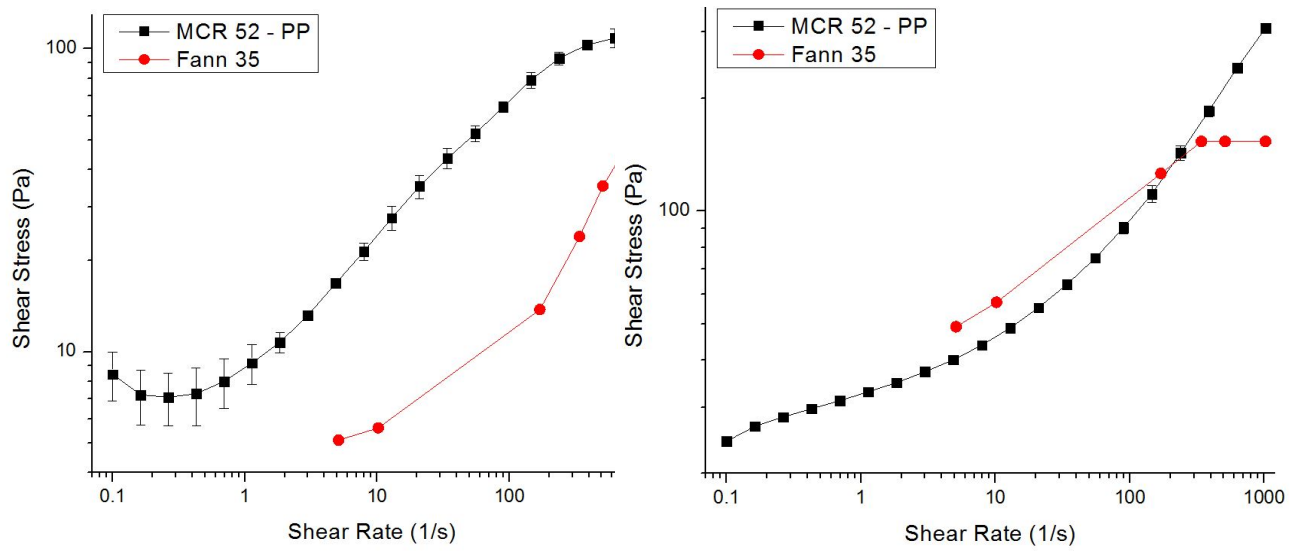

(a) OCF S1 (b) OBM S1

Figure B.79. True & Cohesive Slip Determination: O:W = 50:50, C_{surf} = 3 wt.%, T = 75 °C.

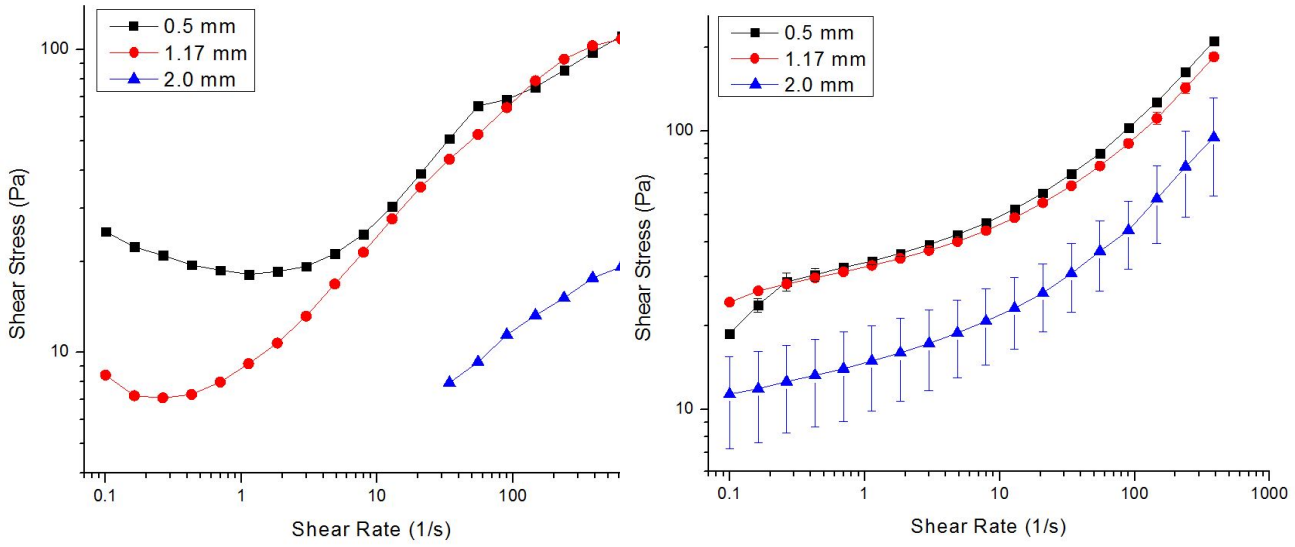

(a) OCF S1 (b) OBM S1

Figure B.80. Lubrication Slip Determination: O:W = 50:50, C_{surf} = 3 wt.%, T = 75 °C.

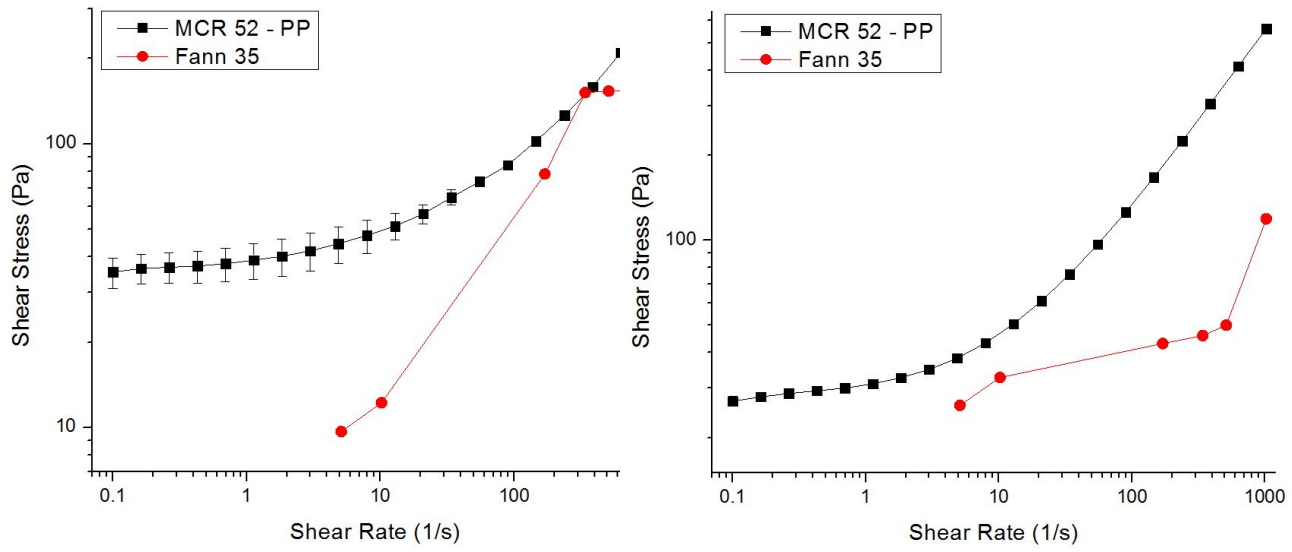

(a) OCF S2 (b) OBM S2

Figure B.81. True & Cohesive Slip Determination: O:W = 60:40, C_{surf} = 3 wt.%, T = 25 °C.

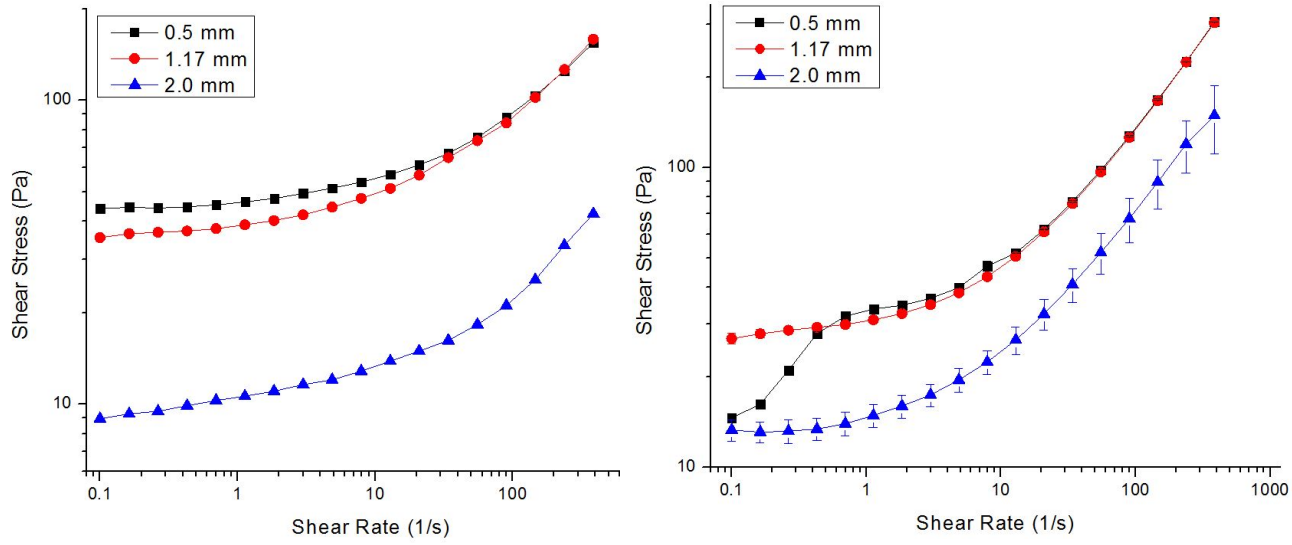

(a) OCF S2 (b) OBM S2

Figure B.82. Lubrication Slip Determination: O:W = 60:40, C_{surf} = 3 wt.%, T = 25 °C.

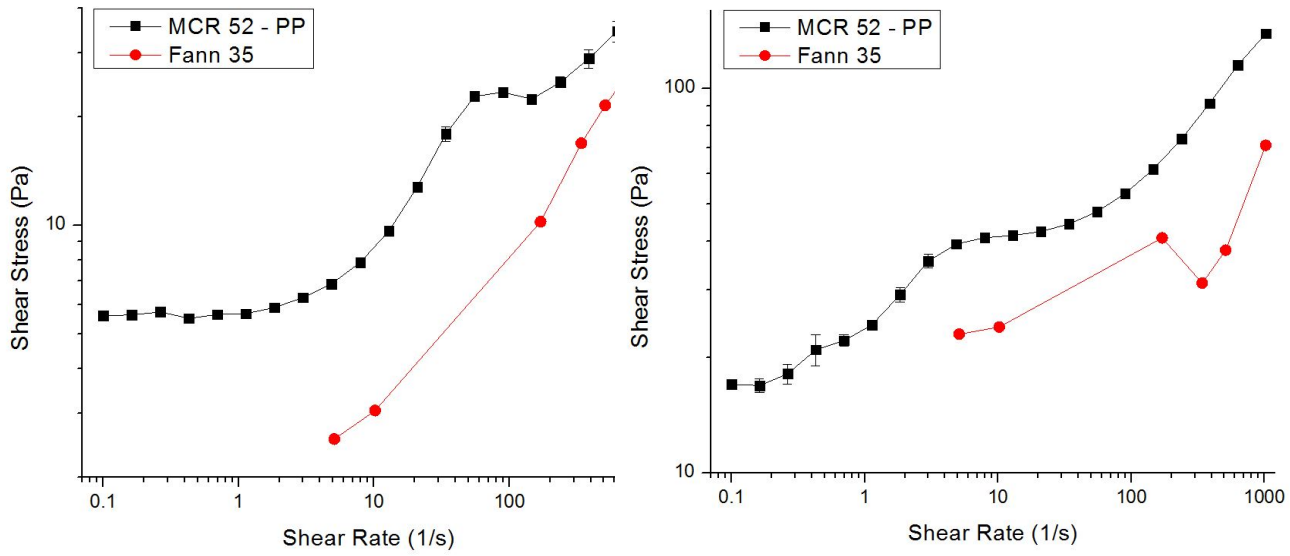

(a) OCF S2 (b) OBM S2

Figure B.83. True & Cohesive Slip Determination: O:W = 60:40, C_{surf} = 3 wt.%, T = 75 °C.

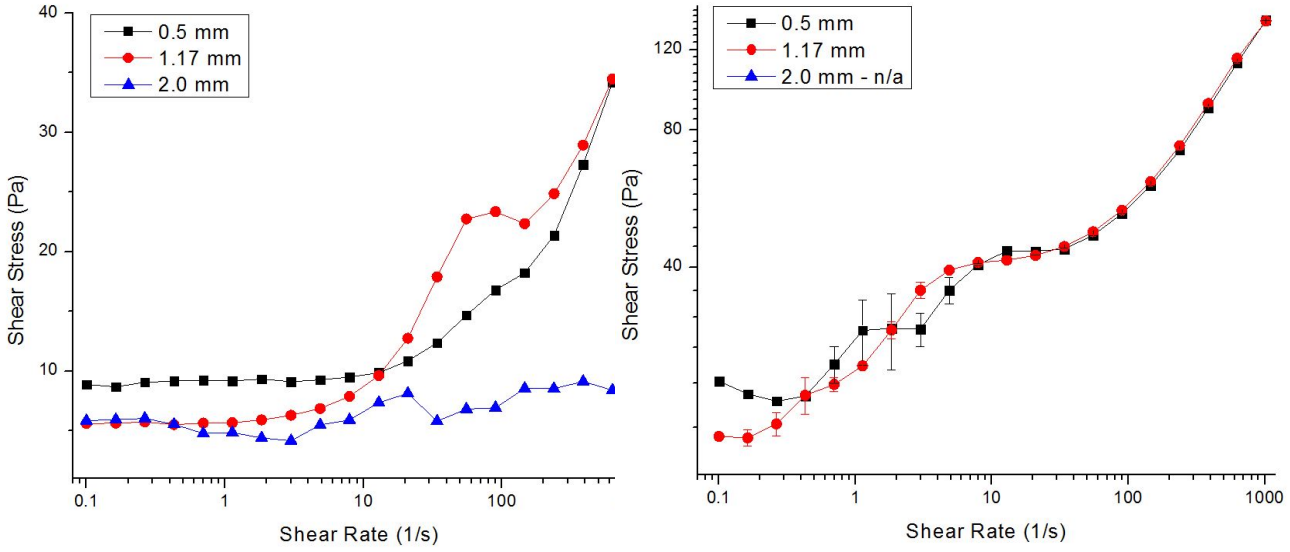

(a) OCF S2 (b) OBM S2

Figure B.84. Lubrication Slip Determination: O:W = 60:40, C_{surf} = 3 wt.%, T = 75 °C.

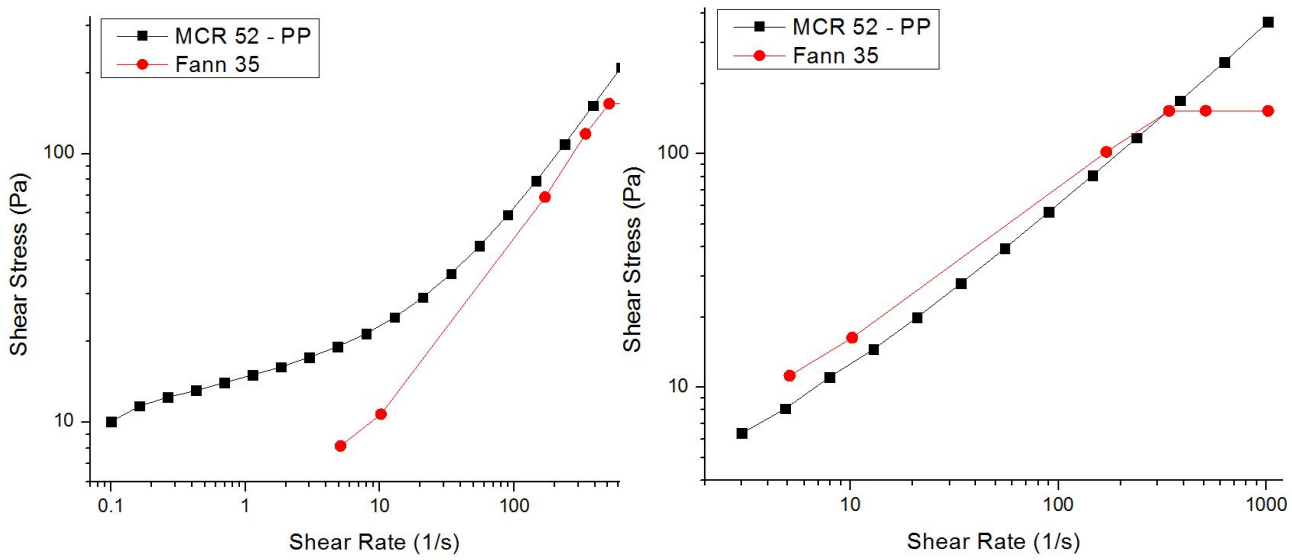

(a) OCF S2 (b) OBM S2

Figure B.85. True & Cohesive Slip Determination: O:W = 70:30, C_{surf} = 3 wt.%, T = 25 °C.

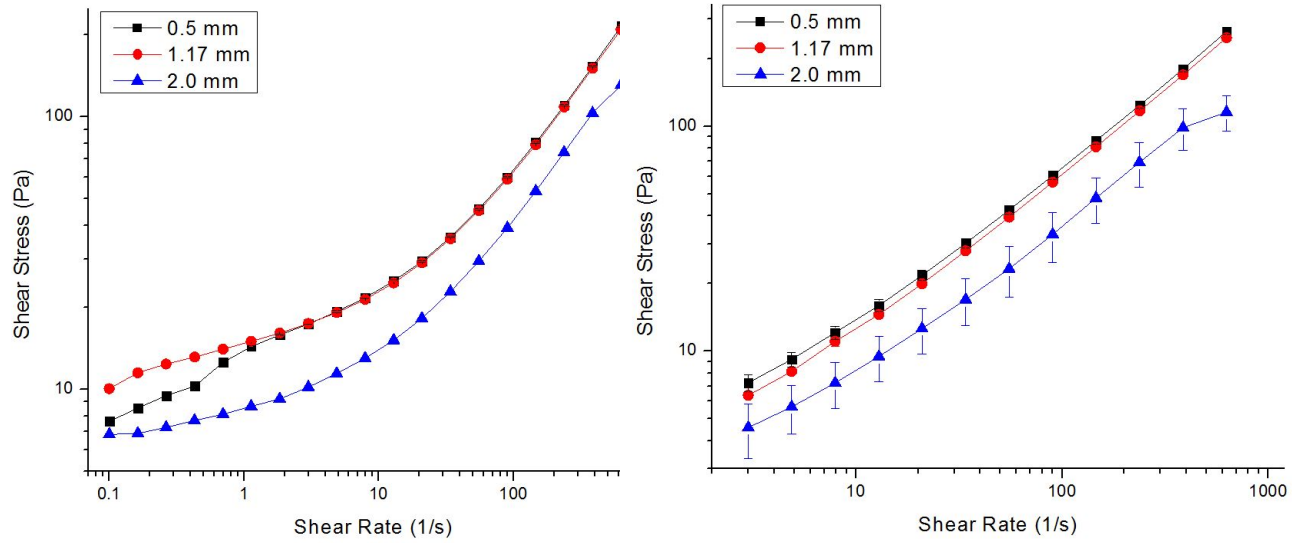

(a) OCF S2 (b) OBM S2

Figure B.86. Lubrication Slip Determination: O:W = 70:30, C_{surf} = 3 wt.%, T = 25 °C.

Vita

Gilles Numkam was born in Cameroon where he grew up and completed his education till his Bachelor's degree in Chemistry, obtained at the University of Buea in 2011. He then traveled to Belgium in Leuven, where he completed his Master's degree in Chemical Engineering at the Katholieke Universiteit Leuven, where his thesis was focused on the effect of microgaps on the shear flow of microstructured systems. Upon completion, he enrolled at the Craft & Hawkins Department of Petroleum Engineering at Louisiana State University in 2014 to pursue his Doctoral degree in Petroleum Engineering, with his research interest focused on the rheology of emulsion-suspension complex fluids.